Hawke's Bay 3D Aquifer Mapping Project:

Numerical Groundwater Modelling experiments using SkyTEM data in the Heretaunga Plains

February 2025
Hawkes Bay Regional Council Publication No. 5676

HAWKES BAY
REGIONAL COUNCIL
TE KAUNIHERA Ā-ROHE O TE MATAU-A-MĀUI

ISSN 2703-2051 (Online)
ISSN 2703-2043 (Print)

HAWKES BAY REGIONAL COUNCIL
TE KAUNIHERA Ā-ROHE O TE MATAU-A-MĀUI

(06) 835 9200
0800 108 838
Private Bag 6006 Napier 4142
159 Dalton Street . Napier 4110

Environmental Science

Hawke's Bay 3D Aquifer Mapping Project:

Numerical Groundwater Modelling experiments using SkyTEM data in the Heretaunga Plains

February 2025
Hawkes Bay Regional Council Publication No. 5676

Prepared By:

GNS Science

BJC Hemmings CR Moore
ZJ Rawlinson M Taves

For: Hawke's Bay Regional Council

Reviewed by:
S Harper, Hawke's Bay Regional Council
A Elwan, Hawke's Bay Regional Council
T Wilson, Hawke's Bay Regional Council
L Chambers, GNS Science
SG Cameron, GNS Science

.

ISSN 2703-2051 (Online)
ISSN 2703-2043 (Print)

Hawke's Bay 3D Aquifer Mapping Project: Numerical groundwater modelling experiments using SkyTEM data in the Heretaunga Plains

BJC Hemmings
ZJ Rawlinson
CR Moore
MW Taves

GNS Science Consultancy Report 2025/06
February 2025

DISCLAIMER

This report has been prepared by the Institute of Geological and Nuclear Sciences Limited (GNS Science) exclusively for and under contract to Hawke's Bay Regional Council. Unless otherwise agreed in writing by GNS Science, GNS Science accepts no responsibility for any use of or reliance on any contents of this report by any person other than Hawke's Bay Regional Council and shall not be liable to any person other than Hawke's Bay Regional Council, on any ground, for any loss, damage or expense arising from such use or reliance.

Use of Data:

Date that GNS Science can use associated data: January 2025

BIBLIOGRAPHIC REFERENCE

Hemmings BJC, Moore CR, Rawlinson ZJ, Taves MW. 2025. Hawke's Bay 3D Aquifer Mapping Project: Numerical groundwater modelling experiments using SkyTEM data in the Heretaunga Plains. Wairakei (NZ): GNS Science. 297 p. Consultancy Report 2025/05.

CONTENTS

FIGURES

TABLES

APPENDICES

APPENDIX FIGURES

APPENDIX TABLES

EXECUTIVE SUMMARY

As part of the Hawke's Bay 3D Aquifer Mapping Project (3DAMP), this report focuses on exploring how airborne electromagnetic (AEM; e.g. SkyTEM) data can be utilised within numerical groundwater model construction and the impact of its inclusion in the modelling workflow on predictive uncertainty. The Heretaunga Plains numerical groundwater model (hereafter referred to as 'Heretaunga GW model') was primarily utilised for this exploration, and a scripted framework was developed to facilitate future modelling. An additional simpler and smaller-scale numerical groundwater model was also used for data-worth experiments (the Bridge Pā GW model). This is the final in a series of Heretaunga Plains reports produced by the Hawke's Bay 3D Aquifer Mapping Project (3DAMP).

The Heretaunga GW model used was the steady-state Heretaunga GW model developed as part of the GNS-Science-led Te Whakaheke o Te Wai (TWOTW) Ministry of Business, Innovation & Employment (MBIE) Endeavour Programme. This model used a 3D geological model as its primary base for defining model layers and properties. As part of this study, the Heretaunga GW model was updated, primarily with SkyTEM-derived hydrogeological-interpretation models.

These hydrogeological-interpretation models were informed by electrical-resistivity models that were developed from SkyTEM data. The workflow presented in this report has been specifically targeted at AEM that collect datasets over large areas; hereafter, the terminology 'AEM data' is used. However, although the workflow and results presented may be relevant to resistivity models developed from systems other than SkyTEM, only SkyTEM data has been utilised within this assessment.

Additionally, the type of geology, lithology and freshness/salinity of groundwater impacts the applicable results and relationship of the resistivity model(s) to hydraulic conductivity. The area investigated is a primarily fresh groundwater resource hosted within unconsolidated sediments, where hydraulic conductivity is strongly controlled by the degree of clay versus gravel content.

The following model parameters (initial values and their uncertainty estimates) were updated with the incorporation of AEM data: hydraulic conductivity (in both horizontal and vertical directions), streambed hydraulic conductivity, drain conductance and porosity. Additional parameters defined on the basis of hydraulic conductivity were also modified. These include general head boundary (GHB) conductance and elevation around the inland boundary of the model, as well as the coastal GHB conductance. Additionally, the following model structures were updated on the basis of AEM-based hydrogeological interpretation: model layering and depth to basement. To promote consistency in the different regional model experiments in this study, prior uncertainty on parameters (expressed as multipliers) were the same for all models; however, two versions of the models utilised AEM-derived data and models to pre-condition (algorithmically modify) initial (prior) parameter uncertainty estimates for hydraulic conductivity and porosity. In total, four different Heretaunga GW model versions were developed utilising the AEM-based hydrogeological interpretation models – (i) parameters updated, (ii) parameters updated and pre-conditioning undertaken, (iii) parameters and layers updated and (iv) parameters and layers updated and pre-conditioning undertaken.

The figures generated herein are used to highlight the differences between the model versions. The updated Heretaunga GW model contains significantly greater property variation than the original Heretaunga GW model (e.g. in hydraulic conductivity) over short spatial scales, owing to the high spatial resolution of the AEM data. The incorporation of the AEM data modifies the mean values of prior parameter distributions and also the parameter uncertainty (distribution standard deviation). The extent to which initial (prior) parameter distributions were modified, on the basis of the AEM data, varies across the modelled domain. In many locations, the incorporation of AEM data reduced prior parameter standard deviation, while, in other locations, prior parameter standard deviations were increased. Some changes are subtle, while others are more pronounced.

History-matching to hydrological and hydrogeological system observations (e.g. groundwater levels) and simulation of five scenarios was undertaken to explore differences in prior (before history-matching) and posterior (after history-matching) uncertainty for specific predictions between the different models. **The added benefit of AEM-derived models is most significant for predictions that are sensitive to smaller-scale flow paths. It is also most significant wherever the prior parameter uncertainty distribution was previously under-estimated.**

Two different types of analyses were also undertaken to explore changes in model predictions using AEM data, conventional hydrogeological data (e.g. groundwater levels, etc.) and less conventional tritium measurements: (i) history-matching outputs when using tritium data with AEM data and (ii) data-worth analyses. The tritium plus AEM analysis looked at the impact of history-matching to a full dataset with and without tritium and AEM. In contrast, the data-worth analysis simply explores the worth of data using a one-at-a-time approach, therefore isolating the impact of prediction-relevant information in AEM data where we assume that either: (i) there is no existing data and AEM data is added in or (ii) there is 'all' existing data and each dataset is removed one at a time. The data-worth analysis focused on stream flow, groundwater level and groundwater–surface-water-exchange predictions.

As would be expected, with the inclusion of tritium age-tracer data, predictions of groundwater age were impacted. In most cases, the uncertainty of these age predictions was reduced for model versions that combined AEM and tritium data, relative to model versions that either excluded tritium data or did not incorporate the AEM data. This is an interesting result, indicating that **AEM-informed models appear to enhance the ability to extract valuable information from data sources that are influenced by fine-scale system complexity, such as tritium**. Therefore, the simulated equivalents are impacted by parameter detail that may be illuminated by AEM data.

The data-worth analysis confirms what we already know – that, if there is no data, then the best data to gather is that of the same type as the prediction. However, in the context of exploring a range of predictions, the model results indicate that, unlike other data, **AEM-derived hydraulic conductivity data would improve the reliability (reduce the uncertainty) of all predictions explored** – no other single dataset was able to achieve this. This indicates the general utility of AEM data in providing information that enhances the reliability of all prediction types to a significant degree.

1.0 Introduction

The objectives of this report are to explore how airborne electromagnetic (AEM; e.g. SkyTEM) data can be utilised within numerical groundwater model construction and the impacts of its inclusion in the numerical workflow on predictive uncertainty. The Heretaunga Plains numerical groundwater model (hereafter referred to as 'Heretaunga GW model'; Figure 1.1) is primarily utilised for this exploration, and a scripted framework is developed to enable rapid future modelling. An additional simpler and smaller-scale numerical groundwater model is also used for data-worth experiments (the Bridge Pā GW model; see Section 1.2.2). This is the final in a series of Heretaunga Plains reports produced by the Hawke's Bay 3D Aquifer Mapping Project (3DAMP).

3DAMP is a five-year initiative (2019–2024) jointly funded by the Provincial Growth Fund (PGF), Hawke's Bay Regional Council (HBRC) and GNS Science's (GNS) Groundwater Strategic Science Investment Fund (SSIF) research programme. The project applies SkyTEM technology to improve mapping and modelling of groundwater resources within the Heretaunga Plains, Ruataniwha Plains and Poukawa and Ōtāne basins. 3DAMP involves collaboration between HBRC, GNS and the Aarhus University HydroGeophysics Group (HGG). This numerical groundwater modelling work is also co-funded by the GNS-Science-led Te Whakaheke o Te Wai (TWOTW) Ministry of Business, Innovation & Employment (MBIE) Endeavour Programme.

SkyTEM (a type of AEM data-collection system) datasets are used to create resistivity models. Resistivity models can be developed from a large number of different types of instruments (both airborne and ground-based) with different depth penetrations, resolutions and sensitivities. The workflow presented in this report has been specifically targeted at AEM that collect datasets over large areas; hereafter, the terminology 'AEM data' is used. However, although the workflow and results presented may be relevant to resistivity models developed from systems other than SkyTEM, only SkyTEM data has been utilised within this assessment (as provided by Rawlinson et al. [2024]).

The primary objectives for the modelling refinement work undertaken are as follows:

1. Explore:
    a. how AEM data can be utilised in numerical groundwater model construction, and
    b. how the utilisation of AEM affects the associated predictive uncertainty, using the Heretaunga GW model as a case study.
2. Develop a new numerical model scripted framework incorporating AEM data, using the Heretaunga GW model as a case study.

Hemmings et al. (in prep.) describes an update of the Heretaunga GW model to assimilate groundwater age data as part of TWOTW. The report herein builds on Hemmings et al. (in prep.) and further extends Rawlinson et al. (2024), which briefly described the update of the reference TWOTW Heretaunga GW model using SkyTEM-derived hydrogeological models as part of 3DAMP.

This work does not intend to re-develop the existing numerical groundwater model developed by HBRC (Rakowski and Knowling 2018). Learnings and outputs from this modelling work are intended to act as a guide for updating existing or future numerical groundwater models should HBRC wish to do so for scientific or policy-development purposes.

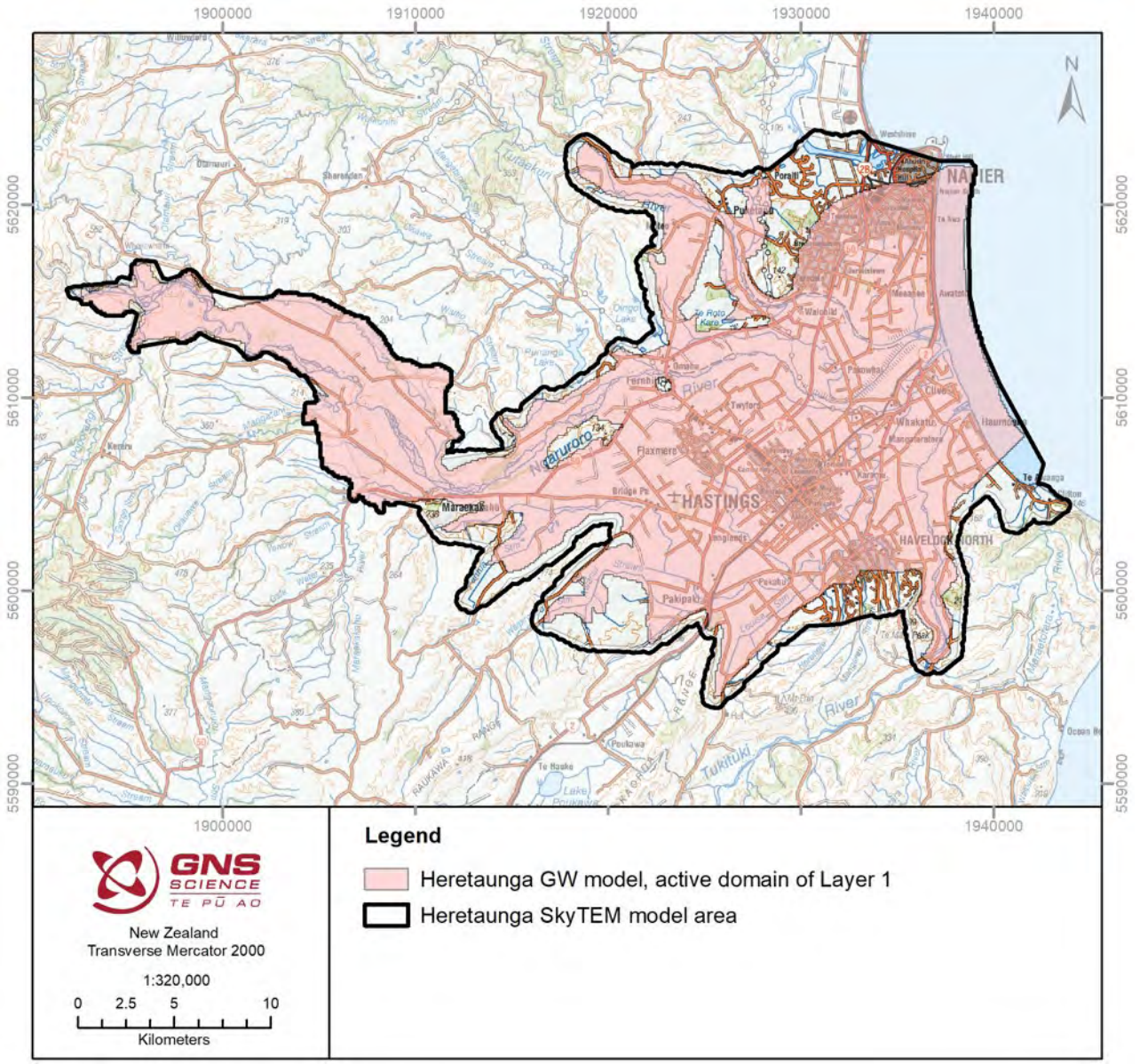

Figure 1.1 Heretaunga GW model area, shown as the active domain of Layer 1. Also shown for comparison is the Heretaunga SkyTEM model area (extent of the 3D models derived from the SkyTEM data).

1.1 Brief Overview of Important Numerical Groundwater Modelling and Uncertainty Analysis Definitions

The following definitions are important to understand for the concepts presented in this report:

- **Simulated outputs:** Model-derived outputs, either to match to system observations or to track as predictions.
- **Budget components:** Broad-scale model outputs that aggregate net components of the hydrological budget (e.g. total recharge, total offshore groundwater flow, total surface water–groundwater exchange).
- **Model parameters:** Model input values that, if adjusted, can modify simulated outputs; these are used as containers of model uncertainty (e.g. hydraulic conductivity).
- **Prior parameter uncertainty:** Definition of the initial uncertainty in model parameters, based on expert knowledge and literature values. The mean of this distribution results in the base model parameters.

- **Prior prediction uncertainty:** Initial uncertainty in model predictions and simulated output values; derived through the propagation of model prior parameter uncertainty through the numerical model.
- **Base model parameters:** Mean of the prior parameter probability distribution.
- **Observations:** Historical system observations (data) that can have a numerical simulated counterpart (e.g. groundwater levels, stream flows).
- **History-matching:** Calibration or conditioning of model parameters through matching simulated outputs to historical system observations (observations; data).
- **Pre-conditioning:** Steps taken prior to history-matching to improve the definition of the prior parameter uncertainty.
- **Posterior uncertainty:** Uncertainty in model parameters after conditioning to observations. The propagation of this uncertainty through to simulated outputs provides the posterior prediction uncertainty.
- **Scenarios:** Alternative system stress conditions that are explored with the numerical model, under uncertainty.
- **Data worth:** Ability of an observation or observation type to reduce the uncertainty of a prediction made by a model.
- **Realisation:** A single set of model parameter values or associated simulated outputs.
- **Ensemble:** A collection of realisations that provides a representation of model uncertainty.

1.2 Input Models

The reference model used is the steady-state Heretaunga GW model developed as part of TWOTW (Hemmings et al., in prep.). This model used a 3D geological model (Begg et al. 2022) combined with expert knowledge and literature values as its primary base for defining model layers and properties (e.g. hydraulic conductivity). In the subsequent text, it will be referred to as the TWOTW or '*geo*' model version. The Heretaunga GW model was further updated here with SkyTEM-derived hydrogeological interpretation models developed in Rawlinson (2023).

1.2.1 Te Whakaheke o Te Wai (TWOTW) Heretaunga Numerical Groundwater Model (Heretaunga GW Model)

The *geo* model version (TWOTW; Hemmings et al., in prep.) was built on the numerical model presented in Rakowski and Knowling (2018) as part of the TANK (Tutaekuri, Ahuriri, Ngaruroro and Karama rivers) Plan Change (Baker et al. 2020). The lateral extent of the active domain is the same as the TANK model (Figure 1.1), and the spatial discretisation remains at 100 x 100 m with a density-corrected, offshore boundary condition. However, the TWOTW model extends the TANK numerical model in a number of aspects. This is discussed in detail in Hemmings et al. (in prep.) and is briefly summarised here:

- **Conversion of the numerical simulation from MODFLOW-2005 to MODFLOW6.**
- **Extension of simulated domain to the ground surface.** The TANK model was focused on system behaviour within the Quaternary aquifer units (Q2–Q7). As such, the model top was at the geologically inferred base of the Holocene sediment confining unit (where present). As the variable competency of the confining unit may have a control on the predictions of interest, the confining unit has been explicitly simulated in the TWOTW update of the model. As identified in Rakowski and Knowling (2018), the inclusion of this surficial unit in the numerical simulation has a significant impact on numerical complexity and therefore on model simulation time.
- **Lateral extension of the coastal general head boundary condition (GHB) in the surface layer to cover the entire offshore portion of the domain.** This extension was applied because the surface layer now reflects the submarine surface in the offshore portion and to allow development of upward flow in the nearshore region. The offshore boundary in deeper layers is still only defined for the most distal offshore cells.

- **Explicit simulation of recharge in the confined portion of the domain.** The TANK model excluded recharge in this portion. Base (prior mean) recharge is now derived from a NIWA (National Institute of Water & Atmospheric Research) TOPNET simulation (e.g. Yang 2017).
- **Increased vertical discretisation.** With a major objective of the TWOTW model being to explore the impact of assimilating tritium, the number of model layers discretising the numerical domain was increased from two to nine (after Knowling et al. [2020]). These were aligned to inferred (hydro)geological units from the 2022 Leapfrog geological model (Begg et al. 2022).
- **Definition of encircling GHB.** Combined groundwater age, chemistry and stable-isotope analyses suggest that budgetary contributions to the plains from the surrounding hillslope may be significant (Morgenstern et al. 2018). This boundary condition allows groundwater inflow (or outflow) from the surrounding hillslopes.
- **Re-specification of the surface-water network (Rivers) to use the MODFLOW6 SFR (Surface Flow Routing) package.** This was done to allow two-way exchange between surface water and groundwater and transport of that flow downstream. Base river inflows into the domain were derived from a NIWA TOPNET simulation (e.g. Yang 2017). Incomplete specification of all fine-scale surface-water flow features was accommodated by combining the MODFLOW6 Drain (DRN) and Mover (MVR) packages.
- **Updated groundwater-abstraction records and estimates as provided by HBRC (July 2022).**

The TWOTW simulation consists of a MODFLOW6 steady-state groundwater flow model and (optional) transient tritium transport and age models for exploring predictions of groundwater age and the assimilation of tritium data. Here, focus is placed on the flow model for the predictions outlined in Section 1.3.

As introduced in Section 1.1, numerical model analysis is undertaken through the lens of model uncertainty. This approach uses realisations of the numerical model parameters (representing parameter uncertainty) to quantify the uncertainty in model predictions.

1.2.2 Te Whakaheke o Te Wai (TWOTW) Bridge Pā Numerical Groundwater Model (Bridge Pā GW Model)

The Bridge Pā GW model domain occurs over a subset of the Heretaunga GW model and then also extends further up into the foothill area to include the full Paritua stream catchment (Figure 1.2). The Bridge Pā model has also been developed as part of the TWOTW programme and is the subject of a draft publication (Moore 2025, pers. comm.) that will be made available to HBRC once completed. The Bridge Pā model is a one-layer model developed to explore the flows within the Paritua Stream and its interaction with the underlying aquifer under a range of stress regimes.

For this report, the Bridge Pā GW model has been used for data-worth explorations only (see Section 3.2). The ‘worth’ of data refers to the ability of an observation type to reduce the uncertainty of predictions made by a model. In this case, the observation type of interest is the set of AEM-derived hydrogeological interpretation models resulting from SkyTEM data acquisition and resistivity modelling.

The details of the Bridge Pā GW model will be discussed in detail in the aforementioned draft publication (Moore 2025, pers. comm.); however, a brief summary is provided below for clarity.

The modelled recharge is derived from the same NIWA TOPNET simulation as used by the Heretaunga GW model.

The bottom of the single model layer was defined by the SkyTEM basement definition, except in areas where the basement outcrops at surface. Where the basement outcrops at the surface, a fixed layer thickness of 30 m was defined, allowing for the assumption that the hydraulic conductivity in these hill catchments takes on an abstract meaning.

A GHB boundary is used to represent: (i) the Ngaruroro River to the north of the model domain, (ii) the groundwater flow streamline co-incident with the pre-1867 Ngaruroro River course to the east of the model domain and (iii) the Awanui Stream south of the model domain. The spatially varying GHB boundary conductances are parameterised using pilot points spaced at approximately every fifth model GHB boundary cell. The GHB elevations are determined by the average stage height over each model stress period for river boundaries or by the average groundwater levels for the groundwater-flow streamlines.

A no-flow boundary surrounds the hillslopes part of the model domain, which is consistent with the Paritua Stream catchment boundary. Groundwater age, chemistry and stable-isotope analyses suggest that most flow into the upper part of the model domain is derived from the hillslopes in the southeast of the domain (Morgenstern et al. 2018). This boundary condition allows overland and groundwater inflow (or outflow) from the surrounding hillslopes. It is possible that additional groundwater enters the surface catchment boundary – this is currently omitted from the model; however, the most significant mass balance terms (recharge across the catchment, groundwater pumping and stream outflow) suggest that this additional inflow is sufficiently minor in terms of the key prediction that this model has been constructed to simulate.

A total of nine sequential steady-state stress periods have been defined, spanning pre-European to current catchment conditions. These are defined as:

- **SP1:** Pre-European stress period.
- **SP2:** Initial land-clearing stress period.
- **SP3:** Changing the course of the Ngaruroro River in 1867 flood stress period.
- **SP4:** Initial land-drainage stress period.
- **SP5:** July 1970 – July 1990, border-dyke irrigation stress period.
- **SP6:** July 2005 – July 2022, average stress period.
- **SP7:** July 2018 – July 2019, wet stress period.
- **SP8:** July 2020 – July 2021, dry stress period.
- **SP9:** Dry stress period augmented by water released from dam.

1.2.3 Airborne Electromagnetic (AEM)-Derived Models (from SkyTEM)

Groundwater model updates presented in this report primarily utilise AEM-derived hydrogeological interpretation models developed in Rawlinson (2023) after SkyTEM acquisition and resistivity modelling.

The Heretaunga GW model was updated using a model of estimated hydraulic conductivity (*KH_initial_basehigh* model; Rawlinson 2023) and a model of the fraction of coarse material (CC model; Rawlinson 2023). These models were derived using a combination of resistivity model values, large-scale manual interpretation of resistivity based on geology (to determine consolidated versus unconsolidated material), lithological log information, hydraulic conductivity information from pumping tests and hydraulic conductivity information informed by expert knowledge. For unconsolidated material, a linear relationship is assumed between resistivity and hydraulic conductivity, as well as coarse material fraction and hydraulic conductivity. For consolidated material, resistivity values were utilised to estimate likely locations of mudstone, sandstone and limestone, and uniform values were set for each of these geology types based on a combination of pumping-test data and expert knowledge. Additionally, the clusters describing permeability, and their associated silhouette index, were used as part of pre-conditioning of parameter priors (utilising the point dataset underlying the 500 hydrostratigraphic realisations of Foged [2022] and Rawlinson [2023]), hereafter termed '*clusters_dataset*'. See Rawlinson (2023) for further details.

The Bridge Pā GW model is a one-layer model. As such, averages of the models were utilised for the data-worth explorations undertaken (see Section 3.2). Specifically, these data-worth analyses explore the worth of SkyTEM-derived hydraulic conductivity estimates as data, using:

- The geometric mean of *KH_initial_basehigh* (Rawlinson 2023) through the vertical column of either the unconsolidated sediments or the consolidated sediments (selected based on which type of sediment is present at the surface).
- The harmonic mean of the upper 5 m of *KH_initial_basehigh* (Rawlinson 2023).

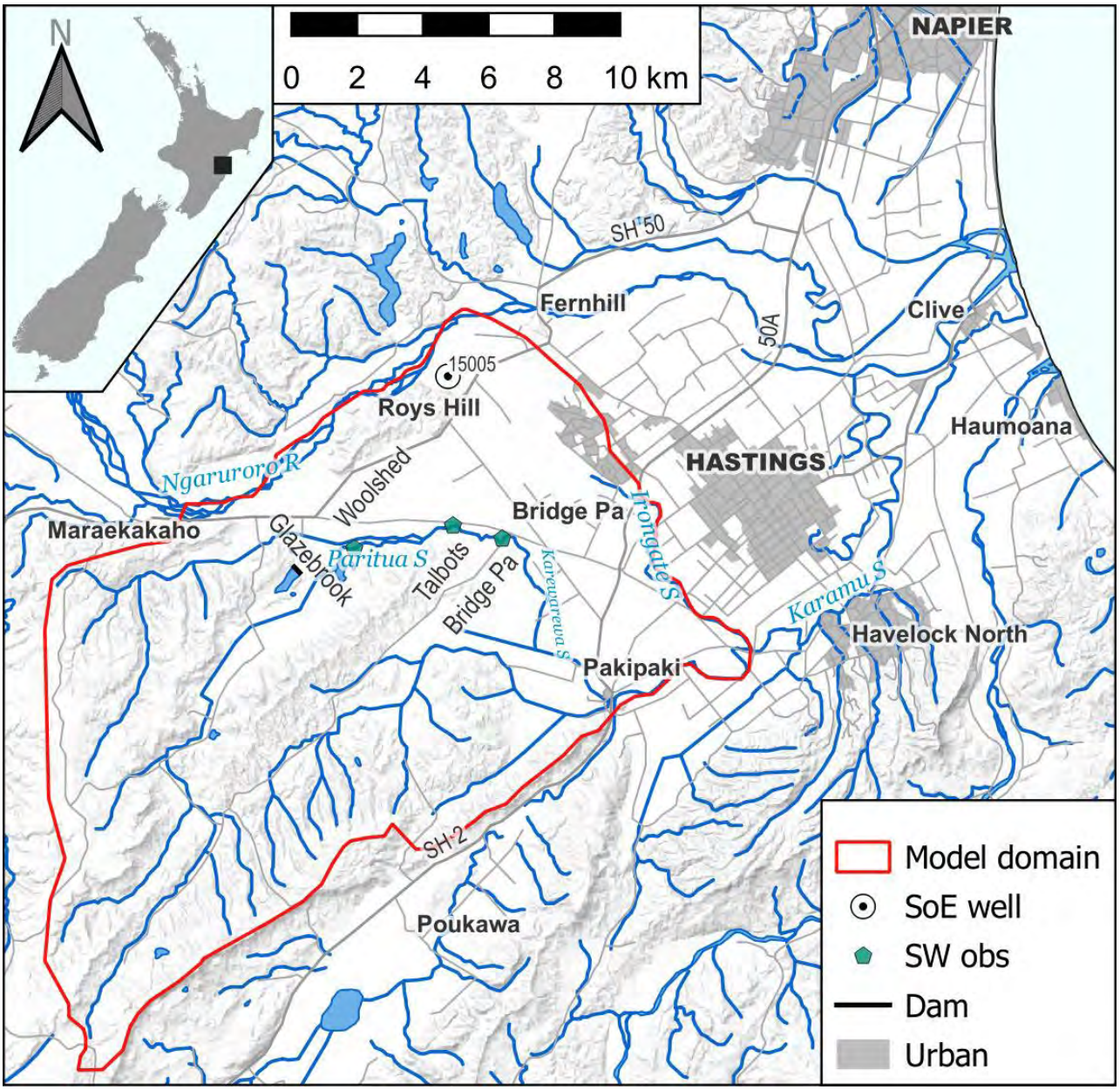

Figure 1.2 Location of the Bridge Pā model domain and specific predictions explored within the data-worth assessment (SW obs = surface-water observations; SoE well = groundwater-level observations).

1.3 Predictions

1.3.1 Heretaunga GW Model

This work primarily aims to explore the impact on a numerical model workflow and resultant predictive uncertainty through the incorporation of additional system information derived from AEM surveys. As such, a broad range of predictions are explored (Figure 1.3):

- Budgetary components of the groundwater system:
  - Net offshore groundwater flow.
  - Net flow across hillslope boundaries (to or from the model domain).
  - Net groundwater–surface-water exchange.
- Zonal disposition of the offshore groundwater flow, along the coast, divided into three zones: north, middle and south (see Figure 1.3; blue, orange and green, respectively).
- Specific groundwater–surface-water exchange along a single Ngaruroro River segment between Maraekakaho and Roys Hill.
- Stream flows at specific locations of interest that relate to spring-fed stream systems:
  - Tutaekuri-Waimate Stream at Goods Bridge.
  - Ruapare Stream at Ormond Road.
  - Karamu River at the floodgates.
- Groundwater levels at eight locations across the domain.

Changes in these predictions are explored under:

- Base long-term averaged conditions, approximately aggregating the period from the 1970s to 2022.
- Dry and wet climate scenarios.
- Modified groundwater abstraction scenarios.

More detail on the scenarios is provided in Section 2.4.

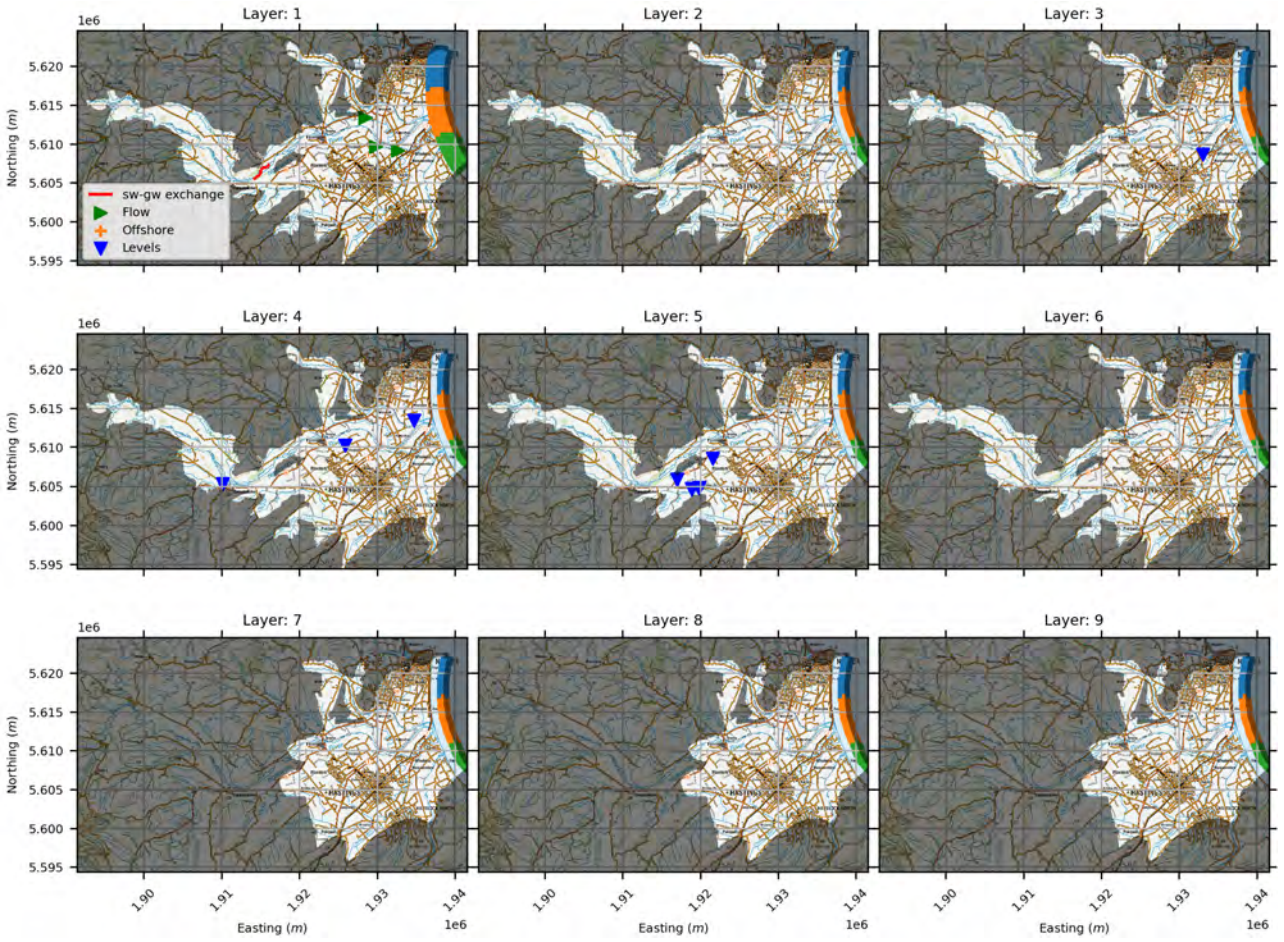

Figure 1.3 Prediction locations. Offshore flow prediction zones are denoted by three different colours; blue in the north, orange in the middle and green in the south. Net budgetary predictions for boundary flow and surface-water–groundwater exchange are not drawn. Note that layer locations of level predictions are in the modified model structure and may differ from those in Hemmings et al. (in prep.).

1.3.2 Bridge Pā GW Model

The Bridge Pā GW model predictions occur in one of nine different stress periods. Each stress period represents large-scale catchment changes from pre-European times through to present day, and these are identified where relevant. Four specific predictions are explored:

- Groundwater–surface-water exchange flux along the Ngaruroro River segment between Maraekakaho and Roys Hill ('sw-gw exchange'), during pre-European times (Stress period 1).
- Groundwater–surface-water exchange flux along the Paritua Stream losing reach, which is defined for this study as between the Woolshed and Talbots monitoring sites ('SW obs' in Figure 1.2), during the dry summer of 2020/21 (Stress period 8).
- Stream flow in the Paritua Stream ('SW obs' in Figure 1.2), as measured at Bridge Pā, during the period where border dyke irrigation was prevalent in the catchment (Stress period 5).
- Groundwater levels at Well 15005 ('SoE well' in Figure 1.2) during the dry summer of 2020/21 (Stress period 8).

2.0 Methods

2.1 General Framework

The following framework was followed:

1. Different and iterative regional model adjustments were explored. For each version:
    a. An ensemble of regional model predictive scenario simulations were undertaken representing prior parameter uncertainty.
    b. The model was history-matched to long-term average groundwater-level data, stream flows and surface-water–groundwater exchange approximately reflecting the period 1972–2021.
    c. Posterior parameter uncertainty (after history-matching) was propagated to posterior prediction uncertainty through simulation of predictive scenarios.
2. Data-worth assessments were made using the Bridge Pā GW model.

The numerical modelling and pre- and post-processing was undertaken in a scripted framework, utilising widely-used, open-source Python libraries:

- Flopy (Hughes et al. 2024; Bakker et al. 2016).
- Pyemu (White et al. 2016, 2021).
- Surface Water Network (Toews and Hemmings 2019).

Regional model uncertainty propagation and history-matching was undertaken using PEST++IES (IES; iterative ensemble smoother; White et al. 2018). IES supports efficient history-matching with high dimensional parametrisation (expressing uncertainty for many thousands of parameters). The parametrisation approach and history-matching methodology is described in detail in Hemmings et al. (in prep.).

In this report, focus is placed on the modifications made to the model structure and base-realisation parameter values on the basis of information contained within the AEM-derived models.

2.2 Regional Model Updates

2.2.1 Base Model Modifications

Four different approaches for incorporating the information from the AEM-derived models into the Heretaunga GW model were explored. The (stochastic) numerical model predictions for these tests are compared to those for the reference model (TWOTW/*geo* model; Hemmings et al., in prep.).

The two primary updates tested were:

- '*skytem-k*', or simply '*k*', model – where only model properties (e.g. hydraulic conductivity, boundary-condition conductance) were modified, relative to the reference model (Table 2.1).
- '*skytem-lays*', or '*lays*', model – where a (re)interpretation of aquifer structure was also incorporated in a re-definition of model layers (Tables 2.1–2.2; Figures 3.1–3.3).

The base-realisation property definition for the *skytem-lays* model was equivalent to the *skytem-k* model, with minor differences per layer associated with the different aggregation to different layer definition.

Table 2.1 Update of Heretaunga GW model parameters.

Parameter	*geo* Model (Hemmings et al., in prep.)	*skytem-k* and *skytem-lays* Models
Horizontal hydraulic conductivity (HK)	Uniform values based on literature values and expert knowledge set to different geological model units (Begg et al. 2022). Low HK buffer added to basin edges to enable model fit to tritium data. Lower HK added to the western extent of Ngaruroro River to fit to groundwater levels. Geological model did not extend offshore; uniform values set based on expectation of confining layer extension in layer 1, gravel layers in layers 2–6 and medium permeability geology in layers 7–9.*	SkyTEM-derived estimates of HK (geometric mean, clipped to a minimum of 5 x 10^{-4} m/day): *KH_initial_basehigh* model (Rawlinson 2023)
Vertical hydraulic conductivity (K33 or VK)	Uniform VK/HK ratios based on literature values and expert knowledge set to different geological model units (Begg et al. 2022).	SkyTEM-derived estimates of coarse-fraction (CC model; Rawlinson 2023) and HK (*KH_initial_basehigh* model; Rawlinson 2023) converted to K33. K33 = HK*$10^{(4*CC)-4}$. Assumed minimum value of HK*10^{-4}. (Vertical anisotropy assumed to have a log-linear relationship to clay content.)
Coastal boundary conductance (GHB)	Derived from HK and K33 (for layer 1) and the cell dimensions to convert to conductance (C) (C = HKA/b, where A is the area of which flow is occurring, and b is the thickness of the boundary with hydraulic conductivity HK).	Derived from HK and K33 (for layer 1) and the cell dimensions to convert to conductance (C) (C = HKA/b, where A is the area of which flow is occurring, and b is the thickness of the boundary with hydraulic conductivity HK).
Hillslope boundary conductance (GHB)	A combined analysis of out-of-domain recharge (to estimate boundary fluxes) and the hydrogeological model informed hydraulic conductivity (HK).	A combined analysis of out-of-domain recharge (to estimate boundary fluxes) and the hydrogeological model informed hydraulic conductivity (HK). In this instance, *KH_initial_basehigh* model provides further guidance of HK distribution associated with, for example, likely limestone occurrence, influencing boundary fluxes.
Streambed hydraulic conductivity (RK)	Values based on VK of layer 1, with linear-scaling adjustment between assumed minimum and maximum values (0.01 and 200 m/day, respectively).	Calculated same as K33 but using the upper 4 m of the SkyTEM-derived models (arithmetic mean of CC and geometric mean of *KH_initial_basehigh*; Rawlinson 2023), with linear-scaling adjustment between assumed minimum and maximum values (0.01 and 200 m/day, respectively).
Drain conductance (DC)	Values based on VK of layer 1, with adjustment to convert to conductance (using cell dimensions and thickness) and linear-scaling adjustment between assumed minimum and maximum values (10 and 2 x 10^5 m^2/day, respectively).	Calculated same as K33 but using the upper 4 m of the SkyTEM-derived models (arithmetic mean of CC and geometric mean of *KH_initial_basehigh*; Rawlinson 2023), with adjustment to convert to conductance (using cell dimensions and thickness) and linear-scaling adjustment between assumed minimum and maximum values (10 and 2 x 10^5 m^2/day, respectively).

*This assumption was applied to all original model parameters.

Table 2.2 Update of Heretaunga GW model structure. Visual comparisons are provided in Figures 3.1–3.3.

Groundwater Model Layers	***geo* and *skytem-k* Models**	***skytem-lays* Model**	**Comment**
	Hydrogeological Model Units (Begg et al. 2022)	**SkyTEM-Assisted Hydrogeological Interpretation (Sahoo et al. 2023; Rawlinson 2023)**	
Model layers L1–L3	Awatoto member	Hydrogeological Unit 1	Minimum thickness (6 m base of L3) set where non-existent.
	Younger river gravels		
	Wider Heretaunga formation		
Model layers L4–L6	Maraekakaho Formation and riverbed and river mouth gravels	Hydrogeological Unit 2	Minimum thickness (45 m base of L6) set where non-existent.
Model layers L7–L9	Early to middle Pleistocene	Hydrogeological Unit 3	Minimum thickness (120 m base of L9) set where non-existent.
Basement	Undifferentiated Paleocene–Pleistocene	Hydrogeological Unit 4	Cut-off for base of L9 set at -270 m below sea level.

2.2.2 Parameter Uncertainty

The base model parameters define only the mean of the prior parameter distributions. Although these mean values may differ greatly between the *skytem-k, skytem-lays* and *geo* models, the definition of uncertainty was approached identically for all models. This was done purposefully to provide a fair comparison between the models.

As detailed in Hemmings et al. (in prep.), for history-matching and uncertainty analysis most parameters are specified as multi-scale multiplier parameters. Other parameters (e.g. drain elevation) are specified through multi-scale additive parameters. These multiplier and additive parameters combine to act on individual model-parameter values (such as the hydraulic conductivity of a model cell). The use of nested, multi-scale multiplier and additive parameters supports the definition of parameter uncertainty at multiple scales (e.g. layer-scale, pilot-point scale and cell-by-cell). It also allows relatively localised conditioning of parameters, only where informed by data (e.g. McKenna 2019; White et al. 2020a). For the *skytem-k* and *skytem-lays* tests, the prior parameter uncertainty of these multiplier (or additive) parameters were defined equivalently to the *geo* model (Table 2.3), although the base realisation of model-parameter values that these multipliers or additive parameters act on may be significantly different.

The AEM-informed parameter fields were more spatially heterogeneous than the TWOTW/*geo* model parameter fields, which resulted in additional challenges with model convergence. As such, more prior realisations (600) were required to ensure sufficient realisations in the posterior predicted ensemble. As detailed in Hemmings et al. (in prep.), realisations were drawn via Monte Carlo sampling of the block diagonal prior parameter co-variance matrix. Diagonal values of the prior parameter co-variance matrix are the standard deviations of individual parameters (listed in Table 2.3); off-diagonals express the expected relationship between parameters within the same group, defined according to their separation distance. These relationships were expressed through stationary geostructures defined by variograms, with range parameter (a) detailed in Table 2.3, and a sill proportional to the standard deviations of individual parameters (also detailed in Table 2.3).

2.2.3 Parameter Pre-Conditioning

Two further tests attempted to incorporate additional information from the AEM-derived models to pre-condition the prior parameter uncertainty definition. These versions are referred to as *skytem-k-precond* (*k-pc*) and *skytem-lays-precond* (*lays-pc*).

For these tests, the 600 prior realisations were conditioned through a precursory, independent IES exercise. Here, the observations were set as loose inequality constraints reflecting the expected minimum or maximum hydraulic properties associated with hydrogeological formations identified through the AEM interpretation. The same multiplier parameters detailed in Section 2.2.2 were conditioned to fit these expected conditions.

In these tests, the *clusters_dataset* (Rawlinson 2023) was used to identify model cells estimated to have a high probability of containing gravels (cluster 0 where the silhouette index is greater than 0.58 [the mean silhouette index]). The log-transform of hydraulic conductivity in these cells was then conditioned to a minimum value of 2.30 (200 m/day). Cells identified as high probability of cluster 2 or 3 (low permeability) (with silhouette index greater than 0.58) were conditioned to expected maximum log-transformed hydraulic conductivity of 2.78 (600 m/day). Constraint values were determined from an assessment of clusters and estimated hydraulic conductivity from pumping tests (see pumping-test dataset in Rawlinson [2023]). To prevent over-adjustment of the large-scale parameters (e.g. layer-scale multipliers), additional loose constraints were put on layer average hydraulic conductivity for cells identified as cluster 0, 2 or 3: cluster 0 cells layer average log-transformed hydraulic conductivity was constrained to less than 3.70 (5000 m/day), while the target for cluster 2 and 3 layer average was greater than -1 (0.1 m/day).

The pre-conditioning was undertaken on 1000 parameter realisations with three IES iterations. A 600-realisation sub-sample of the subsequent pre-conditioned realisations were then history-matched in the same manner as the other tests (*skytem-k* and *skytem-lays*).

Table 2.3 Parameter group summary. Note: parameters are expressed as multipliers or are additive, acting on initial model-input values, and are unitless. Bounds and standard deviations for groups marked as 'log' transformed are in log_{10} space. Ultimate bounds are specified as un-transformed and related to model-input values (after multiplier and additive parameters have been applied).

Group Name	Verbose Name	Style	Type	Transform	Count	Initial Value	Lower Bound	Upper Bound	Standard Deviation	a (m)	Ultimate Lower Bound	Ultimate Upper Bound
drn-cond-cnst_inst:0	Drain conductance	Multiplier	Global-constant	log	1	0	-2.000	2.000	0.667	-	1e-2 m2d-1	1e9 m2d-1
drn-cond-grd_inst:0	Drain conductance	Multiplier	Grid	log	151,302	0	-2.000	2.000	0.667	10,000		
drn-elev-cnst_inst:0	Drain elevation	Additive	Global-constant	None	1	0	-1.000	1.000	0.333	-	-	-
drn-elev-grd_inst:0	Drain elevation	Additive	Grid	None	151,302	0	-1.000	1.000	0.333	10,000	-	-
dumpar_inst:0	Dummy, insensitive parameter	Multiplier	Constant	log	1	0	-1.000	1.000	0.333	-	-	-
ghbboundc-cnst_inst:0	Boundary conductance	Multiplier	Global-constant	log	1	0	-2.000	2.000	0.667	-	1e-10 m2d-1	1e3 m2d-1
ghbboundc-grid_inst:0	Boundary conductance	Multiplier	Grid	log	15,534	0	-3.000	3.000	1.000	10,000		
ghbboundc-layer_inst:0	Boundary conductance	Multiplier	Layer-constant	log	9	0	-2.000	2.000	0.667	-		
ghbboundc-zone_inst:0	Boundary conductance	Multiplier	Zone-constant	log	6	0	-3.000	3.000	1.000	-		
ghbboundh-grid_inst:0	Boundary head	Additive	Grid	None	15,534	0	-10.000	10.000	3.333	10,000	-	-
ghbboundh-layer_inst:0	Boundary head	Additive	Layer-constant	None	9	0	-5.000	5.000	1.667	-	-	-
ghbboundh-zone_inst:0	Boundary head	Additive	Zone-constant	None	6	0	-5.000	5.000	1.667	-	-	-
ghbcoastc-grid_inst:0	Offshore conductance	Multiplier	Grid	log	3894	0	-3.000	3.000	1.000	10,000	-	-
ghbcoastc-layer_inst:0	Offshore conductance	Multiplier	Layer-constant	log	9	0	-2.000	2.000	0.667	-	-	-
hk-cn_k:0	Horizontal hydraulic conductivity, Layer: 0	Multiplier	Global-constant	log	1	0	-2.000	2.000	0.667	-	1e-5 md-1	1e5 md-1
hk-cn_k:1	Horizontal hydraulic conductivity, Layer: 1	Multiplier	Global-constant	log	1	0	-2.000	2.000	0.667	-		
hk-cn_k:2	Horizontal hydraulic conductivity, Layer: 2	Multiplier	Global-constant	log	1	0	-2.000	2.000	0.667	-		
hk-cn_k:3	Horizontal hydraulic conductivity, Layer: 3	Multiplier	Global-constant	log	1	0	-2.000	2.000	0.667	-		

Group Name	Verbose Name	Style	Type	Transform	Count	Initial Value	Lower Bound	Upper Bound	Standard Deviation	a (m)	Ultimate Lower Bound	Ultimate Upper Bound
hk-cn_k:4	Horizontal hydraulic conductivity, Layer: 4	Multiplier	Global-constant	log	1	0	-2.000	2.000	0.667	-		
hk-cn_k:5	Horizontal hydraulic conductivity, Layer: 5	Multiplier	Global-constant	log	1	0	-2.000	2.000	0.667	-		
hk-cn_k:6	Horizontal hydraulic conductivity, Layer: 6	Multiplier	Global-constant	log	1	0	-2.000	2.000	0.667	-		
hk-cn_k:7	Horizontal hydraulic conductivity, Layer: 7	Multiplier	Global-constant	log	1	0	-2.000	2.000	0.667			
hk-cn_k:8	Horizontal hydraulic conductivity, Layer: 8	Multiplier	Global-constant	log	1	0	-2.000	2.000	0.667	-		
hk-gr_k:0	Horizontal hydraulic conductivity, Layer: 0	Multiplier	Grid	log	51,016	0	-3.000	3.000	1.000	10,000		
hk-gr_k:1	Horizontal hydraulic conductivity, Layer: 1	Multiplier	Grid	log	51,016	0	-3.000	3.000	1.000	10,000		
hk-gr_k:2	Horizontal hydraulic conductivity, Layer: 2	Multiplier	Grid	log	51,016	0	-3.000	3.000	1.000	10,000		
hk-gr_k:3	Horizontal hydraulic conductivity, Layer: 3	Multiplier	Grid	log	51,016	0	-3.000	3.000	1.000	10,000		
hk-gr_k:4	Horizontal hydraulic conductivity, Layer: 4	Multiplier	Grid	log	51,016	0	-3.000	3.000	1.000	10,000		
hk-gr_k:5	Horizontal hydraulic conductivity, Layer: 5	Multiplier	Grid	log	51,016	0	-3.000	3.000	1.000	10,000	1e-5 md-1	1e5 md-1
hk-gr_k:6	Horizontal hydraulic conductivity, Layer: 6	Multiplier	Grid	log	36,578	0	-3.000	3.000	1.000	10,000		
hk-gr_k:7	Horizontal hydraulic conductivity, Layer: 7	Multiplier	Grid	log	36,578	0	-3.000	3.000	1.000	10,000		

Group Name	Verbose Name	Style	Type	Transform	Count	Initial Value	Lower Bound	Upper Bound	Standard Deviation	a (m)	Ultimate Lower Bound	Ultimate Upper Bound
hk-gr_k:8	Horizontal hydraulic conductivity, Layer: 8	Multiplier	Grid	log	36,578	0	-3.000	3.000	1.000	10,000		
hk-pp_k:0	Horizontal hydraulic conductivity, Layer: 0	Multiplier	Pilot point	log	511	0	-2.000	2.000	0.667	10,000		
hk-pp_k:1	Horizontal hydraulic conductivity, Layer: 1	Multiplier	Pilot point	log	511	0	-2.000	2.000	0.667	10,000		
hk-pp_k:2	Horizontal hydraulic conductivity, Layer: 2	Multiplier	Pilot point	log	511	0	-2.000	2.000	0.667	10,000		
hk-pp_k:3	Horizontal hydraulic conductivity, Layer: 3	Multiplier	Pilot point	log	511	0	-2.000	2.000	0.667	10,000		
hk-pp_k:4	Horizontal hydraulic conductivity, Layer: 4	Multiplier	Pilot point	log	511	0	-2.000	2.000	0.667	10,000		
hk-pp_k:5	Horizontal hydraulic conductivity, Layer: 5	Multiplier	Pilot point	log	511	0	-2.000	2.000	0.667	10,000		
hk-pp_k:6	Horizontal hydraulic conductivity, Layer: 6	Multiplier	Pilot point	log	365	0	-2.000	2.000	0.667	10,000		
hk-pp_k:7	Horizontal hydraulic conductivity, Layer: 7	Multiplier	Pilot point	log	365	0	-2.000	2.000	0.667	10,000	1e-5 md-1	1e5 md-1
hk-pp_k:8	Horizontal hydraulic conductivity, Layer: 8	Multiplier	Pilot point	log	365	0	-2.000	2.000	0.667	10,000		
rech-cn_inst:0	Recharge	Multiplier	Global-constant	log	1	0	-0.523	0.477	0.167	-	0 md^{-1}	-
rech-gr_inst:0	Recharge	Multiplier	Grid	log	51,016	0	-1.000	1.000	0.333	10,000		-
sfrhk_inst:0	Horizontal hydraulic conductivity	Multiplier	Grid	log	5074	0	-2.000	2.000	0.667	10,000	1e-10 md-1	1e4 md-1
sfrhk_inst:1	Horizontal hydraulic conductivity	Multiplier	Global-constant	log	1	0	-2.000	2.000	0.667	-		
sfrin_inst:0	Stream inflow	Multiplier	Grid	log	19	0	-0.301	0.301	0.100	10,000	-	-

Group Name	Verbose Name	Style	Type	Transform	Count	Initial Value	Lower Bound	Upper Bound	Standard Deviation	a (m)	Ultimate Lower Bound	Ultimate Upper Bound
sfrin_inst:1	Stream inflow	Multiplier	Global-constant	log	1	0	-0.301	0.301	0.100	-	-	-
vka-cn_k:0	$\frac{\text{Vertical hydraulic conductance}}{\text{Horizontal hydraulic conductance}}$ Layer: 0	Multiplier	Global-constant	log	1	0	-2.000	2.000	0.667	-	1e-6	100
vka-cn_k:1	$\frac{\text{Vertical hydraulic conductance}}{\text{Horizontal hydraulic conductance}}$ Layer: 1	Multiplier	Global-constant	log	1	0	-2.000	2.000	0.667	-		
vka-cn_k:2	$\frac{\text{Vertical hydraulic conductance}}{\text{Horizontal hydraulic conductance}}$ Layer: 2	Multiplier	Global-constant	log	1	0	-2.000	2.000	0.667	-		
vka-cn_k:3	$\frac{\text{Vertical hydraulic conductance}}{\text{Horizontal hydraulic conductance}}$ Layer: 3	Multiplier	Global-constant	log	1	0	-2.000	2.000	0.667	-		
vka-cn_k:4	$\frac{\text{Vertical hydraulic conductance}}{\text{Horizontal hydraulic conductance}}$ Layer: 4	Multiplier	Global-constant	log	1	0	-2.000	2.000	0.667			
vka-cn_k:5	$\frac{\text{Vertical hydraulic conductance}}{\text{Horizontal hydraulic conductance}}$ Layer: 5	Multiplier	Global-constant	log	1	0	-2.699	2.699	0.900	-		
vka-cn_k:6	$\frac{\text{Vertical hydraulic conductance}}{\text{Horizontal hydraulic conductance}}$ Layer: 6	Multiplier	Global-constant	log	1	0	-2.699	2.699	0.900	-		
vka-cn_k:7	$\frac{\text{Vertical hydraulic conductance}}{\text{Horizontal hydraulic conductance}}$ Layer: 7	Multiplier	Global-constant	log	1	0	-2.699	2.699	0.900	-	1e-6	100
vka-cn_k:8	$\frac{\text{Vertical hydraulic conductance}}{\text{Horizontal hydraulic conductance}}$ Layer: 8	Multiplier	Global-constant	log	1	0	-2.699	2.699	0.900	-		
vka-gr_k:0	$\frac{\text{Vertical hydraulic conductance}}{\text{Horizontal hydraulic conductance}}$ Layer: 0	Multiplier	Grid	log	51,016	0	-2.000	2.000	0.667	10,000		
vka-gr_k:1	$\frac{\text{Vertical hydraulic conductance}}{\text{Horizontal hydraulic conductance}}$ Layer: 1	Multiplier	Grid	log	51,016	0	-2.000	2.000	0.667	10,000		
vka-gr_k:2	$\frac{\text{Vertical hydraulic conductance}}{\text{Horizontal hydraulic conductance}}$ Layer: 2	Multiplier	Grid	log	51,016	0	-2.000	2.000	0.667	10,000		

Group Name	Verbose Name	Style	Type	Transform	Count	Initial Value	Lower Bound	Upper Bound	Standard Deviation	a (m)	Ultimate Lower Bound	Ultimate Upper Bound
vka-gr_k:3	$\frac{\text{Vertical hydraulic conductance}}{\text{Horizontal hydraulic conductance}}$ Layer: 3	Multiplier	Grid	log	51,016	0	-2.000	2.000	0.667	10,000		
vka-gr_k:4	$\frac{\text{Vertical hydraulic conductance}}{\text{Horizontal hydraulic conductance}}$ Layer: 4	Multiplier	Grid	log	51,016	0	-2.000	2.000	0.667	10,000		
vka-gr_k:5	$\frac{\text{Vertical hydraulic conductance}}{\text{Horizontal hydraulic conductance}}$ Layer: 5	Multiplier	Grid	log	51,016	0	-2.699	2.699	0.900	10,000		
vka-gr_k:6	$\frac{\text{Vertical hydraulic conductance}}{\text{Horizontal hydraulic conductance}}$ Layer: 6	Multiplier	Grid	log	36,578	0	-2.699	2.699	0.900	10,000		
vka-gr_k:7	$\frac{\text{Vertical hydraulic conductance}}{\text{Horizontal hydraulic conductance}}$ Layer: 7	Multiplier	Grid	log	36,578	0	-2.699	2.699	0.900	10,000		
vka-gr_k:8	$\frac{\text{Vertical hydraulic conductance}}{\text{Horizontal hydraulic conductance}}$ Layer: 8	Multiplier	Grid	log	36,578	0	-2.699	2.699	0.900	10,000		
welflux_inst:0	Pump rate	Multiplier	Grid	log	1543	0	-0.155	0.114	0.045	-	-	-

2.3 Regional Model History-Matching

2.3.1 Observations for History-Matching

Parameters were conditioned through history matching to observations of system behaviour. See Figure 2.1 for observation locations. The observation data was composed of:

- **138 groundwater level (head) observations** (Table A2.1; Figure A2.1) – long-term average (mean) over the period January 1972 – July 2021 (extracted from the file *gwl_hpm.parquet*, provided by HBRC). Note, some level data could not be used due to the absence of adequate bore information or ambiguous measurement datum.
- **Six (6) stream-flow observations** (Table A2.2; Figure A2.2) – long-term average (median flow) over the period ~1970–2022 (extracted from the file *HY_2223_HPlainsGaugingsAndFlows.xlsx* provided by HBRC).
- **Six (6) surface-water–groundwater-exchange estimates** (Table A2.3; Figure A2.3) – groundwater-exchange estimates from Wilding (2018).

See Hemmings et al. (in prep.) for a discussion on observation weighting and re-balancing. Consistent with the history-matching undertaken in Hemmings et al. (in prep.), three IES iterations were completed to condition parameters and provide posterior parameter ensembles for scenarios analyses. Note that Hemmings et al. (in prep.) explored the incorporation of tritium data in the history-matching effort for the prediction of groundwater age. While the work presented here is not focused toward tritium and groundwater age, the results of a preliminary and supplementary exploration of combined AEM and tritium are included (see Section 3.1.5).

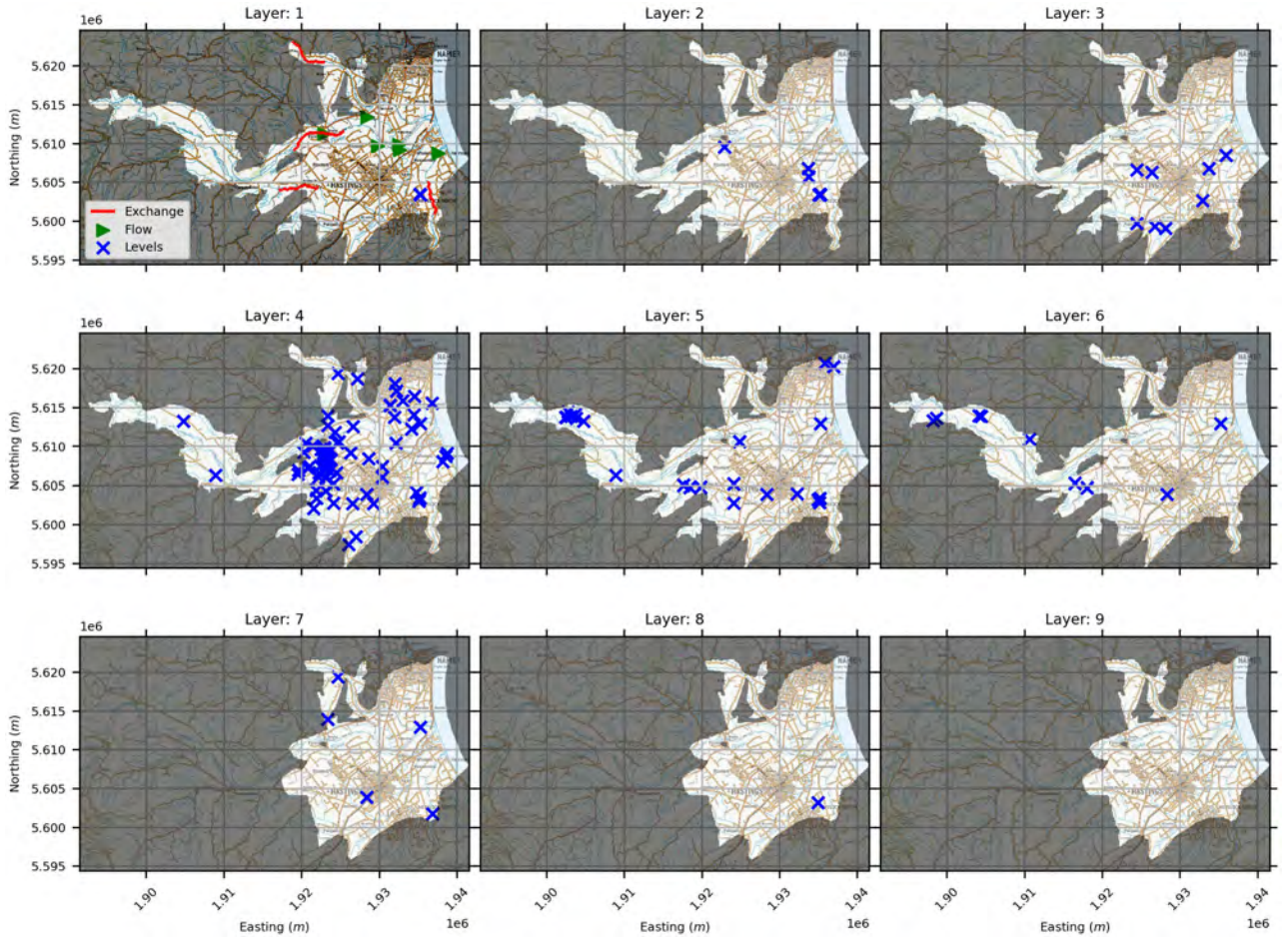

Figure 2.1 History-matching observation locations. Note that layer locations are in the modified model structure for the *skytem-lays* model and may differ from the layer locations for the *skytem-k* model and those in Hemmings et al. (in prep.).

2.4 Scenarios

The scenarios investigated are the same as those presented in Hemmings et al. (in prep.).

- **Base:** Continuation of current long-term average stresses (approximately aggregating the period 1970–2022).
- **Dry:** Reflecting a dry climate future where the recharge and stream inflow is decreased. Stresses were taken from a relatively dry historical period (July 2020 – July 2021) and extended as a steady-state condition.
- **Wet:** Reflecting a wet climate future where the recharge and stream inflow is increased. Stresses were taken from a relatively wet historical period (July 2009 – July 2011) and extended as a steady-state condition.
- **Pump80:** Where groundwater abstraction is reduced by 20%.
- **Pump120:** Where groundwater abstraction is increased by 20%.

Prior and posterior (after three iterations) parameter ensembles for each model version (*skytem-k*, *skytem-lays*, *skytem-k-pc* and *skytem-lays-pc*) were run through predictive flow and age simulations for the five scenarios.

2.5 Data-Worth Assessment

Data-worth analyses allow data of disparate types to be compared in terms of their ability to increase the reliability of model-based predictions. These analyses can then be used to inform data-collection strategies, highlighting which data-acquisition strategy provides the greatest return for investment. Similarly, the relative merits of making measurements at different locations and times can be assessed. The results offer useful insights even though they are based on approximate estimates for uncertainties (parameter and measurement uncertainty estimates) and the assumption of linear relationships implicit in the data-worth analysis (Moore and Doherty 2005; Dausman et al. 2010).

This section uses data-worth analyses to explore the ability of SkyTEM-derived hydraulic conductivity estimates to reduce the uncertainty of different predictions using the Bridge Pā GW model. This 'worth' is compared with the ability of other existing data types in the area, namely groundwater levels (including current and historic wetland locations), stream flows and groundwater–surface-water-exchange measurements. This allows the worth of data to be considered within a realistic context where other data already exists.

The requirements for a data-worth assessment are as follows:

- A description of the uncertainty of model parameters (e.g. hydraulic conductivity, streambed conductivity, etc). These are based on *a priori* estimates of parameter uncertainty.
- Calculated sensitivities of the prediction to the measurements, which are calculated with the model.
- A description of the uncertainty of measurements used in the model, for example, groundwater levels, stream flows, groundwater–stream-exchange fluxes, SkyTEM-derived observations of hydraulic conductivity, etc.

Because of these requirements, data-worth assessments can be undertaken both on models that are history-matched and those that are not. Typically, in our experience, the results do not differ significantly between prior and history-matched models. Ideally, the analyses are checked for both pre and post-history-matched models, but, in this work, we have only explored data worth for the pre-history-matched model.

The uncertainty of groundwater levels and flow data is based on estimates of current measurement accuracy: a standard error of 1 cm was adopted for groundwater levels and a 10% standard error was adopted for surface-water flow. These values were then adjusted using a propagation-of-error formula

to accommodate the fact that transient measurements were being used to provide an estimate of steady-state observations. A propagation-of-error formula was also used to estimate the groundwater–surface-water-exchange-flux standard errors.

The analysis of data worth is somewhat sensitive to the estimated uncertainty of the observations. Despite efforts to assign realistic estimates of uncertainty, it is still possible that these are under- or over-estimated – for example, that the uncertainty of flux estimates in this analysis are over-estimated or that the uncertainty of the groundwater-level measurements are under-estimated.

The uncertainty of SkyTEM-derived observations of hydraulic conductivity is more involved and is a combination of:

- The resistivity model error (i.e. the mis-fit between the forward-modelled voltage data from the resistivity model versus the measured voltage), estimated to have a standard error of 0.66 (Rawlinson et al. [2021]).
- The kriging interpolation errors (to interpolate between 1D resistivity model locations and a 3D model grid; *resvar* from Rawlinson [2023]). This has a scale-dependant error that has a mean of 0.51 and a median of 0.47 and varies between 0.1 and 4.67 within the model domain.
- The uncertainty in the relationship between resistivity and hydraulic conductivity, estimated to have a standard error of 0.54 in the log-log domain (Rawlinson 2023).

Additional errors in the SkyTEM-derived analyses will relate to differences of scale between the model grid and the resistivity soundings, as well as uncertainties associated with the quality and location of lithological log data and hydraulic-conductivity estimates from pumping tests; these have been ignored in this analysis.

The worth of the SkyTEM data compared to existing data is explored in two ways. Firstly, the case of having no observations available is considered. The exploration then describes the extent to which the addition of each current dataset on its own reduces the uncertainty of the prediction. Secondly, the case of all existing observations being available is considered. The exploration then describes the extent to which the removal of any dataset, one at a time, would increase the uncertainty of the prediction. Differing data-worth relationships between the first and second cases can occur if observation groups are highly correlated.

3.0 Results

3.1 Regional Model Results

3.1.1 Model Structure and Parameter Changes

The regional model upgrades that utilise the AEM-derived (SkyTEM) data and interpretation (as introduced in Section 2.2.1) significantly alter the initial base-realisation model properties, relative to the TWOTW (*geo*) model version, detailed in Hemmings et al. (in prep.). As detailed in Section 2.2.1, the *skytem-lays* models also have altered model-layering structures. A visual comparison of *geo* and *skytem-lays* model structure is presented in Figures 3.1–3.3. A comparison of base-realisation model parameter changes is presented in Figures 3.4–3.9. For reference, a similar comparison between the *skytem-k* and *geo* models is presented in Appendix 1.

Generally, the utilisation of the AEM data in the *skytem* models results in more granular variation in the base-realisation model properties; compare the more zonal base-realisation property variations in the left-hand (*geo*) plots in Figures 3.4–3.9 to the detailed variations (high spatial frequency) in the right-hand plots (*skytem-lays*). For hydraulic conductivity (Figures 3.4 and 3.5) and the hillslope boundary conductance (Figure 3.6), base-realisation values span a greater range of parameter values for the *skytem* models than the *geo* model, and more cells are at the extreme (high and low) values. In some areas, the incorporation of AEM data significantly increased estimates of the hillslope boundary conductance (Figure 3.6).

Base-realisation value ranges for streambed hydraulic conductivity and drain conductance were the same across the different models (due to the consistent scaling method applied [see Table 2.1]). As the *geo* model streambed hydraulic conductivity and drain conductance is derived from VK in layer 1 (see Table 2.1), the distribution of relative high and low streambed hydraulic conductivity and drain conductance resemble each other (left-hand plots in Figures 3.8 and 3.9) and the 'lay 1' plot (left-hand plot, upper left) in Figure 3.5. Similarly, the relative distribution of relatively high and low streambed hydraulic conductivity and drain conductance for *skytem* models resemble each other (right-hand plots in Figures 3.8 and 3.9). In this instance, the values for streambed hydraulic conductivity and drain conductance where derived from processed CC and HK estimates from the AEM data in the upper 4 m (see Section 1.2.3 and Table 2.1), as such similarities can also be seen between the disposition of relative high and low values for *skytem* model streambed hydraulic conductivity and drain conductance and the 'lay 1' VK plot (right-hand plot, upper left) in Figure 3.5. The relationship to estimated VK means that both model versions (*geo* and skytem) generally have higher streambed hydraulic conductivity and drain conductance over the unconfined portion. However, the *skytem* version has lower streambed hydraulic conductivity and drain conductance over a wider area, with the highest streambed hydraulic conductivity and drain conductance confined to along Ngaruroro River, upstream of Fernhill, and along Tutaekuri River, upstream of Waikohiki.

This page left intentionally blank.

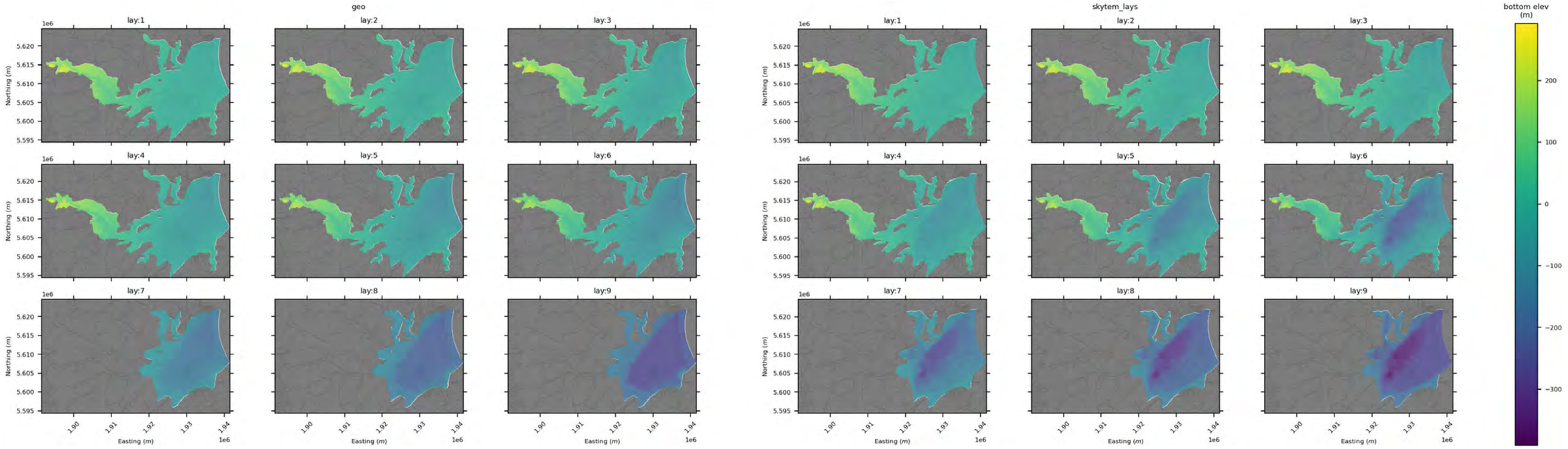

Figure 3.1 Layer bottom elevations (metres above sea level) for the (left) original (TWOTW/*geo*) and (right) SkyTEM-informed (*skytem-lays*) models, with layer adjustment.

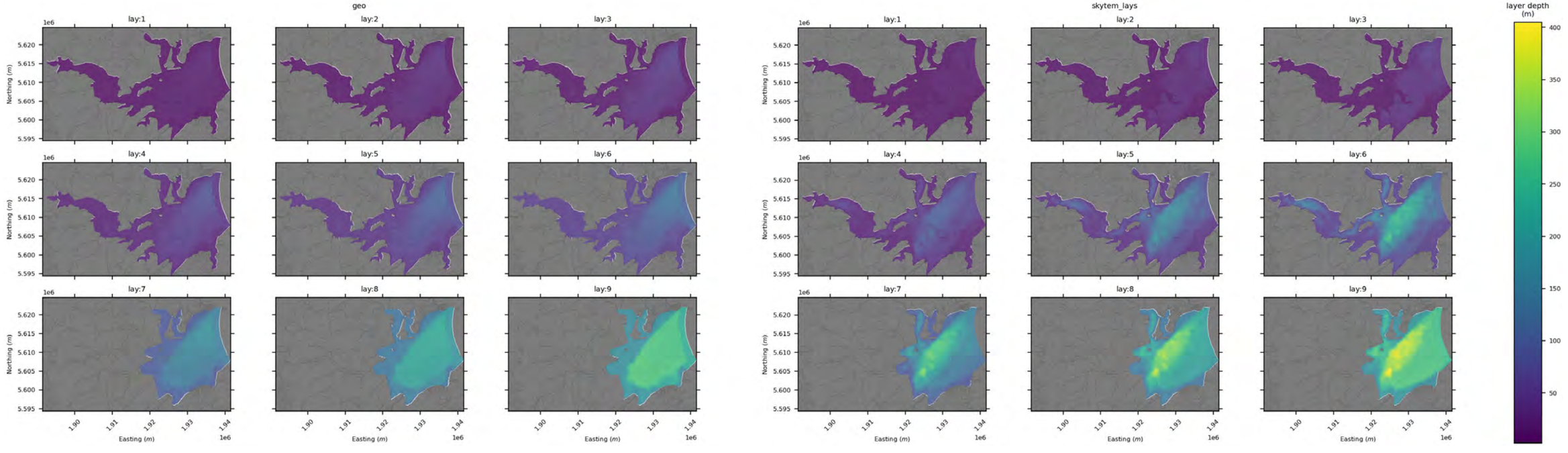

Figure 3.2 Layer bottom depths (metres) for the (left) original (TWOTW/*geo*) and (right) SkyTEM-informed (*skytem-lays*) models, with layer adjustment.

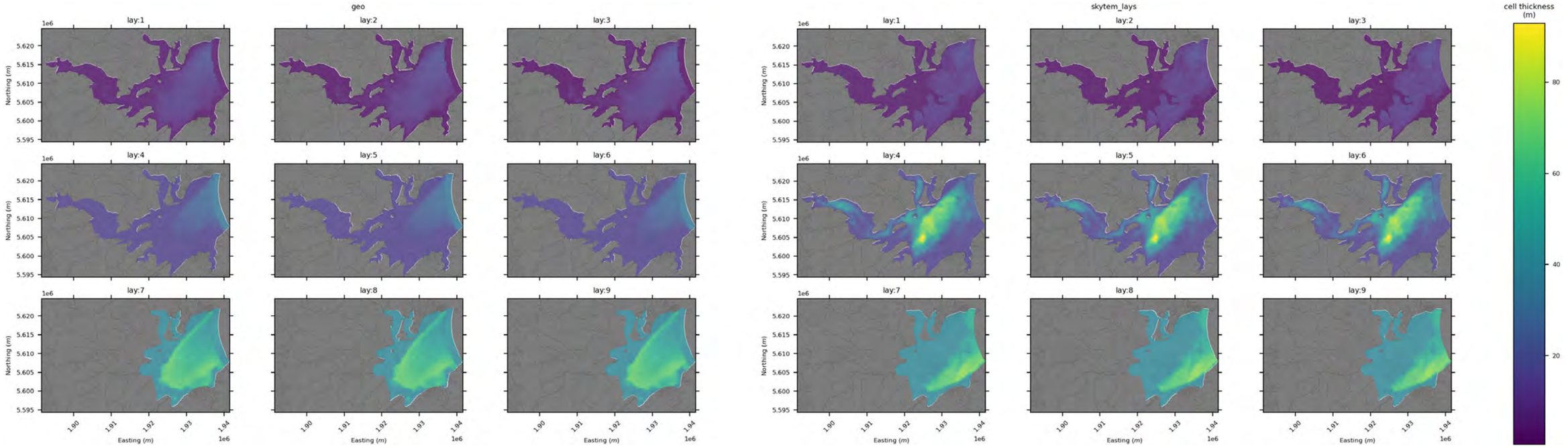

Figure 3.3 Layer bottom thickness (metres) for the (left) original (TWOTW/*geo*) and (right) SkyTEM-informed (*skytem-lays*) models, with layer adjustment.

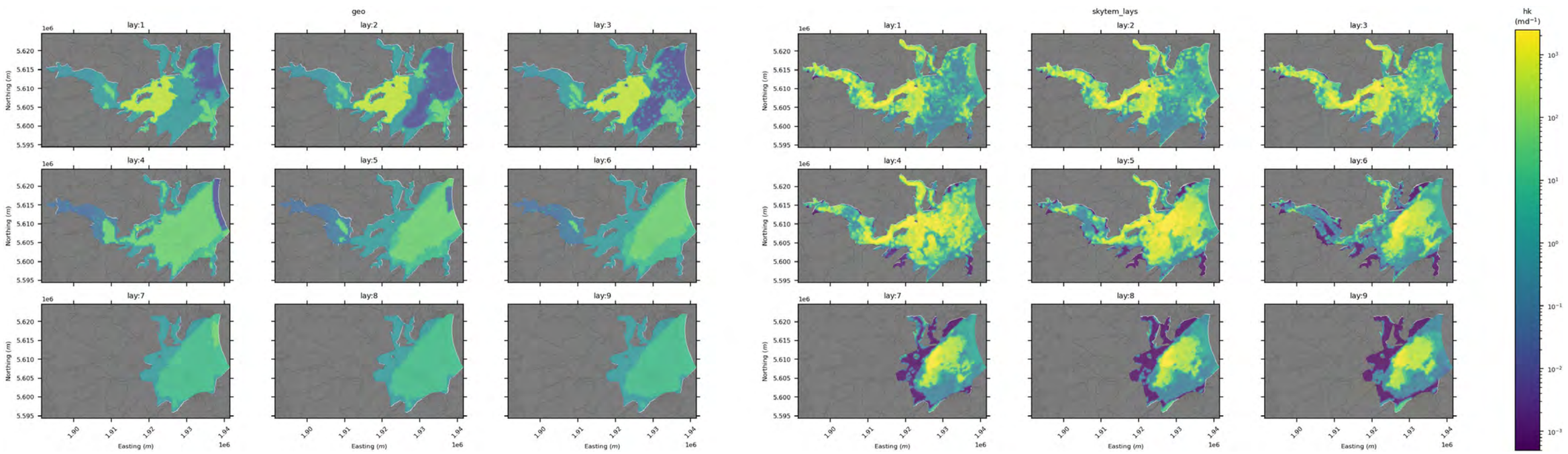

Figure 3.4 Base-realisation horizontal hydraulic conductivity (m/day) for the (left) original (TWOTW/*geo*) and (right) SkyTEM-informed (*skytem-lays*) models, with layer adjustment.

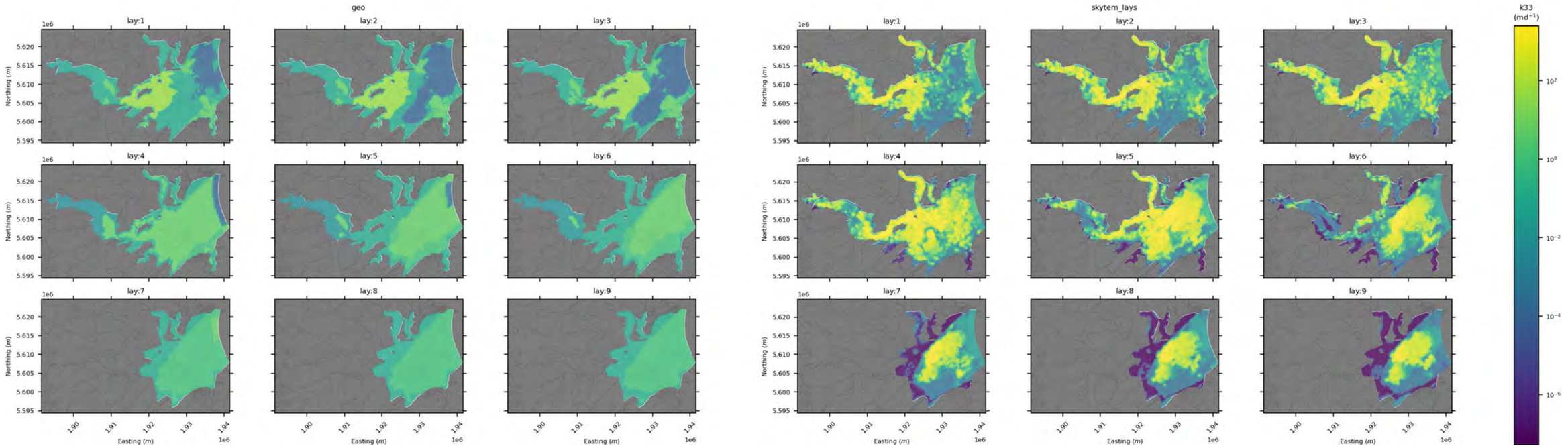

Figure 3.5 Base-realisation vertical hydraulic conductivity (m/day) for the (left) original (TWOTW/*geo*) and (right) SkyTEM-informed (*skytem-lays*) models, with layer adjustment.

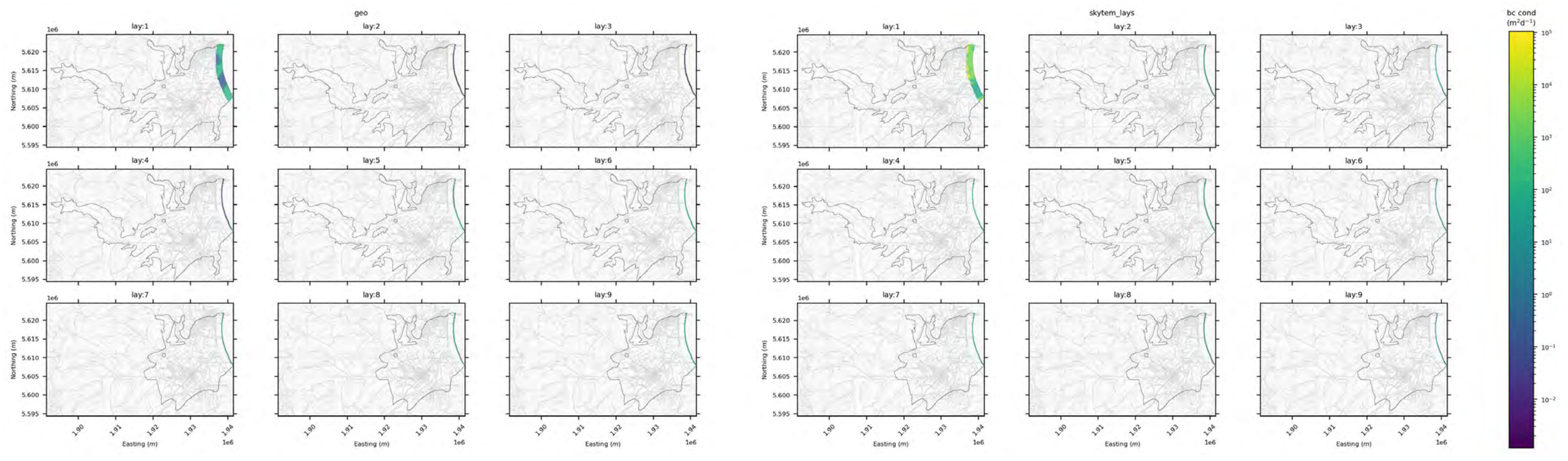

Figure 3.6 Base-realisation coastal general head boundary (GHB) conductance (m^2/day) for the (left) original (TWOTW/*geo*) and (right) SkyTEM-informed (*skytem-lays*) models, with layer adjustment.

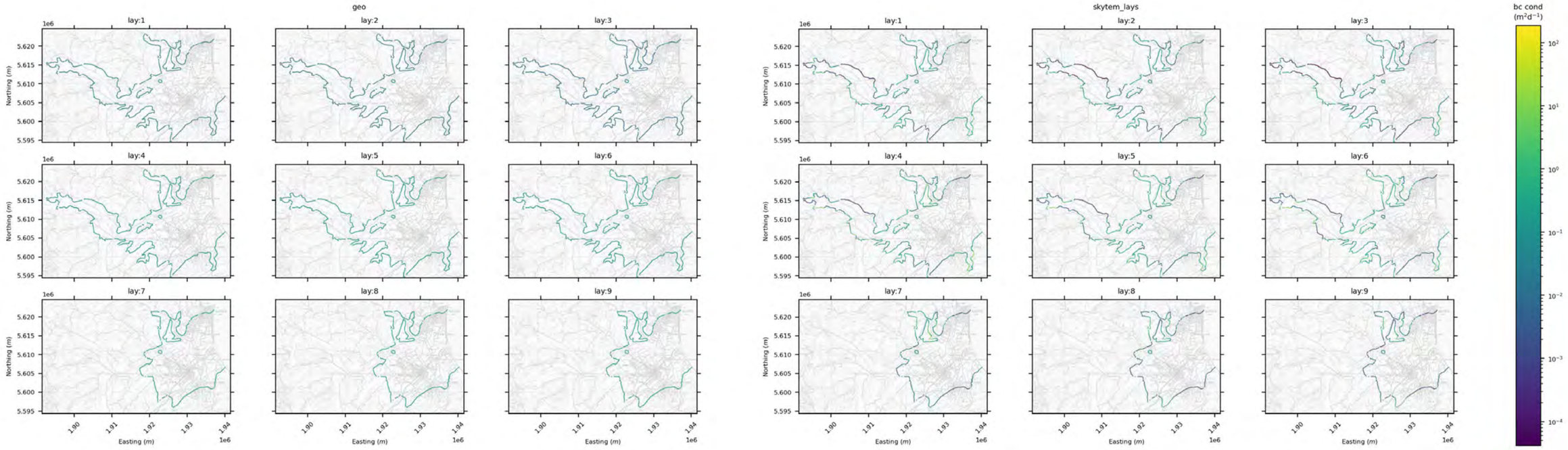

Figure 3.7 Base-realisation hillslope boundary general head boundary (GHB) conductance (m^2/day) for the (left) original (TWOTW/*geo*) and (right) SkyTEM-informed (*skytem-lays*) models, with layer adjustment.

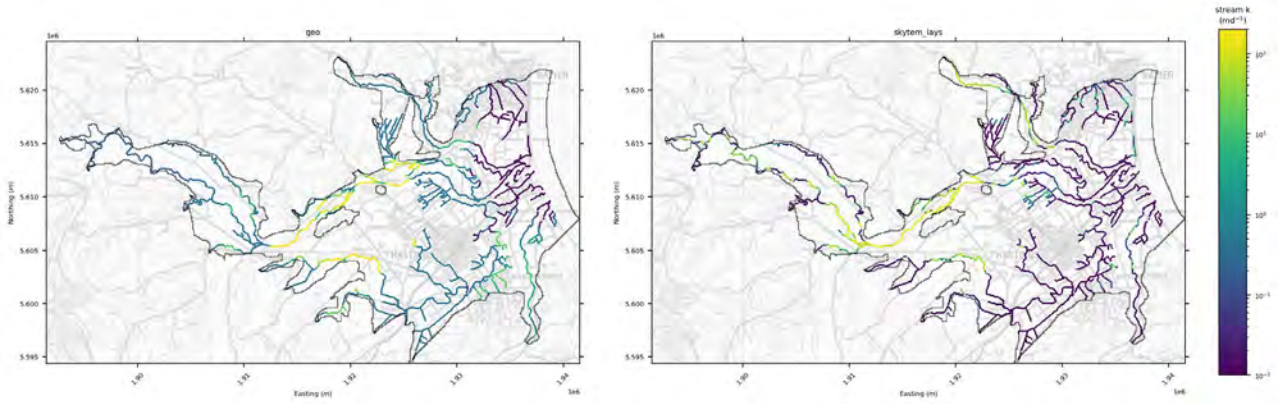

Figure 3.8 Base-realisation stream hydraulic conductivity (m/day) for the (left) original (TWOTW/*geo*) and (right) SkyTEM-informed (*skytem-lays*) models, with layer adjustment.

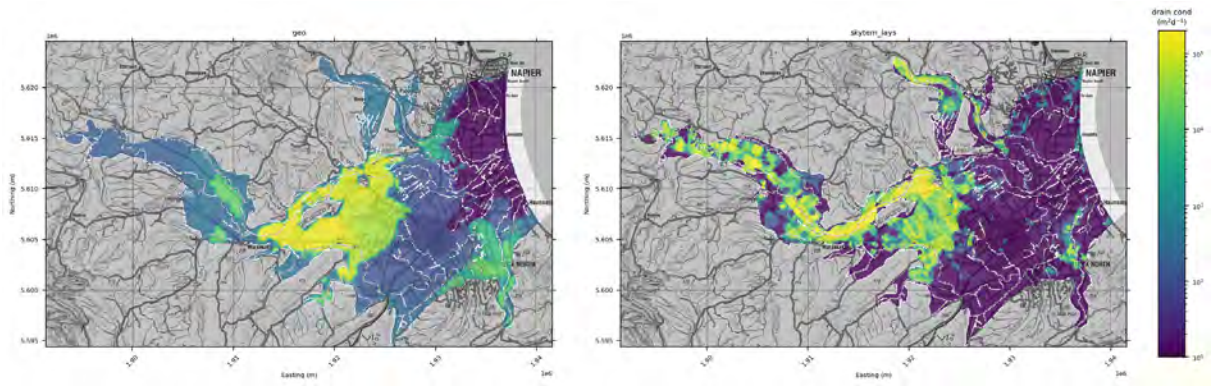

Figure 3.9 Base-realisation drain conductances (m^2/day) for the (left) original (TWOTW/*geo*) and (right) SkyTEM-informed (*skytem-lays*) models, with layer adjustment.

3.1.2 Parameter Pre-Conditioning

A comparison of the statistical descriptors (mean and standard deviation) of the model hydraulic conductivity parameter distributions, before and after pre-conditioning, is provided in Figures 3.10 and 3.11 (*skytem-k* and *skytem-k-precond)* and in Figures 3.12 and 3.13 (*skytem-lays* and *skytem-lays-precond).* Visual inspection of the ensemble mean hydraulic conductivity suggests very minimal change in the hydraulic conductivity fields through pre-conditioning (Figures 3.10 and 3.12). However, the mapped ensemble standard deviations do show significant differences after pre-conditioning (Figures 3.11 and 3.13). Generally, pre-conditioning results in greatly reduced standard deviations, especially around cluster 0 locations (high permeability; red circles in Figures 3.11 and 3.13). However, the use of only inequality constraints in the pre-conditioning results in non-gaussian distributions that may not be well represented by the standard deviation; this is likely to be reason why there are some increases in standard deviation in some locations.

This page left intentionally blank.

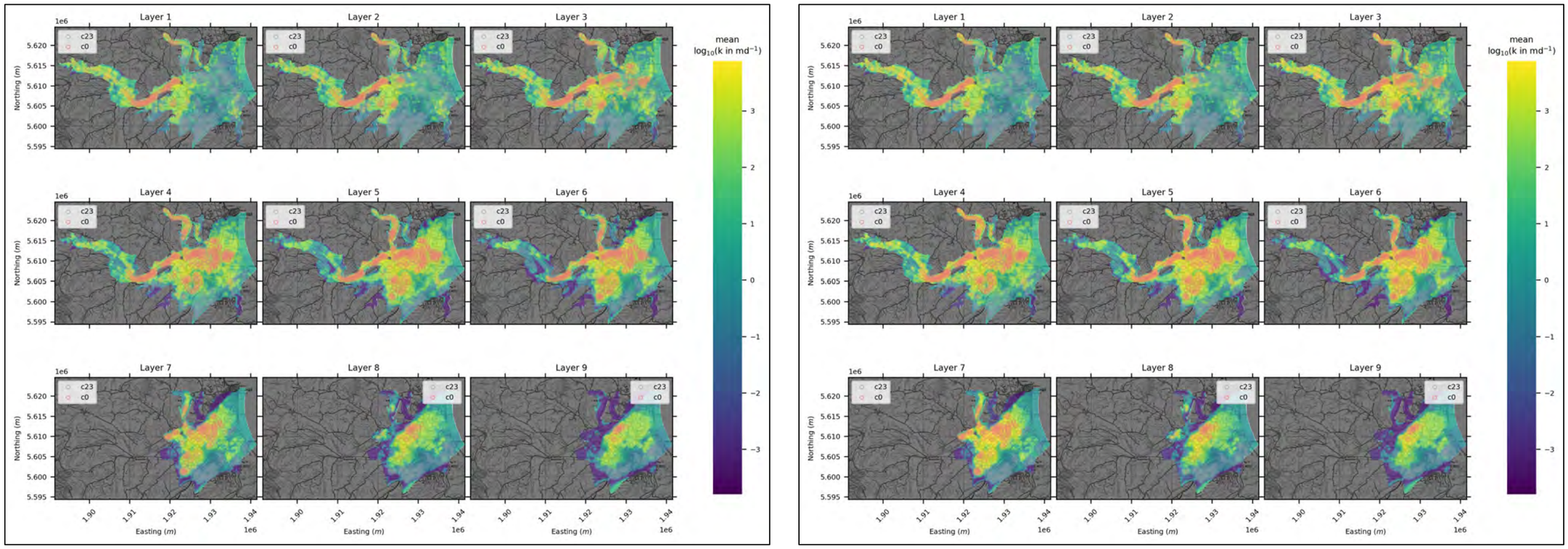

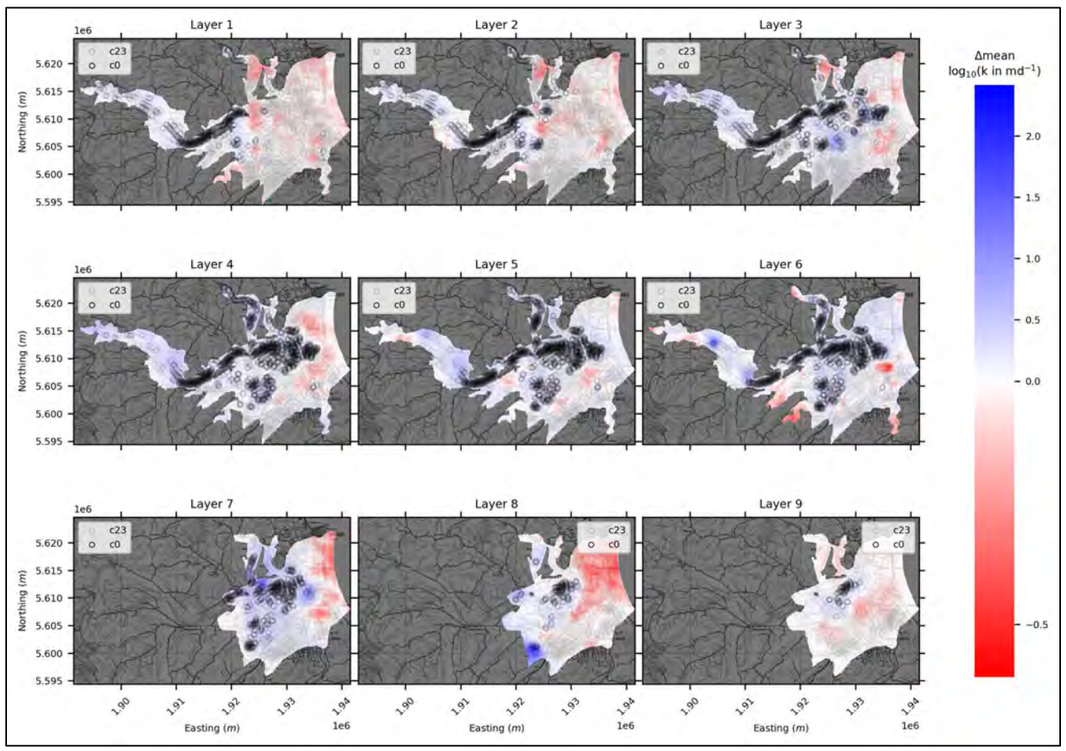

Figure 3.10 Ensemble mean of prior log-transformed HK field for *skytem-k-precond* before (upper left) and after (upper right) pre-conditioning, with the difference between these (right). Identified orange and grey circles identify locations where pre-conditioning was undertaken: c0 = cluster 0 (high permeability); c23 = cluster 2 or cluster 3 (low permeability).

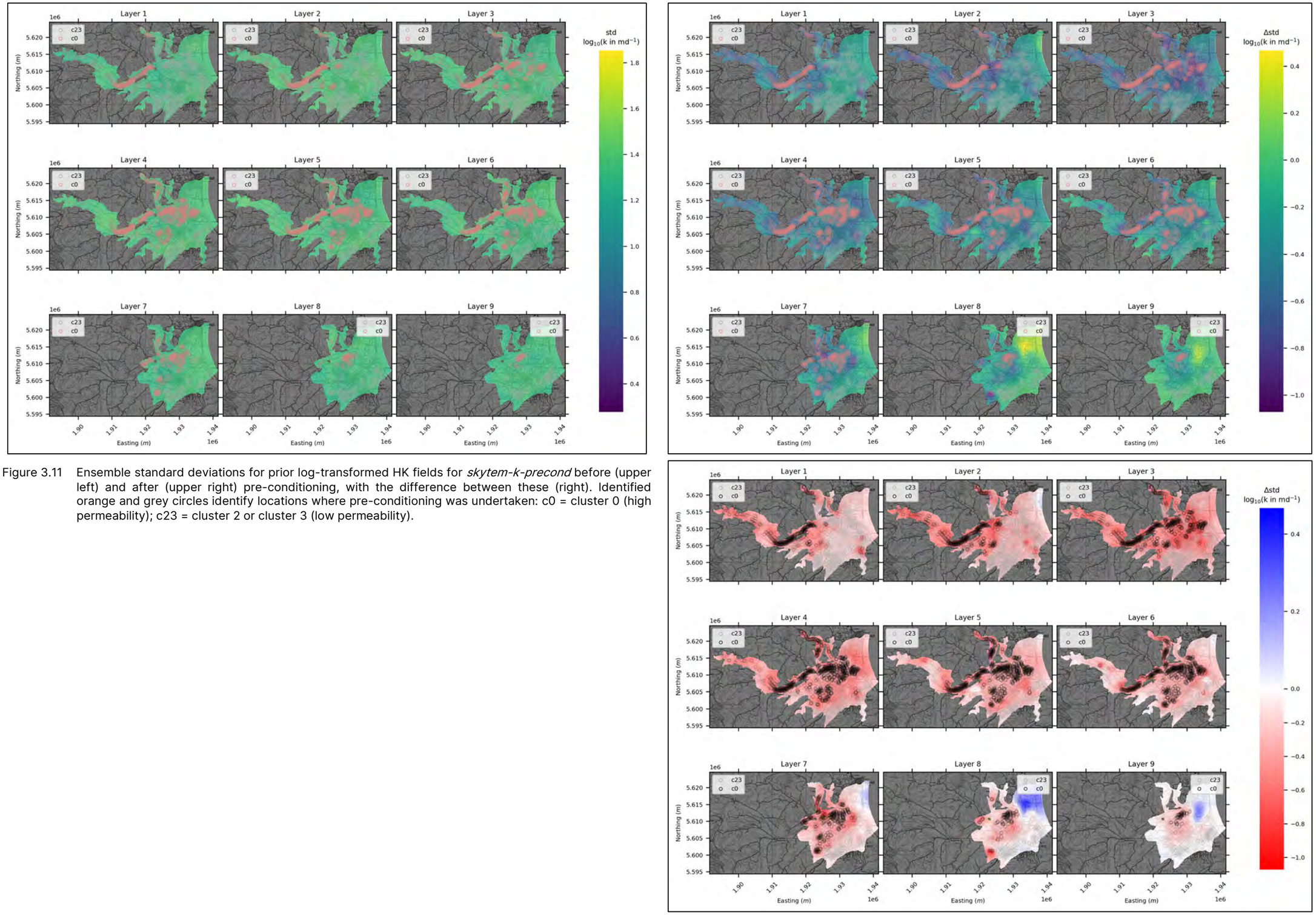

Figure 3.11 Ensemble standard deviations for prior log-transformed HK fields for *skytem-k-precond* before (upper left) and after (upper right) pre-conditioning, with the difference between these (right). Identified orange and grey circles identify locations where pre-conditioning was undertaken: c0 = cluster 0 (high permeability); c23 = cluster 2 or cluster 3 (low permeability).

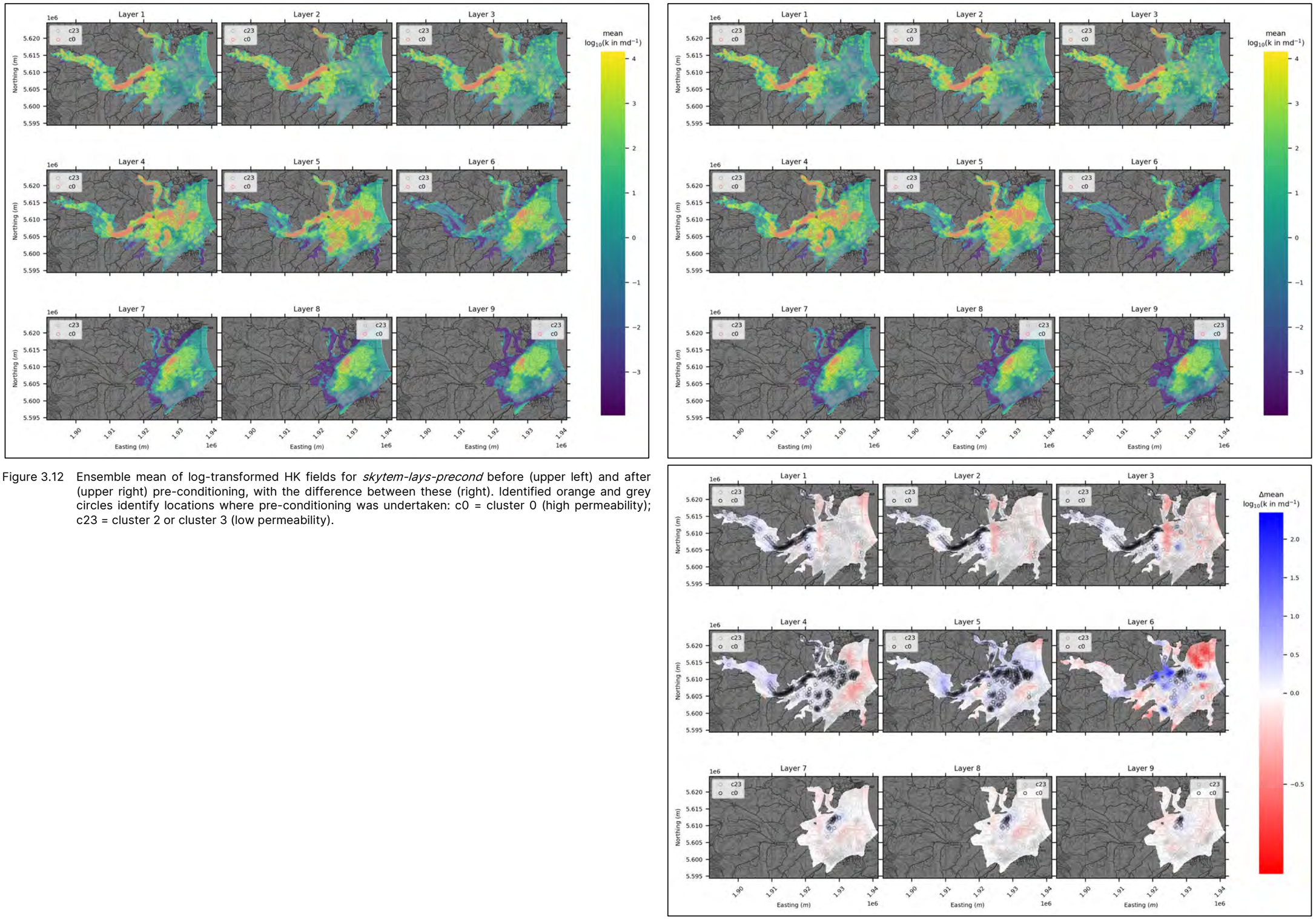

Figure 3.12 Ensemble mean of log-transformed HK fields for *skytem-lays-precond* before (upper left) and after (upper right) pre-conditioning, with the difference between these (right). Identified orange and grey circles identify locations where pre-conditioning was undertaken: c0 = cluster 0 (high permeability); c23 = cluster 2 or cluster 3 (low permeability).

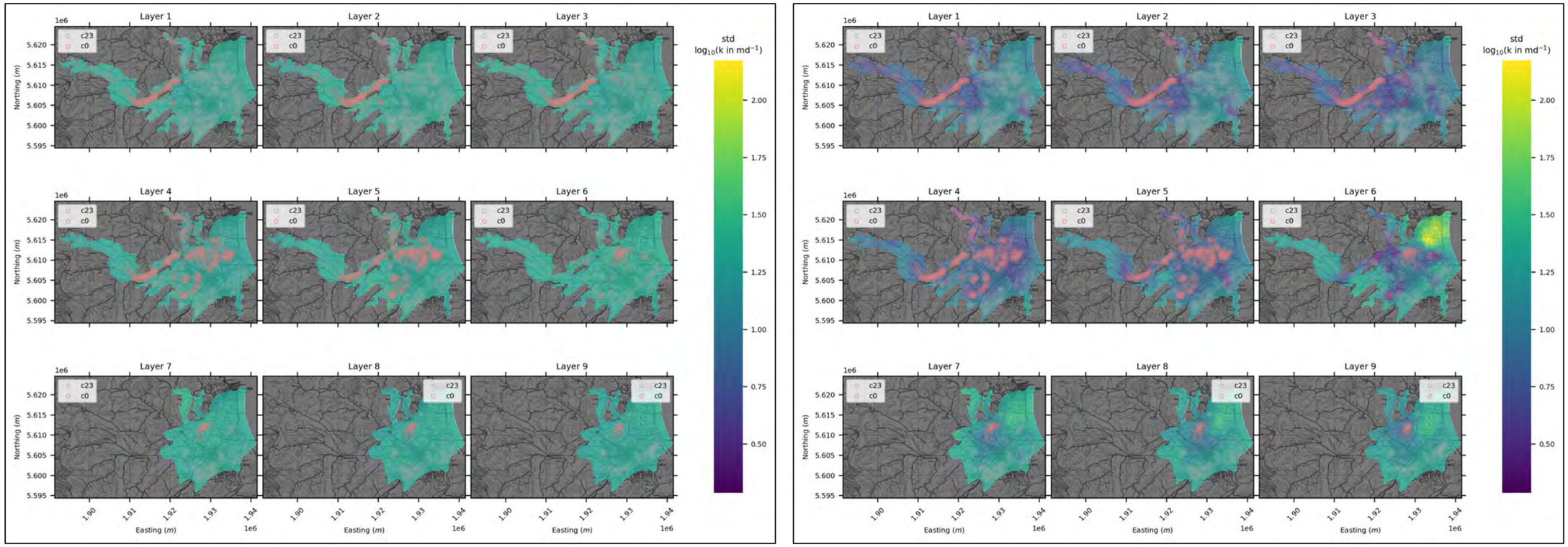

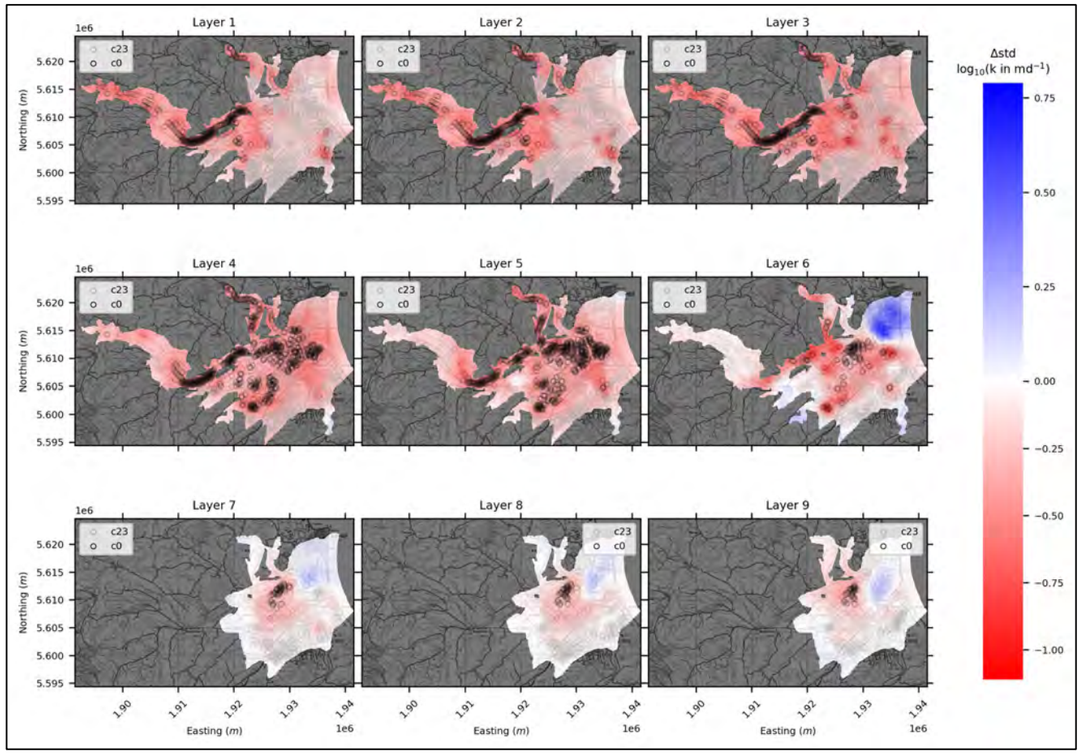

Figure 3.13 Ensemble standard deviation for log-transformed HK fields for *skytem-lays-precond* before (upper left) and after (upper right) pre-conditioning, with the difference between these (right). Identified orange and grey circles identify locations where pre-conditioning was undertaken: c0 = cluster 0 (high permeability); c23 = cluster 2 or cluster 3 (low permeability).

3.1.3 History-Matching

For all model versions, the three history-matching iterations improved the overall ensemble fits to the observations data. Summary plots of the prior and posterior simulated ensembles relative to observed data values are presented in Figure 3.14 (for the history-matching effort with the *geo* model, after Hemmings et al. [in prep.]), Figure 3.15 (for the *skytem-lays* models) and Figure 3.16 (for the preconditioned *skytem-lays-precond* model). Note that the prior ensembles (grey bars) in Figure 3.16 represent the pre-conditioned prior. Similar summary plots for the *skytem-k* models are provided in Appendix 3 (Figures A3.1 and A3.2). Prior and posterior simulated output distributions for individual observations are also provided in Appendix 3 (Section A3.2).

The fits to individual observations vary for the different model versions. Most noticeable from Figures 3.14 and 3.15 is that the posterior simulated outputs (blue bars) for surface-water–groundwater-exchange observations (E and F in Figure 3.15) for the *skytem-lays* model appear to better capture the observed values (accounting for observation noise; red bars) than the equivalent simulated outputs for the *geo* model version (E and F in Figure 3.14), albeit with greater apparent uncertainty in the outputs. Another notable difference between the *skytem-lays* and *geo* simulated outputs is clear in the cluster of higher water-level observations (over 125 m; I and H in both Figures 3.14 and 3.15). For these observations, the outputs for *skytem-lays* model version are generally lower than the equivalent outputs for the *geo* model version.

Generally, the *geo* model struggled to fit water-level observations in the coastal, confined portion of the model domain (e.g. sites 1417, 1450 and 15001; see Appendix 1 in Hemmings et al. [in prep.]). In these regions, the fit to water-level observations mostly improve for the AEM-informed versions of the model (e.g. sites 1417, 1450 and 15001; plots BE, BG and BK in Section A3.2.3.1). However, in other areas, the history-matching of the *geo* model is more able to capture the observed water levels than the AEM-informed model versions, for example, for water-level observations around Brookvale Road, Havelock North (e.g. sites 16557 and 16611; EI and EK in Section A3.2.3.1). Here, while the posterior ensemble for the *skytem-lays* model largely captures observed values, generally the simulated output is greater than the observation value (see EI and EK in Section A3.2.3.1). For these sites, the *geo* model posterior generally fits the observations better (see Appendix 1 in Hemmings et al. [in prep.]). Significant discrepancies in observed water-level values between closely located sites might contribute to challenges fitting these data. For example, sites 16556 and 16557 are closely located and in the same model layer, but have water-level observation discrepancies of up to 1 m. The presence of such discrepancies provides additional justification for pursuing ‘under-fitting’ in the history-matching efforts here. Another example is water-level observations of site 16202, at approximately 11 m depth, and the closely located site 16203, at approximately 22 m depth (DE and DF in Sections A3.2.1.1, A3.2.2.1, A3.2.3.1 and A3.2.4.1). The water-level observations at these two sites suggest a very strong upward head gradient of greater than 0.5 and a localised deep water table (approximately 9 m deep) or low head in the shallow system. These data are very difficult for the model to reproduce – they may reflect a very localised hydrogeological feature or even an erroneous datum for the measurements.

The progress of the iterative ensemble history-matching iterations also indicates some challenges converging on a posterior parameter ensemble that minimises the mis-fit between observations and simulated outputs. This is indicated by the algorithm resorting to ‘partial upgrades’ for a number of iterations for all model version history-matching exercises. Partial upgrades are undertaken where the upgrade of the parameter ensemble, for a given iteration, fails to meet mean objective function improvement criteria (commonly, this is a reduction in the mean objective function across the ensemble). In this instance, parameter upgrades are only applied to realisations that do meet the objective function improvement criteria. It is likely that the inequality observation on water levels, introduced as a pragmatic device to encourage movement of the ensemble toward improved numerical stability, created some strong non-linearity between parameter values and the objective function, as the inequality is contravened.

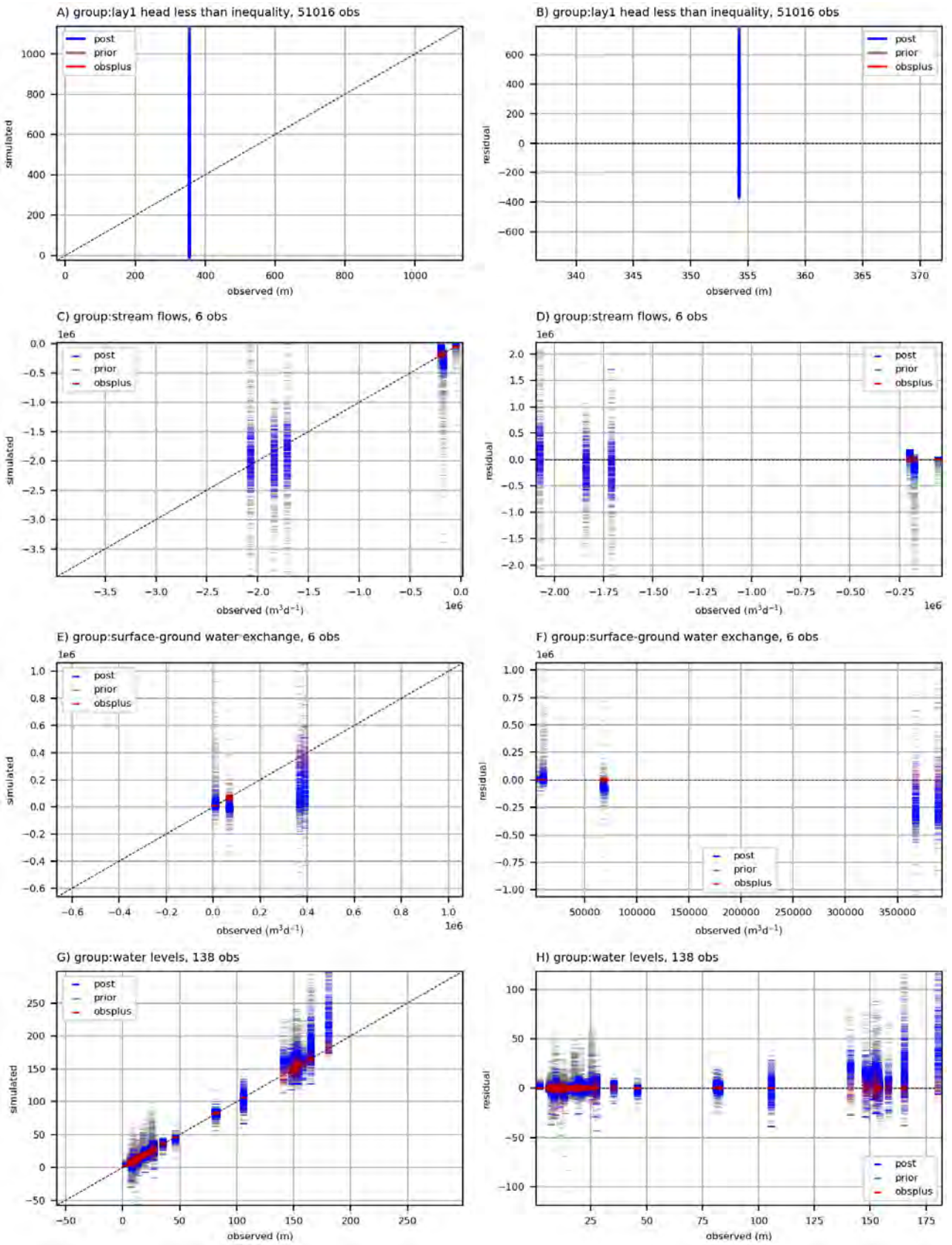

Figure 3.14 Summary of history-matching for the *geo* model, after Hemmings et al. [in prep.]. Left-hand plots (A, C, E, G) are simulated values versus observed values. Right-hand plots (B, D, F, H) are residual values (simulated minus observed) for each observed value. Grey bars represent prior simulated values. Blue bars are posterior simulated values with respect to the same observations. Red bars are the observed values with the inclusion of 'observation noise'. The top two plots (A and B) relate to inequality observations that surface-layer heads should always be below 350 m above sea level, which is a pragmatic observation to try to reduce spurious head spikes in the ensembles.

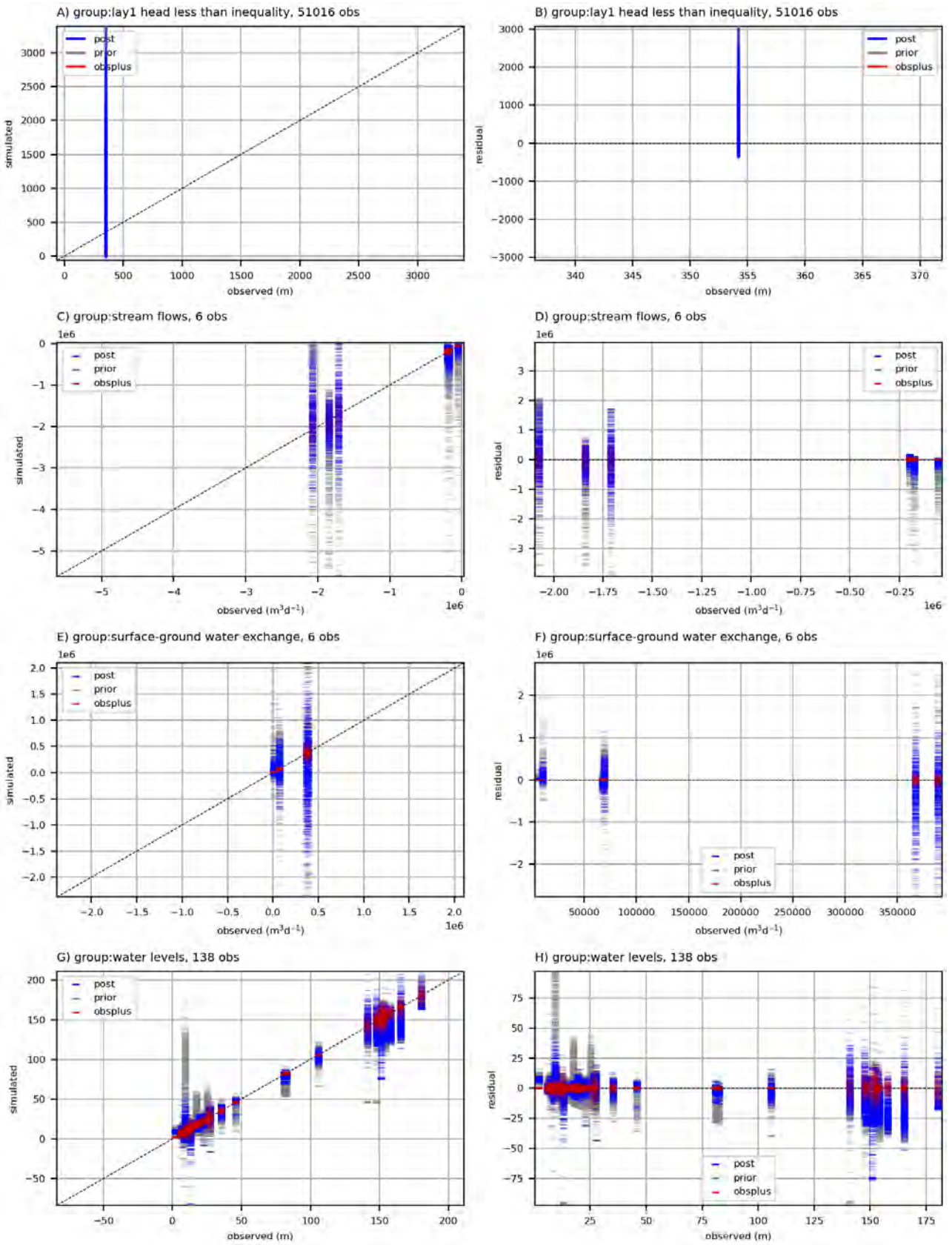

Figure 3.15 Summary of history-matching for the *skytem-lays* model. Left-hand plots (A, C, E, G) are simulated values versus observed values. Right-hand plots (B, D, F, H) are residual values (simulated minus observed) for each observed value. Grey bars represent prior simulated values. Blue bars are posterior simulated values with respect to the same observations. Red bars are the observed values with the inclusion of 'observation noise'. The top two plots (A and B) relate to inequality observations that surface-layer heads should always be below 350 m above sea level, which is a pragmatic observation to try to reduce spurious head spikes in the ensembles.

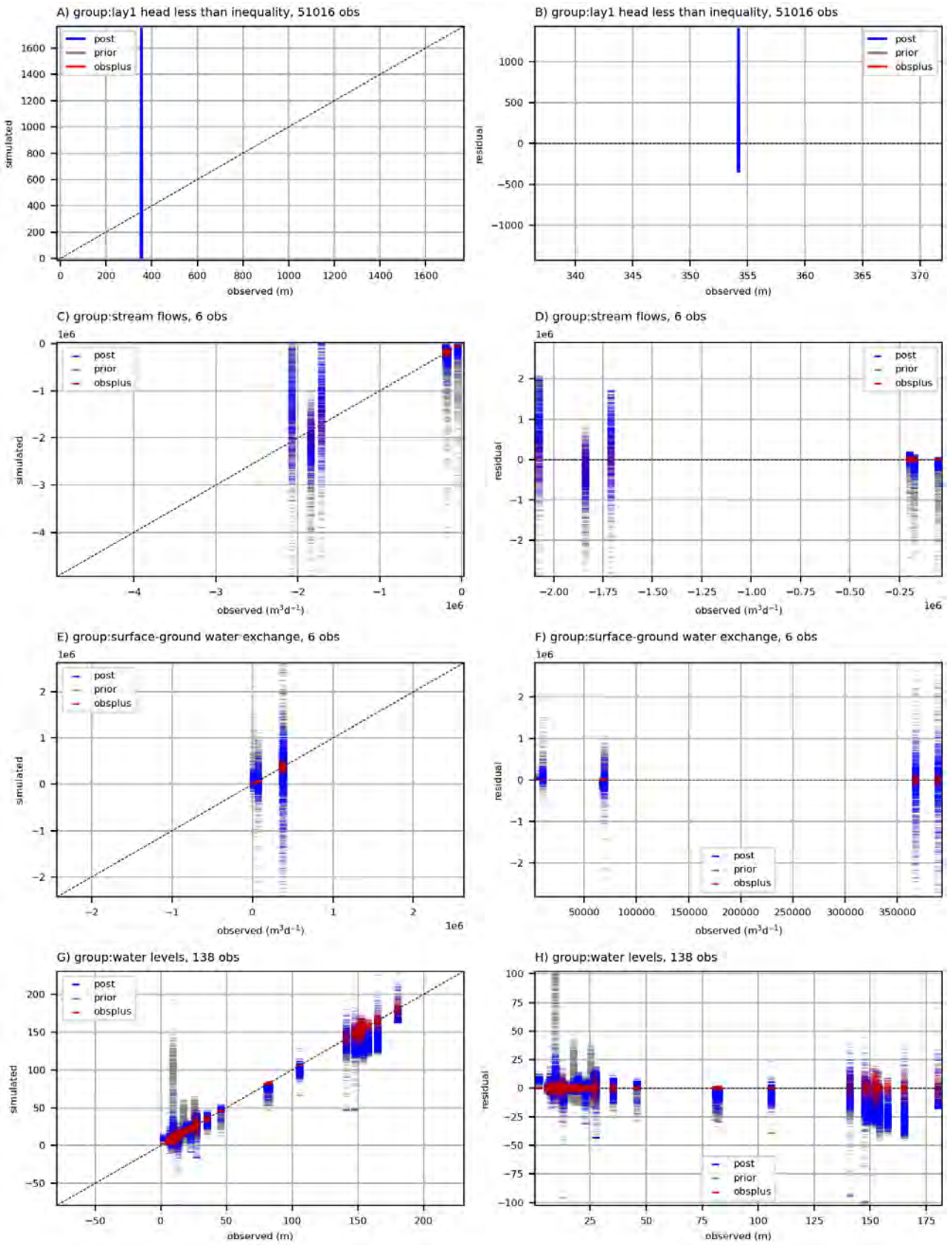

Figure 3.16 Summary of model history-matching for the *skytem-lays-precond* model. Left-hand plots (A, C, E, G) are simulated values versus observed values. Right-hand plots (B, D, F, H) are residual values (simulated minus observed) for each observed value. Grey bars represent prior simulated values. Blue bars are posterior simulated values with respect to the same observations. Red bars are the observed values with the inclusion of 'observation noise'. The top two plots (A and B) relate to inequality observations that surface-layer heads should always be below 350 m above sea level, which is a pragmatic observation to try to reduce spurious head spikes in the ensembles.

3.1.4 Predictive Changes

The subsequent sections detail the propagation of prior and posterior parameter ensembles through predictive model scenarios. Note that the use of a different numerical simulation for each predictive scenario, as well as for the history-matching, results in different patterns of model failure. As such, prior predictive ensembles may contain fewer members than posterior predictive ensembles, and the number of successful realisations may vary between scenarios.

3.1.4.1 Base Scenario

Base scenario prior and posterior distributions for specific predictions are shown in Figures 3.17–3.22. General mapped overviews of some prediction related simulated outputs and the differences in prior and posterior ensemble mean, median and standard deviation are provided in Section A4.1.

The AEM-informed changes to the model increase both the magnitude and uncertainty of the prior prediction of net inflow from the hillslope boundaries (compare lower distributions for *skytem* models to the *geo* model reference in Figure 3.17A). The *geo* model median value of prior prediction distribution for boundary inflow (indicated by a white line on the boxplot in the lower section of the probability distributions plot [labelled *base-geo*] in Figure 3.17A) is 7.2 m^{3s-1}. For all *skytem* models, the prior prediction median increases to over 20 m^{3s-1}. The prior standard deviation for this prediction approximately doubles for the *skytem* models relative to the *geo* model (from ~21 to over 40 m^{3s-1}). The extra boundary inflow predicted in the *skytem* model versions is balanced by increases in predicted exchange from groundwater to surface water (Figure 3.17B) and increases in the predicted offshore groundwater flow (Figure 3.17C).

After history-matching, the posterior distributions for boundary inflow and surface-water exchange predictions (upper plots in Figure 3.17A and B) are all reduced, in magnitude and apparent uncertainty, relative to the prior distributions. Posterior groundwater–surface-water-exchange prediction distributions for the *skytem-k* models move closer to the *geo* model posterior, albeit with greater predictive uncertainty (Figure 3.17B). The *skytem-lays-pc* model posterior also results in a similar posterior median to the *geo* model, although also with greater apparent uncertainty (standard deviation of 13 m^{3s-1} relative to 3.5 m^{3s-1} for the *geo* model). For this model version, more of the proportion of the additional boundary inflow is predicted to discharge offshore through the groundwater system; the posterior median prediction for *skytem-lays-pc* offshore groundwater discharge is 9.5 m^{3s-1}, compared to the posterior median groundwater–surface-water-exchange prediction of 7 m^{3s-1}. The *skytem-lays* model version, without pre-conditioning, maintains an elevated groundwater–surface-water-exchange prediction in the posterior (purple plot in Figure 3.17B), with the distribution median at over 11 m^{3s-1} surface-water gain and relatively low offshore flow (posterior median of 4.4 m^{3s-1}).

For these budget component predictions, notwithstanding the significant differences between the prediction distributions for the different models, median values for each *skytem* model posterior distribution fall well within the posterior distributions for each other *skytem* model. The *geo* model median values also always fall within all other model distributions. However, the *geo* model distributions do not always encompass the *skytem* model median values.

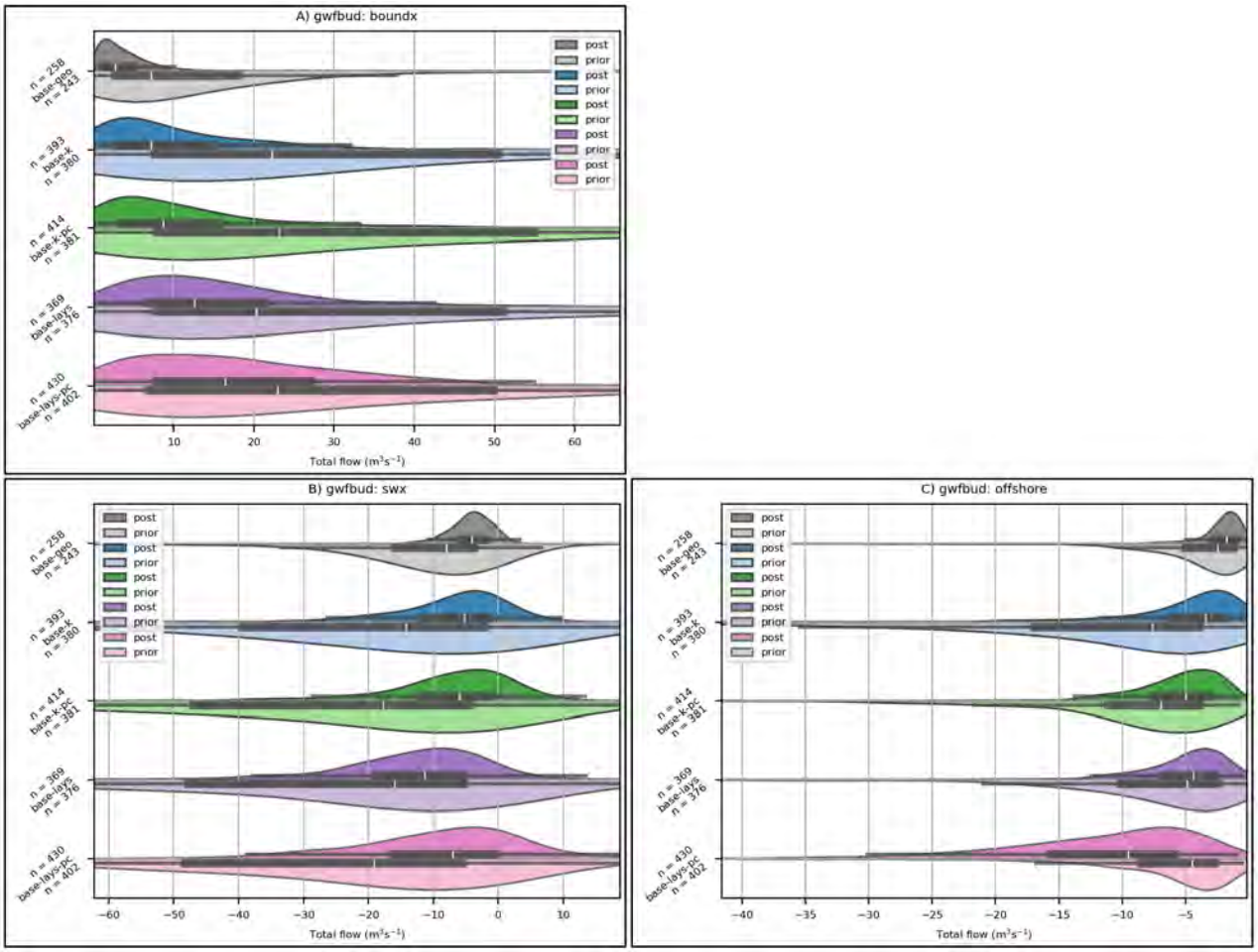

Figure 3.17 Budgetary component *base* scenario prediction distributions for the *geo, skytem-k* and *skytem-lays* models, including pre-conditioned versions (-*pc*). (A) Net flow across hillslope boundaries (to [positive] or from [negative] simulated domain). (B) Net groundwater–surface-water exchange to groundwater (positive) or surface water (negative). Note: this includes groundwater exchange with the explicit routed stream network (SFR package) and flux to model drains (DRN package). (C) Net offshore groundwater flow (positive values are net offshore flow). Violin plots represent kernel density estimation of prediction distributions; inner boxplots indicate quartiles with whiskers extending to 1.5 x the interquartile range. Models shown: *geo* (reference model; grey), *k* (parameter fields updated; blue), *k-pc* (parameter fields updated and preconditioning applied; green), *lays* (layers and parameter fields updated; purple), *lays-pc* (layers and parameter fields updated and pre-conditioning applied; pink). Note: x-axes are clipped to the maximum extent of the posterior distributions.

For the predictions that relate to the apportionment of offshore flow within zones, the AEM data informs a prediction of relatively little offshore groundwater flow in the southern zone (Figures 3.18D and 3.19D). This is even indicated in the prior distributions, although the structural changes in the *skytem-lays* model versions do support greater proportion than the *skytem-k* versions. Low offshore flow prediction in the southern zone for the *skytem* models is commensurate with a prediction of greater offshore flow through the middle zone (Figures 3.18C and 3.19C) and marks a clear difference from *geo* model predictions, which suggest more even distribution of offshore flow and increased prediction uncertainty, especially for the southern zone.

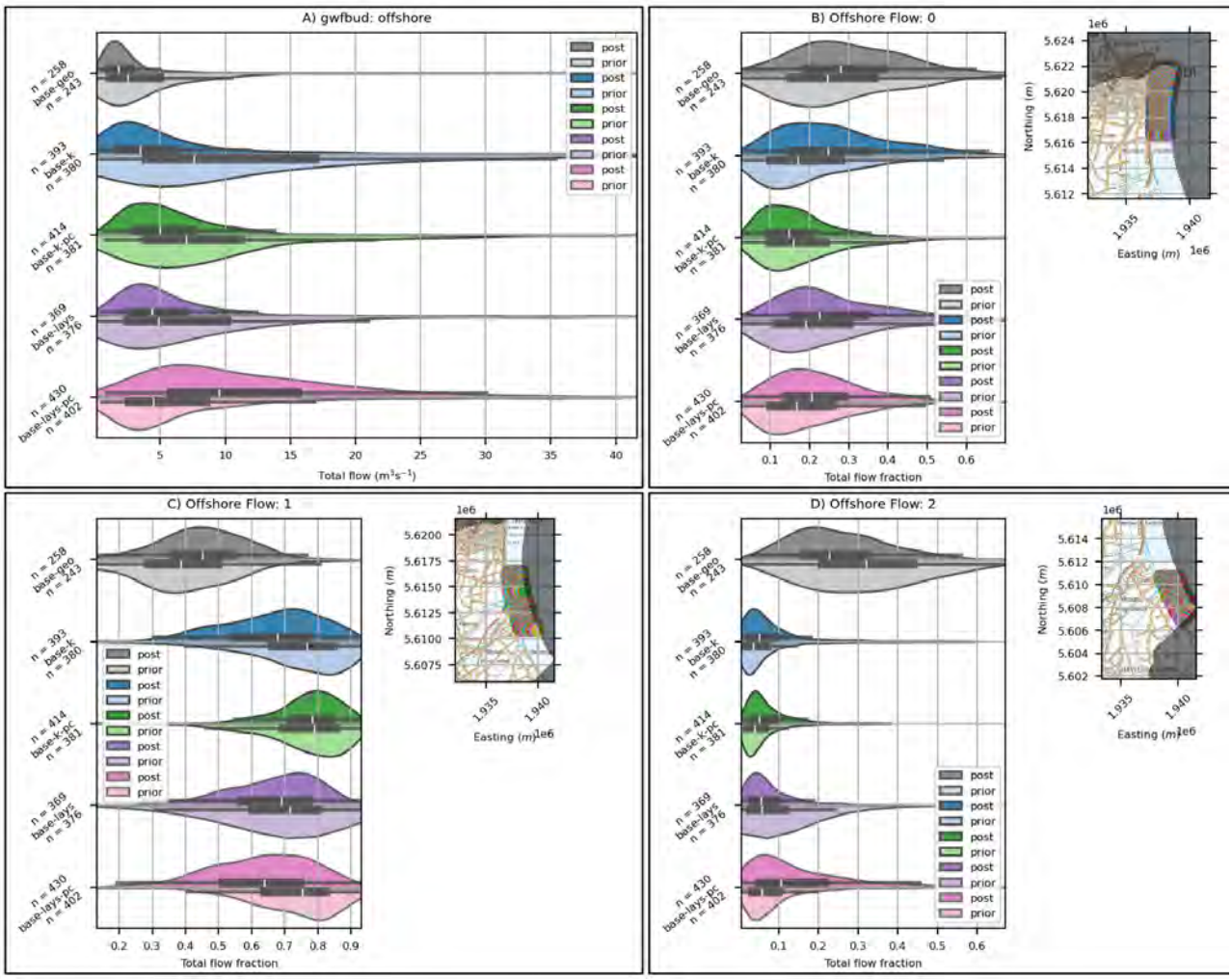

Figure 3.18 Fractional zonal groundwater offshore discharge prediction distributions for the *base* scenario for the *geo, skytem-k* and *skytem-lays* models, including pre-conditioned versions (-*pc*). (A) Total discharge and equivalent to Figure 3.19A. (B–D) Zonal components in the north, middle and south zones, respectively (as shown on inset maps). Note: x-axes are clipped to the maximum extent of the posterior distributions.

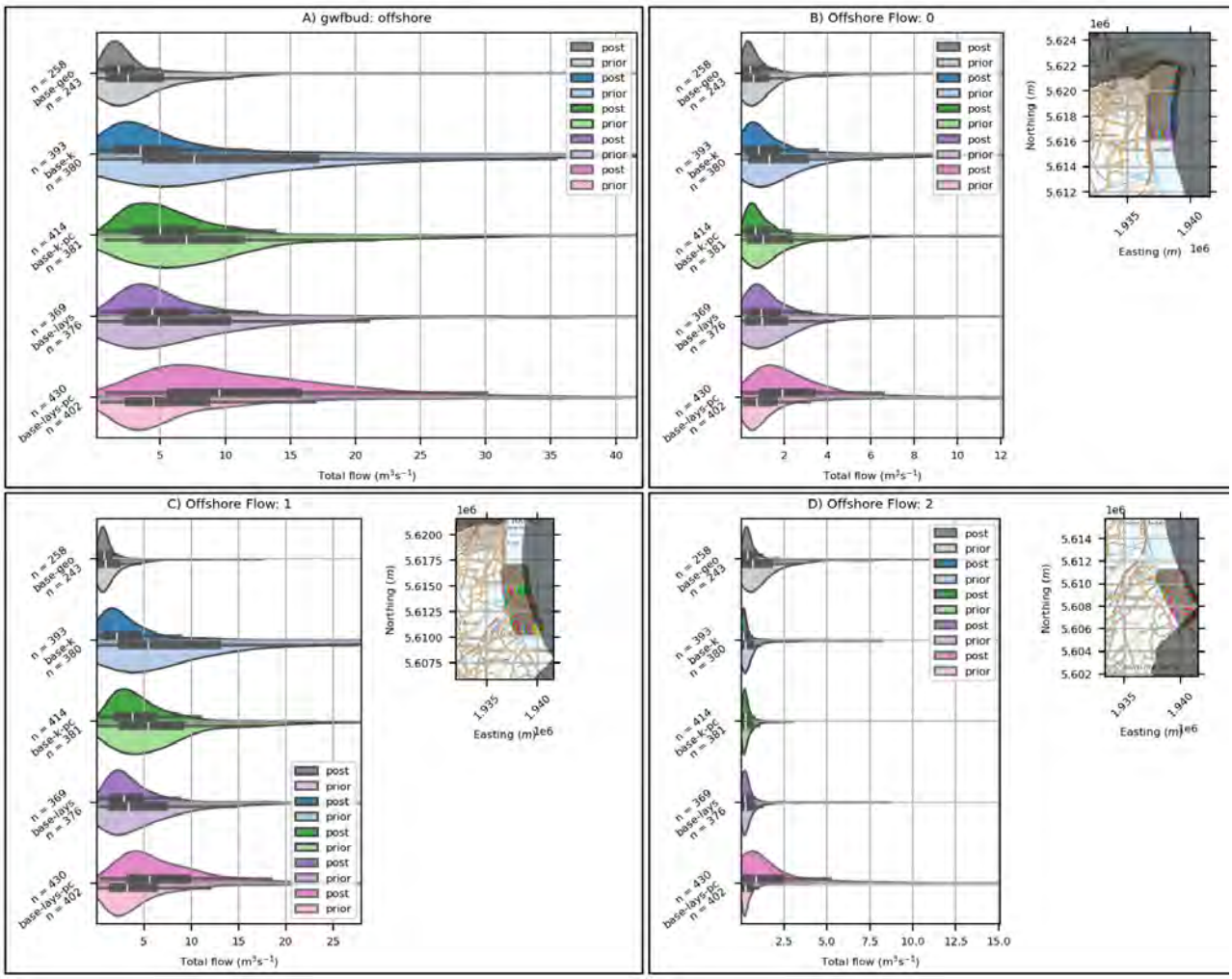

Figure 3.19 Net zonal groundwater offshore discharge prediction distributions for the *base* scenario for the *geo, skytem-k* and *skytem-lays* models, including pre-conditioned versions (-*pc*). (A) Total discharge. (B–D) Zonal components in the north, middle and south zones, respectively (as shown on inset maps). Note that the polarity of the plots is opposite to Figure 3.17C (positive values indicate offshore flow); as such, (A) is the additive inverse of Figure 3.17C. Note: x-axes are clipped to the maximum extent of the posterior distributions.

For the local groundwater–surface-water-exchange prediction along Ngaruroro River, upstream of Roys Hills (grey plots in Figure 3.20A), the *geo* model prior and posterior distributions indicate minor river loss: both prior and posterior distribution median values are at approximately 0.5 m^3s^{-1}, and the middle two quartiles (majority of the distribution) are between 0 and 3.2 (prior) and 0.1 and 1.0 (posterior). For the *skytem* model versions, the prediction distributions move toward favouring river gain from groundwater. The maximum median value is predicted with the *skytem-lays-pc* model version (gain of 3.7 m^3s^{-1}).

The in-stream flow predictions are unique in that there are also history-matching observations at these locations. As such, the violin plots in Figure 3.20B–D are equivalent to plots K, G and A, respectively, in Sections A3.2.1.2, A3.2.2.2, A3.2.3.2 and A3.2.4.2 (with a unit adjustment to m^3s^{-1}). As the predictions form part of the history-matching dataset, the apparent prediction uncertainty is significantly reduced by history-matching. Posterior distribution standard deviations are 70–90% lower than the respective prior distribution standard deviations, which were initially very high. However, few of the posterior distributions are well centred on the observation values. Despite the reduction in posterior prediction standard deviations, the posterior prediction uncertainty remains high for the *skytem* model version. However, this uncertainty allows predictive distributions for all of the *skytem* models to comfortably encompass all of the observation plus noise (red bars in Figure 3.20B–D). In contrast, the *geo* model posterior distributions do not encompass the observation-plus-noise values as effectively.

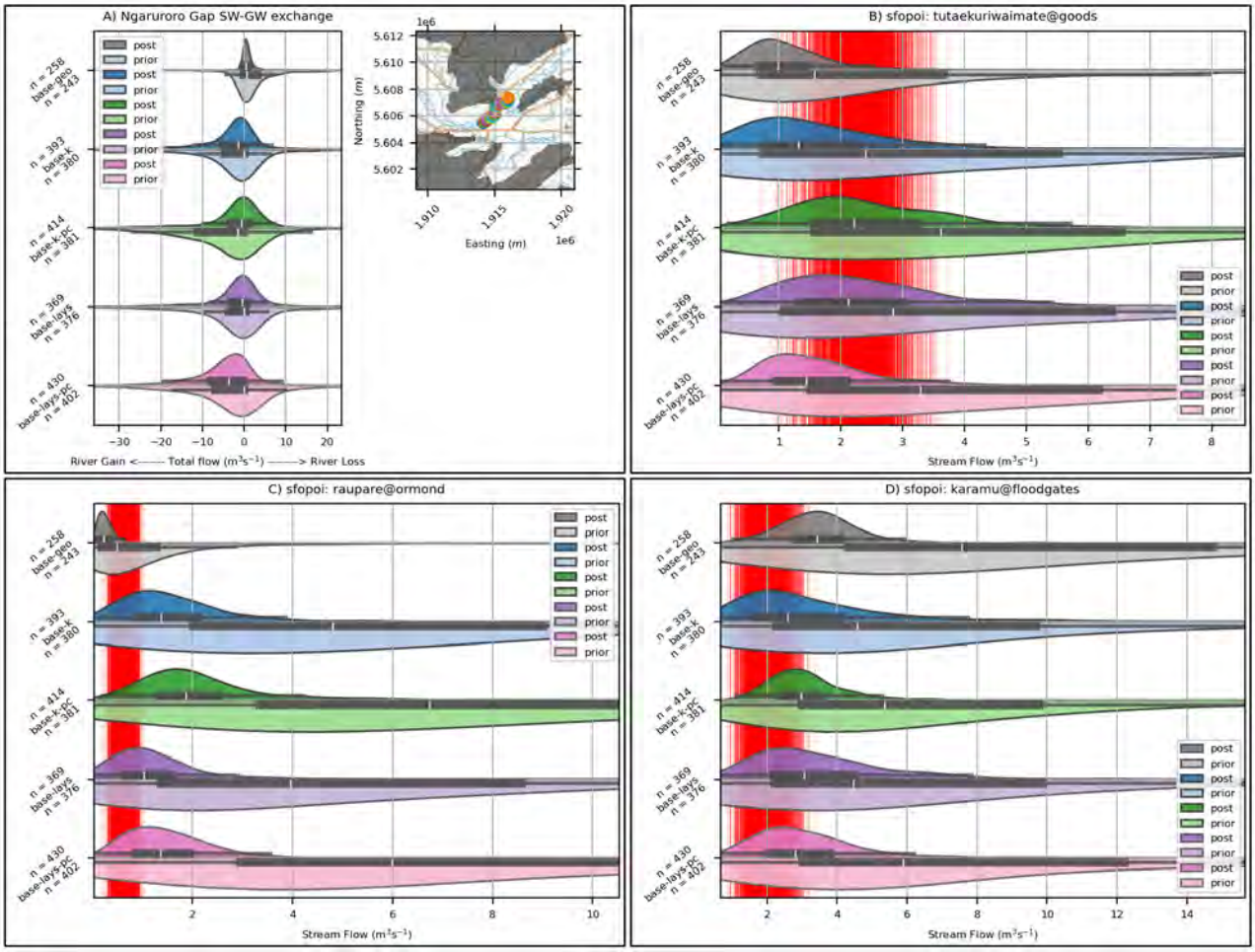

Figure 3.20 Ngaruroro River groundwater exchange between Maraekakaho and Roys Hill (A) and in-stream flow (B–D) *base* scenario prediction distributions for the *geo, skytem-k* and *skytem-lays* models, including pre-conditioned versions (*-pc*). Positive values in (A) indicate simulated surface-water gain along the river reach (explicit SFR package exchange). The red bars in (B–D) represent the realisations of observations plus noise (note that the Ngaruroro River exchange at this location was not a history-matching observation). Note: x-axes are clipped to the maximum extent of the posterior distributions.

For the eight water-level predictions, posterior distributions demonstrate significant reductions in prediction uncertainty for all model versions (Figures 3.21 and 3.22). Generally, *skytem* model version prediction distributions are in good agreement with each other. However there is often reasonable discrepancy between all *skytem* model distribution centres and the *geo* model distribution centres (e.g. at sites 5970, 1865, 10796 and 5368; Figure 3.21A, C, D and Figure 3.22A, respectively). For these water-level predictions, the apparent posterior uncertainty of *skytem* version predictions appears to be similar or reduced, relative to the *geo* model uncertainty.

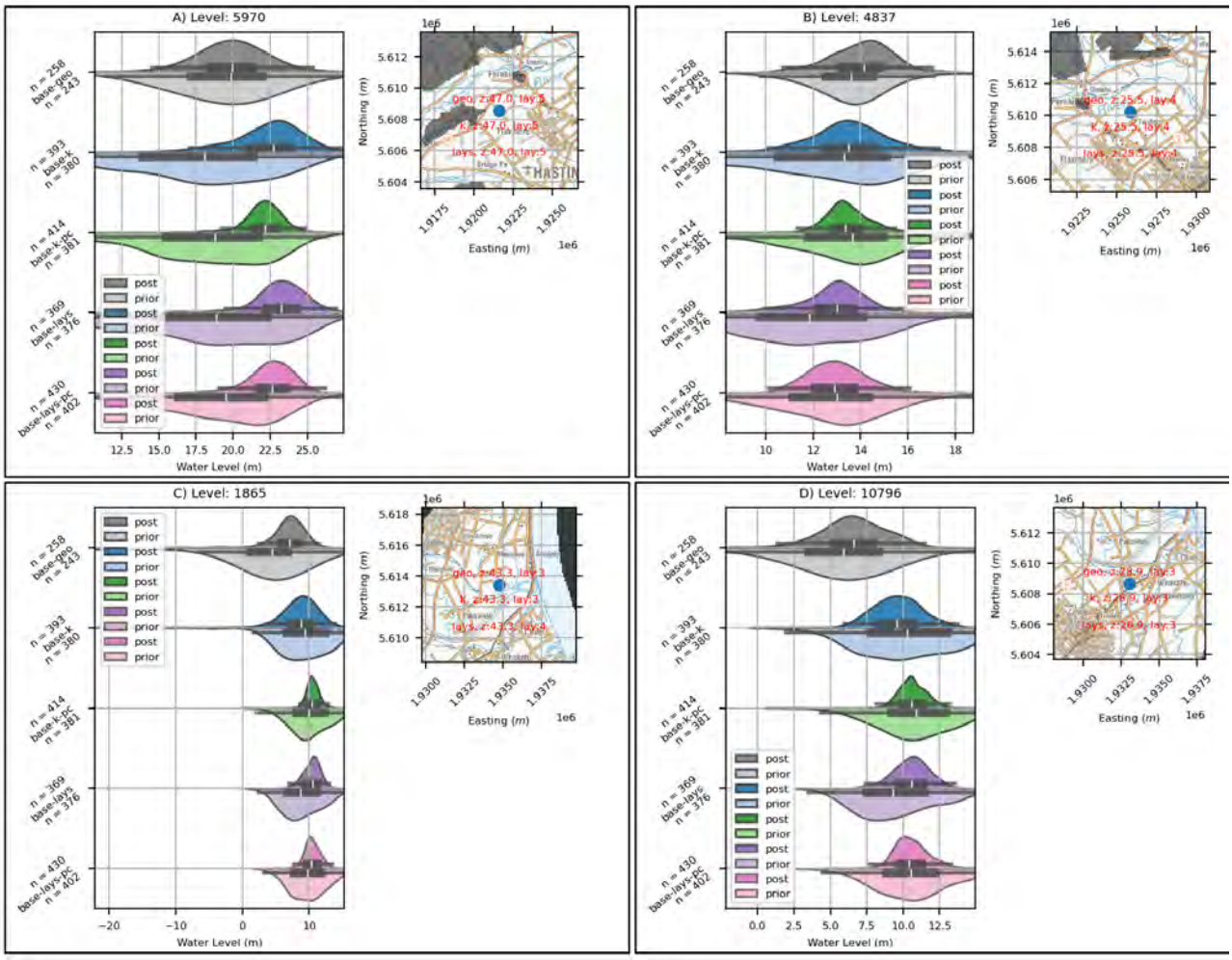

Figure 3.21 Groundwater-level prediction distributions for the *base* scenario for the *geo, skytem-k* and *skytem-lays* models, including pre-conditioned versions (*-pc*). The red text in the inset maps indicates the model layer for the simulated output – this can differ between the *geo* and *skytem-lays* model versions due to changes in the model structure. Note: x-axes are clipped to the maximum extent of the posterior distributions.

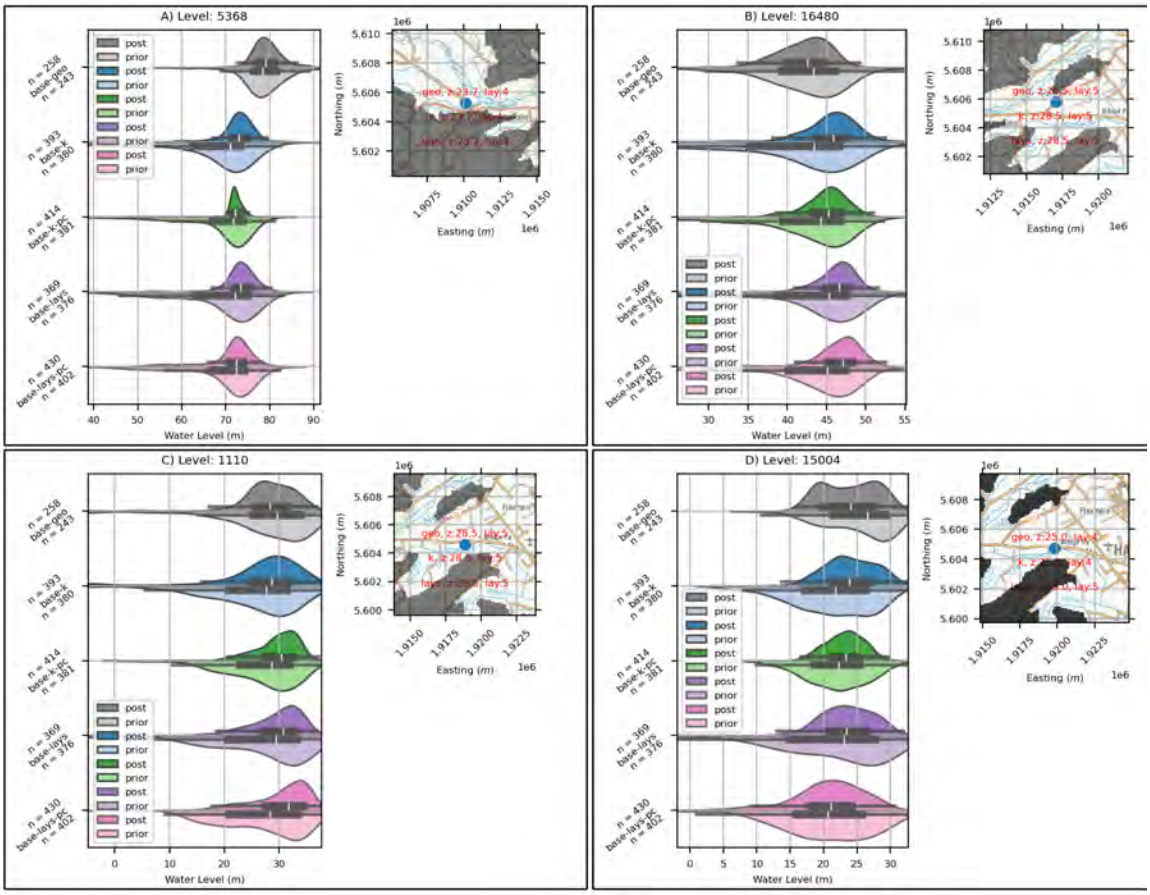

Figure 3.22 Further groundwater-level prediction distributions for the *base* scenario for the *geo, skytem-k* and *skytem-lays* models, including pre-conditioned versions (-*pc*). Red text in inset maps indicates the model layer for the simulated output – this can differ between the *geo* and *skytem-lays* model versions due to changes in the model structure. Note: x-axes are clipped to the maximum extent of the posterior distributions.

3.1.4.2 Scenario Difference Predictions

Scenario analysis (see Section 2.4) included simulation of predictive model realisations for *dry*, *wet*, *increased pumping* and *decreased pumping* conditions. The results for these scenarios are expressed as absolute predictions for the scenarios and difference predictions relative to the *base* scenario. The *dry* climate scenario results for the *skytem-lays* model versions are presented in Figures 3.23–3.28. See Appendix 4 for results associated with the other scenarios and the *skytem-k* model.

Budget predictions for the *dry* scenario (Figure 3.23) include a small increase in predicted flow from hillslope boundaries (Figure 3.23A) for all model versions. The predicted increase is higher for the *skytem* model versions than the *geo* model and with greater apparent uncertainty. However, the posterior prediction distribution is mostly below a 0.1 m^3s^{-1} increase. The *dry* scenario prediction for offshore flow (Figure 3.23C) indicates a similar magnitude of change.

The *dry* scenario does not noticeably alter the zonal partitioning of the offshore flow; the change in the fraction of offshore flow predicted for each zone is close to zero (Figure 3.24). Predicted increases in each zone are approximately proportional to the *base* scenario flow (Figure 3.25).

For the prediction of surface-water–groundwater exchange (Figure 3.23B), the *dry* scenario prediction is for reduced flow from groundwater toward surface water. The predictive distributions for change in exchange are similar for the *geo* and *skytem-lays* model versions (approximately 2 m^3s^{-1} reduction in surface-water gain). However, the distribution median for the *skytem-lays-pc* predictive distribution (pink in Figure 3.23B), and both *skytem-k* model versions (Section A4.3.1), is shifted to less reduction in groundwater flux to surface water for the *dry* scenario (toward 1 m^3s^{-1}).

Along Ngaruroro River between Maraekakho and Roys Hill, the prediction distributions are reasonably even around no change in gain (or loss) for the *dry* scenario (Figure 3.26A). However, the *skytem-lays-pc* model does indicate potential for decreased gain (or increased loss), up to 1 m^3s^{-1}.

For all stream-flow predictions, the models indicate reductions in flow for the *dry* scenario (Figure 3.26B–D). The change predictions are significantly affected by history-matching – the posterior prediction distributions are reduced in magnitude (less reduction in flow) and apparent uncertainty for all model versions relative to the priors. Posterior predictions for change in flow for the *dry* scenario are similar across all model versions. However, the *skytem-lays-pc* and both *skytem-k* models predict that stream flow on Karamu River at the floodgates is marginally less affected by the *dry* scenario (less reduction in flow; Figure 3.26D and Section A4.3.1).

Similarly, the prediction of the effect of the *dry* scenario on water levels (i.e. change in level relative to *base*) is similar across the different model versions. For all sites, the predictions are for reduced water levels in the *dry* scenario (Figures 3.27 and 3.28). Site 5368 shows the greatest discrepancy in the predicted *dry* scenario effect between the *geo* and *skytem* model versions (Figure 3.28A). For sites 5970, 4837 and 10796, the *skytem-lays* and *skytem-lays-pc* posterior predictions of change in level are much reduced relative to the prior, and the posterior distributions align with the *geo* model posterior (Figure 3.27A, B and D).

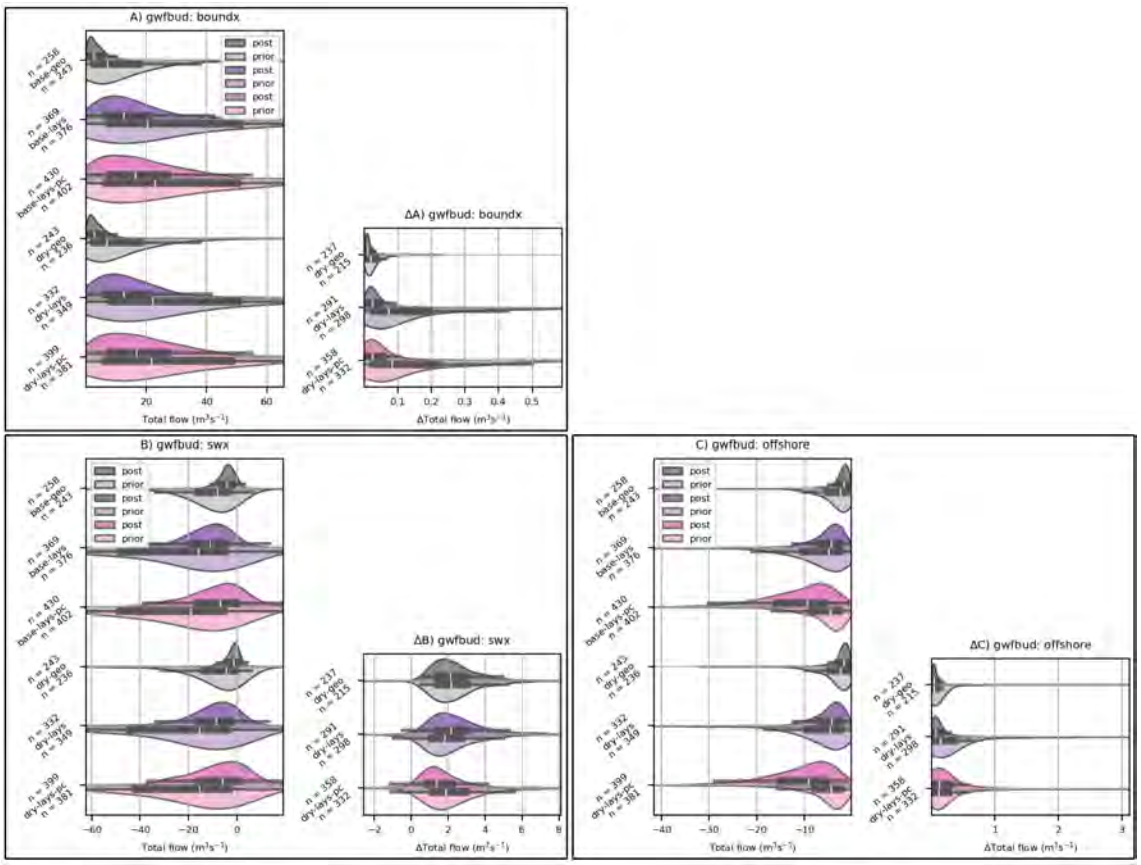

Figure 3.23 Comparison between *base* and *dry* scenario budget component predictions for the *geo* and *skytem-lays* models. Left-hand plots in each panel show prediction distributions for the *base* (upper three plots) and *dry* scenarios (lower three plots). Right-hand plots show the change predictions, calculated as *dry* – *base* for each realisation. (A) Net flow across hillslope boundaries (to [positive] or from [negative] simulated domain). (B) Net groundwater–surface-water exchange to groundwater (positive) or surface water (negative). Note that this includes groundwater exchange with the explicit, routed, stream network (SFR package) and flux to model drains (DRN package). (C) Net offshore groundwater flow (positive values are net offshore flow). Violin plots represent kernel density estimation of prediction distributions; inner boxplots indicate quartiles with whiskers extending to 1.5 x the interquartile range. Models shown: *geo* (reference model; grey), *lays* (layers and parameter fields updated; purple), *lays-pc* (layers and parameter fields updated and pre-conditioning applied; pink). Note: x-axes are clipped to the maximum extent of the posterior distributions.

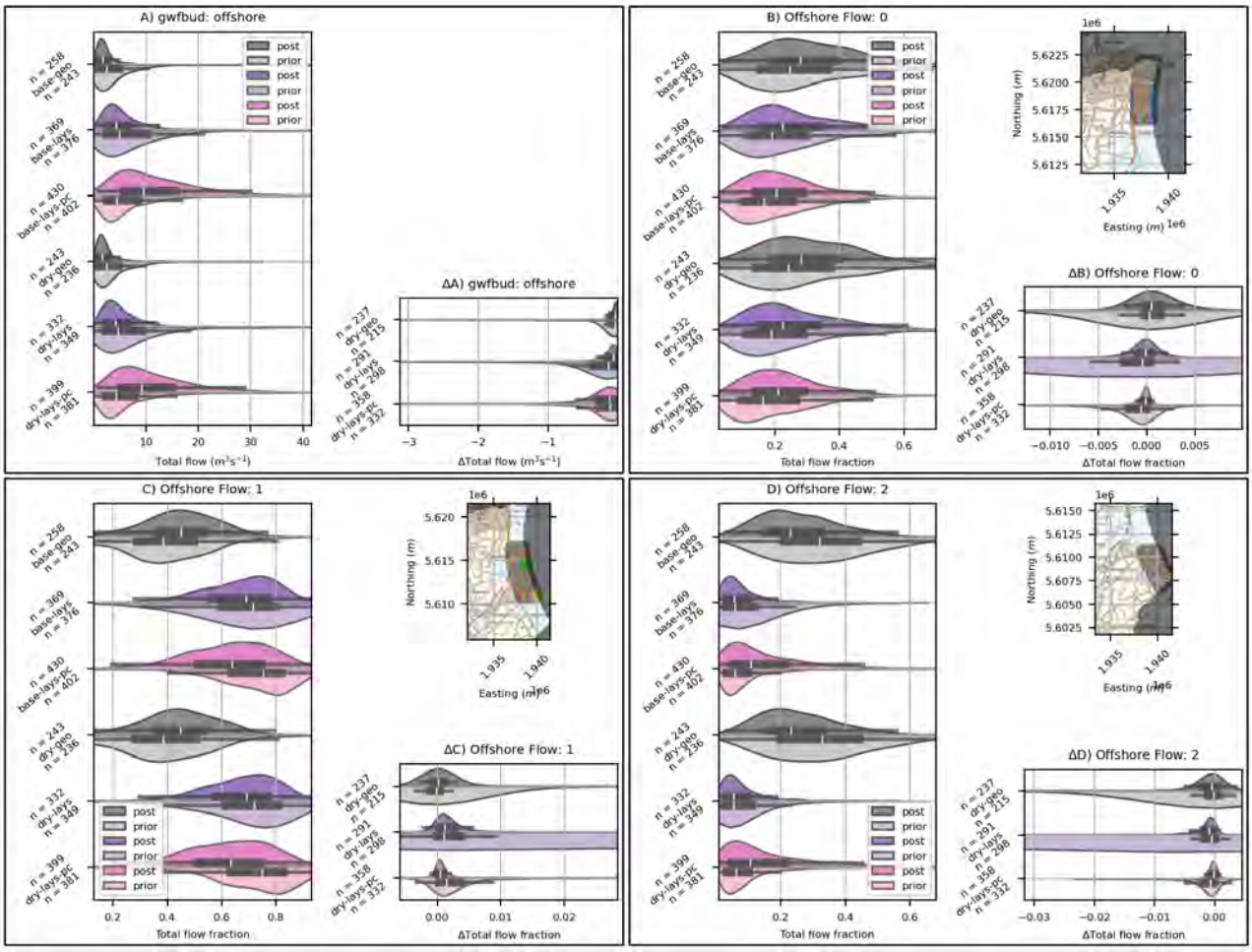

Figure 3.24 Comparison between *base* and *dry* scenarios for the fractional zonal groundwater offshore discharge prediction for the *geo* and *skytem-lays* models. Left-hand plots in each panel show the prediction distribution for the *base* (upper three plots) and *dry* scenarios (lower three plots). Lower right-hand plots show the change predictions, calculated as *dry* – *base* for each realisation. (A) Total discharge and equivalent to Figure 3.25A. (B–D) Zonal components in north, middle and south zones, respectively (as shown on inset maps). Note: x-axes are clipped to the maximum extent of the posterior distributions.

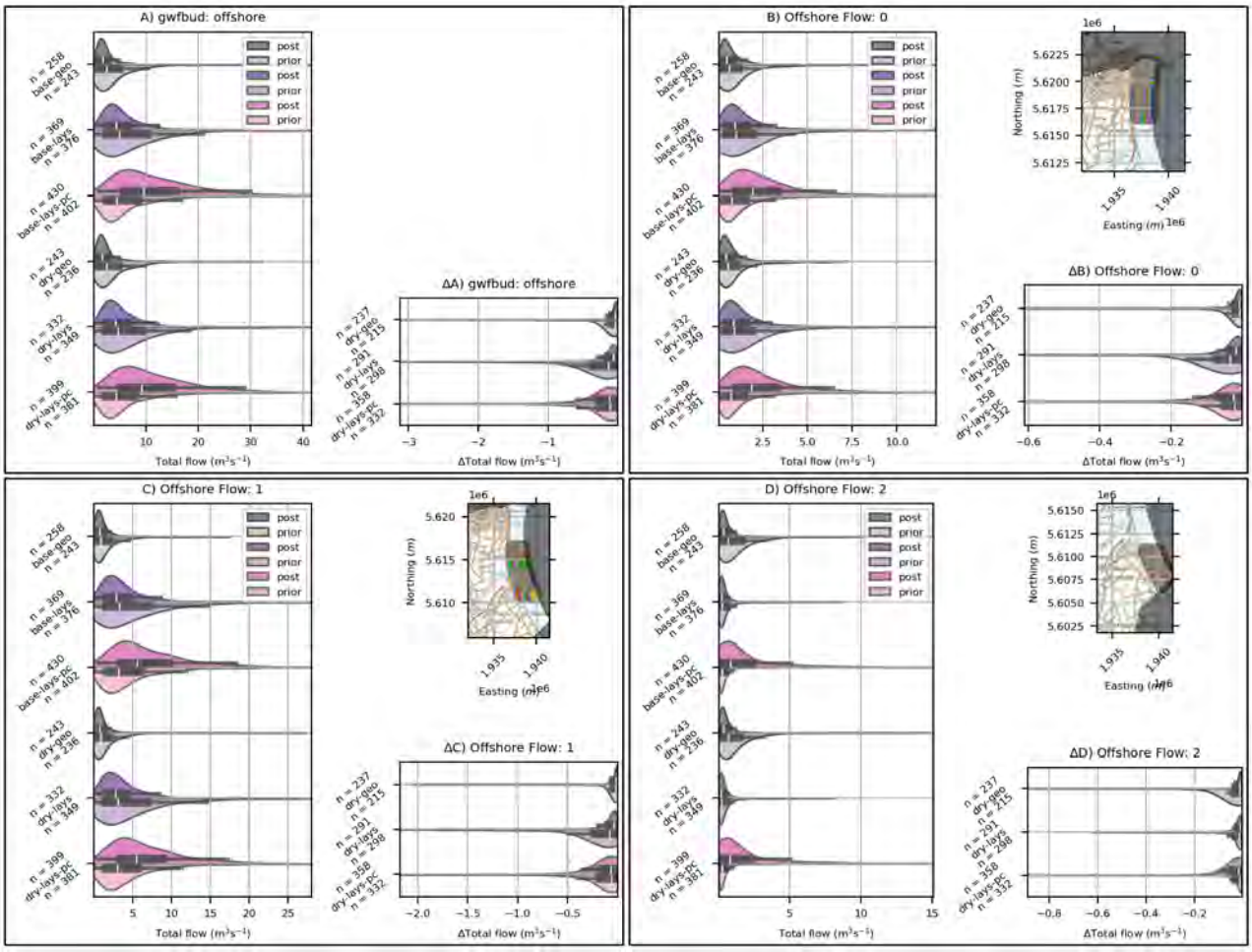

Figure 3.25 Comparison between *base* and *dry* scenarios for the net zonal groundwater offshore discharge prediction, for the *geo* and *skytem-lays* models. Left-hand plots in each panel show the prediction distribution for the *base* (upper three plots) and *dry* scenarios (lower three plots). Lower right-hand plots show the change predictions, calculated as *dry* – *base* for each realisation. (A) Total discharge and equivalent to Figure 3.23A, showing net decrease in flow offshore. (B–D) Zonal components in the north, middle and south zones, respectively (as shown on inset maps). Note: x-axes are clipped to the maximum extent of the posterior distributions.

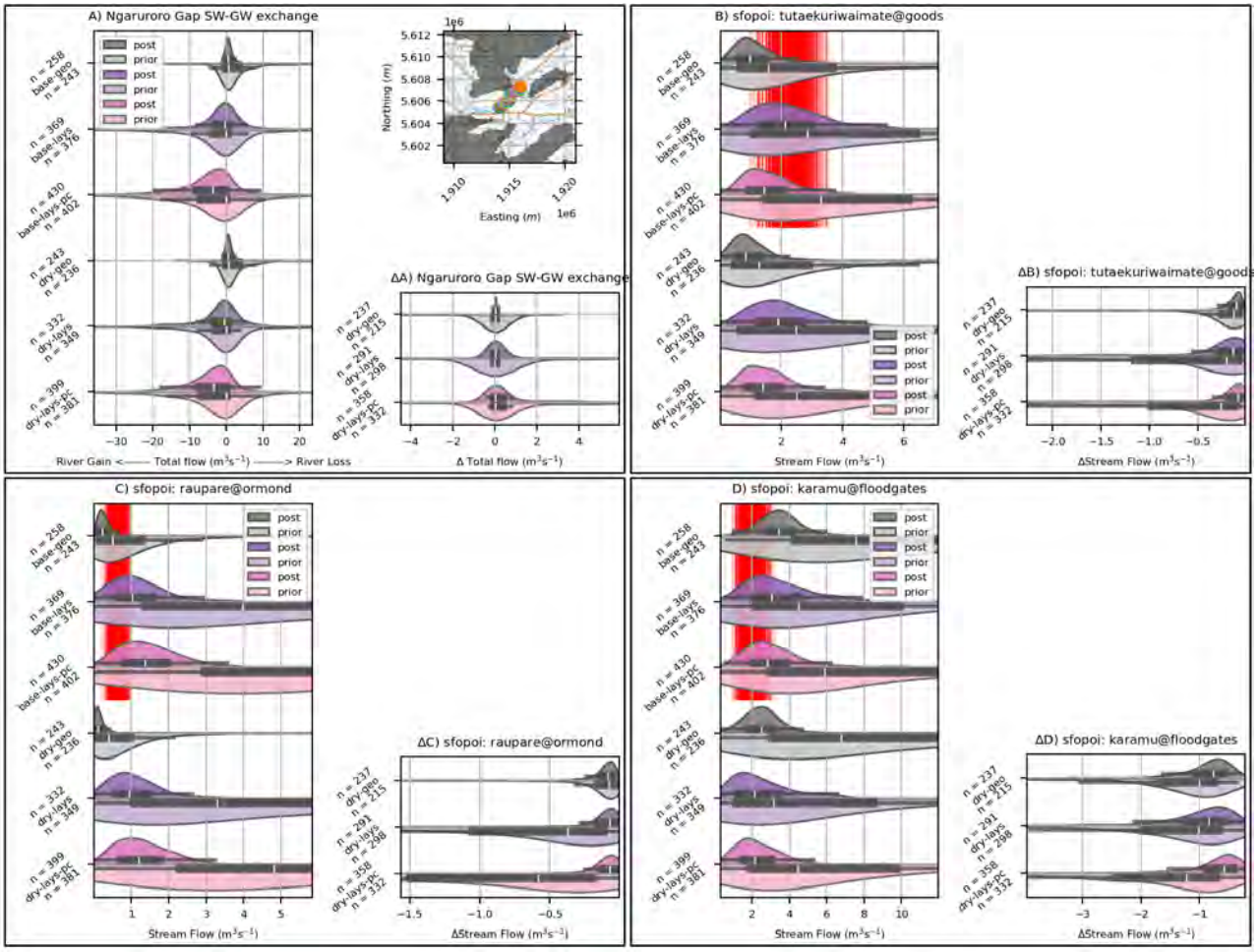

Figure 3.26 Comparison between the *base* and *dry* scenarios for Ngaruroro River groundwater exchange between Maraekakaho and Roys Hill (A) and in-stream flow (B–D) predictions, for the *geo* and *skytem-lays* models. Left-hand plots in each panel show the prediction distribution for the *base* (upper three plots) and *dry* scenarios (lower three plots). Right-hand plots show the change predictions, calculated as *dry* – *base* for each realisation. Positive values in (A) indicate simulated surface-water gain along the river reach (explicit SFR package exchange). Positive values in (A) can mean increased river loss or decreased river gain. Note that, on average in the *geo* model, this stretch of the model was a losing reach, and, in the *skytem-lays* models, became a gaining reach. Red bars in (B–D) represent the realisations of observations plus noise (note that the Ngaruroro River exchange at this location was not a history-matching observation). Note: x-axes are clipped to the maximum extent of the posterior distributions.

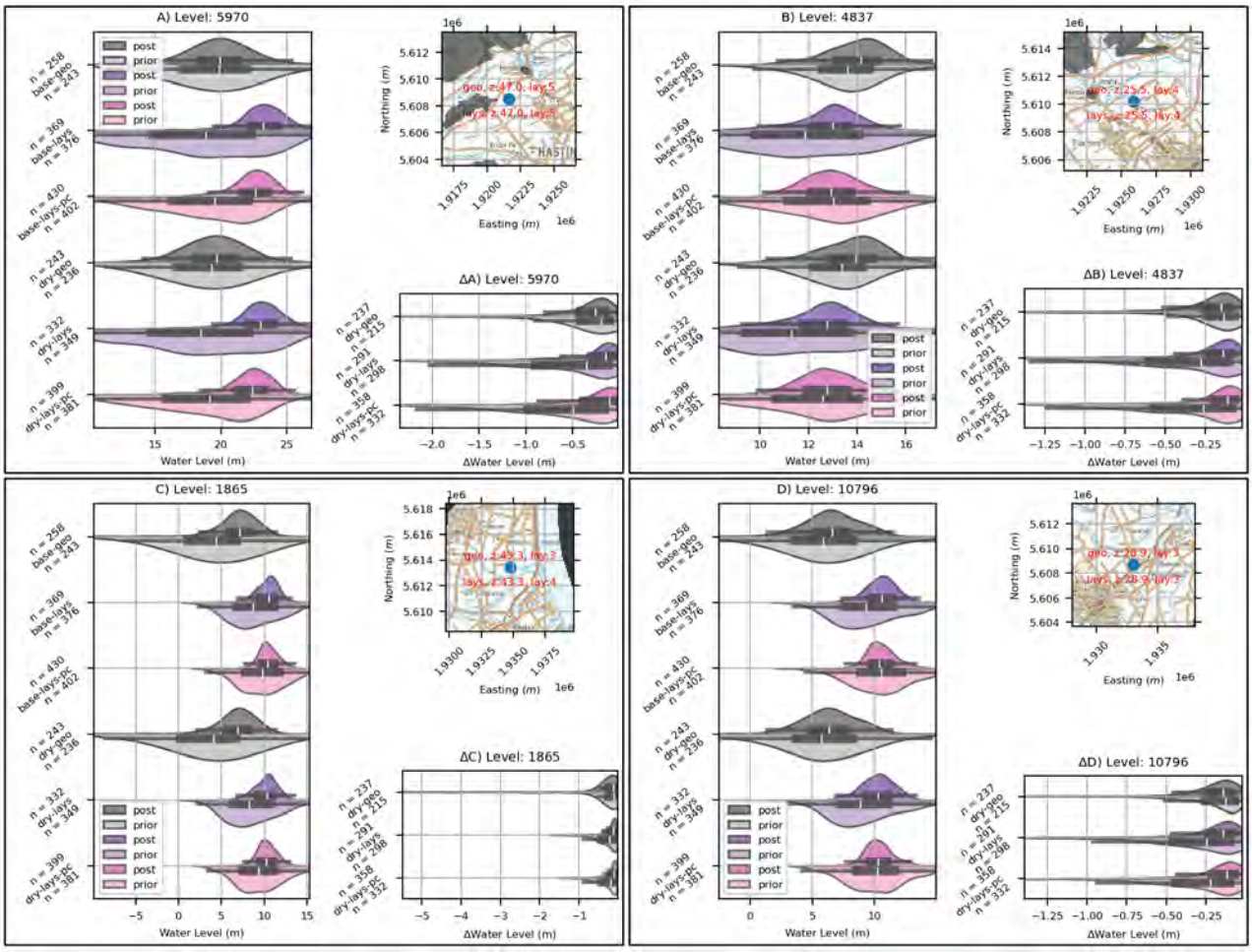

Figure 3.27 Comparison between the *base* and *dry* scenarios for groundwater-level predictions for the *base* scenario for the *geo* and *skytem-lays* models. Left-hand plots in each panel show the prediction distribution for the *base* (upper three plots) and *dry* scenarios (lower three plots). Lower right-hand plots show the change predictions, calculated as *dry* – *base* for each realisation. The red text in the inset maps indicates the model layer for the simulated output – this can differ between the *geo* and *skytem-lays* model versions due to changes in the model structure. Note: x-axes are clipped to the maximum extent of the posterior distributions.

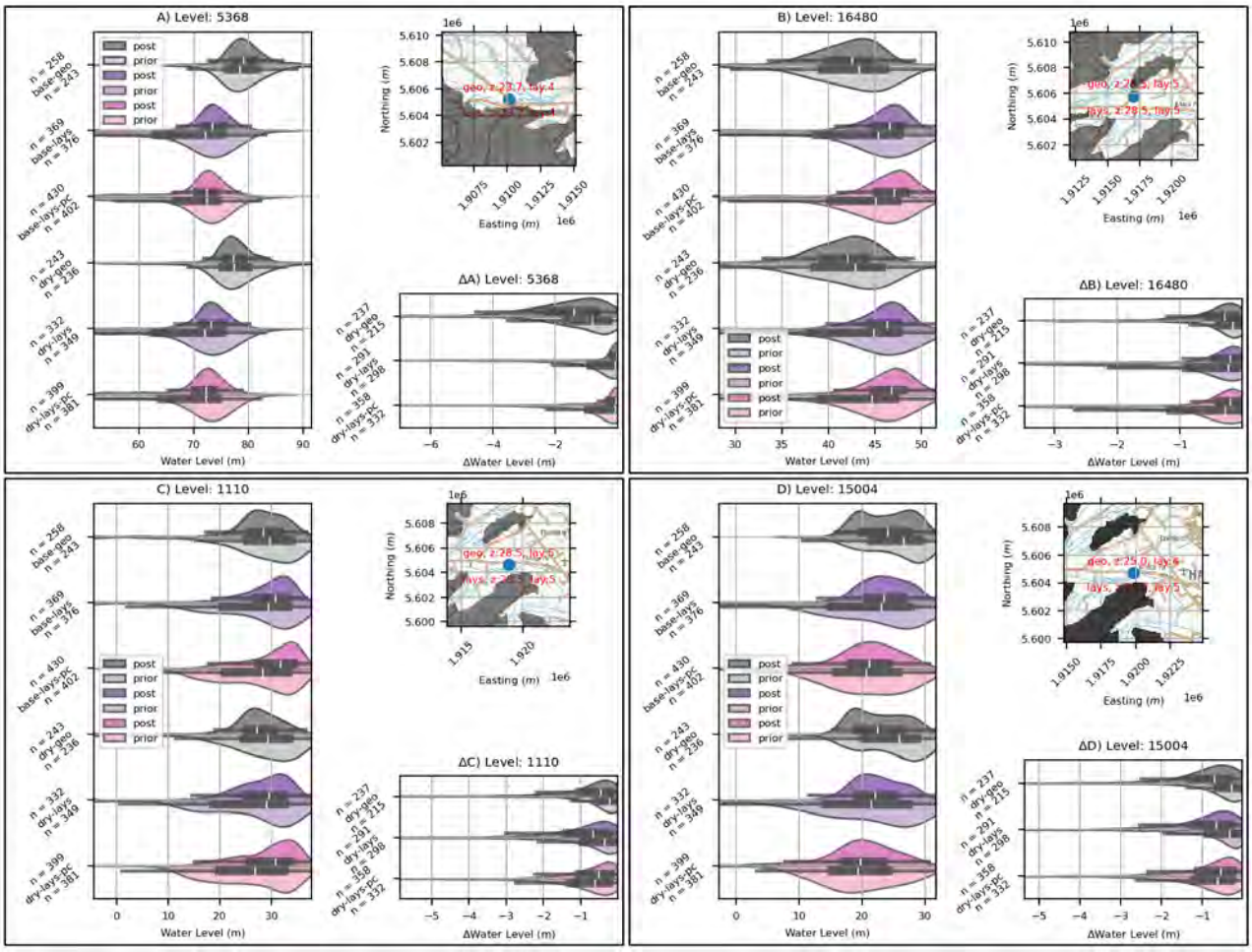

Figure 3.28 Comparison between the *base* and *dry* scenarios for further groundwater-level predictions for the *base* scenario for the *geo* and *skytem-lays* models. Left-hand plots in each panel show the prediction distribution for the *base* (upper three plots) and *dry* scenarios (lower three plots). Lower right-hand plots show the change predictions, calculated as *dry* – *base* for each realisation. The red text in the inset maps indicates the model layer for the simulated output – this can differ between the *geo* and *skytem-lays* model versions due to changes in the model structure. Note: x-axes are clipped to the maximum extent of the posterior distributions.

3.1.5 Preliminary Results when History-Matching to Tritium

For further discussion, the base scenario for the *skytem-lays* model predictions with and without tritium in history-matching, and with and without pre-conditioning, are presented in Figures 3.29–3.39. These include age predictions and porosity pre-conditioning (Hemmings et al., in prep.).

3.1.5.1 Equivalent Flow Model Predictions

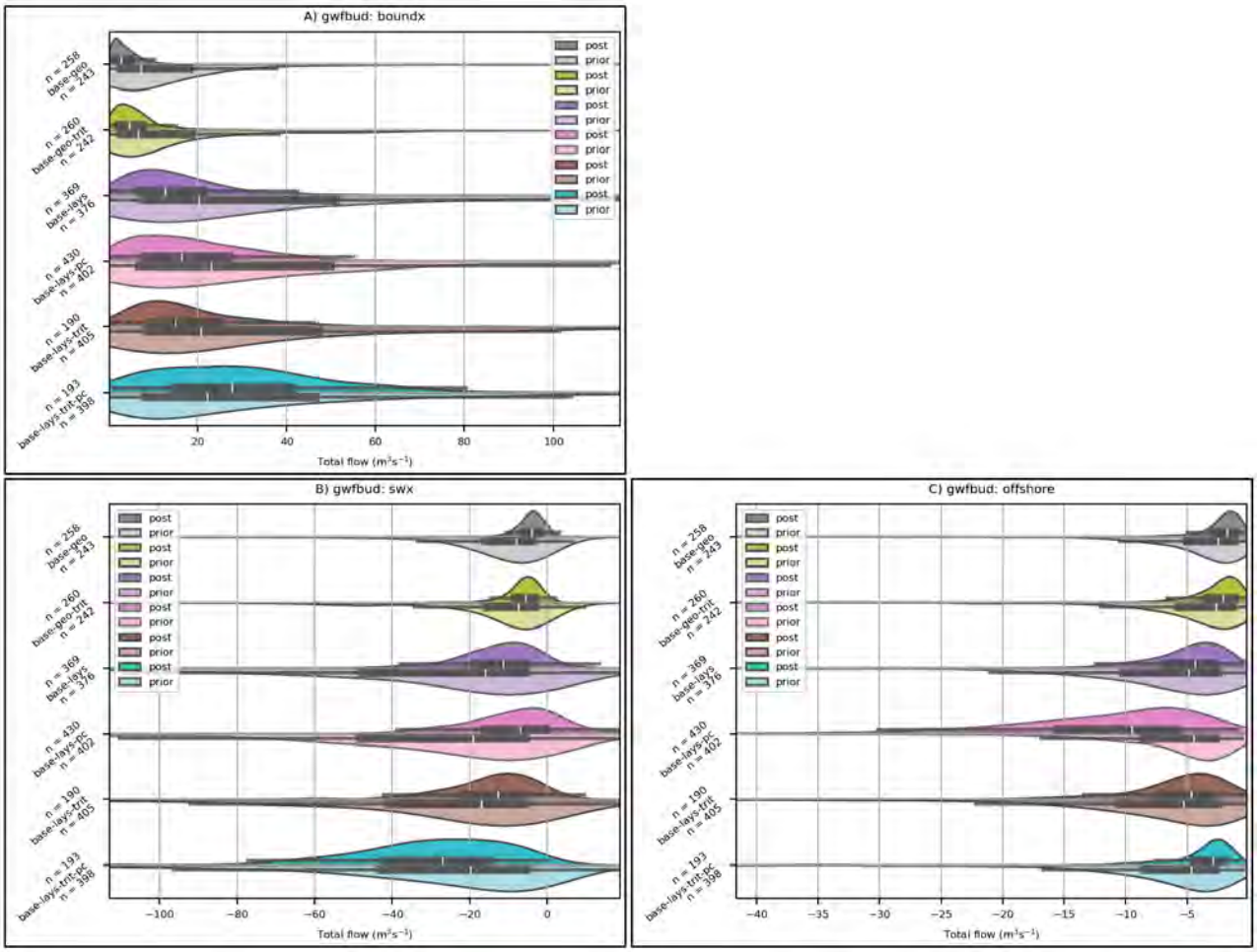

Figure 3.29 Budgetary component *base* scenario prediction distributions for the *geo* and *skytem-lays* models, with and without history-matching to tritium (*-trit*). (A) Net flow across hillslope boundaries (to [positive] or from [negative] simulated domain). (B) Net groundwater–surface-water exchange to groundwater (positive) or surface water (negative). Note that this includes groundwater exchange with the explicit routed stream network (SFR package) and flux to model drains (DRN package). (C) Net offshore groundwater flow ([positive values are net offshore flow). Violin plots represent kernel density estimation of prediction distributions; inner boxplots indicate quartiles with whiskers extending to 1.5 x the interquartile range. Models shown: *geo* (reference model; grey), *geo-trit* (including history matching to tritium; yellow-green), *lays* (layers and parameter fields updated; purple), *lays-pc* (layers and parameter fields updated and pre-conditioning applied; pink), *lays-trit* (layers and parameter fields updated, posterior history matched to tritium; brown), *lays-trit-pc* (layers and parameter fields updated, pre-conditioning applied and tritium included in history-matching; cyan). Note: x-axes are clipped to the maximum extent of the posterior distributions.

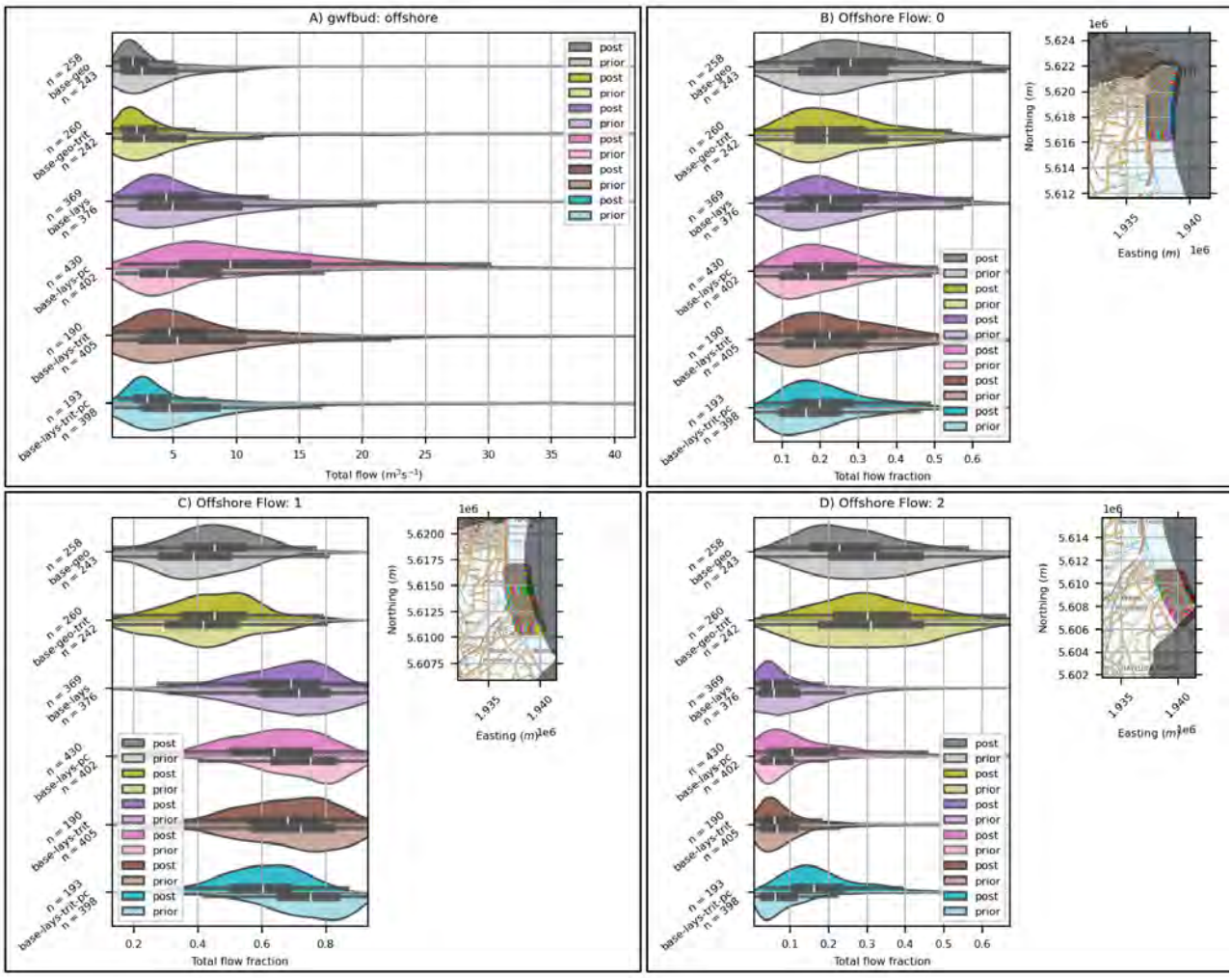

Figure 3.30 Fractional zonal groundwater offshore discharge prediction distributions for the *base* scenario for the *geo* and *skytem-lays* models, with and without tritium in history matching. (A) Total discharge and equivalent to Figure 3.31A. (B–D) Zonal components in the north, middle and south zones, respectively (as shown on inset maps). Note: x-axes are clipped to the maximum extent of the posterior distributions.

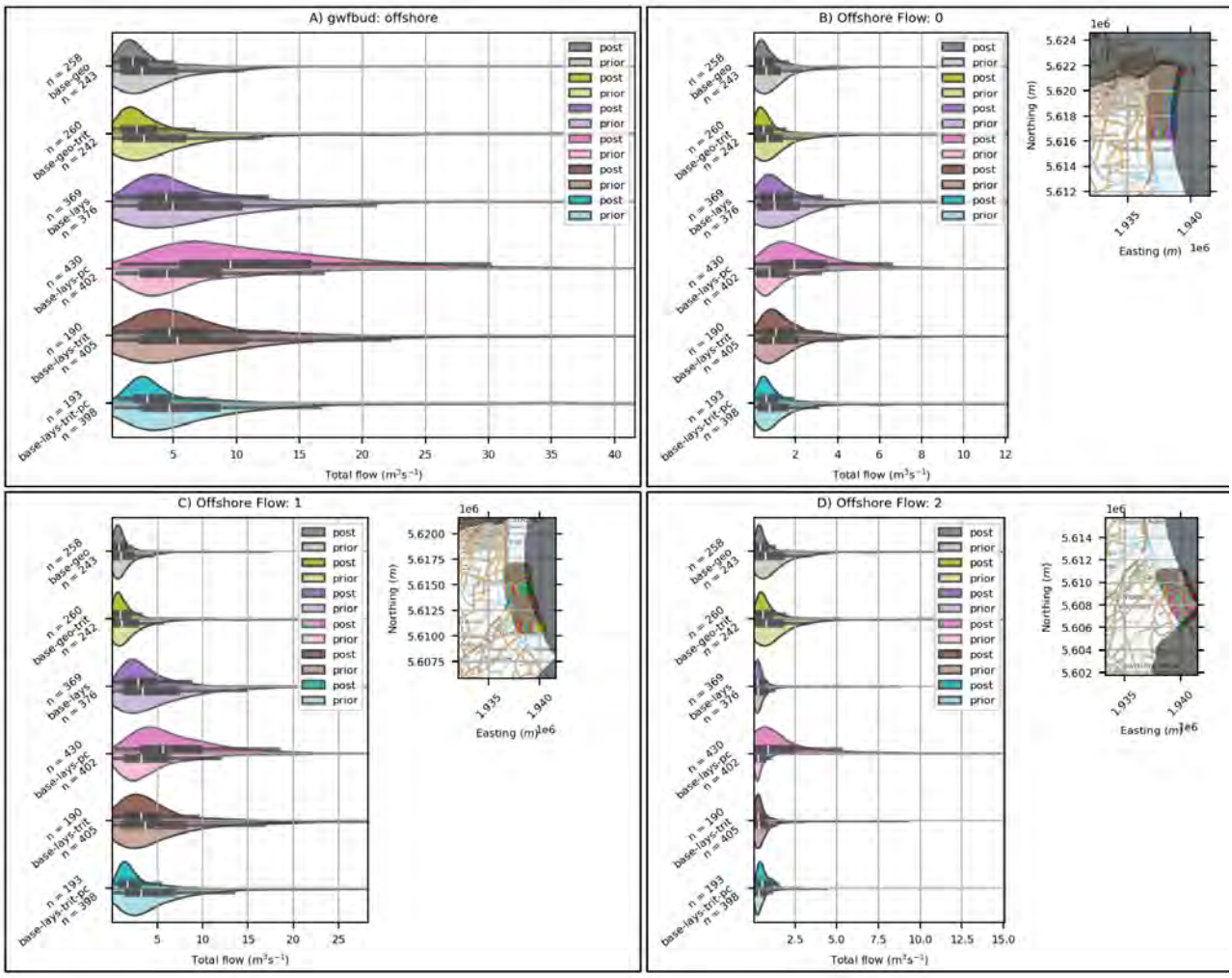

Figure 3.31 Net zonal groundwater offshore discharge prediction distributions for the *base* scenario for the *geo* and *skytem-lays* models, with and without tritium in history-matching. (A) Total discharge. (B–D) Zonal component in the north, middle and south zones, respectively (as shown on inset maps). Note that the polarity of the plots is opposite to Figure 3.29C (positive values indicate offshore flow); as such, (A) is the additive inverse of Figure 3.29C. Note: x-axes are clipped to the maximum extent of the posterior distributions.

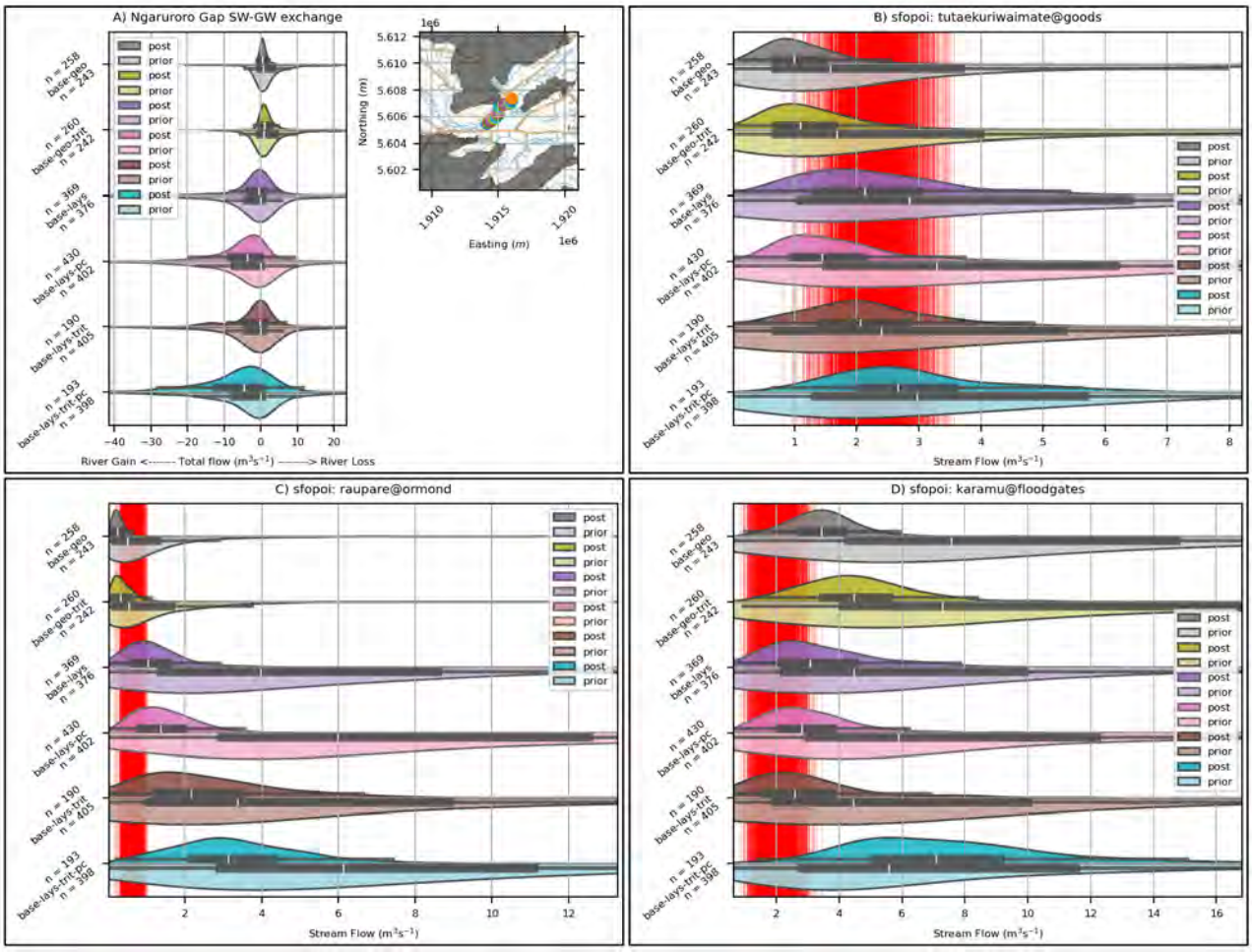

Figure 3.32 Ngaruroro River groundwater exchange between Maraekakaho and Roys Hill (A) and in-stream flow (B–D) *base* scenario prediction distributions for the *base* scenario for the *geo* and *skytem-lays* models, with and without tritium in history-matching. Positive values in (A) indicate simulated surface-water gain along the river reach (explicit SFR package exchange). The red bars in (B–D) represent the realisations of observations plus noise (note that the Ngaruroro River exchange at this location was not a history-matching observation). Note: x-axes are clipped to the maximum extent of the posterior distributions.

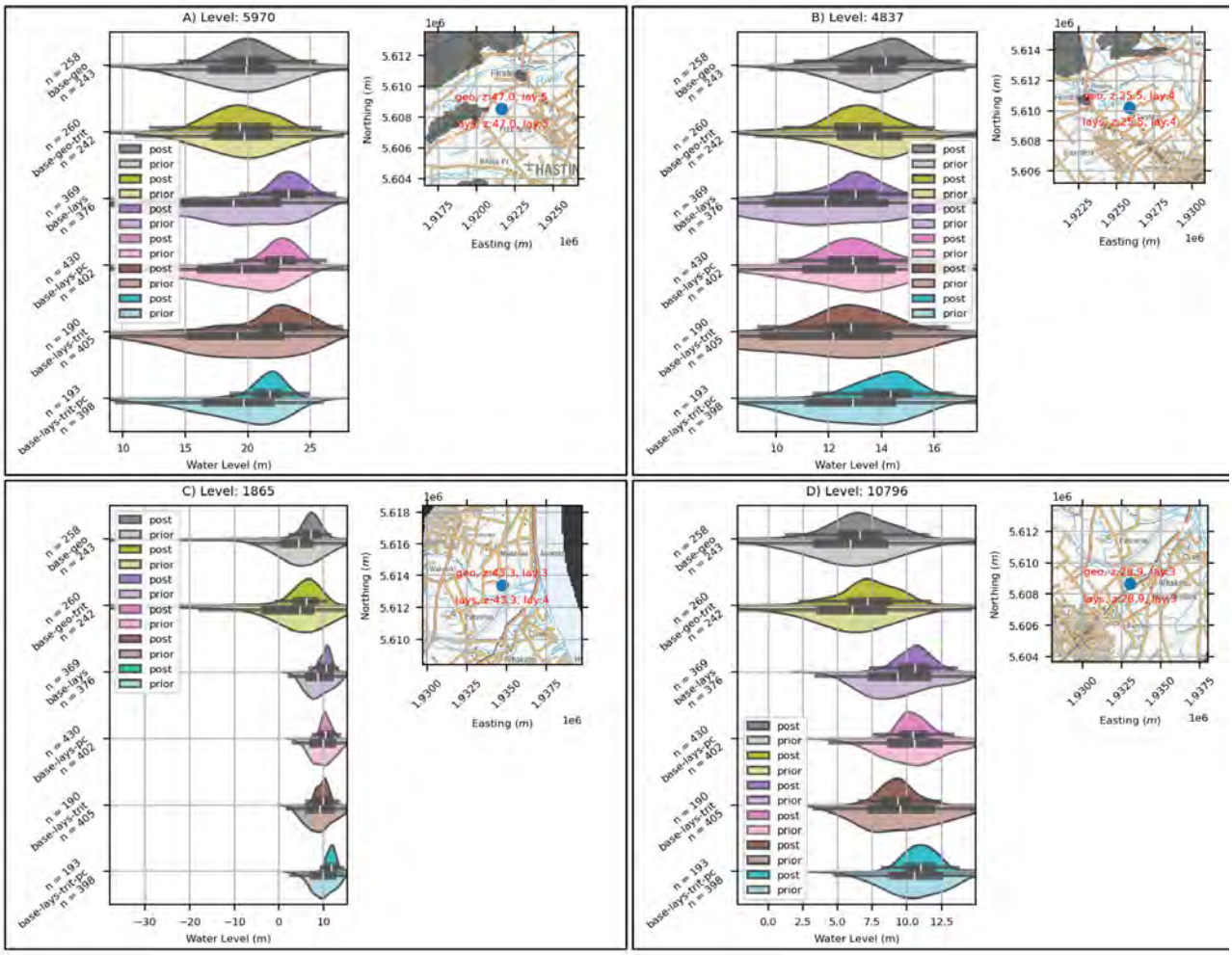

Figure 3.33 Groundwater-level prediction distributions for the *base* scenario for the *geo* and *skytem-lays* models, with and without tritium in history-matching. The red text in the inset maps indicates the model layer for the simulated output – this can differ between the *geo* and *skytem-lays* model versions due to changes in the model structure. Note: x-axes are clipped to the maximum extent of the posterior distributions.

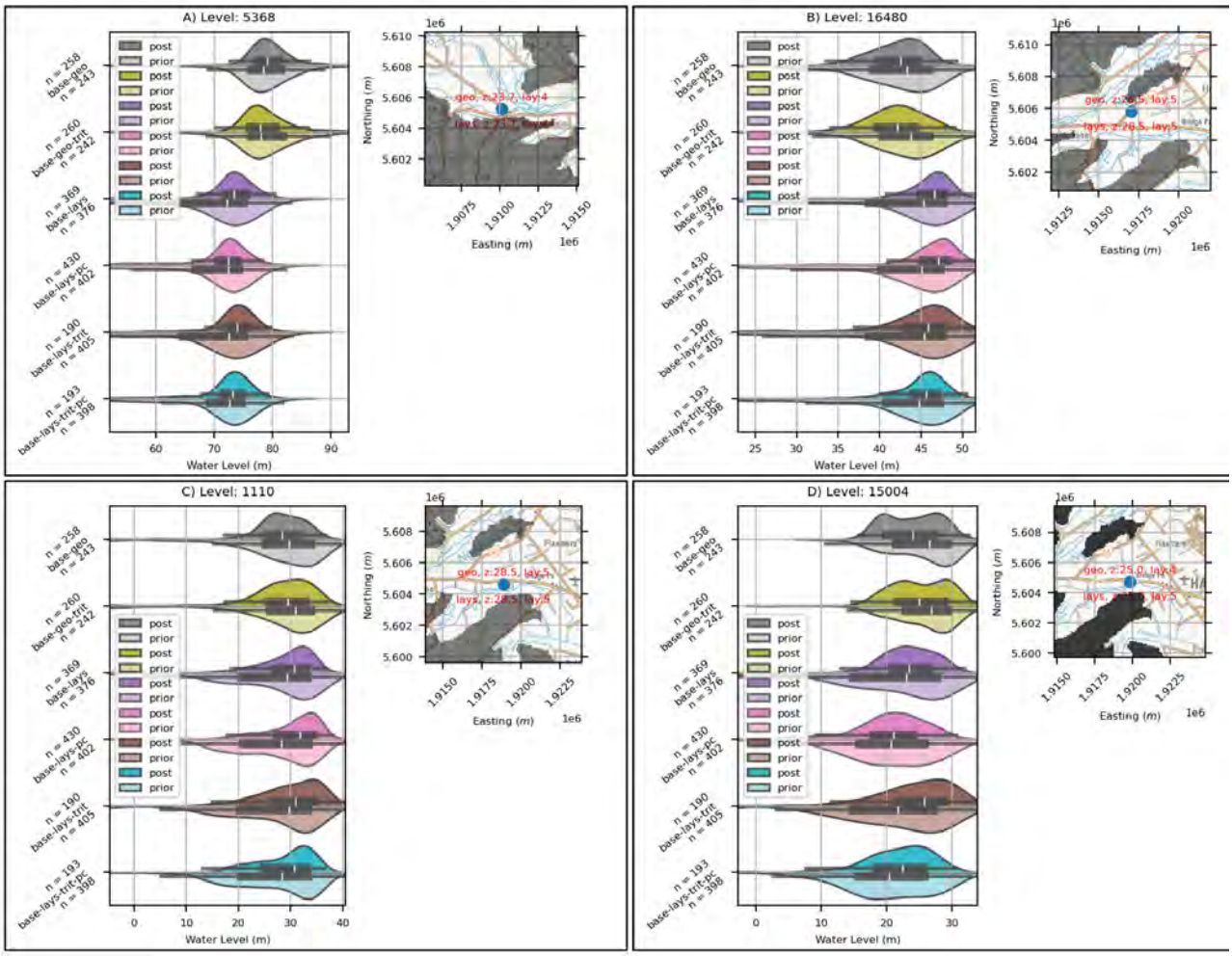

Figure 3.34 Further groundwater-level prediction distributions for the *base* scenario for the *geo* and *skytem-lays* models, with and without tritium in history-matching. The red text in the inset maps indicates the model layer for the simulated output – this can differ between the *geo* and *skytem-lays* model versions due to changes in the model structure. Note: x-axes are clipped to the maximum extent of the posterior distributions.

3.1.5.2 Additional Age Predictions

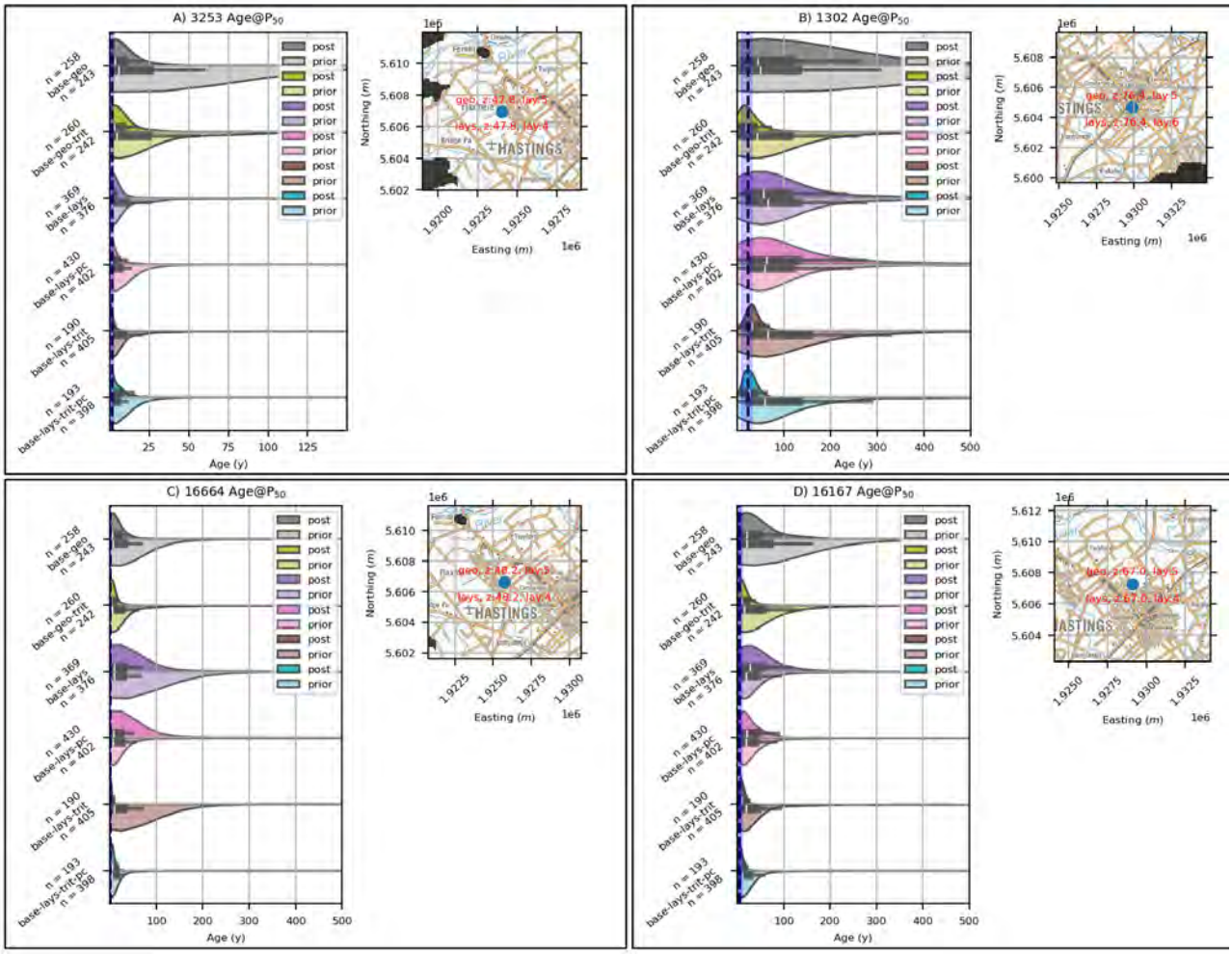

Figure 3.35 Municipal-well-site median age predictions (P_{50}) for the *base* scenario for the *geo* and *skytem-lays* models, with and without tritium in history-matching. The dashed black line is the lumped parameter model estimate of median age and the blue-shaded area is the associated broad age bin (Morgenstern et al. 2018; Morgenstern 2021) (note that there are two estimates for site 16167). The red text in the inset maps indicates the model layer for the simulated output – this can differ between the *geo* and *skytem-lays* model versions due to changes in the model structure. Note: x-axes are clipped to the maximum extent of the posterior distributions.

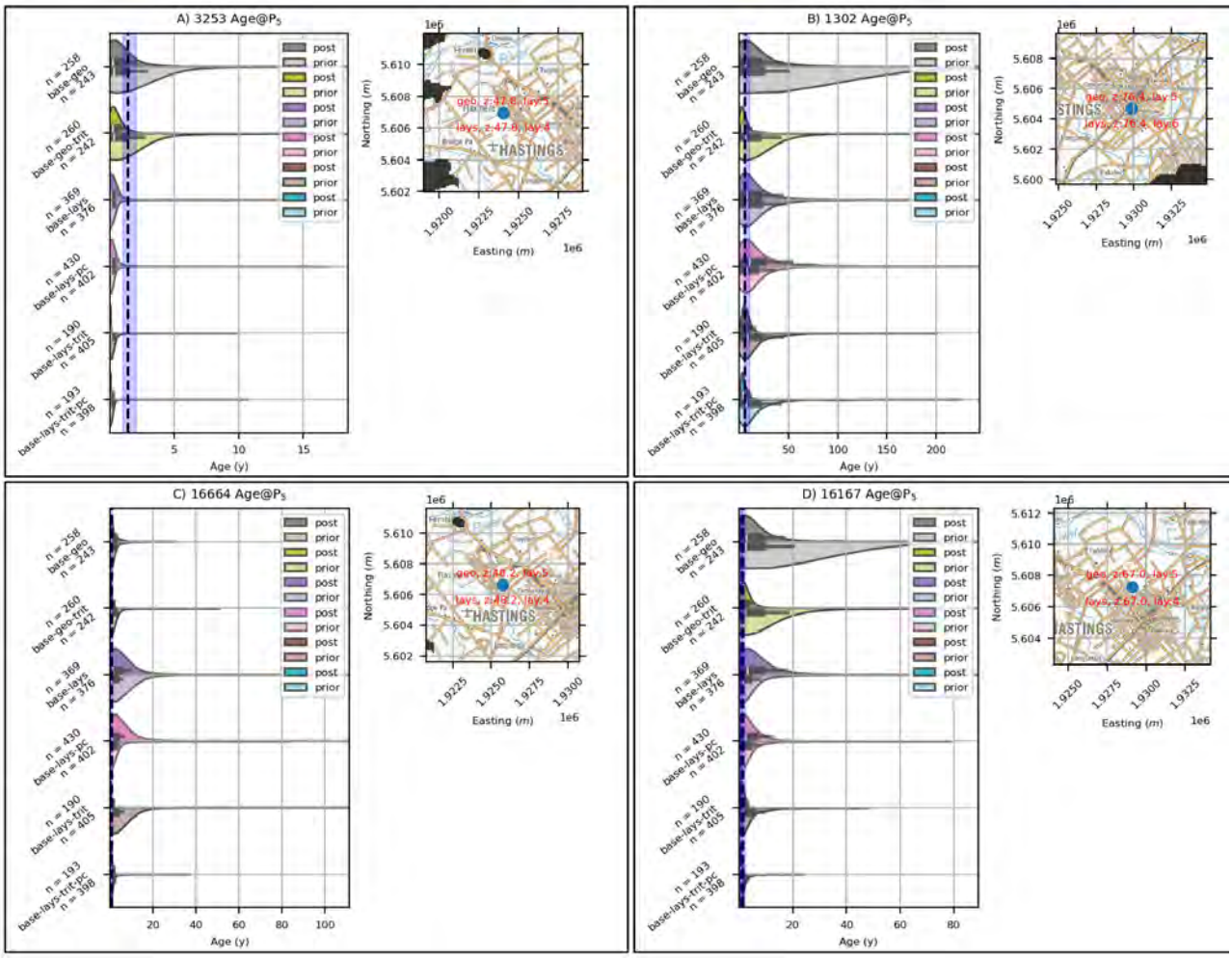

Figure 3.36 Municipal-well-sites fifth age percentile prediction (P_5) for the *base* scenario for the *geo* and *skytem-lays* models, with and without tritium in history-matching. The dashed black line is the lumped parameter model estimate of P_5 and the blue-shaded area is the associated broad age bin (Morgenstern et al. 2018; Morgenstern 2021) (note that there are two estimates for site 16167). The red text in the inset maps indicates the model layer for the simulated output – this can differ between the *geo* and *skytem-lays* model versions due to changes in the model structure. Note: x-axes are clipped to the maximum extent of the posterior distributions.

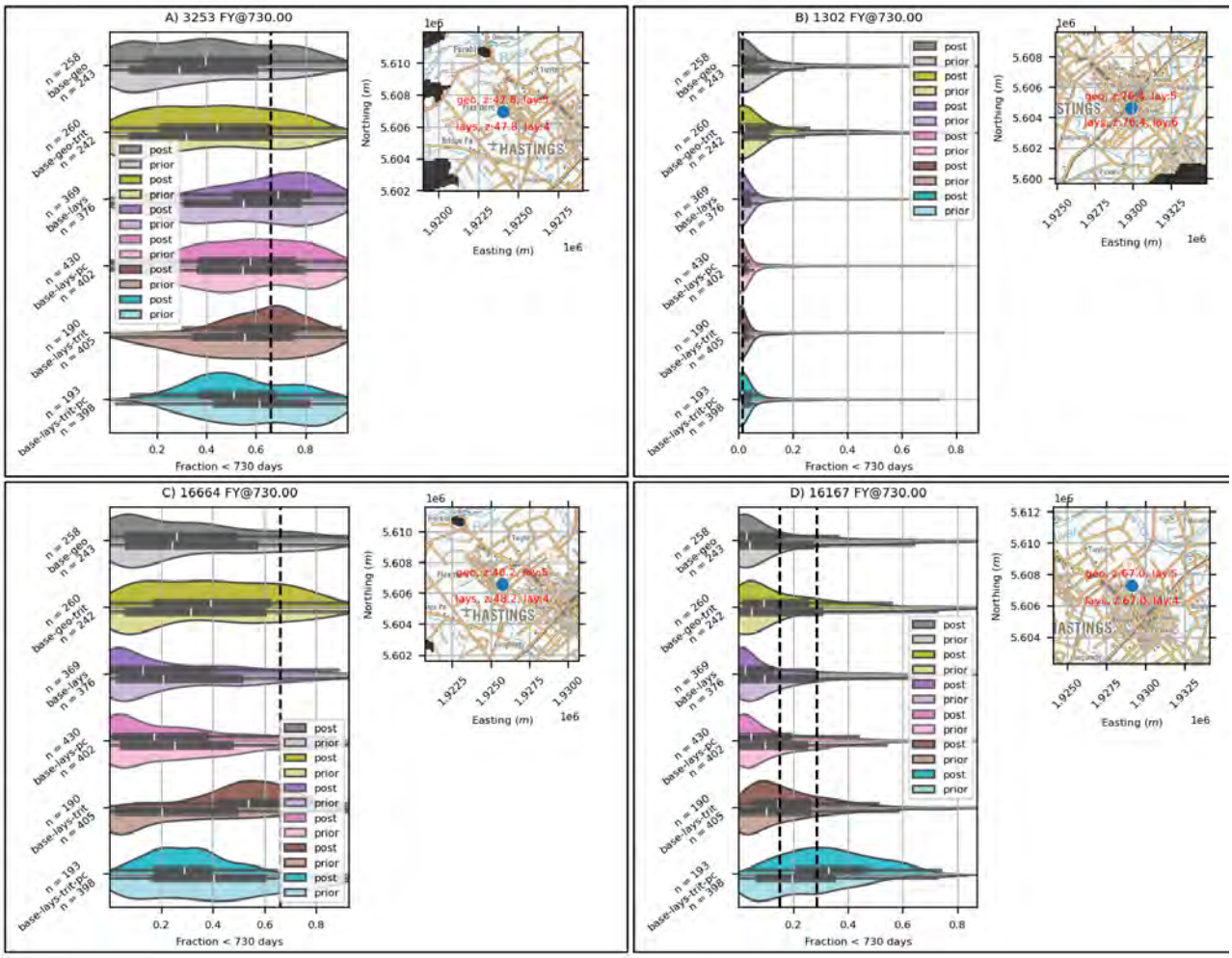

Figure 3.37 Prediction of fraction of water younger than two years at municipal well sites for the *base* scenario for the *geo* and *skytem-lays* models, with and without tritium in history-matching. The dashed black line is the fraction of young water derived from the lumped parameter model estimate (Morgenstern et al. 2018; Morgenstern 2021) (note that there are two estimates for site 16167). The red text in the inset maps indicates the model layer for the simulated output – this can differ between the *geo* and *skytem-lays* model versions due to changes in the model structure. Note: x-axes are clipped to the maximum extent of the posterior distributions.

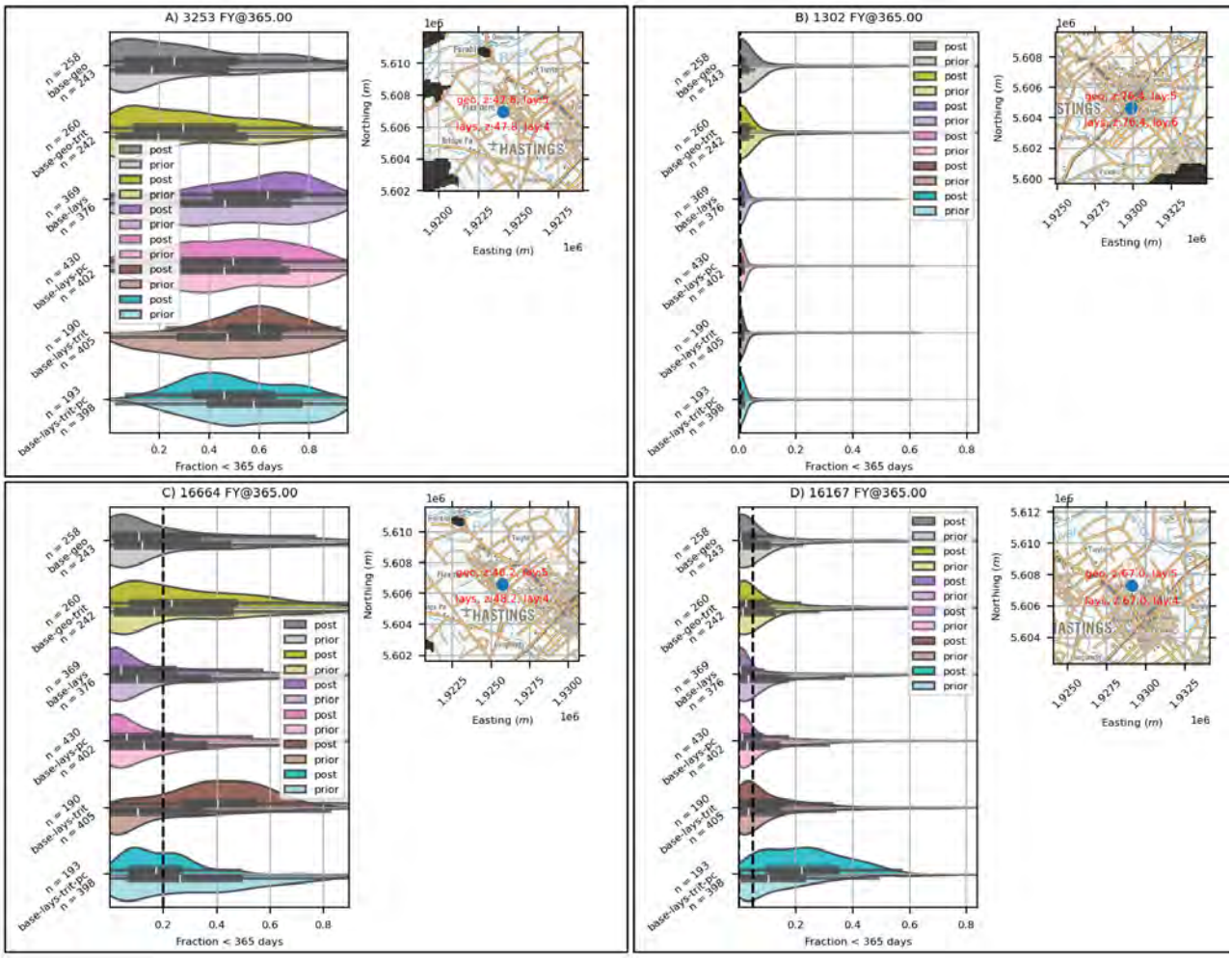

Figure 3.38 Prediction of fraction of water younger than one year at municipal well sites for the *base* scenario for the *geo* and *skytem-lays* models, with and without tritium in history-matching. The dashed black line is the fraction of young water derived from the lumped parameter model estimate (Morgenstern et al. 2018; Morgenstern 2021) (note that there are two estimates for site 16167, and that the estimate for 3253 is zero). The red text in the inset maps indicates the model layer for the simulated output – this can differ between the *geo* and *skytem-lays* model versions due to changes in the model structure. Note: x-axes are clipped to the maximum extent of the posterior distributions.

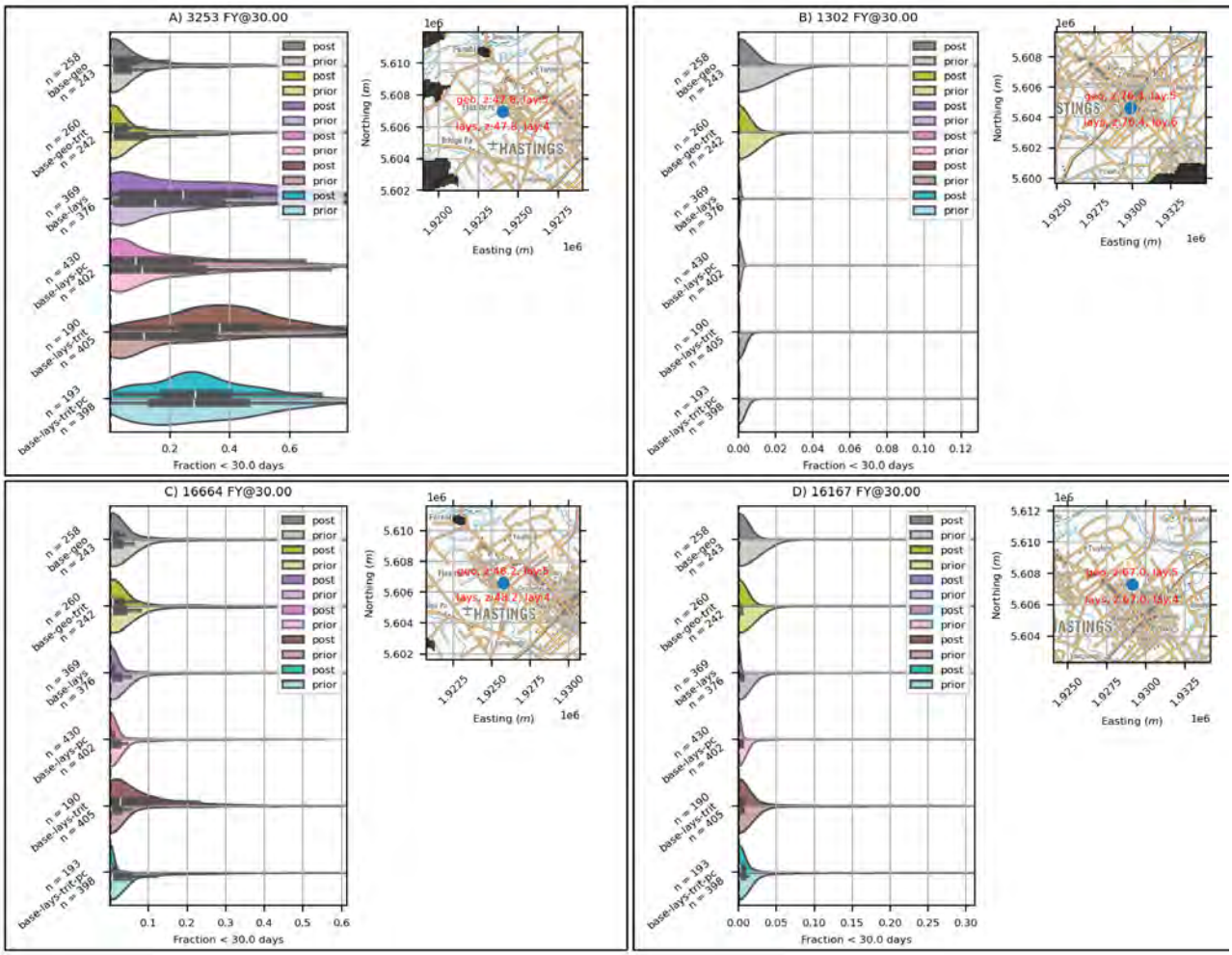

Figure 3.39 Prediction of fraction of water younger than 30 days at municipal well sites for the *base* scenario for the *geo* and *skytem-lays* models, with and without tritium in history-matching. The dashed black line is the fraction of young water derived from the lumped parameter model estimate (Morgenstern et al. 2018; Morgenstern 2021) (note that there are two estimates for site 16167) – these estimates place the young fraction very close to zero for all sites. The red text in the inset maps indicates the model layer for the simulated output – this can differ between the *geo* and *skytem-lays* model versions due to changes in the model structure. Note: x-axes are clipped to the maximum extent of the posterior distributions.

3.2 Data-Worth Assessment

Using the Bridge Pā model, an exploration was undertaken on the relative worth of existing observation data in terms of the extent to which these informed four selected predictions, as discussed below (see also Section 1.3.2 for the list of predictions). The four selected predictions serve as exemplars of predictions for which aquifer structure and parameter knowledge acquired through AEM data are likely to be of importance. If other predictions are of interest, the analysis can be repeated in future work.

Five observation data groups were used, as listed below:

- Historical groundwater-level observations throughout the model domain.
- Stream flow observations in Paritua Stream.
- Stream–groundwater exchange flux data along Paritua Stream.
- Stream–groundwater exchange flux data along Ngaruroro River.
- Historical wetland locations (from soil data maps).
- SkyTEM-informed hydraulic conductivity estimates ('AEM data').

The data-worth analysis explored the relative worth of each data group in two ways; firstly, the extent to which history-matching to a specific data group reduced the *prior* uncertainty of a prediction; and, secondly, the extent to which the *posterior* uncertainty would increase if the same data group was removed from the history-matching dataset. Assessing the two approaches together is informative. Where the results are similar, this indicates that there is insufficient prediction-relevant information across the history-matching dataset. If results differ, this indicates redundancy in the history-matching dataset, caused by correlation in the prediction-relevant information found in data groups.

Prediction 1: Groundwater–Stream-Exchange Fluxes in Paritua Stream along the Losing Reach during a Dry Year (SP8)

History-matching to all available data was estimated to reduce the uncertainty of this prediction of groundwater–stream exchange along the losing reach in Paritua Stream by more than 99.5%, that is, the posterior uncertainty is 0.05% of the prior uncertainty.

The data-worth analysis showed that a history-matching dataset comprising either only AEM data or groundwater–stream exchange flux data would reduce the prior uncertainty of this prediction by approximately 30% (Figure 3.40). A history-matching dataset comprising groundwater levels or Paritua Stream flow data would reduce the prior uncertainty by 25% and 7%, respectively. The remaining data groups made no significant difference to the calculated prior uncertainty.

In contrast, assuming that all existing history-matching data was available, then removing the Paritua Stream – groundwater flux data group would effectively double the posterior uncertainty. The removal of other data groups from the history-matching dataset had no significant impact on the posterior uncertainty, indicating that there is significant correlation in the prediction-relevant information found in the remaining data groups.

Prediction 2: Groundwater Level at Well 15005 during a Dry Year (SP8)

History-matching to all available data was again estimated to reduce the uncertainty of predicted groundwater level in Well 15005 by more than 97.5% of the prior uncertainty.

The data-worth analysis showed that history-matching to groundwater-level data would reduce the prior uncertainty by 47%. Both AEM data or Ngaruroro River groundwater–surface-water-exchange fluxes in the minor and major recharge zones reduced the prior uncertainty of this prediction by approximately 20% (Figure 3.41). Other data would not inform this prediction to any significant extent.

In contrast, removal of the groundwater-level data group from the full history-matching dataset doubled the posterior uncertainty, indicating the unique prediction-relevant information in this data group. The removal of all other data groups produced negligible changes in the posterior uncertainty, indicating that any relevant information in these data groups was highly correlated with existing data.

Prediction 3: Paritua Stream Flow at Bridge Pā during a Dry Year (SP8)

History-matching to all available data was estimated to reduce the prior uncertainty of the prediction of Paritua Stream flow at Bridge Pā during the border dyke irrigation period to approximately 95%.

Data-worth analysis showed that a history-matching dataset comprising either AEM data, groundwater-level data, Paritua streamflow data or Paritua groundwater–surface-water-exchange flux data would each reduce the prior uncertainty of the prediction from 22 to 27%, respectively (Figure 3.42). Other data groups would not inform this prediction to any significant extent.

Removal of the Paritua Stream flow data from an otherwise full history-matching dataset would almost double the posterior uncertainty, indicating the unique prediction-salient information in this dataset. Removing Paritua Stream – groundwater-exchange flux data would increase the posterior uncertainty by approximately 8%. Removing the AEM data and groundwater-level data would increase the posterior uncertainty by approximately 4%. This indicates that only Paritua Stream flow data has unique prediction-relevant information, while additional information is somewhat correlated in the other data groups.

Prediction 4: Surface-Water–Groundwater Flux Aquifer in the Major Recharge Area between Roys Hill and Fernhill during a Dry Year (SP8)

History-matching to all available data was estimated to reduce the prior uncertainty of the prediction of the flux of water from Ngaruroro River into the aquifer in the area between Roys Hill and Fernhill during a dry stress period by 95%. Recall that Ngaruroro River is represented as a GHB boundary (see Section 2.2.2), with an assumed head elevation and estimated (uncertain) conductance.

The analysis shows that a history-matching dataset comprising groundwater–surface-water flux in the major recharge zone provides the greatest reduction in the prior uncertainty of this prediction by 38% (Figure 3.43). If groundwater levels or AEM data are acquired, each dataset would reduce the uncertainty of the prediction by 27% and 23%, respectively. The Paritua Stream – groundwater-exchange flux data would reduce the uncertainty by 6%. Other data could reduce this uncertainty by less than 4%.

Removal of the groundwater–surface-water flux information for the major recharge zone from an otherwise full history-matching dataset would increase the posterior uncertainty by approximately 32%. Removing groundwater-level data would increase the posterior uncertainty by 30%. Removing AEM data from the dataset would increase the uncertainty by 31%. This indicates that there is unique prediction-relevant information in each of these datasets.

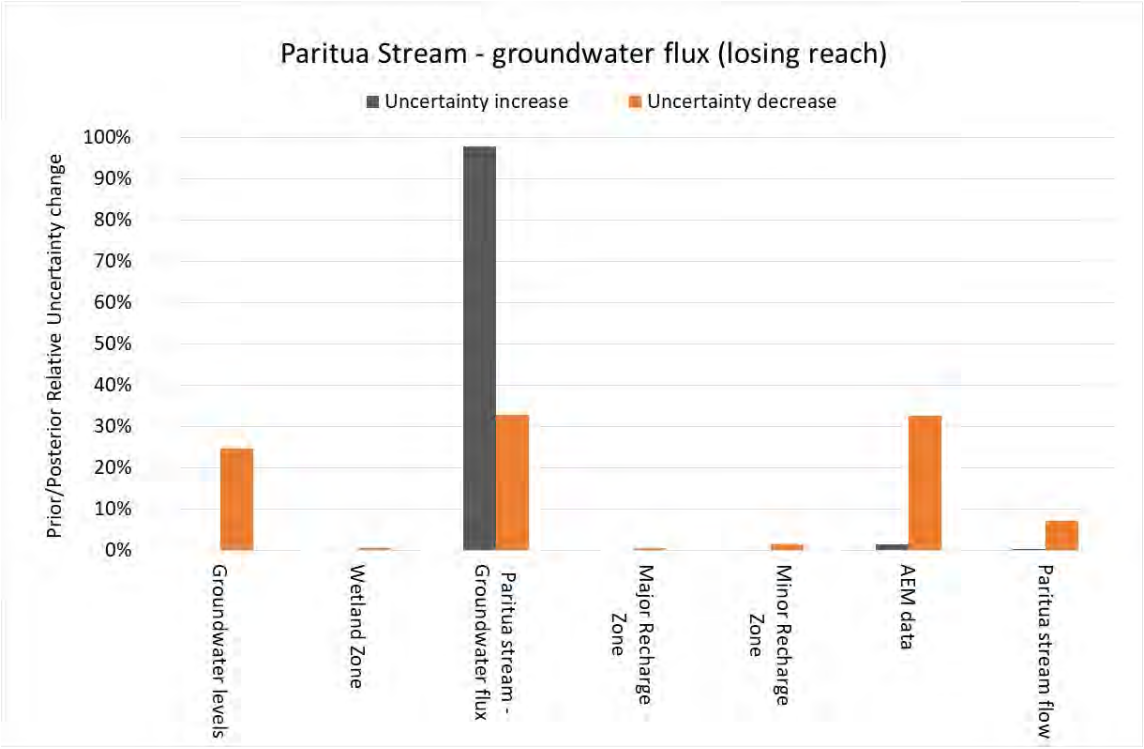

Figure 3.40 Paritua Stream losing reach prediction data-worth results, where the relative worth of different datasets is described in the context of a particular prediction, for example, the Paritua Stream losses along the defined losing reach. The figure depicts the reduction in uncertainty due to adding a dataset when no other data are available (orange) and the increase in uncertainty due to removing data but retaining all other datasets (grey). The y-axis describes the relative change in the prior uncertainty (orange) or posterior uncertainty (grey).

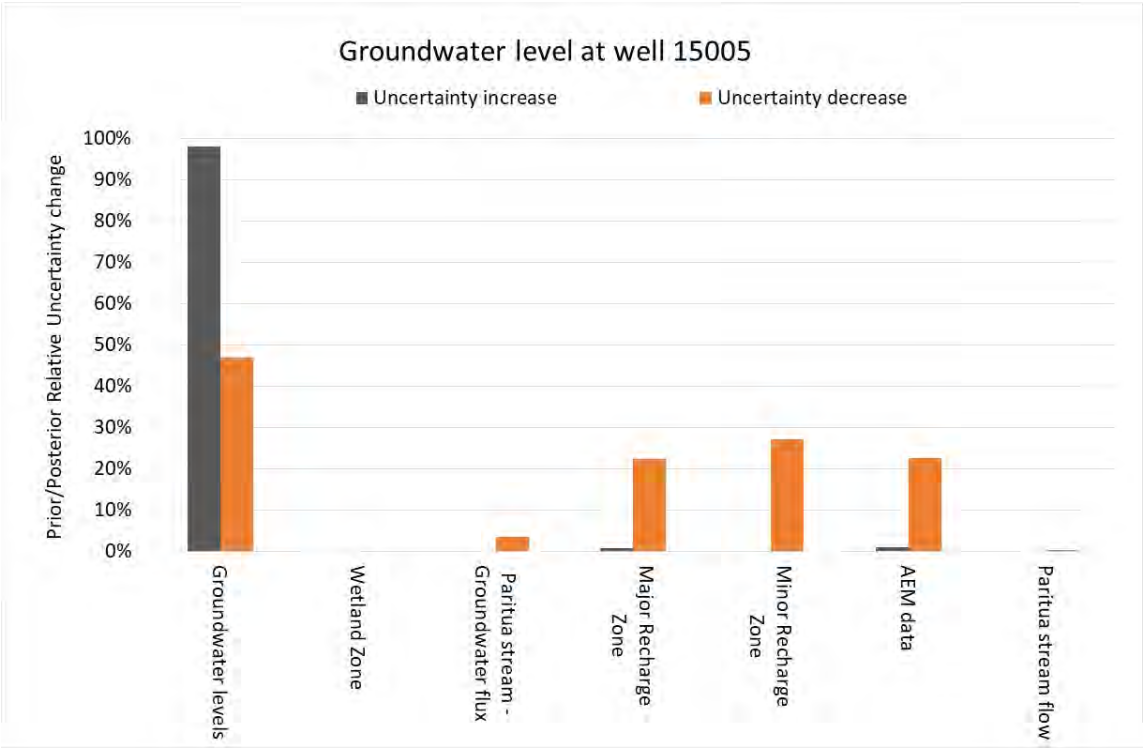

Figure 3.41 Groundwater level at well 15005 prediction data-worth, where the relative worth of different datasets is described in the context of a particular prediction, for example, the groundwater levels at well 15005. The figure depicts the reduction in prior uncertainty due to adding a dataset when no other data are available (orange) and the increase in posterior uncertainty due to removing data but retaining all other data sets (grey). The y-axis describes the relative change in the prior uncertainty (orange) or posterior uncertainty (grey).

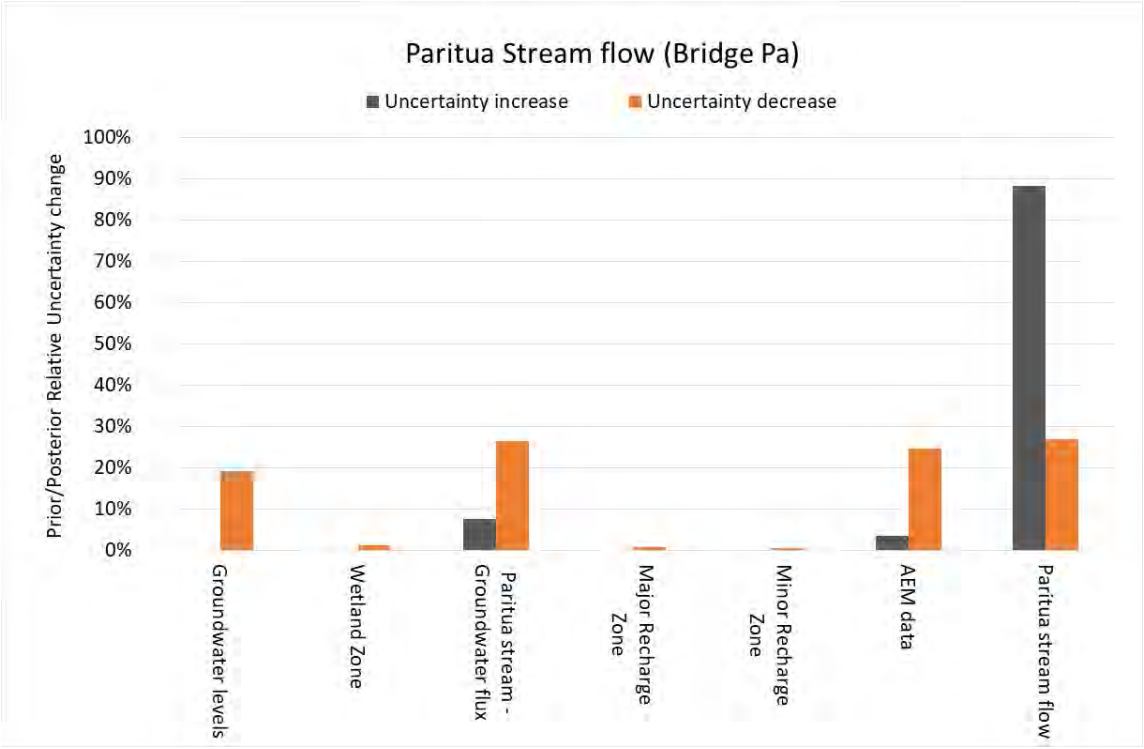

Figure 3.42 Stream flow at Bridge Pā prediction data-worth, where the relative worth of different datasets is described in the context of a particular prediction, for example, the Paritua Stream flow at Bride Pā. The figure depicts the reduction in prior uncertainty due to adding a dataset when no other data are available (orange) and the increase in posterior uncertainty due to removing data but retaining all other datasets (grey). The y-axis describes the relative change in the prior uncertainty (orange) or posterior uncertainty (grey).

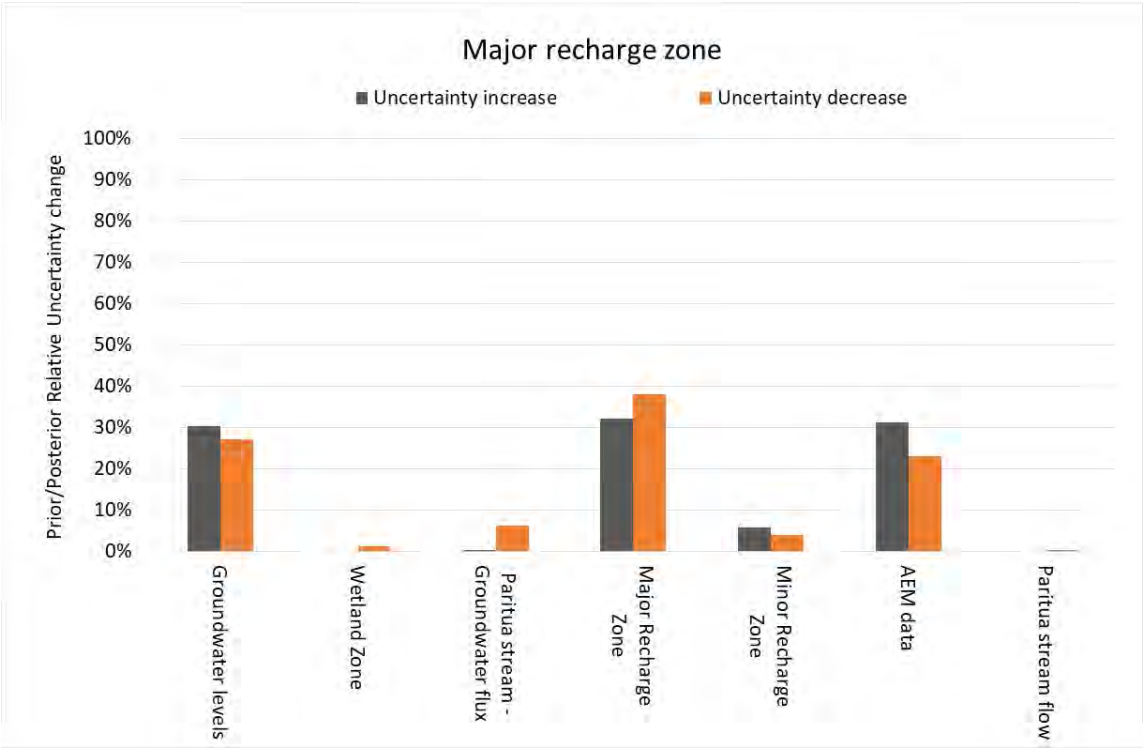

Figure 3.43 Groundwater–surface-water exchange in the minor recharge zone prediction data-worth, where the relative worth of different datasets is described in the context of a particular prediction, for example, the flow along the major recharge zone between Roys Hill and Fernhill. The figure depicts the reduction in prior uncertainty due to adding a dataset when no other data are available (orange) and the increase in posterior uncertainty due to removing data but retaining all other data sets (grey). The y-axis describes the relative change in the prior uncertainty (orange) or posterior uncertainty (grey).

4.0 Discussion

Within the Heretaunga Plains, AEM data provided detail on hydrogeological structure, aquifer system boundaries and the distribution of hydraulic properties with a broader three-dimensional coverage than can currently be achieved through other methods. In this study, we have explored both approaches for incorporating these data within numerical groundwater models and the value of this information (derived from SkyTEM data processing and modelling) in numerical groundwater model predictions.

SkyTEM datasets are used to create resistivity models. Resistivity models can be developed from a large number of different types of instruments (both airborne and ground-based) with different depth penetrations, resolutions and sensitivities. The workflow presented in this report has been specifically targeted at AEM that collect datasets over large areas. While the workflow and results presented may be relevant to resistivity models developed from systems other than SkyTEM, only SkyTEM data has been utilised within this assessment.

The type of geology, lithology and freshness/salinity of the groundwater impacts the relationship of the resistivity model(s) to hydraulic conductivity. The area investigated is a primarily fresh groundwater resource hosted within unconsolidated sediments where hydraulic conductivity is strongly controlled by the degree of clay versus gravel content. See Rawlinson (2023) for further discussion on the linear relationship between hydraulic conductivity and resistivity found within the Heretaunga Plains.

Herein, a number of prediction types and methods were explored to assess the value of AEM data within a numerical groundwater modelling context. The AEM data was used to inform numerical model parameter values, aquifer structure and the uncertainty of these properties. The value of the AEM data was explored, somewhat quantitatively, in terms of changes to regional model predictions (with the Heretaunga GW model). The scripts that execute these developments and experiments have been provided as digital datasets to HBRC. The value of the AEM data was also formally explored, more quantitatively, using a data-worth analysis in the context of more local predictions simulated using a local model (Bridge Pā GW model).

The magnitude of the impact of the AEM-informed model changes on specific model predictions varies for different prediction types and locations within the aquifer system. Many regional model predictions (and uncertainty distributions) were significantly modified after the inclusion of AEM data in both the model, parameterisation and construction. However, depending on how the prior parameter distribution was defined, the predictive uncertainty was not necessarily reduced. This, and the fact that AEM-informed parameters show much more variation and span than originally reflected in the original model parameter uncertainty definitions, provides an indication that the previous definition of prior parameter uncertainty may under-represent the true uncertainty in individual parameter values (particularly model domain boundary conditions).

The AEM data appears to strongly inform the spatial apportionment of offshore groundwater flow. The inclusion of AEM data in the regional model also raises conceptual questions about the relative contributions of hillslope inflows to the regional groundwater budget, with downstream implications for other budgetary components. The results indicate that there would be significant value in exploring the collection of additional data that might provide improved definition of the hillslope contribution volumes to the Heretaunga Plains groundwater system.

Inclusion of the AEM data in the local Bridge Pā GW model was shown to provide a universal data worth of a similar magnitude to the most informative data across all predictions. Where existing data is available, the relative worth of AEM data fluctuates depending on whether or not other, more prediction-relevant, information is available in the history-matching dataset.

These results, their implications, workflow considerations and future work are explored in the following sections.

4.1 Airborne Electromagnetic (AEM) and Regional Model Experiments

4.1.1 Updated Model

The regional model experiments explore two representations of the AEM data in the groundwater model. The first, *skytem-k*, uses AEM-derived information to inform groundwater model hydraulic conductivity and other boundary-condition properties (e.g. streambed hydraulic conductivity, drain conductance, offshore and hillslope boundary conductance), within the existing *geo* model structure. The second, *skytem-lays*, incorporates AEM-informed hydrogeological unit definitions to update the groundwater model layer structure (while maintaining the grid discretisation: 100 x 100 m cells and nine layers) and updates properties in this new structure. Both AEM-informed models result in significantly altered base-realisation properties relative to the *geo* model version. Generally, the AEM-informed properties are more spatially varied and span a greater value range. Higher hydraulic conductivity at depth and generally increased model thickness in the *skytem-lays* model version results in higher overall transmissivity beneath the central plains. Overall, greater detail in property, boundary condition and, for *skytem-lays,* model-layer definition was afforded by the inclusion of AEM data compared to the *geo* model.

The base model parameter updates mean that there are higher instances of base parameters at the limits of what may have previously been expressed as the likely range of model parameter values. For example, the AEM-informed high hydraulic conductivity in a region that was previously defined as moderate or even low hydraulic conductivity may be close to, or even exceed, that expressed by the prior uncertainty in the *geo* model. As such, this may be evidence that the *geo* model uncertainty was understated. An ill-defined prior can prevent appropriate assimilation of history-matching data and propagate to predictive bias and poor representation of prediction uncertainty (in both a prior and posterior sense). Consideration of this should be given when evaluating the results herein.

4.1.2 Pre-Conditioning

As indicated above, the definition of prior parameter uncertainty is important for both history-matching and robust predictions. To promote consistency in the different regional model experiments in this study, prior uncertainty on parameters (expressed as multipliers) was the same for the *geo* and *skytem* models. However, in an effort to extract some further information from the AEM data and subsequent processing workflow, we explored a way of updating, or conditioning, the prior parameter uncertainty. The approach used was to honour the categorised *clusters_dataset* (Rawlinson 2023), which indicates locations with a high probability of high-conductivity gravels and locations with a high probability of low-conductivity clay-bound sediments.

The pre-conditioning had minimal effect on the hydraulic conductivity ensemble means. This is due to base parameter values for the *skytem* models, around which the realisations of prior uncertainty were drawn, and the cluster definitions for prior conditioning being sourced from the same underlying data (interpreted AEM resistivity). However, the prior conditioning does result in a significant change in ensemble standard deviations. Generally, for both models, standard deviations were decreased through pre-conditioning; in some areas, this decrease is over an order of magnitude. However, there are areas, particularly in deeper layers beneath the Napier region, where standard deviations increased through prior conditioning. This is an area with few conditioning datapoints due to a lack of SkyTEM data coverage; therefore, the pre-conditioning may be causing a variance increase in an effort to satisfy the secondary (layer-mean) conditioning targets. This increase is somewhat unexpected and may be a reflection of the development of non-gaussian parameter distributions or unintended consequence of the inequality targets used in the pre-conditioning.

4.1.3 Matching Data

The fits to history-matching observations vary with the different model versions. Generally, the relative history-matching performance of the different model versions was mixed. In some areas, water-level fits were improved in the AEM-informed *skytem* model versions, while, in others, the model updates with the AEM data resulted in poorer reproductions of observations. Generally, greater uncertainty in simulated outputs is maintained in the *skytem* model version posterior distributions than in the *geo* model posterior.

As well as informing hydraulic conductivity, AEM data was also used to modify the definition of base model streambed hydraulic conductivity and drain conductance. This appears to have had an impact on fitting stream-related observations. Overall, AEM-informed *skytem* models better capture the surface-water observations (in-stream flow and surface-water–groundwater exchange). However, the posterior simulated outputs that relate to observations are again more uncertain, in almost all instances. This posterior uncertainty is not significantly affected by pre-conditioning.

The generally greater posterior simulated output uncertainty in the AEM-informed models is likely to be a function of the greater prior uncertainty range expressed in the AEM-informed *skytem* model. It also provides potential indication of tension in the observation dataset, as well as strong parameter non-uniqueness, whereby a range of parameter combinations can effectively fit observation data (or at least reduce the objective function value).

Where fits are improved by the *skytem* model versions and their broader definition of prior uncertainty, it may be a further indication that the parameter uncertainty expressed in the *geo* model version was under-estimated.

4.1.4 Airborne Electromagnetic (AEM) Informing Predictions

In general, an aquifer system with greater heterogeneity can be expected to increase the uncertainty of some model predictions, for example, transport model predictions and local-field dependent predictions. Therefore, by enhancing our understanding of sub-surface detail, we can expect our quantification of the uncertainty of predictions to be more realistic, and, where we had previously under-estimated this heterogeneity, we can expect that prediction uncertainty may increase. The analyses depicted in the prediction figures based on these AEM-informed models (in Section 3.4 and the appendices) indicate that this has occurred for many of the predictions explored.

The extent to which the greater structural detail and modified parameter uncertainty definition changes the uncertainty of model predictions was dependent on the predictions. Prior predictive distributions for the AEM-informed models suggest 2–3 times higher (and more uncertain) inflow from the hillslope boundary. This is potentially a consequence of regions where the AEM-informed boundary conductance is elevated, relative to the *geo* model, to values that not only promote higher inflow but are also in a more sensitive region in parameter space.

Increases in AEM-informed boundary inflow are accommodated by increases in both discharge to surface water (surface-water–groundwater exchange) and offshore. In the prior, discharge to surface water takes up most of this extra component of inflow. In the posterior distributions (after history-matching), the increase in hillslope boundary inflow is reduced (although less significantly for the *skytem-lays* models) and the relative portioning to surface water and offshore discharge is evened-out, although significant predictive uncertainty remains.

Interestingly, the broader posterior uncertainty in simulated outputs that relate to history-matching observations for the *skytem* model versions does not necessarily translate to significantly higher posterior prediction uncertainty for all predictions. While the budget term predictions are more uncertain for the AEM-informed models, uncertainty for many other predictions is similar or reduced (e.g. water-level predictions). Many of the water-level predictions do show significant changes in posterior prediction distributions between the *geo* model and AEM-informed *skytem* versions. The most extreme changes in mean and median predictions are concentrated close to the boundary of the domain, often in areas

where prediction uncertainty (ensemble standard deviation) also increases. This is consistent with the changes seen in boundary inflow predictions when informing base model condition parameters with AEM data. However, there are also AEM-informed water-level prediction changes in the interior domain. Across much of the model domain, AEM-informed predictions of water levels are higher than the *geo* model predictions. However, in the Twyford region the AEM-informed water-level predictions are generally lower. These spatial variations in water-level prediction differences between the different models appear to be coincident with the simulated boundary between confined and unconfined aquifer conditions. Here, the AEM-informed models are potentially providing more detail on the location and sharpness of this important hydrogeological transition.

Scenario-change predictions demonstrated minimal impact from incorporating the AEM data in the model workflow. Change-prediction distributions were largely centred on the same value for the different model versions and generally also demonstrated similar predictive uncertainty between models. The reduced insensitivity of change predictions has been observed in many other studies (e.g. Knowling et al. 2019) and highlights that exploring relative change predictions provides some insurance against both model defects and parameter uncertainty. However, we have only explored large-scale prediction scenarios that are influenced by a spatial average of the entire aquifer (homogenous change in stress applied). A heterogeneous stress application may reveal a different result; additionally, where parameter detail (e.g. high-resolution flow paths) is critical for a prediction, change predictions are less able to compensate for model defects.

Predications that are expected to be more sensitive to parameter detail are preliminarily explored in Section 3.1.5, where results are presented for model predictions using the *geo* and *skytem-lays* models with and without tritium data (as per Hemmings et al. [in prep.]). In many, but not all cases, the uncertainty of predictions was reduced when history-matched to tritium data in addition to the original history-matching dataset. Often, but not always, this reduction in uncertainty was greatest for the AEM-informed pre-conditioned case. This analysis also included predictions of groundwater age (median age [P_{50}] and fifth percentile [P_5]), as well as young fraction predictions. While predictions of the fraction of young water remain complex (as detailed in Hemmings et al. [in prep.]), the combined use of AEM data and tritium in the numerical model workflow clearly reduced P_{50} and P_5 prediction uncertainty relative to models that only used one of these data sources (i.e. the *geo* model with tritium or *skytem-lays* without tritium). These results indicate that AEM-informed models enhance the processing of information that is influenced by parameter detail, such as tritium age-tracer data.

4.1.5 Workflow Considerations

The effort of this study focused on exploring the incorporation of AEM-derived hydrogeological information into the numerical groundwater model workflow. AEM data was used to define base model parameter values (which effectively became the mean values of the different prior parameter ensembles), modify model structure and attempt to refine the parameter uncertainty before history-matching.

As briefly discussed above, the evaluation of the AEM data, on its own, may indicate that the parameter uncertainty applied in the *geo* model version was insufficient to appropriately represent the true uncertainty – for example, where AEM-informed hydraulic conductivity estimates approach or eclipse the limits anticipated in the *geo* model. Potentially, on the basis of the parameter variability insights gained from interpreting the AEM data, the *geo* model parameter uncertainty should be amended (increased).

If the *geo* model uncertainty is under-estimated or misrepresented, the prediction uncertainty may not show an apparent improvement for AEM-informed models by way of uncertainty reduction. However, the under-representation of uncertainty can lead to erroneous predictions. Unfortunately, in a real-world setting, such erroneous predictions are difficult to identify, as the 'truth' is rarely known.

Additionally, it could also be considered that the AEM-informed hydraulic-conductivity estimates are less uncertain (at least in some locations) than the estimates provided for the *geo* model, which were based on geological zonation and literature values. The prior conditioning effort attempted to reflect additional information around the (variable) uncertainty of AEM-informed parameter values. However, there would

be considerable value in continuing to explore the definition of uncertainty in AEM-derived property estimates. For this study, we wanted to isolate the AEM information from the *geo* model workflow and maintain consistency in our initial definition of property uncertainty. As such, we have maintained the same prior uncertainty definition for multiplier parameters across the experiments.

The history-matching then undertaken in the experiments was general and limited. The emphasis was placed on maintaining consistency in the workflow between history-matching efforts using the different base models. In an effort to maintain a consistent and conservative representation of uncertainty in the posterior (after history-matching), a conservative noise model was applied to observation targets. As discussed in Hemmings et al. (in prep.), this is designed to accommodate the representativeness of long-term-averaged observations in a single steady-state model stress period. Additionally, the level of fit that was sought in the history-matching was also conservative.

As well as providing a consistent basis for the different history-matching efforts, this relatively limited history-matching may also have helped guard against bias or corruption of predictions through inappropriate fitting of historical data in an imperfect model (Hemmings et al. 2020; White et al. 2020b). Through more bespoke definition of observation weights, a more detailed analysis of individual target observations values and more exhaustive history-matching, it may be possible to improve the level of fit for any of the history-matching efforts and therefore potentially improve the model predictive capacity. This should be an important consideration before direct use of the results presented herein in decision-making processes.

Also discussed in Hemmings et al. (in prep.), the IES process in these experiments was not as efficient at reducing the objective function as is often observed (e.g. White et al. 2018). Hemmings et al. (in prep.) cites that challenges in reducing the objective function potentially result from non-linearities introduced through use of the inequality constraints on water levels as a measure to combat numerical instability. Further investigation into the parameter combinations that results in this instability might allow for mitigation within the forward model and alleviate the need for the inequality constraint. This could allow for more efficient history-matching. Improvements to numerical stability resulting in reduced forward model failure rate would also support a reduced number of prior realisations, again, providing a further efficiency gain.

The success of the prior conditioning efforts was mixed. While the results showed that the IES algorithm can effectively condition parameters to fit expectations about the distribution of specific materials, the formulation of the objective function with only inequality constraints, which cause a natural non-linearity, likely impacted the reliability of the conditioning. Some pre-conditioned parameter distributions became quite non-gaussian, and potentially large-scale parameters were able to be heavily conditioned, without penalty, to represent what could be relatively fine-scale features. The method shows promise, but more work is needed to ensure appropriate objective function formulation.

Work is underway to explore including expression and parametrisation of the non-stationary geostructures in the workflow. Potentially, this is another avenue where valuable information can be derived from AEM data that relates to the relative spatial variation in material properties.

One of the major differences between the *geo* model and the AEM-informed *skytem* models was the simulated increase in boundary inflow. The increase is expected to be related to AEM-informed boundary condition properties (e.g. increased conductance from predicted locations of limestone), allowing greater inflow. The AEM-informed boundary conditions also appear to move base parameter values to a more sensitive part of parameter space. Consequently, the uncertainty around the predicted hillslope inflow contribution to the groundwater budgets is also increased. This uncertainty is not well constrained by the current history-matching dataset. The collection or inclusion of data to help reduce this uncertainty could potentially provide significant improvements to the models predictive capacity.

4.2 Data Worth in Locally Focused Model

The data-worth analysis explored the worth of data using a one-at-a-time approach, thereby isolating the prediction-relevant information in AEM data where we assume either that: (i) there is no existing data and AEM data is added in or (ii) there is 'all' existing data and each dataset is removed one at a time.

The data-worth analysis confirms what we already know – that, if there is no data, then the best to gather is that of the same type as the prediction. However, in the context of exploring a range of predictions, the analysis indicated that AEM-derived hydraulic-conductivity data would improve the reliability of all four predictions explored (Section 1.3.2) to a level commensurate with the most informative data in each prediction context – no other single dataset was able to achieve this. This indicates the general utility of AEM data in providing information that enhances the reliability of many prediction types to a significant degree in any context where very little data exists. Contrast this with other data that is generally most relevant to a specific prediction.

Isolating the relative worth of AEM data as part of existing hydrogeological-monitoring data (e.g. groundwater levels, stream flows, etc.) varies depending on the prediction-data context. We note that the regional modelling work indicates that often the maximal value of AEM data may be achieved in groundwater systems with existing hydrological and hydrogeological datasets.

While not easy to quantify with data-worth methods, AEM data also brought changes in the system conceptualisation and the resulting design of the local Bridge Pā model. The AEM data shows a large vertical drop-off in the model basement along the Awanui Fault delineation. This new basement elevation, coupled with an initial AEM-informed parameter distribution, provided a much improved starting point for history-matching.

4.3 General Future Work

The updated boundary-condition properties raise questions of significant unknowns in the budgetary contribution of hillslope boundary inflow. As shown in this study, uncertainty around boundary inflows propagates to uncertainty in surface-water–groundwater exchange and offshore flow, neither of which is well constrained by the current system observations. Estimation of the expected boundary flow contribution to the groundwater budget (at any spatial scale) would be beneficial for model history-matching and predictions. This may be possible from the analysis of existing data, such as chemical end-member analysis or stable-isotope analysis. While assimilation of chemical data from point samples in time and space presents challenges of non-uniqueness, similar to those presented for tritium in Hemmings et al. (in prep.) and Knowling et al. (2019), pre-processing this sort of data to give broad-scale budgetary estimates might provide sufficient and effective information to help constrain influential parameters.

Although the results presented herein indicate that there is significant value in the AEM data for improving groundwater models, the level of detail for property definition that is provided by the AEM data may not be maximally leveraged by the nature of the groundwater model predictions explored here. The budgetary component predictions are naturally complex aggregations of whole-system behaviour. Stream flow and exchange predictions are also integrations of sub-regional conditions, i.e. along a collection of stream reaches and upstream and downstream hydrogeological conditions. Even though water-level observations are point-specific, these are only minimally sensitive to small-scale property features; water levels tend to be locally smooth and therefore are sensitive to the hydrogeological properties variations across a broad area. Even greater value in the AEM data might be elicited for predictions that are more sensitive to the local-scale features that the data resolves, such as groundwater age.

This report presented a preliminary exploration of combining AEM data with tritium data, which should be expanded on. Improved utilisation of the finer-scale property definition provided by the AEM data and associated better extraction of information contained within the tritium data may also be facilitated

by supporting less stationarity in the geostructures that define the spatial relationships between parameters (e.g. defining spatially varying anisotropy). Including adjustable and conditionable spatially varying geostructure definition parameters as uncertainty super-parameters may support the definition and evolution (through history-matching) of fine-scale flow features that data and predictions might be sensitive to.

The use of non-stationary geostructures in model parameterisation may also present an additional opportunity to incorporate information from AEM. The broad coverage of the AEM data potentially contains unique information on the variability in the relationships between parameters (or co-variance). This could be used to condition geostructure super-parameters (i.e. spatially varying range and anisotropy) in a joint inversion or a similar pre-conditioning exercise to the one presented here. However, whether using joint inversion or pre-conditioning, the results presented here indicate that additional consideration is required when formulating the objective function using the AEM-derived data. Additionally, as noted previously, the same prior uncertainty definition was maintained for multiplier parameters across the experiments in this study. However, more formal uncertainty bounds could be derived from the SkyTEM data.

5.0 Summary of Conclusions

Some of the changes introduced through incorporating AEM data in numerical groundwater models are explicitly quantifiable, while others are more qualitative. Some of the changes are subtle, while others appear more pronounced.

AEM data was used to update numerical groundwater flow models in the Heretaunga Plains as follows:

- Re-definition of model hydrogeological properties with values, detail and coverage that was previously unavailable (initial values and their uncertainty estimates for hydraulic conductivity in both horizontal and vertical directions, streambed hydraulic conductivity, drain conductance, porosity). Additional parameters defined on the basis of hydraulic conductivity were also modified. These include, general head boundary (GHB) conductance and elevation around the inland boundary of the model, as well as the coastal GHB conductance.
- Modification of the groundwater model grid-layering structure to better represent the thickness of potentially hydrogeologically active units.
- Refinement of parameter uncertainty (pre-conditioning) according to the probabilistic presence of end-member hydrogeological materials (gravel and clay).

Note that, for this study, the intention was to isolate the AEM information and maintain consistency in the initial definition of property uncertainty. As such, the same prior uncertainty definition was maintained for multiplier parameters across the experiments.

Assessments undertaken included:

- Comparison of four different Heretaunga GW model versions: (i) parameters updated; (ii) parameters updated and pre-conditioning undertaken; (iii) parameters and layers updated; (iv) parameters and layers updated and pre-conditioning undertaken.
- Comparison with the inclusion of history-matching to tritium data.
- Data-worth analyses to isolate the impact of prediction-relevant information in AEM data where we assume either that: (i) there is no existing data and AEM data is added in or (ii) there is ‘all’ existing data and each dataset is removed one at a time.

These assessments indicate that:

- Overall, greater detail in property, boundary condition and, for *skytem-lays*, model-layer definition was afforded by the inclusion of AEM data compared to the *geo* model.
- The variation in AEM-derived property values indicates that previous parameter uncertainty was likely under-represented. This could have implications for history-matching and the reliability of predictions. Therefore, the inclusion of AEM data is expected to have increased prediction reliability even where apparent prediction uncertainty has not been reduced.
- The added benefit of AEM-derived models is most significant for predictions that are sensitive to smaller-scale flow paths. It is also most significant wherever the prior parameter uncertainty distribution was previously under-estimated.
- AEM-informed models appear to enhance the ability to extract valuable information from data sources that are influenced by fine-scale system complexity, such as tritium.
- Property updates imply greater potential for groundwater contributions from hillslope boundaries.
- Data-worth analyses indicate that the AEM data provides information that enhances the reliability of many prediction types to a significant degree in any context where very little data exists. This is in contrast with most other commonly available data that is generally most relevant to a specific prediction.

Recommendations for further work include:

- Further studies should explore data collection and analysis that may help reduce the uncertainty in boundary contributions to the regional and local groundwater budget, for example, boundary flux estimates utilising chemistry data in end-member mixing boundary conditions and associated rejection sampling in the numerical GW model.
- There are further opportunities presented by the broad-coverage yet detailed 3D AEM-derived system information that may allow for an even greater extraction of value in terms of model predictive capacity, for example, defining spatially varying anisotropy. These warrant further investigation.
- The data-worth analyses could be extended to formally assess optimal combinations of different data types, rather than the simple one-at-a-time analyses described herein.
- As noted above, in this study, the same prior uncertainty definition was maintained for multiplier parameters across the experiments. However, more formal uncertainty bounds could be derived from the SkyTEM data.

6.0 Digital Deliverables

The zip file *tw_heretaunga-main.zip* contains scripts and functions for:

- Building TWOTW and SkyTEM-informed versions of Heretaunga Plains groundwater simulations:
  - Steady-state flow model +
  - Tritium transport +
  - Combined young fraction and mean age transport.
- Constructing PEST interfaces for running history-matching (with and without tritium data) and uncertainty analysis.
- Undertaking uncertainty analysis on predictive scenarios.
- Processing simulation and uncertainty analysis results and comparing between different model and history-matching versions.

Within the zip file, *README* contains a brief look at running the main workflow, while more detailed guidance is provided in *docs/_build/latex/twotwheretaungaregionalmodelling.pdf.*

7.0 Acknowledgements

This work has been jointly funded by the New Zealand Government's Provincial Growth Fund, Hawke's Bay Regional Council, and GNS Science's (GNS) Strategic Science Investment Fund (Ministry of Business, Innovation & Employment; Programme Investment Contract C05X1702). The groundwater modelling component of this work was co-funded by the GNS-led programme Te Whakaheke o te Wai, funded by the New Zealand Ministry of Business, Innovation & Employment (MBIE; grant no. C05X1803).

Thank you to Simon Harper of Hawke's Bay Regional Council and Jeff Smith (previously at Hawke's Bay Regional Council) for their contributions to this project. Thank you to Amanda Langley of Project Haus for project management support.

Thank you to Simon Harper, Ahmed Elwan, Tom Wilson, Lee Chambers and Stewart Cameron for providing report reviews.

8.0 References

Baker M-A, Edmonds C. 2020. Proposed Plan Change 9: Tūtaekurī, Ahuriri, Ngaruroro and Karamū Catchments. Napier (NZ): Hawke's Bay Regional Council. Publication Number 5456.

Bakker M, Post V, Langevin CD, Hughes JD, White JT, Starn JJ, Fienen MN. 2016. Scripting MODFLOW model development using Python and FloPy. *Groundwater*. 54(5):733–739. https://doi.org/10.1111/gwat.12413

Begg JG, Jones KE, Lee JM, Tschritter C. 2022. 3D geological map of the Napier-Hastings urban area [explanatory text]. Lower Hutt (NZ): GNS Science. 21 p. (GNS Science geological map; 7b). https://doi.org/10.21420/QFEK-9369

Dausman AM, Doherty J, Langevin CD, Sukop MC. 2010. Quantifying data worth toward reducing predictive uncertainty. *Groundwater*. 48(5):729–740. https://doi.org/10.1111/j.1745-6584.2010.00679.x

Foged N. 2022. Hawke's Bay 3D Aquifer Mapping Project: Heretaunga Plains, 3D hydrostratigraphic modelling. Aarhus (DK): Aarhus University HydroGeophysics Group. 27 p. Prepared for Hawke's Bay Regional Council.

Hemmings B, Knowling MJ, Moore CR. 2020. Early uncertainty quantification for an improved decision support modeling workflow: a streamflow reliability and water quality example. *Frontiers in Earth Science*. 8. https://doi.org/10.3389/feart.2020.565613

Hemmings BJC, Moore CR, Rawlinson ZJ. In prep. Te Whakaheke o te Wai Programme – Heretaunga Plains regional groundwater model update: age and flow predictions and uncertainty. Lower Hutt (NZ): GNS Science. (GNS Science report; 2024/44).

Hughes JD, Langevin CD, Paulinski SR, Larsen JD, Brakenhoff D. 2024. FloPy workflows for creating structured and unstructured MODFLOW models. *Groundwater*. 62(1):124–139. https://doi.org/10.1111/gwat.13327

Knowling MJ, White JT, Moore CR. 2019. Role of model parameterization in risk-based decision support: an empirical exploration. *Advances in Water Resources*. 128:59–73. https://doi.org/10.1016/j.advwatres.2019.04.010

Knowling MJ, White JT, Moore CR, Rakowski P, Hayley K. 2020. On the assimilation of environmental tracer observations for model-based decision support. *Hydrology and Earth System Sciences*. 24(4):1677–1689. https://doi.org/10.5194/hess-24-1677-2020

McKenna SA, Akhriev A, Echeverría Ciaurri D, Zhuk S. 2020. Efficient uncertainty quantification of reservoir properties for parameter estimation and production forecasting. *Mathematical Geosciences*. 52:233–251. https://doi.org/10.1007/s11004-019-09810-y

Moore CR. 2025. Personal communication. Senior Groundwater Modeller, GNS Science; Lower Hutt, NZ.

Moore C, Doherty J. 2005. Role of the calibration process in reducing model predictive error. *Water Resources Research*. 41(5):W05020. https://doi.org/10.1029/2004WR003501

Morgenstern U. 2021. Personal communication. Principal Scientist Environmental Chemistry, GNS Science; Lower Hutt, NZ.

Morgenstern U, Begg JG, van der Raaij RW, Moreau M, Martindale H, Daughney CJ, Franzblau RE, Stewart MK, Knowling MJ, Toews MW, et al. 2018. Heretaunga Plains aquifers: groundwater dynamics, source and hydrochemical processes as inferred from age, chemistry, and stable isotope tracer data. Lower Hutt (NZ): GNS Science. 82 p. (GNS Science report; 2017/33). https://doi.org/10.21420/G2Q92G

Rakowski P, Knowling MJ. 2018. Heretaunga aquifer groundwater model: development report. Napier (NZ): Hawke's Bay Regional Council. 182 p. HRBC Report RM18-14.

Rawlinson ZJ. 2023. Hawke's Bay 3D Aquifer Mapping Project: 3D hydrogeological models from SkyTEM data in the Heretaunga plains. Lower Hutt (NZ): GNS Science. 77 p. Consultancy Report 2023/57. Prepared for Hawke's Bay Regional Council.

Rawlinson ZJ, Foged N, Westerhoff RS, Kellett RL. 2021. Hawke's Bay 3D Aquifer Mapping Project: Heretaunga Plains SkyTEM data processing and resistivity models. Wairakei (NZ): GNS Science. 90 p. Consultancy Report 2021/93. Prepared for Hawke's Bay Regional Council.

Rawlinson ZJ, Hemmings BJC, Moore CR. 2024. Hawke's Bay 3D aquifer mapping project: Heretaunga Plains numerical groundwater model updates using SkyTEM data. Wairakei (NZ): GNS Science. 14 p. Consultancy Report 2024/10LR. Prepared for Hawke's Bay Regional Council.

Sahoo TR, Rawlinson ZJ, Kellett RL. 2023. Hawke's Bay 3D Aquifer Mapping Project: delineation of major hydrological units within the Heretaunga Plains from SkyTEM-derived resistivity models. Lower Hutt (NZ): GNS Science. 55 p. Consultancy Report 2022/30. Prepared for Hawke's Bay Regional Council.

Toews MW, Hemmings B. 2019. A surface water network method for generalising streams and rapid groundwater model development [abstract]. In: *New Zealand Hydrological Society Conference: oral abstracts*; 2019 Dec 3–6; Rotorua, NZ. Wellington (NZ): New Zealand Hydrological Conference. p. 166–167.

White JT, Fienen MN, Doherty JE. 2016. A python framework for environmental model uncertainty analysis. *Environmental Modelling & Software*. 85:217–228. https://doi.org/10.1016/j.envsoft.2016.08.017

White JT, Fienen MN, Barlow PM, Welter DE. 2018. A tool for efficient, model-independent management optimization under uncertainty. *Environmental Modelling & Software*. 100:213–221. https://doi.org/10.1016/j.envsoft.2017.11.019

White JT, Foster LK, Fienen MN, Knowling MJ, Hemmings B, Winterle JR. 2020a. Toward reproducible environmental modeling for decision support: a worked example. *Frontiers in Earth Science*. 8:50. https://doi.org/10.3389/feart.2020.00050

White JT, Knowling MJ, Moore CR. 2020b. Consequences of groundwater-model vertical discretization in risk-based decision-making. *Groundwater*. 58(5):695–709. https://doi.org/10.1111/gwat.12957

White JT, Hemmings B, Fienen MN, Knowling MJ. 2021. Towards improved environmental modeling outcomes: enabling low-cost access to high-dimensional, geostatistical-based decision-support analyses. *Environmental Modelling & Software*. 139:105022. https://doi.org/10.1016/j.envsoft.2021.105022

Wilding T. 2018. Heretaunga Springs: gains and losses of stream flow to groundwater on the Heretaunga Plains. Napier (NZ): Hawke's Bay Regional Council. HBRC Report RM18-13 – 4996.

Yang J, McMillan H, Zammit C. 2017. Modeling surface water–groundwater interaction in New Zealand: model development and application. *Hydrological Processes*. 31(4):925–934. https://doi.org/10.1002/hyp.11075

APPENDICES

This page left intentionally blank.

APPENDIX 1 Comparison of *skyTEM-k* and *geo* Models

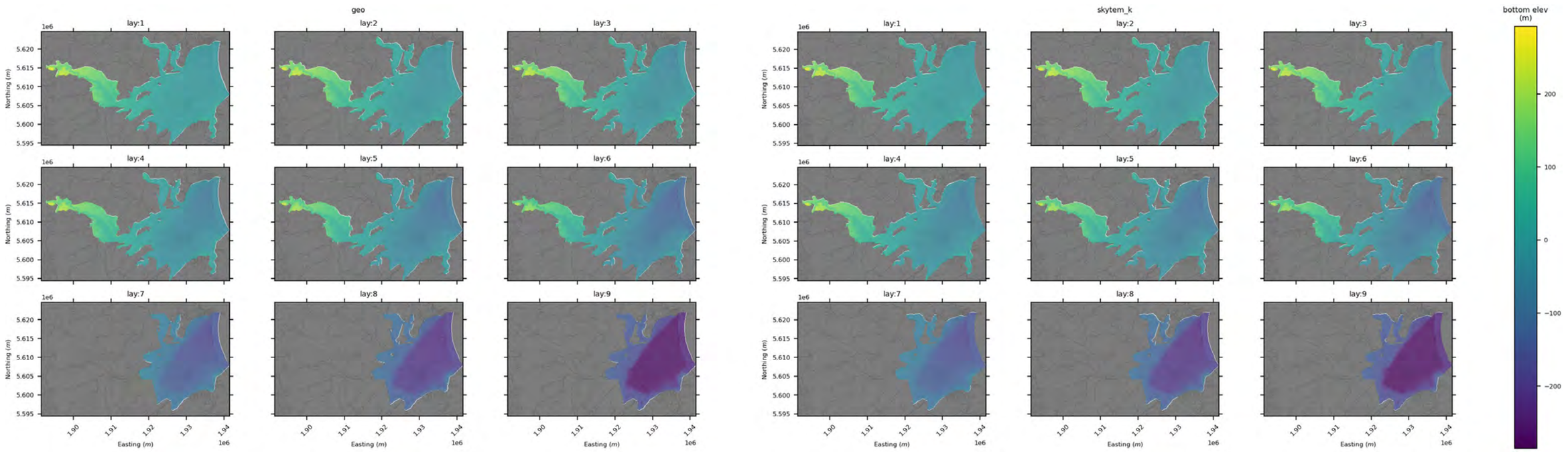

Figure A1.1 Layer bottom elevations (metres above sea level) for the (left) original (TWOTW/*geo*) and (right) SkyTEM-informed (*skytem-k*) models.

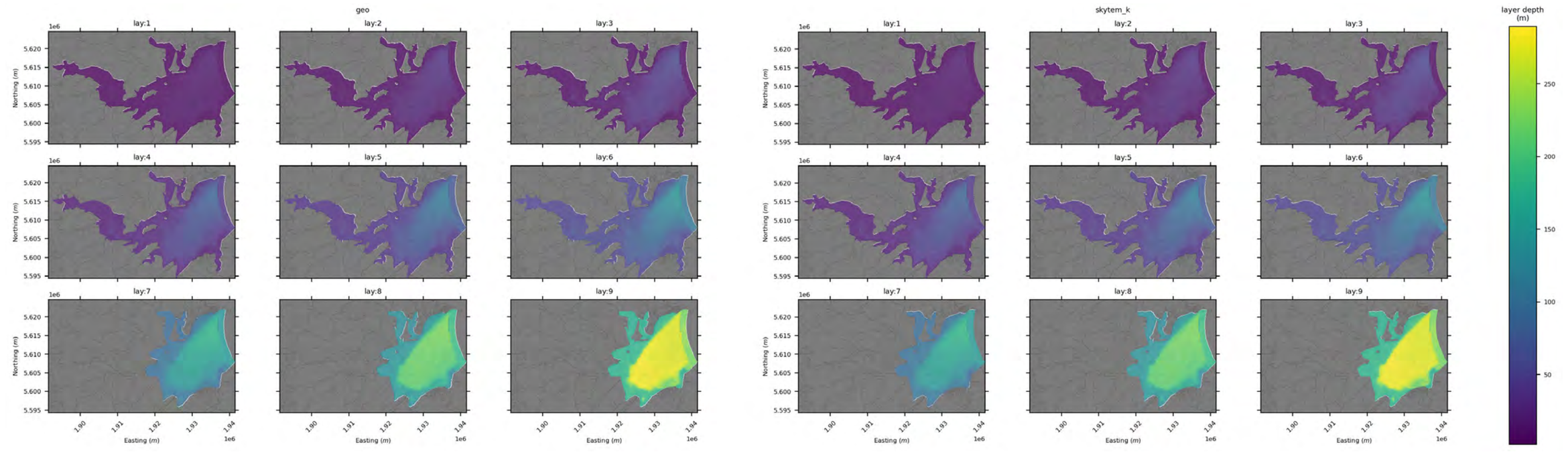

Figure A1.2 Layer bottom depths (metres) for the (left) original (TWOTW/*geo*) and (right) SkyTEM-informed (*skytem-k*) models.

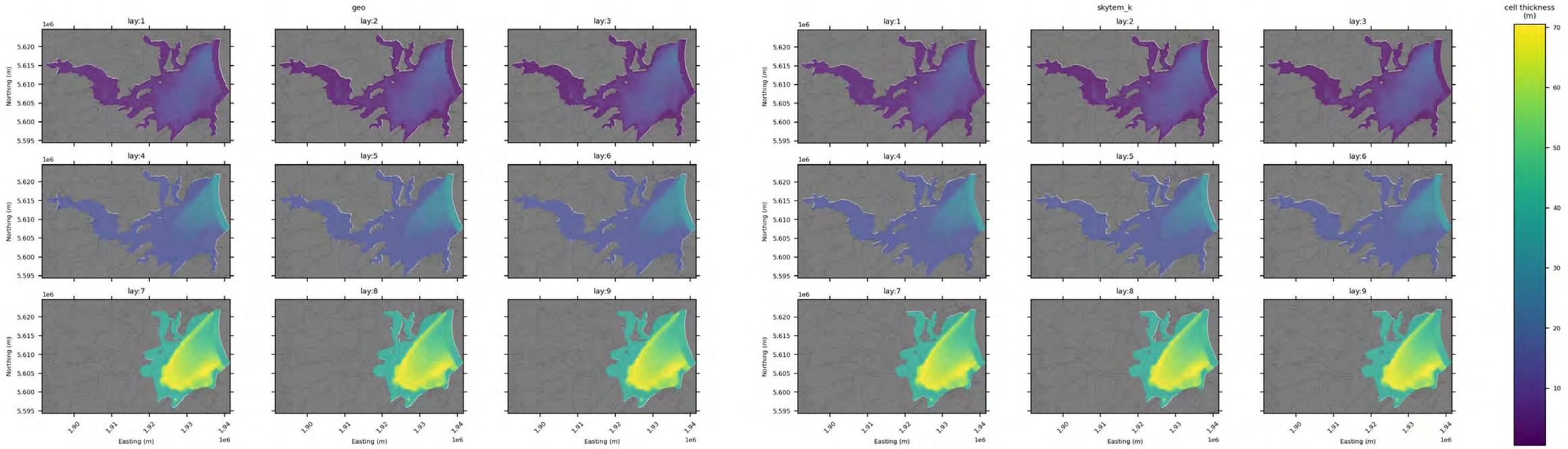

Figure A1.3 Layer bottom thickness (metres) for the (left) original (TWOTW/*geo*) and (right) SkyTEM-informed (*skytem-k*) models.

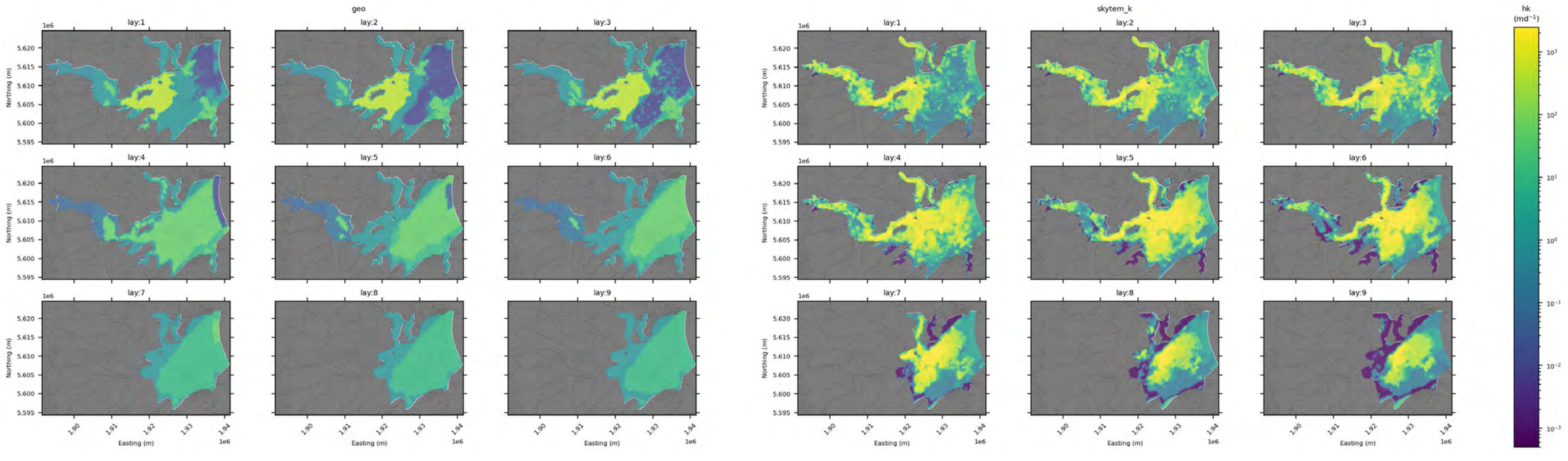

Figure A1.4 Base-realisation horizontal hydraulic conductivity (m/day) for the (left) original (TWOTW/*geo*) and (right) SkyTEM-informed (*skytem-k*) models.

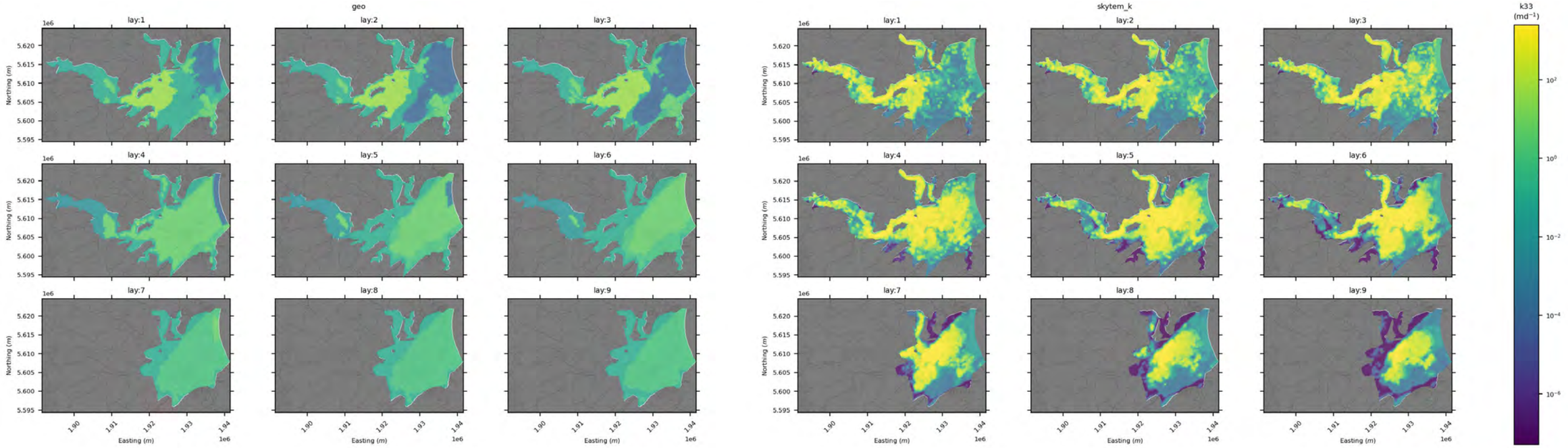

Figure A1.5 Base-realisation vertical hydraulic conductivity (m/day) for the (left) original (TWOTW/*geo*) and (right) SkyTEM-informed (*skytem-k*) models.

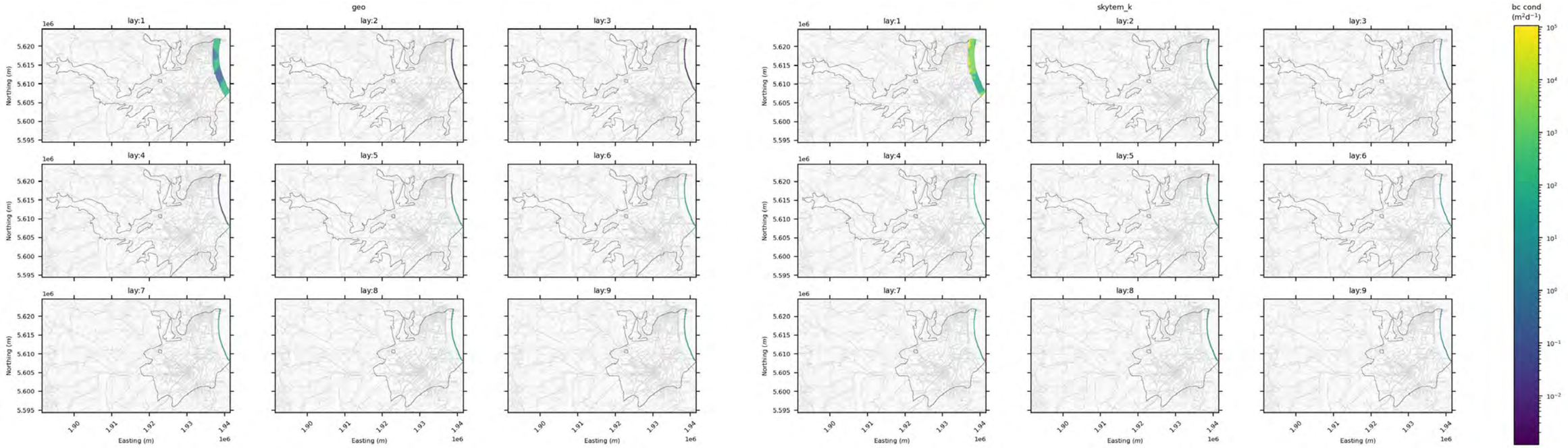

Figure A1.6 Base-realisation coastal general head boundary (GHB) conductance (m^2/day) for the (left) original (TWOTW/*geo*) and (right) SkyTEM-informed (*skytem-k*) models.

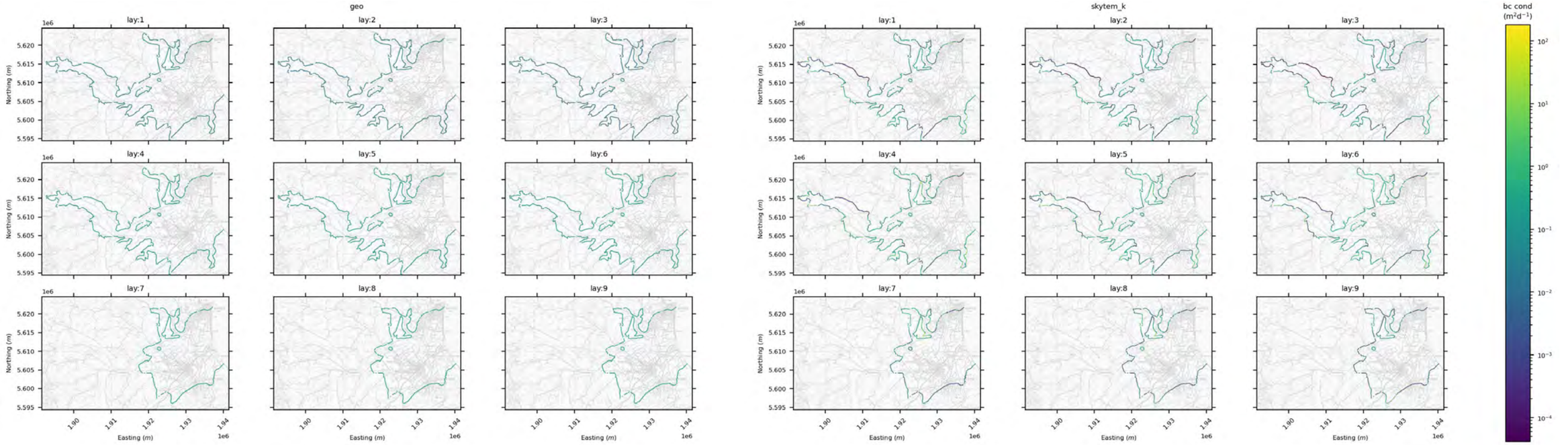

Figure A1.7 Base-realisation hillslope boundary general head boundary (GHB) conductance (m²/day) for the (left) original (TWOTW/*geo*) and (right) SkyTEM-informed (*skytem-k*) models.

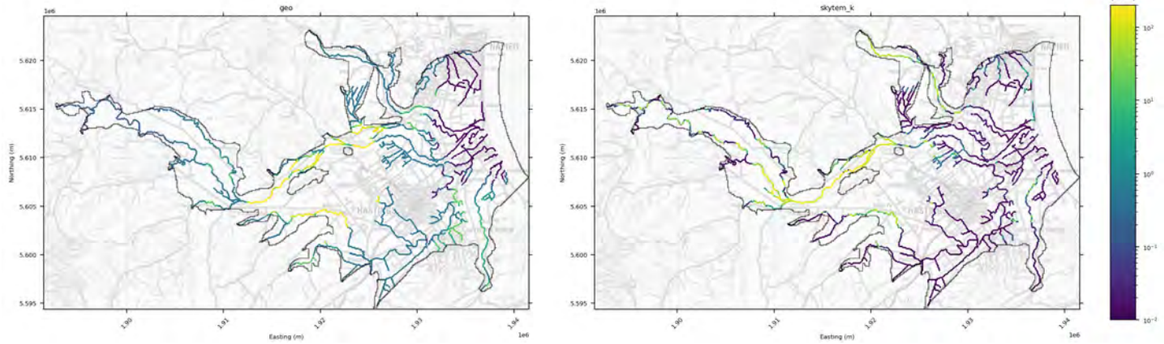

Figure A1.8 Base-realisation stream hydraulic conductivity (m/day) for the (left) original (TWOTW/*geo*) and (right) SkyTEM-informed (*skytem-k*) models.

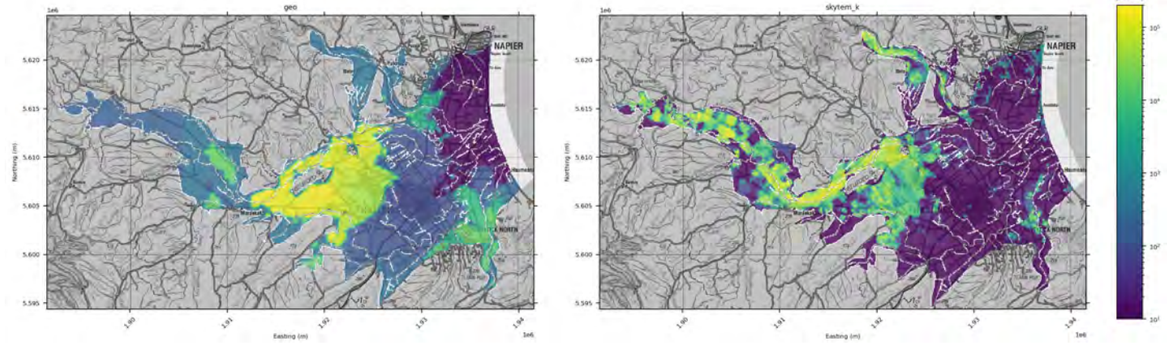

Figure A1.9 Base-realisation drain conductances (m²/day) for the (left) original (TWOTW/*geo*) and (right) SkyTEM-informed (*skytem-k*) models.

APPENDIX 2 History-Matching Observations

Table A2.1 Water-level (head) observations used in history-matching. Note: 'adjusted standard deviation' refers to the implied observation error accounting for the number of samples in the long-term average data value (the temporal coverage of the record). 'bs' = below surface; 'amsl' = above mean sea level.

Site Bore ID	Easting NZTM (m)	Northing NZTM (m)	Bore Depth (m bs)	Data Start Date	Data End Date	Sample Count	Data Mean, Target Value (m amsl)	Data Standard Deviation (m)	Adjusted Standard Deviation (m)
113	1928183	5599057	23.8	1991-02-19	2000-06-28	69	12.31	1.20	2.36
164	1923630	5606859	9.8	1975-09-18	1986-08-26	9353	17.99	0.31	0.31
222	1936826	5615559	59.1	1995-01-12	2021-07-07	25,5180	7.84	0.64	0.64
244	1926431	5606310	29.6	1991-04-12	2000-06-28	108	13.65	0.44	0.87
271	1933015	5615890	50.5	1991-02-14	2000-06-28	124	9.53	0.72	1.42
413	1936992	5620242	82.6	2001-07-03	2014-09-09	8	13.06	3.83	7.64
605	1921569	5602066	18.3	1991-03-22	2005-07-20	148	13.54	0.50	0.97
611	1931423	5615292	39.3	1995-05-17	2018-06-14	14	10.05	2.81	5.61
705	1930387	5607408	40.5	1983-01-19	2018-02-01	72,213	11.24	1.05	1.05
913	1931939	5613728	41.5	1991-02-14	2000-02-09	140,474	10.23	0.60	0.60
938	1938187	5608002	26.8	1991-02-19	2000-06-28	110	7.45	0.64	1.26
990	1926553	5602674	36.6	1991-02-19	2021-07-07	369	13.29	0.75	1.40
995	1929290	5602707	35.5	1991-02-19	2002-04-02	128	12.81	0.76	1.49
1001	1926661	5612540	21.6	1991-02-25	2015-04-29	120,983	11.95	1.00	1.00
1003	1921892	5604378	9.8	2009-04-23	2021-07-07	416,722	15.56	1.41	1.41
1053	1932150	5610421	37.5	1991-02-19	1998-09-24	101	11.13	0.67	1.31
1129	1935128	5602829	21.2	1991-02-19	2003-03-05	138	7.91	0.57	1.11
1191	1919581	5606894	21.9	1998-06-17	2020-03-19	28	19.43	0.92	1.83
1210	1935226	5603433	18.0	2016-09-30	2017-01-26	16,843	6.87	0.20	0.45
1320	1932922	5602633	16.8	2009-12-17	2010-05-20	7	6.85	0.37	1.66
1329	1935187	5603357	22.0	2016-09-29	2016-12-21	39,992	8.44	0.66	1.48
1412	1934548	5616458	56.7	1991-02-14	2006-12-06	196	8.73	0.92	1.77
1417	1934507	5614019	53.6	1991-02-22	2021-07-07	368	9.12	0.69	1.29
1450	1934175	5612199	49.8	1991-02-19	2021-07-07	363	10.35	0.66	1.23
1459	1932238	5603941	53.0	1995-02-28	2016-06-08	11	9.72	0.67	1.33
1501	1924441	5599661	26.0	1991-02-19	2021-07-07	369	13.18	0.87	1.63
1674	1928675	5608417	38.0	1991-04-12	2021-07-07	383	12.46	0.61	1.13
1695	1924330	5611791	22.5	1994-08-24	2015-11-06	238	17.23	0.29	0.55
1703	1923396	5612645	16.3	1995-02-18	2008-11-11	160	18.84	0.20	0.40
1799	1935938	5608506	32.6	1995-04-28	2014-09-11	19	8.09	1.26	2.50
1890	1935139	5603281	21.0	2016-09-30	2016-11-16	16,859	7.35	0.23	0.53
1940	1936870	5601729	66.4	1997-09-03	2020-03-18	64	9.27	0.69	1.37

Site Bore ID	Easting NZTM (m)	Northing NZTM (m)	Bore Depth (m bs)	Data Start Date	Data End Date	Sample Count	Data Mean, Target Value (m amsl)	Data Standard Deviation (m)	Adjusted Standard Deviation (m)
2106	1935087	5603273	24.0	2016-09-29	2016-12-22	39,986	9.07	0.46	1.03
2801	1920543	5610381	11.8	1990-11-23	2021-07-07	409,431	27.18	0.61	0.61
3148	1919547	5606374	32.0	1995-07-27	2000-06-28	53	19.48	0.64	1.91
3336	1928377	5603869	47.5	1995-04-24	2021-07-07	70,476	12.94	0.73	0.73
3337	1918450	5604755	36.0	2009-12-17	2010-05-20	7	26.43	1.59	7.14
3453	1908915	5606242	27.3	2003-09-02	2021-01-20	194,168	81.03	0.43	0.43
3525	1927030	5598449	31.5	1997-10-27	2018-06-05	246,909	12.31	1.03	1.03
3697	1928377	5603869	89.5	1995-03-14	2021-07-07	127,990	12.90	0.68	0.68
3698	1924122	5605227	14.2	1996-12-09	2021-07-07	194,860	13.63	0.72	0.72
3737	1924483	5606575	29.2	1974-05-07	2021-07-07	866,197	14.58	0.51	0.51
3738	1924484	5606576	5.8	1974-06-06	2003-10-15	13,478	15.16	0.21	0.21
3739	1917655	5604982	21.3	1975-06-09	1979-06-11	8148	35.30	1.52	2.38
3742	1921457	5610003	8.2	1982-03-19	1982-12-01	918	23.02	0.22	0.84
3749	1938567	5608691	32.0	1981-12-18	2020-12-04	37,290	5.99	0.57	0.57
3779	1935832	5620724	64.0	1995-11-30	2000-06-29	67,187	7.13	1.02	1.53
3781	1932018	5618064	38.1	1999-04-07	2020-03-19	25	8.38	0.93	1.85
4151	1934987	5603184	26.5	2016-10-07	2016-11-29	25,437	7.16	0.19	0.42
4333	1903848	5613617	61.0	2000-10-24	2008-12-22	62	157.98	2.13	4.21
4362	1904774	5613227	15.5	2013-05-09	2020-08-07	16	148.44	1.70	3.38
4375	1903164	5613861	24.0	2001-07-16	2009-01-26	59	151.09	4.21	8.33
4384	1902441	5613741	57.5	2001-05-22	2009-09-29	51	152.66	3.38	6.69
4393	1902586	5613730	57.5	2001-05-22	2009-09-29	60	152.28	4.95	9.78
4559	1898703	5613606	54.4	2002-10-16	2010-04-30	47	165.22	3.80	7.53
4614	1898264	5613295	49.0	2002-05-01	2017-11-22	68	180.31	3.94	7.77
4618	1918086	5604724	44.4	2009-12-17	2010-05-20	7	27.44	1.57	7.06
4650	1902796	5614412	60.0	2003-04-24	2008-09-26	45	165.22	0.48	0.95
4707	1903719	5614084	24.2	2004-03-17	2006-08-24	22	153.57	2.66	7.96
4959	1910632	5610931	56.1	2003-09-26	2008-09-26	35	105.73	0.21	0.42
5023	1904771	5613219	54.0	2003-10-23	2020-08-07	38,024	154.14	1.17	1.17
5390	1904470	5613860	53.7	2006-05-16	2015-09-25	71	141.03	3.72	7.35
5453	1904146	5613900	54.0	2006-09-27	2015-09-25	68	147.69	4.24	8.38
5988	1924134	5602752	109.0	2010-01-21	2021-07-07	233,454	12.34	0.89	0.89
6502	1922828	5608760	27.1	1972-12-20	1976-03-10	118	19.50	0.39	1.14
6505	1922828	5609060	19.8	1973-02-07	1976-03-10	118	19.15	0.36	1.06
6506	1923129	5609061	27.0	1972-11-22	1976-03-10	118	19.26	0.42	1.24
7980	1924608	5610388	20.1	1991-02-13	2020-11-03	368	16.35	0.45	0.84
8512	1923124	5604296	29.8	1973-03-15	1976-03-11	114	14.41	0.42	1.23

Site Bore ID	Easting NZTM (m)	Northing NZTM (m)	Bore Depth (m bs)	Data Start Date	Data End Date	Sample Count	Data Mean, Target Value (m amsl)	Data Standard Deviation (m)	Adjusted Standard Deviation (m)
8515	1923120	5607127	27.1	1973-02-14	1976-03-11	114	17.78	0.41	1.21
8517	1922243	5606600	18.3	1973-03-15	1976-03-11	109	18.33	0.43	1.26
8521	1923103	5605947	30.5	1997-12-08	2020-03-18	84	16.01	0.76	1.50
8523	1922428	5607459	18.3	1973-03-15	1976-03-11	76	18.15	0.31	0.91
8524	1923029	5607859	30.0	1973-02-07	1975-10-09	106	18.27	0.41	1.22
8525	1923229	5607459	30.5	1973-02-14	1975-10-09	106	17.91	0.46	1.35
8527	1922213	5606017	17.7	1973-03-15	1976-03-11	104	18.50	0.49	1.44
9068	1931400	5615240	45.1	1997-07-25	2021-07-07	277,755	12.05	0.53	0.53
10212	1932190	5617087	38.1	1990-01-01	2003-03-05	332,867	8.70	0.87	0.87
10313	1921929	5603355	25.0	1973-03-27	1976-03-11	80	14.51	0.56	1.65
10340	1922962	5609398	16.5	1997-05-23	2000-06-28	42,515	19.10	0.52	0.78
10344	1923829	5608260	22.9	1973-03-27	1976-03-10	108	17.72	0.37	1.09
10345	1922928	5609861	30.1	1973-02-28	1973-05-17	12	20.60	0.25	1.14
10348	1922928	5609561	4.8	1973-05-12	1976-03-10	107	21.00	0.10	0.31
10349	1922928	5609661	17.7	1973-05-24	1976-03-10	100	19.64	0.33	0.98
10356	1921054	5607416	30.0	1973-02-21	2020-01-17	430	19.37	0.85	1.57
10357	1923729	5609561	26.4	1973-03-15	1976-03-10	109	18.62	0.33	0.97
10358	1923629	5609461	15.6	1973-09-13	1976-03-10	85	18.65	0.33	0.97
10359	1923729	5609461	14.3	1973-09-13	1976-03-10	87	18.36	0.32	0.96
10362	1923329	5608260	30.7	1973-01-17	1976-03-10	115	18.23	0.40	1.17
10363	1922829	5608360	22.7	1973-01-24	1975-10-09	112	18.96	0.38	1.10
10365	1923129	5609161	12.8	1973-08-29	1976-03-10	89	19.62	0.37	1.09
10370	1922928	5609861	13.1	1974-02-08	1976-03-10	63	21.42	0.35	1.03
10371	1922467	5609565	13.4	1972-01-01	2021-07-07	823,092	20.13	0.67	0.67
10496	1935134	5602998	8.3	2003-05-28	2018-02-01	186	7.89	0.31	0.59
10773	1933796	5605715	12.8	1991-03-22	2006-02-10	240,455	8.92	0.58	0.58
15001	1935267	5612895	161.5	1995-08-29	2021-07-07	200,910	11.44	0.48	0.48
15002	1935267	5612895	103.5	1995-08-29	2021-07-07	217,353	9.74	0.56	0.56
15003	1935267	5612895	65.5	1995-09-15	2021-07-07	226,827	9.65	0.56	0.56
15004	1919828	5604728	25.0	1991-02-13	2021-07-07	713,979	22.74	1.93	1.93
15005	1920276	5609193	17.6	1992-06-02	2021-07-07	430,114	25.19	1.32	1.32
15006	1926345	5609156	30.2	1991-02-19	2018-06-05	152,014	13.55	0.51	0.51
15007	1908915	5606242	16.5	2013-05-09	2021-01-20	150,074	82.66	1.03	1.03
15008	1908915	5606242	19.8	2013-05-09	2021-01-20	179,625	81.56	0.55	0.55
15009	1924122	5605227	74.8	1996-12-09	2021-07-07	91	13.69	0.66	1.30
15010	1924122	5605227	48.0	1996-12-09	2021-07-07	201,312	13.21	0.73	0.73
15011	1924122	5605227	114.0	1996-09-20	2021-07-07	270,325	13.37	0.58	0.58

Site Bore ID	Easting NZTM (m)	Northing NZTM (m)	Bore Depth (m bs)	Data Start Date	Data End Date	Sample Count	Data Mean, Target Value (m amsl)	Data Standard Deviation (m)	Adjusted Standard Deviation (m)
15012	1928377	5603869	114.0	1997-04-08	2021-07-07	59	12.22	0.89	1.76
15018	1928377	5603869	152.5	2021-02-24	2021-07-07	6	11.83	0.49	2.18
15022	1935267	5612895	40.5	1995-09-15	2021-07-07	226,358	9.63	0.57	0.57
15464	1924134	5602752	81.5	2010-01-21	2021-07-07	175,890	12.40	0.89	0.89
15465	1924134	5602752	15.0	2010-01-21	2021-07-07	236,396	11.52	0.50	0.50
15684	1927202	5618662	13.2	2010-06-10	2021-07-07	177,311	20.64	0.24	0.24
15794	1924708	5619382	90.0	2011-04-07	2021-07-07	106,977	25.22	0.31	0.31
15795	1923396	5613907	96.0	2011-06-10	2019-11-29	166,737	17.47	0.17	0.17
15796	1923396	5613907	37.7	2011-06-10	2021-07-07	176,388	17.63	0.22	0.22
15884	1924706	5619380	10.4	2011-08-08	2021-07-07	171,267	25.42	0.22	0.22
16078	1916483	5605275	40.0	2014-01-08	2021-07-07	202,085	45.86	0.72	0.72
16202	1933728	5606795	11.2	2014-10-15	2021-07-07	218,160	2.19	0.27	0.27
16203	1933732	5606796	22.2	2014-10-15	2021-07-07	227,979	8.34	0.68	0.68
16300	1924834	5610619	98.0	2015-04-23	2021-07-07	88	14.42	0.31	0.61
16360	1924829	5610617	65.3	2015-04-23	2021-07-07	134,478	15.21	0.31	0.31
16361	1924829	5610618	23.9	2015-04-23	2021-07-07	186,928	15.68	0.33	0.33
16383	1934943	5603162	150.0	2016-03-24	2021-07-07	62	8.17	0.21	0.41
16432	1926069	5597417	12.0	1995-11-07	2000-06-28	25,140	9.96	0.25	0.37
16550	1935285	5603381	1.5	2016-10-11	2017-01-26	11	7.04	0.18	0.81
16551	1935277	5603376	3.0	2016-10-07	2017-01-26	29,818	7.86	0.22	0.50
16552	1935274	5603375	4.1	2016-10-07	2017-01-26	13,431	7.74	0.20	0.45
16553	1935220	5603429	1.5	2016-10-07	2017-01-26	13,428	8.48	0.03	0.07
16554	1935220	5603427	3.0	2016-10-07	2017-01-26	13,426	8.23	0.16	0.37
16555	1935222	5603427	4.0	2016-10-13	2017-01-26	10	7.01	0.64	2.88
16556	1935112	5603397	3.0	2016-10-07	2017-01-26	47,081	8.53	0.18	0.40
16557	1935111	5603391	4.1	2016-10-07	2017-01-26	13,452	7.69	0.17	0.40
16611	1934764	5604127	18.0	2017-08-08	2021-07-07	97,442	7.97	0.39	0.58
16641	1930387	5606036	45.0	2017-08-08	2021-07-07	47	11.59	0.62	1.85
16729	1926320	5609177	27.0	2018-02-01	2021-07-07	86,484	13.78	0.49	0.74
16758	1926750	5599330	26.5	2018-02-22	2021-07-07	108,803	12.03	1.39	2.08
16772	1920804	5607186	29.7	2018-05-01	2021-07-07	102,956	18.52	0.65	0.97
16965	1938727	5609085	34.0	2020-03-05	2021-07-07	19	6.38	0.53	1.60

Table A2.2 Stream-flow observations used in history-matching.

Site	Easting NZTM (m)	Northing NZTM (m)	Target Value (m^3/d) [m^3/s]	Standard Deviation (m^3/d)
Karamu at the floodgates	1932689	5609195	172,800.0 [2.00]	34,560.0
Ngaruroro at Chesterhope	1932539	5609866	2,073,600.0 [24.00]	414,720.0
Ngaruroro at State Highway 50	1922945	5611244	1,710,720.0 [19.80]	342,144.0
Raupare at Ormond	1929836	5609665	54,432.0 [0.63]	10,886.4
Tukituki at Blackbridge	1937610	5608740	1,840,320.0 [21.30]	368,064.0
Tutaekuriwaimate at Goods	1928467	5613386	198,720.0 [2.30]	39,744.0

Table A2.3 Surface-water–groundwater-exchange observations used in history-matching.

Reach	River Loss Target (m^3/d) [m^3/s]	Standard Deviation (m^3/d)
Ngaruroro Roys Hill – Fernhill	367,200.0 [4.25]	73,440.0
Ngaruroro D/S Fernhill	10,368.0 [0.12]	2073.6
Ngaruroro loss combined	388,800.0 [4.50]	77,760.0
Paritua Upstream of Bridge Pā	6,912.0 [0.08]	1382.4
Tukituki River Road – Tennant Road	67,392.0 [0.78]	13,478.4
Tutaekuri Hakowi – Silverford	69,120.0 [0.8]	13,824.0

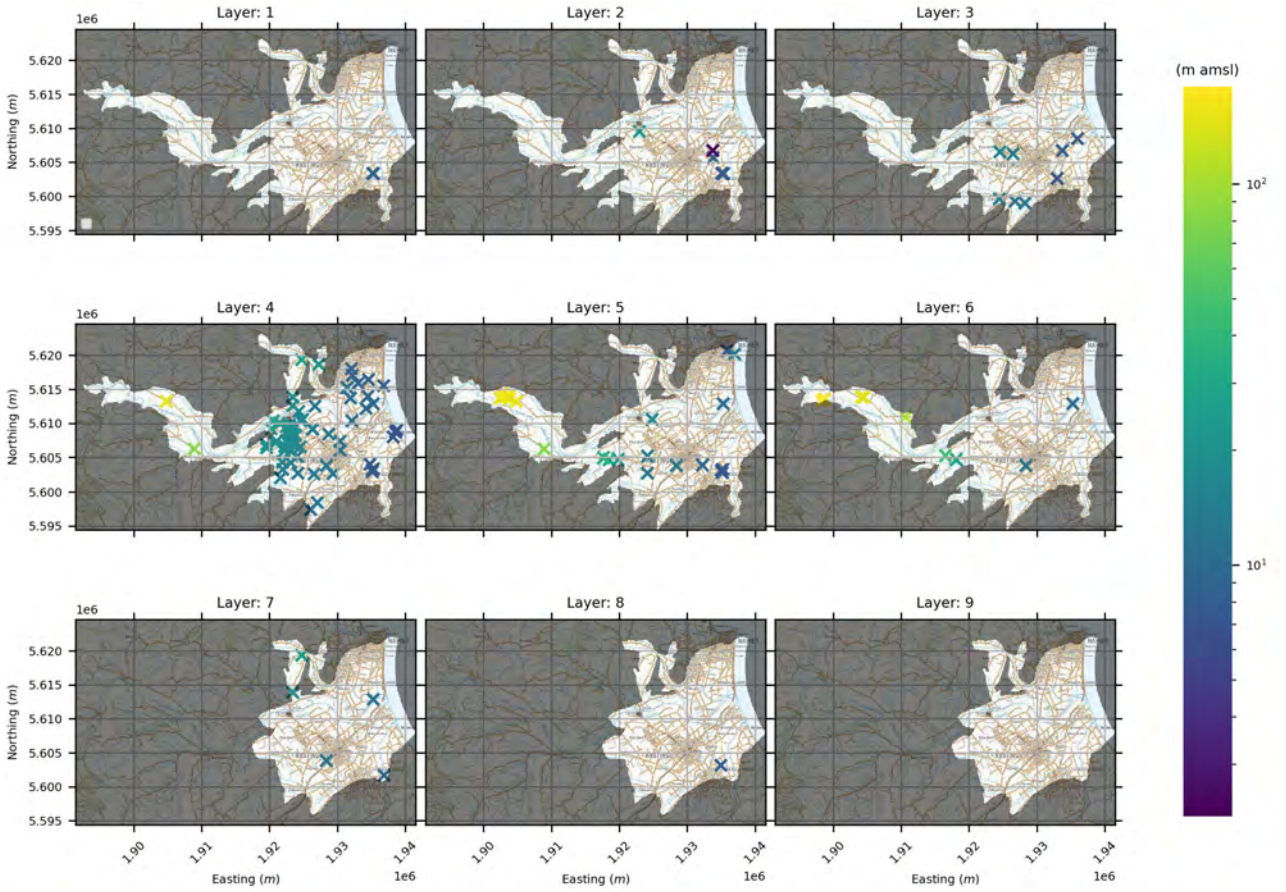

Figure A2.1 Water-level observations across all layers.

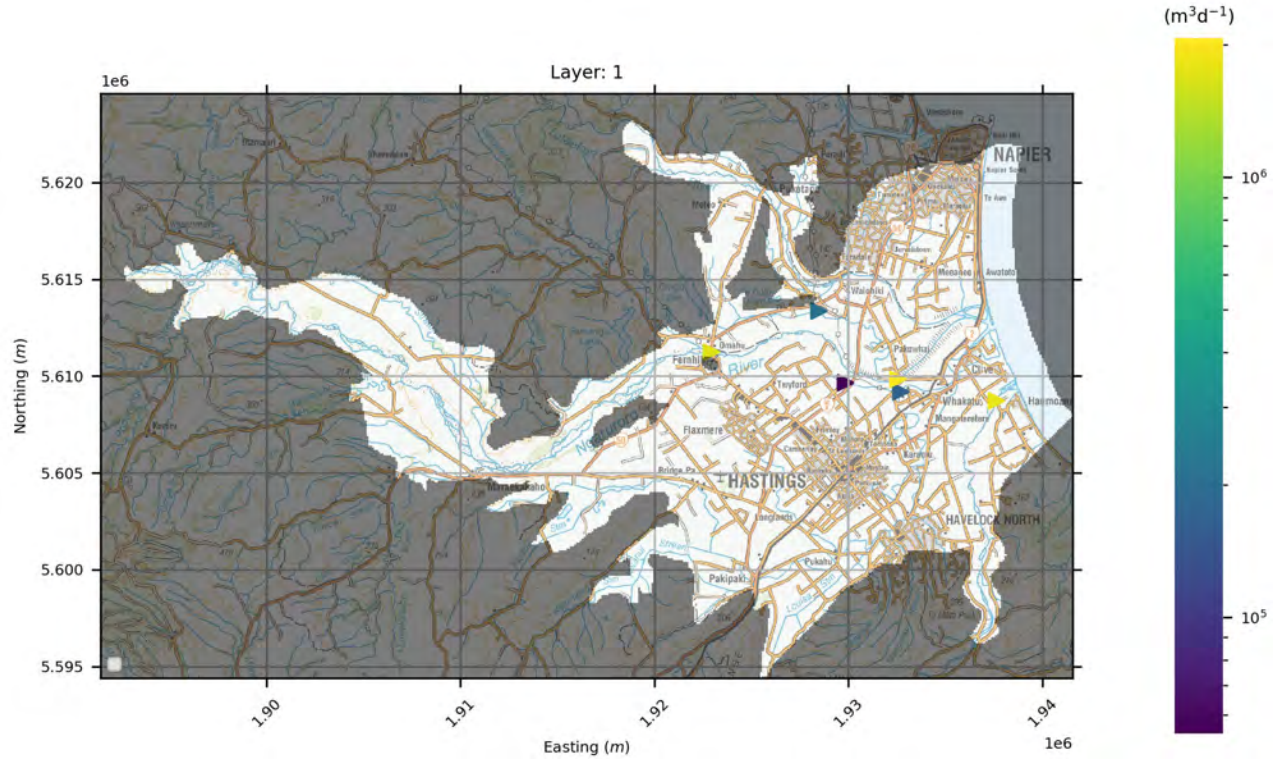

Figure A2.2 Stream-flow observations.

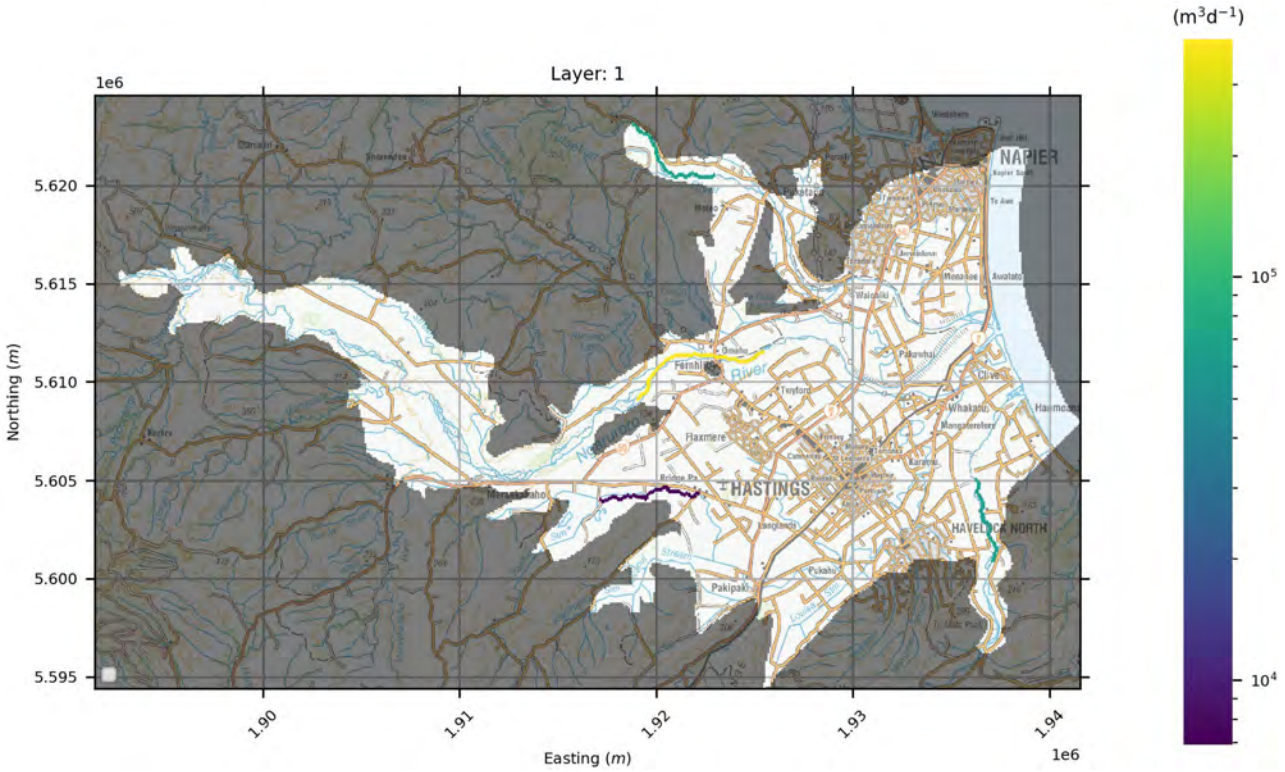

Figure A2.3 Surface-water–groundwater-exchange estimates.

APPENDIX 3 Simulated Output versus Observations

A3.1 *skytem-k* and *skytem-k-precond* Summaries

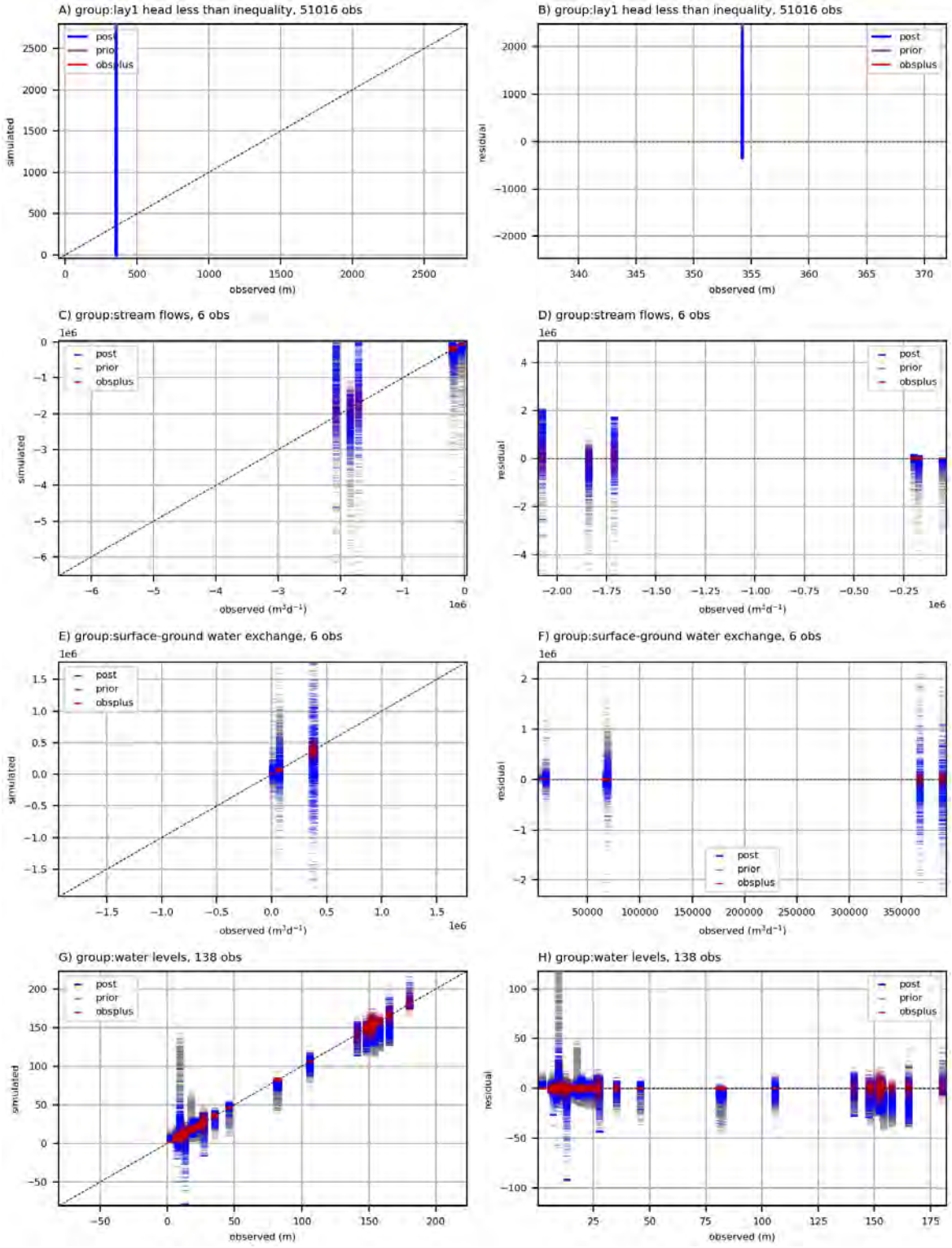

Figure A3.1 Summary of history-matching results for the *skytem-k* model. Left-hand plots (A, C, E, G) are simulated values versus observed values. Right-hand plots (B, D, F, H) are residual values (simulated – observed) for each observed value. Grey bars represent prior simulated values. Blue bars are posterior simulated values with respect to the same observations. Red bars are the observed values with the inclusion of 'observation noise'. The top two plots (A and B) relate to inequality observations that surface-layer heads should always be below 350 m above sea level, which is a pragmatic observation to try to reduce spurious head spikes in the ensembles.

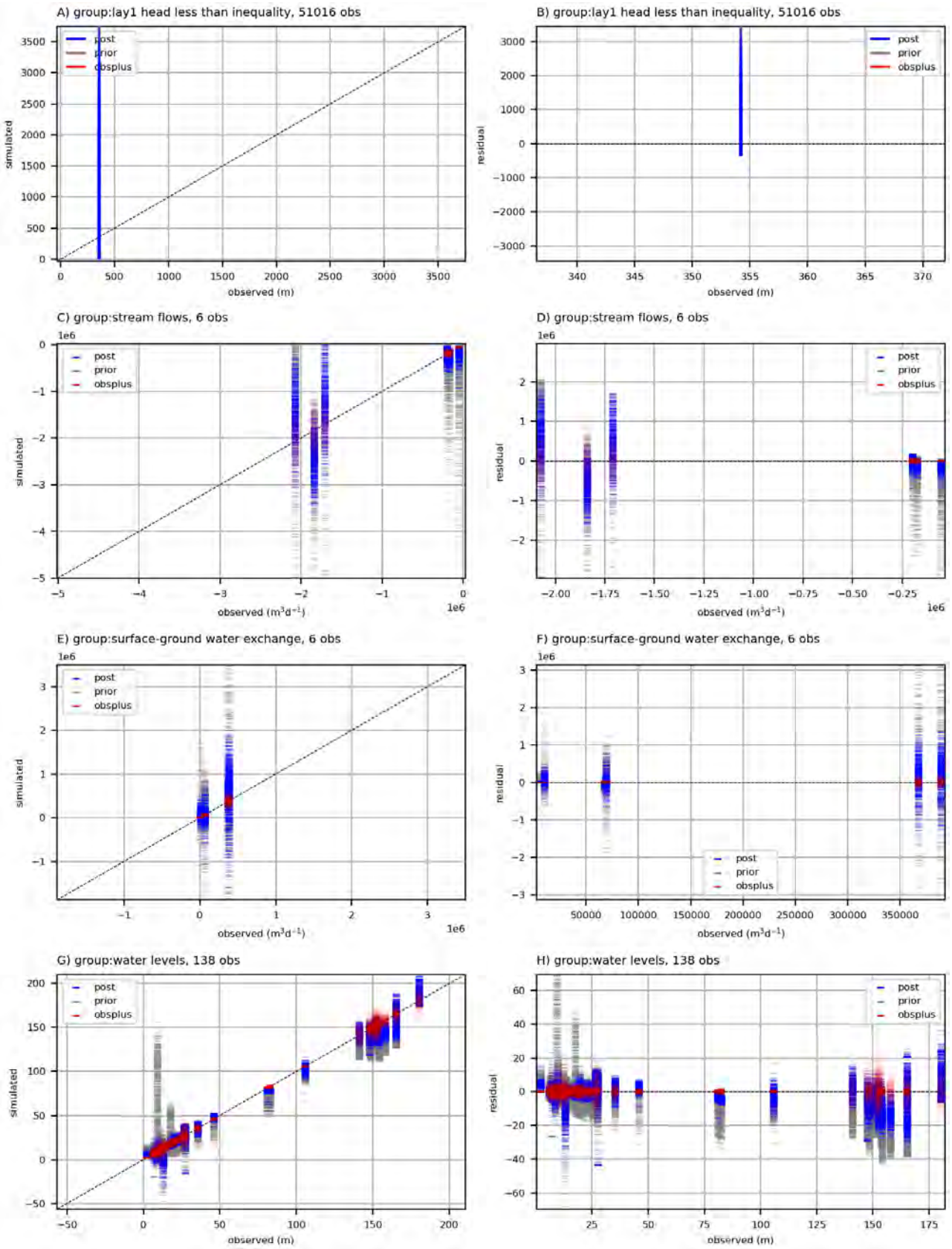

Figure A3.2 Summary of model history-matching for the *skytem-k-precond* model. Left-hand plots (A, C, E, G) are simulated values versus observed values. Right-hand plots (B, D, F, H) are residual values (simulated – observed) for each observed value. Grey bars represent prior simulated values. Blue bars are posterior simulated values with respect to the same observations. Red bars are the observed values with the inclusion of 'observation noise'. The top two plots (A and B) relate to inequality observations that surface-layer heads should always be below 350 m above sea level, which is a pragmatic observation to try to reduce spurious head spikes in the ensembles.

A3.2 Individual Observation Fits

Note that, for comparison, individual observation fit plots for the *geo* model are provided in Hemmings et al. (in prep.).

A3.2.1 *skytem-k*

A3.2.1.1 Levels

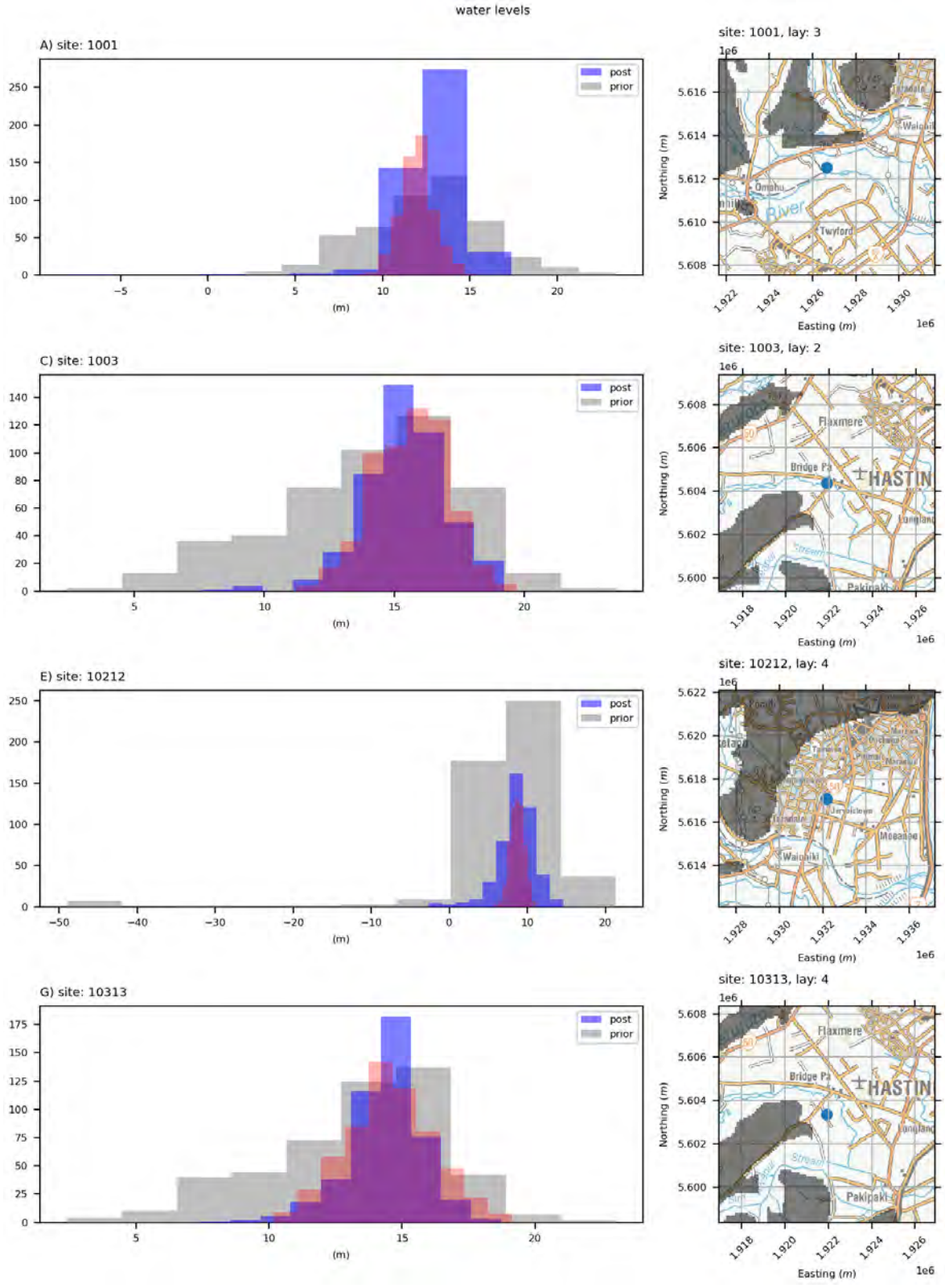

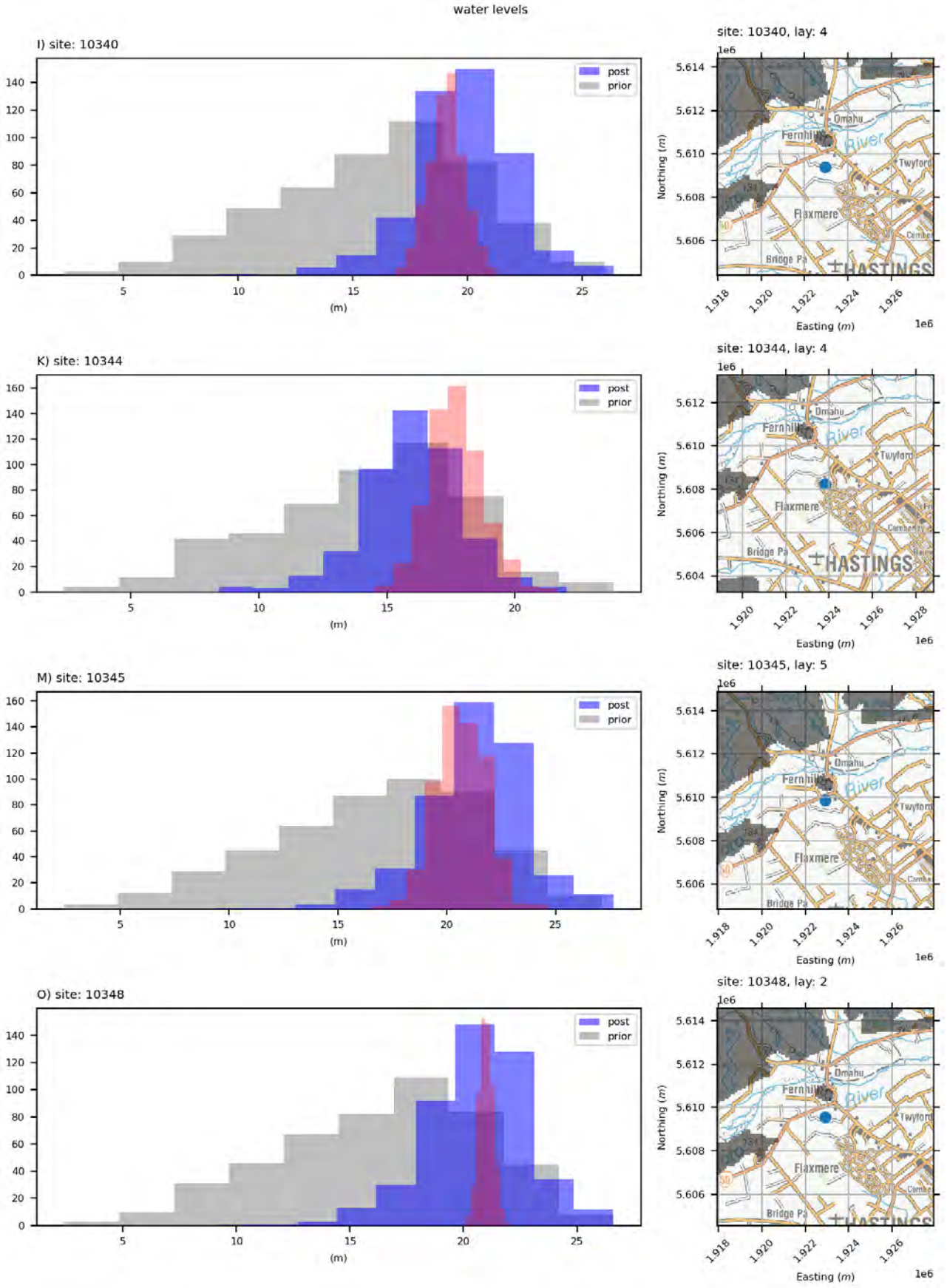
water levels
I) site: 10340
post
prior
(m)
site: 10340, lay: 4
Northing (m)
Easting (m)
1e6
K) site: 10344
site: 10344, lay: 4
M) site: 10345
site: 10345, lay: 5
O) site: 10348
site: 10348, lay: 2
Omahu
Fernhill
River
Twyford
Flaxmere
Bridge Pa
HASTINGS

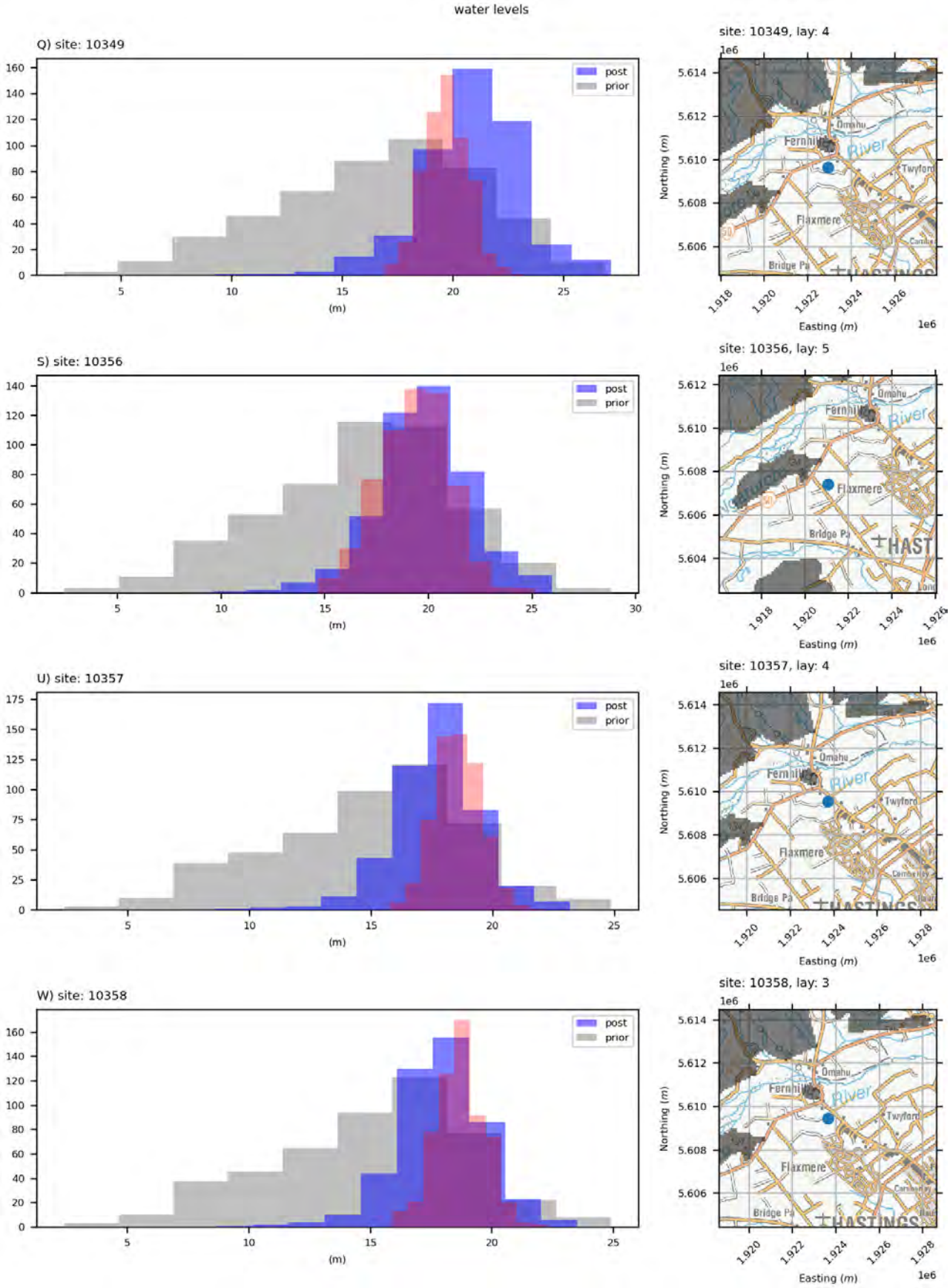
water levels
Q) site: 10349
post
prior
(m)
site: 10349, lay: 4
1e6
Northing (m)
Easting (m)
Omahu
Fernhill
River
Twyford
Flaxmere
Bridge Pa
HASTINGS
S) site: 10356
site: 10356, lay: 5
U) site: 10357
site: 10357, lay: 4
W) site: 10358
site: 10358, lay: 3

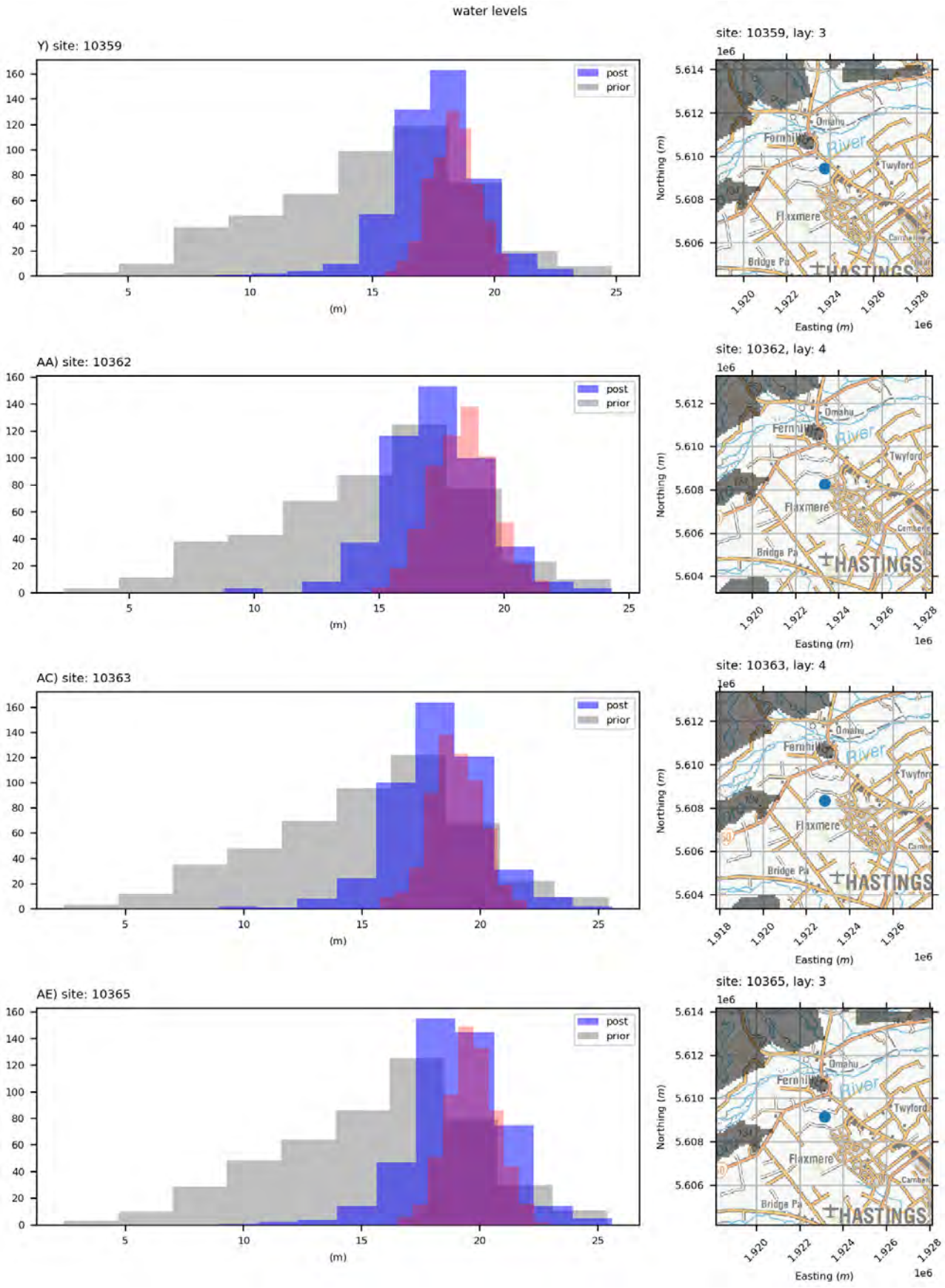
water levels
Y) site: 10359
post
prior
(m)
site: 10359, lay: 3
1e6
Northing (m)
Easting (m)
Omahu
Fernhill
River
Twyford
Flaxmere
Bridge Pa
HASTINGS
AA) site: 10362
site: 10362, lay: 4
AC) site: 10363
site: 10363, lay: 4
AE) site: 10365
site: 10365, lay: 3

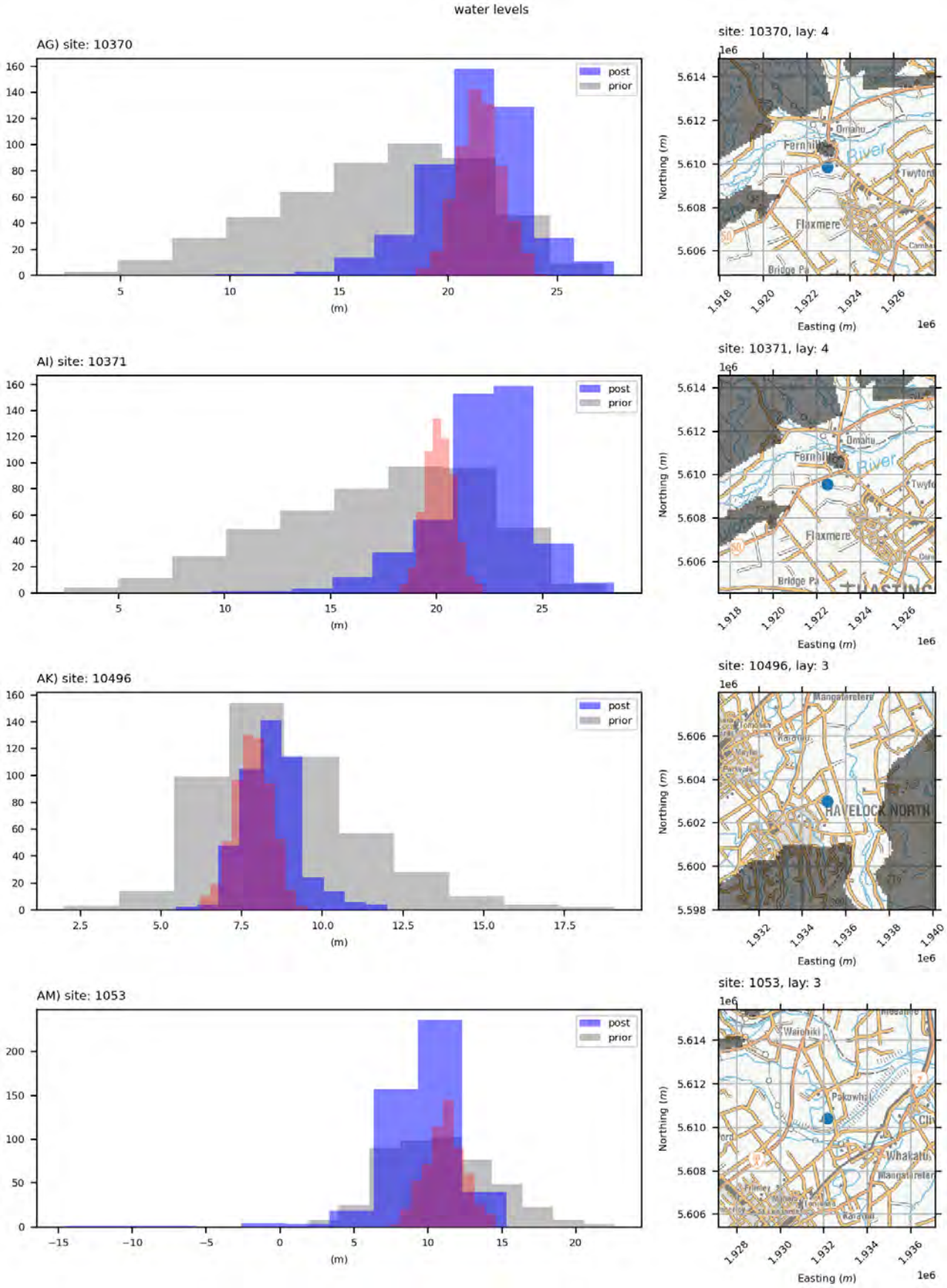
water levels
AG) site: 10370
post
prior
(m)
site: 10370, lay: 4
1e6
Northing (m)
Easting (m)
AI) site: 10371
post
prior
(m)
site: 10371, lay: 4
1e6
Northing (m)
Easting (m)
AK) site: 10496
post
prior
(m)
site: 10496, lay: 3
1e6
Northing (m)
Easting (m)
AM) site: 1053
post
prior
(m)
site: 1053, lay: 3
1e6
Northing (m)
Easting (m)

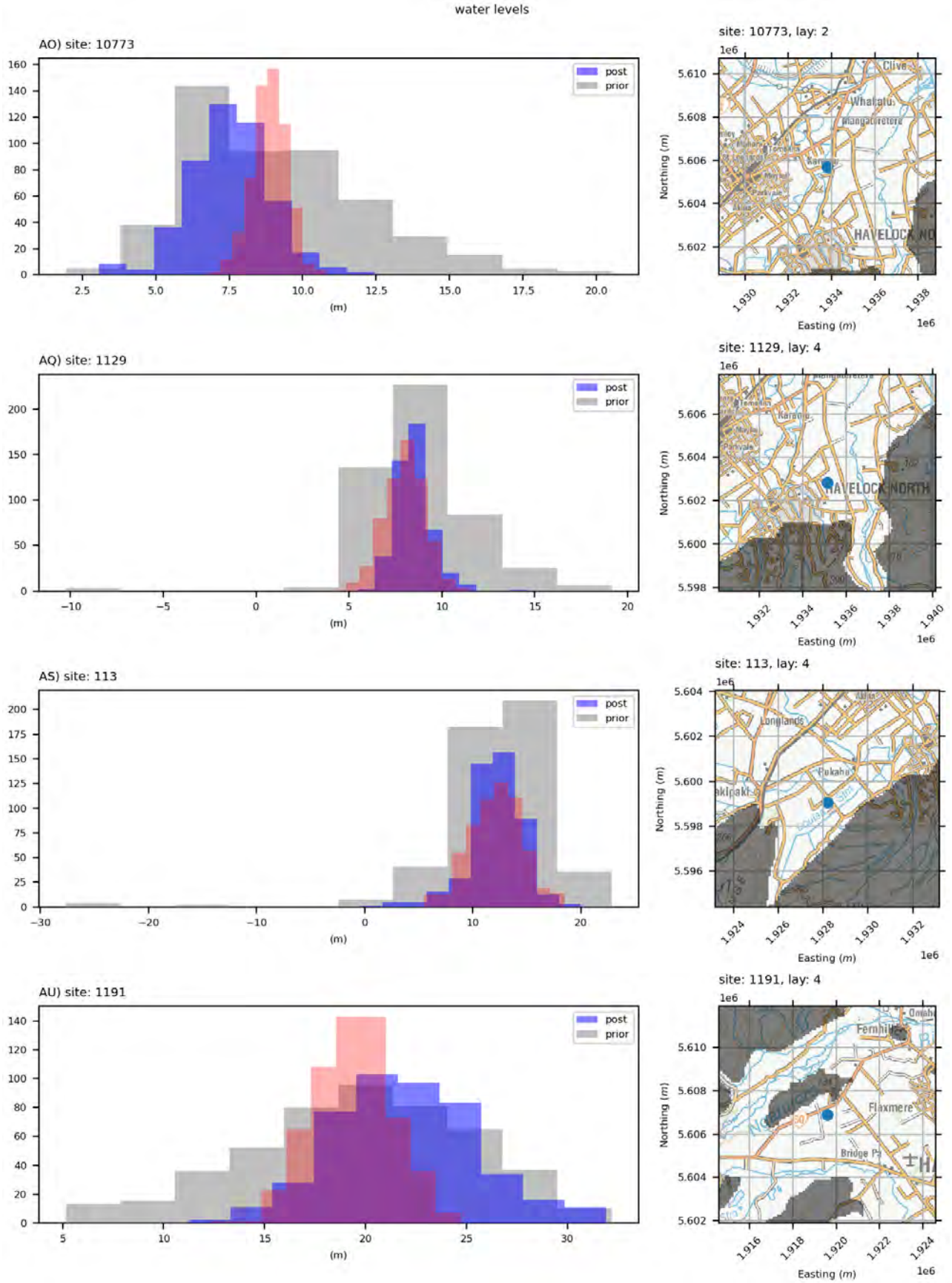
water levels
AO) site: 10773
post
prior
(m)
site: 10773, lay: 2
Northing (m)
Easting (m)
1e6
AQ) site: 1129
site: 1129, lay: 4
AS) site: 113
site: 113, lay: 4
AU) site: 1191
site: 1191, lay: 4

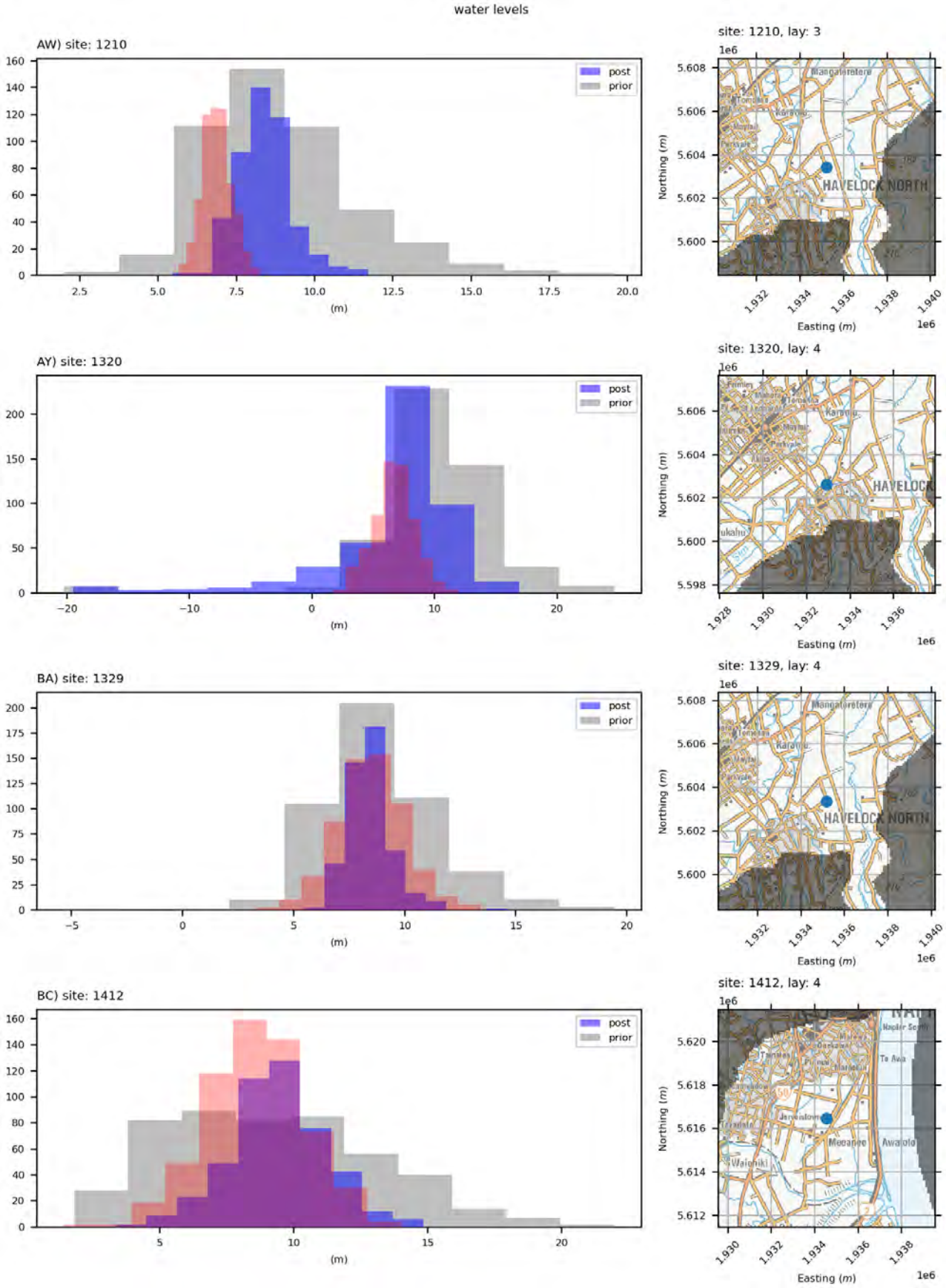
water levels
AW) site: 1210
post
prior
(m)
site: 1210, lay: 3
1e6
Northing (m)
Easting (m)
HAVELOCK NORTH
AY) site: 1320
site: 1320, lay: 4
HAVELOCK
BA) site: 1329
site: 1329, lay: 4
BC) site: 1412
site: 1412, lay: 4
Napier South
Te Awa
Meeanee
Awatoto

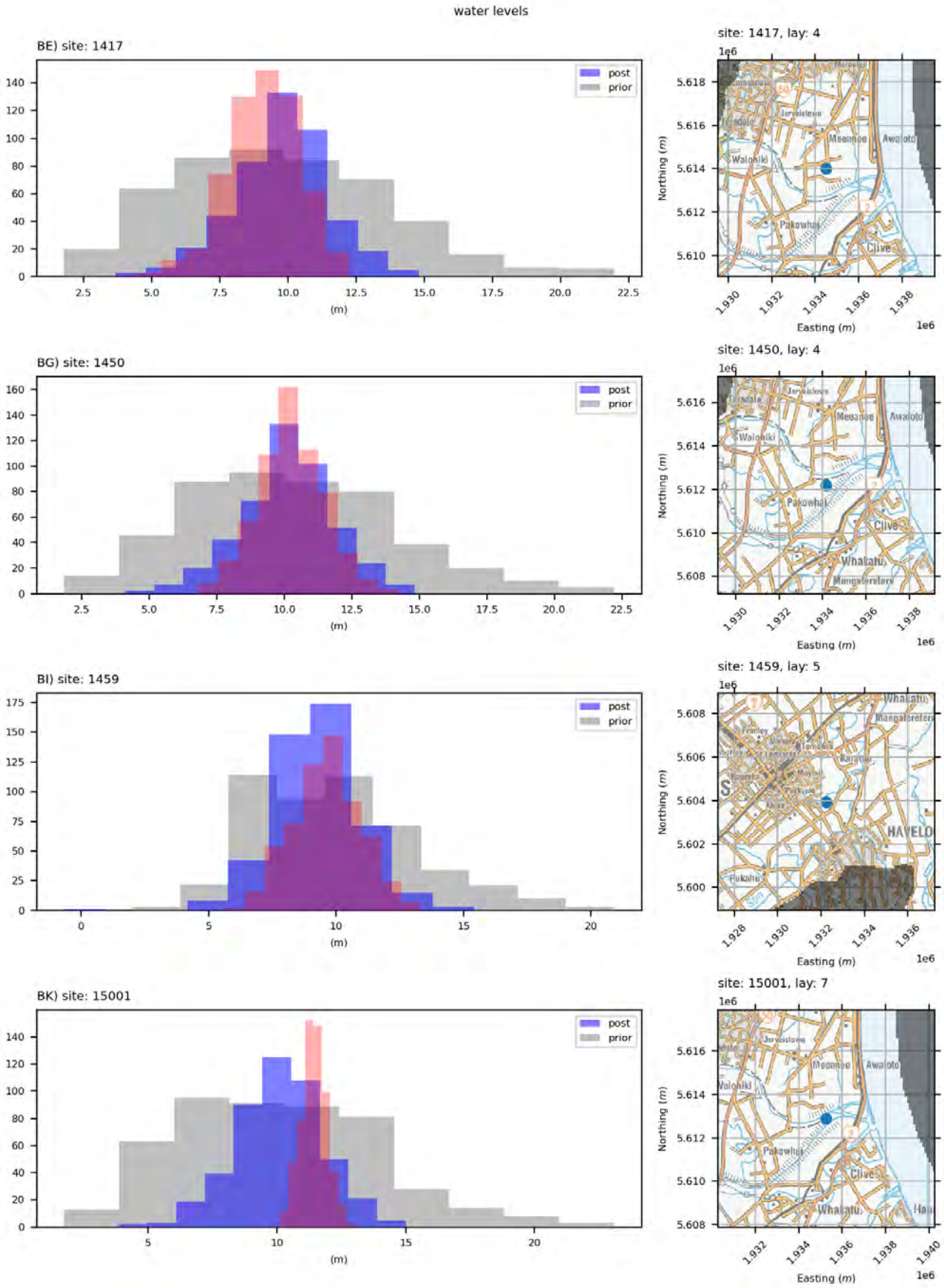
water levels
BE) site: 1417
post
prior
(m)
site: 1417, lay: 4
1e6
Northing (m)
Easting (m)
BG) site: 1450
post
prior
(m)
site: 1450, lay: 4
1e6
Northing (m)
Easting (m)
BI) site: 1459
post
prior
(m)
site: 1459, lay: 5
1e6
Northing (m)
Easting (m)
BK) site: 15001
post
prior
(m)
site: 15001, lay: 7
1e6
Northing (m)
Easting (m)

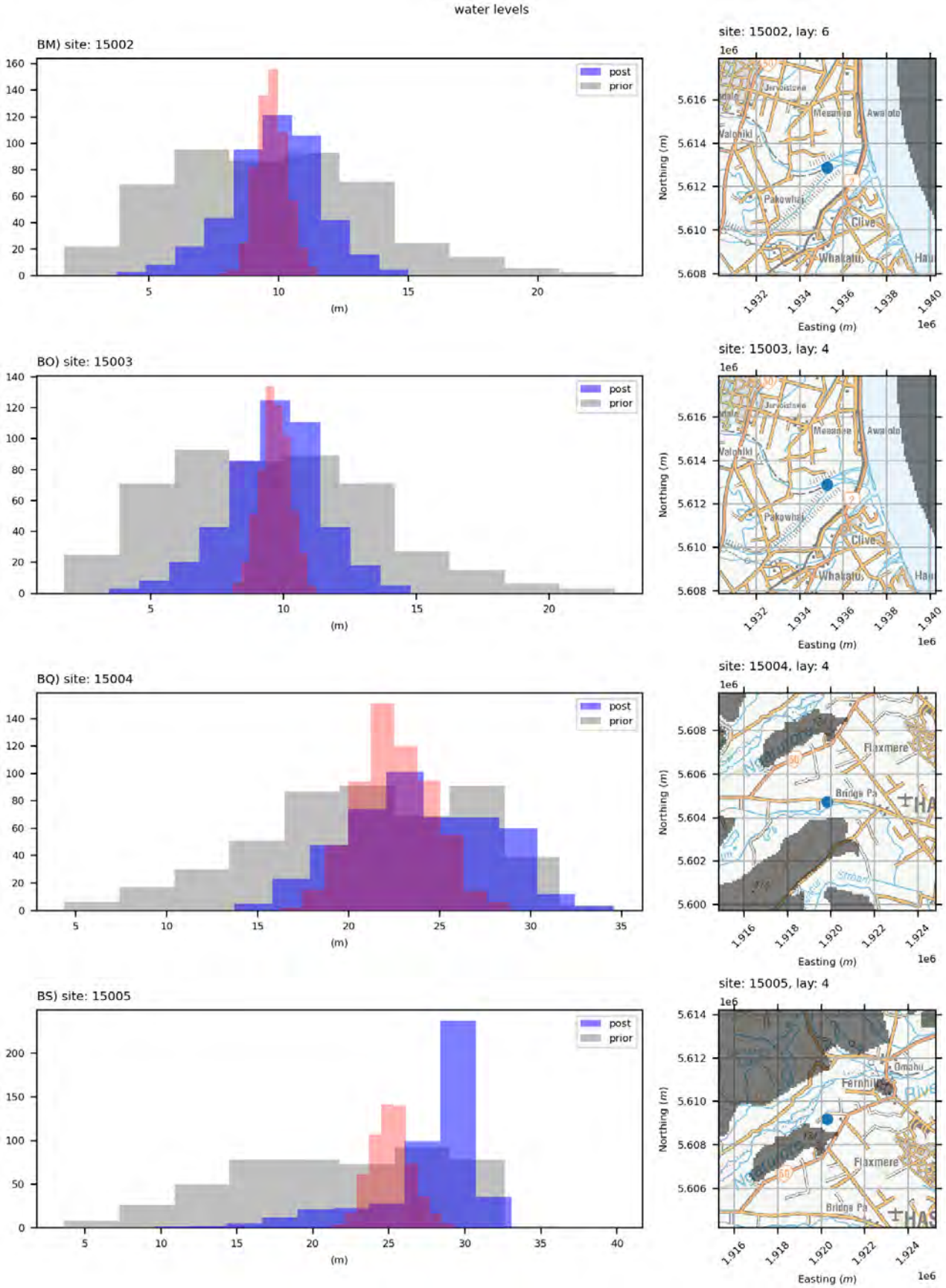
water levels
BM) site: 15002
post
prior
(m)
site: 15002, lay: 6
1e6
Northing (m)
Easting (m)
Pakowhai
Clive
Whakatu
BO) site: 15003
site: 15003, lay: 4
BQ) site: 15004
site: 15004, lay: 4
Flaxmere
Bridge Pa
BS) site: 15005
site: 15005, lay: 4
Fernhill
Omahu

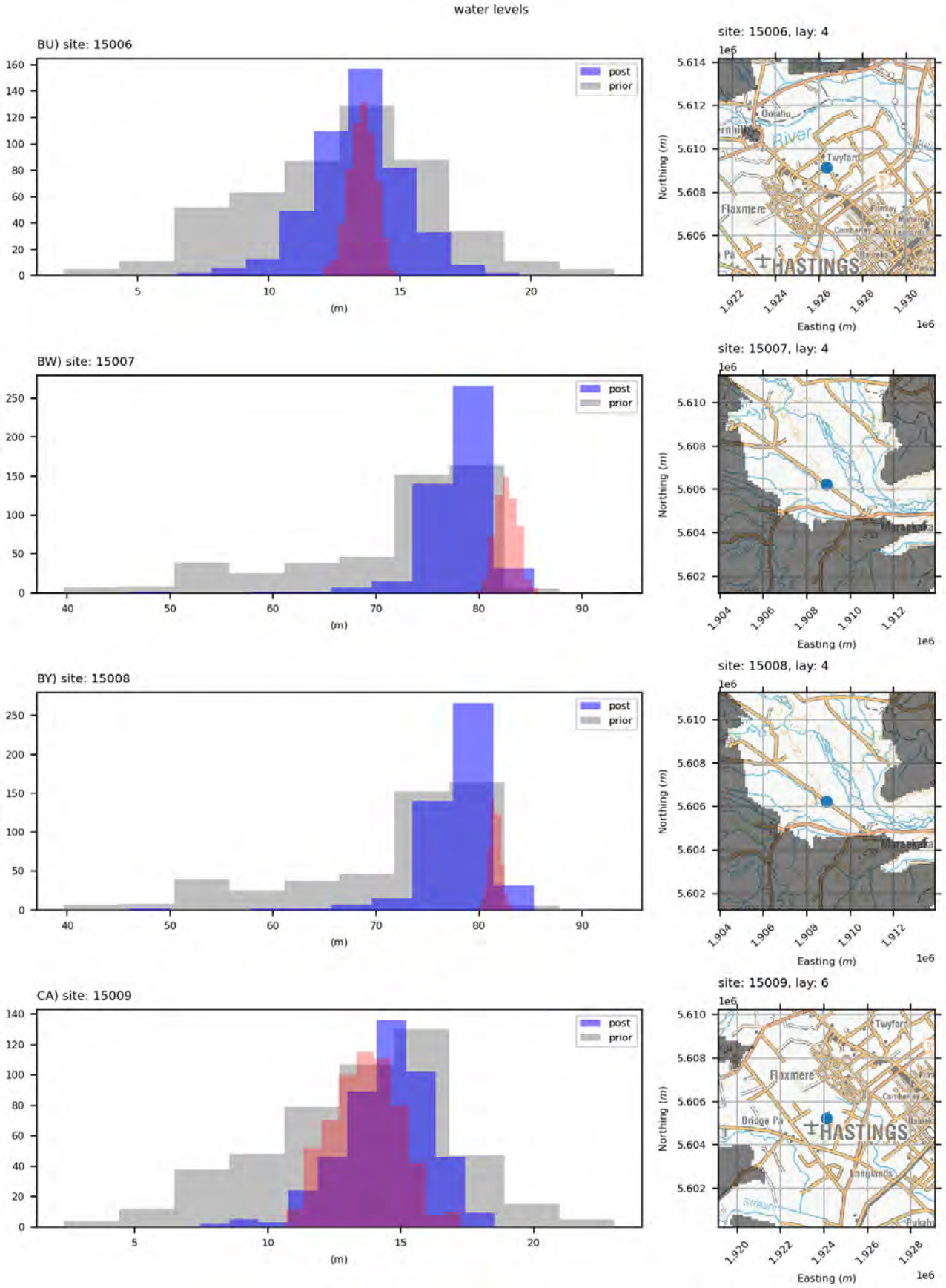
water levels
BU) site: 15006
post
prior
(m)
site: 15006, lay: 4
1e6
Northing (m)
Easting (m)
Omahu
Twyford
Flaxmere
HASTINGS
BW) site: 15007
site: 15007, lay: 4
Maraekakaho
BY) site: 15008
site: 15008, lay: 4
CA) site: 15009
site: 15009, lay: 6
Bridge Pa
Lyndhurst

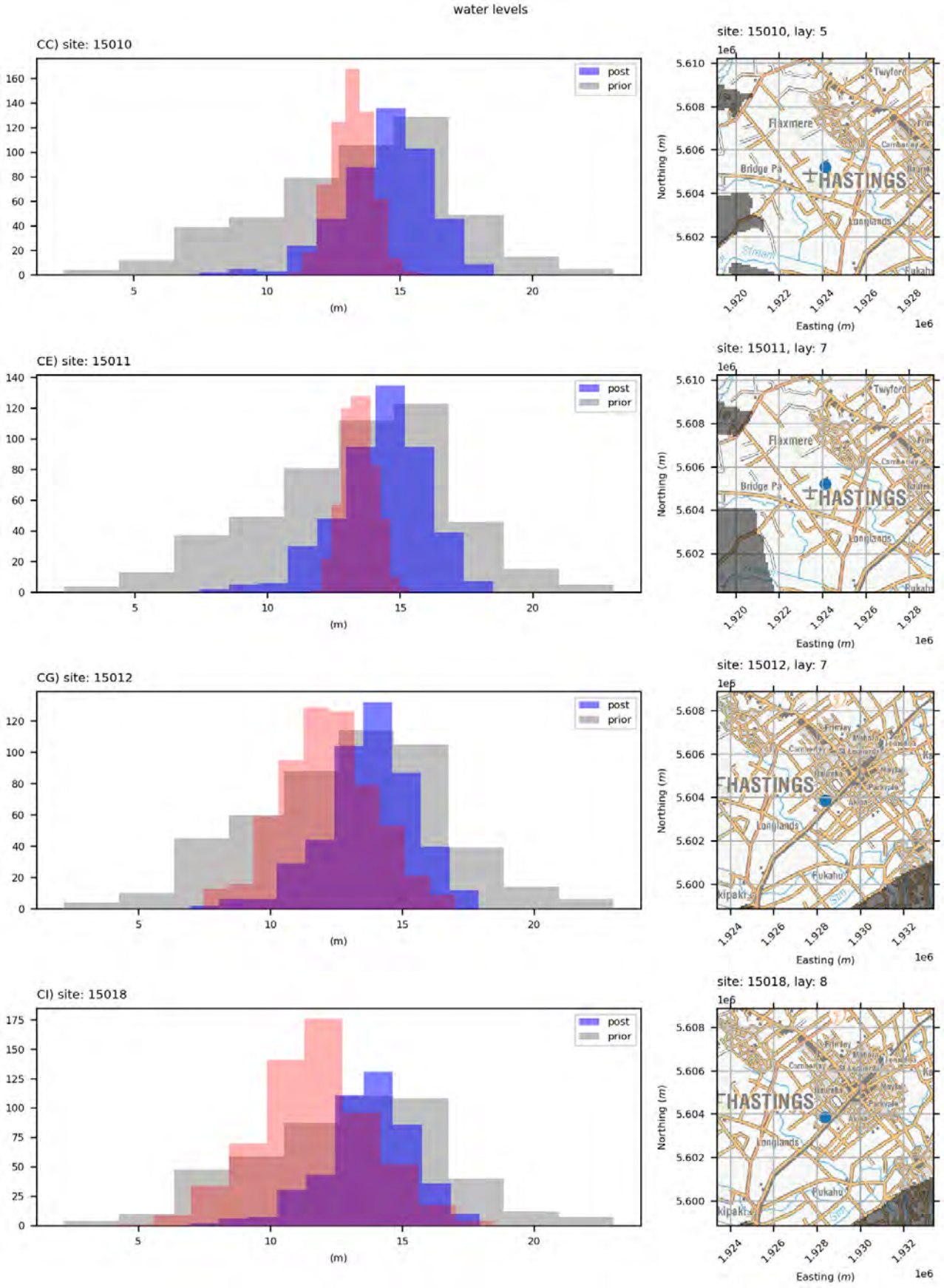
water levels
CC) site: 15010
post
prior
(m)
site: 15010, lay: 5
Northing (m)
Easting (m)
1e6
Twyford
Flaxmere
Bridge Pa
HASTINGS
Longlands
Fukahu
CE) site: 15011
site: 15011, lay: 7
CG) site: 15012
site: 15012, lay: 7
CI) site: 15018
site: 15018, lay: 8

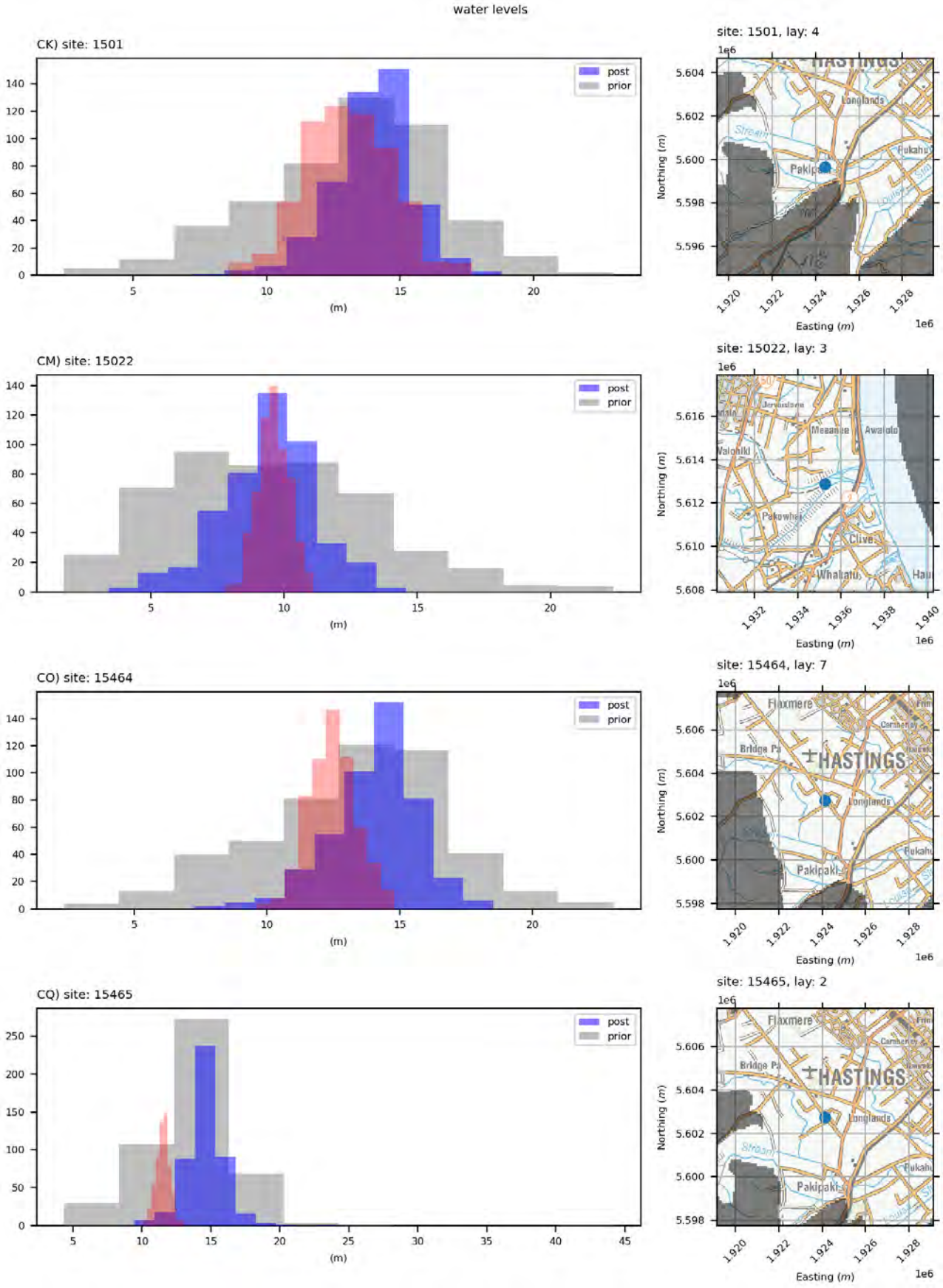
water levels
CK) site: 1501
post
prior
(m)
site: 1501, lay: 4
1e6
Northing (m)
Easting (m)
CM) site: 15022
site: 15022, lay: 3
CO) site: 15464
site: 15464, lay: 7
CQ) site: 15465
site: 15465, lay: 2
HASTINGS
Flaxmere
Longlands
Pakipaki
Pukahu
Awatoto
Clive
Whakatu

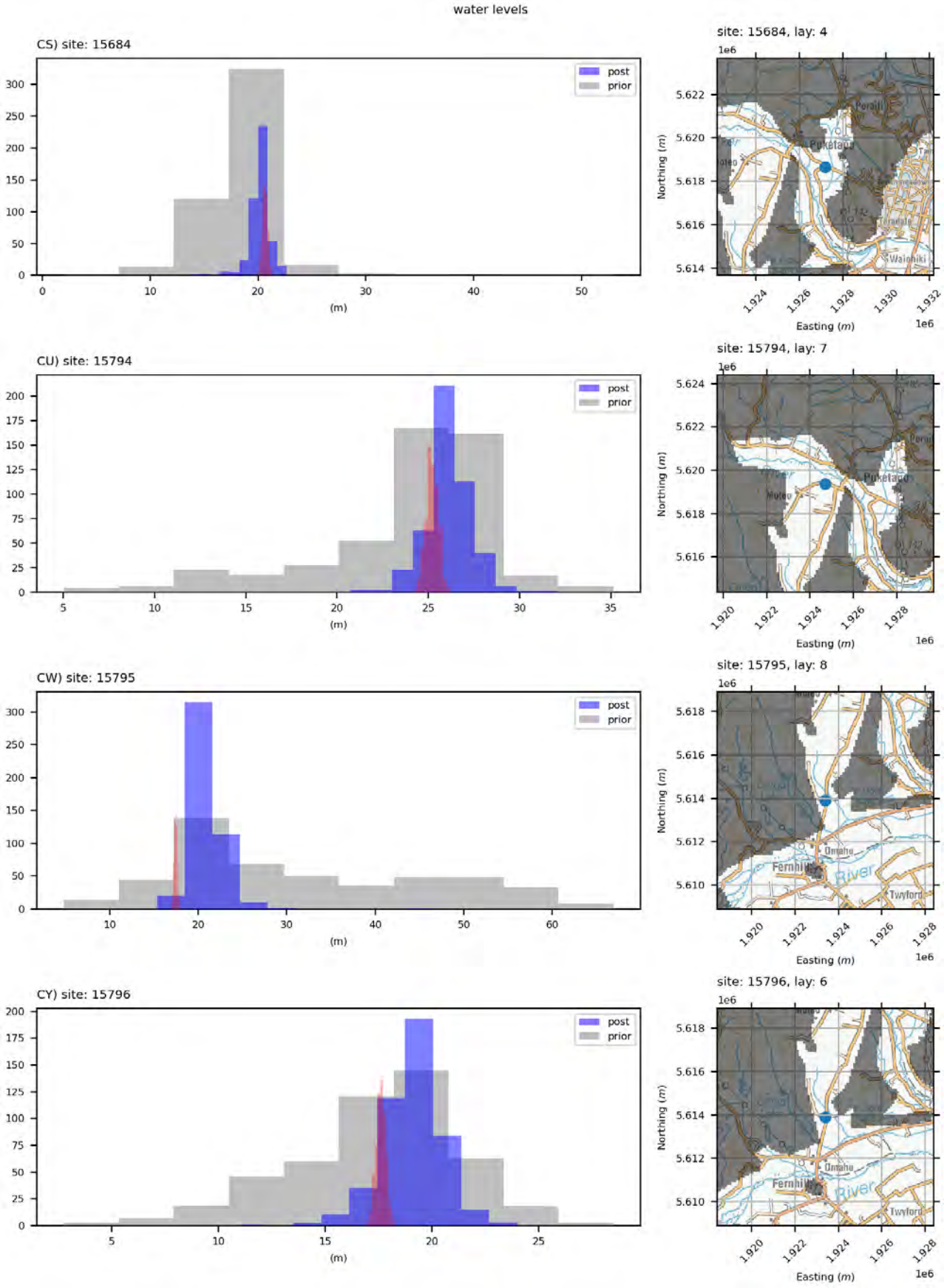
water levels
CS) site: 15684
post
prior
(m)
site: 15684, lay: 4
1e6
Northing (m)
Easting (m)
Pukekaha
Waiohiki
CU) site: 15794
site: 15794, lay: 7
Pukekaha
Muteo
CW) site: 15795
site: 15795, lay: 8
Omahu
Fernhill
River
Twyford
CY) site: 15796
site: 15796, lay: 6

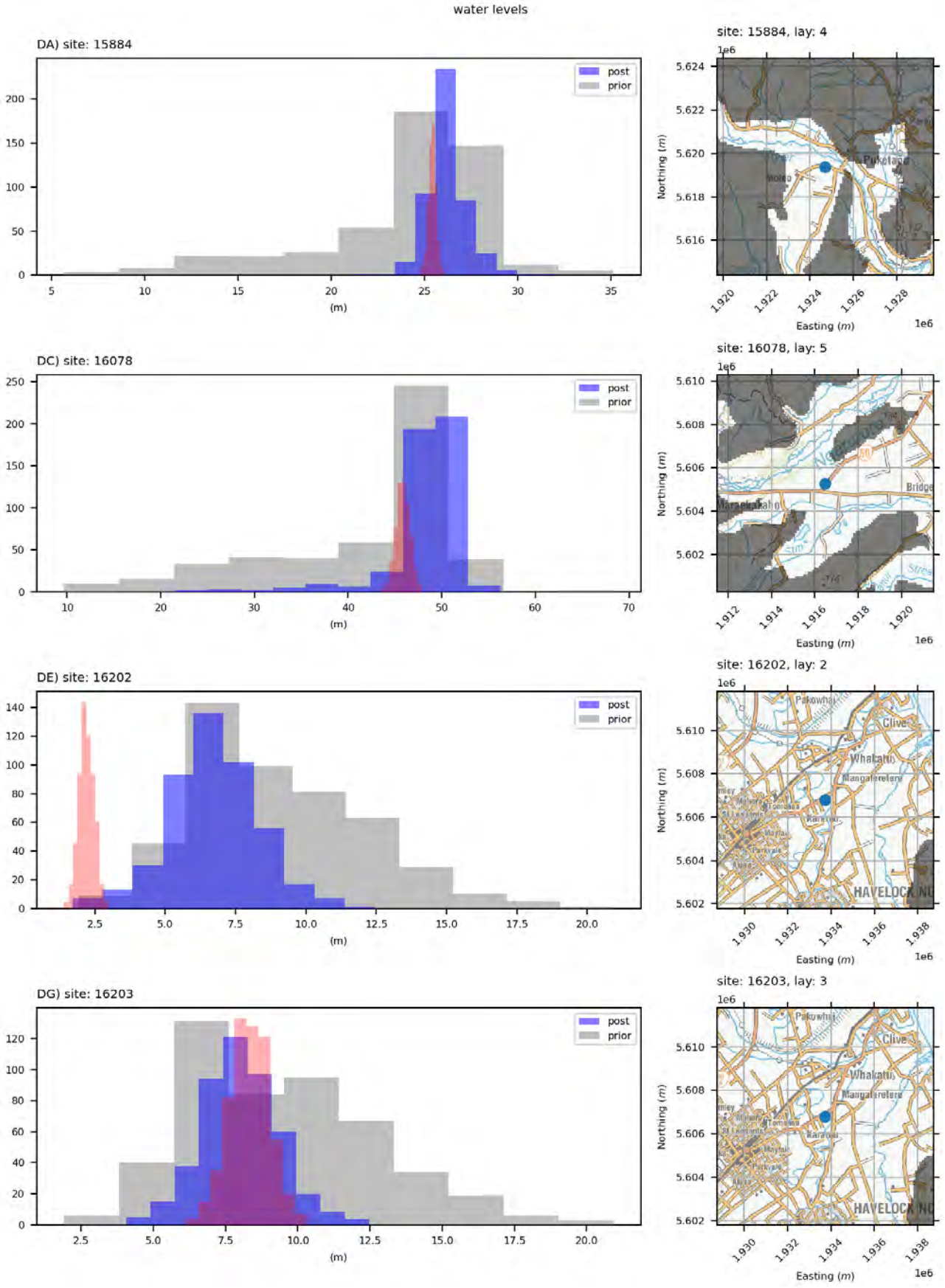
water levels
DA) site: 15884
post
prior
(m)
site: 15884, lay: 4
Northing (m)
Easting (m)
1e6
DC) site: 16078
post
prior
(m)
site: 16078, lay: 5
Northing (m)
Easting (m)
1e6
DE) site: 16202
post
prior
(m)
site: 16202, lay: 2
Northing (m)
Easting (m)
1e6
DG) site: 16203
post
prior
(m)
site: 16203, lay: 3
Northing (m)
Easting (m)
1e6

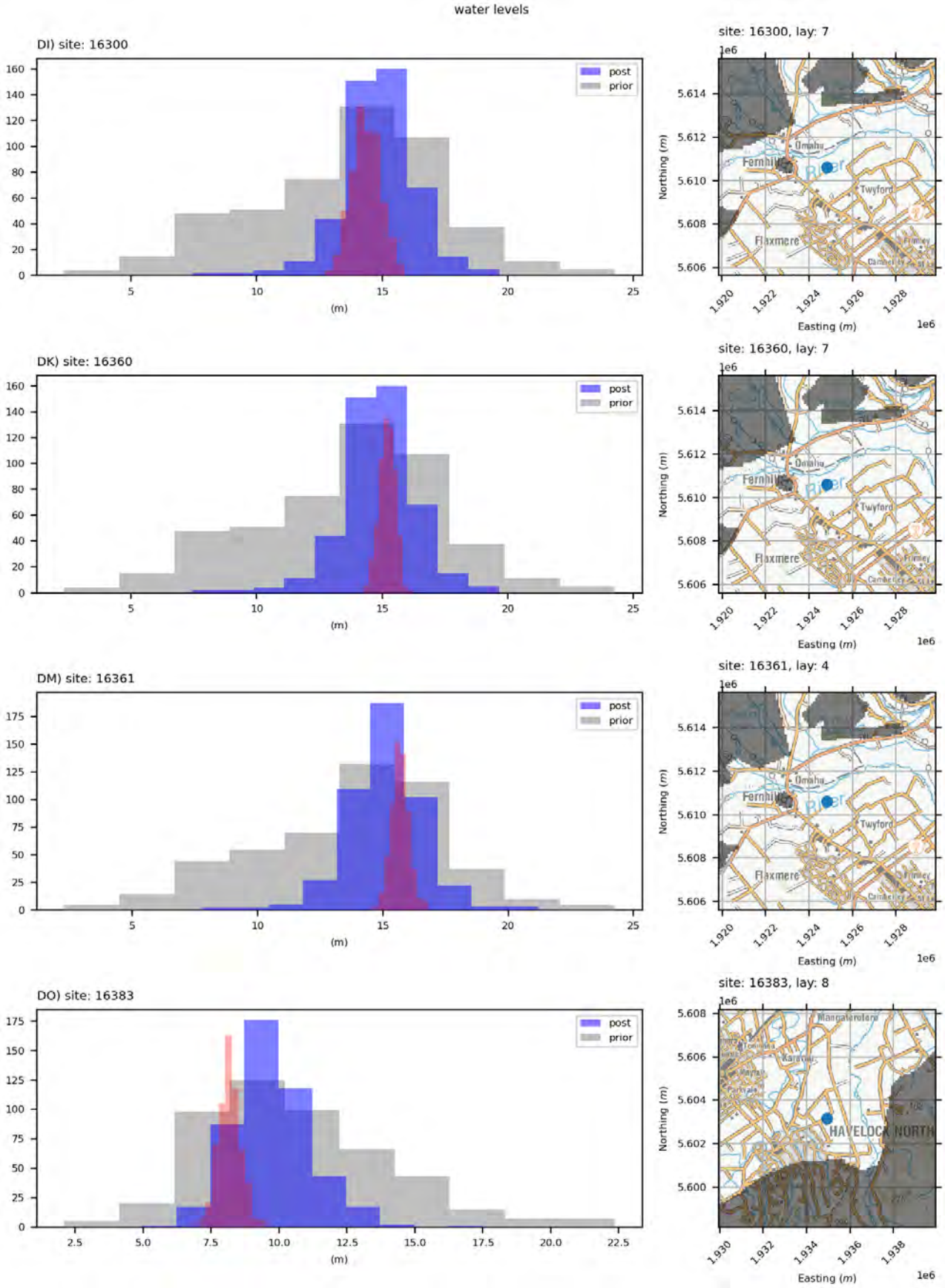
water levels
DI) site: 16300
post
prior
(m)
site: 16300, lay: 7
Northing (m)
Easting (m)
DK) site: 16360
site: 16360, lay: 7
DM) site: 16361
site: 16361, lay: 4
DO) site: 16383
site: 16383, lay: 8
HAVELOCK NORTH

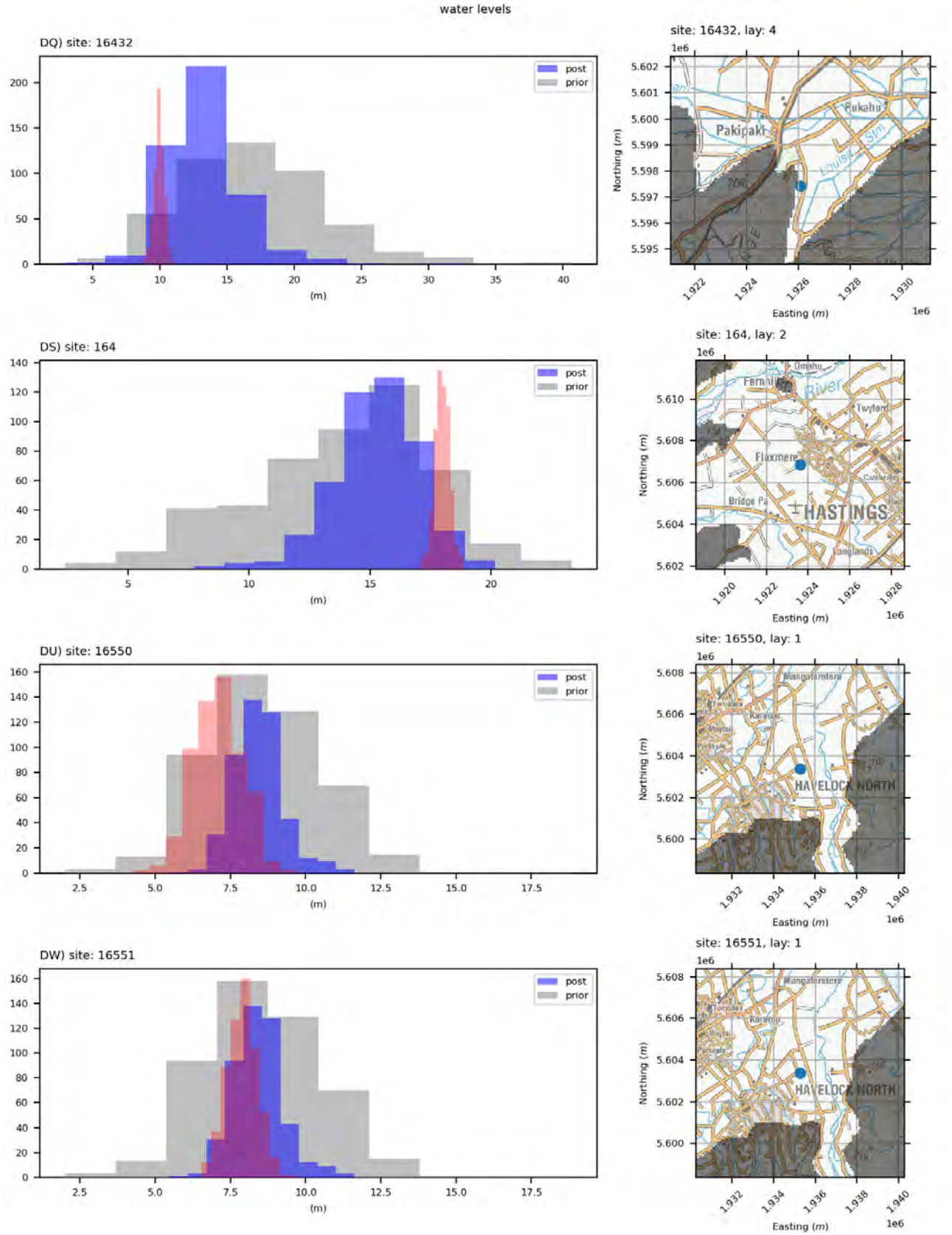
water levels
DQ) site: 16432
post
prior
(m)
site: 16432, lay: 4
1e6
Pukahu
Pakipaki
Louise Stm
Northing (m)
Easting (m)
DS) site: 164
site: 164, lay: 2
Omahu
Fernhill
River
Twyford
Flaxmere
Bridge Pa
HASTINGS
Longlands
DU) site: 16550
site: 16550, lay: 1
Mangateretere
HAVELOCK NORTH
DW) site: 16551
site: 16551, lay: 1

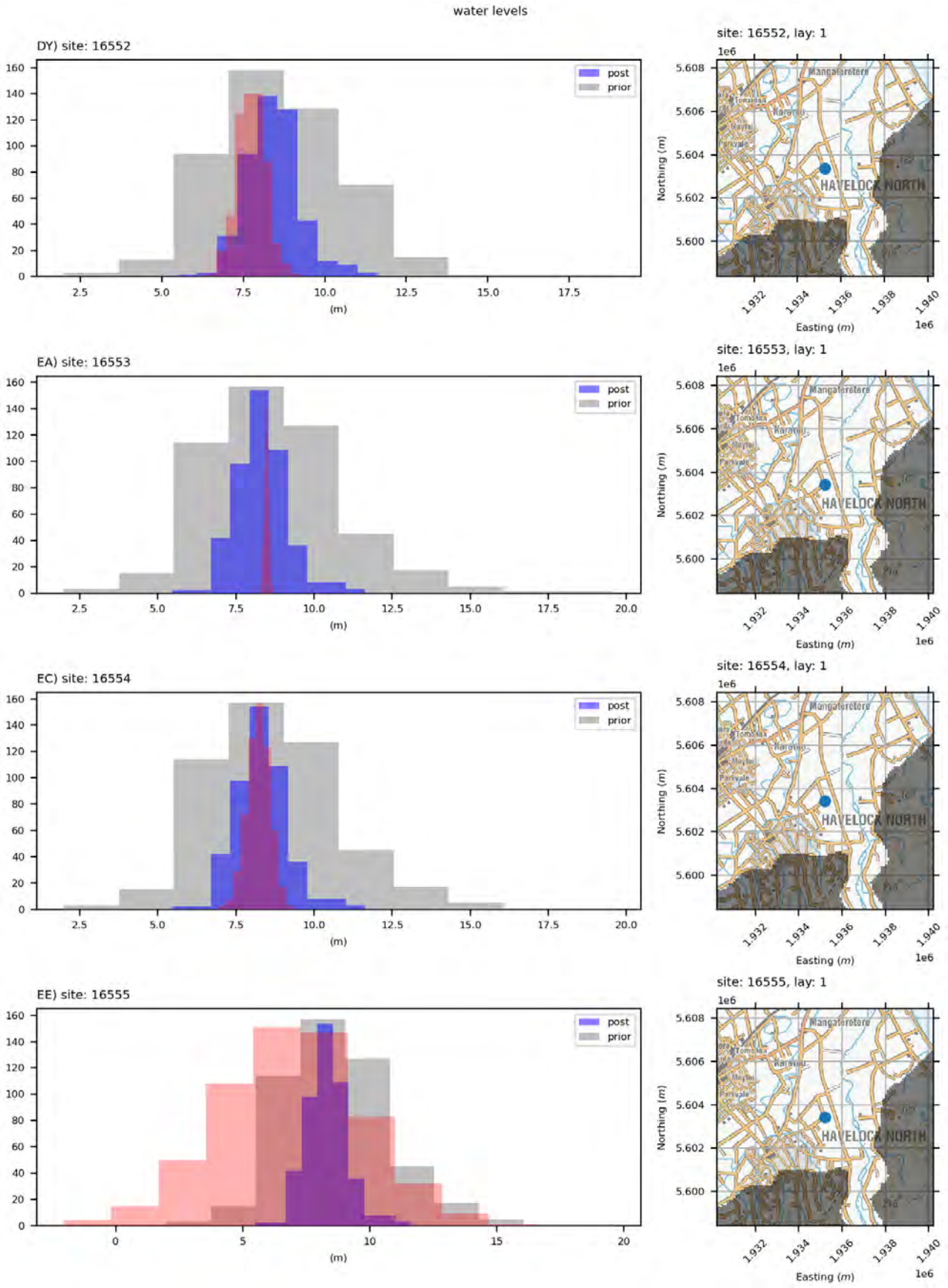
water levels
DY) site: 16552
post
prior
(m)
site: 16552, lay: 1
1e6
Northing (m)
Easting (m)
HAVELOCK NORTH
EA) site: 16553
site: 16553, lay: 1
EC) site: 16554
site: 16554, lay: 1
EE) site: 16555
site: 16555, lay: 1

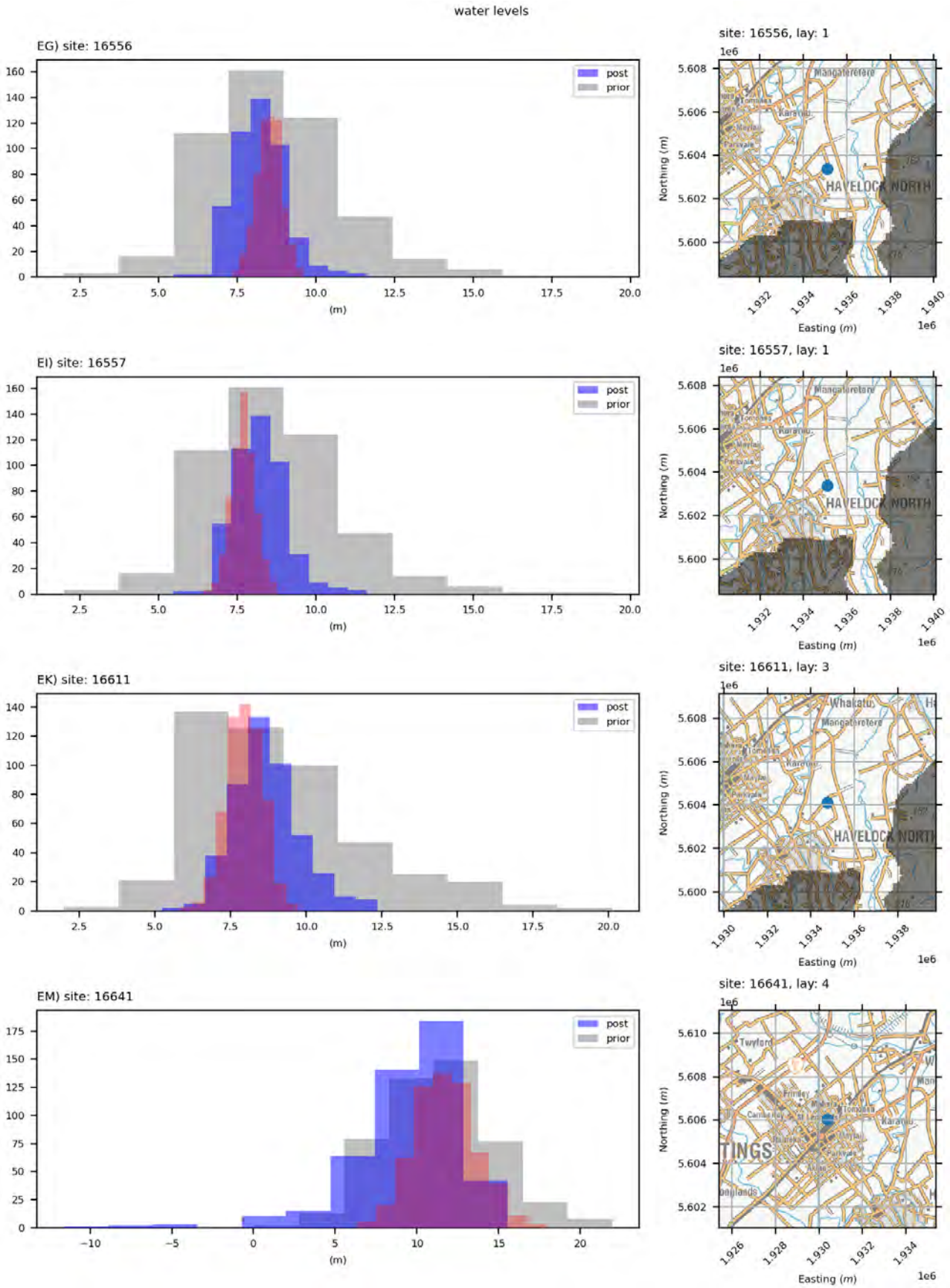
water levels
EG) site: 16556
post
prior
(m)
site: 16556, lay: 1
1e6
Northing (m)
Easting (m)
HAVELOCK NORTH
EI) site: 16557
post
prior
(m)
site: 16557, lay: 1
1e6
Northing (m)
Easting (m)
HAVELOCK NORTH
EK) site: 16611
post
prior
(m)
site: 16611, lay: 3
1e6
Northing (m)
Easting (m)
HAVELOCK NORTH
EM) site: 16641
post
prior
(m)
site: 16641, lay: 4
1e6
Northing (m)
Easting (m)
TINGS

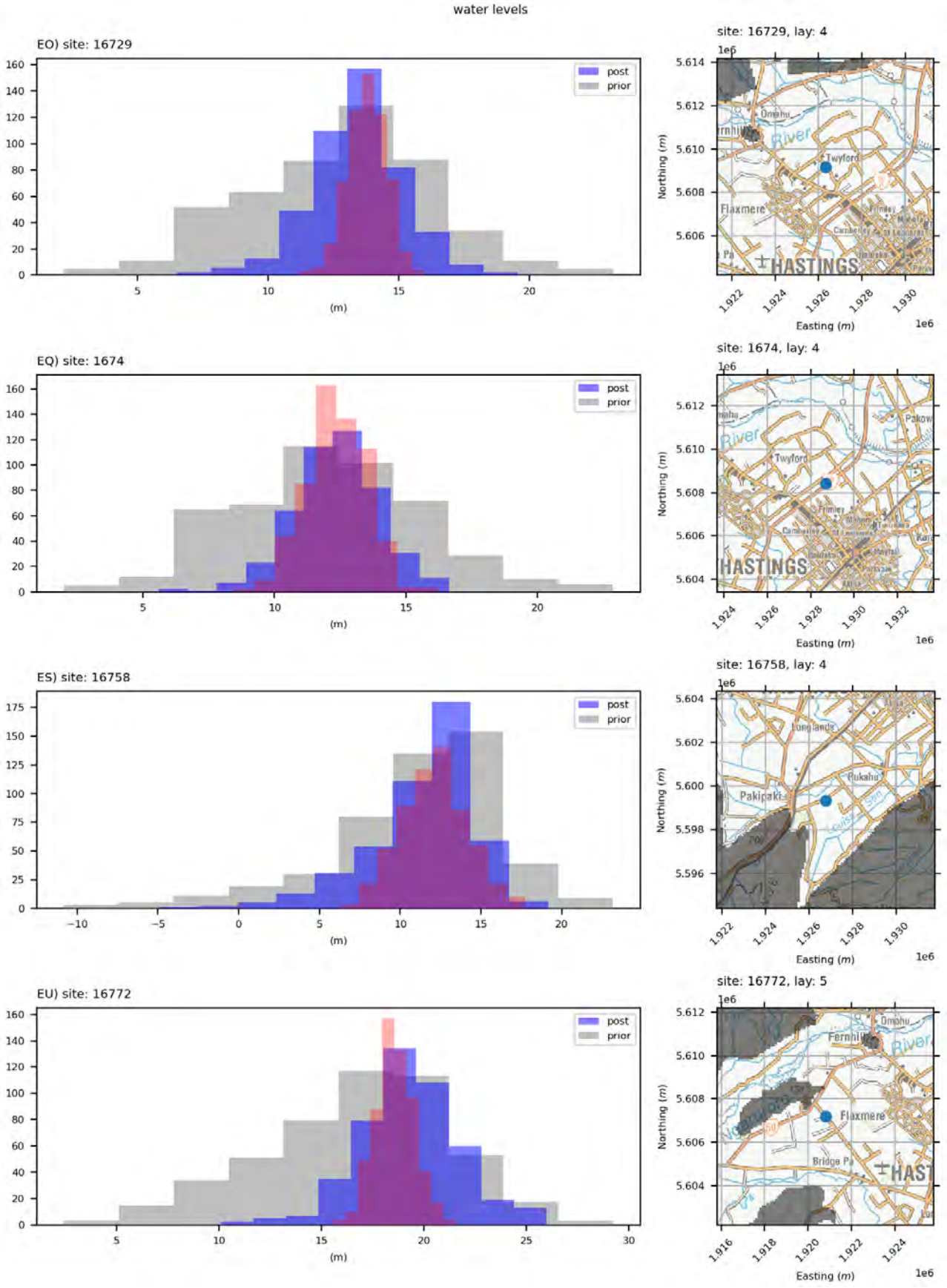
water levels
EO) site: 16729
post
prior
(m)
site: 16729, lay: 4
1e6
Northing (m)
Easting (m)
Omahu
Twyford
Flaxmere
HASTINGS
EQ) site: 1674
site: 1674, lay: 4
Pakowhai
ES) site: 16758
site: 16758, lay: 4
Longlands
Pukahu
Pakipaki
EU) site: 16772
site: 16772, lay: 5
Fernhill
Bridge Pa

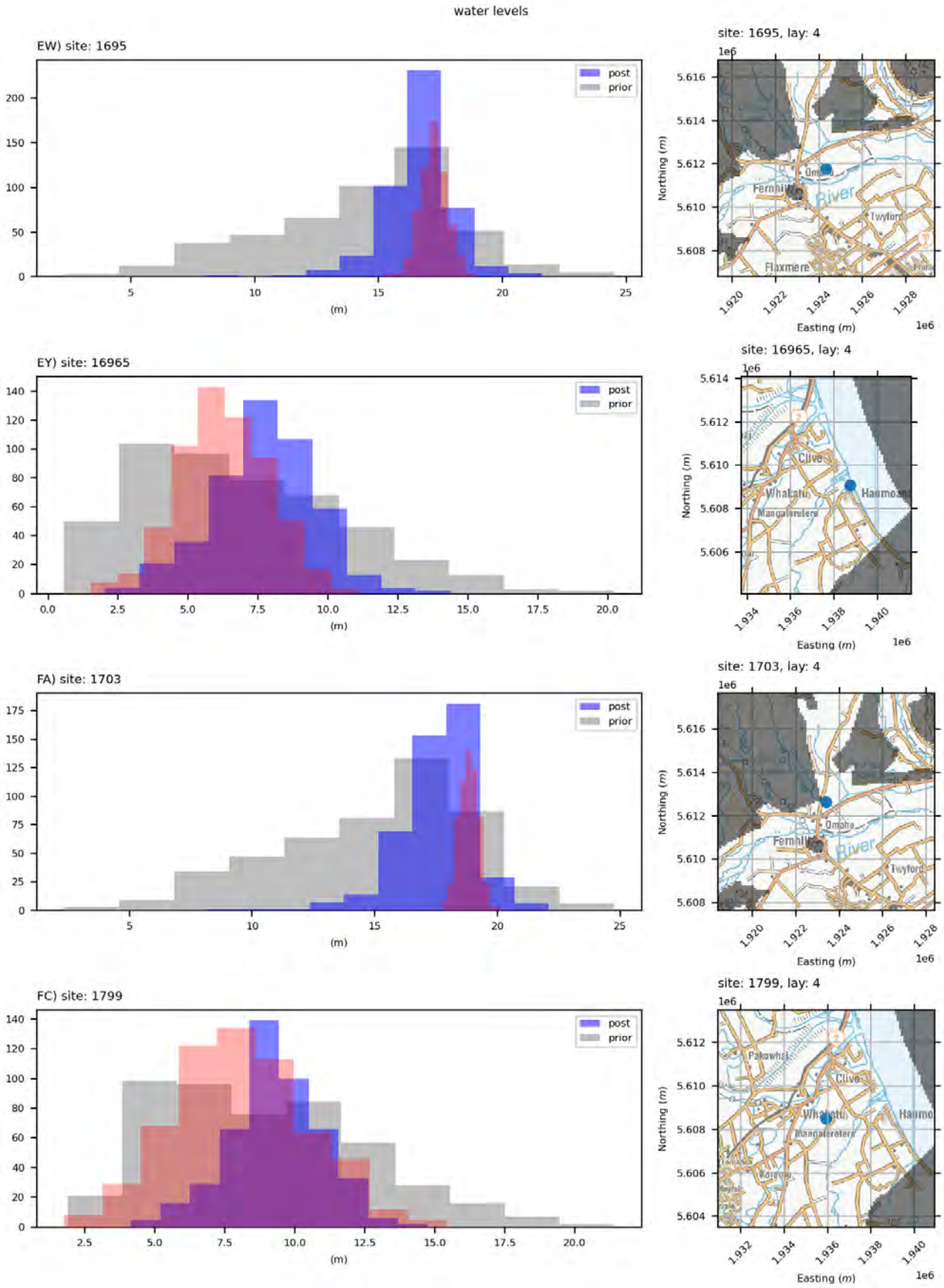
water levels
EW) site: 1695
post
prior
(m)
site: 1695, lay: 4
Northing (m)
Easting (m)
1e6
Omaha
Fernhill
River
Twyford
Flaxmere
EY) site: 16965
site: 16965, lay: 4
Clive
Whakatu
Hawkes Bay
Mangateretere
FA) site: 1703
site: 1703, lay: 4
FC) site: 1799
site: 1799, lay: 4
Pakowhai
Haumo

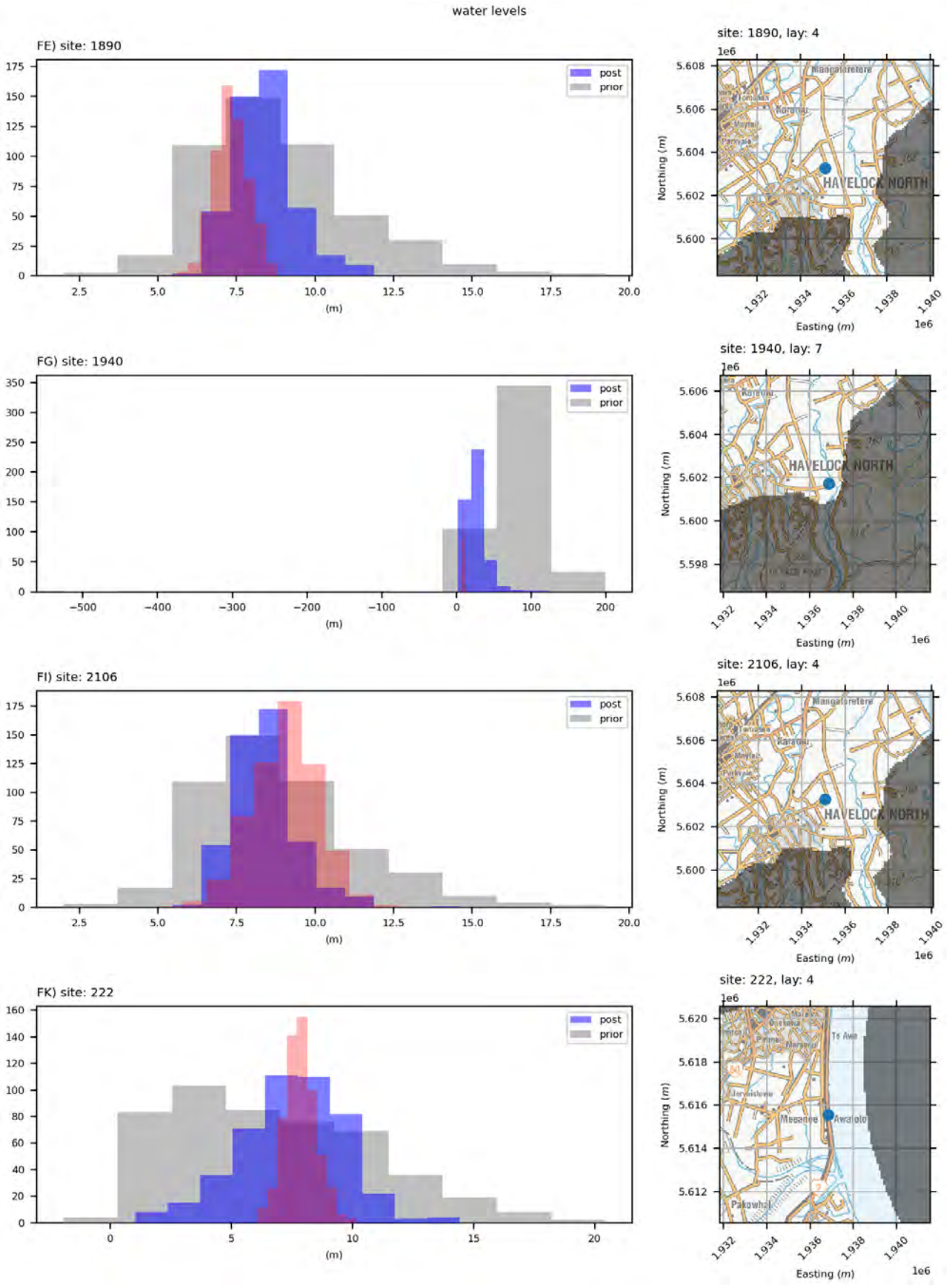
water levels
FE) site: 1890
post
prior
(m)
site: 1890, lay: 4
1e6
Northing (m)
Easting (m)
HAVELOCK NORTH
FG) site: 1940
post
prior
(m)
site: 1940, lay: 7
1e6
Northing (m)
Easting (m)
HAVELOCK NORTH
FI) site: 2106
post
prior
(m)
site: 2106, lay: 4
1e6
Northing (m)
Easting (m)
HAVELOCK NORTH
FK) site: 222
post
prior
(m)
site: 222, lay: 4
1e6
Northing (m)
Easting (m)
Te Awa
Awatoto
Meeanee
Pakowhai

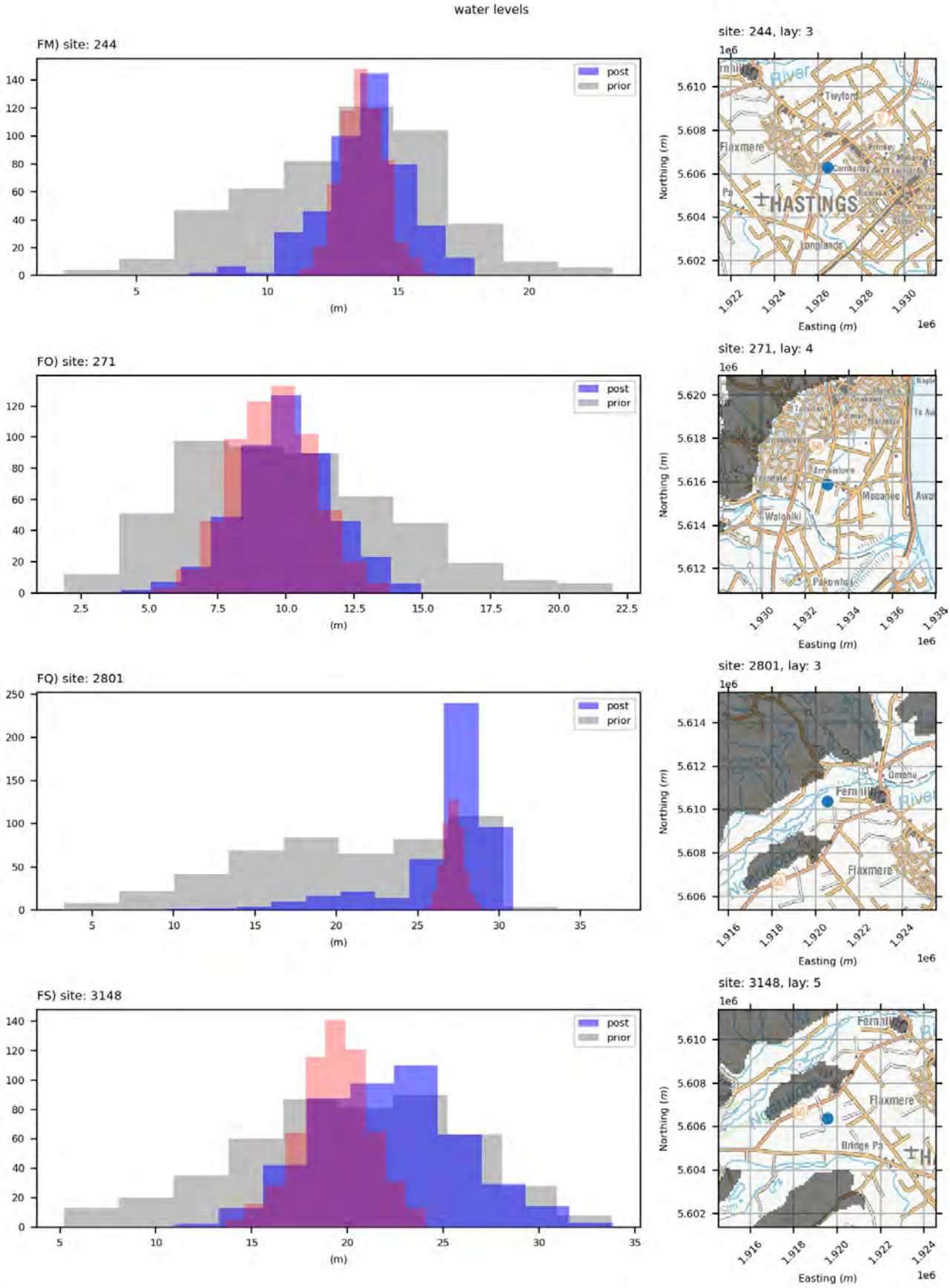
water levels
FM) site: 244
post
prior
(m)
site: 244, lay: 3
Northing (m)
Easting (m)
1e6
Twyford
Flaxmere
HASTINGS
Longlands
FO) site: 271
site: 271, lay: 4
Meeanee
Waiohiki
Pakowhai
FQ) site: 2801
site: 2801, lay: 3
Fernhill
Omahu
Flaxmere
FS) site: 3148
site: 3148, lay: 5
Bridge Pa

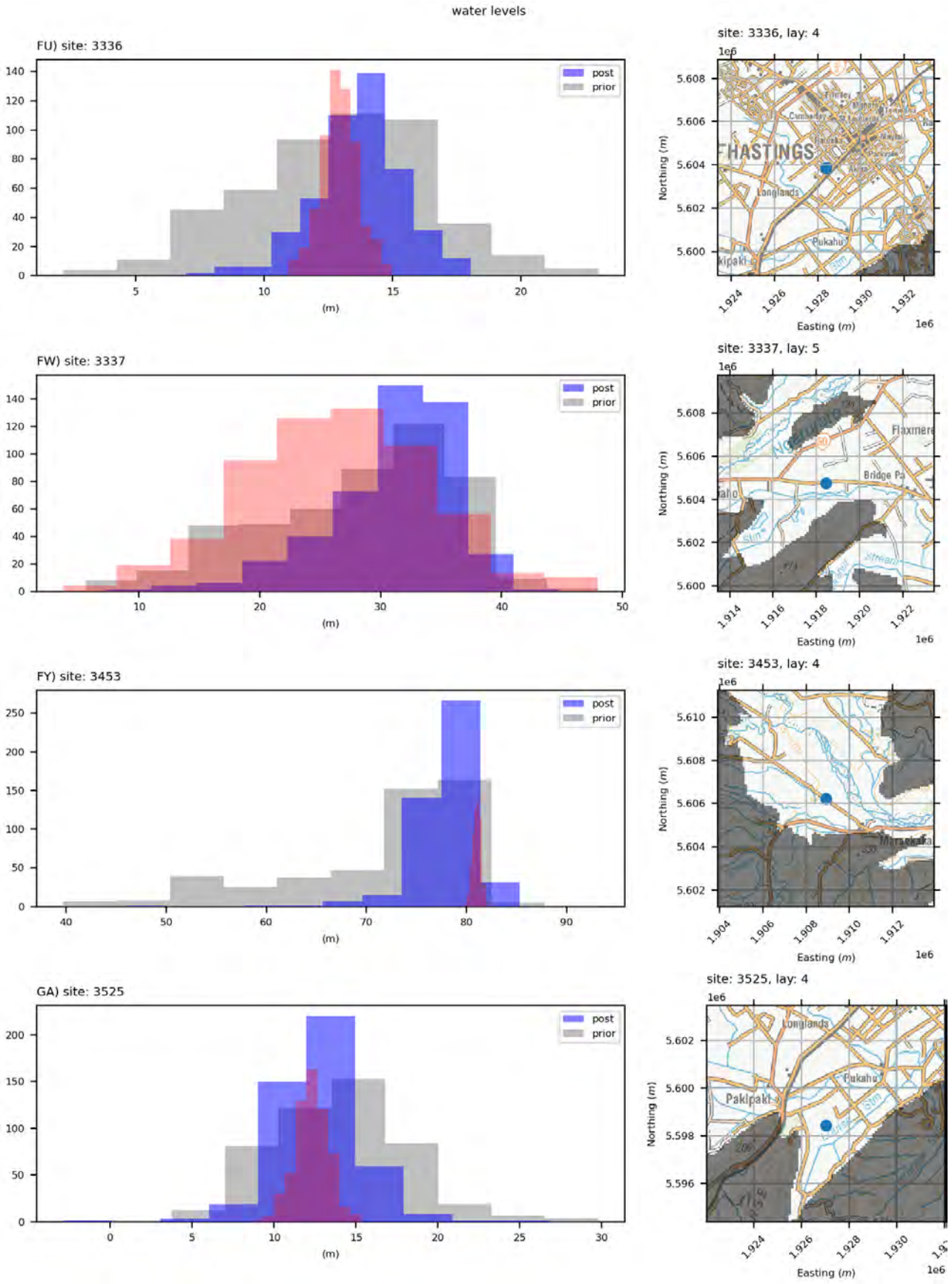
water levels
FU) site: 3336
post
prior
(m)
site: 3336, lay: 4
1e6
Northing (m)
Easting (m)
HASTINGS
Longlands
Pukahu
FW) site: 3337
site: 3337, lay: 5
Flaxmere
Bridge Pa
FY) site: 3453
site: 3453, lay: 4
GA) site: 3525
site: 3525, lay: 4
Pakipaki

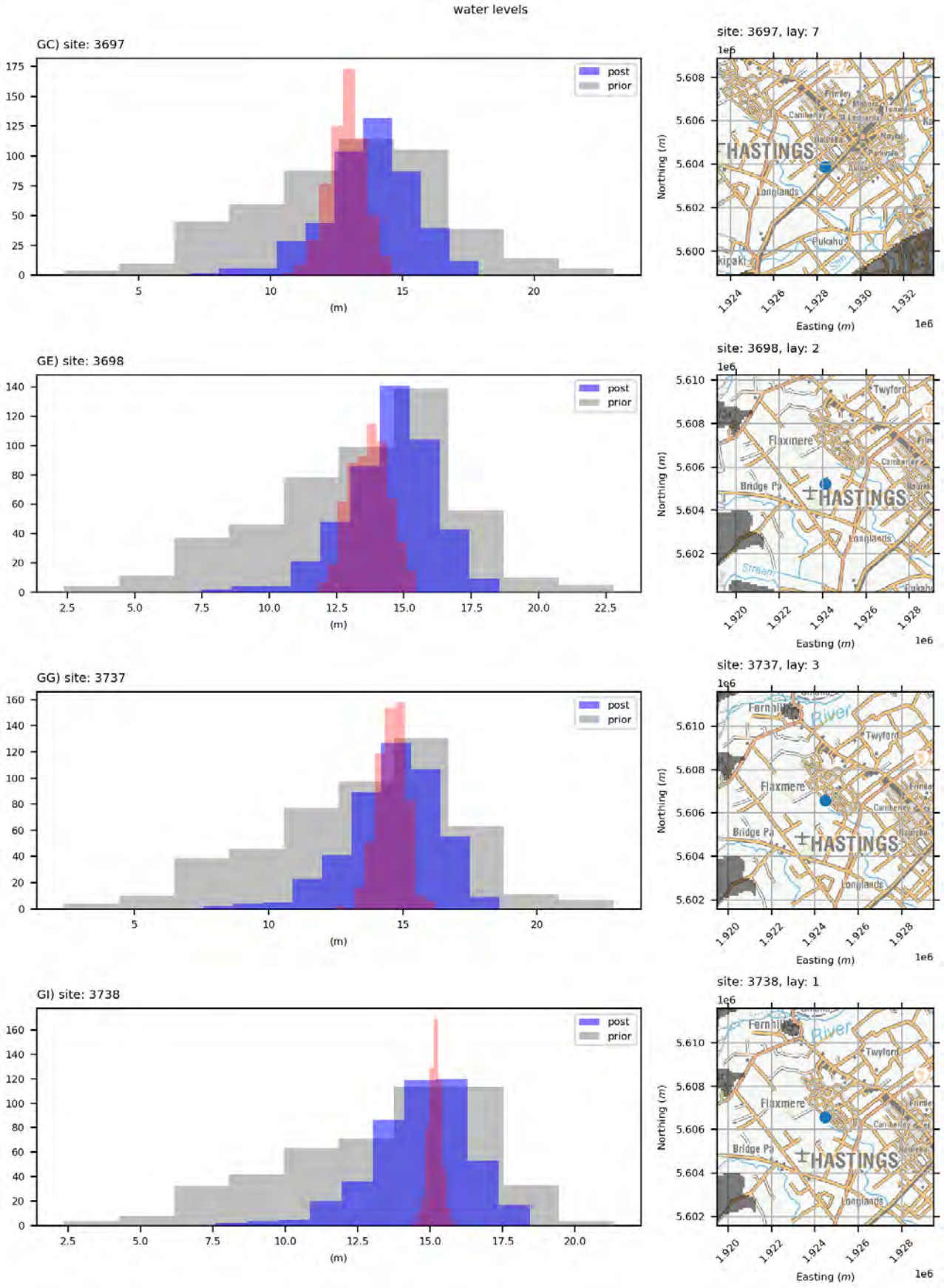
water levels
GC) site: 3697
post
prior
(m)
site: 3697, lay: 7
Northing (m)
Easting (m)
HASTINGS
GE) site: 3698
site: 3698, lay: 2
GG) site: 3737
site: 3737, lay: 3
GI) site: 3738
site: 3738, lay: 1

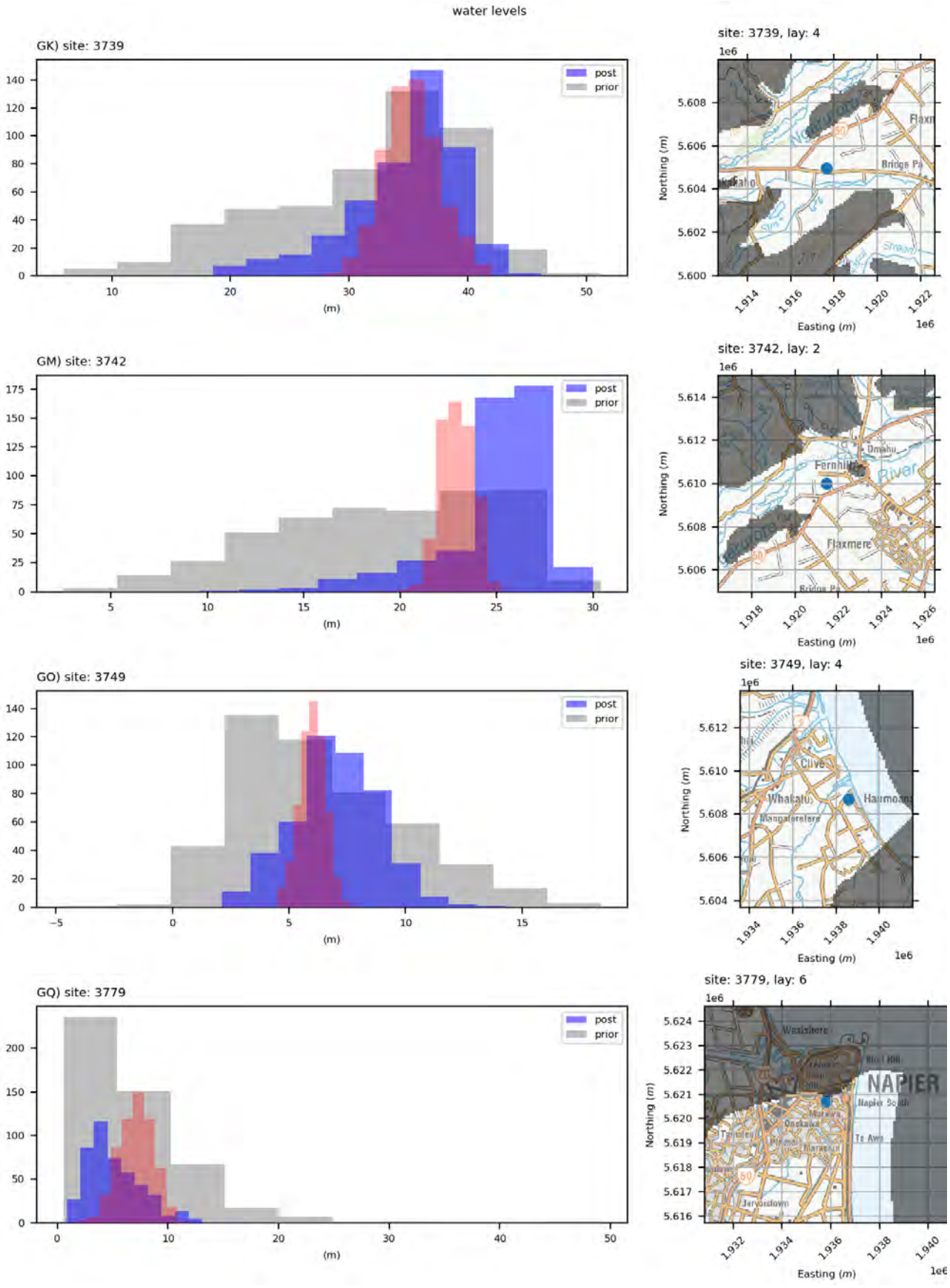
water levels
GK) site: 3739
post
prior
(m)
site: 3739, lay: 4
1e6
Northing (m)
Easting (m)
GM) site: 3742
site: 3742, lay: 2
Fernhill
Flaxmere
River
GO) site: 3749
site: 3749, lay: 4
Clive
Whakatu
Haumoana
GQ) site: 3779
site: 3779, lay: 6
NAPIER
Westshore
Napier South
Onekawa
Te Awa
Taradale
Jervoistown

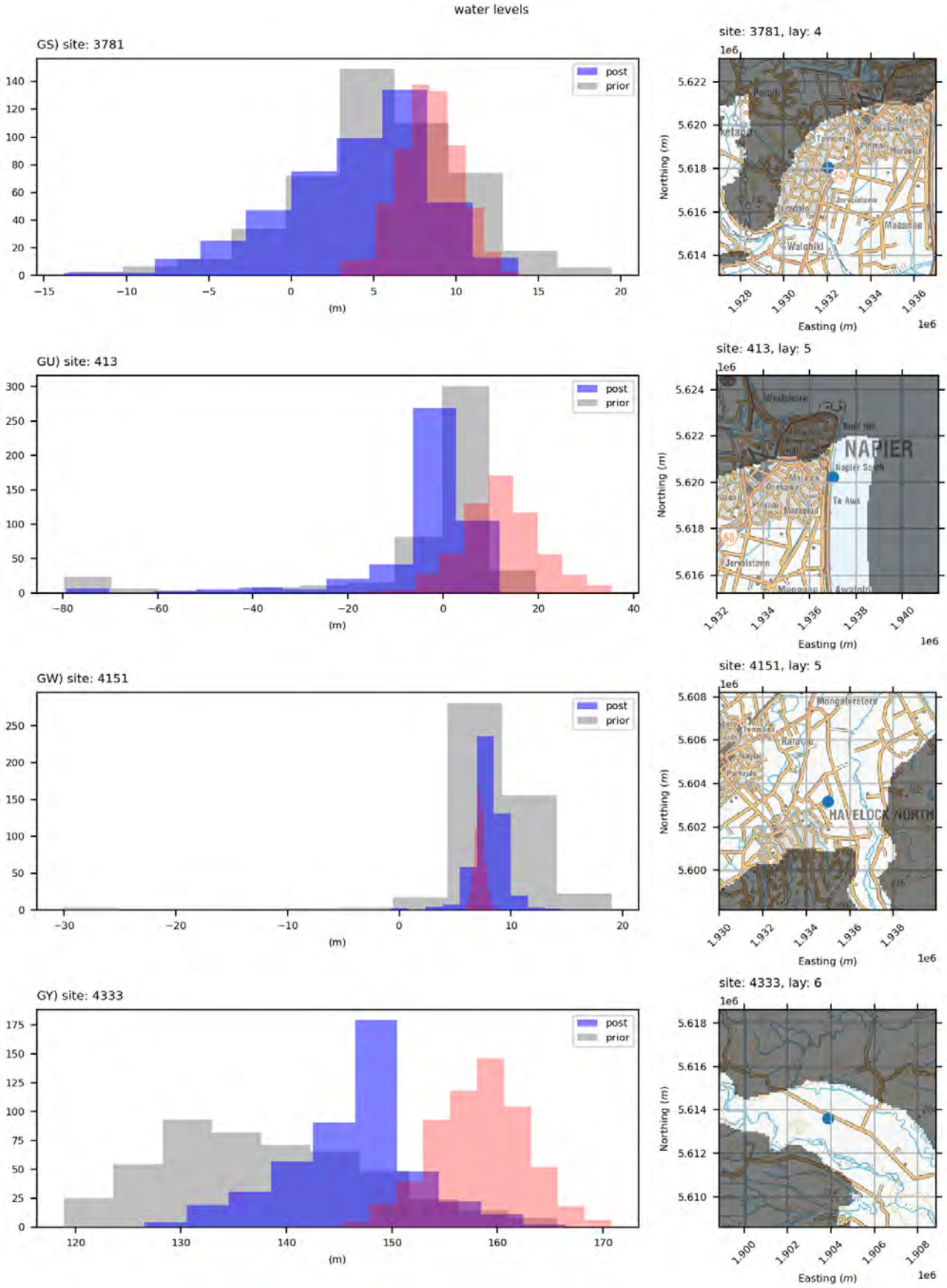
water levels
GS) site: 3781
post
prior
(m)
site: 3781, lay: 4
1e6
Northing (m)
Easting (m)
GU) site: 413
site: 413, lay: 5
NAPIER
Napier South
Te Awa
Jervoistown
GW) site: 4151
site: 4151, lay: 5
HAVELOCK NORTH
GY) site: 4333
site: 4333, lay: 6

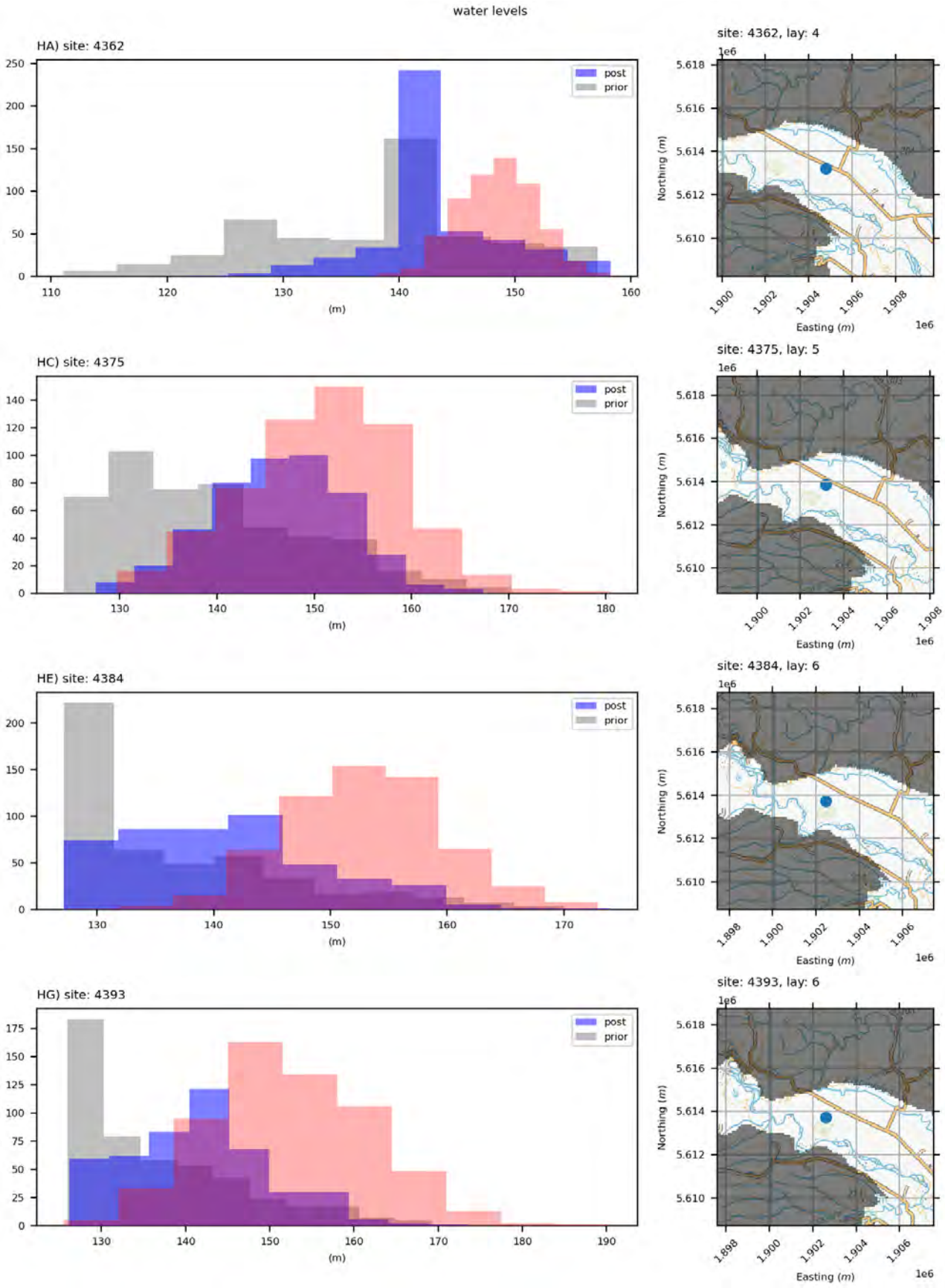
water levels
HA) site: 4362
post
prior
(m)
site: 4362, lay: 4
1e6
Northing (m)
Easting (m)
HC) site: 4375
site: 4375, lay: 5
HE) site: 4384
site: 4384, lay: 6
HG) site: 4393
site: 4393, lay: 6

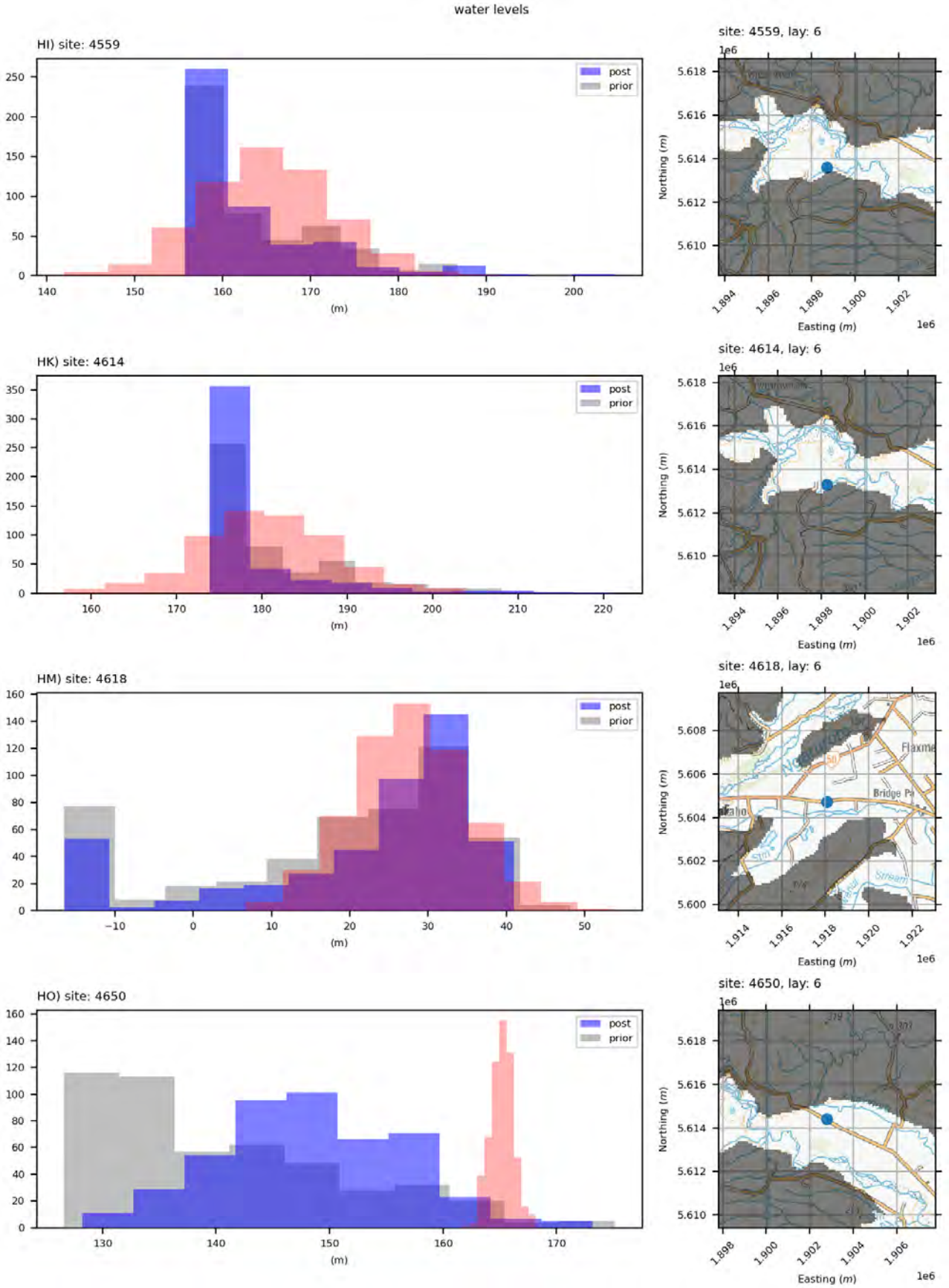
water levels
HI) site: 4559
post
prior
(m)
site: 4559, lay: 6
1e6
Northing (m)
Easting (m)
HK) site: 4614
post
prior
(m)
site: 4614, lay: 6
1e6
Northing (m)
Easting (m)
HM) site: 4618
post
prior
(m)
site: 4618, lay: 6
1e6
Northing (m)
Easting (m)
HO) site: 4650
post
prior
(m)
site: 4650, lay: 6
1e6
Northing (m)
Easting (m)

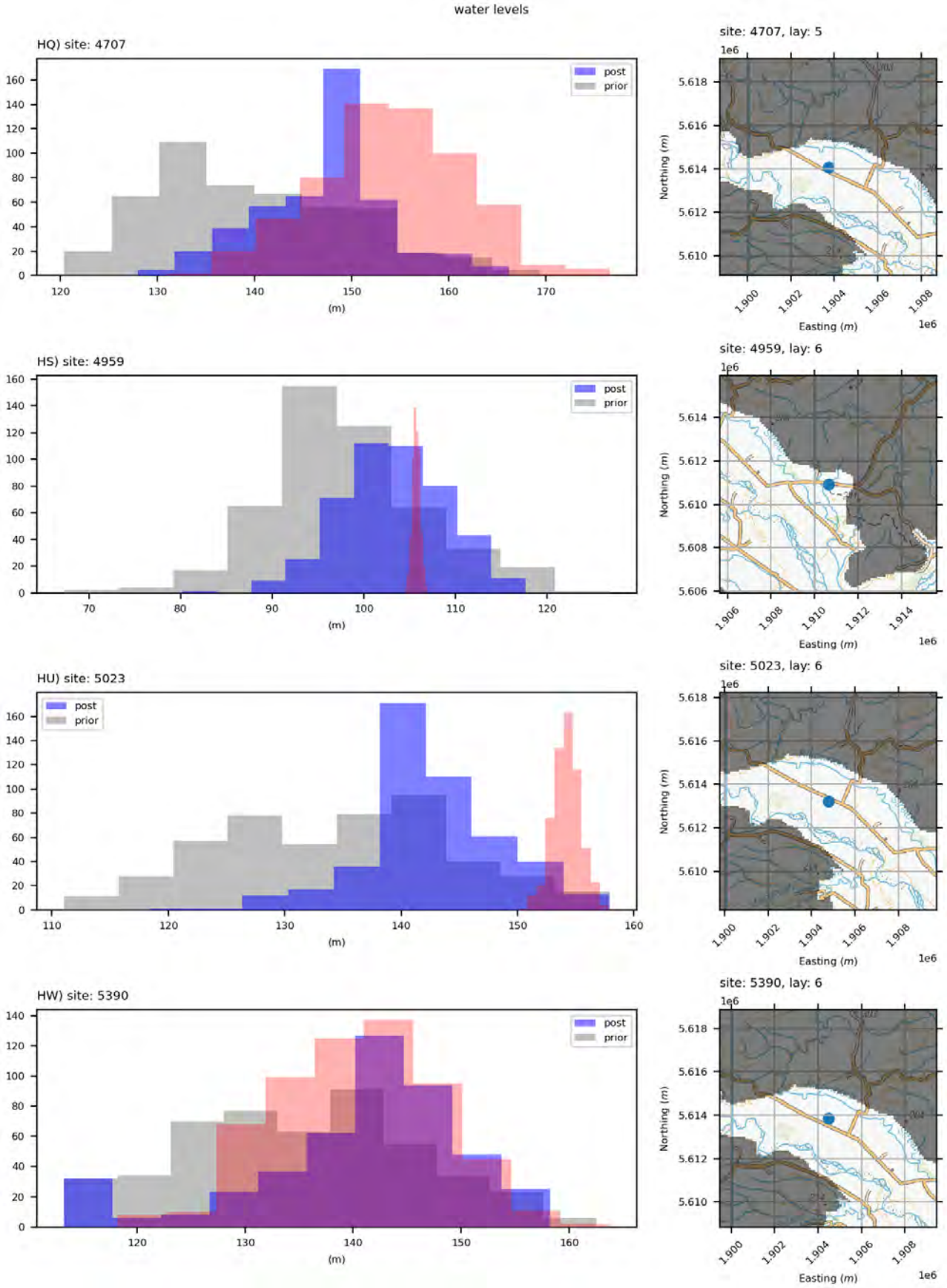
water levels
HQ) site: 4707
post
prior
(m)
site: 4707, lay: 5
1e6
Northing (m)
Easting (m)
HS) site: 4959
site: 4959, lay: 6
HU) site: 5023
site: 5023, lay: 6
HW) site: 5390
site: 5390, lay: 6

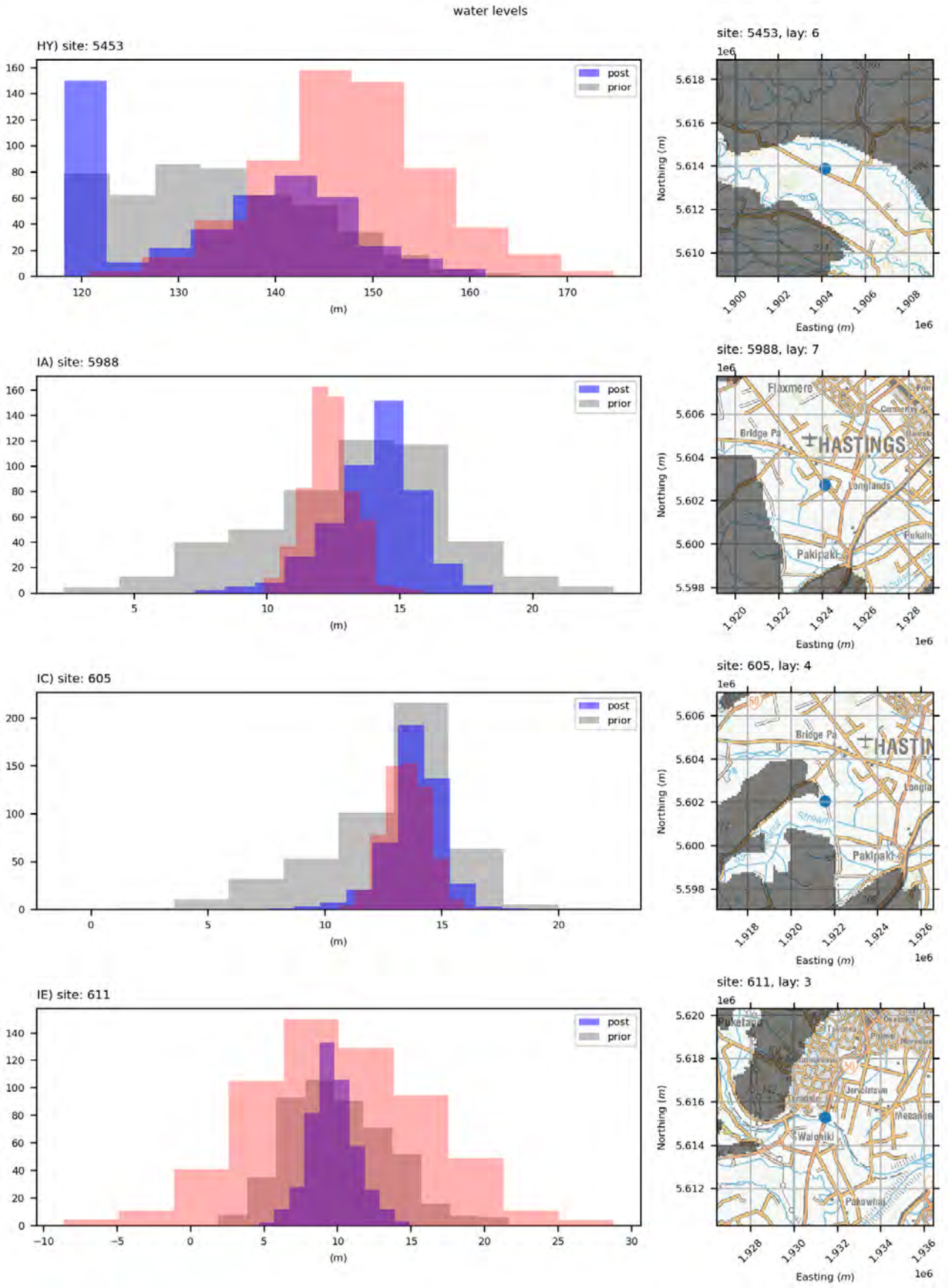
water levels
HY) site: 5453
post
prior
(m)
site: 5453, lay: 6
1e6
Northing (m)
Easting (m)
IA) site: 5988
site: 5988, lay: 7
Flaxmere
HASTINGS
Longlands
Pakipaki
IC) site: 605
site: 605, lay: 4
IE) site: 611
site: 611, lay: 3
Waiohiki

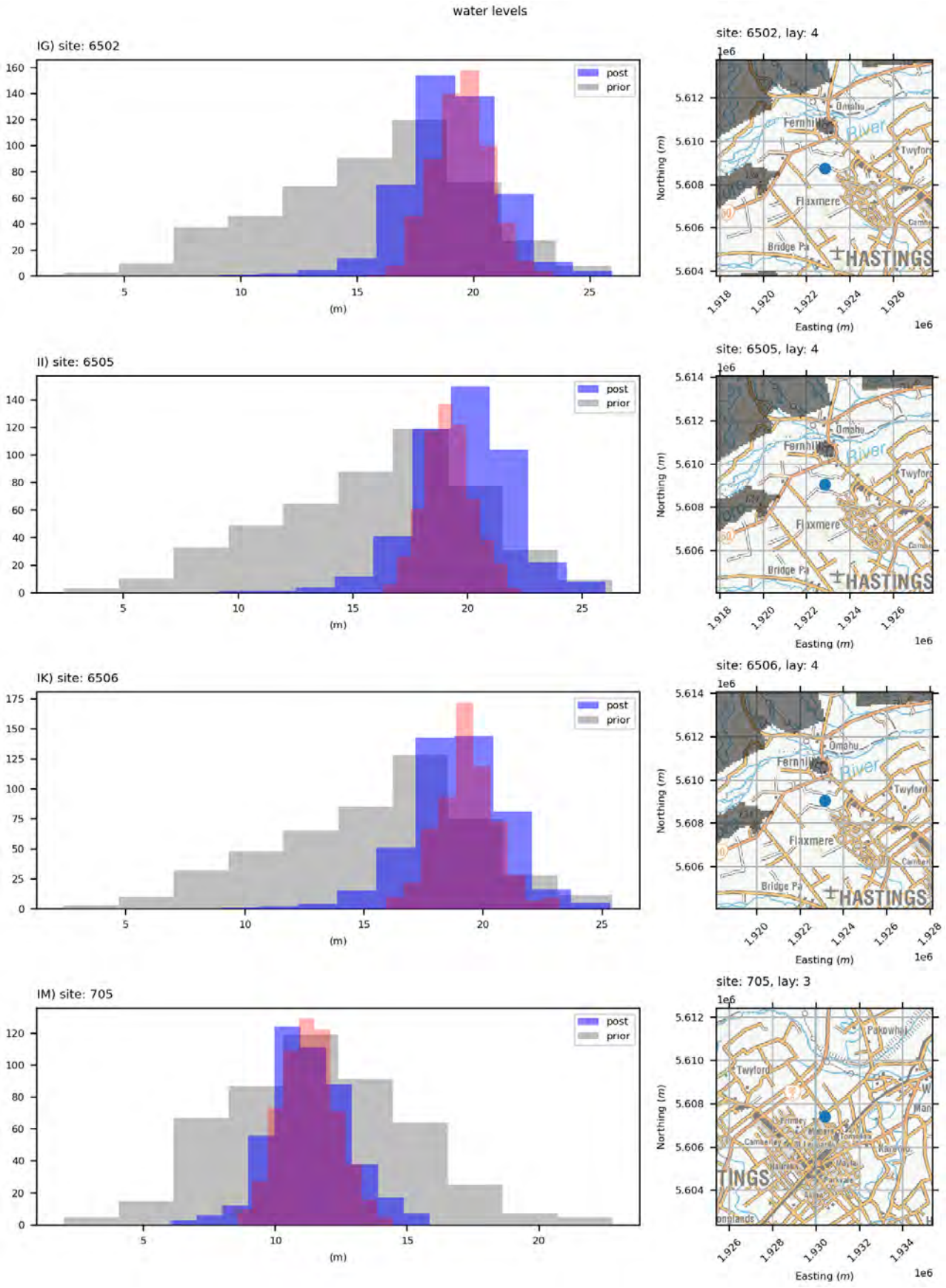
water levels
IG) site: 6502
post
prior
(m)
site: 6502, lay: 4
Northing (m)
Easting (m)
1e6
II) site: 6505
site: 6505, lay: 4
IK) site: 6506
site: 6506, lay: 4
IM) site: 705
site: 705, lay: 3
Omahu
Fernhill
River
Twyford
Flaxmere
Bridge Pa
HASTINGS
Pakowhai

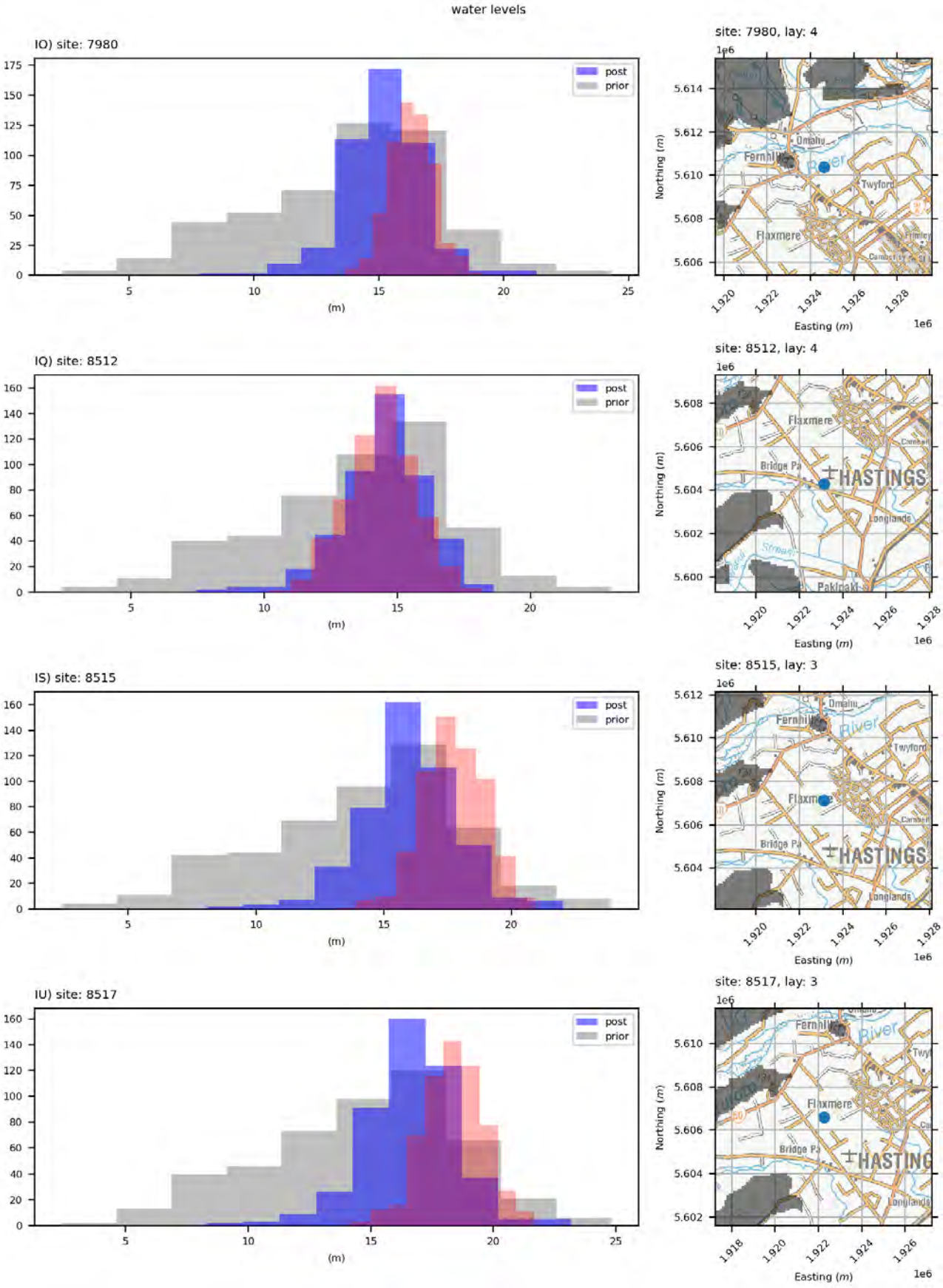
water levels
IO) site: 7980
post
prior
(m)
site: 7980, lay: 4
1e6
Northing (m)
Easting (m)
IQ) site: 8512
site: 8512, lay: 4
Flaxmere
Bridge Pa
HASTINGS
Longlands
IS) site: 8515
site: 8515, lay: 3
Fernhill
Twyford
IU) site: 8517
site: 8517, lay: 3

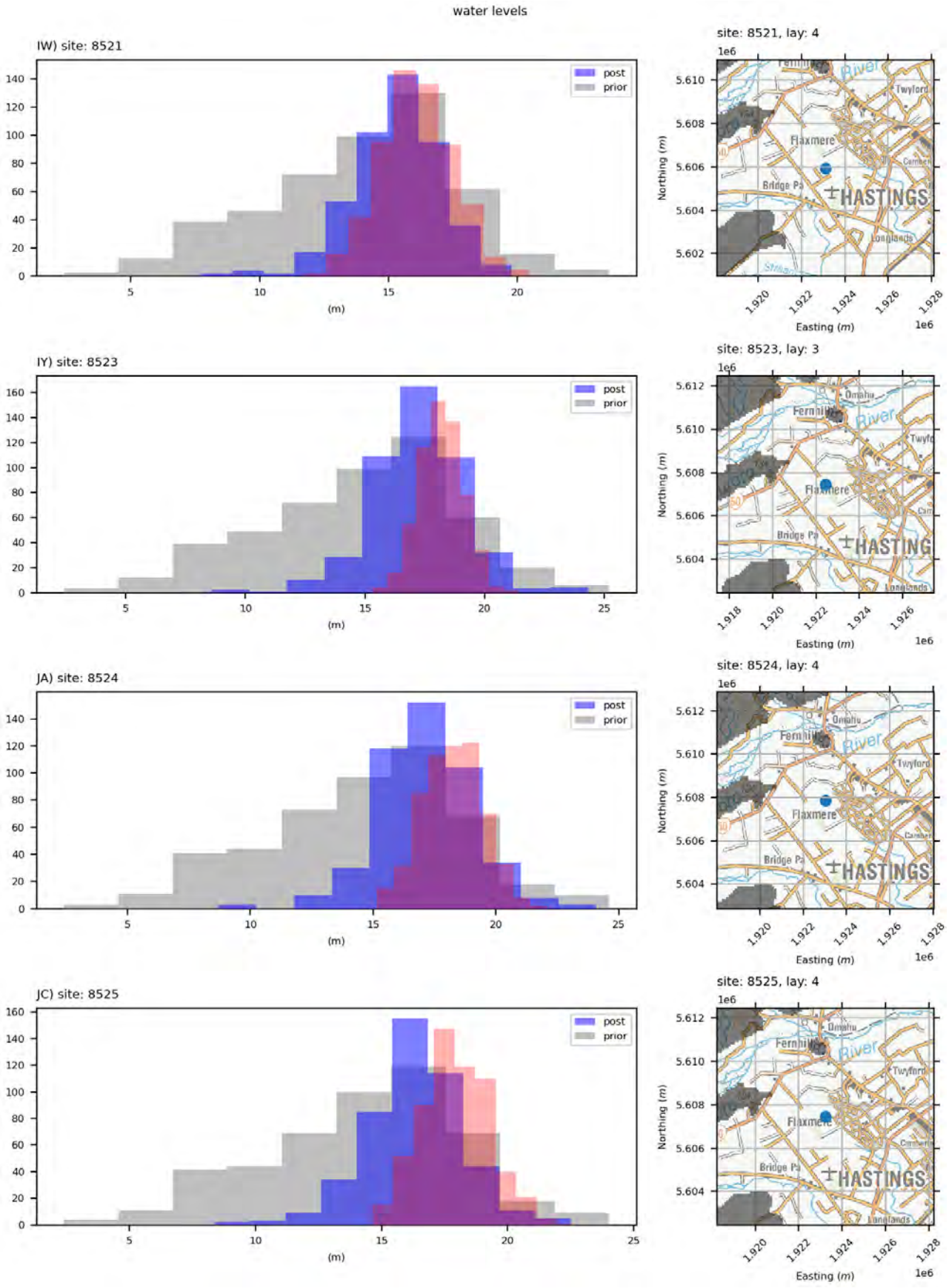
water levels
IW) site: 8521
post
prior
(m)
site: 8521, lay: 4
1e6
Northing (m)
Easting (m)
IY) site: 8523
site: 8523, lay: 3
JA) site: 8524
site: 8524, lay: 4
JC) site: 8525
site: 8525, lay: 4
Flaxmere
HASTINGS

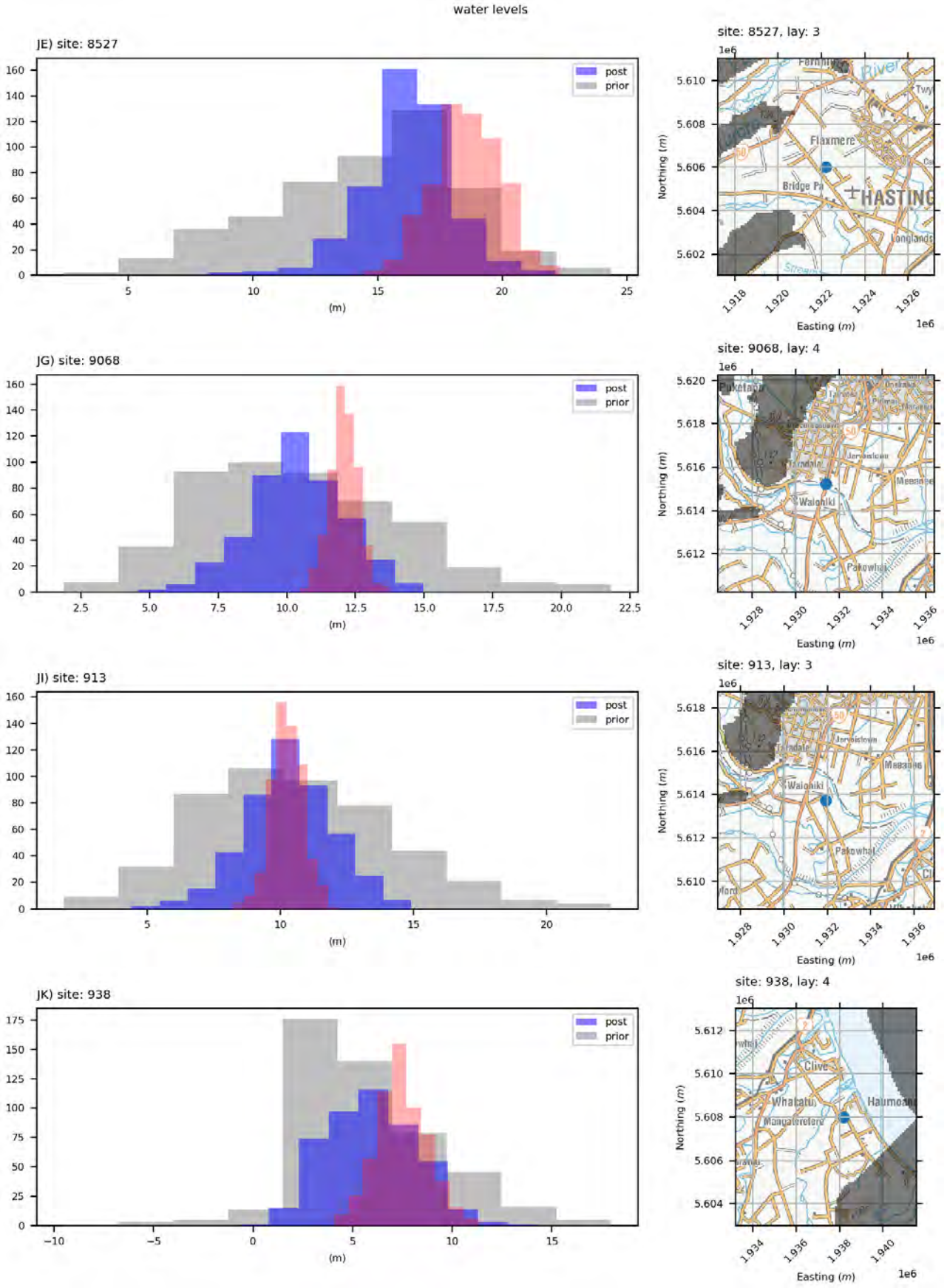
water levels
JE) site: 8527
post
prior
(m)
site: 8527, lay: 3
Northing (m)
Easting (m)
JG) site: 9068
site: 9068, lay: 4
JI) site: 913
site: 913, lay: 3
JK) site: 938
site: 938, lay: 4
Flaxmere
Waiohiki
Pakowhai
Clive
Whakatu
Haumoana

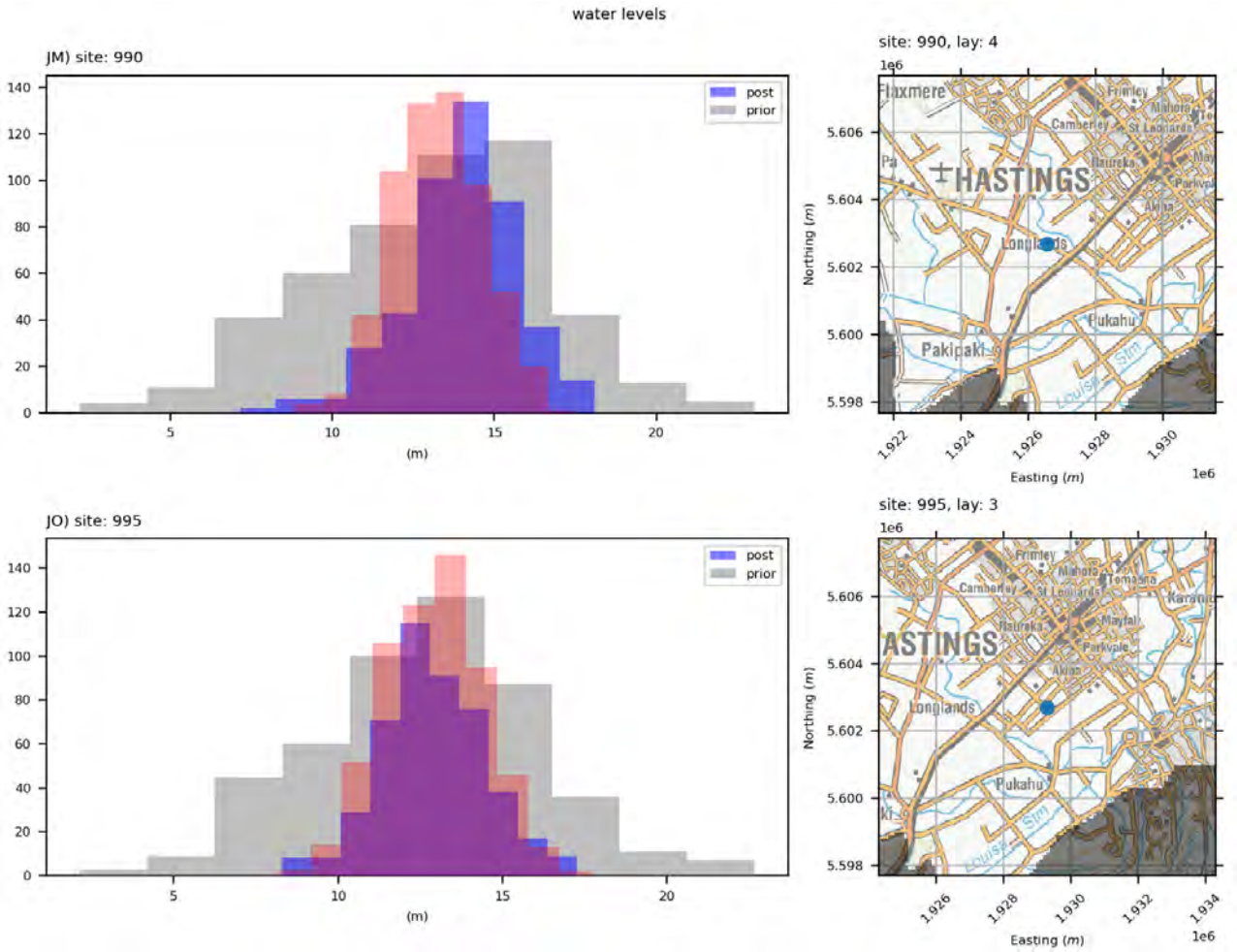
water levels
JM) site: 990
post
prior
(m)
site: 990, lay: 4
1e6
Flaxmere
HASTINGS
Longlands
Pukahu
Pakipaki
Northing (m)
Easting (m)
JO) site: 995
post
prior
(m)
site: 995, lay: 3
1e6
ASTINGS
Longlands
Pukahu
Northing (m)
Easting (m)

A3.2.1.2 Stream Flows

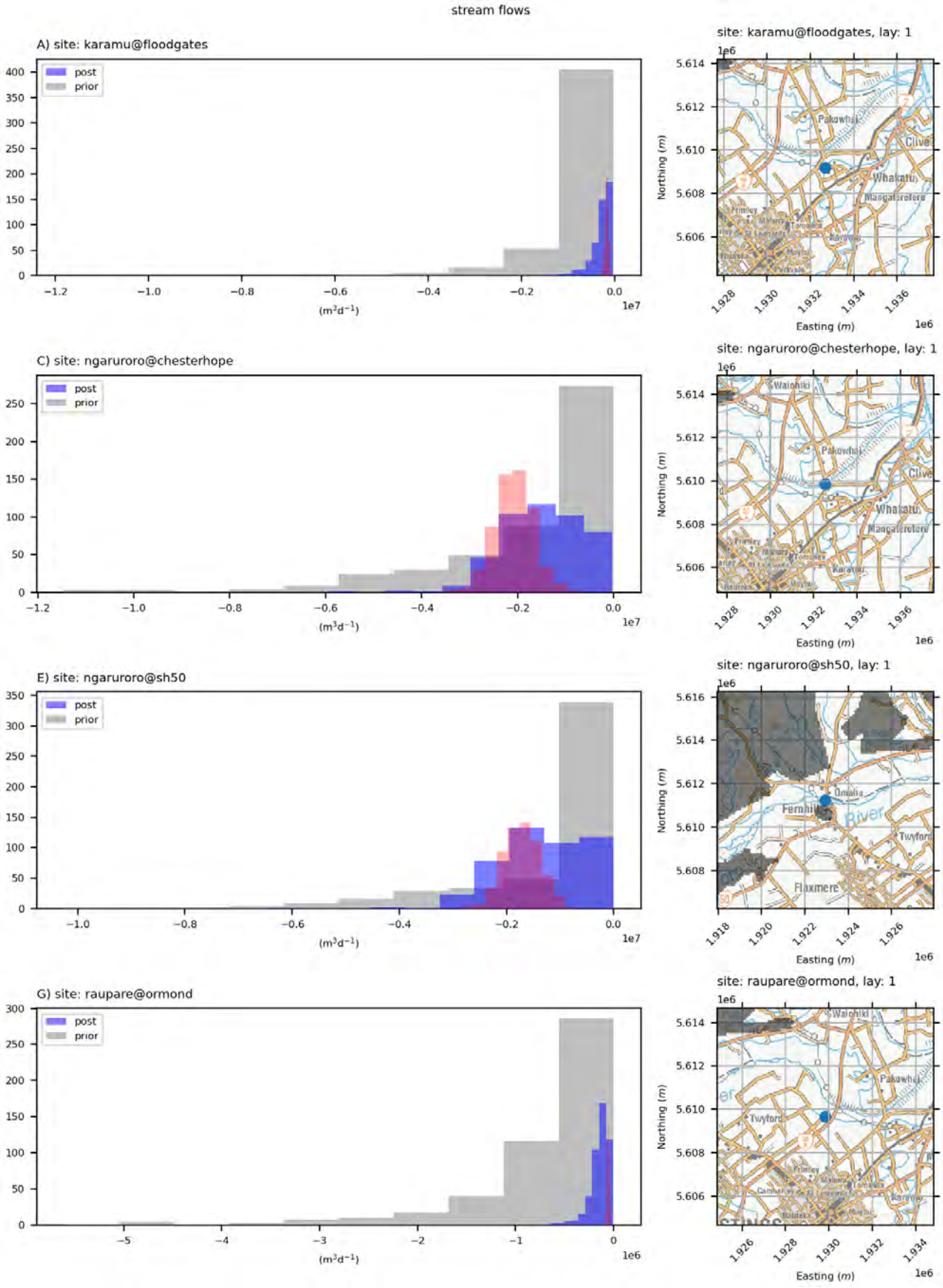

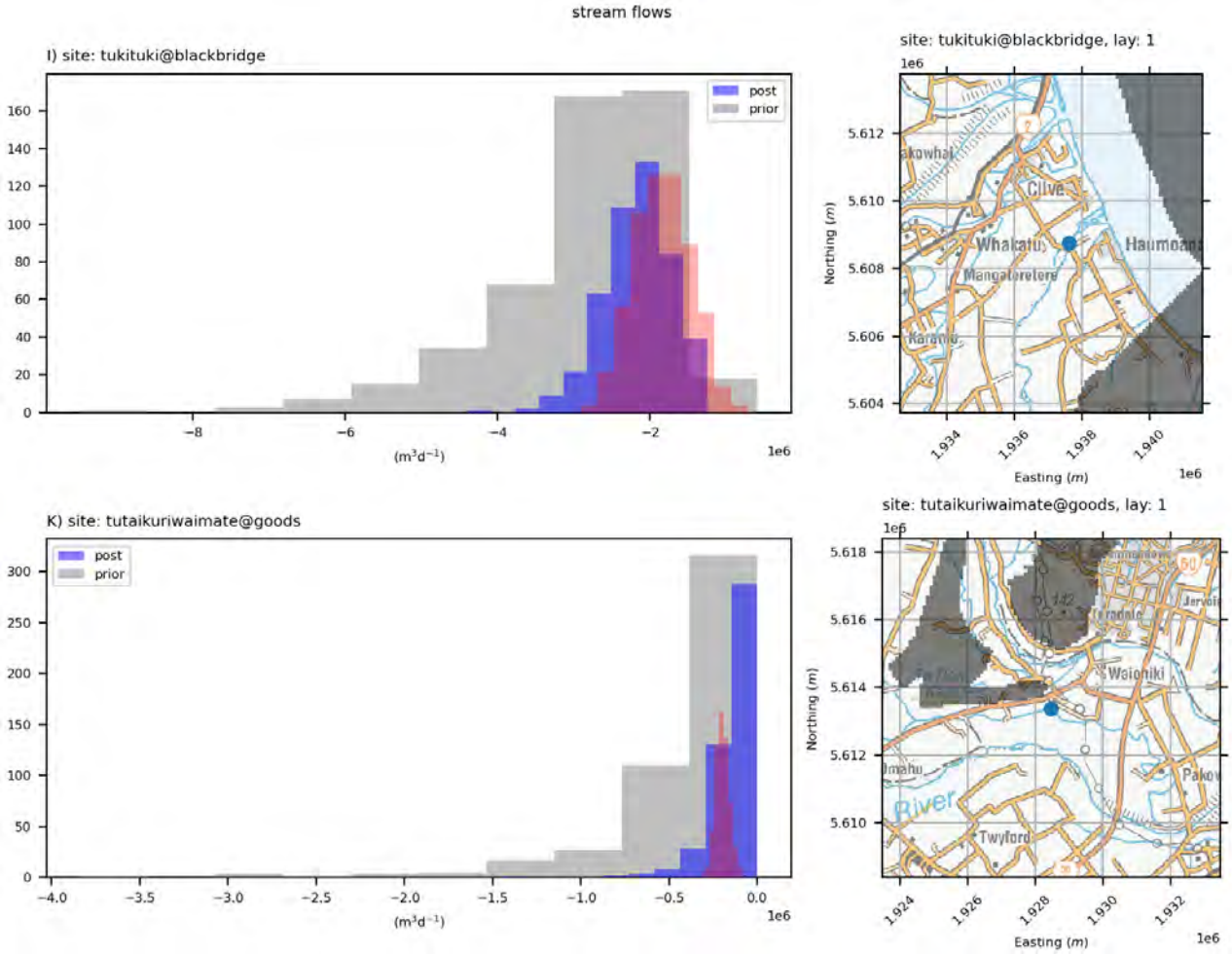
stream flows
I) site: tukituki@blackbridge
post
prior
(m³d⁻¹)
1e6
site: tukituki@blackbridge, lay: 1
Northing (m)
Easting (m)
Clive
Whakatu
Mangateretere
Haumoana
K) site: tutaikuriwaimate@goods
site: tutaikuriwaimate@goods, lay: 1
Waioniki
Twyford
River

A3.2.1.3 Surface-Water–Groundwater Exchange

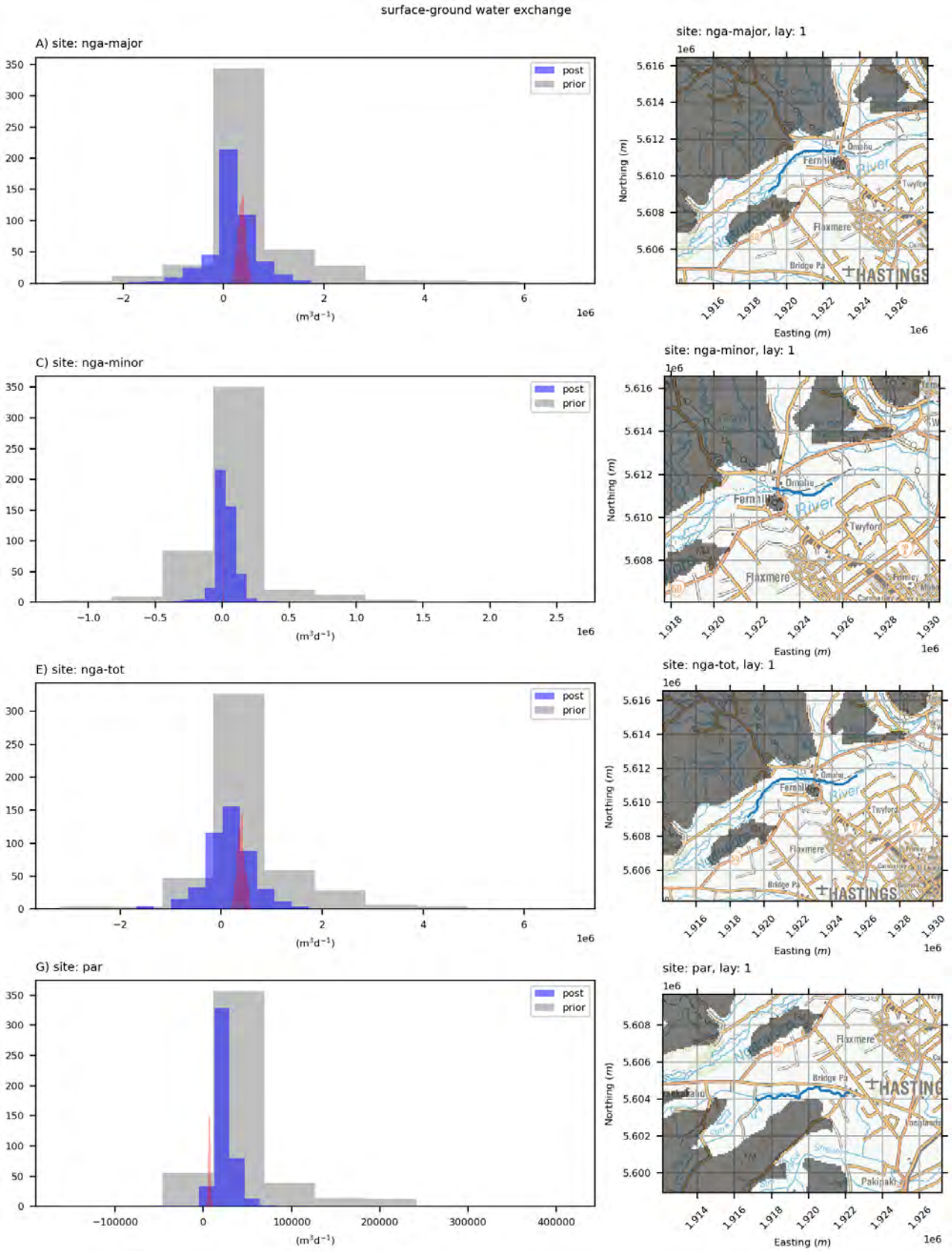

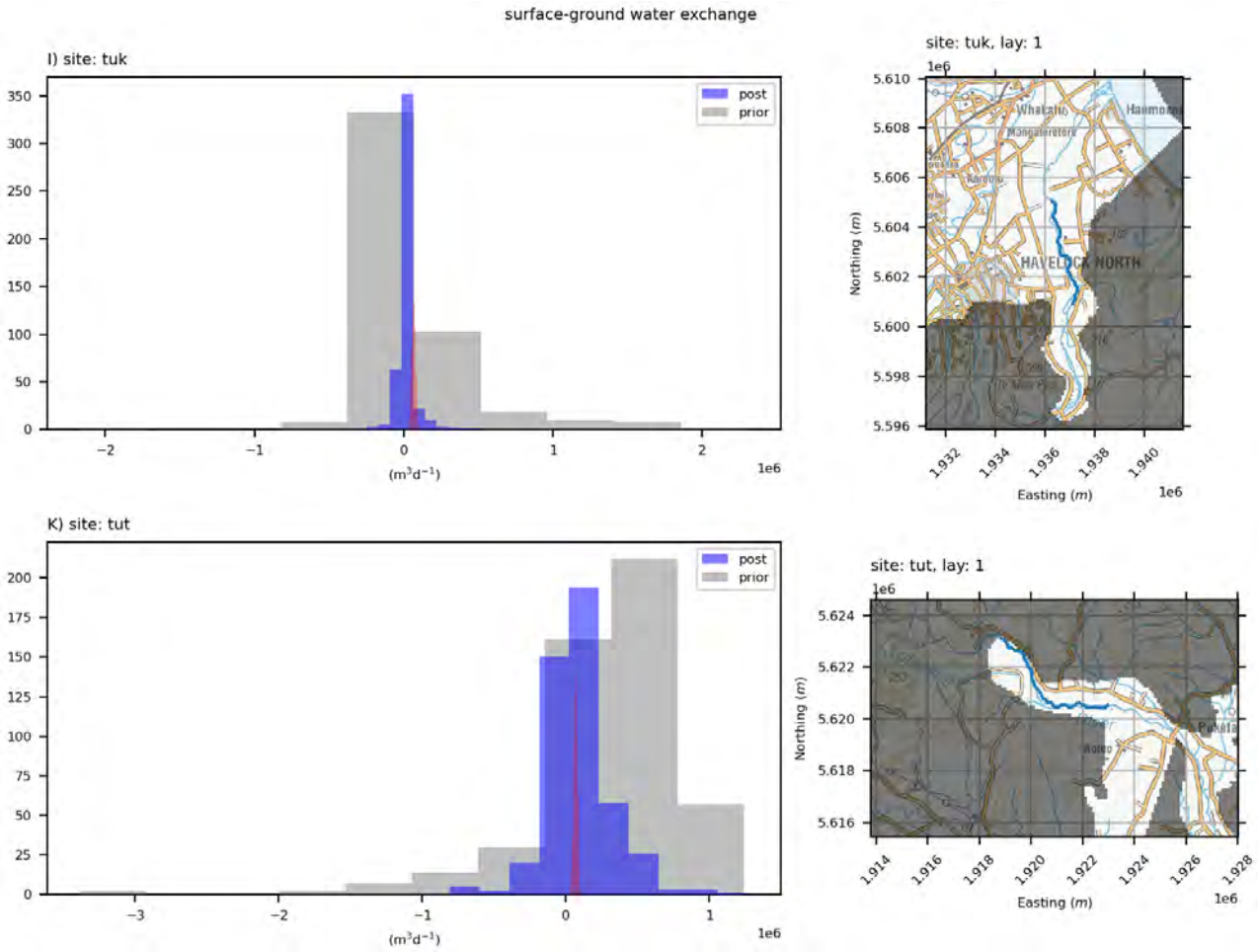
surface-ground water exchange
l) site: tuk
post
prior
(m³d⁻¹)
1e6
site: tuk, lay: 1
Northing (m)
Easting (m)
HAVELOCK NORTH
K) site: tut
site: tut, lay: 1

A3.2.2 *skytem-k-precond*

A3.2.2.1 Levels

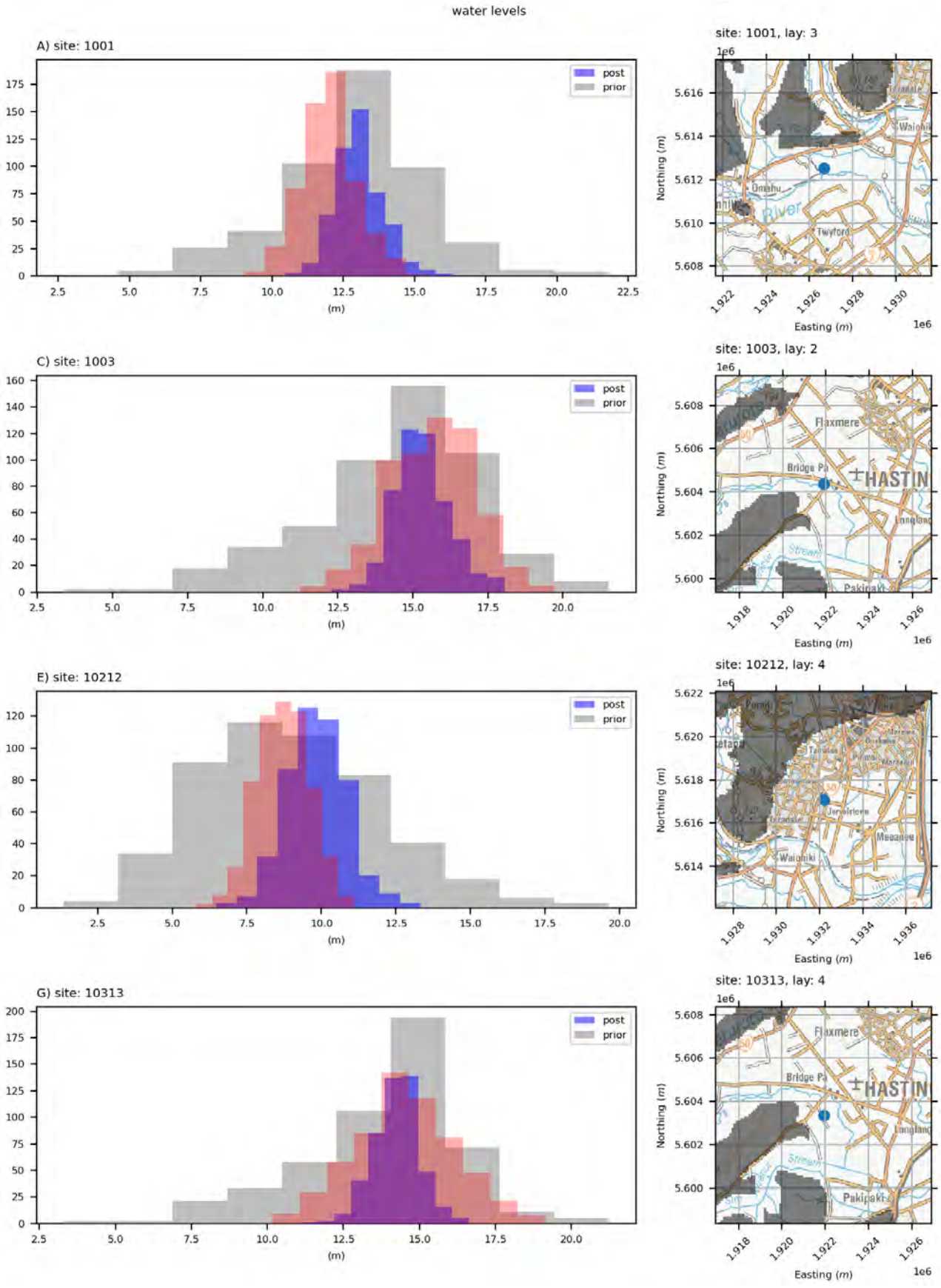

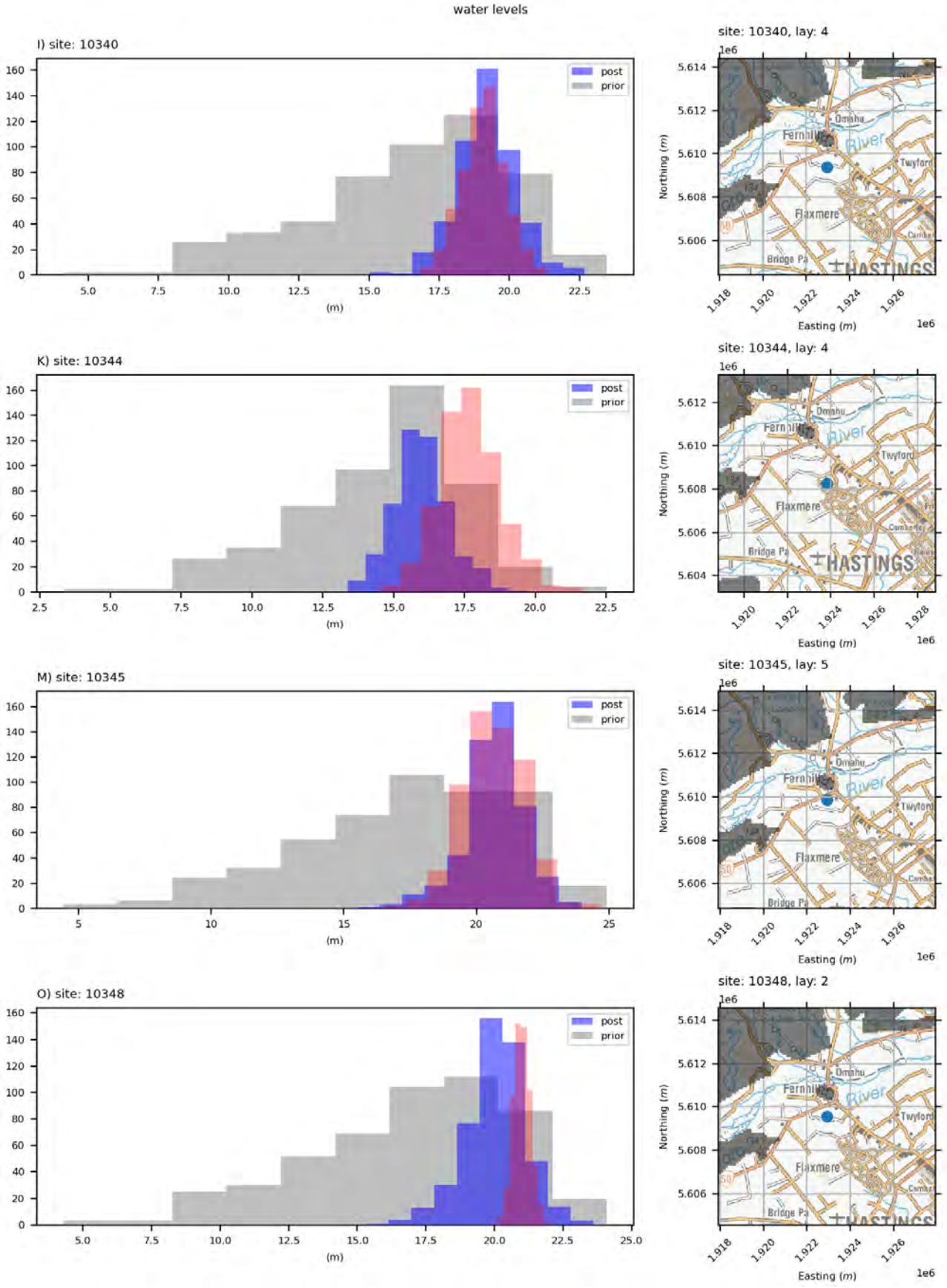
water levels
I) site: 10340
post
prior
(m)
site: 10340, lay: 4
1e6
Northing (m)
Easting (m)
Omahu
Fernhill
River
Twyford
Flaxmere
Bridge Pa
HASTINGS
K) site: 10344
site: 10344, lay: 4
M) site: 10345
site: 10345, lay: 5
O) site: 10348
site: 10348, lay: 2

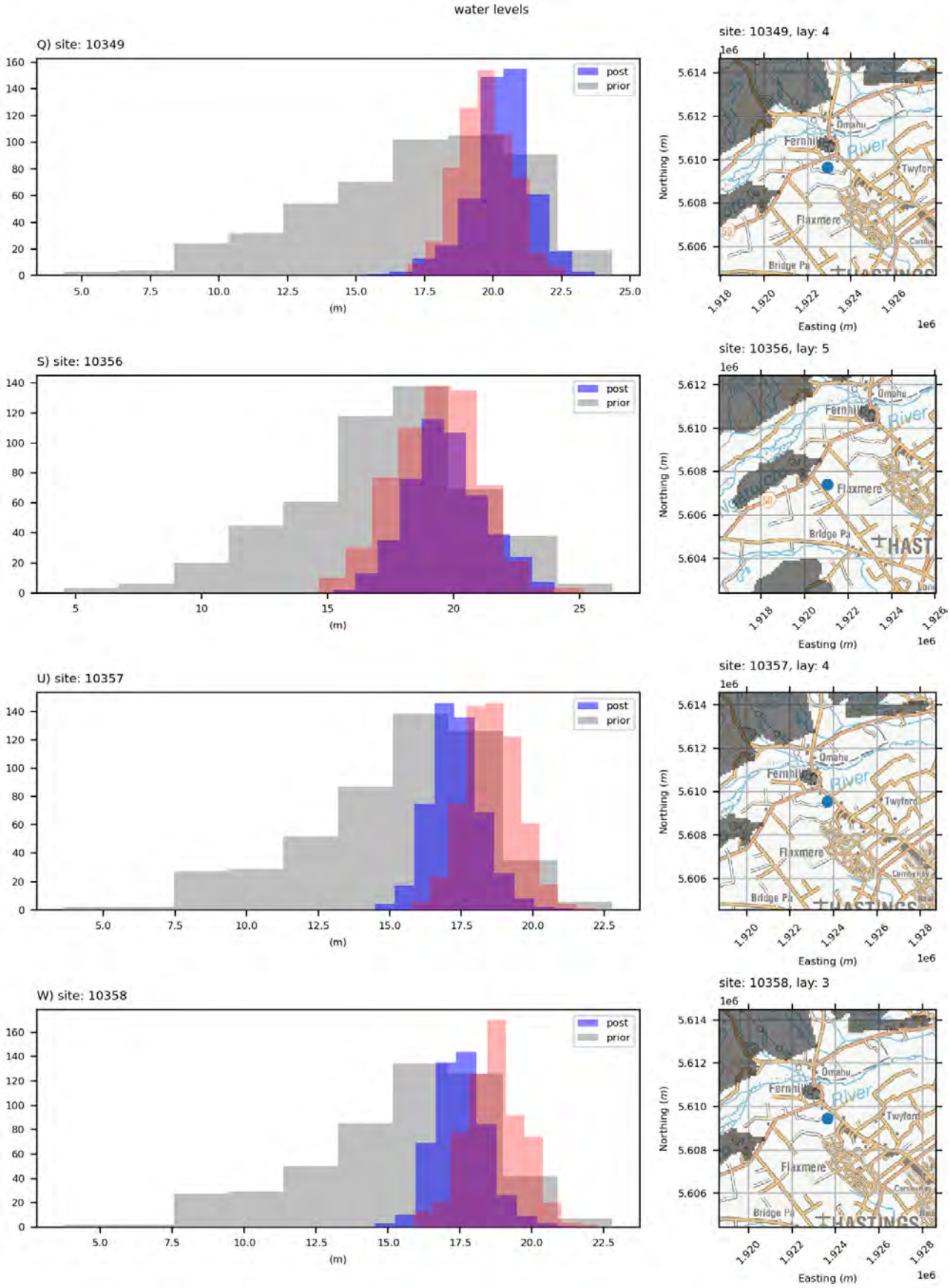
water levels
Q) site: 10349
post
prior
(m)
site: 10349, lay: 4
Northing (m)
Easting (m)
1e6
Omahu
Fernhill
River
Twyford
Flaxmere
Bridge Pa
S) site: 10356
site: 10356, lay: 5
U) site: 10357
site: 10357, lay: 4
W) site: 10358
site: 10358, lay: 3

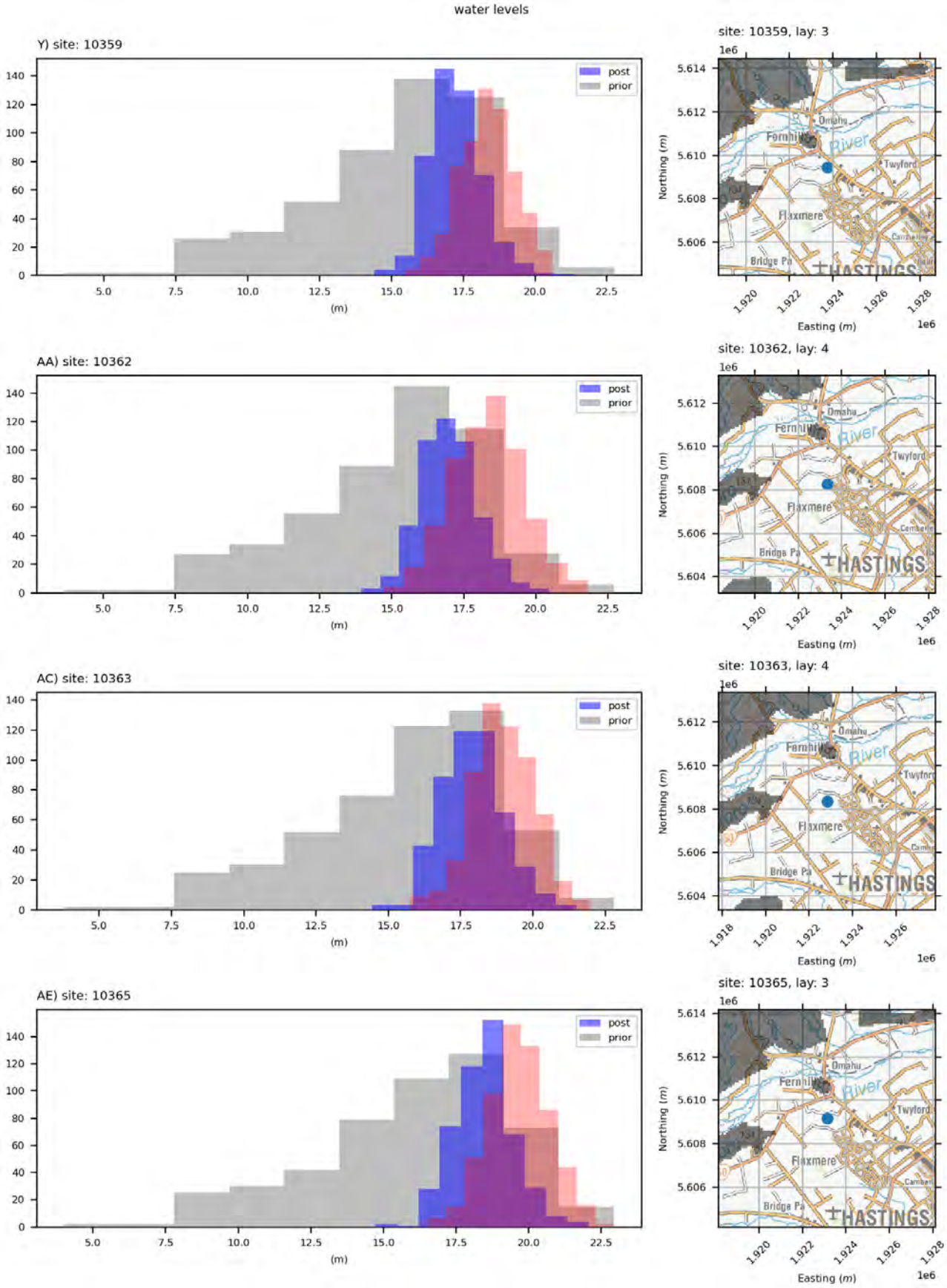
water levels
Y) site: 10359
post
prior
(m)
site: 10359, lay: 3
1e6
Northing (m)
Easting (m)
Omahu
Fernhill
River
Twyford
Flaxmere
Bridge Pa
HASTINGS
AA) site: 10362
site: 10362, lay: 4
AC) site: 10363
site: 10363, lay: 4
AE) site: 10365
site: 10365, lay: 3

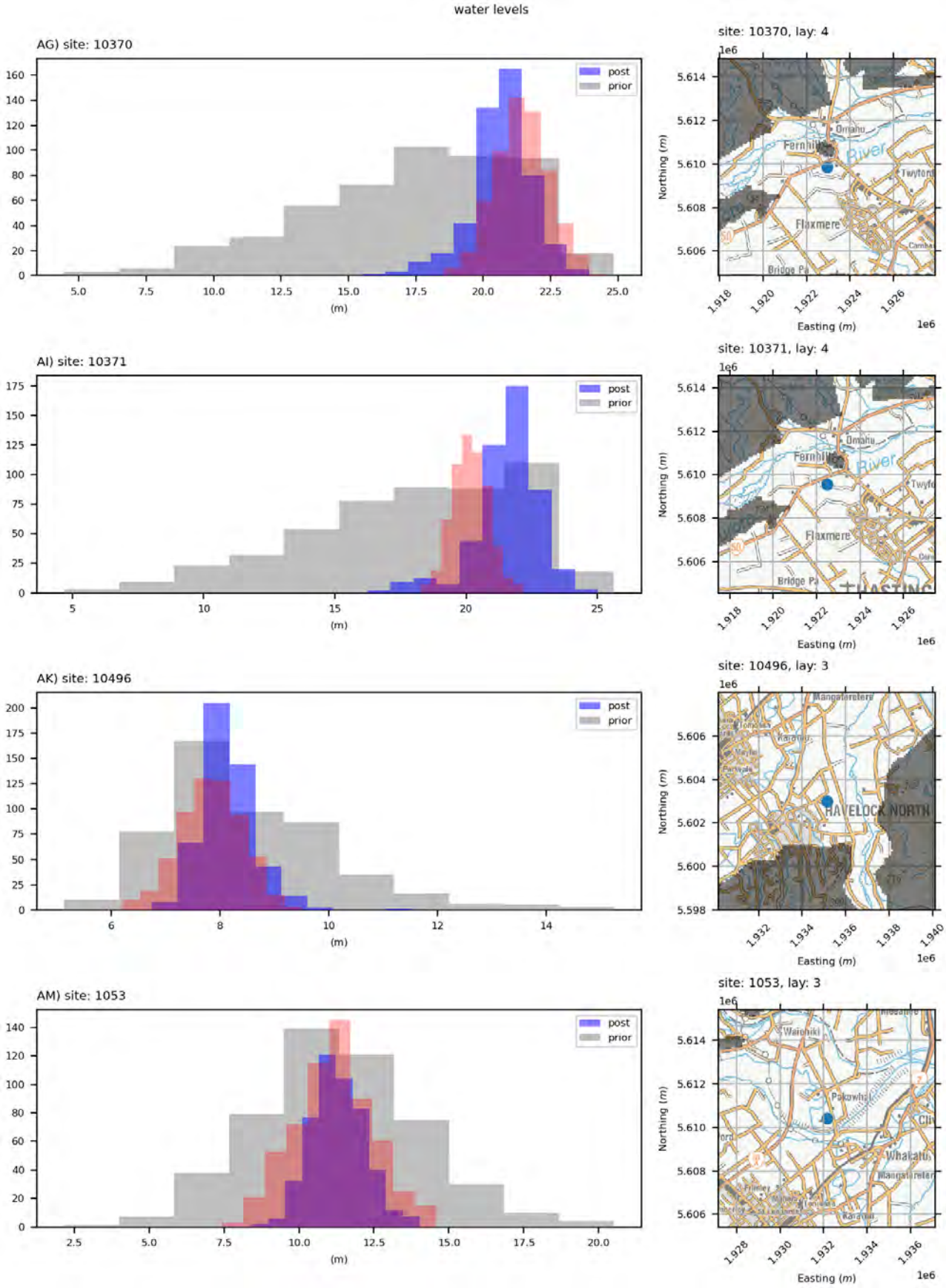
water levels
AG) site: 10370
post
prior
(m)
site: 10370, lay: 4
Northing (m)
Easting (m)
1e6
AI) site: 10371
post
prior
(m)
site: 10371, lay: 4
Northing (m)
Easting (m)
1e6
AK) site: 10496
post
prior
(m)
site: 10496, lay: 3
HAVELOCK NORTH
Northing (m)
Easting (m)
1e6
AM) site: 1053
post
prior
(m)
site: 1053, lay: 3
Northing (m)
Easting (m)
1e6

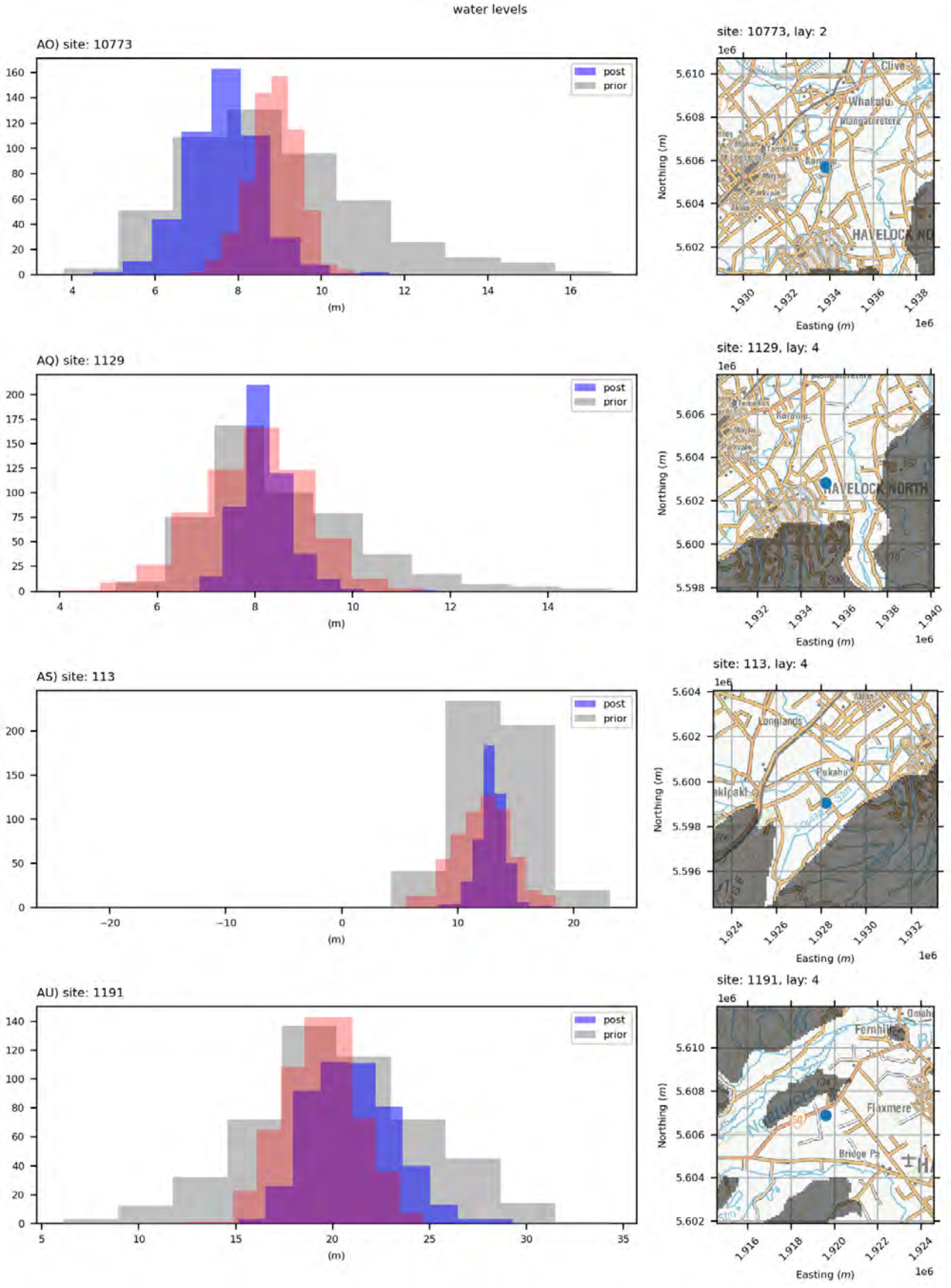
water levels
AO) site: 10773
post
prior
(m)
site: 10773, lay: 2
1e6
Northing (m)
Easting (m)
AQ) site: 1129
site: 1129, lay: 4
AS) site: 113
site: 113, lay: 4
AU) site: 1191
site: 1191, lay: 4

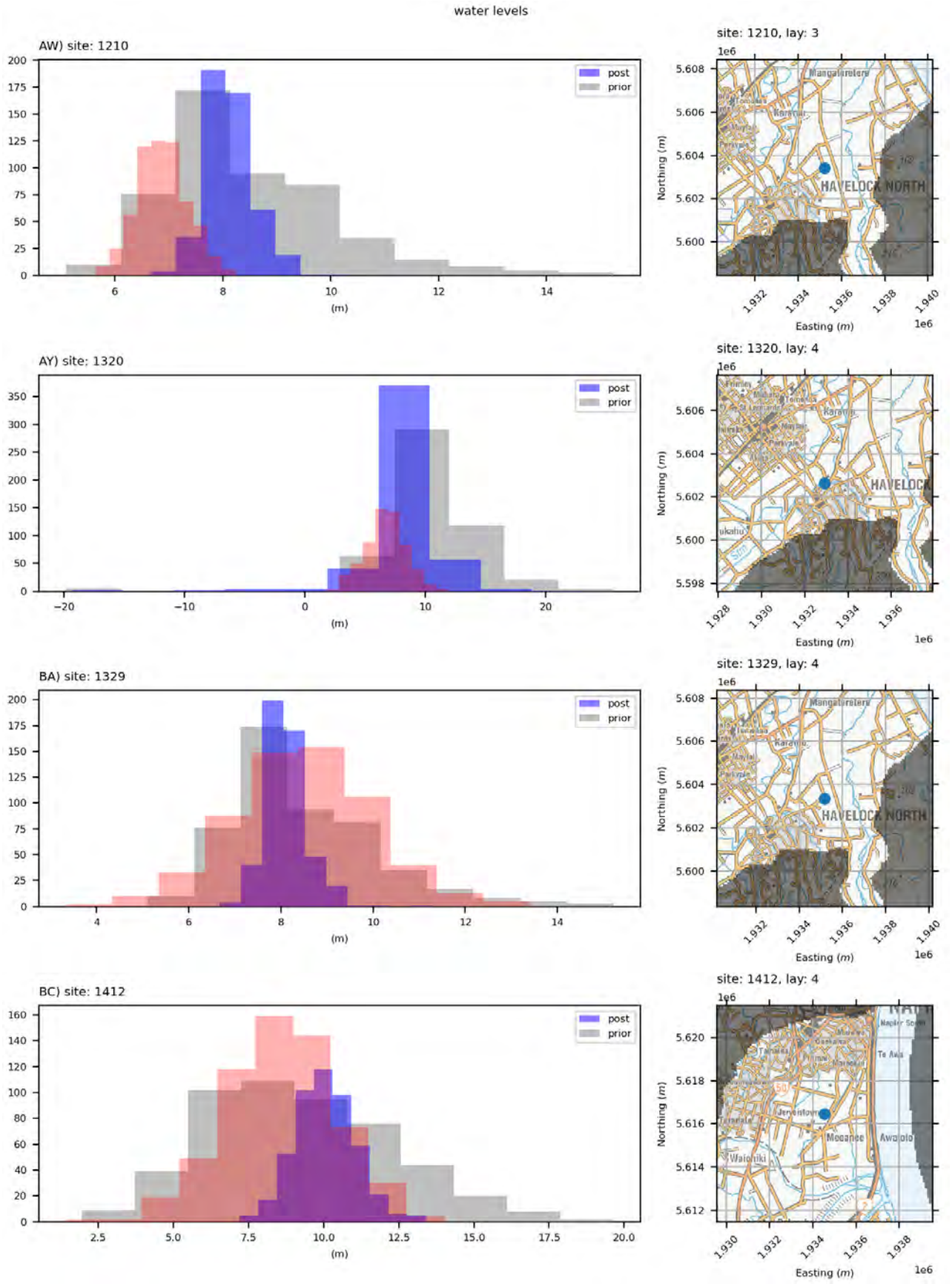
water levels
AW) site: 1210
post
prior
(m)
site: 1210, lay: 3
1e6
Northing (m)
Easting (m)
HAVELOCK NORTH
AY) site: 1320
site: 1320, lay: 4
HAVELOCK
BA) site: 1329
site: 1329, lay: 4
HAVELOCK NORTH
BC) site: 1412
site: 1412, lay: 4
Meeanee
Awatoto
Waiohiki

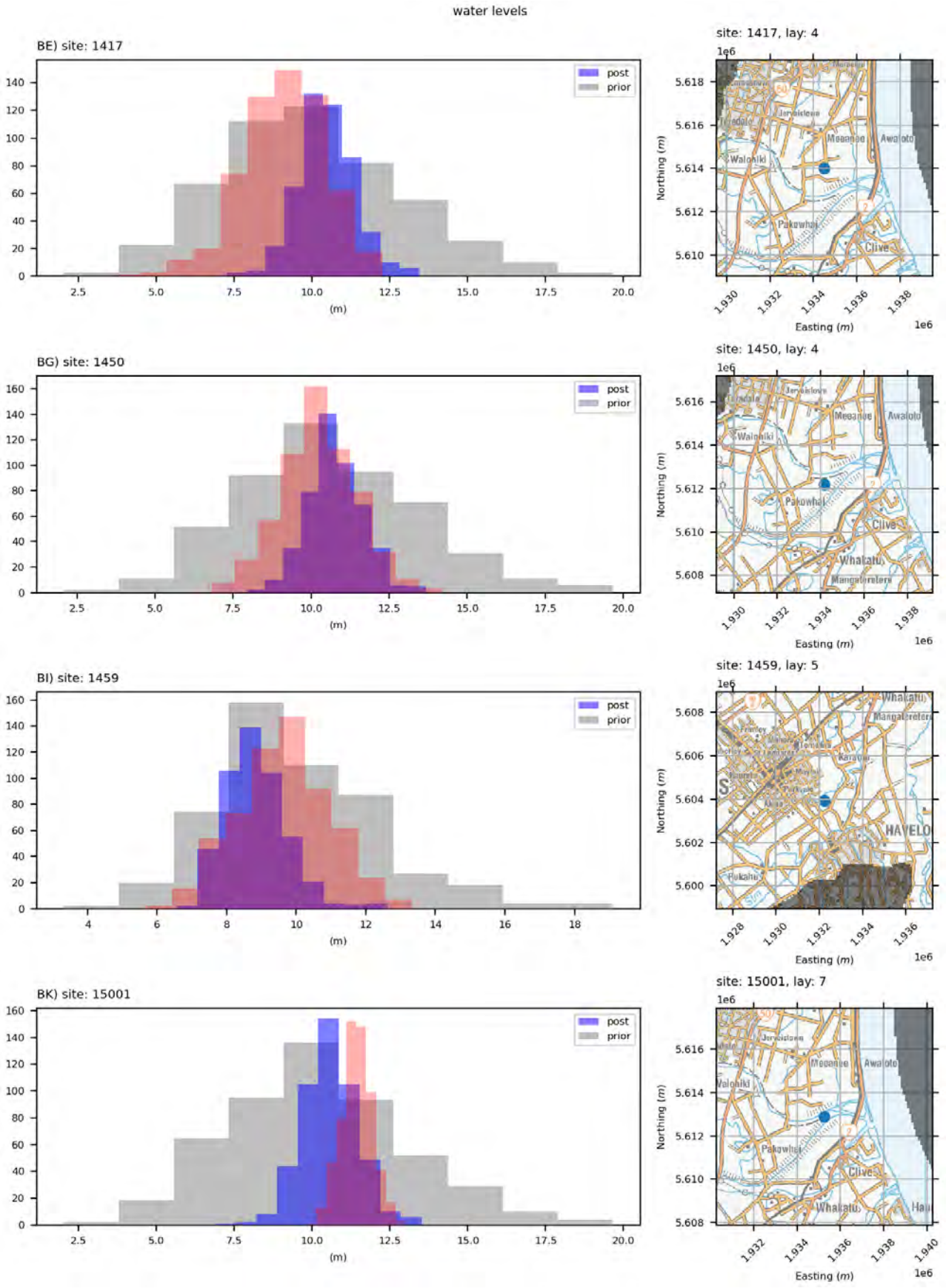
water levels
BE) site: 1417
post
prior
(m)
site: 1417, lay: 4
1e6
Northing (m)
Easting (m)
BG) site: 1450
site: 1450, lay: 4
BI) site: 1459
site: 1459, lay: 5
BK) site: 15001
site: 15001, lay: 7

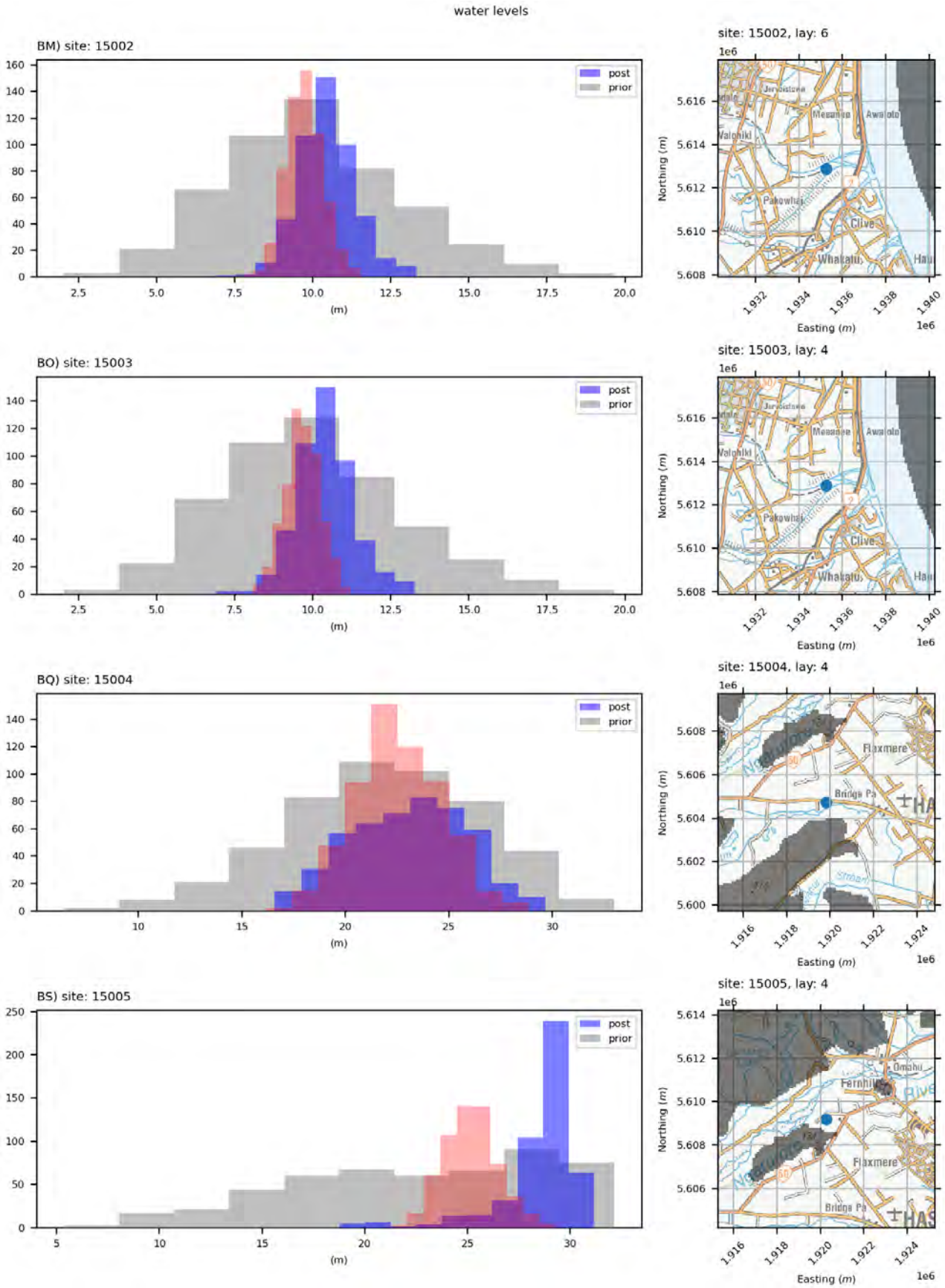
water levels
BM) site: 15002
post
prior
(m)
site: 15002, lay: 6
1e6
Northing (m)
Easting (m)
1e6
BO) site: 15003
post
prior
(m)
site: 15003, lay: 4
1e6
Northing (m)
Easting (m)
1e6
BQ) site: 15004
post
prior
(m)
site: 15004, lay: 4
1e6
Northing (m)
Easting (m)
1e6
BS) site: 15005
post
prior
(m)
site: 15005, lay: 4
1e6
Northing (m)
Easting (m)
1e6

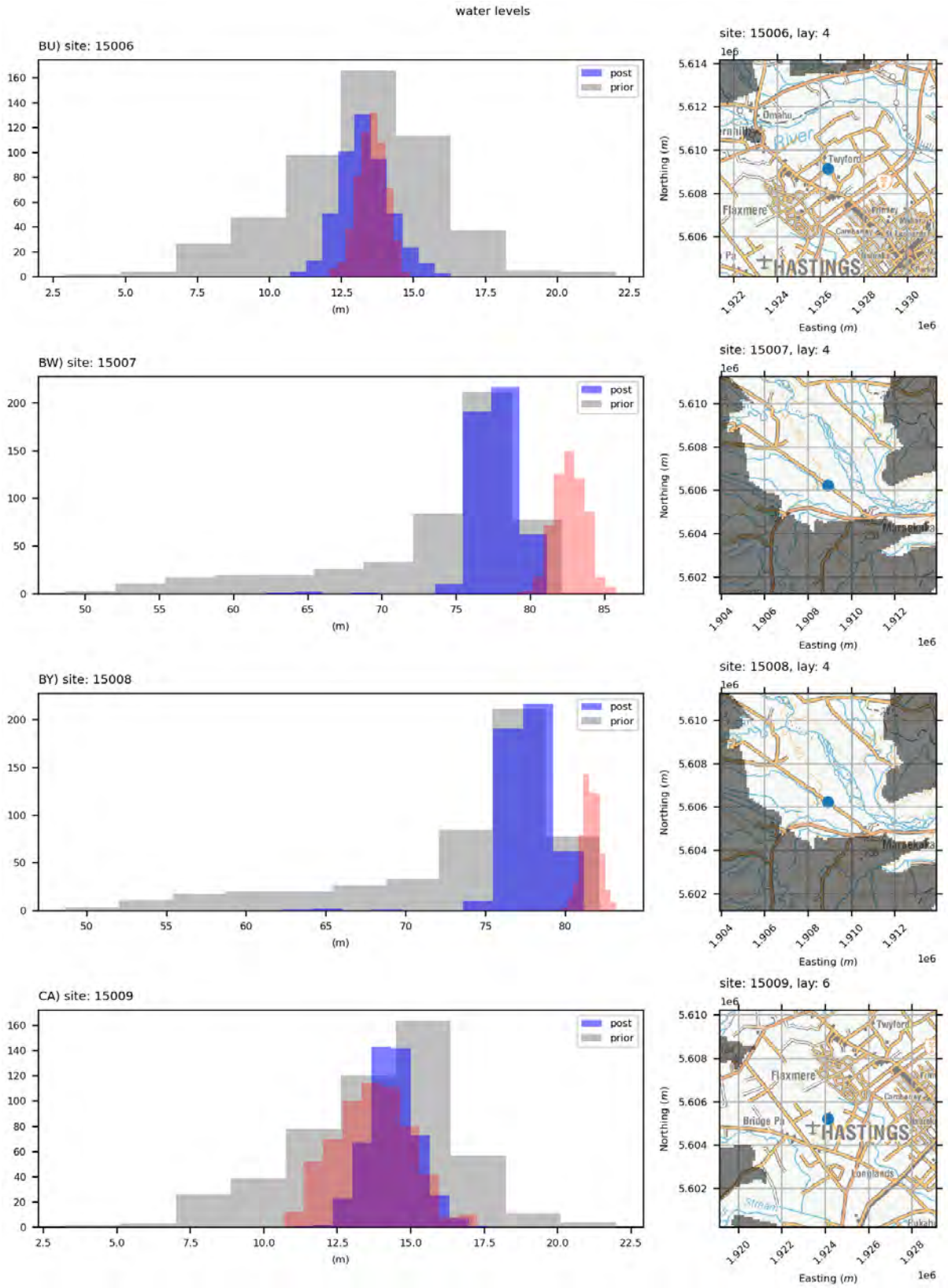
water levels
BU) site: 15006
post
prior
(m)
site: 15006, lay: 4
1e6
Northing (m)
Easting (m)
HASTINGS
Flaxmere
Twyford
Omahu
River
BW) site: 15007
site: 15007, lay: 4
BY) site: 15008
site: 15008, lay: 4
CA) site: 15009
site: 15009, lay: 6
Bridge Pa

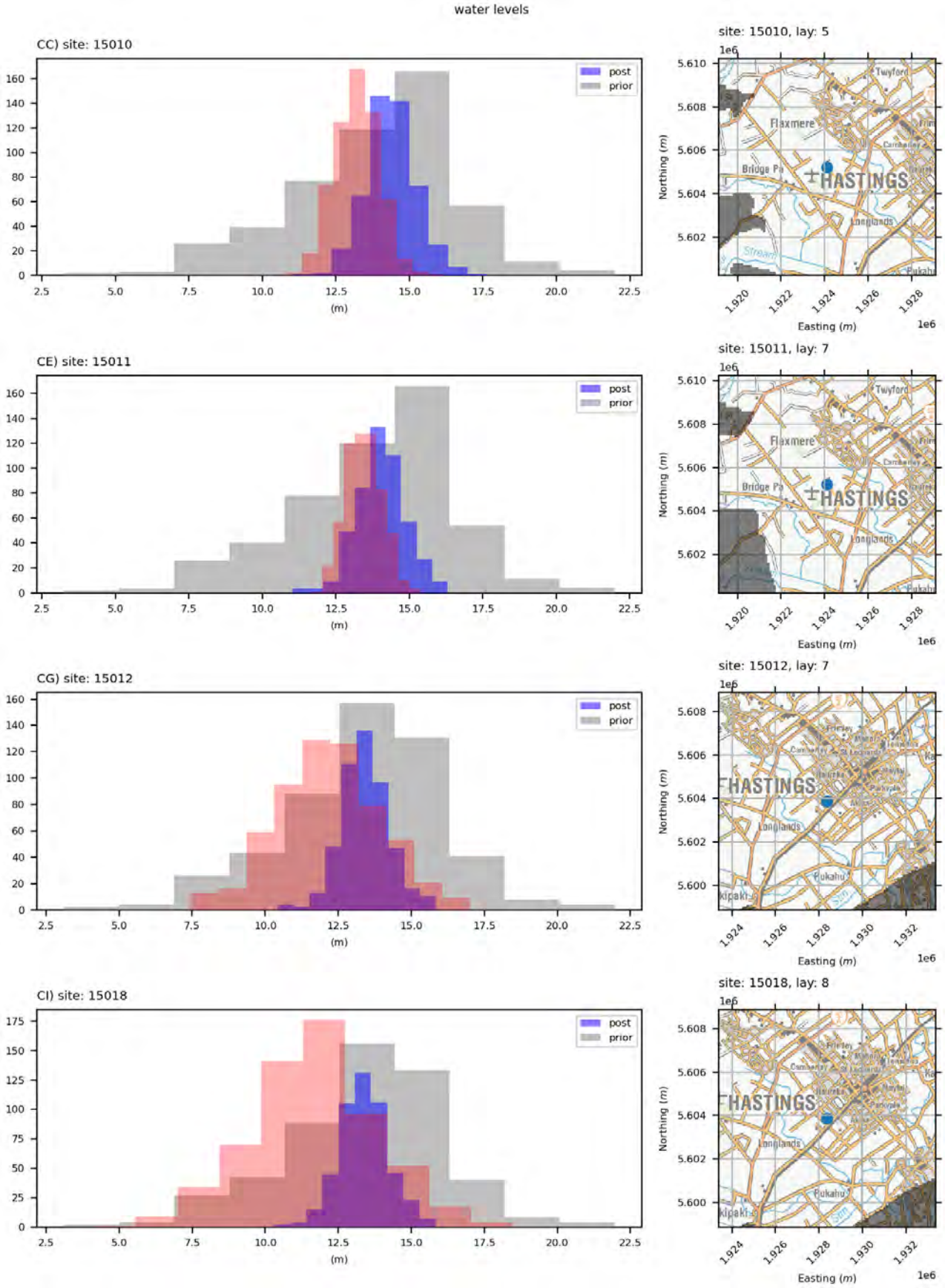
water levels
CC) site: 15010
CE) site: 15011
CG) site: 15012
CI) site: 15018
post
prior
(m)
site: 15010, lay: 5
site: 15011, lay: 7
site: 15012, lay: 7
site: 15018, lay: 8
Northing (m)
Easting (m)
1e6
HASTINGS
Flaxmere
Twyford
Longlands
Pukahu

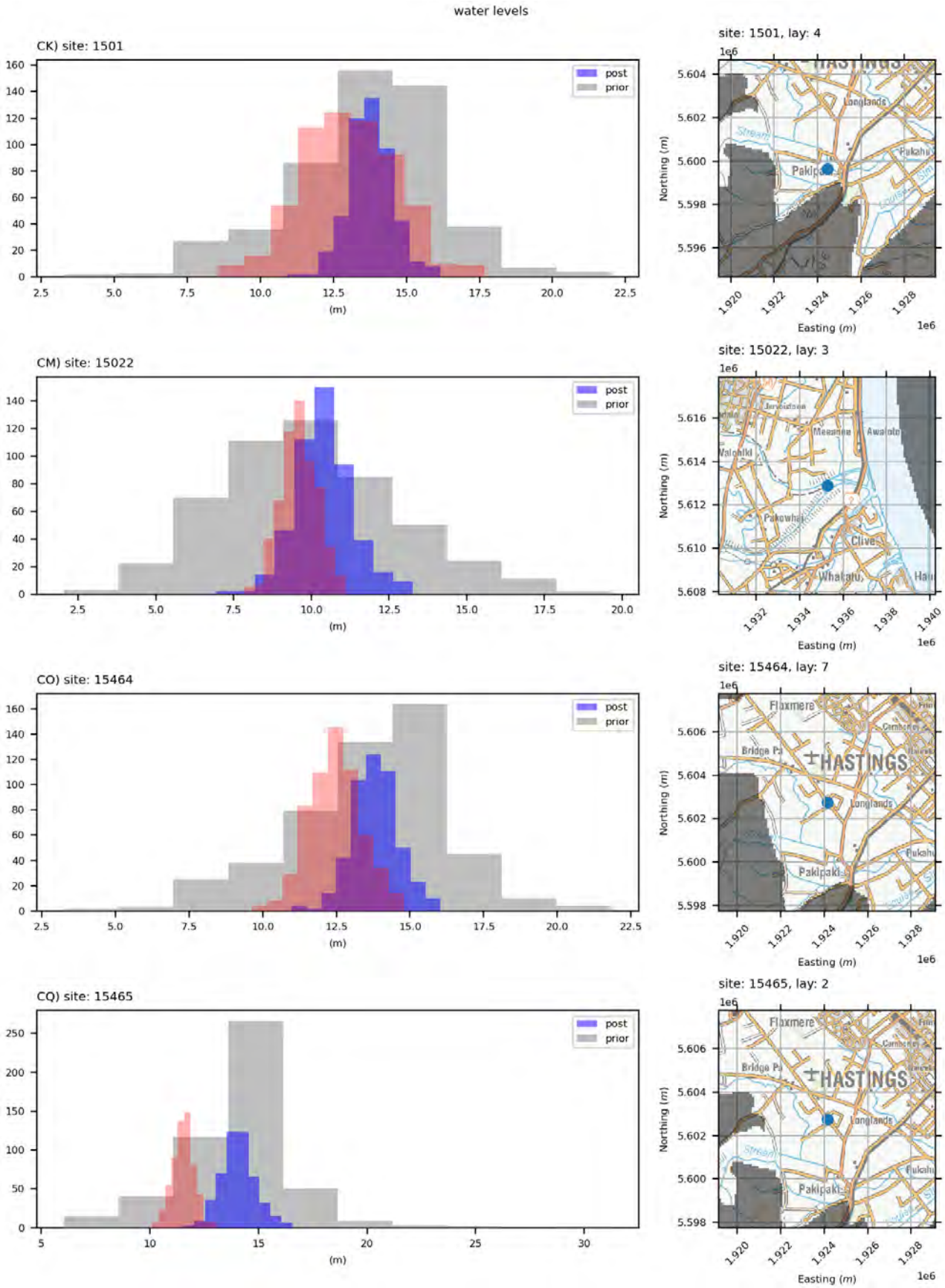
water levels
CK) site: 1501
post
prior
(m)
site: 1501, lay: 4
1e6
Northing (m)
Easting (m)
CM) site: 15022
site: 15022, lay: 3
CO) site: 15464
site: 15464, lay: 7
CQ) site: 15465
site: 15465, lay: 2
HASTINGS
Longlands
Pakipaki
Clive
Whakatu
Meeanee
Awatoto
Valhalla
Pakowhai
Floxmere

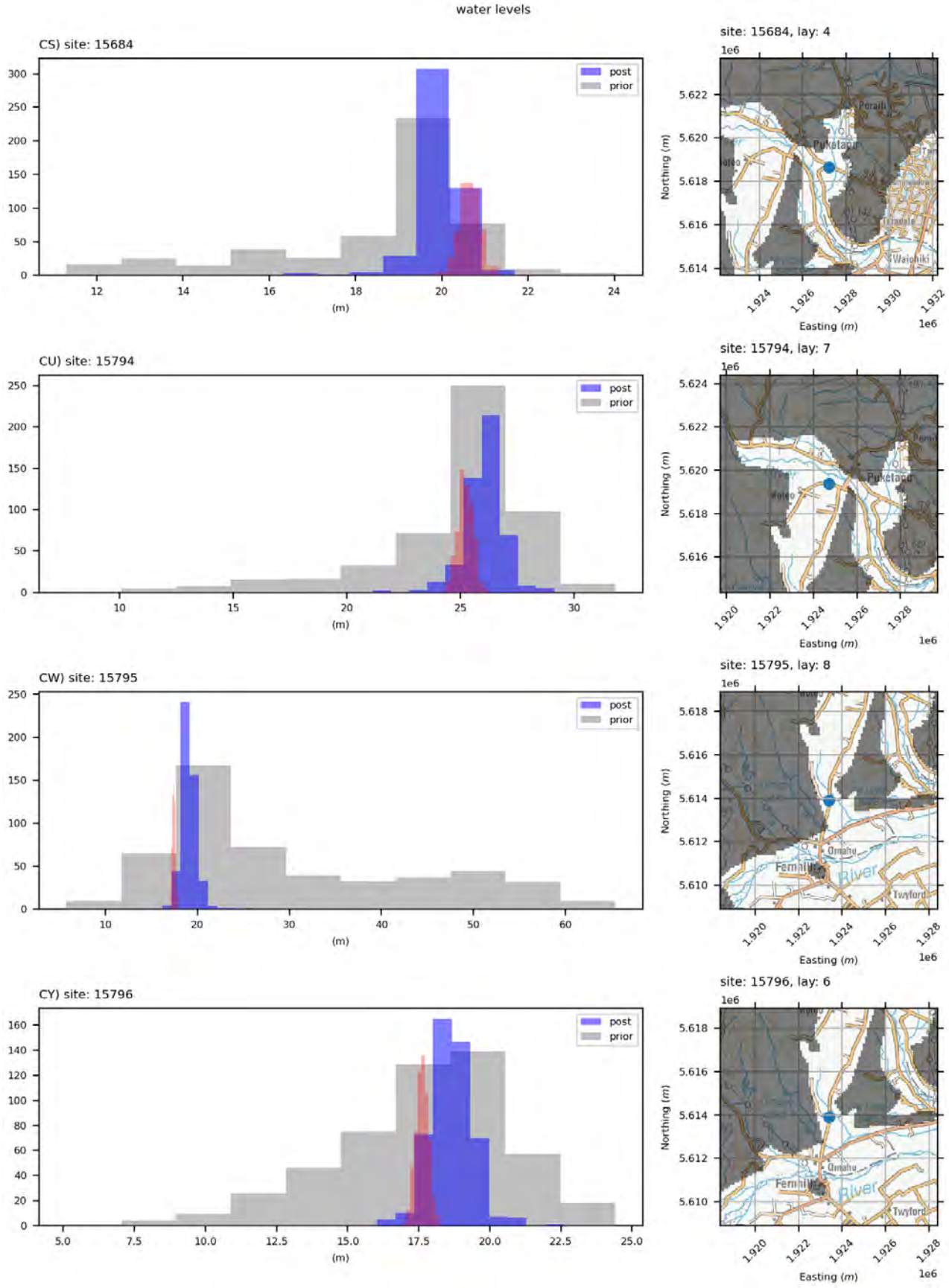
water levels
CS) site: 15684
post
prior
(m)
site: 15684, lay: 4
1e6
Northing (m)
Easting (m)
Pukeiaro
Waionuku
CU) site: 15794
site: 15794, lay: 7
CW) site: 15795
site: 15795, lay: 8
Omahu
Fernhill
Twyford
CY) site: 15796
site: 15796, lay: 6

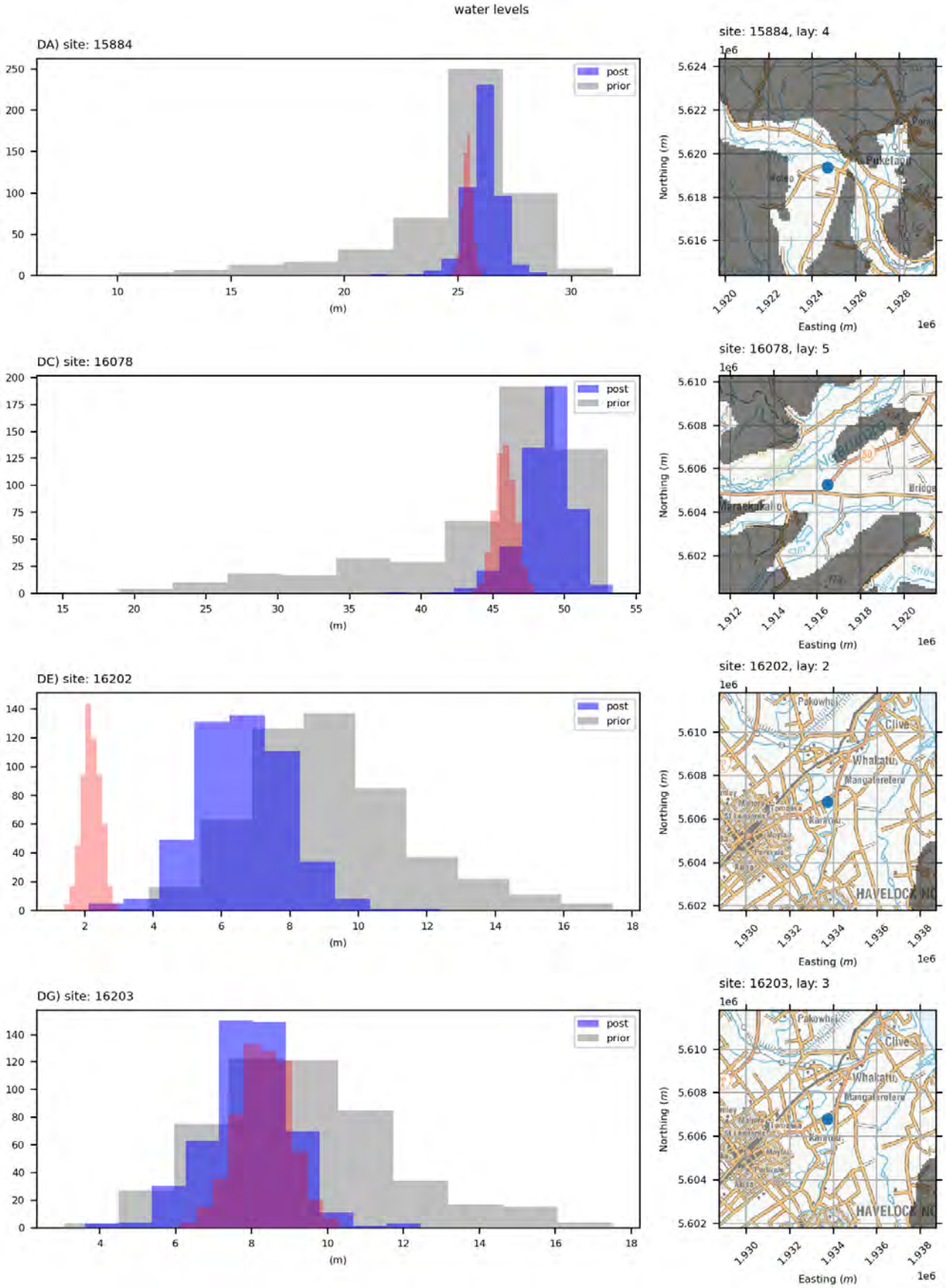
water levels
DA) site: 15884
post
prior
(m)
site: 15884, lay: 4
1e6
Northing (m)
Easting (m)
DC) site: 16078
site: 16078, lay: 5
DE) site: 16202
site: 16202, lay: 2
Pakowhai
Clive
Whakatu
Mangateretere
HAVELOCK NO
DG) site: 16203
site: 16203, lay: 3

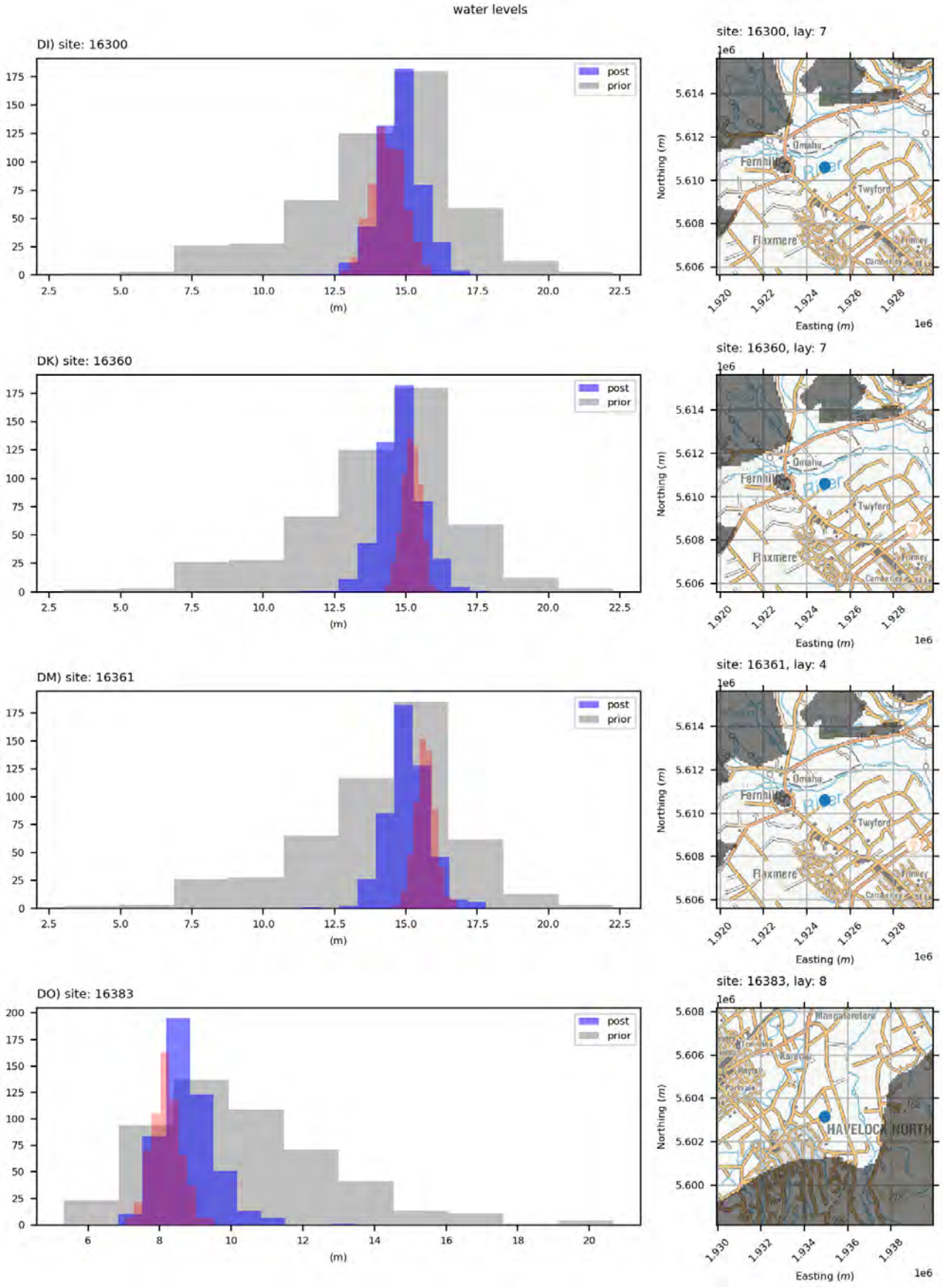
water levels
DI) site: 16300
DK) site: 16360
DM) site: 16361
DO) site: 16383
post
prior
(m)
site: 16300, lay: 7
site: 16360, lay: 7
site: 16361, lay: 4
site: 16383, lay: 8
Northing (m)
Easting (m)
1e6
Omahu
Fernhill
Twyford
Flaxmere
Frimley
HAVELOCK NORTH

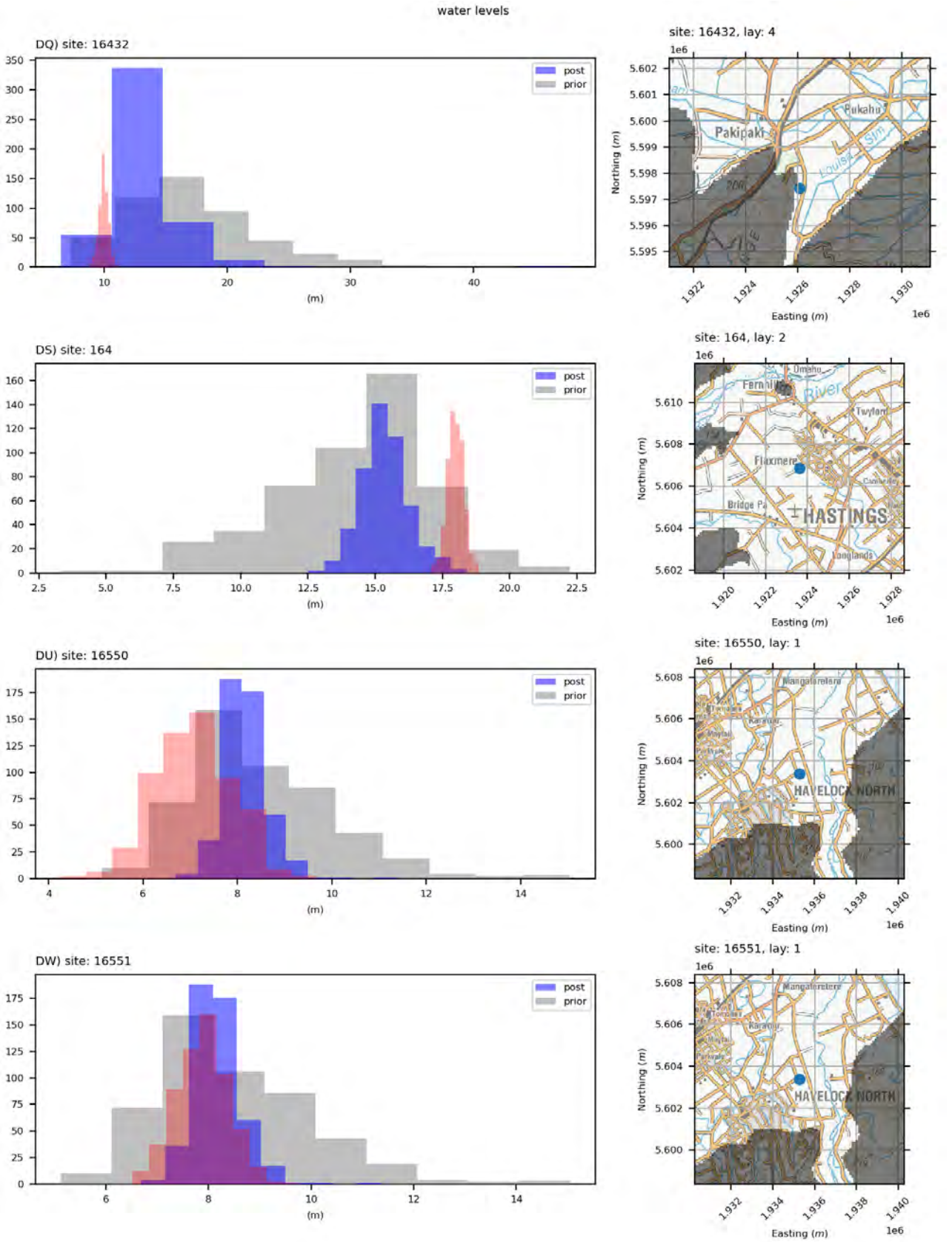
water levels
DQ) site: 16432
post
prior
(m)
site: 16432, lay: 4
1e6
Pukahu
Pakipaki
Northing (m)
Easting (m)
DS) site: 164
site: 164, lay: 2
Omahu
Fernhill
River
Twyford
Flaxmere
Bridge Pa
HASTINGS
Northing (m)
Easting (m)
DU) site: 16550
site: 16550, lay: 1
Mangateretere
HAVELOCK NORTH
Northing (m)
Easting (m)
DW) site: 16551
site: 16551, lay: 1
Mangateretere
HAVELOCK NORTH
Northing (m)
Easting (m)

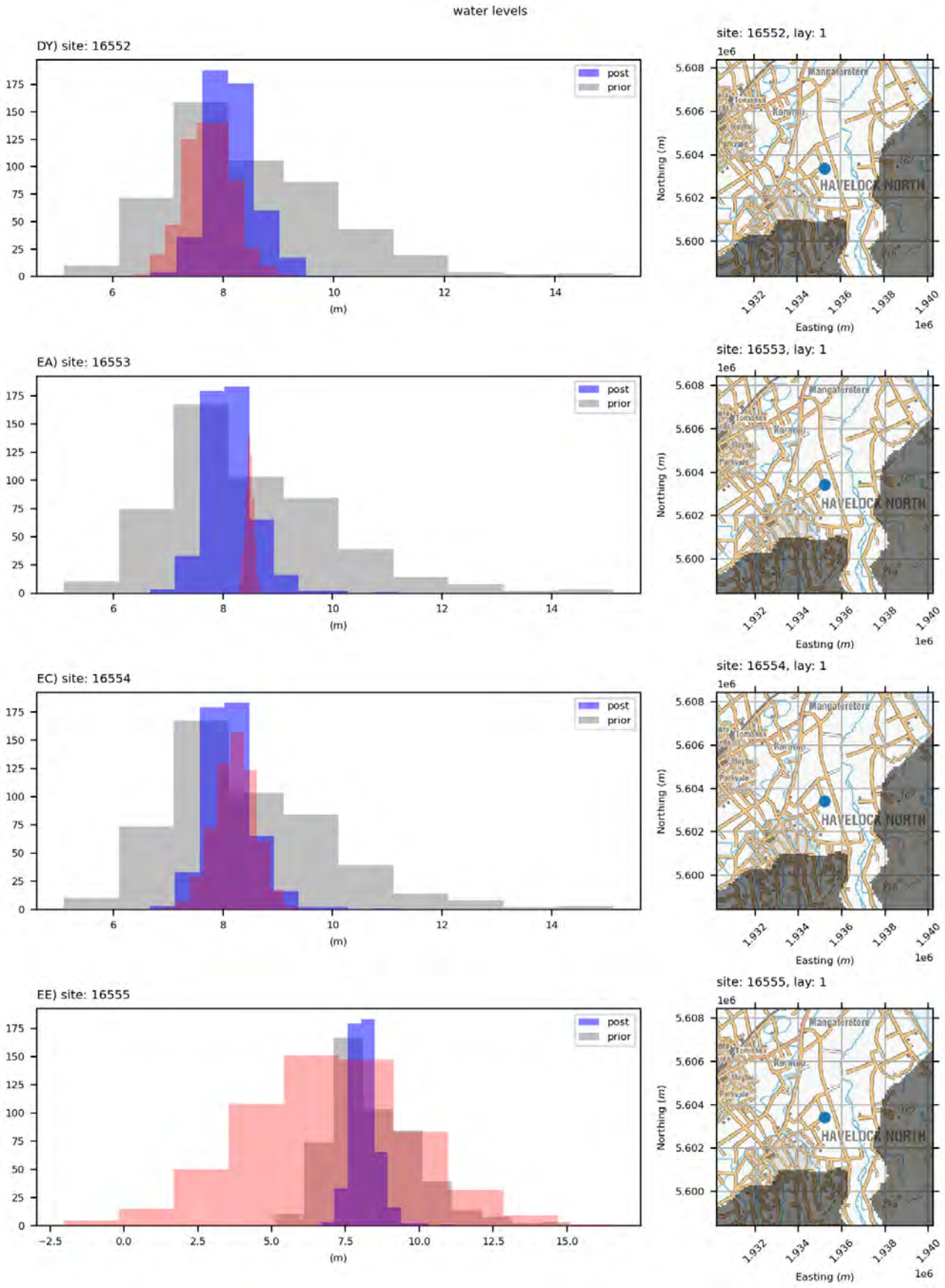
water levels
DY) site: 16552
EA) site: 16553
EC) site: 16554
EE) site: 16555
post
prior
(m)
site: 16552, lay: 1
site: 16553, lay: 1
site: 16554, lay: 1
site: 16555, lay: 1
1e6
Northing (m)
Easting (m)
HAVELOCK NORTH
Mangateretere

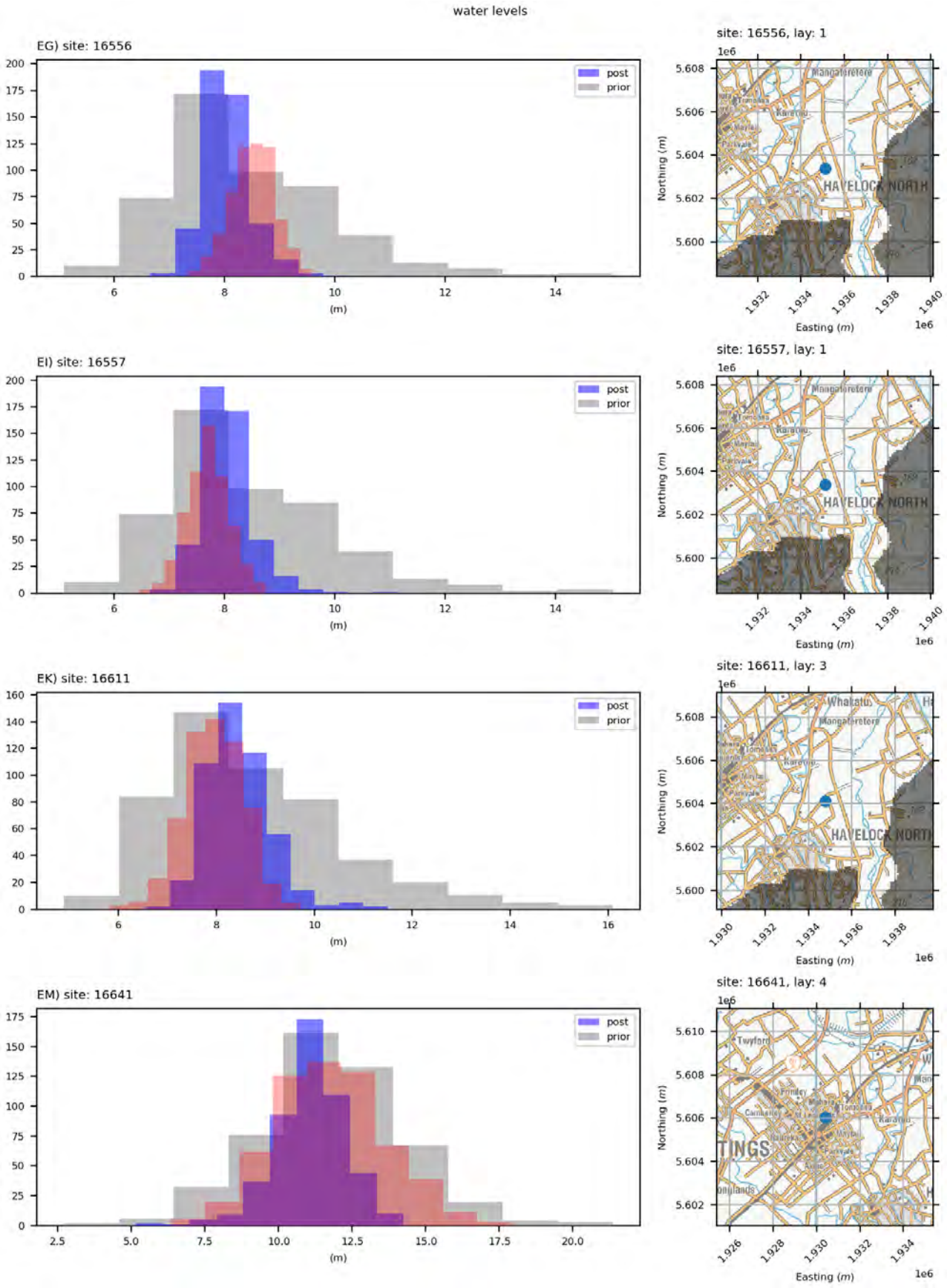
water levels
EG) site: 16556
post
prior
(m)
site: 16556, lay: 1
1e6
Northing (m)
Easting (m)
HAVELOCK NORTH
EI) site: 16557
site: 16557, lay: 1
EK) site: 16611
site: 16611, lay: 3
EM) site: 16641
site: 16641, lay: 4
TINGS

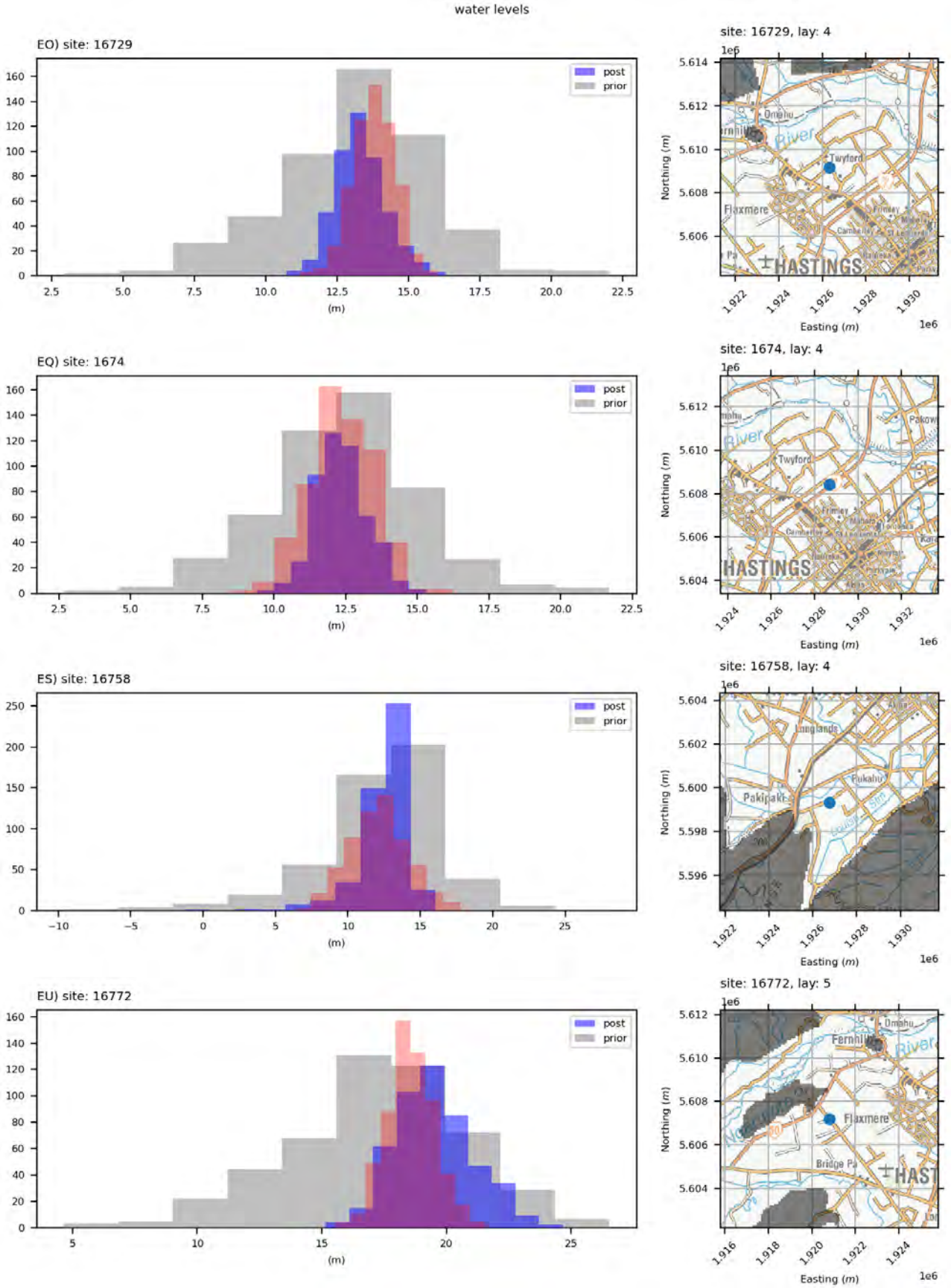
water levels
EO) site: 16729
post
prior
(m)
site: 16729, lay: 4
1e6
Northing (m)
Easting (m)
Omahu
Twyford
Flaxmere
HASTINGS
EQ) site: 1674
site: 1674, lay: 4
ES) site: 16758
site: 16758, lay: 4
Pakipaki
Pukahu
EU) site: 16772
site: 16772, lay: 5
Fernhill
Bridge Pa

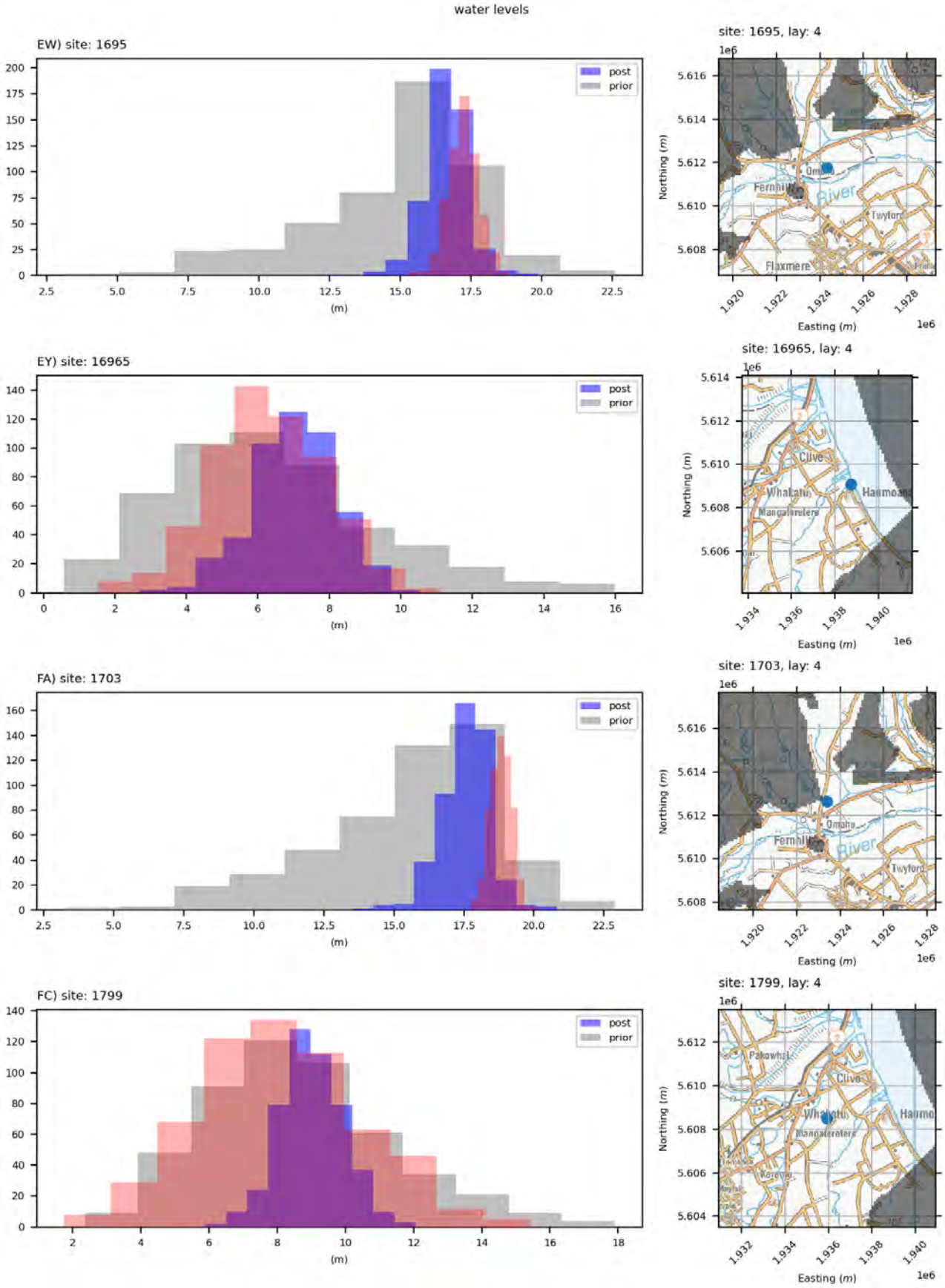
water levels
EW) site: 1695
post
prior
(m)
site: 1695, lay: 4
Northing (m)
Easting (m)
1e6
Omaha
Fernhill
River
Twyford
Flaxmere
EY) site: 16965
site: 16965, lay: 4
Clive
Whakatu
Hawkes Bay
Mangateretere
FA) site: 1703
site: 1703, lay: 4
FC) site: 1799
site: 1799, lay: 4
Pakowhai
Haumo
Korokipo

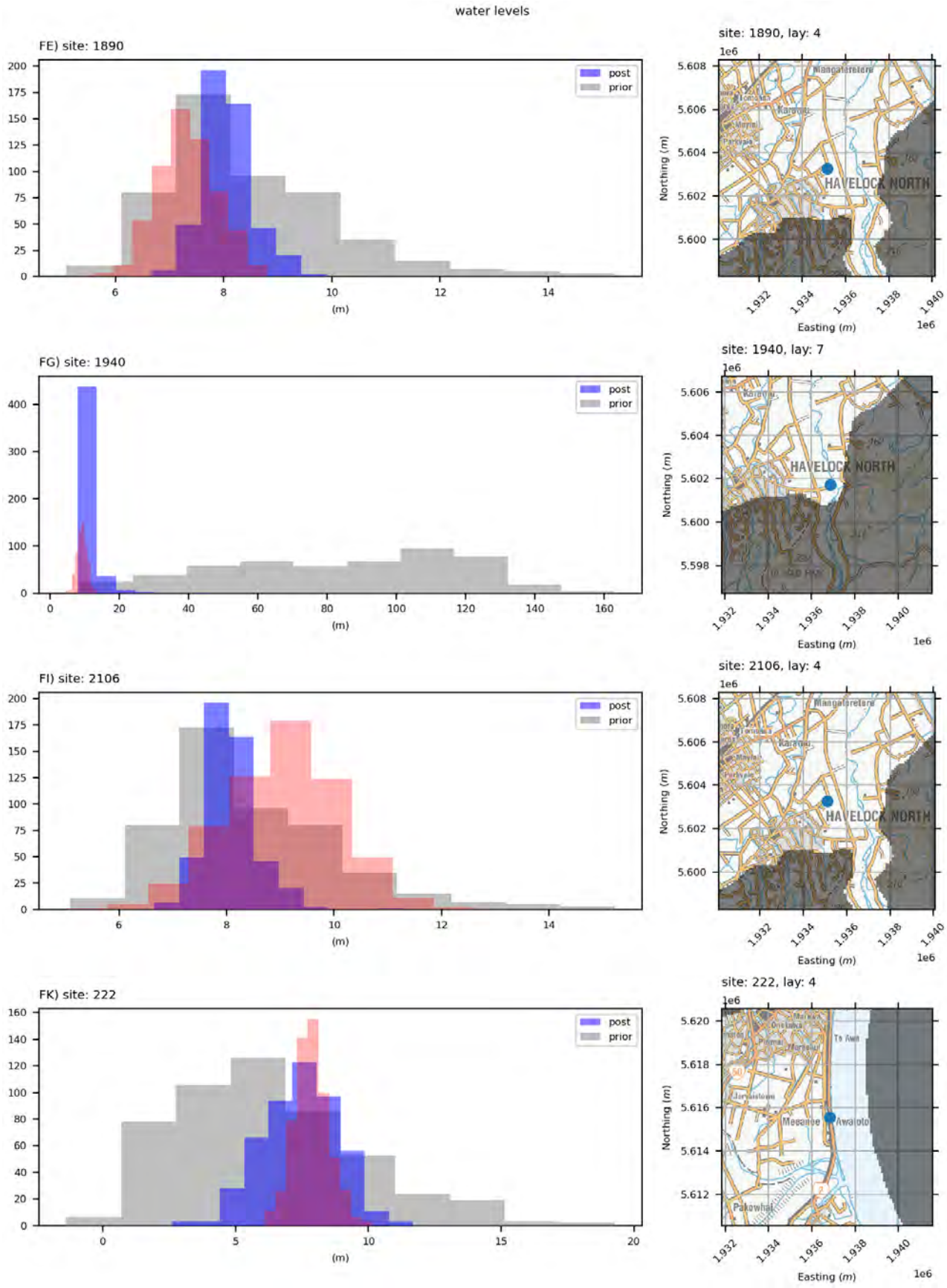
water levels
FE) site: 1890
post
prior
(m)
site: 1890, lay: 4
1e6
HAVELOCK NORTH
Northing (m)
Easting (m)
FG) site: 1940
site: 1940, lay: 7
FI) site: 2106
site: 2106, lay: 4
FK) site: 222
site: 222, lay: 4
Mangateretere
Karamu
Meeanee
Awapoto
Pakowhai
To Awa

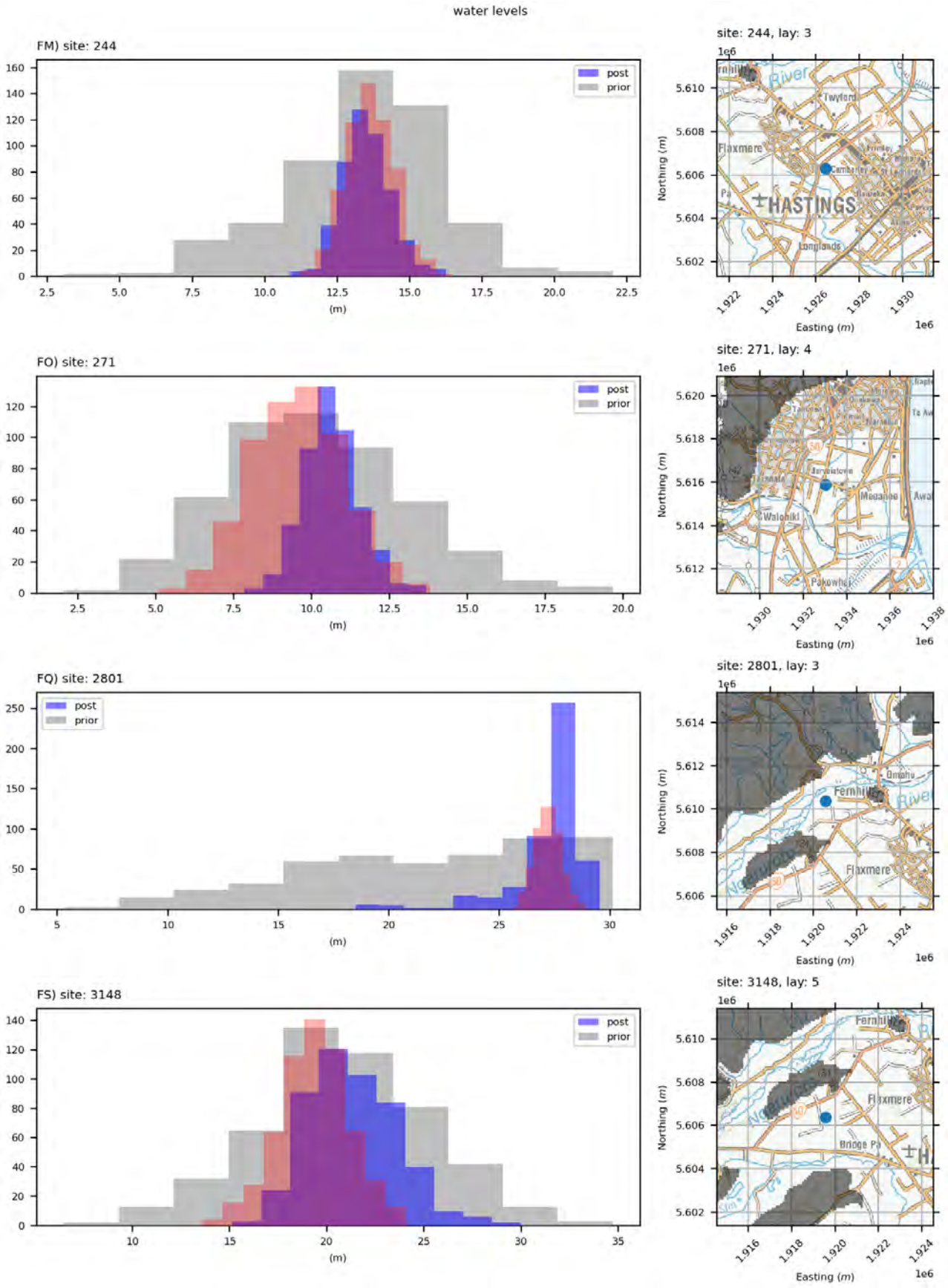
water levels
FM) site: 244
post
prior
(m)
site: 244, lay: 3
1e6
Twyford
Flaxmere
HASTINGS
Longlands
Northing (m)
Easting (m)
FO) site: 271
post
prior
(m)
site: 271, lay: 4
1e6
Waiohiki
Pakowhai
Northing (m)
Easting (m)
FQ) site: 2801
post
prior
(m)
site: 2801, lay: 3
1e6
Fernhill
Flaxmere
Northing (m)
Easting (m)
FS) site: 3148
post
prior
(m)
site: 3148, lay: 5
1e6
Fernhill
Flaxmere
Northing (m)
Easting (m)

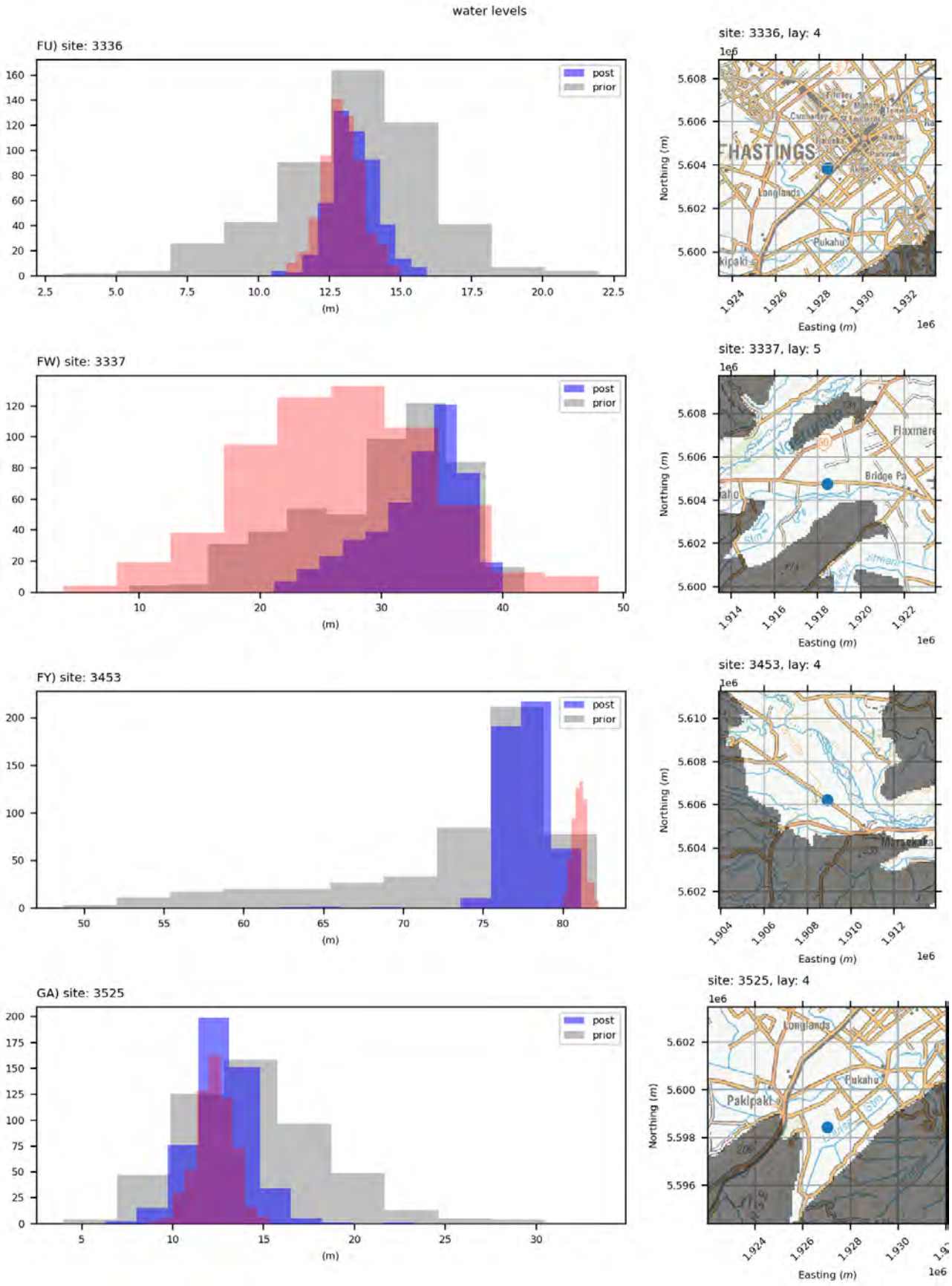
water levels
FU) site: 3336
post
prior
(m)
site: 3336, lay: 4
1e6
HASTINGS
Longlands
Pukahu
Northing (m)
Easting (m)
FW) site: 3337
site: 3337, lay: 5
Flaxmere
Bridge Pa
FY) site: 3453
site: 3453, lay: 4
GA) site: 3525
site: 3525, lay: 4
Pakipaki

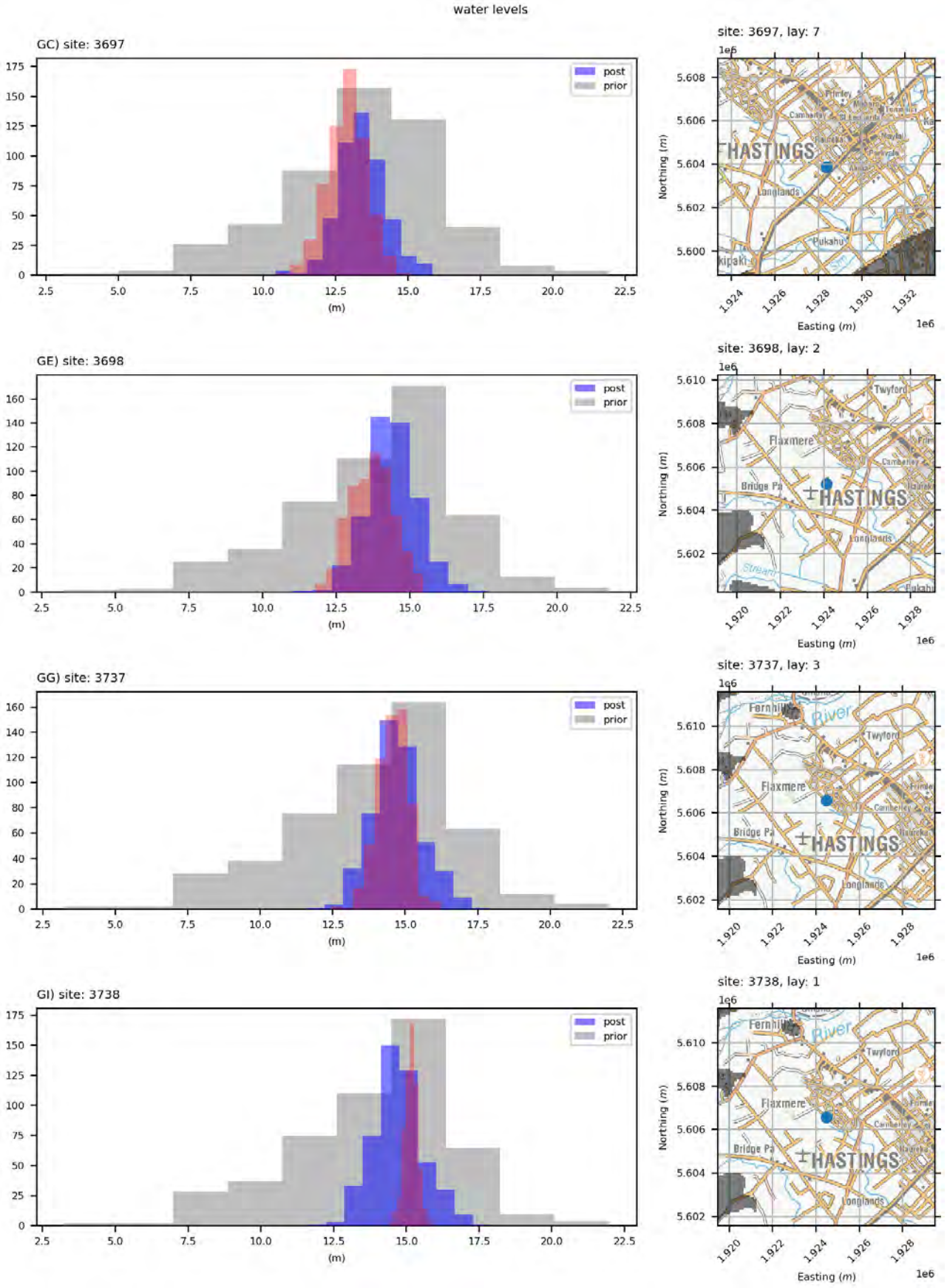
water levels
GC) site: 3697
GE) site: 3698
GG) site: 3737
GI) site: 3738
post
prior
(m)
site: 3697, lay: 7
site: 3698, lay: 2
site: 3737, lay: 3
site: 3738, lay: 1
Northing (m)
Easting (m)
1e6
HASTINGS
Flaxmere
Twyford
Fernhill
Longlands
Bridge Pa
Pukahu

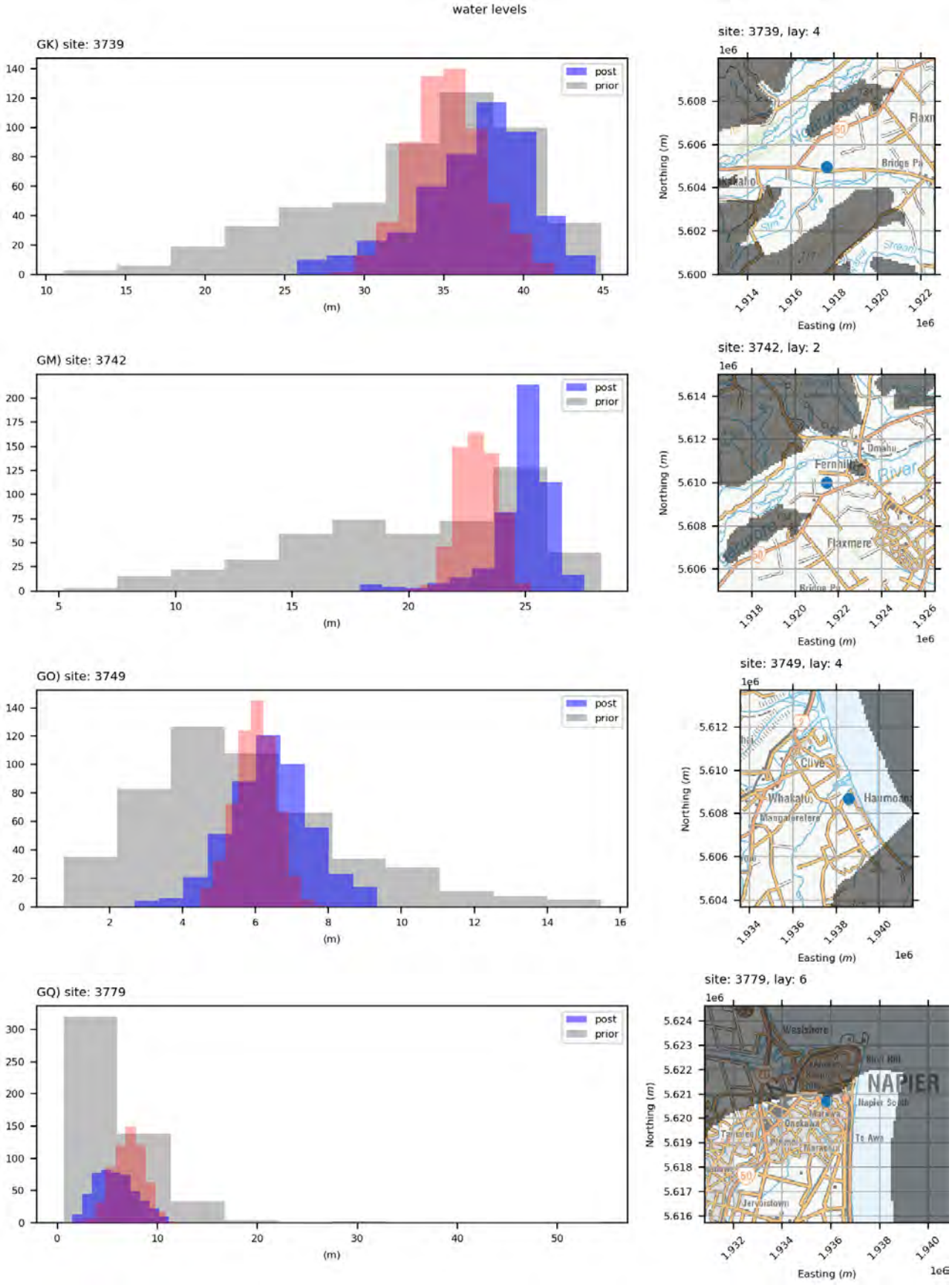
water levels
GK) site: 3739
post
prior
(m)
site: 3739, lay: 4
Northing (m)
Easting (m)
1e6
GM) site: 3742
post
prior
(m)
site: 3742, lay: 2
Northing (m)
Easting (m)
1e6
GO) site: 3749
post
prior
(m)
site: 3749, lay: 4
Northing (m)
Easting (m)
1e6
GQ) site: 3779
post
prior
(m)
site: 3779, lay: 6
Northing (m)
Easting (m)
1e6

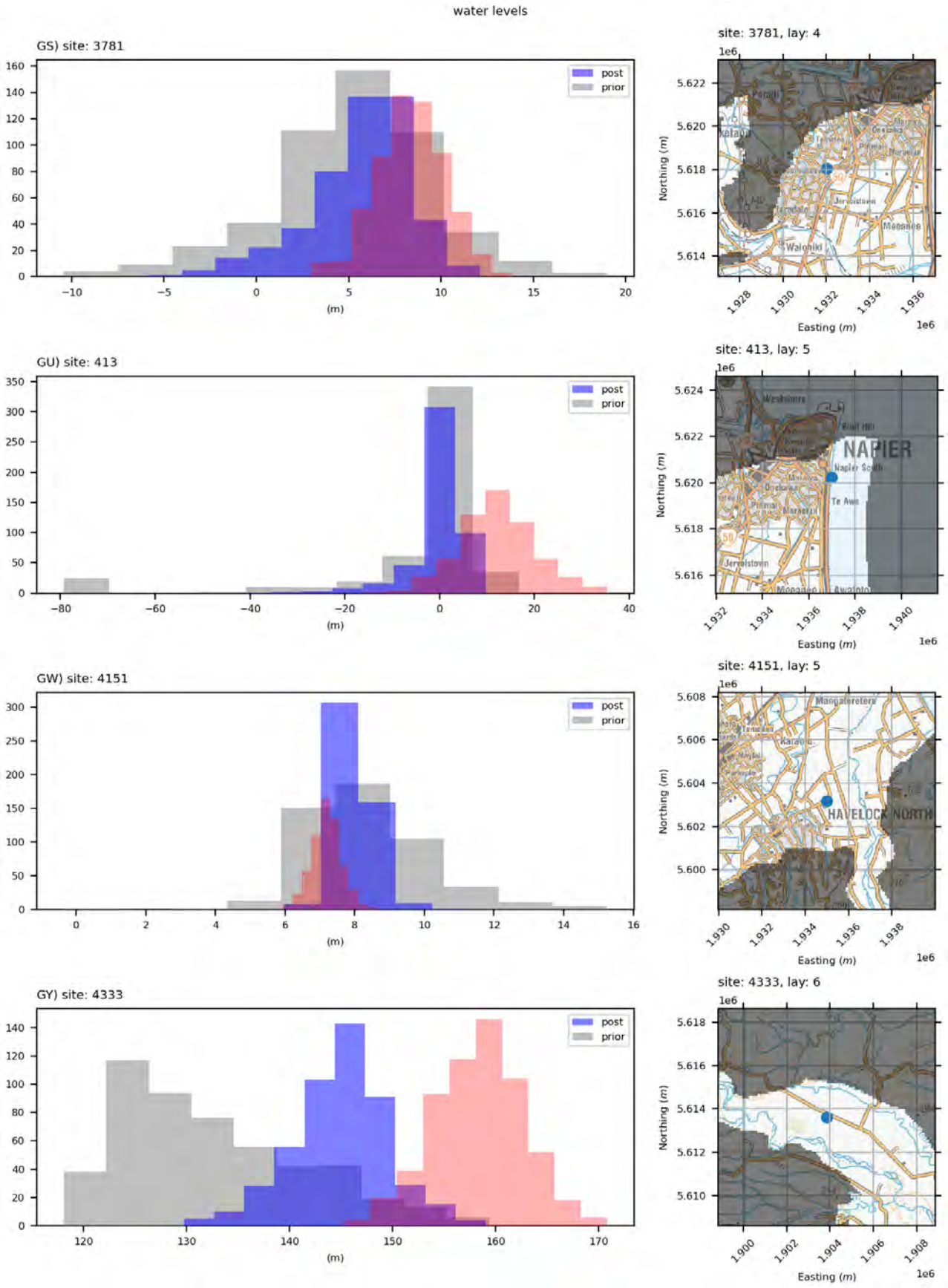
water levels
GS) site: 3781
post
prior
(m)
site: 3781, lay: 4
1e6
Northing (m)
Easting (m)
GU) site: 413
site: 413, lay: 5
NAPIER
GW) site: 4151
site: 4151, lay: 5
HAVELOCK NORTH
GY) site: 4333
site: 4333, lay: 6

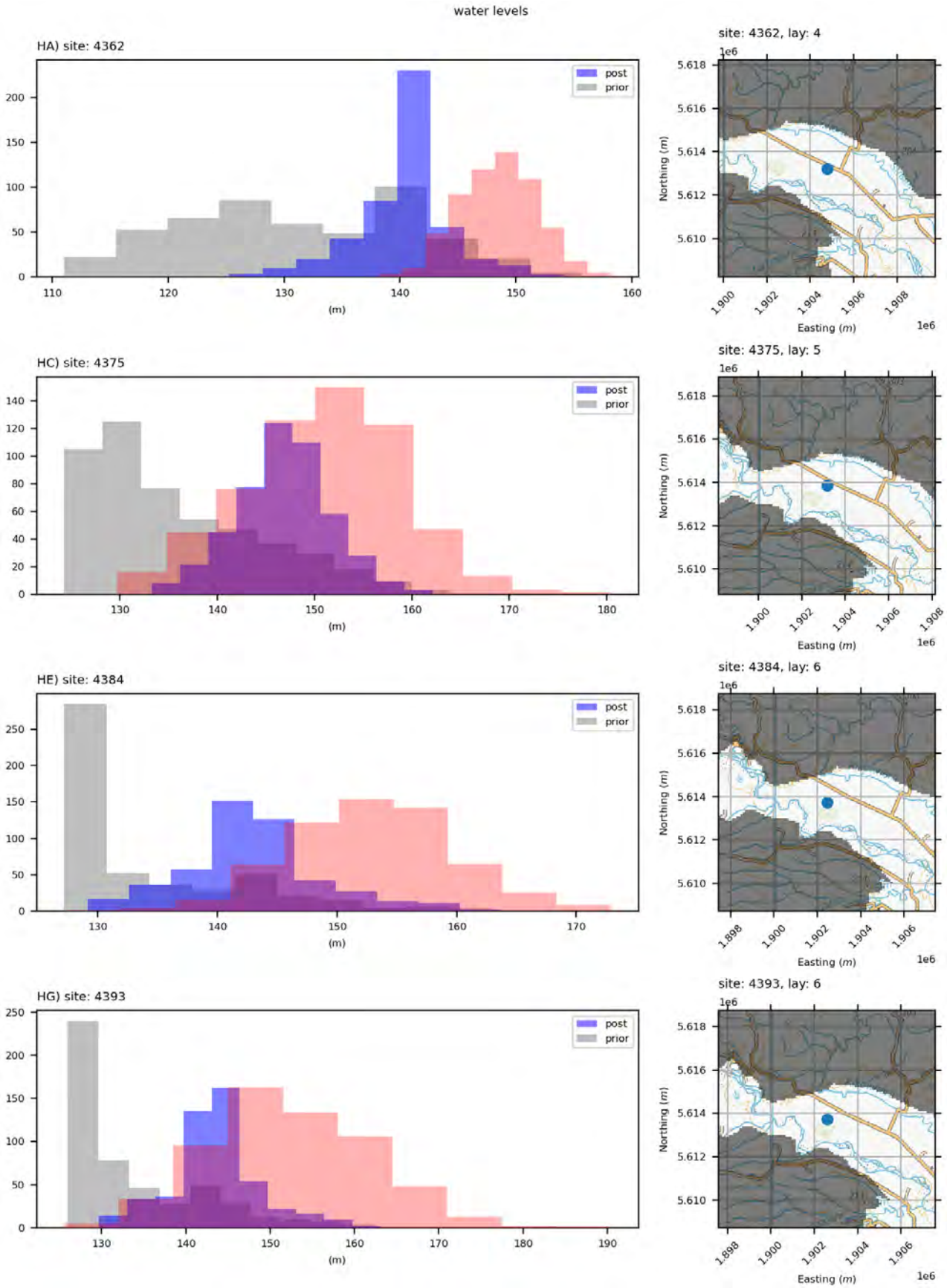
water levels
HA) site: 4362
post
prior
(m)
site: 4362, lay: 4
1e6
Northing (m)
Easting (m)
HC) site: 4375
site: 4375, lay: 5
HE) site: 4384
site: 4384, lay: 6
HG) site: 4393
site: 4393, lay: 6

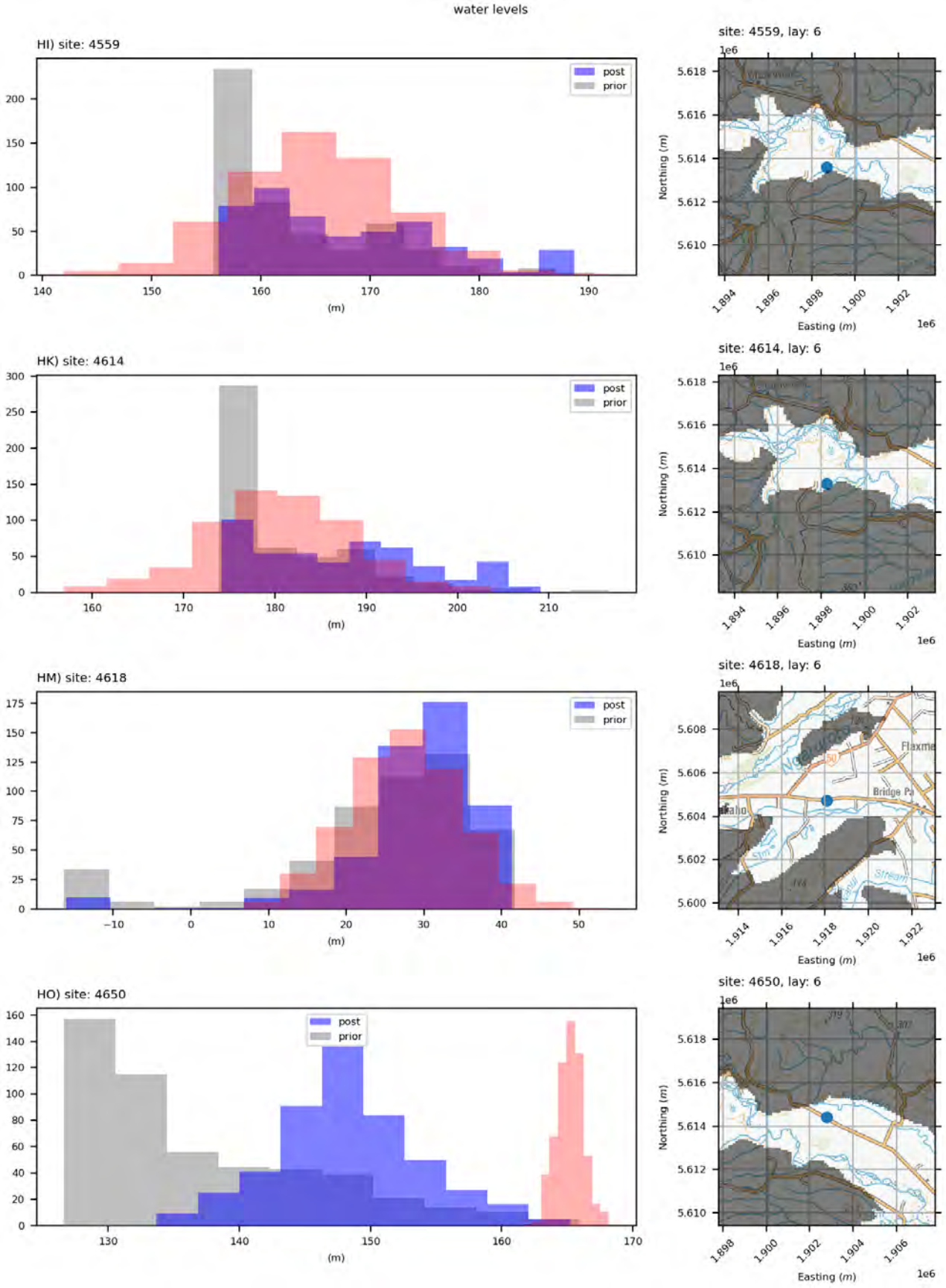
water levels
HI) site: 4559
post
prior
(m)
site: 4559, lay: 6
1e6
Northing (m)
Easting (m)
HK) site: 4614
site: 4614, lay: 6
HM) site: 4618
site: 4618, lay: 6
HO) site: 4650
site: 4650, lay: 6

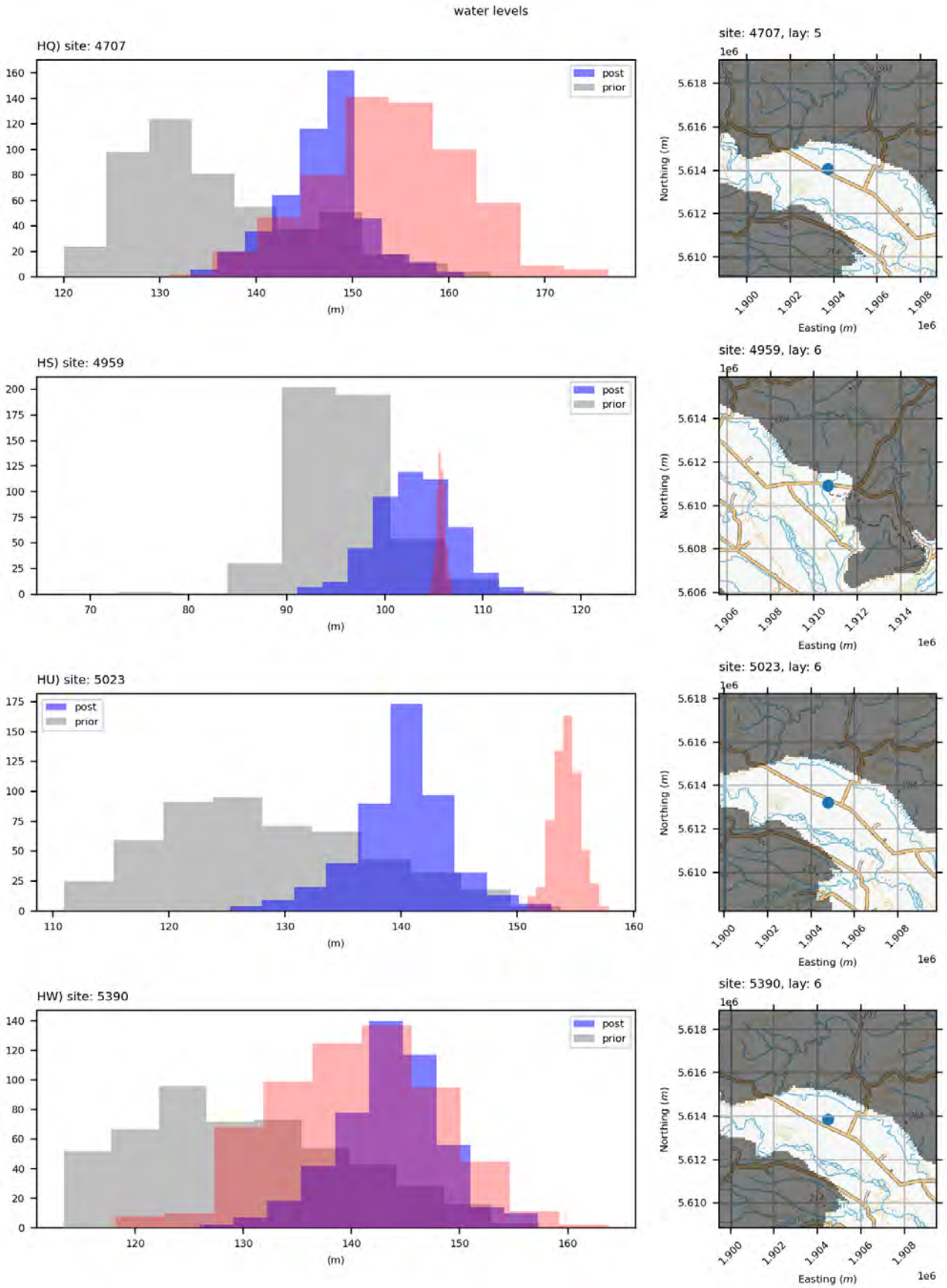
water levels
HQ) site: 4707
post
prior
(m)
site: 4707, lay: 5
1e6
Northing (m)
Easting (m)
HS) site: 4959
site: 4959, lay: 6
HU) site: 5023
site: 5023, lay: 6
HW) site: 5390
site: 5390, lay: 6

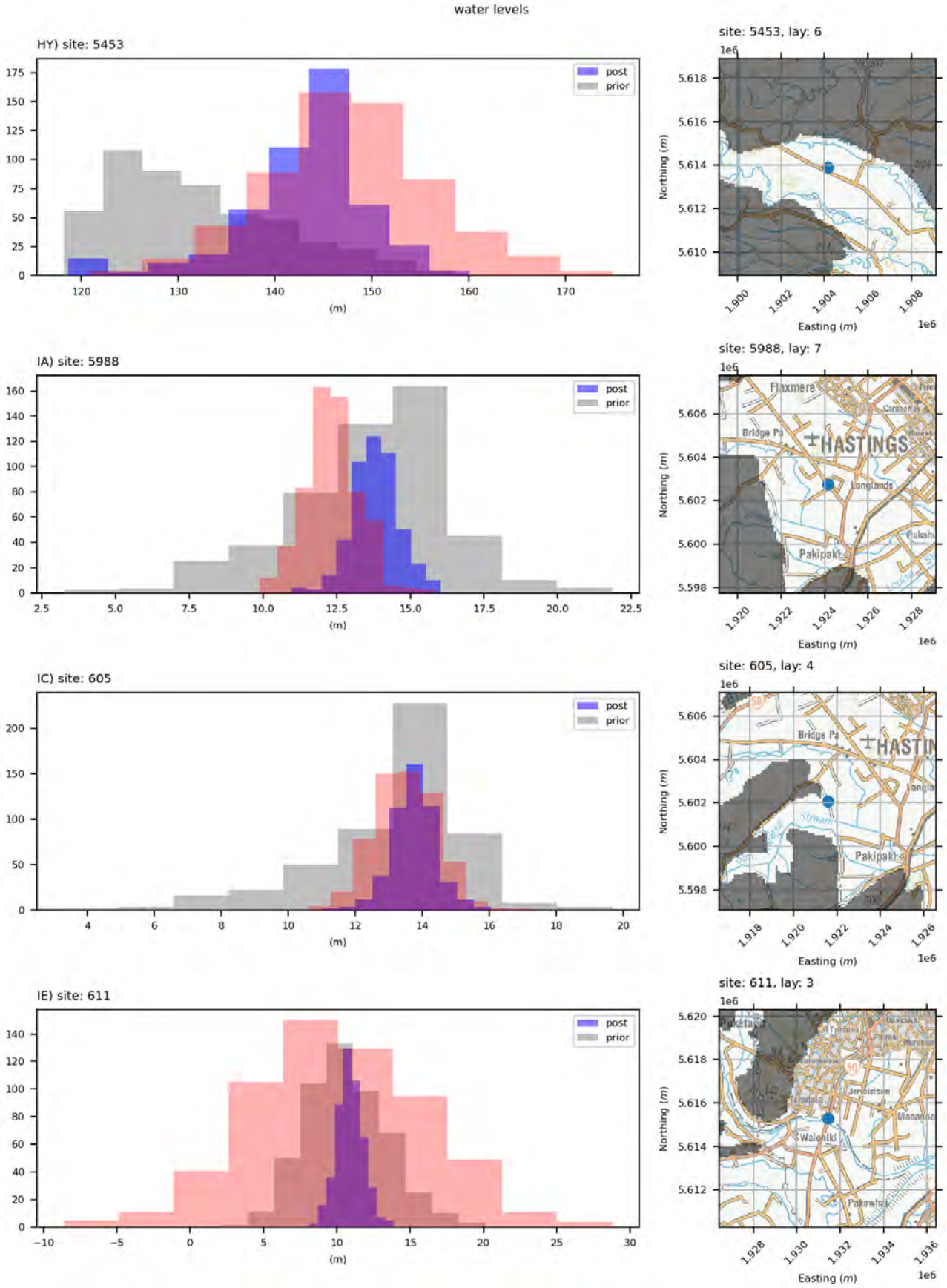
water levels
HY) site: 5453
post
prior
(m)
site: 5453, lay: 6
1e6
Northing (m)
Easting (m)
IA) site: 5988
site: 5988, lay: 7
Flaxmere
Bridge Pa
HASTINGS
Longlands
Pakipaki
IC) site: 605
site: 605, lay: 4
IE) site: 611
site: 611, lay: 3
Waiohiki
Pakowhai

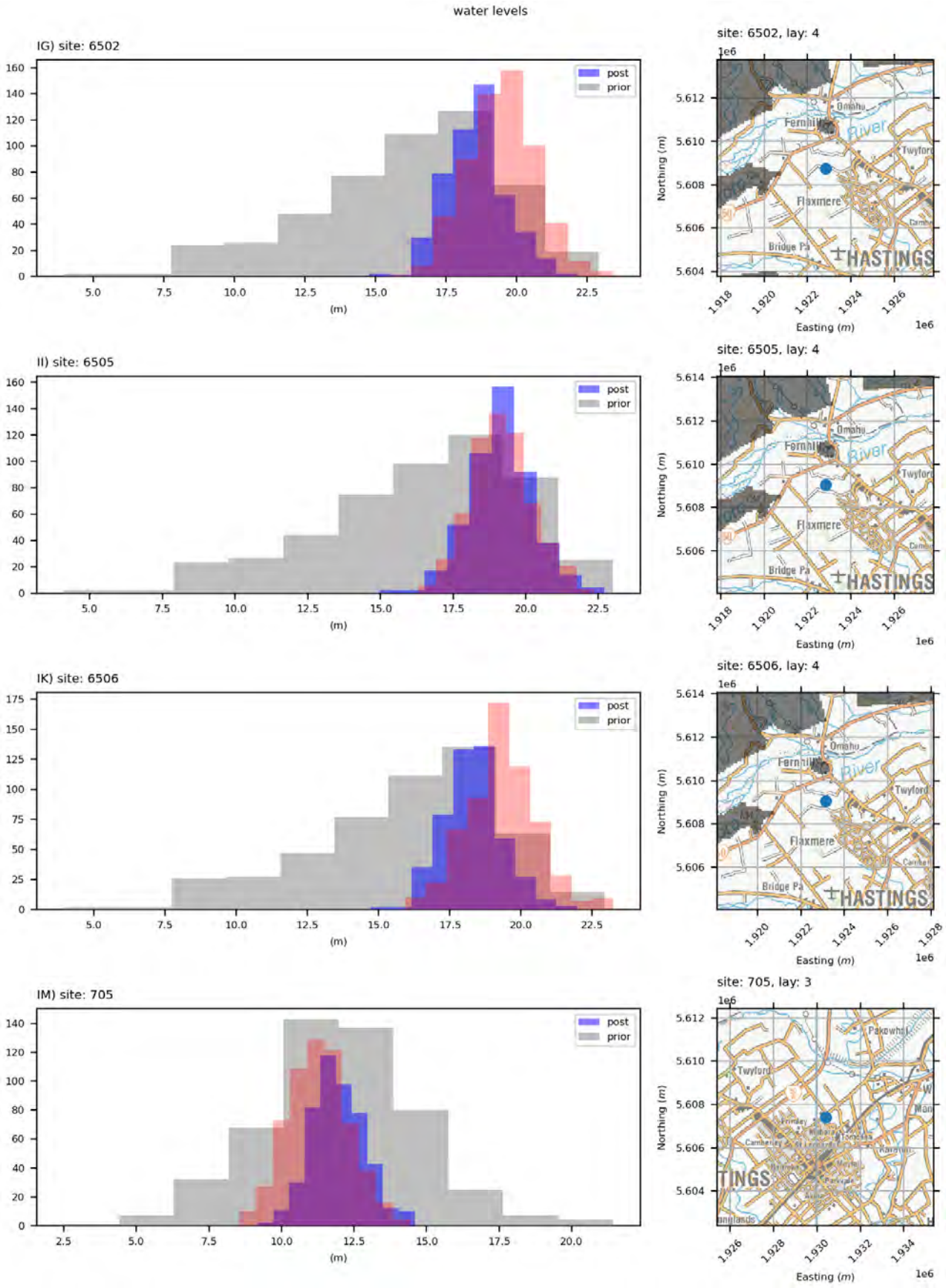
water levels
IG) site: 6502
post
prior
(m)
site: 6502, lay: 4
1e6
Northing (m)
Easting (m)
Omaha
Fernhill
River
Twyford
Flaxmere
Bridge Pa
HASTINGS
II) site: 6505
site: 6505, lay: 4
IK) site: 6506
site: 6506, lay: 4
IM) site: 705
site: 705, lay: 3
Pakowhai
Camberley

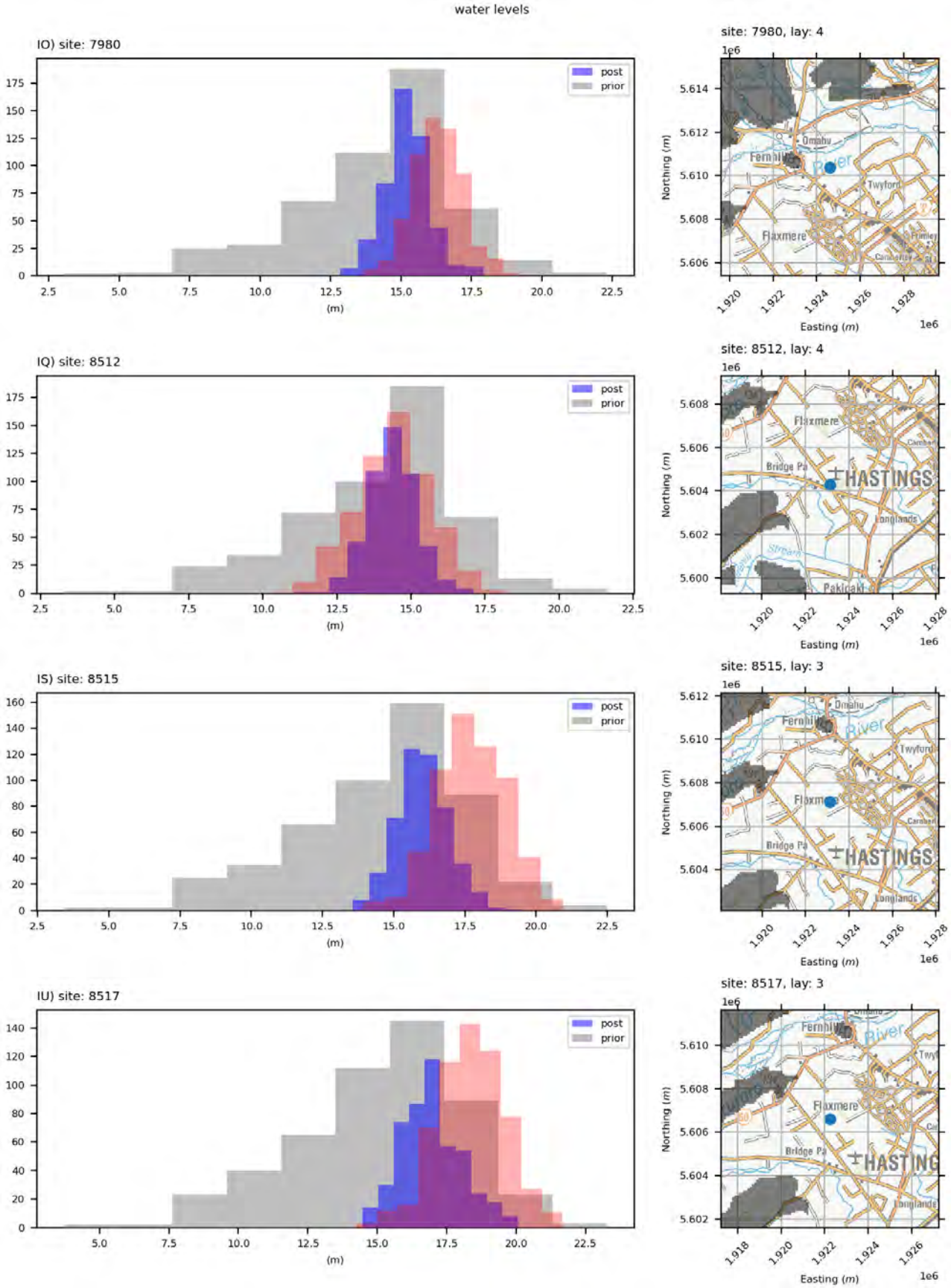
water levels
IO) site: 7980
post
prior
(m)
site: 7980, lay: 4
1e6
Northing (m)
Easting (m)
Omahu
Twyford
Flaxmere
IQ) site: 8512
site: 8512, lay: 4
Bridge Pa
HASTINGS
IS) site: 8515
site: 8515, lay: 3
IU) site: 8517
site: 8517, lay: 3

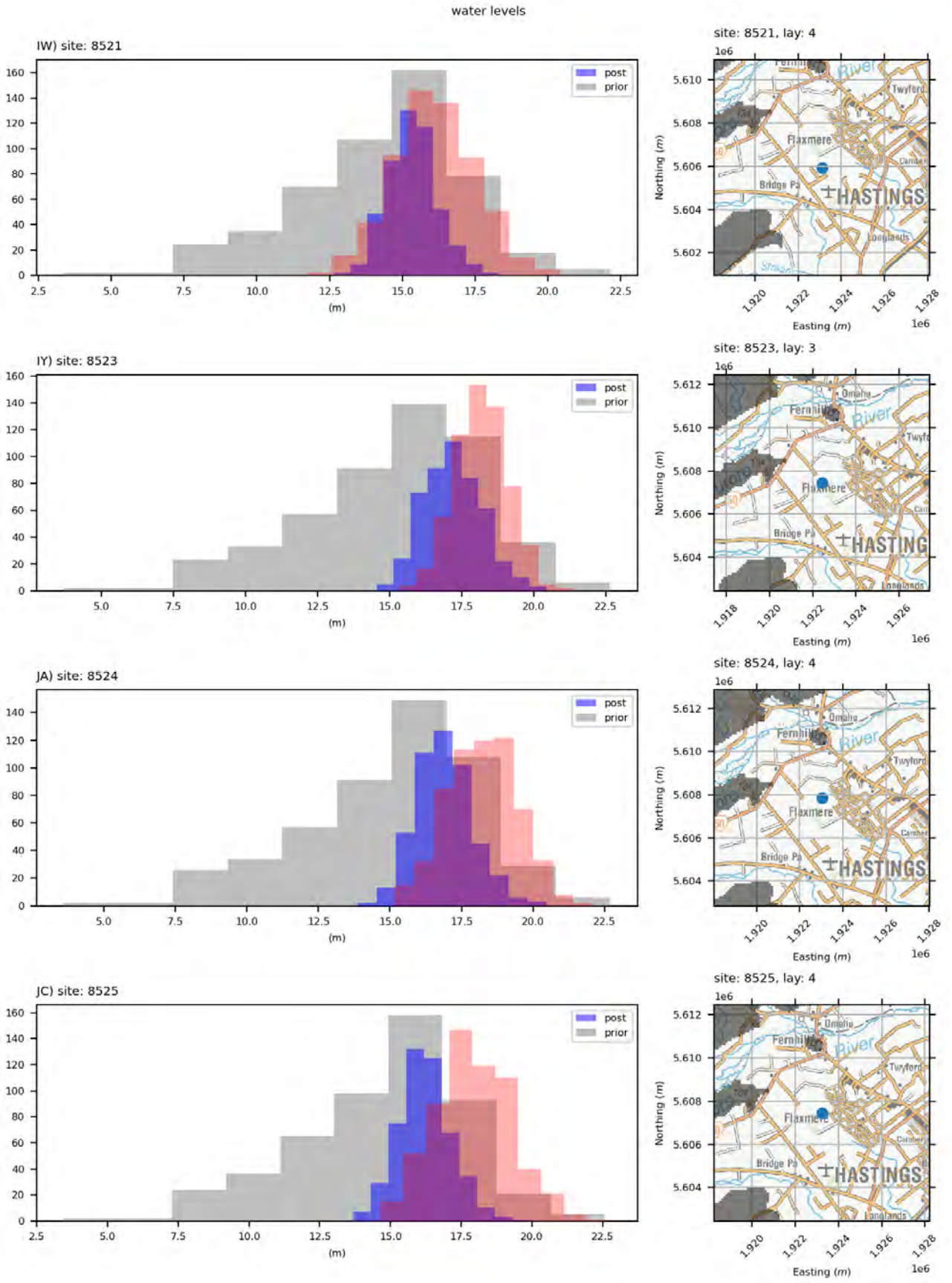
water levels
IW) site: 8521
post
prior
(m)
site: 8521, lay: 4
1e6
Northing (m)
Easting (m)
IY) site: 8523
site: 8523, lay: 3
JA) site: 8524
site: 8524, lay: 4
JC) site: 8525
site: 8525, lay: 4
HASTINGS
Flaxmere
Twyford
Bridge Pa

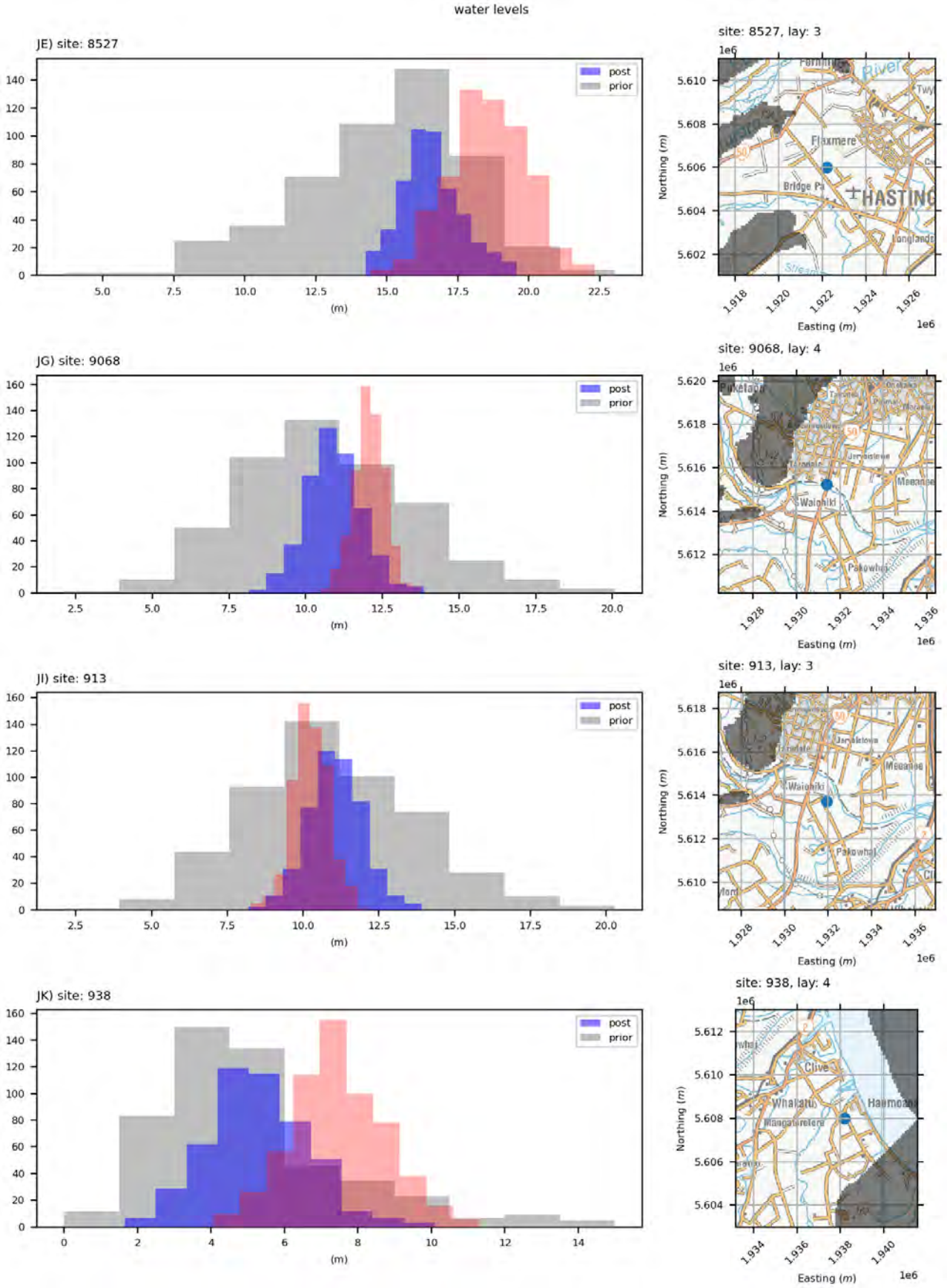
water levels
JE) site: 8527
post
prior
(m)
site: 8527, lay: 3
1e6
Northing (m)
Easting (m)
JG) site: 9068
site: 9068, lay: 4
JI) site: 913
site: 913, lay: 3
JK) site: 938
site: 938, lay: 4
Flaxmere
HASTING
Waiohiki
Pakowhai
Clive
Whakatu
Haumoana

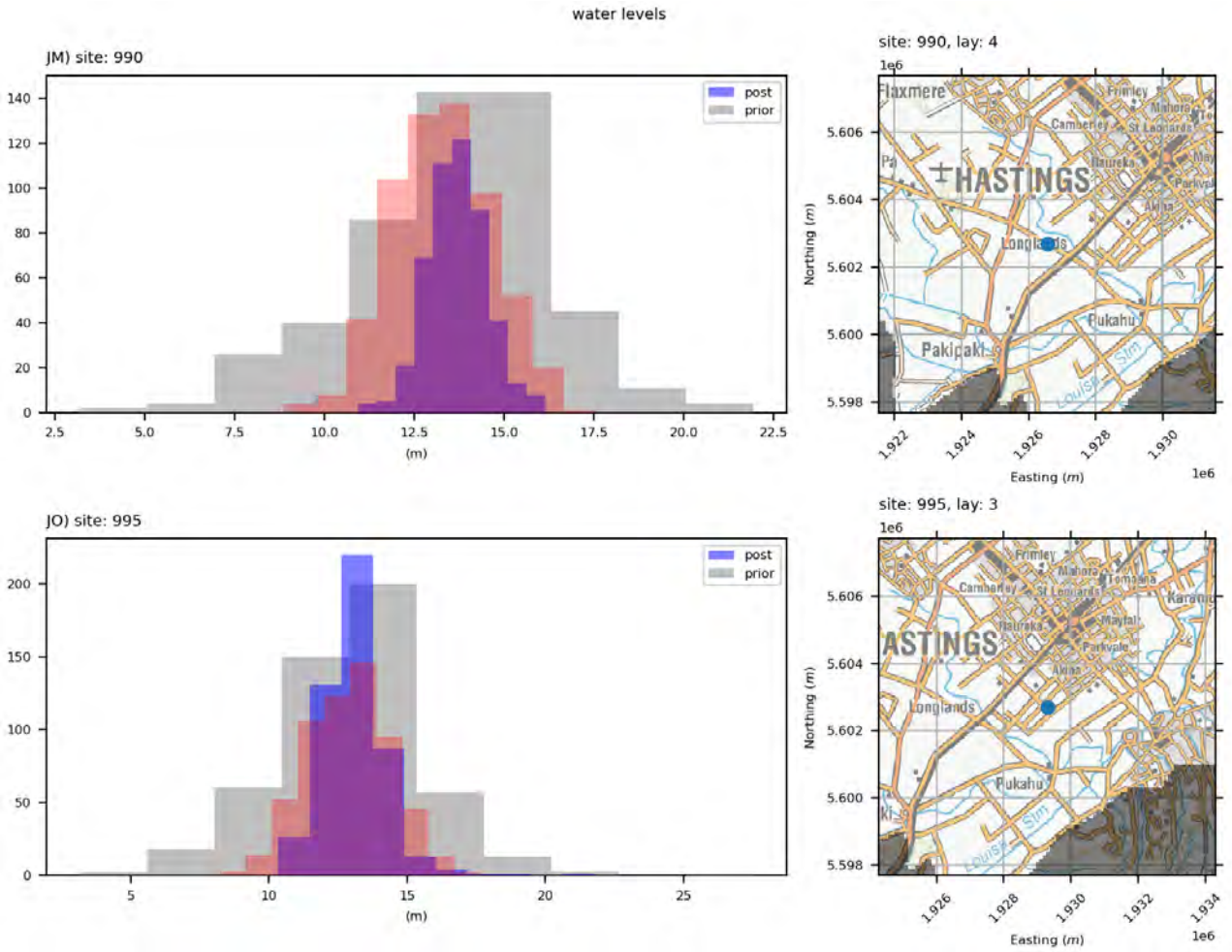
water levels
JM) site: 990
post
prior
(m)
site: 990, lay: 4
1e6
Flaxmere
HASTINGS
Longlands
Pukahu
Pakipaki
Northing (m)
Easting (m)
JO) site: 995
post
prior
(m)
site: 995, lay: 3
1e6
HASTINGS
Longlands
Pukahu
Northing (m)
Easting (m)

A3.2.2.2 Stream Flows

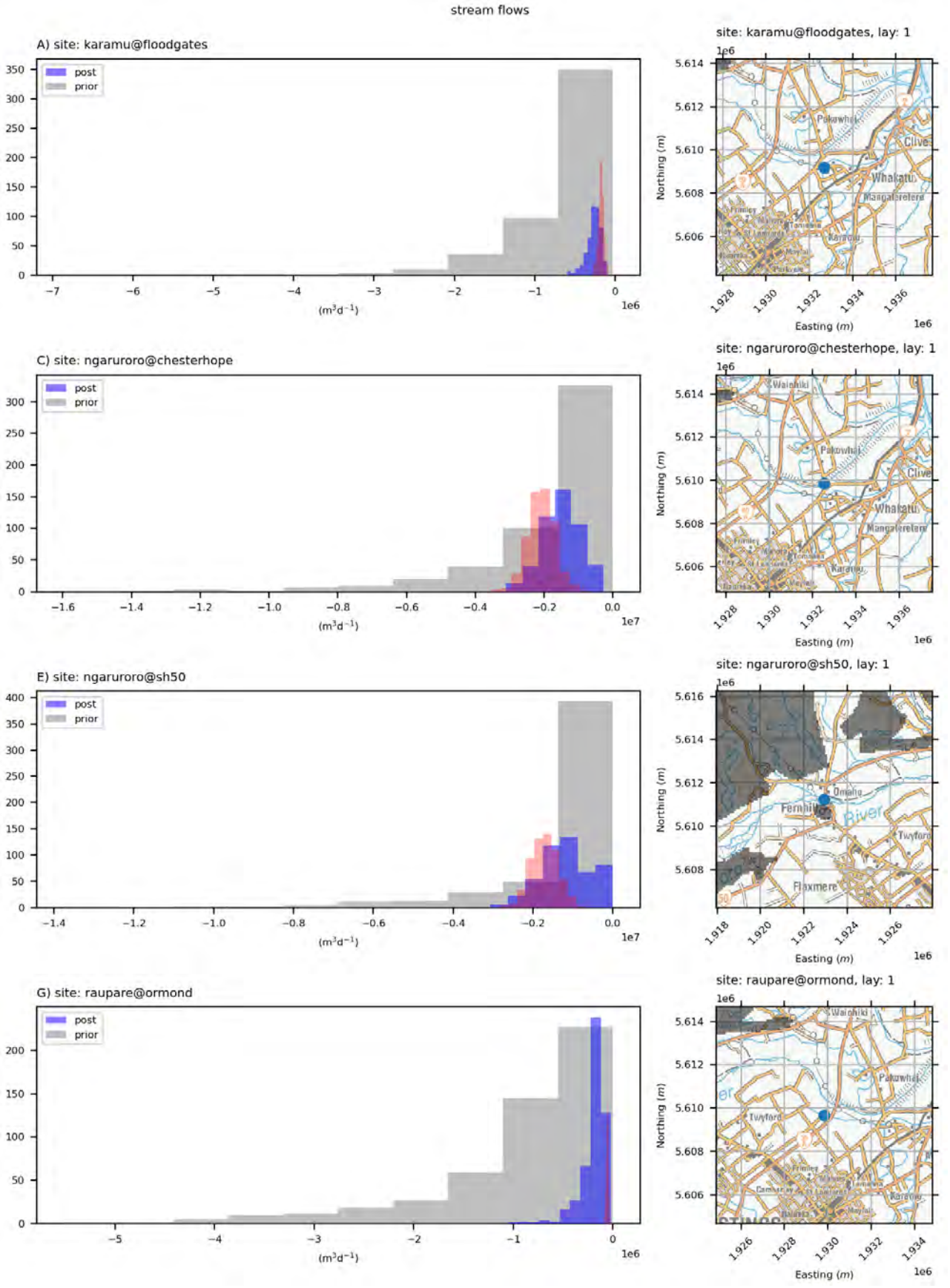

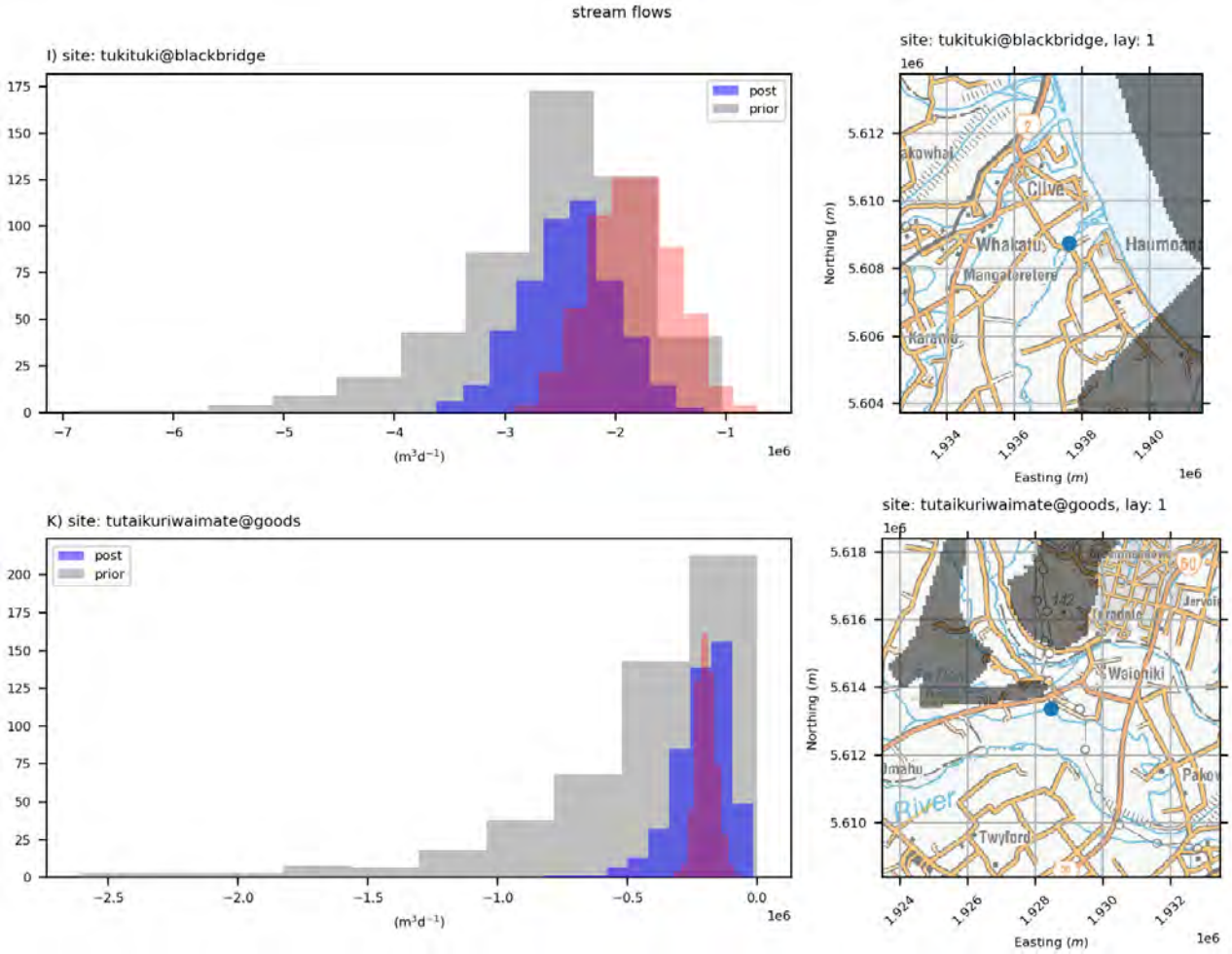
stream flows
I) site: tukituki@blackbridge
post
prior
(m³d⁻¹)
1e6
site: tukituki@blackbridge, lay: 1
Northing (m)
Easting (m)
Clive
Whakatu
Mangateretere
Haumoana
K) site: tutaikuriwaimate@goods
site: tutaikuriwaimate@goods, lay: 1
Waioniki
Twyford
River

A3.2.2.3 Surface-Water–Groundwater Exchange

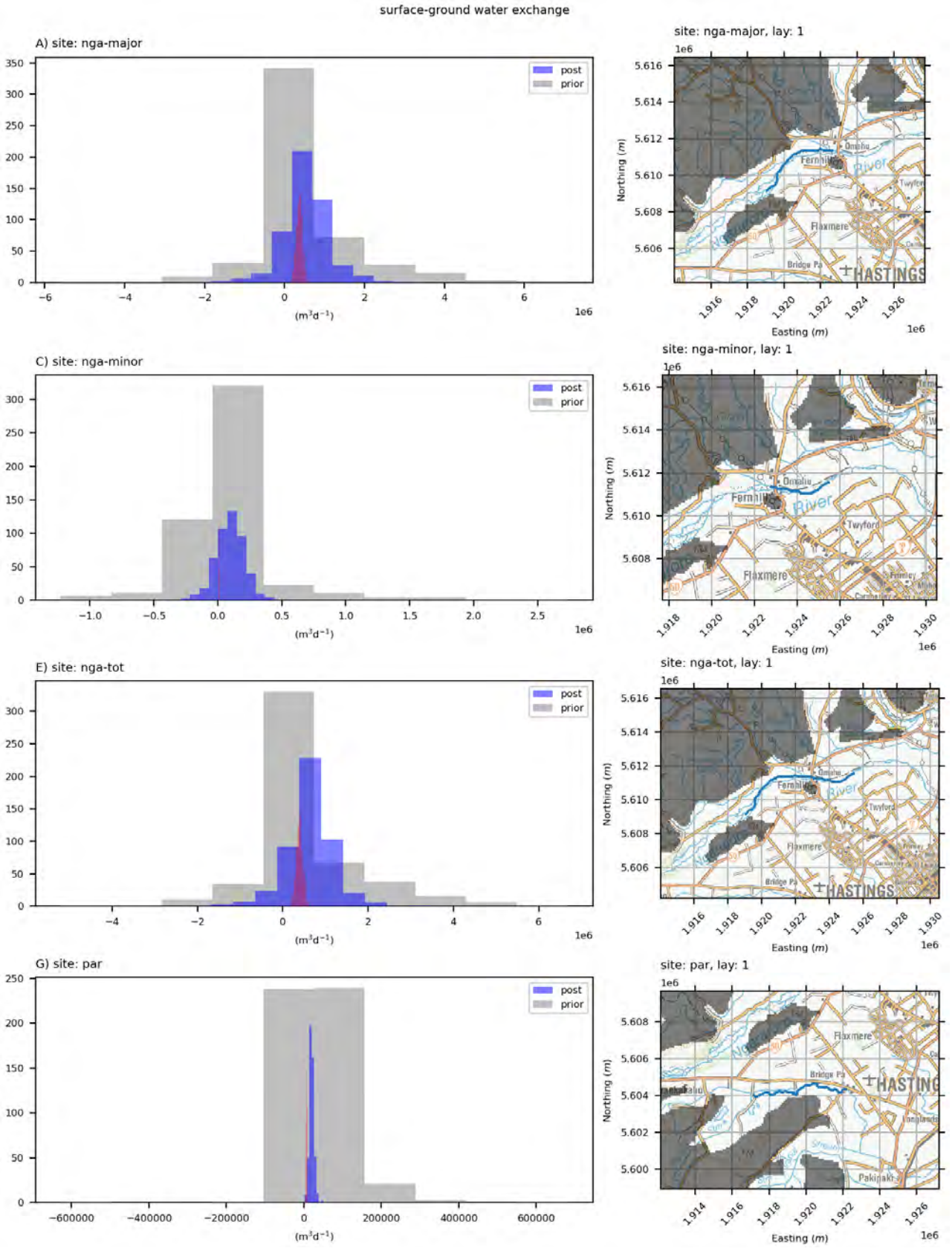

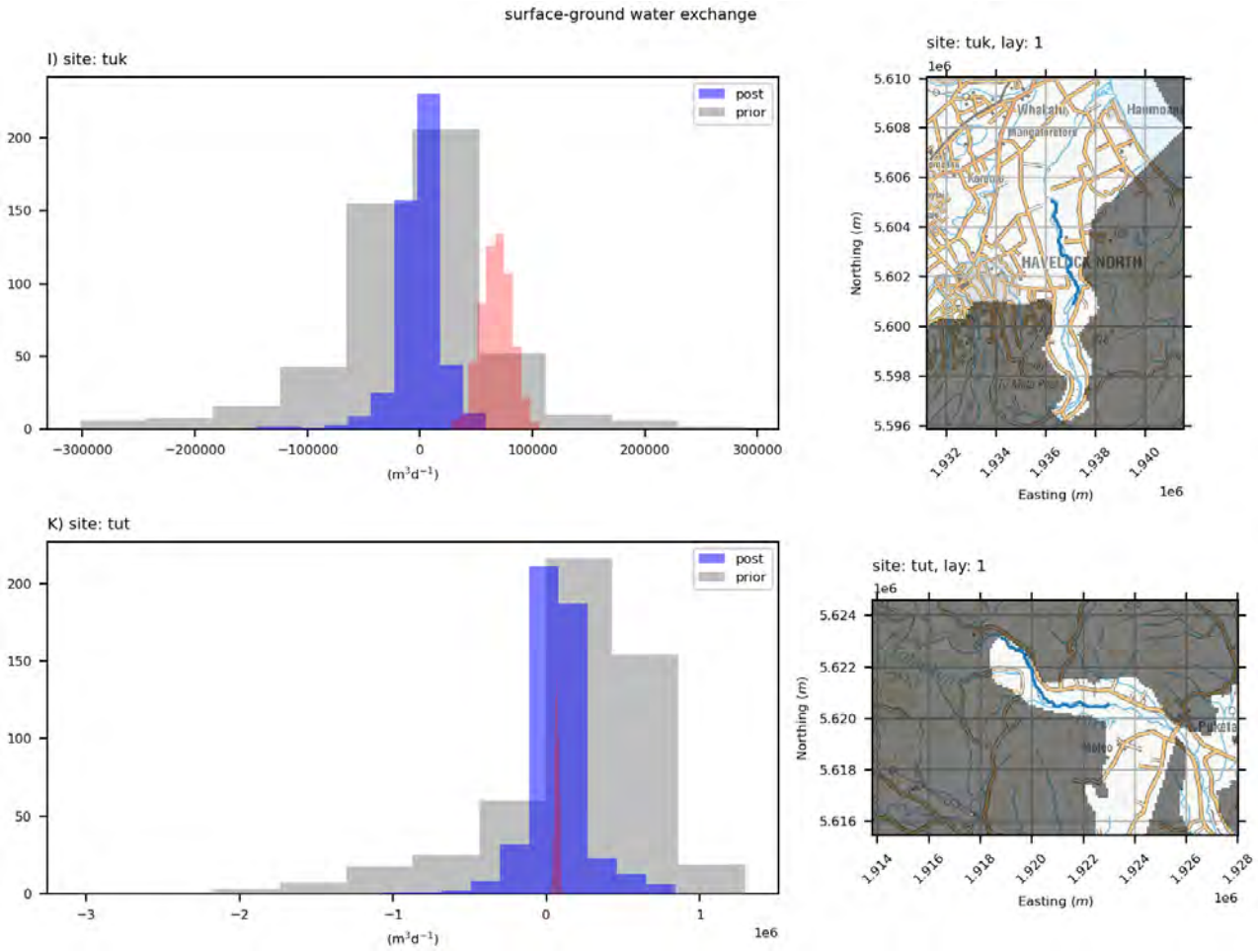
surface-ground water exchange
l) site: tuk
post
prior
200
150
100
50
0
−300000
−200000
−100000
0
100000
200000
300000
(m³d⁻¹)
site: tuk, lay: 1
1e6
5.610
5.608
5.606
5.604
5.602
5.600
5.598
5.596
Northing (m)
Whatatiri
Haumoana
Mangateretere
Karamu
HAVELOCK NORTH
1.932
1.934
1.936
1.938
1.940
Easting (m)
1e6
K) site: tut
post
prior
200
150
100
50
0
−3
−2
−1
0
1
(m³d⁻¹)
1e6
site: tut, lay: 1
1e6
5.624
5.622
5.620
5.618
5.616
Northing (m)
Puketa
Mahia
1.914
1.916
1.918
1.920
1.922
1.924
1.926
1.928
Easting (m)
1e6

A3.2.3 *skytem-lays*

A3.2.3.1 Levels

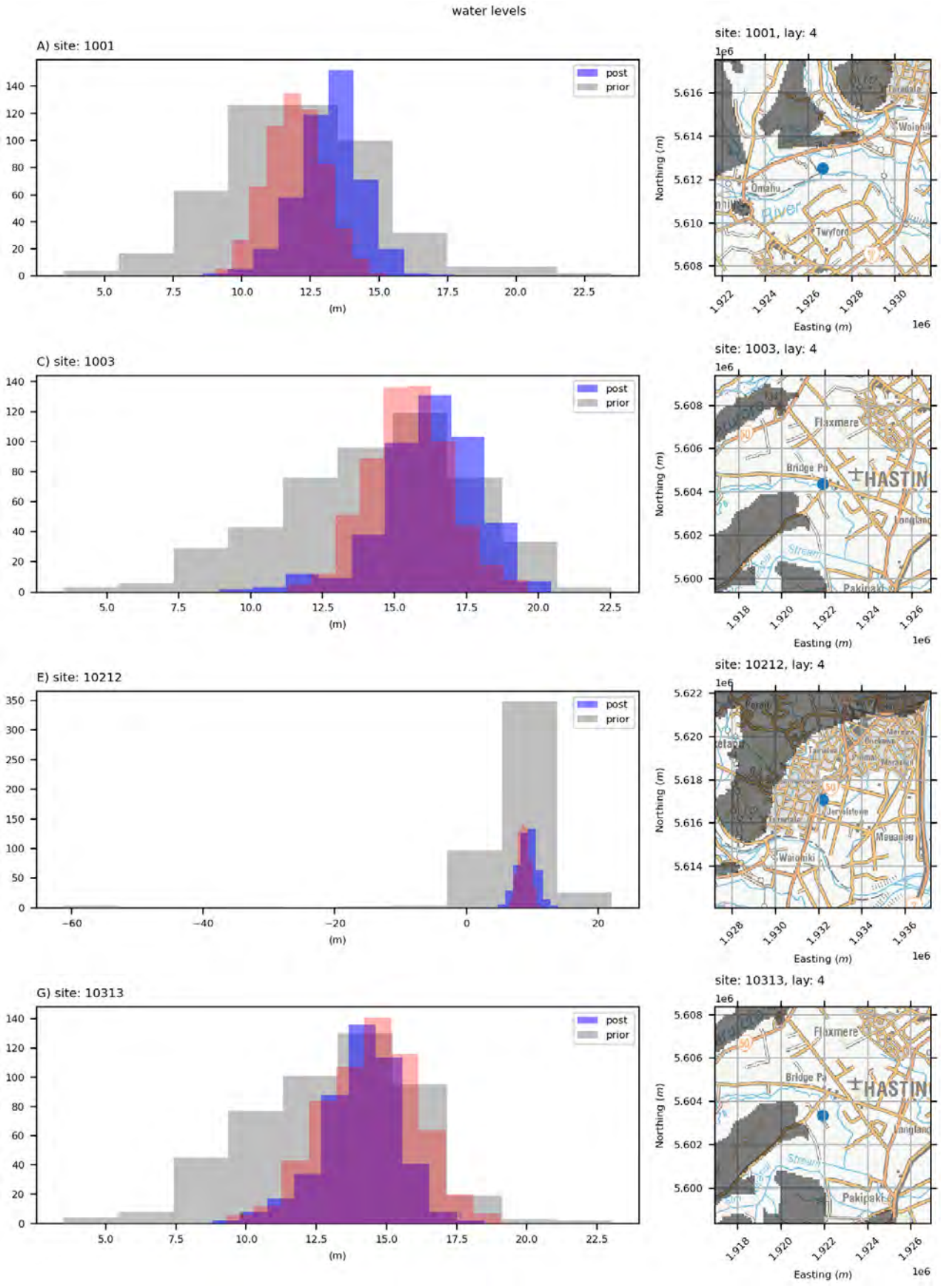

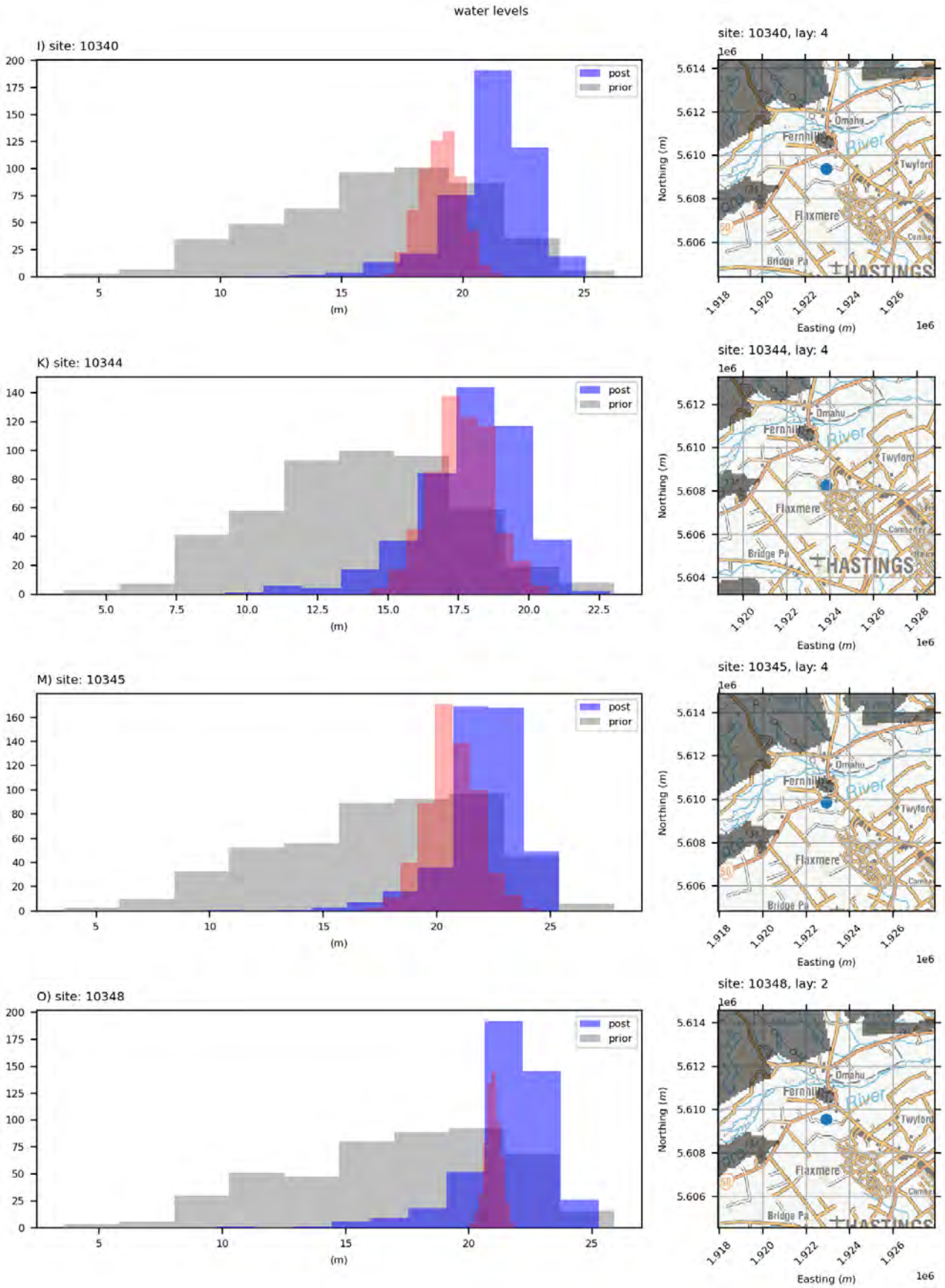
water levels
I) site: 10340
post
prior
(m)
site: 10340, lay: 4
Northing (m)
Easting (m)
1e6
K) site: 10344
post
prior
(m)
site: 10344, lay: 4
Northing (m)
Easting (m)
1e6
M) site: 10345
post
prior
(m)
site: 10345, lay: 4
Northing (m)
Easting (m)
1e6
O) site: 10348
post
prior
(m)
site: 10348, lay: 2
Northing (m)
Easting (m)
1e6

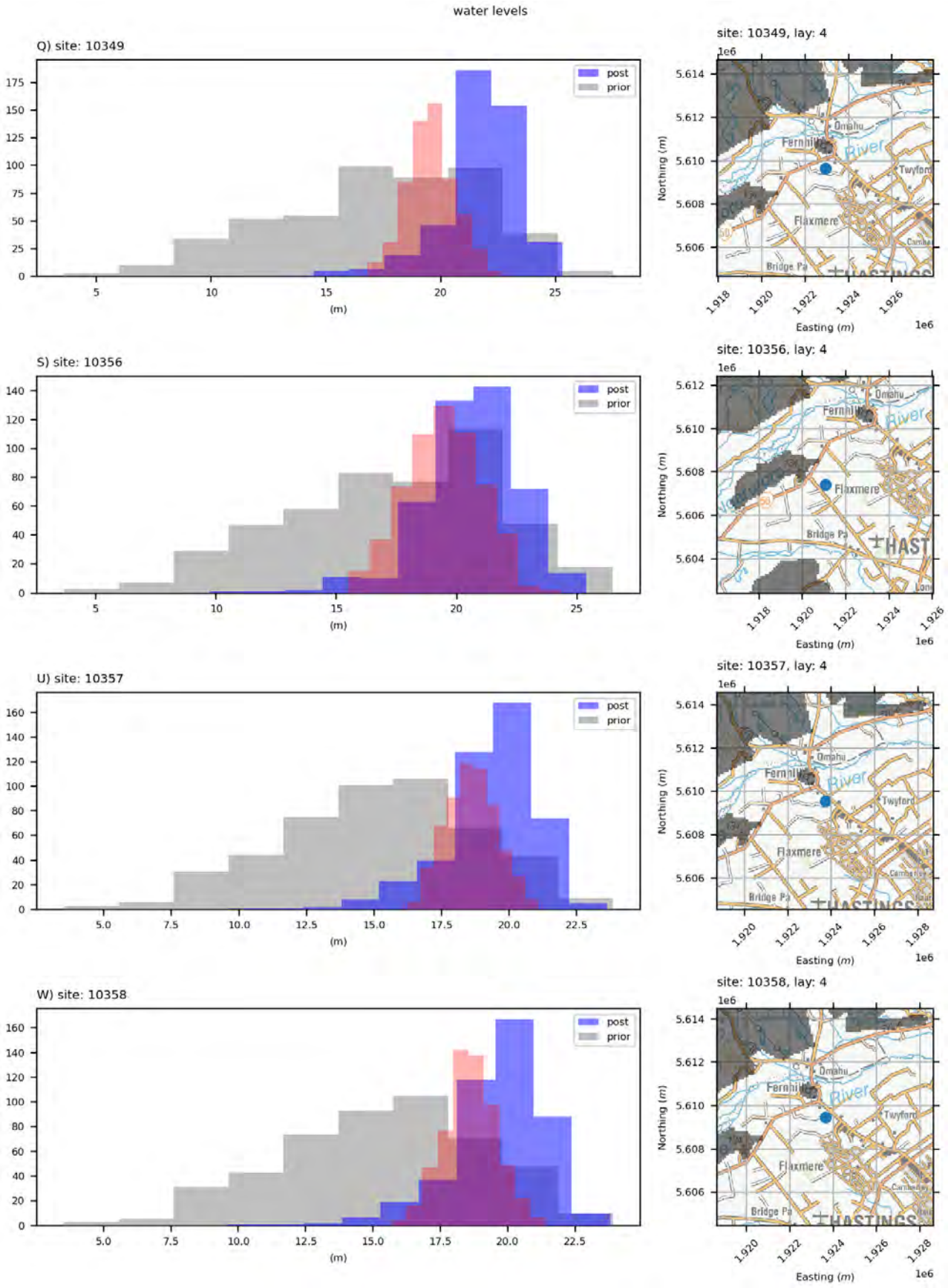
water levels
Q) site: 10349
post
prior
(m)
site: 10349, lay: 4
1e6
Northing (m)
Easting (m)
Omahu
Fernhill
River
Twyford
Flaxmere
Bridge Pa
S) site: 10356
site: 10356, lay: 4
U) site: 10357
site: 10357, lay: 4
W) site: 10358
site: 10358, lay: 4

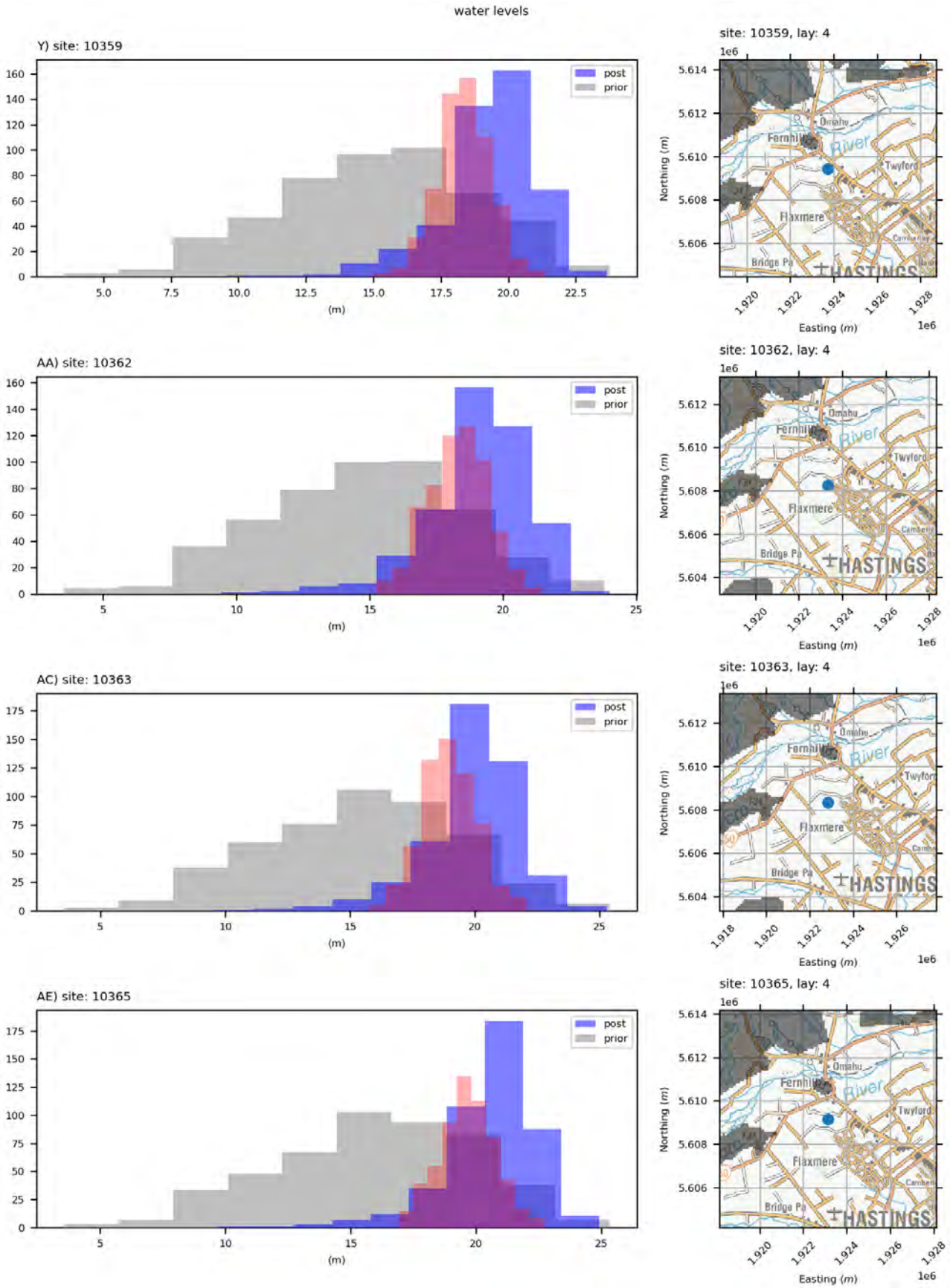
water levels
Y) site: 10359
post
prior
(m)
site: 10359, lay: 4
1e6
Northing (m)
Easting (m)
Omahu
Fernhill
River
Twyford
Flaxmere
Bridge Pa
HASTINGS
AA) site: 10362
site: 10362, lay: 4
AC) site: 10363
site: 10363, lay: 4
AE) site: 10365
site: 10365, lay: 4

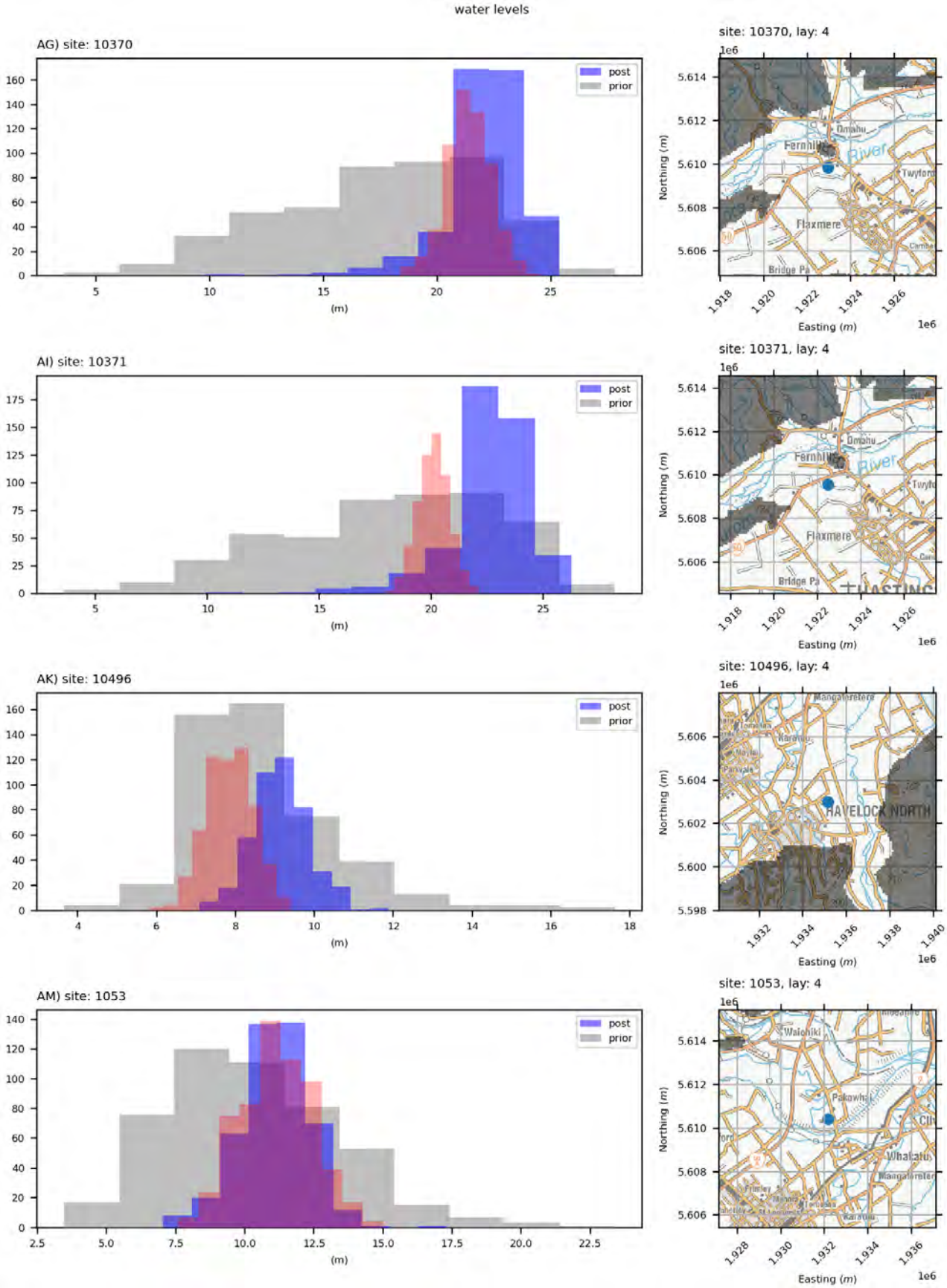
water levels
AG) site: 10370
post
prior
(m)
site: 10370, lay: 4
1e6
Northing (m)
Easting (m)
Fernhill
Flaxmere
Bridge Pa
River
AI) site: 10371
site: 10371, lay: 4
AK) site: 10496
site: 10496, lay: 4
HAVELOCK NORTH
AM) site: 1053
site: 1053, lay: 4
Waiohiki
Pakowhai
Whakatu

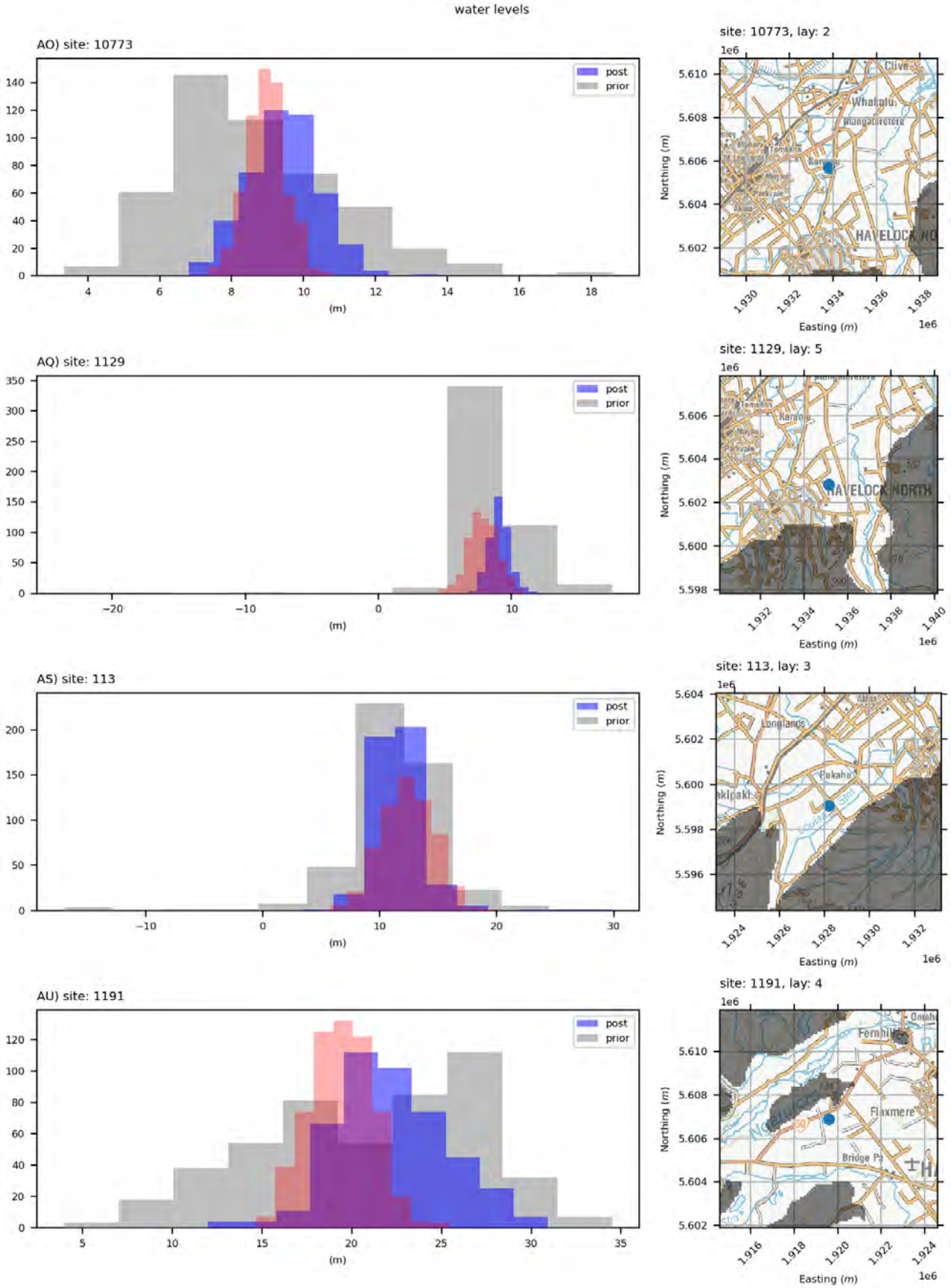
water levels
AO) site: 10773
post
prior
(m)
site: 10773, lay: 2
1e6
Northing (m)
Easting (m)
AQ) site: 1129
site: 1129, lay: 5
AS) site: 113
site: 113, lay: 3
AU) site: 1191
site: 1191, lay: 4

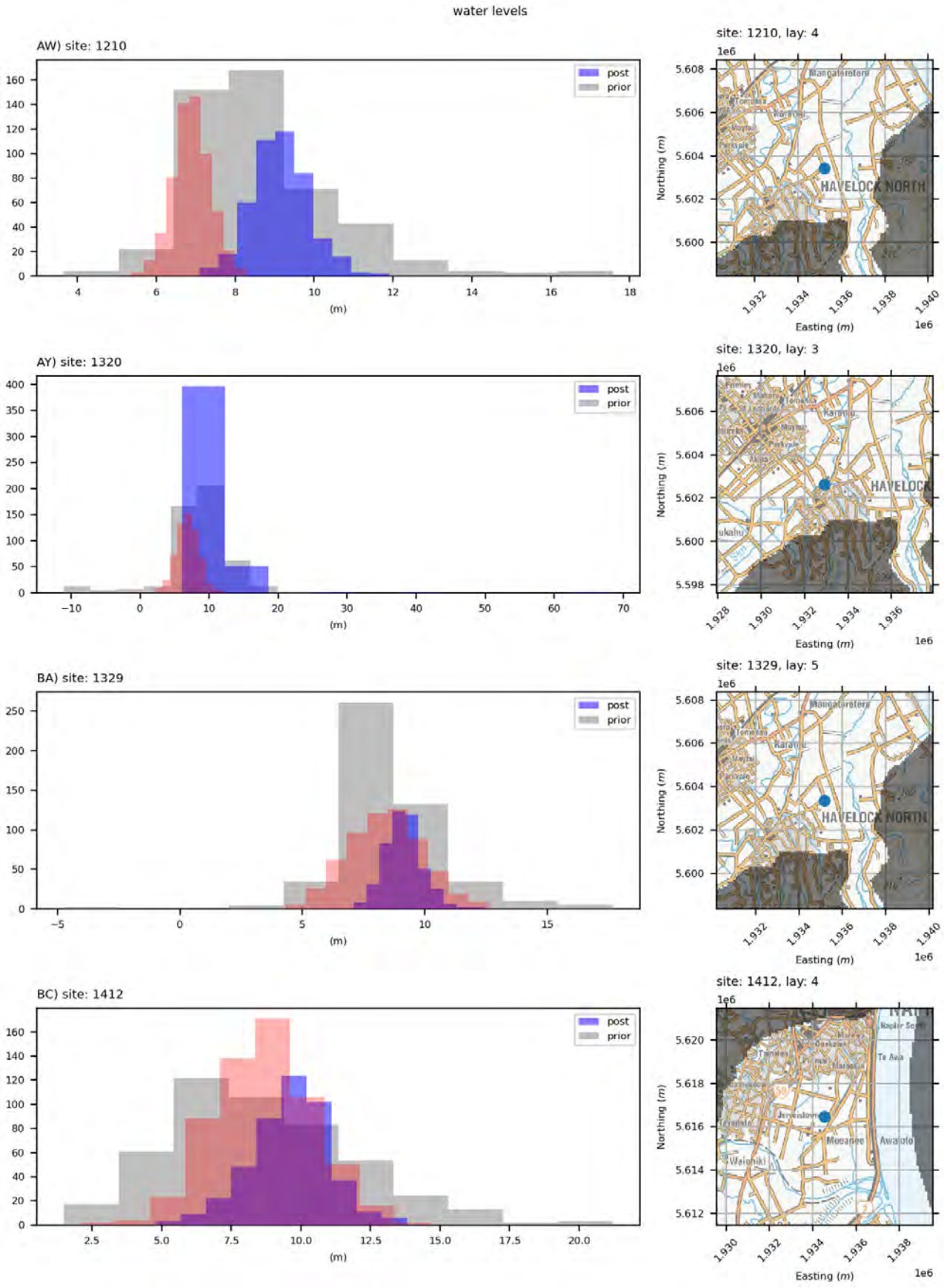
water levels
AW) site: 1210
post
prior
(m)
site: 1210, lay: 4
1e6
Northing (m)
Easting (m)
HAVELOCK NORTH
AY) site: 1320
site: 1320, lay: 3
HAVELOCK
BA) site: 1329
site: 1329, lay: 5
HAVELOCK NORTH
BC) site: 1412
site: 1412, lay: 4
Meeanee
Awatoto

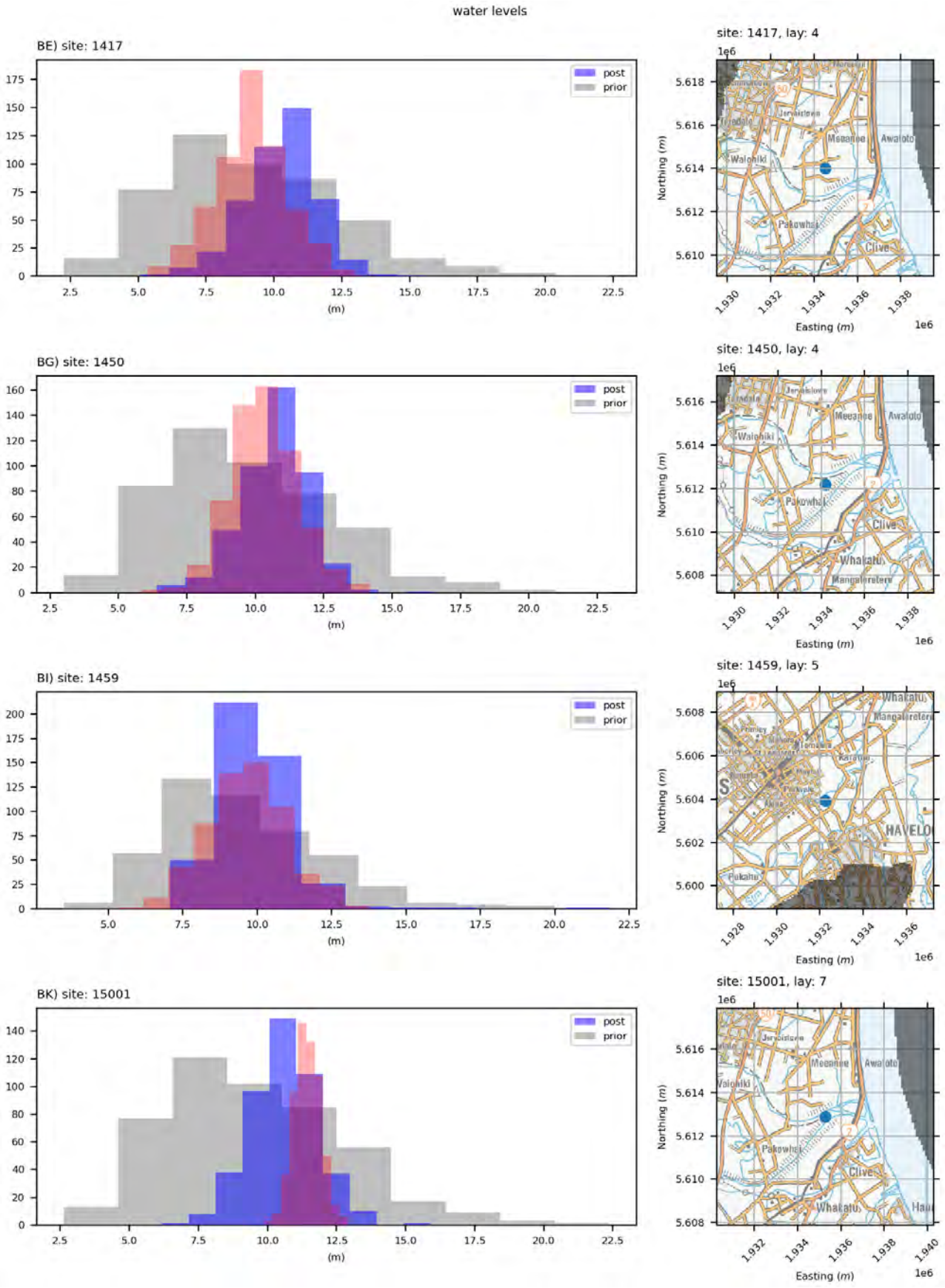
water levels
BE) site: 1417
post
prior
(m)
site: 1417, lay: 4
Northing (m)
Easting (m)
BG) site: 1450
post
prior
(m)
site: 1450, lay: 4
Northing (m)
Easting (m)
BI) site: 1459
post
prior
(m)
site: 1459, lay: 5
Northing (m)
Easting (m)
BK) site: 15001
post
prior
(m)
site: 15001, lay: 7
Northing (m)
Easting (m)

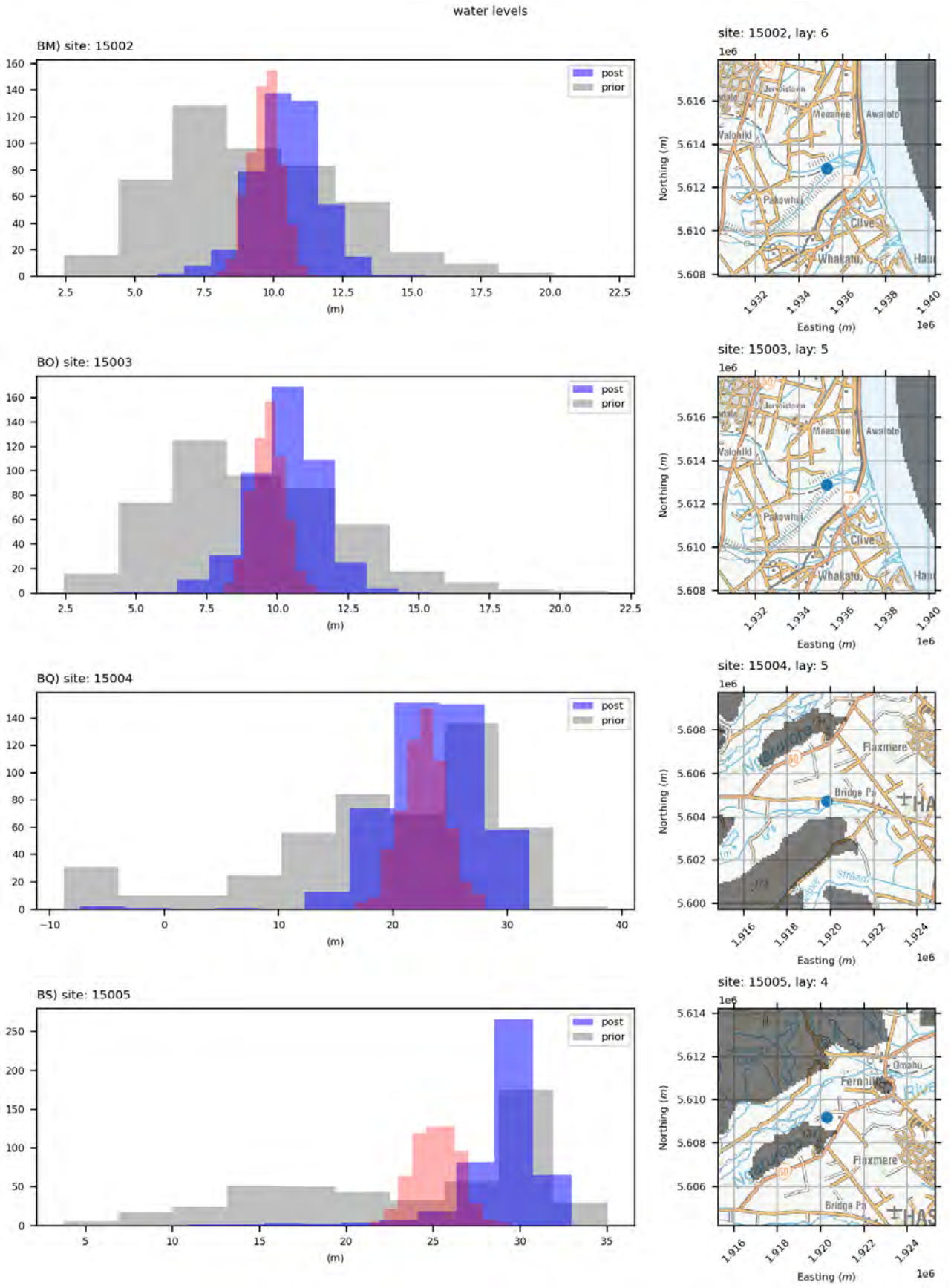
water levels
BM) site: 15002
post
prior
(m)
site: 15002, lay: 6
1e6
Northing (m)
Easting (m)
BO) site: 15003
post
prior
(m)
site: 15003, lay: 5
1e6
Northing (m)
Easting (m)
BQ) site: 15004
post
prior
(m)
site: 15004, lay: 5
1e6
Flaxmere
Bridge Pa
Northing (m)
Easting (m)
BS) site: 15005
post
prior
(m)
site: 15005, lay: 4
1e6
Omahu
Flaxmere
Bridge Pa
Northing (m)
Easting (m)

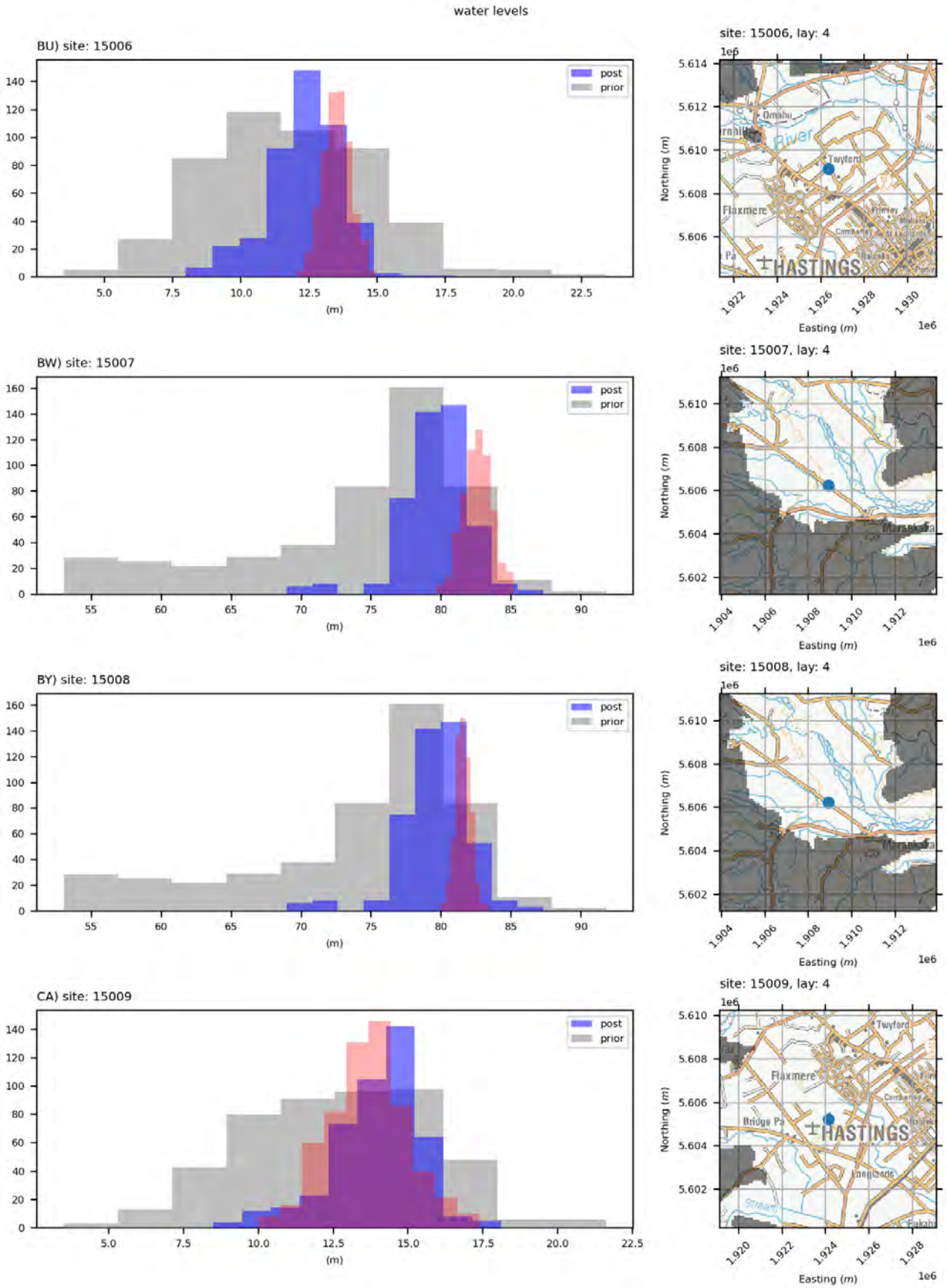
water levels
BU) site: 15006
post
prior
(m)
site: 15006, lay: 4
1e6
Northing (m)
Easting (m)
Twyford
Flaxmere
HASTINGS
River
BW) site: 15007
site: 15007, lay: 4
BY) site: 15008
site: 15008, lay: 4
CA) site: 15009
site: 15009, lay: 4

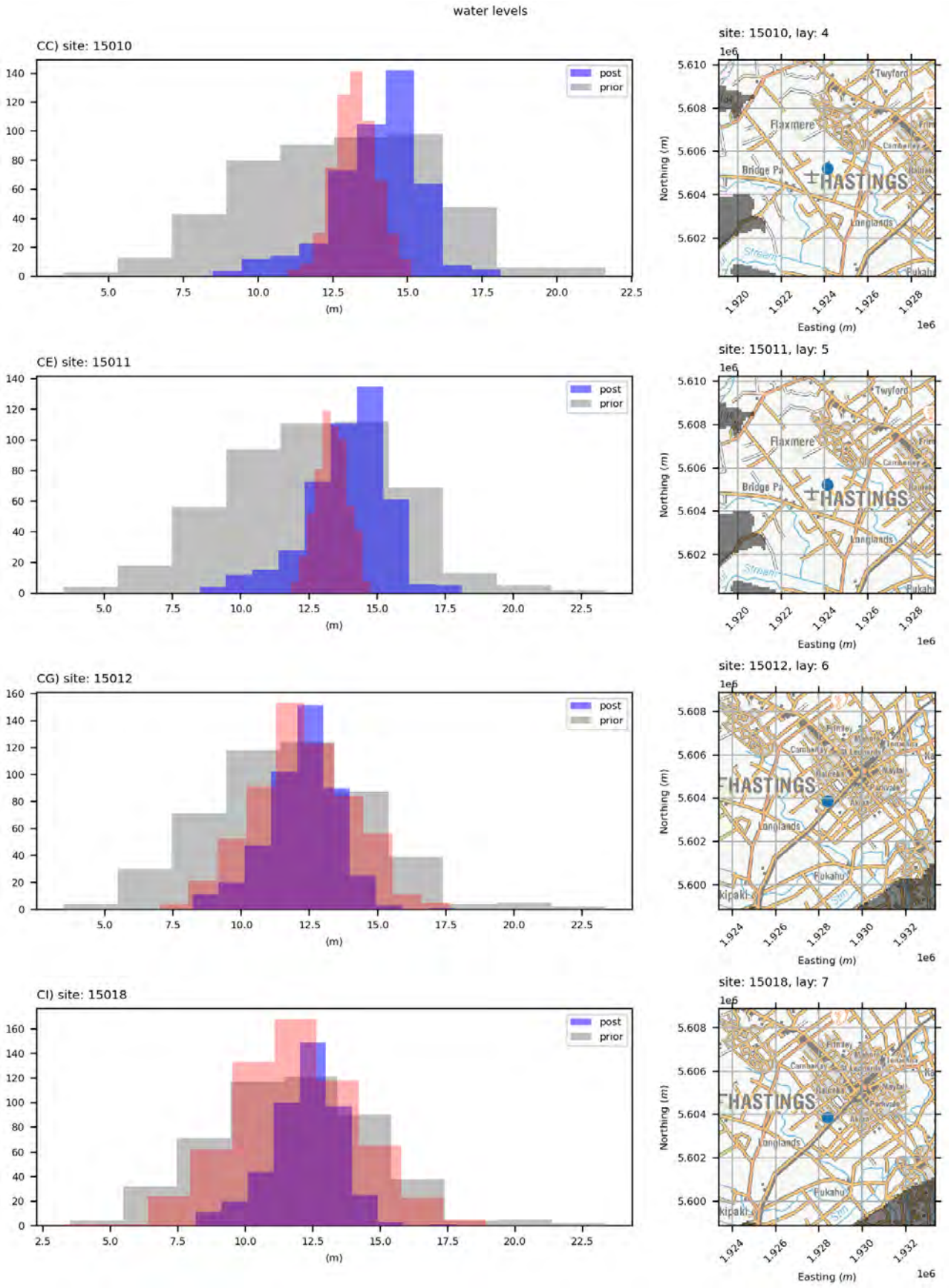
water levels
CC) site: 15010
post
prior
(m)
site: 15010, lay: 4
1e6
Northing (m)
Easting (m)
Twyford
Flaxmere
Bridge Pa
HASTINGS
Longlands
CE) site: 15011
site: 15011, lay: 5
CG) site: 15012
site: 15012, lay: 6
Pukahu
CI) site: 15018
site: 15018, lay: 7

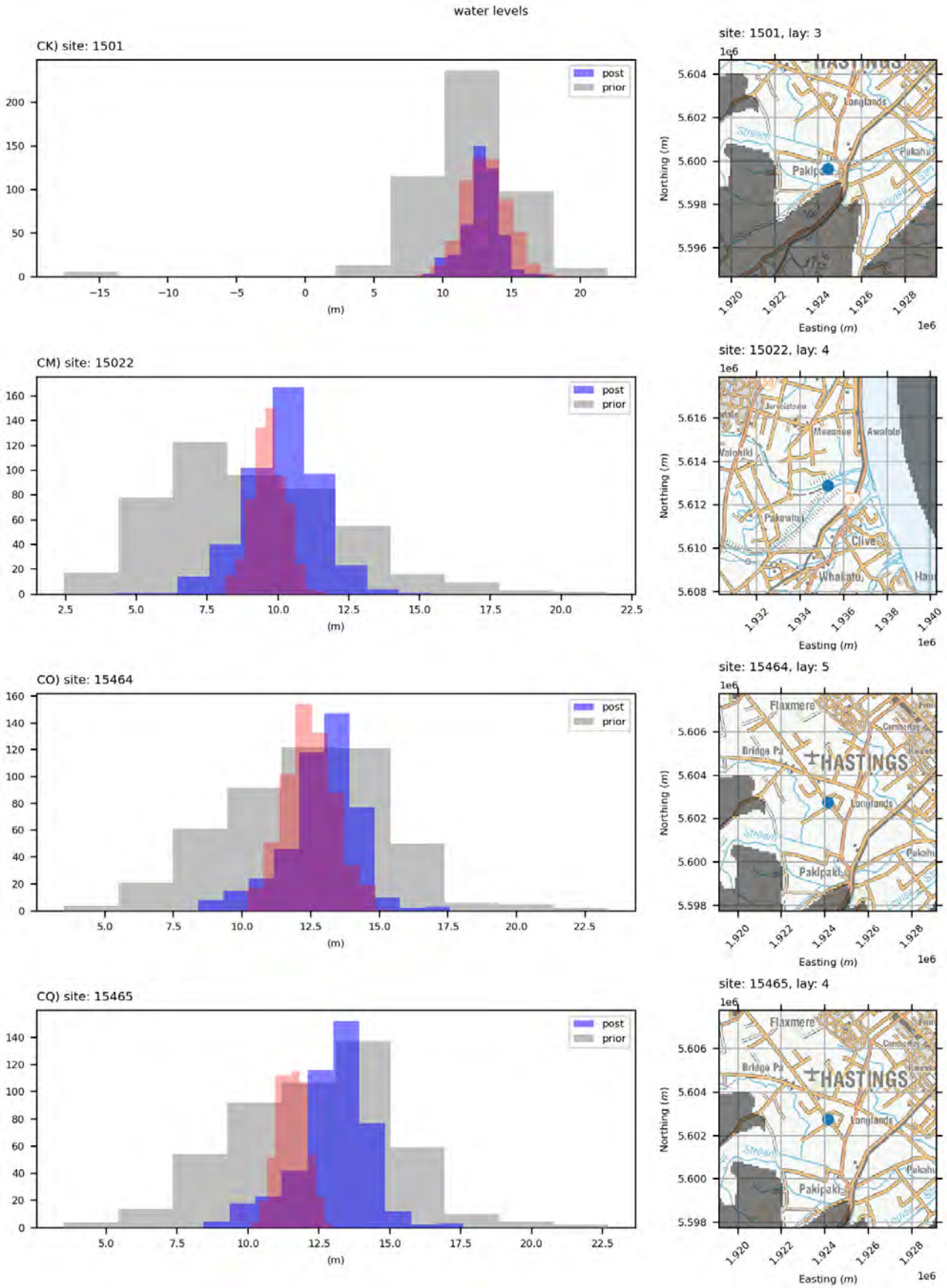
water levels
CK) site: 1501
post
prior
(m)
site: 1501, lay: 3
1e6
Northing (m)
Easting (m)
CM) site: 15022
site: 15022, lay: 4
CO) site: 15464
site: 15464, lay: 5
CQ) site: 15465
site: 15465, lay: 4
HASTINGS
Flaxmere
Longlands
Clive
Whakatu

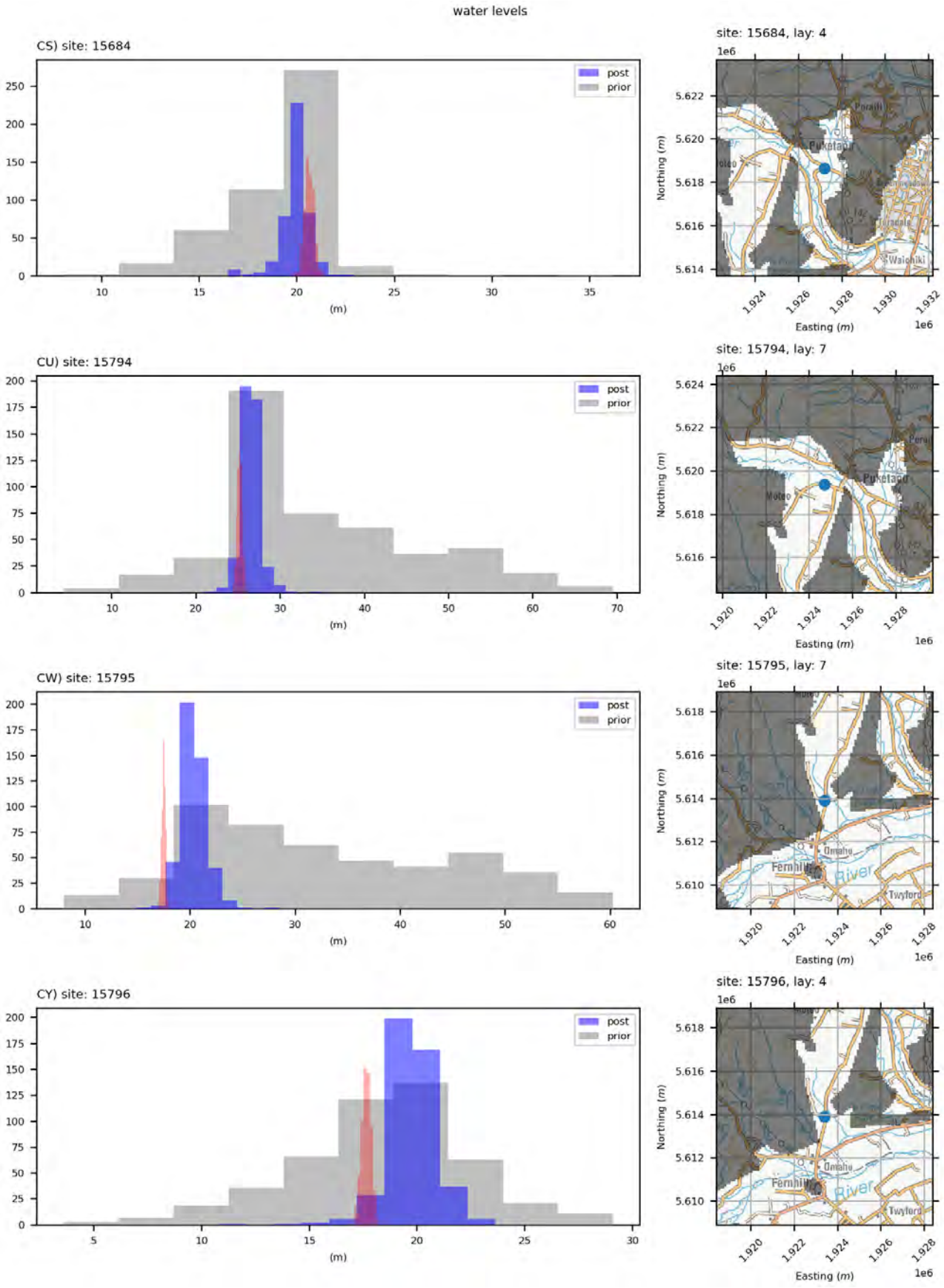
water levels
CS) site: 15684
post
prior
(m)
site: 15684, lay: 4
1e6
Northing (m)
Easting (m)
Pyketago
Waioiki
CU) site: 15794
post
prior
(m)
site: 15794, lay: 7
1e6
Northing (m)
Easting (m)
Pyketago
Moteo
CW) site: 15795
post
prior
(m)
site: 15795, lay: 7
1e6
Northing (m)
Easting (m)
Omahu
Fernhill
River
Twyford
CY) site: 15796
post
prior
(m)
site: 15796, lay: 4
1e6
Northing (m)
Easting (m)
Omahu
Fernhill
River
Twyford

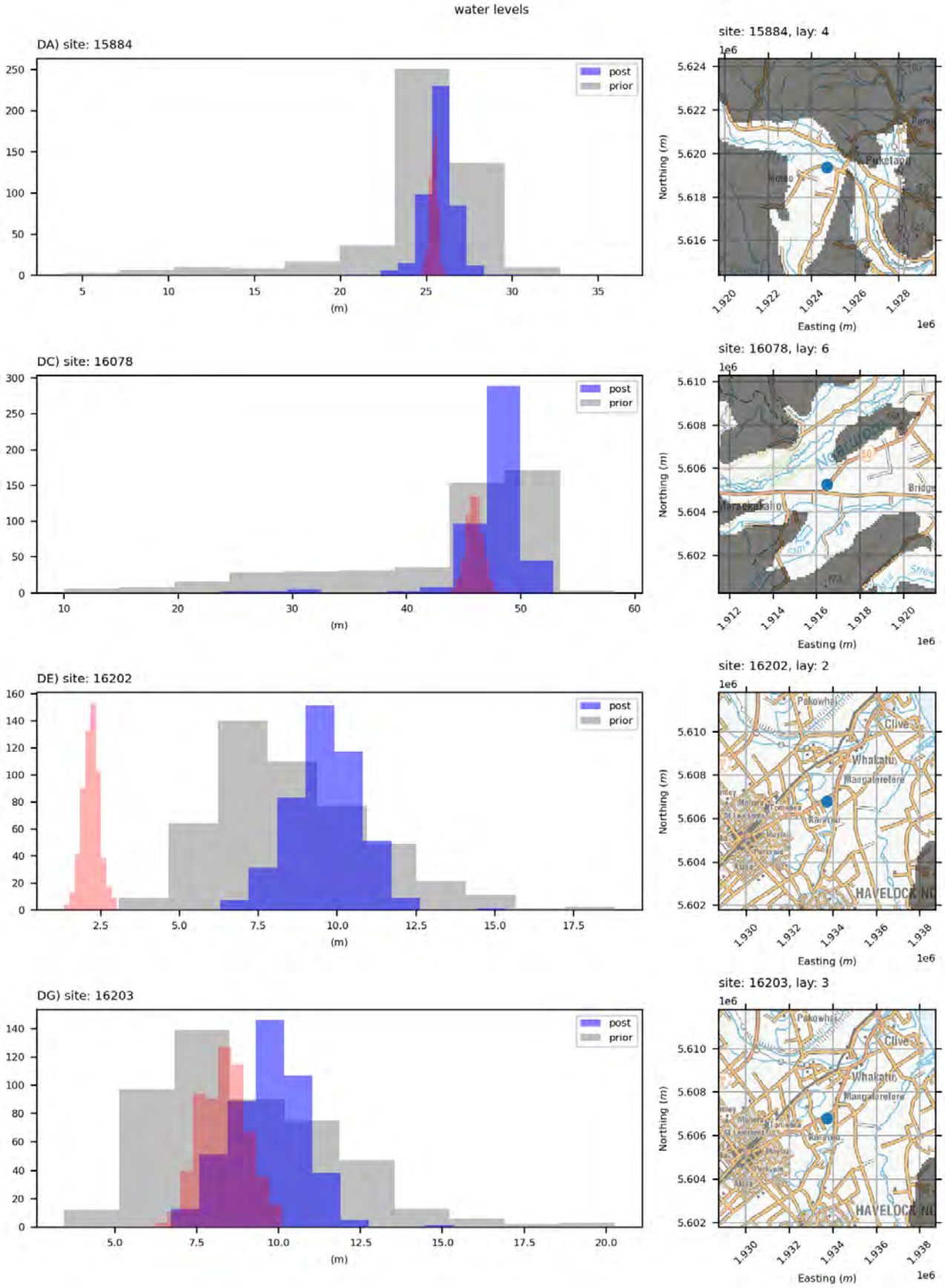
water levels
DA) site: 15884
post
prior
(m)
site: 15884, lay: 4
1e6
Northing (m)
Easting (m)
DC) site: 16078
post
prior
(m)
site: 16078, lay: 6
1e6
Northing (m)
Easting (m)
DE) site: 16202
post
prior
(m)
site: 16202, lay: 2
1e6
Pakowhai
Clive
Whakatu
Mangaoreretera
HAVELOCK NO
Northing (m)
Easting (m)
DG) site: 16203
post
prior
(m)
site: 16203, lay: 3
1e6
Pakowhai
Clive
Whakatu
Mangaoreretera
HAVELOCK NO
Northing (m)
Easting (m)

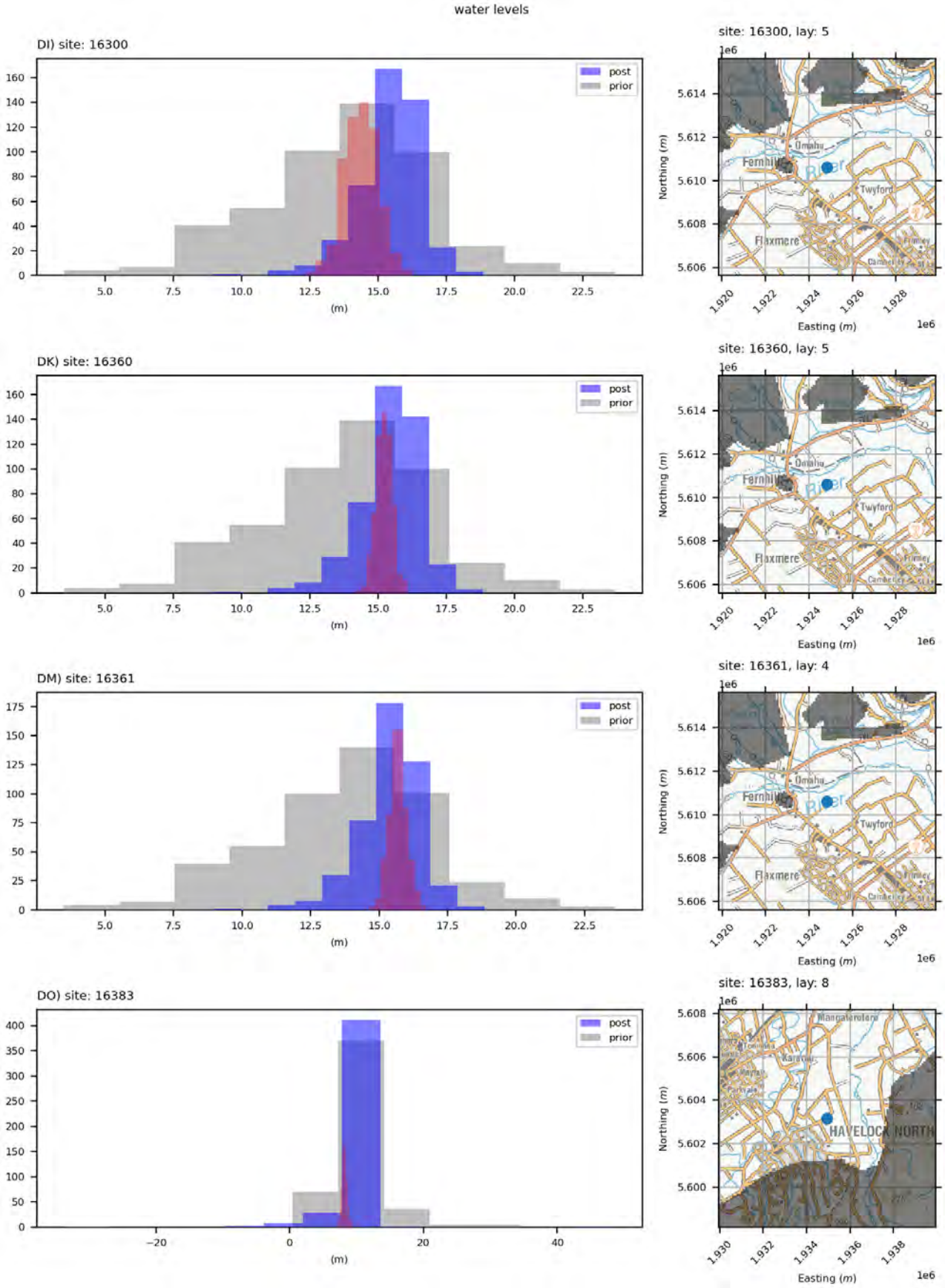
water levels
DI) site: 16300
post
prior
(m)
site: 16300, lay: 5
1e6
Northing (m)
Easting (m)
Omahu
Twyford
Flaxmere
DK) site: 16360
site: 16360, lay: 5
DM) site: 16361
site: 16361, lay: 4
DO) site: 16383
site: 16383, lay: 8
HAVELOCK NORTH

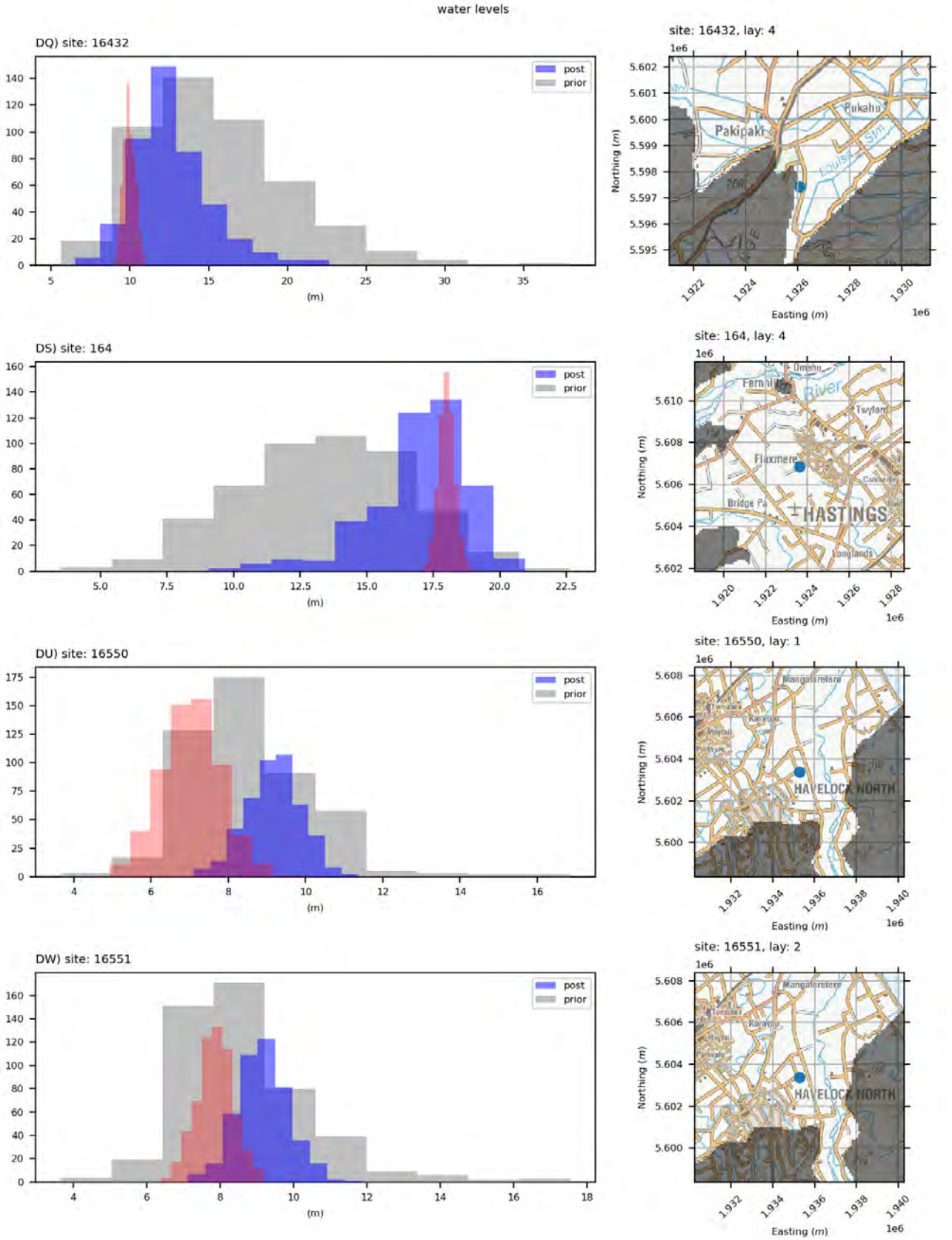
water levels
DQ) site: 16432
post
prior
(m)
site: 16432, lay: 4
1e6
Pukahu
Pakipaki
Louise Stm
Northing (m)
Easting (m)
DS) site: 164
post
prior
(m)
site: 164, lay: 4
Omahu
Fernhill
River
Twyford
Flaxmere
Bridge Pa
HASTINGS
Longlands
Northing (m)
Easting (m)
DU) site: 16550
post
prior
(m)
site: 16550, lay: 1
Mangateretere
HAVELOCK NORTH
Northing (m)
Easting (m)
DW) site: 16551
post
prior
(m)
site: 16551, lay: 2
Mangateretere
HAVELOCK NORTH
Northing (m)
Easting (m)

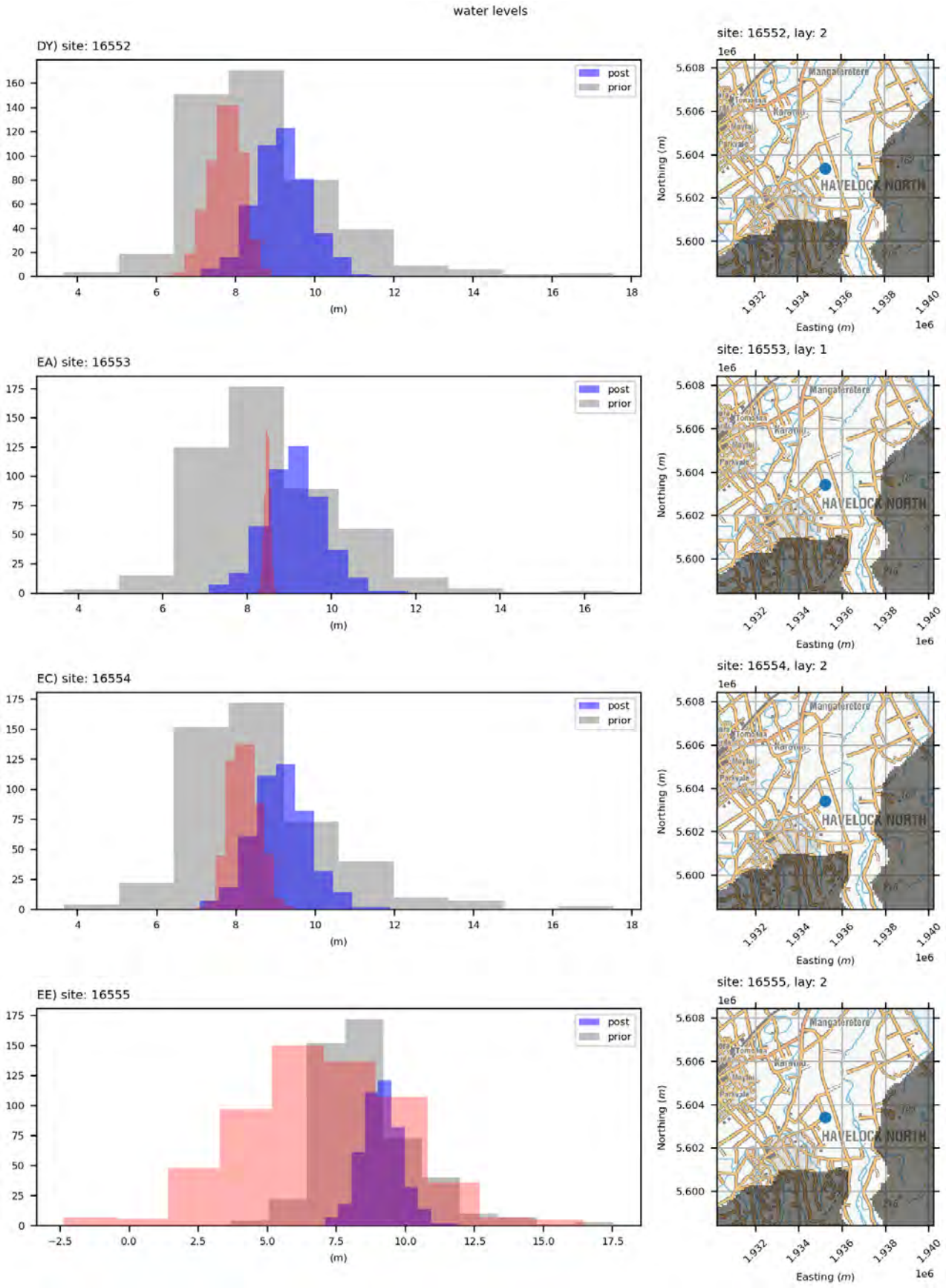
water levels
DY) site: 16552
post
prior
(m)
site: 16552, lay: 2
1e6
Northing (m)
Easting (m)
HAVELOCK NORTH
EA) site: 16553
site: 16553, lay: 1
EC) site: 16554
site: 16554, lay: 2
EE) site: 16555
site: 16555, lay: 2

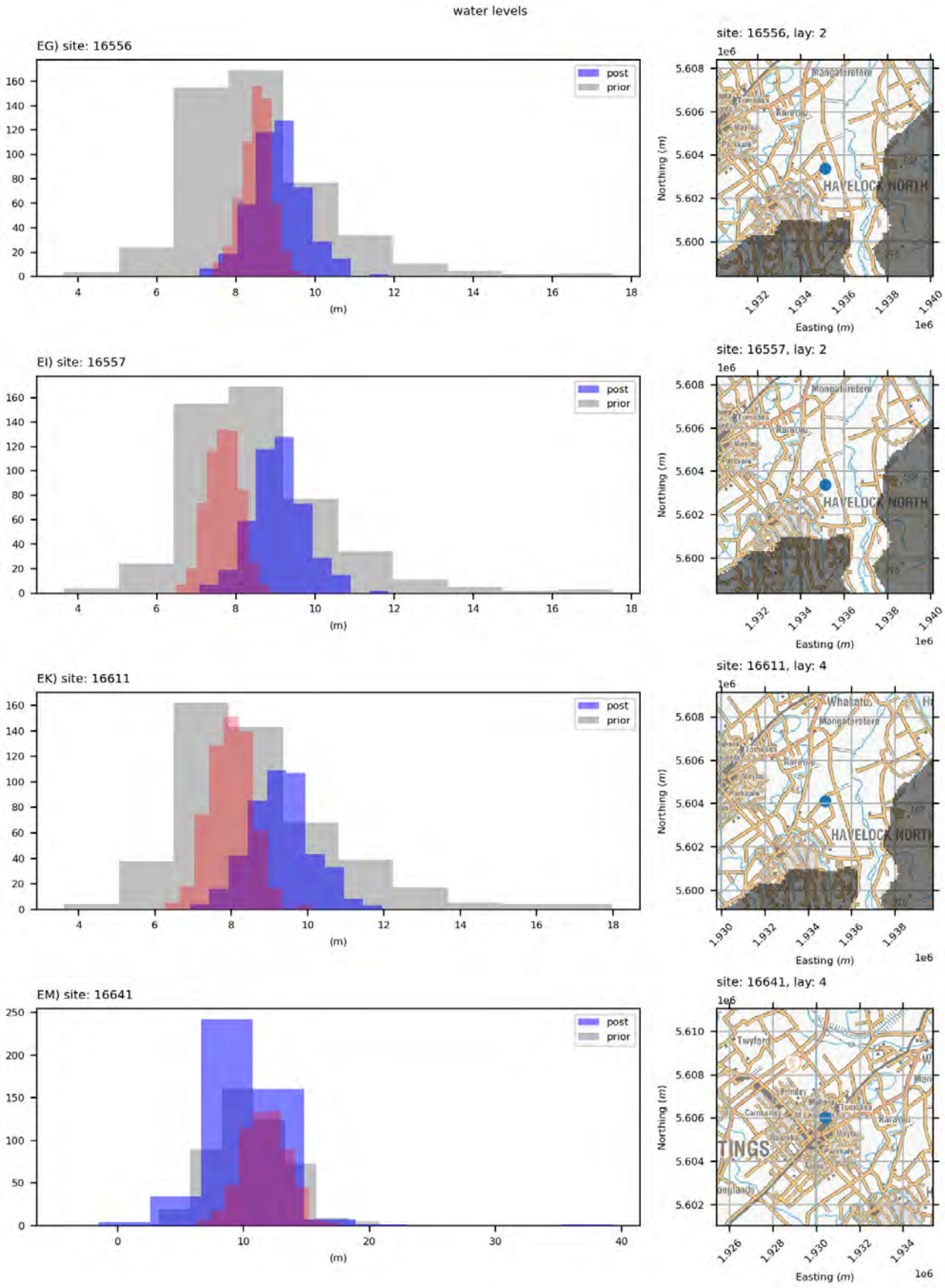
water levels
EG) site: 16556
post
prior
(m)
site: 16556, lay: 2
1e6
Northing (m)
Easting (m)
HAVELOCK NORTH
EI) site: 16557
post
prior
(m)
site: 16557, lay: 2
1e6
Northing (m)
Easting (m)
HAVELOCK NORTH
EK) site: 16611
post
prior
(m)
site: 16611, lay: 4
1e6
Northing (m)
Easting (m)
HAVELOCK NORTH
EM) site: 16641
post
prior
(m)
site: 16641, lay: 4
1e6
Northing (m)
Easting (m)
TINGS

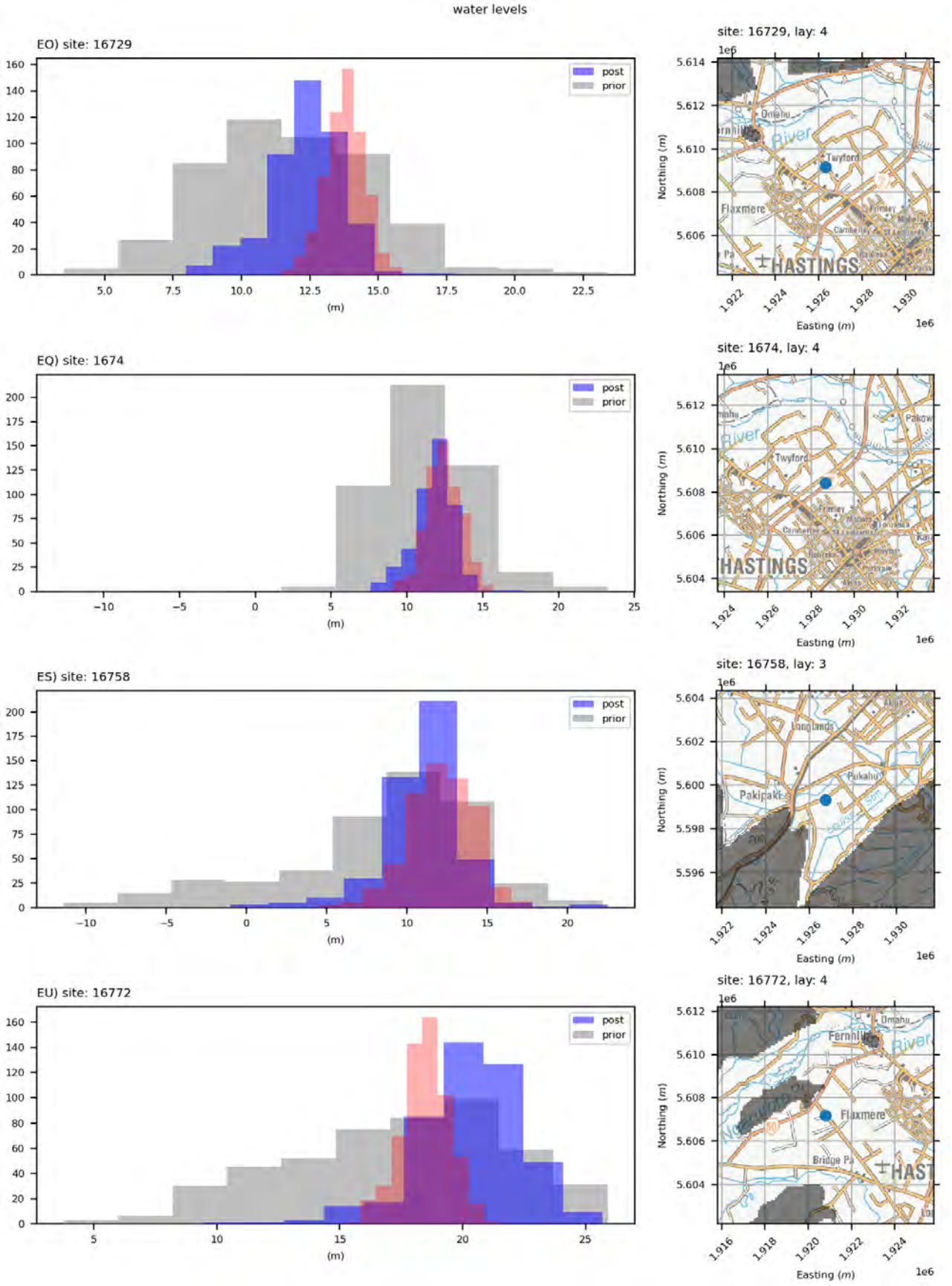
water levels
EO) site: 16729
post
prior
(m)
site: 16729, lay: 4
1e6
Northing (m)
Easting (m)
Omahu
Twyford
Flaxmere
HASTINGS
EQ) site: 1674
site: 1674, lay: 4
Pakowhai
ES) site: 16758
site: 16758, lay: 3
Longlands
Pukahu
Pakipaki
EU) site: 16772
site: 16772, lay: 4
Fernhill
Bridge Pa

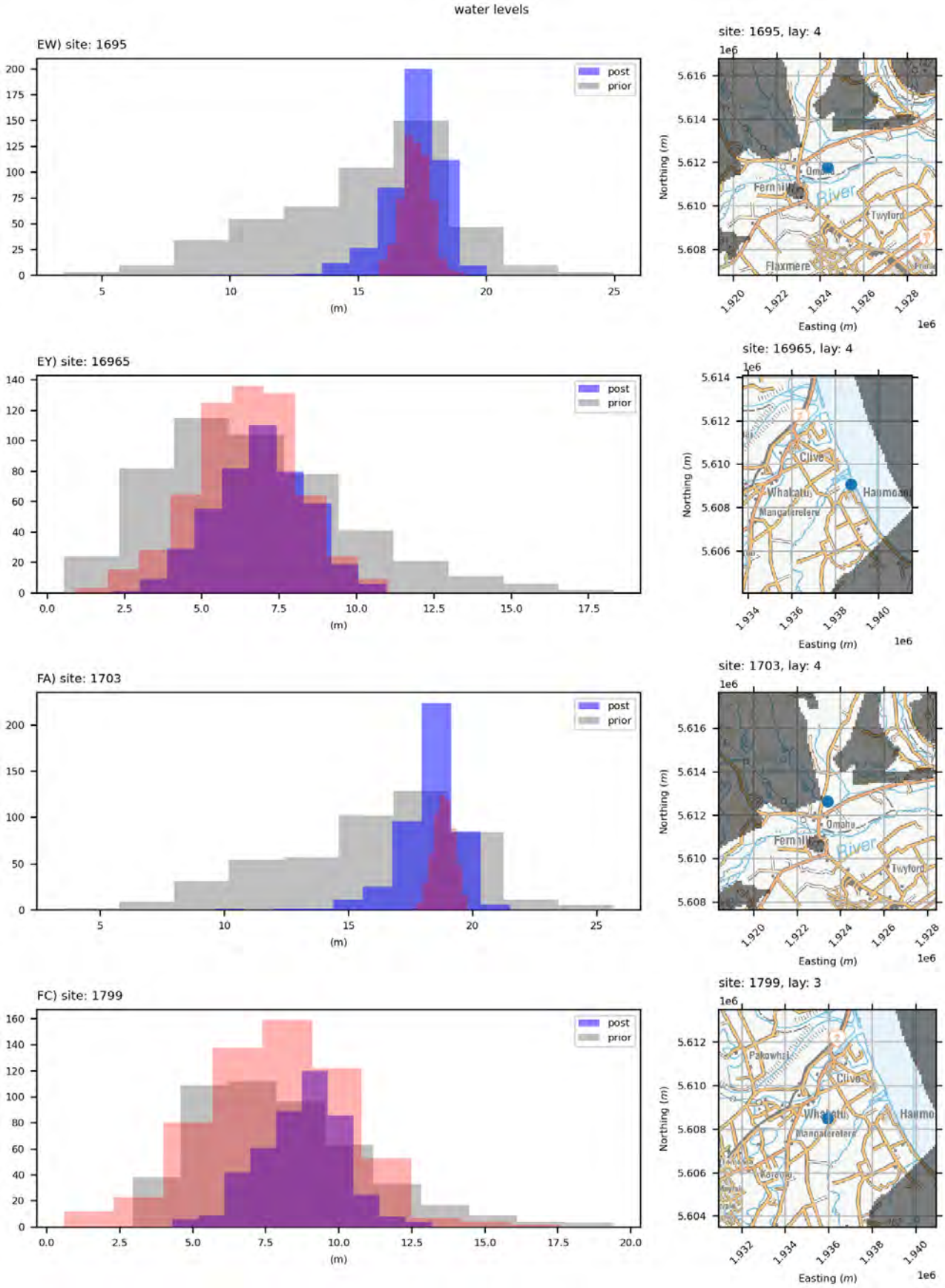
water levels
EW) site: 1695
post
prior
(m)
site: 1695, lay: 4
Northing (m)
Easting (m)
1e6
Fernhill
Twyford
Flaxmere
River
EY) site: 16965
site: 16965, lay: 4
Clive
Whakatu
Haumoana
Mangateretere
FA) site: 1703
site: 1703, lay: 4
Omahu
FC) site: 1799
site: 1799, lay: 3
Pakowhai
Haumo
Korongo

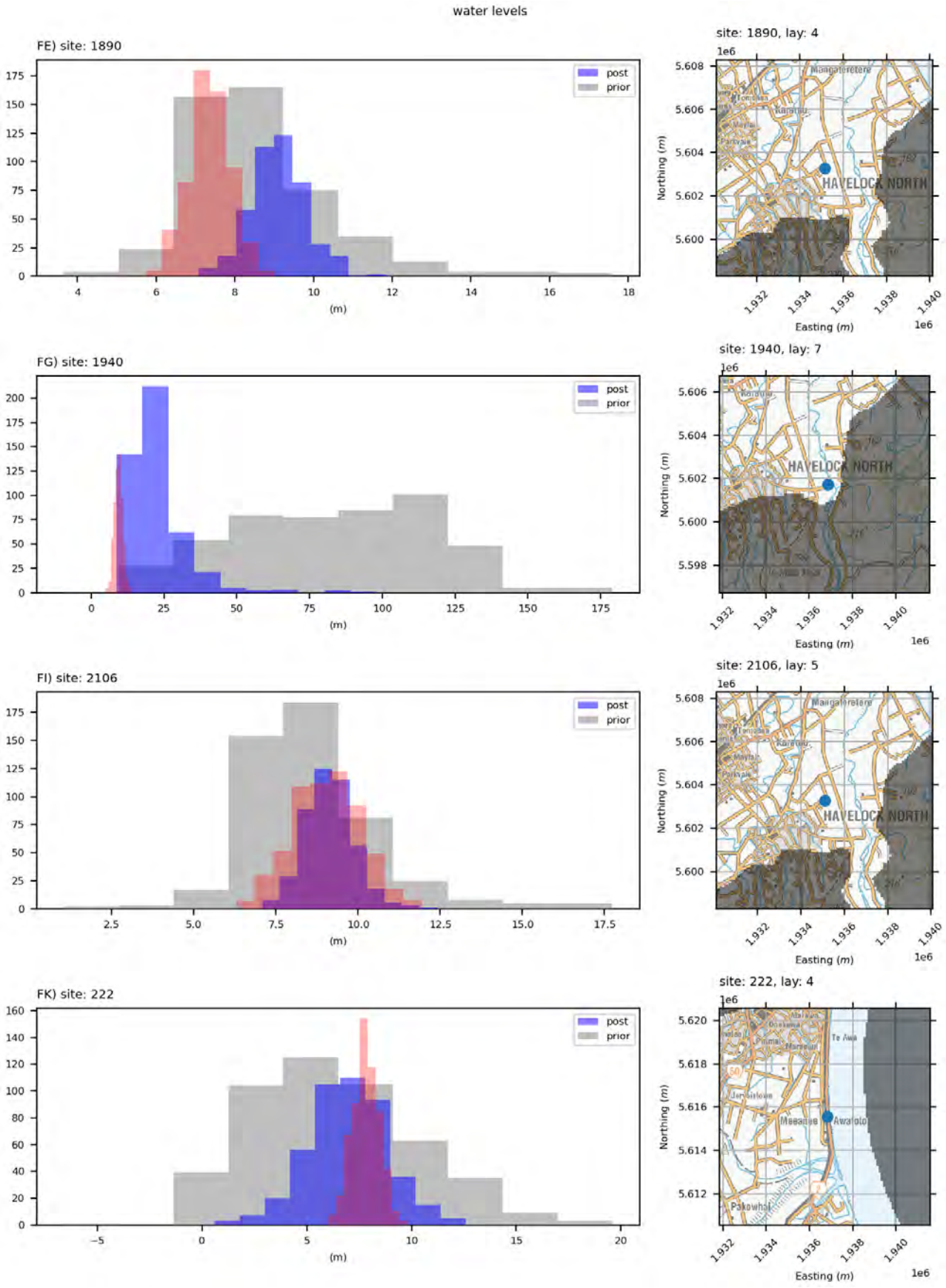
water levels
FE) site: 1890
post
prior
(m)
site: 1890, lay: 4
1e6
HAVELOCK NORTH
Northing (m)
Easting (m)
FG) site: 1940
site: 1940, lay: 7
FI) site: 2106
site: 2106, lay: 5
FK) site: 222
site: 222, lay: 4
Meeanee
Awatoto
Pakowhai

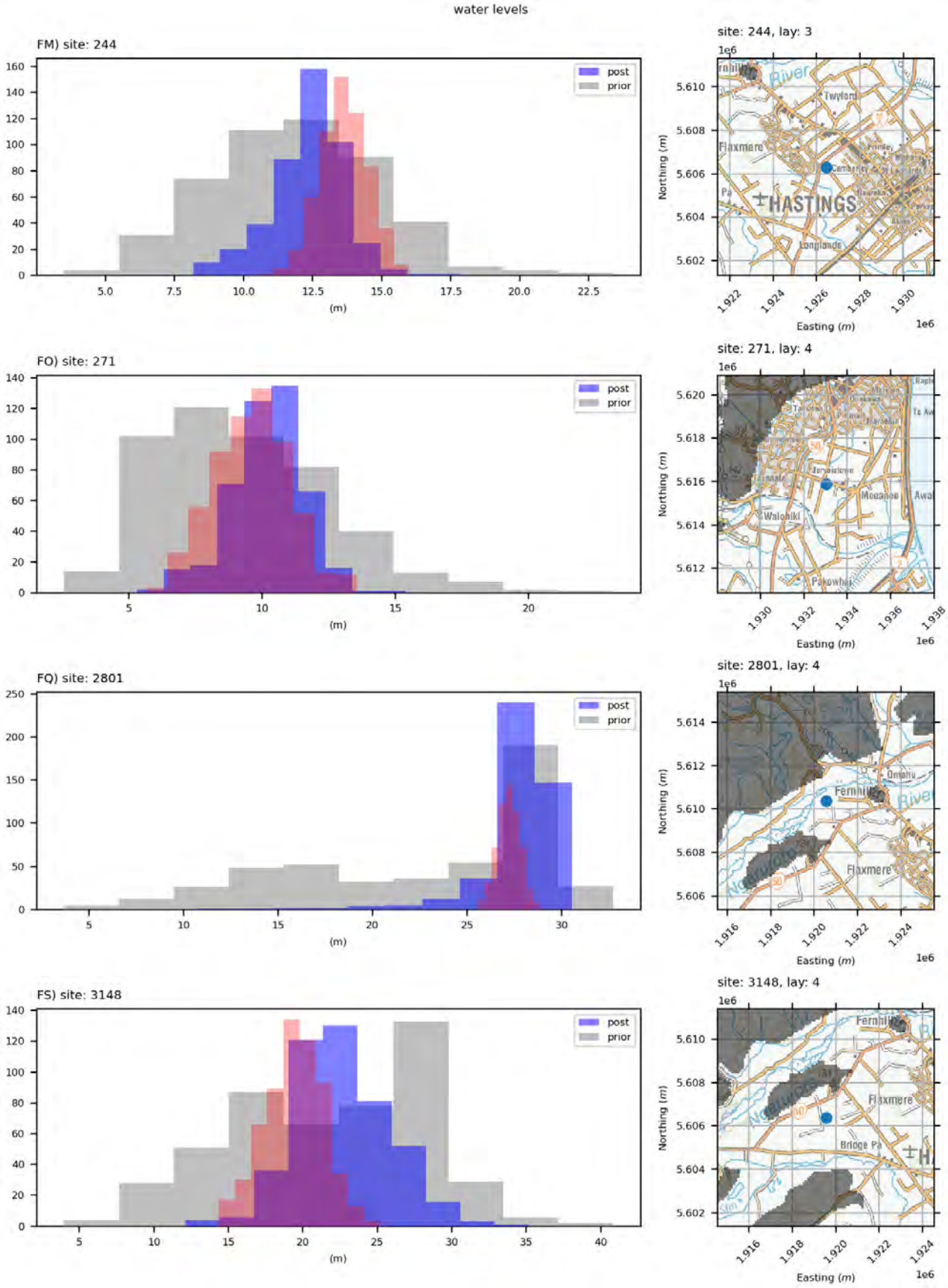
water levels
FM) site: 244
post
prior
(m)
site: 244, lay: 3
1e6
Northing (m)
Easting (m)
Twyford
Flaxmere
HASTINGS
Longlands
FO) site: 271
site: 271, lay: 4
Waiohiki
Pakowhai
FQ) site: 2801
site: 2801, lay: 4
Omahu
Fernhill
Flaxmere
FS) site: 3148
site: 3148, lay: 4
Bridge Pa

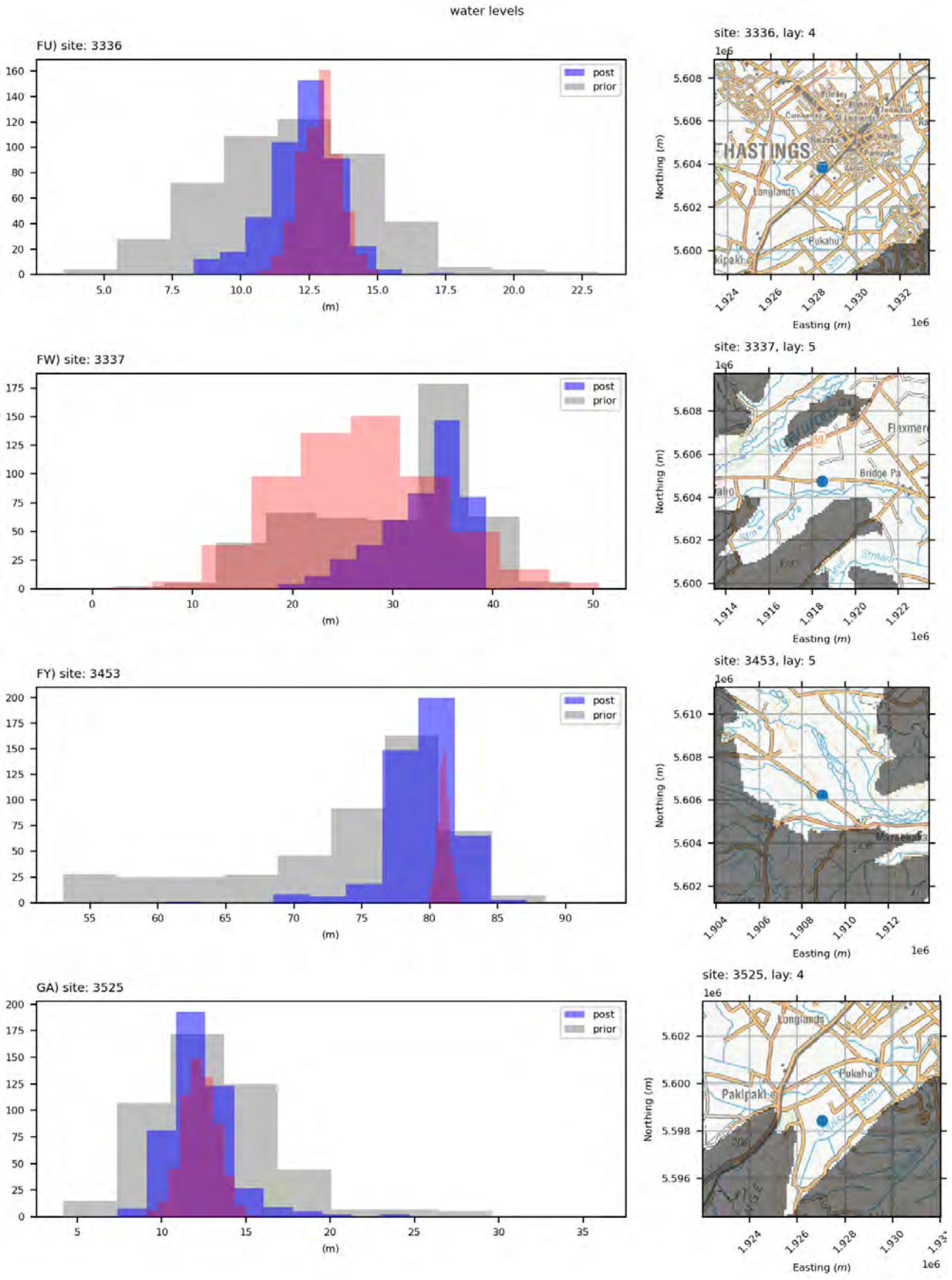
water levels
FU) site: 3336
post
prior
(m)
site: 3336, lay: 4
1e6
Northing (m)
Easting (m)
HASTINGS
Longlands
Pukahu
FW) site: 3337
site: 3337, lay: 5
Bridge Pa
FY) site: 3453
site: 3453, lay: 5
GA) site: 3525
site: 3525, lay: 4

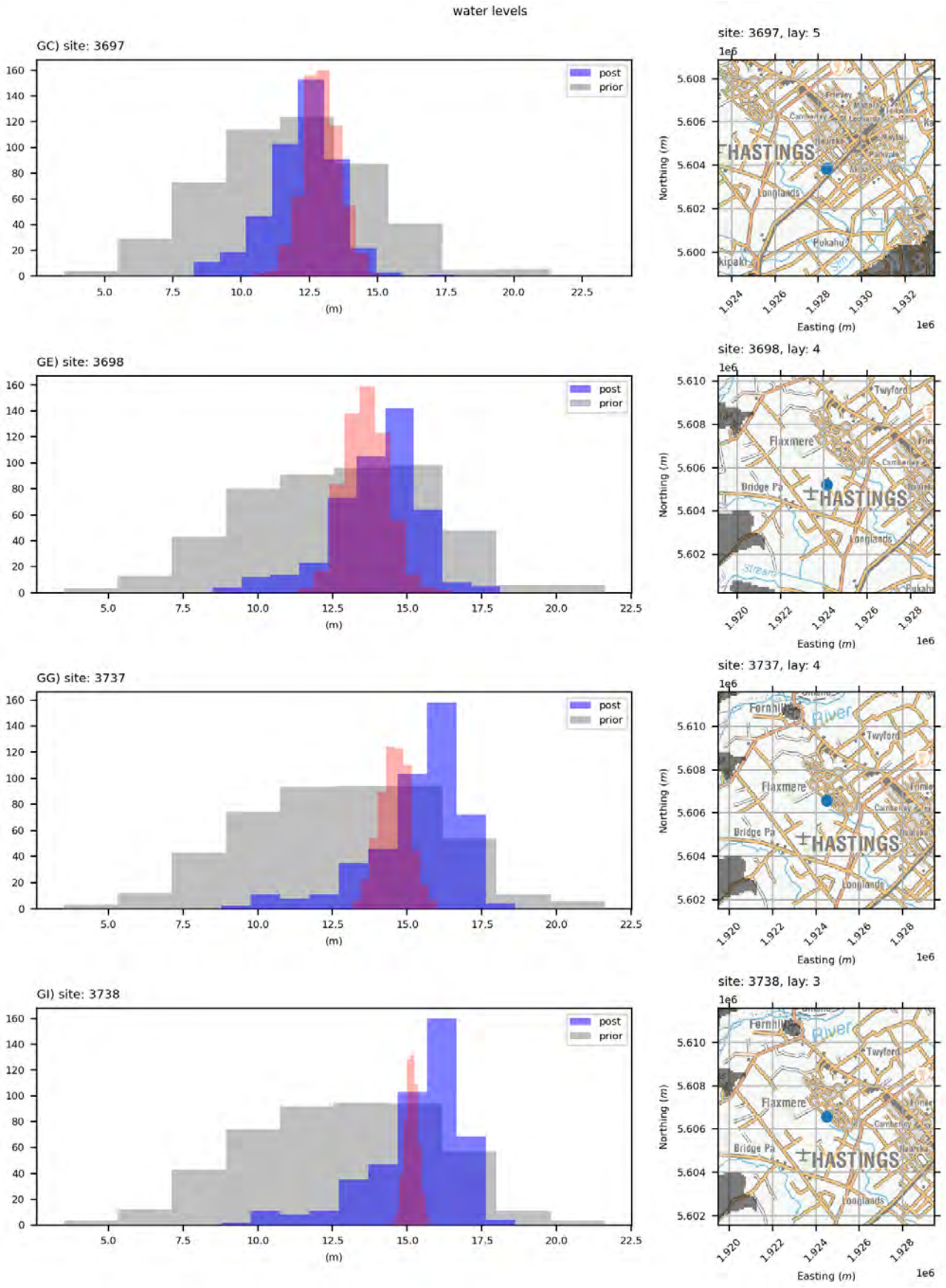
water levels
GC) site: 3697
GE) site: 3698
GG) site: 3737
GI) site: 3738
post
prior
(m)
site: 3697, lay: 5
site: 3698, lay: 4
site: 3737, lay: 4
site: 3738, lay: 3
Northing (m)
Easting (m)
1e6
HASTINGS
Flaxmere
Twyford
Longlands
Bridge Pa

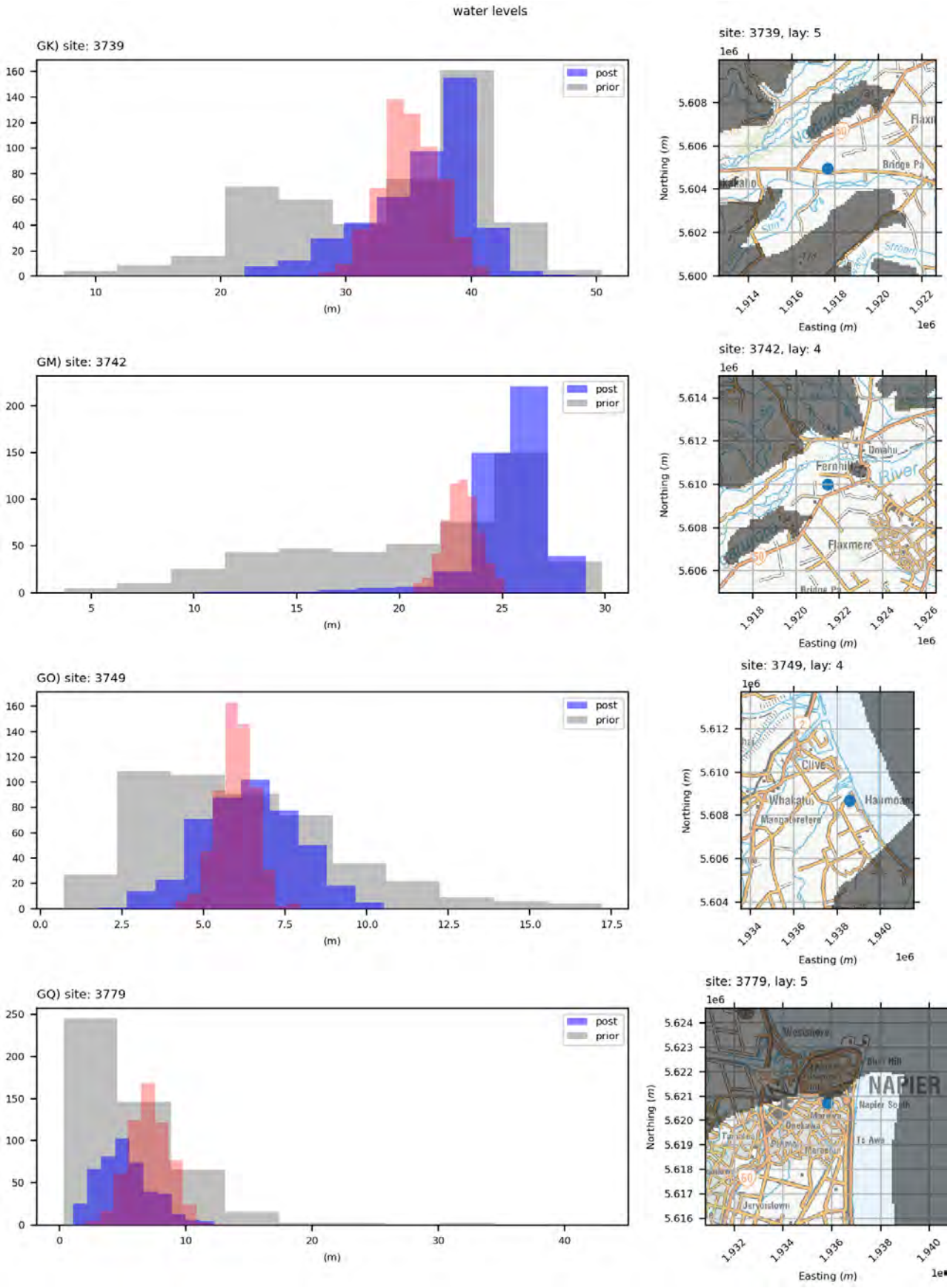
water levels
GK) site: 3739
post
prior
(m)
site: 3739, lay: 5
1e6
Northing (m)
Easting (m)
GM) site: 3742
post
prior
(m)
site: 3742, lay: 4
1e6
Northing (m)
Easting (m)
GO) site: 3749
post
prior
(m)
site: 3749, lay: 4
1e6
Northing (m)
Easting (m)
GQ) site: 3779
post
prior
(m)
site: 3779, lay: 5
1e6
Northing (m)
Easting (m)

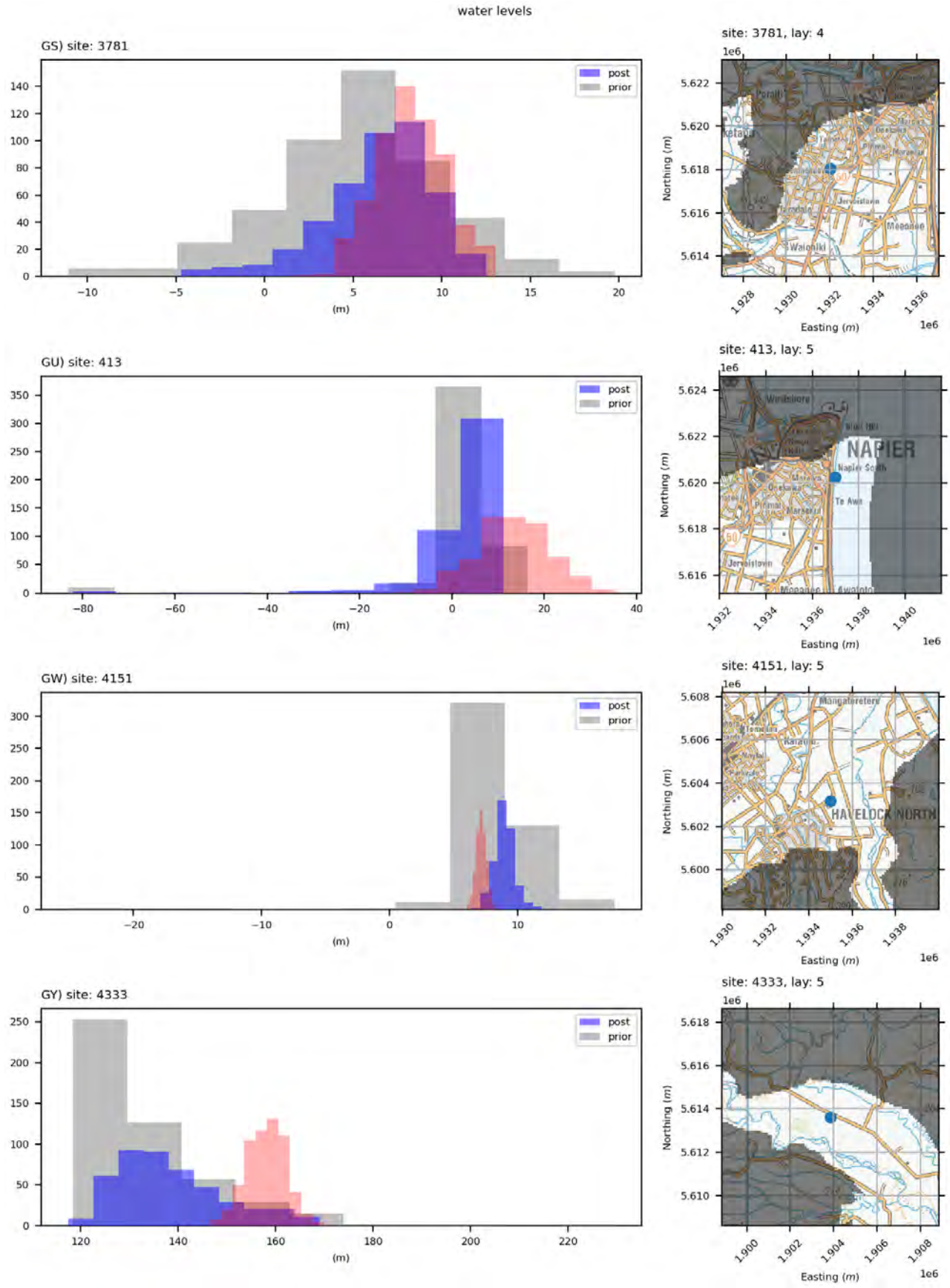
water levels
GS) site: 3781
post
prior
(m)
site: 3781, lay: 4
1e6
Northing (m)
Easting (m)
GU) site: 413
site: 413, lay: 5
NAPIER
GW) site: 4151
site: 4151, lay: 5
HAVELOCK NORTH
GY) site: 4333
site: 4333, lay: 5

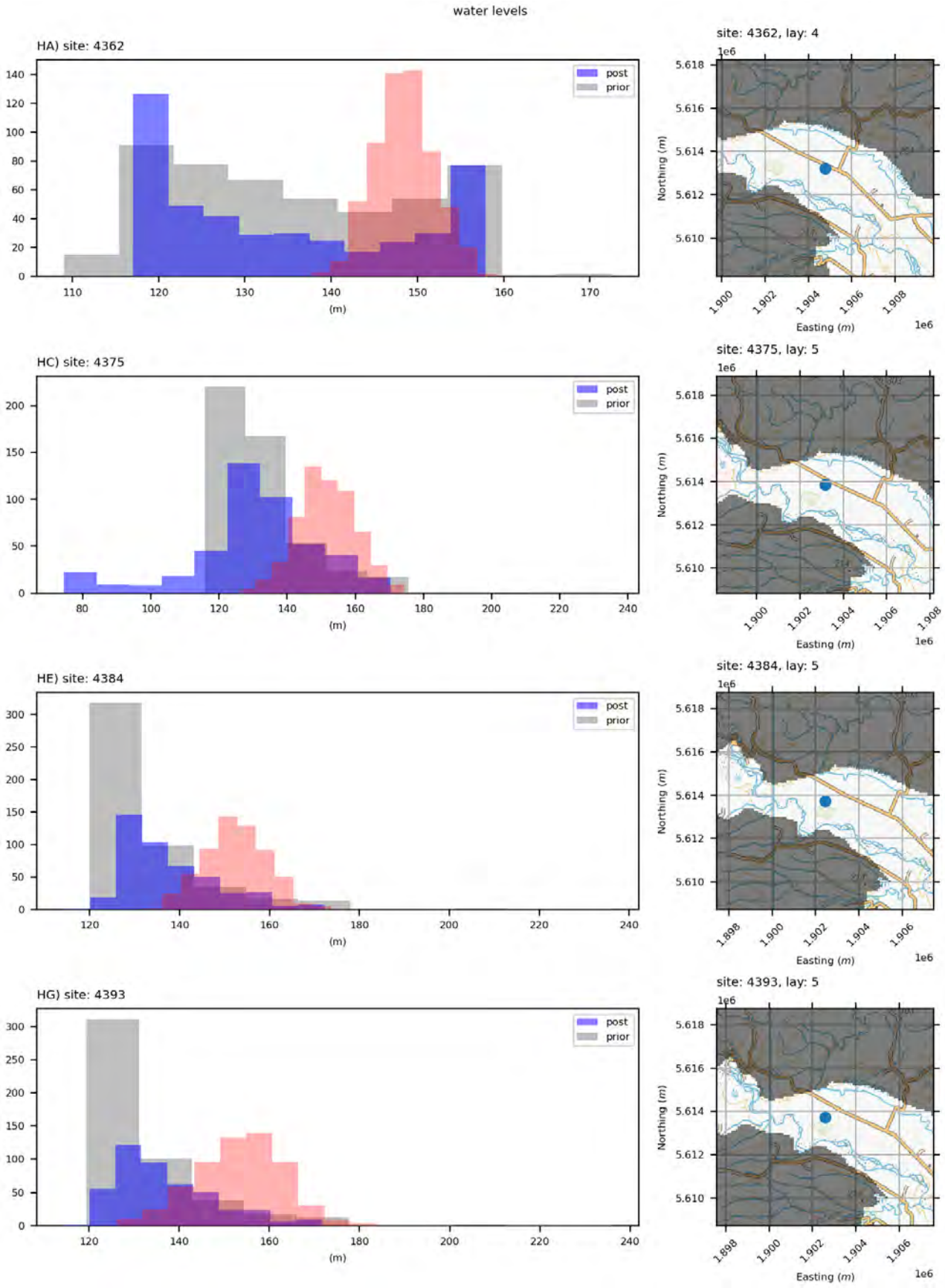
water levels
HA) site: 4362
post
prior
(m)
site: 4362, lay: 4
1e6
Northing (m)
Easting (m)
HC) site: 4375
site: 4375, lay: 5
HE) site: 4384
site: 4384, lay: 5
HG) site: 4393
site: 4393, lay: 5

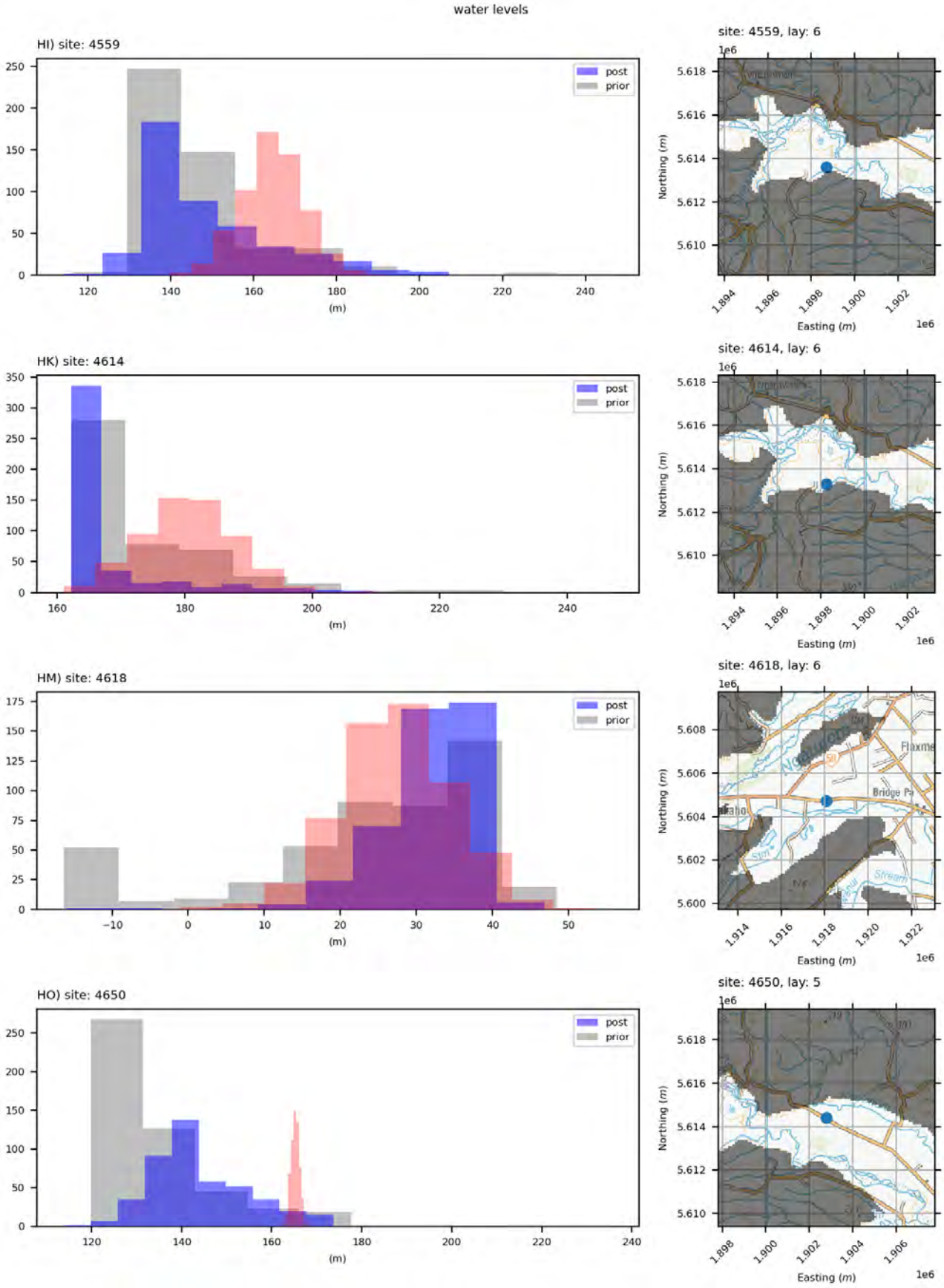
water levels
HI) site: 4559
post
prior
(m)
site: 4559, lay: 6
1e6
Northing (m)
Easting (m)
HK) site: 4614
site: 4614, lay: 6
HM) site: 4618
site: 4618, lay: 6
HO) site: 4650
site: 4650, lay: 5

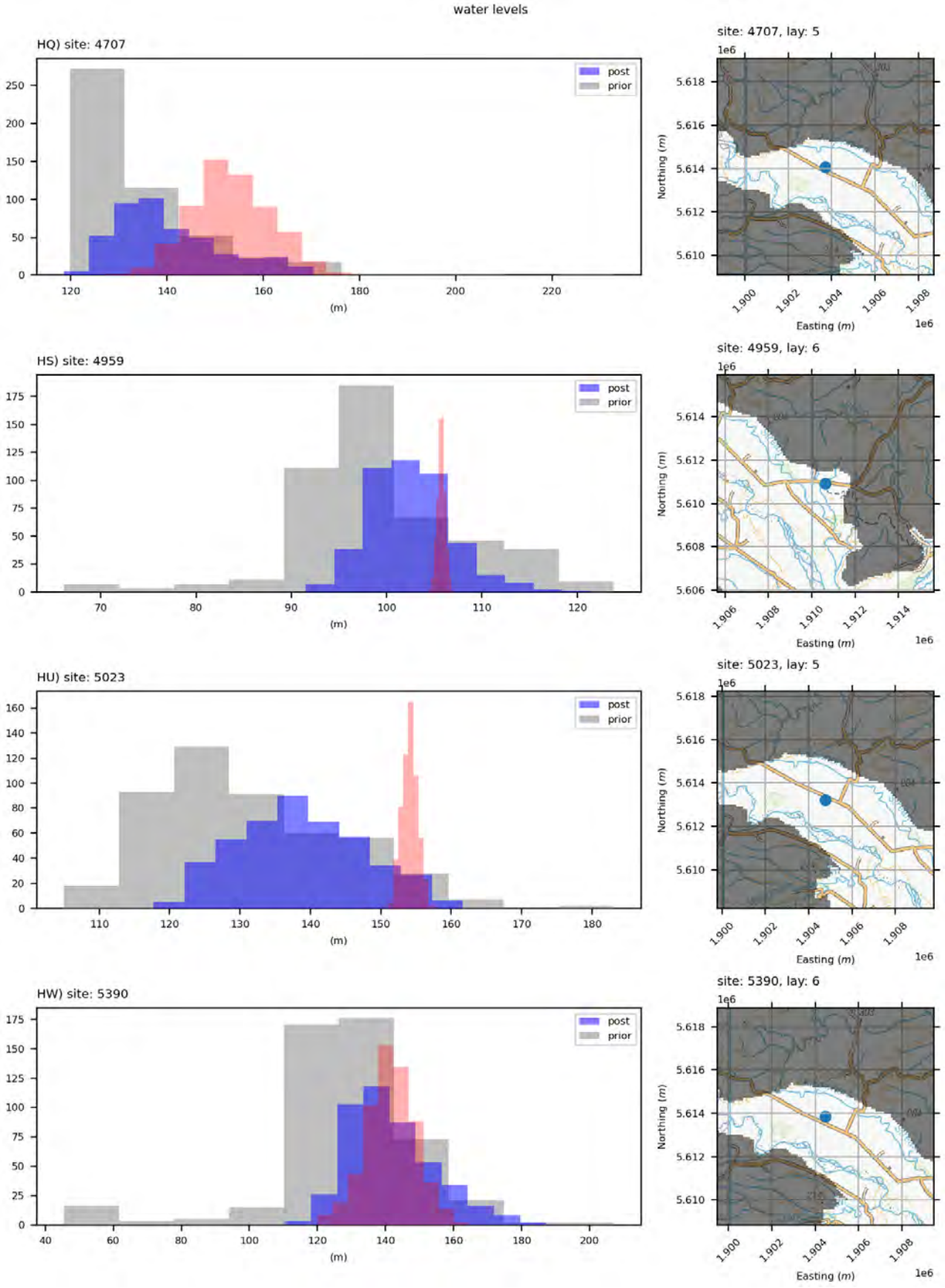
water levels
HQ) site: 4707
post
prior
(m)
site: 4707, lay: 5
1e6
Northing (m)
Easting (m)
HS) site: 4959
site: 4959, lay: 6
HU) site: 5023
site: 5023, lay: 5
HW) site: 5390
site: 5390, lay: 6

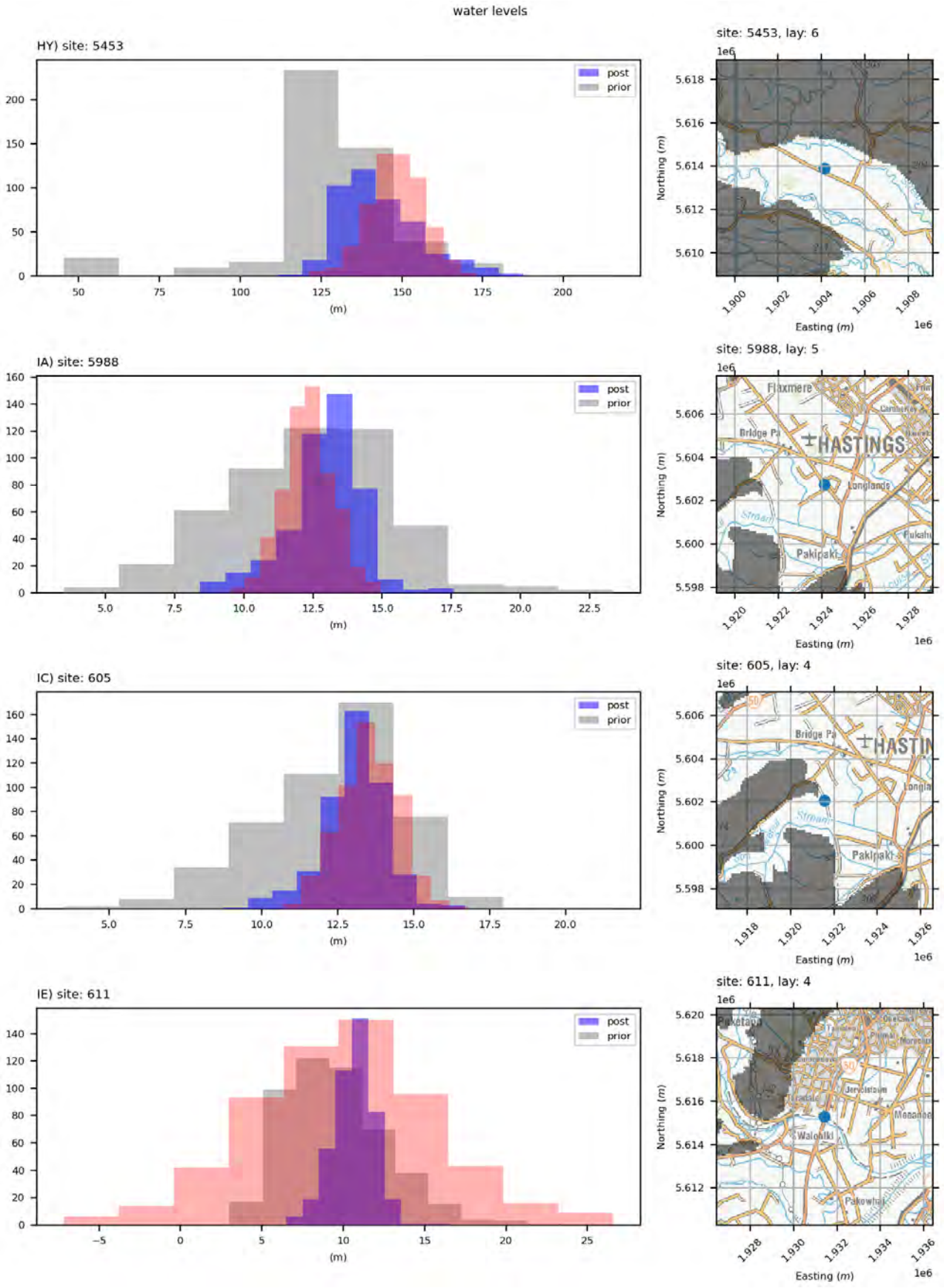
water levels
HY) site: 5453
post
prior
(m)
site: 5453, lay: 6
1e6
Northing (m)
Easting (m)
IA) site: 5988
site: 5988, lay: 5
Flaxmere
HASTINGS
Longlands
Pakipaki
IC) site: 605
site: 605, lay: 4
IE) site: 611
site: 611, lay: 4
Waiohiki

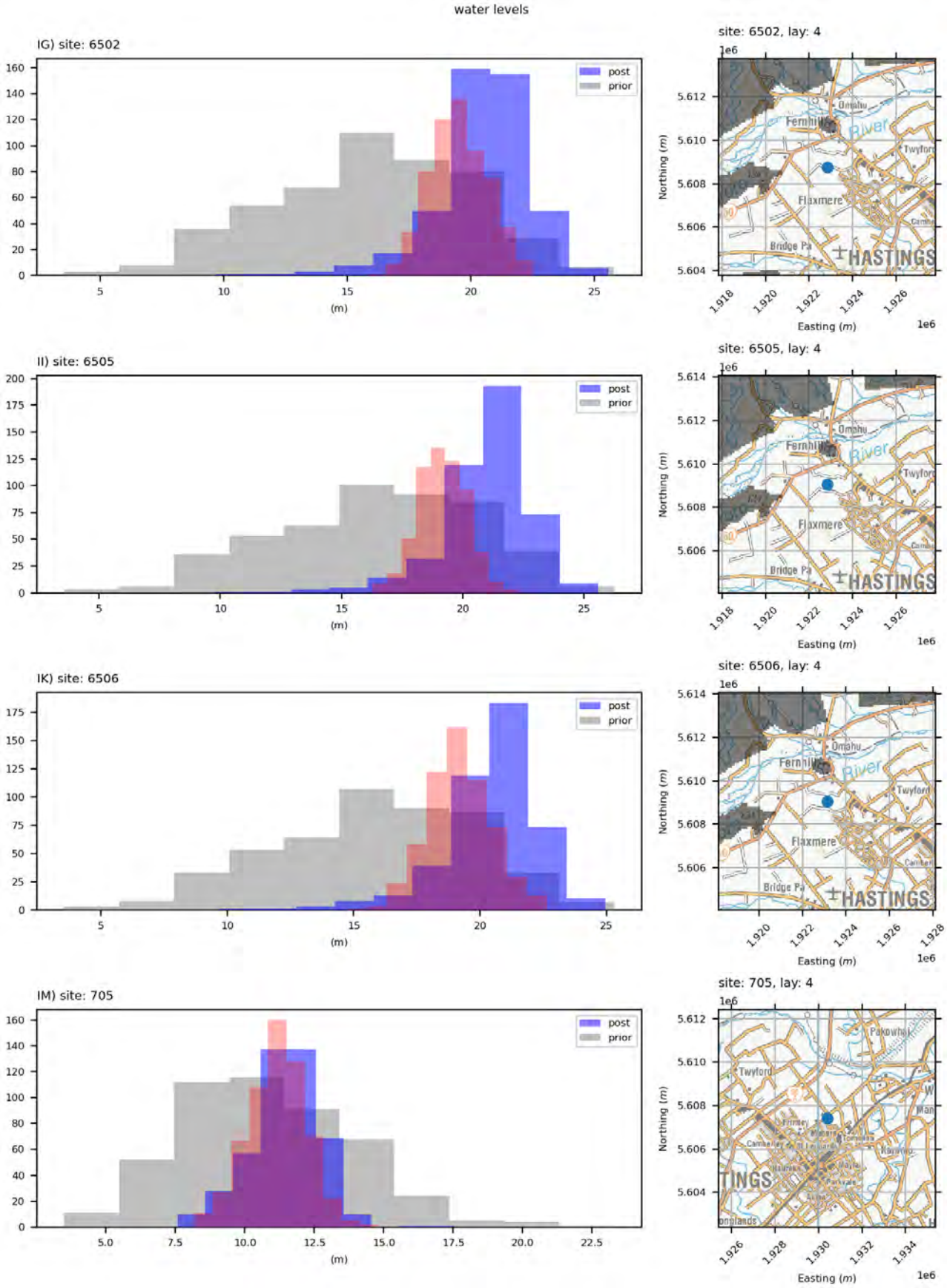
water levels
IG) site: 6502
post
prior
(m)
site: 6502, lay: 4
1e6
Northing (m)
Easting (m)
II) site: 6505
site: 6505, lay: 4
IK) site: 6506
site: 6506, lay: 4
IM) site: 705
site: 705, lay: 4
Omahu
Fernhill
River
Twyford
Flaxmere
Bridge Pa
HASTINGS

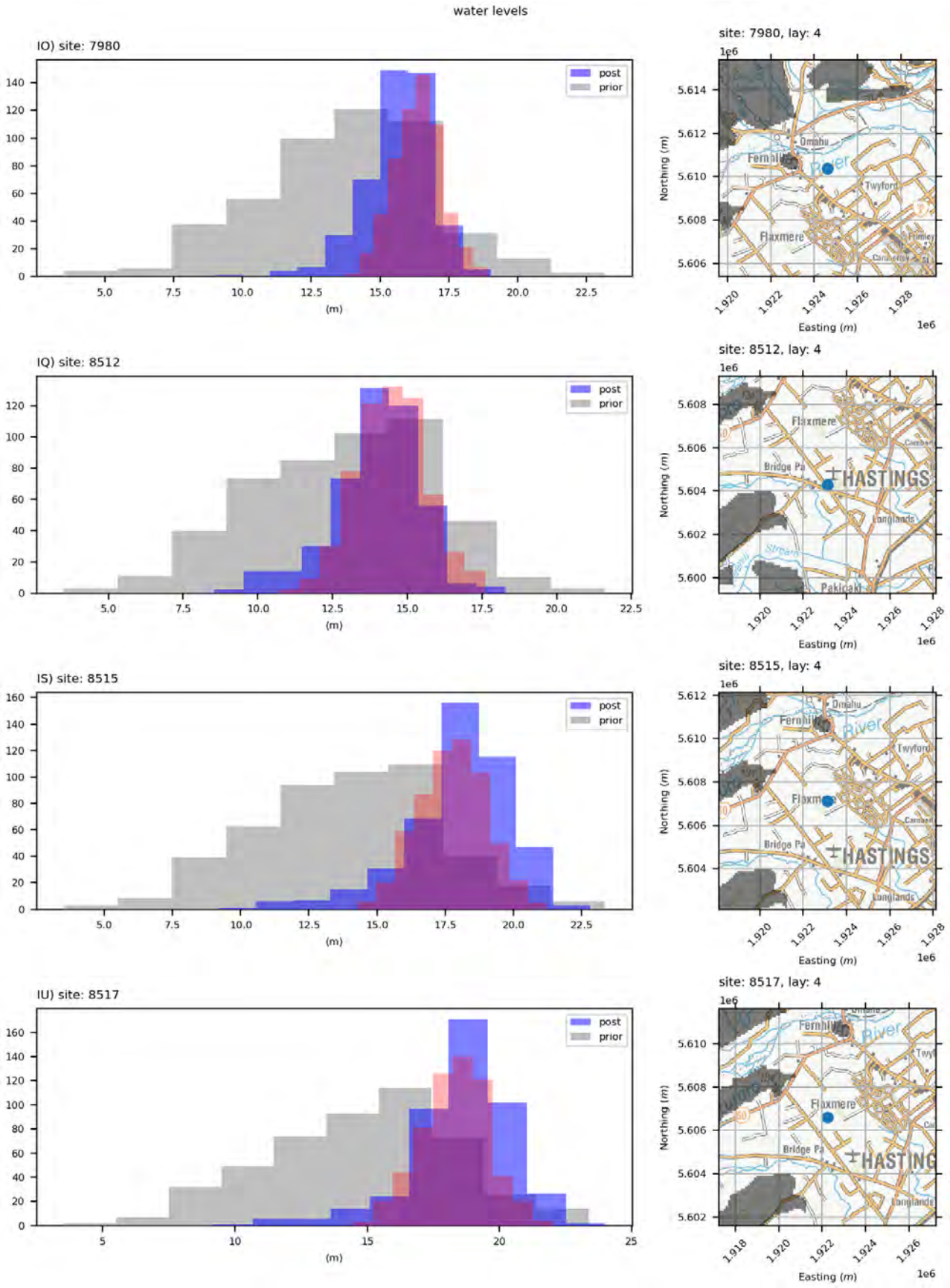
water levels
IO) site: 7980
post
prior
(m)
site: 7980, lay: 4
1e6
Northing (m)
Easting (m)
IQ) site: 8512
site: 8512, lay: 4
IS) site: 8515
site: 8515, lay: 4
IU) site: 8517
site: 8517, lay: 4
Fernhill
Twyford
Flaxmere
HASTINGS
Bridge Pa
Longlands
Pakipaki

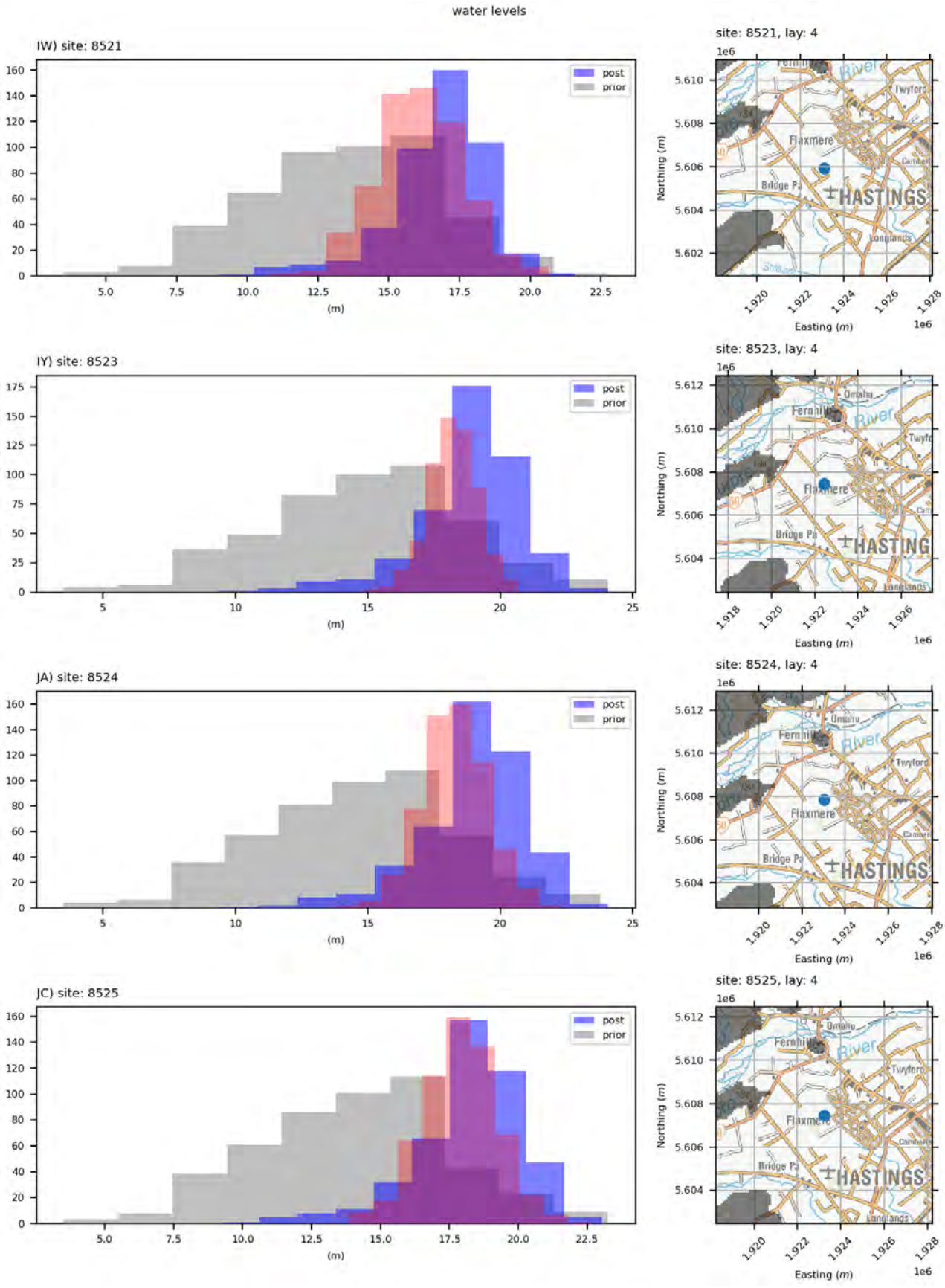
water levels
IW) site: 8521
post
prior
(m)
site: 8521, lay: 4
1e6
Northing (m)
Easting (m)
IY) site: 8523
site: 8523, lay: 4
JA) site: 8524
site: 8524, lay: 4
JC) site: 8525
site: 8525, lay: 4
HASTINGS
Flaxmere
Bridge Pa
Twyford
Fernhill
Omahu
River

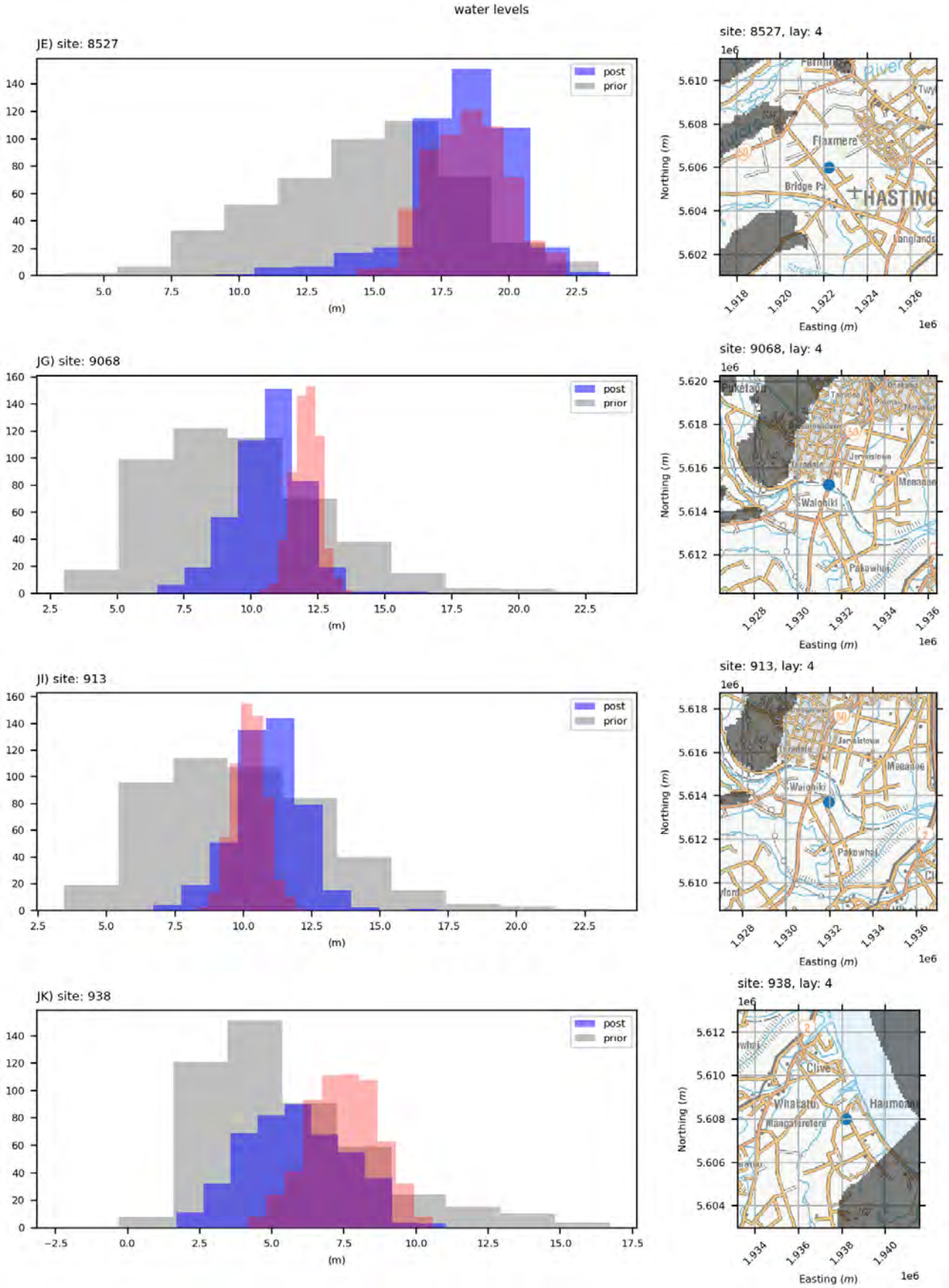
water levels
JE) site: 8527
post
prior
(m)
site: 8527, lay: 4
Northing (m)
Easting (m)
1e6
Flaxmere
HASTING
JG) site: 9068
site: 9068, lay: 4
Waiohiki
Pakowhai
JI) site: 913
site: 913, lay: 4
JK) site: 938
site: 938, lay: 4
Clive
Whakatu
Haumoana

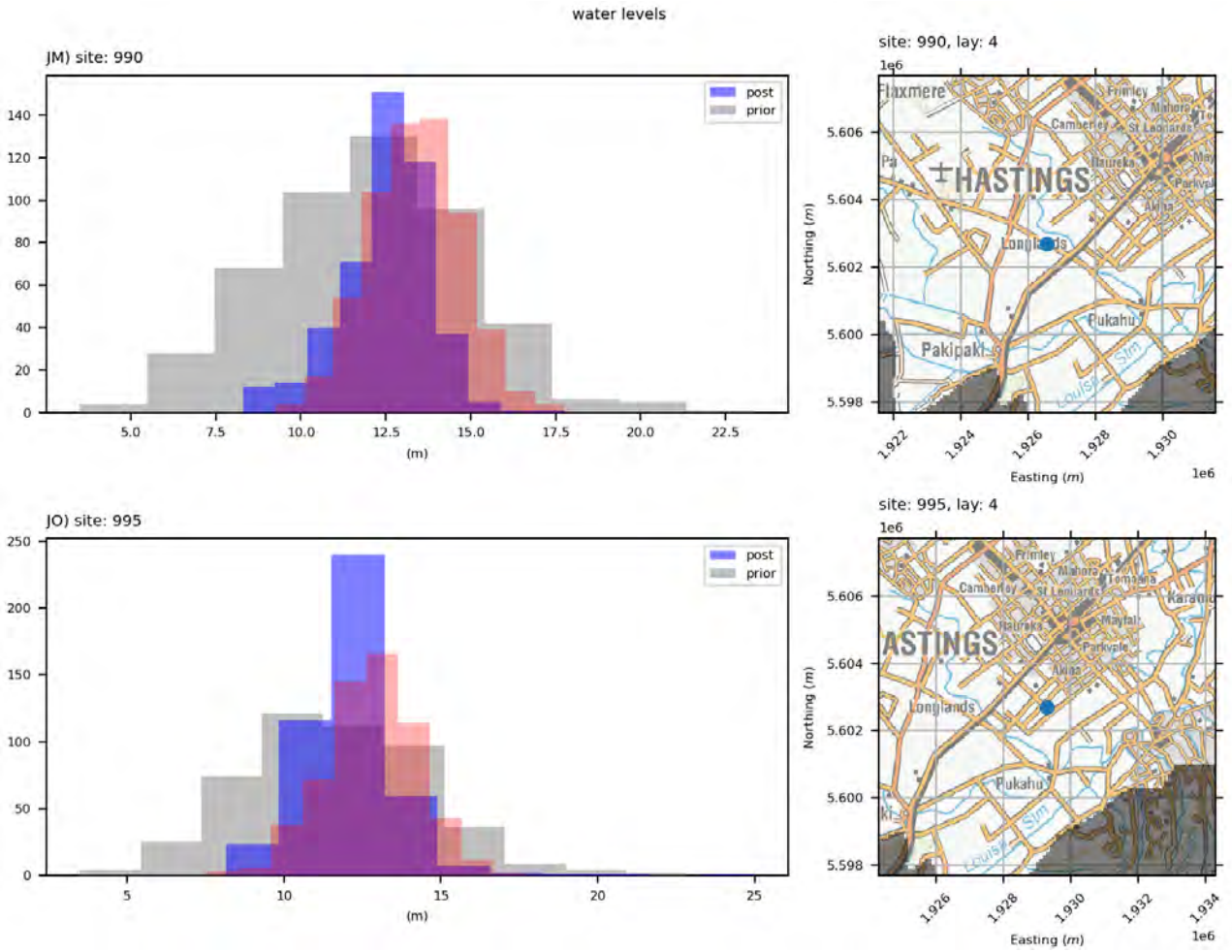
water levels
JM) site: 990
post
prior
(m)
site: 990, lay: 4
1e6
Flaxmere
HASTINGS
Pukahu
Pakipaki
Northing (m)
Easting (m)
JO) site: 995
post
prior
(m)
site: 995, lay: 4
1e6
ASTINGS
Longlands
Pukahu
Northing (m)
Easting (m)

A3.2.3.2 Stream Flows

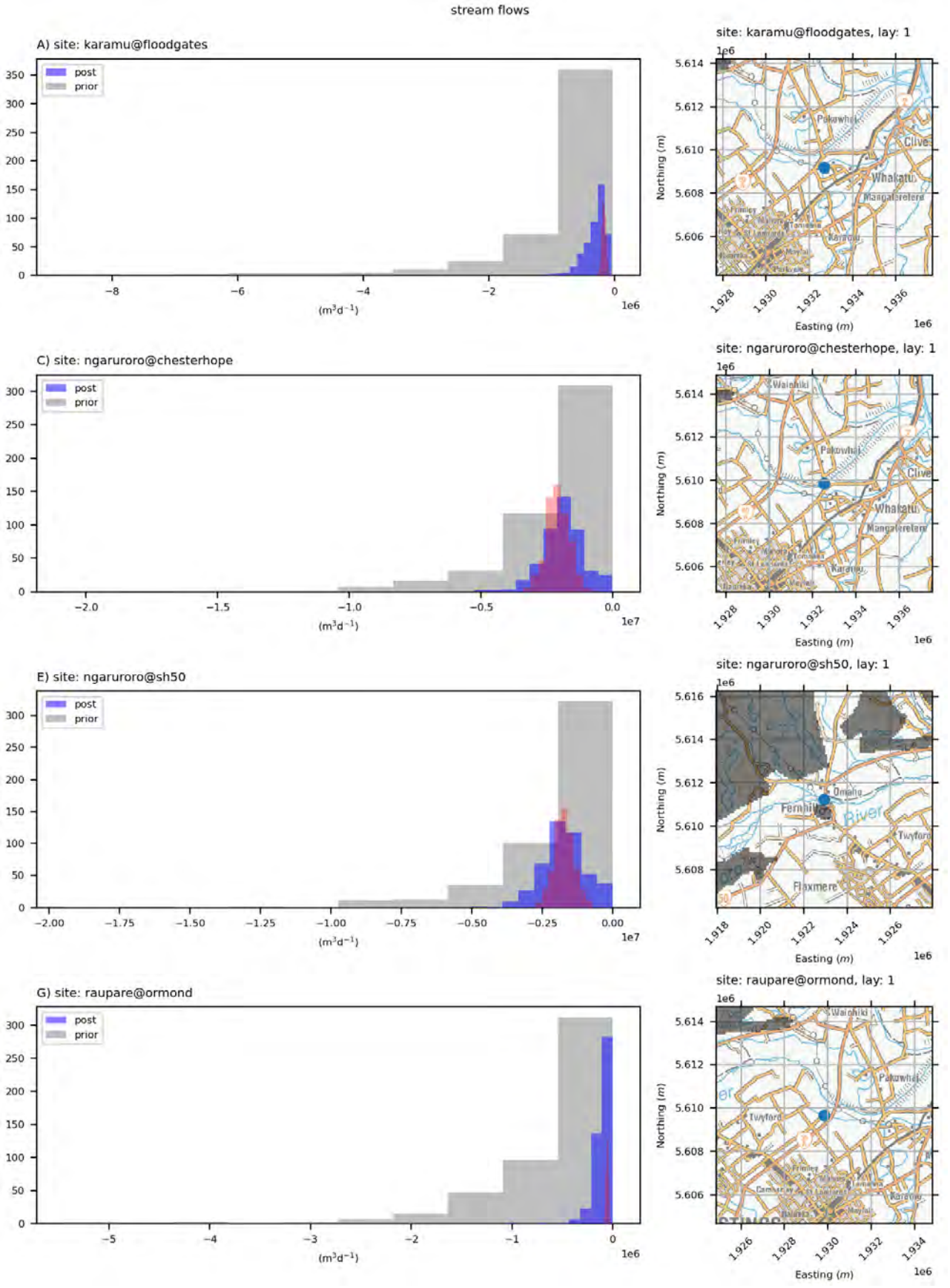

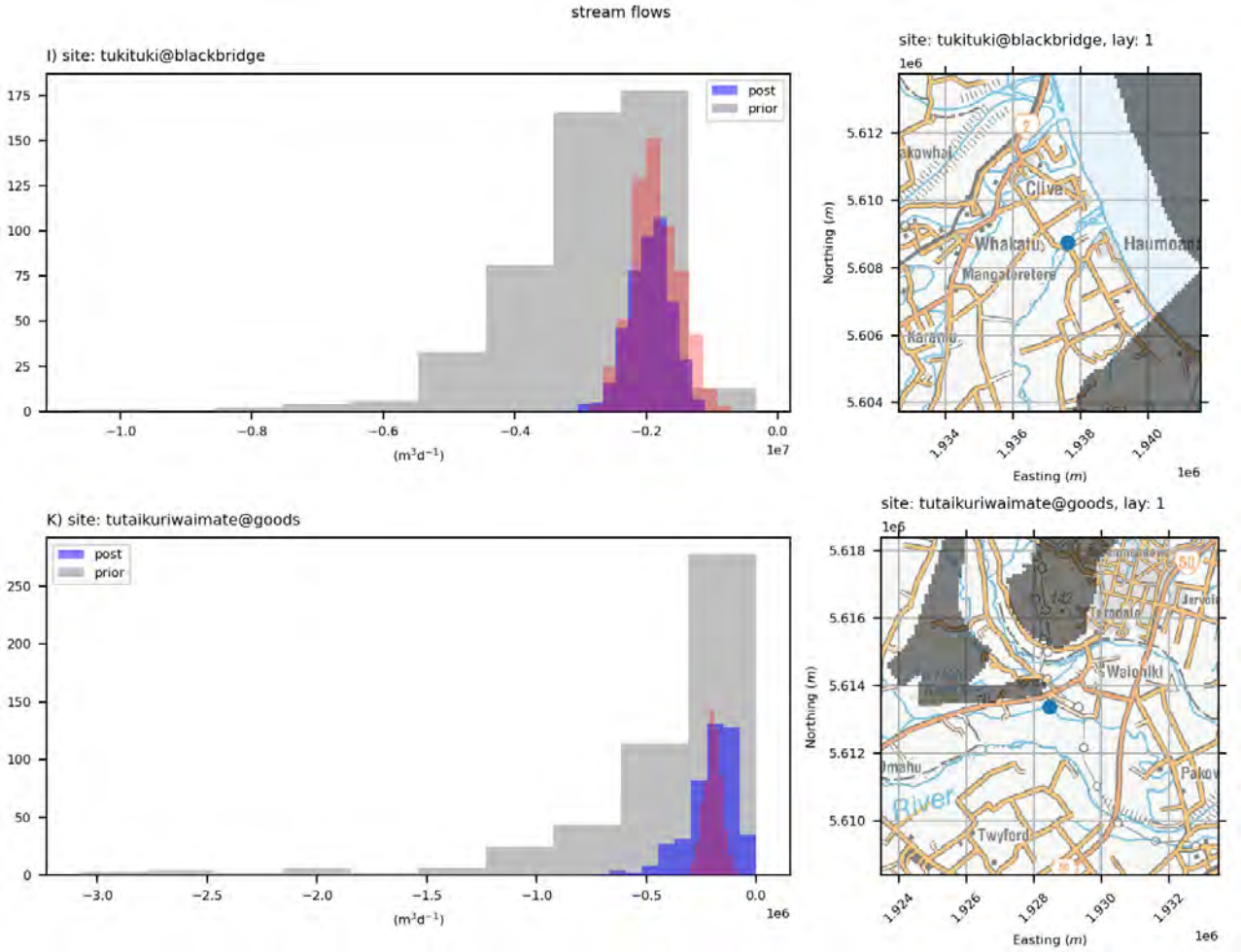
stream flows
I) site: tukituki@blackbridge
post
prior
(m³d⁻¹)
1e7
site: tukituki@blackbridge, lay: 1
Northing (m)
Easting (m)
Clive
Whakatu
Mangateretere
K) site: tutaikuriwaimate@goods
post
prior
(m³d⁻¹)
1e6
site: tutaikuriwaimate@goods, lay: 1
Northing (m)
Easting (m)
Waioriki
Twyford
River

A3.2.3.3 Surface-Water–Groundwater Exchange

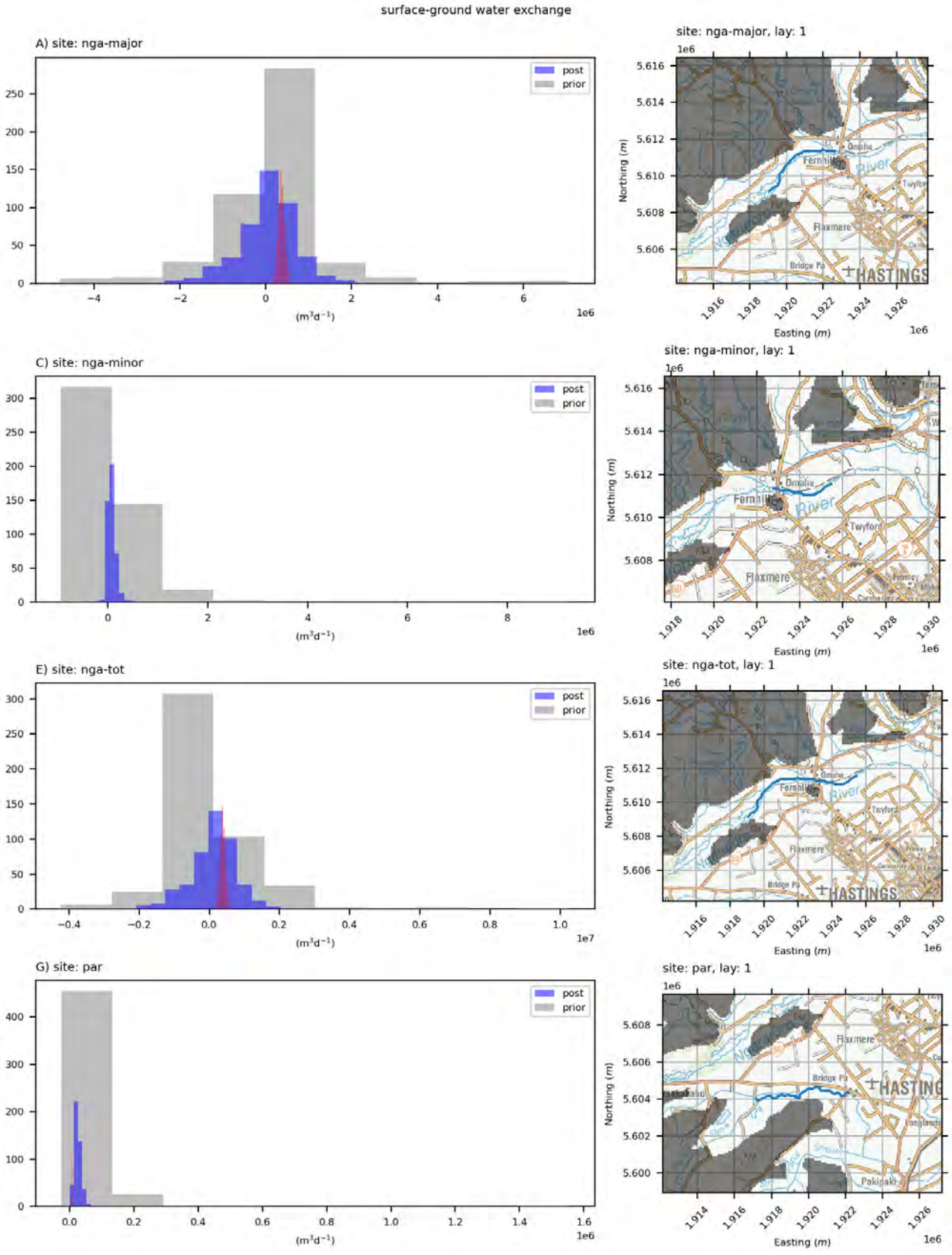

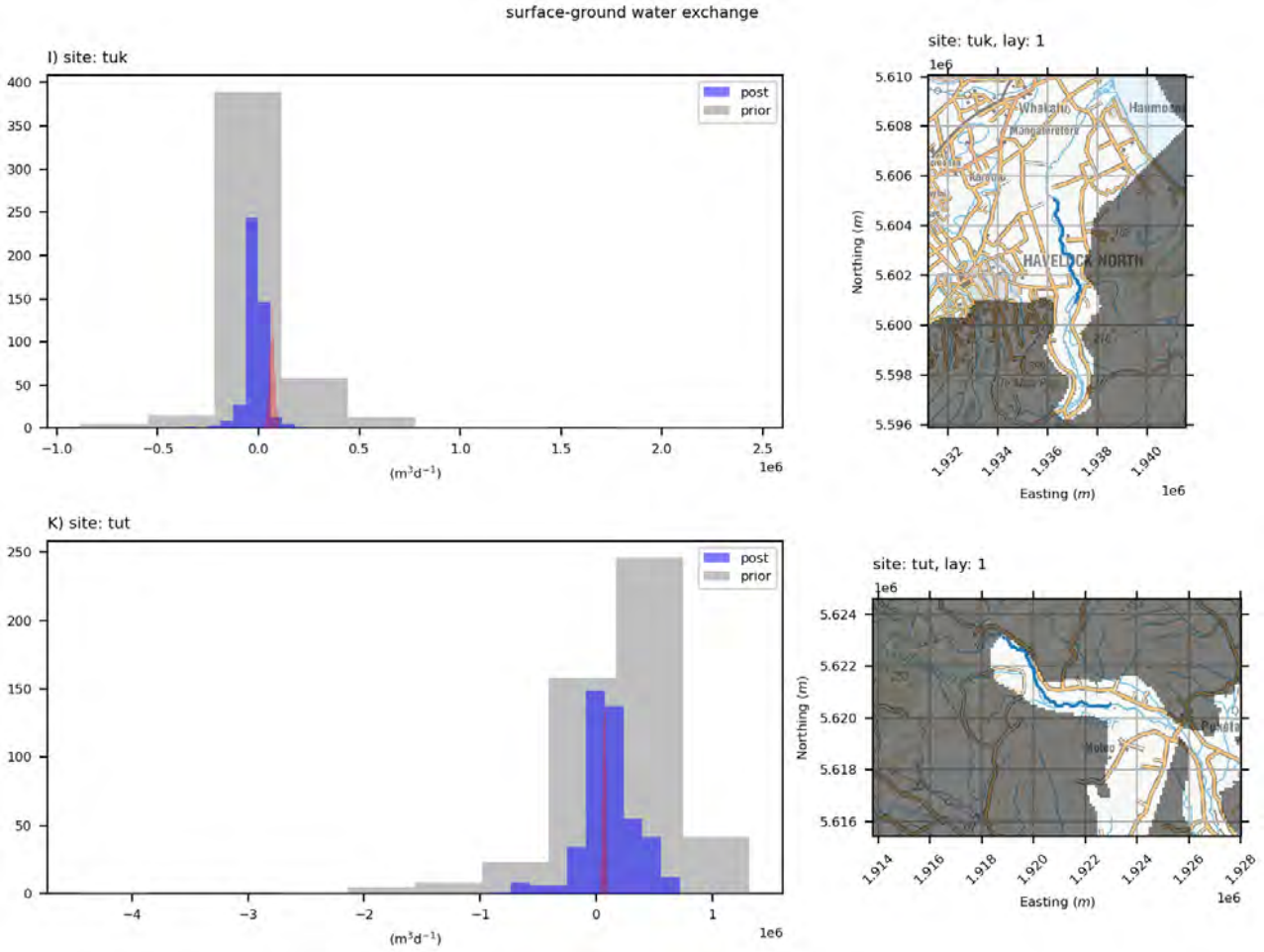
surface-ground water exchange
I) site: tuk
post
prior
(m³d⁻¹)
1e6
site: tuk, lay: 1
Northing (m)
Easting (m)
HAVELOCK NORTH
K) site: tut
post
prior
(m³d⁻¹)
1e6
site: tut, lay: 1
Northing (m)
Easting (m)

A3.2.4 *skytem-lay-precond*

A3.2.4.1 Levels

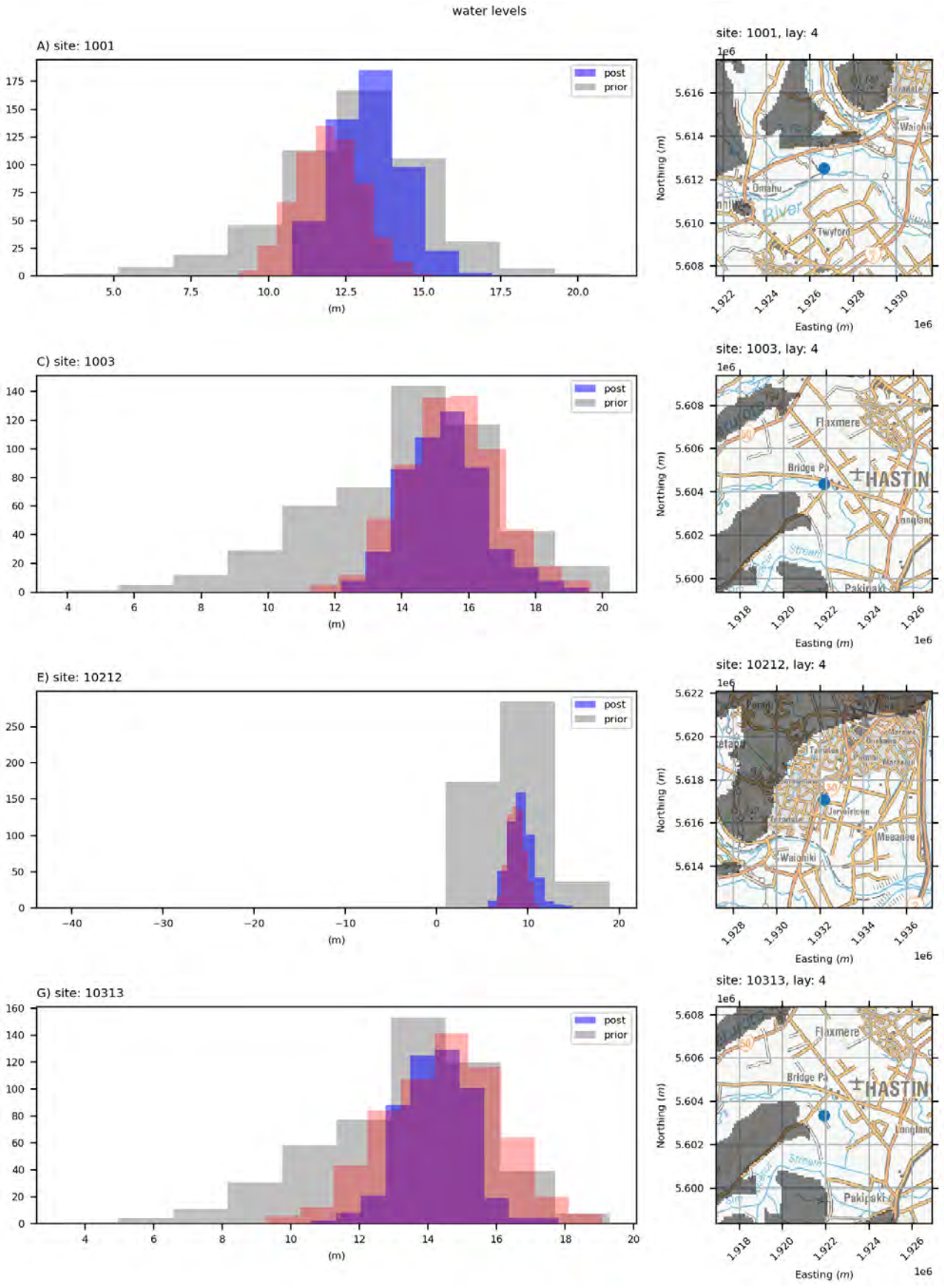

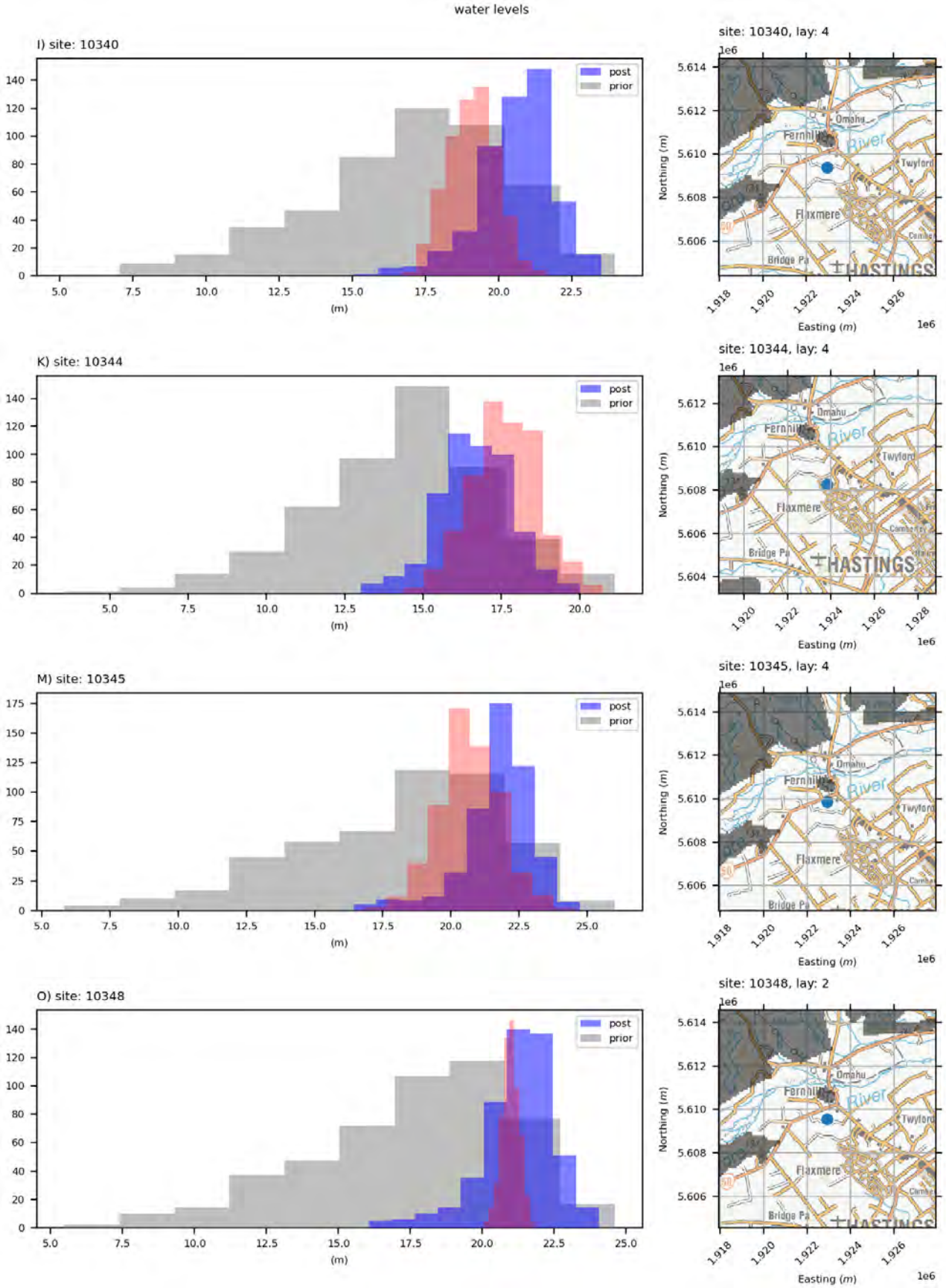
water levels
I) site: 10340
post
prior
(m)
site: 10340, lay: 4
1e6
Northing (m)
Easting (m)
Omahu
Fernhill
River
Twyford
Flaxmere
Bridge Pa
HASTINGS
K) site: 10344
site: 10344, lay: 4
M) site: 10345
site: 10345, lay: 4
O) site: 10348
site: 10348, lay: 2

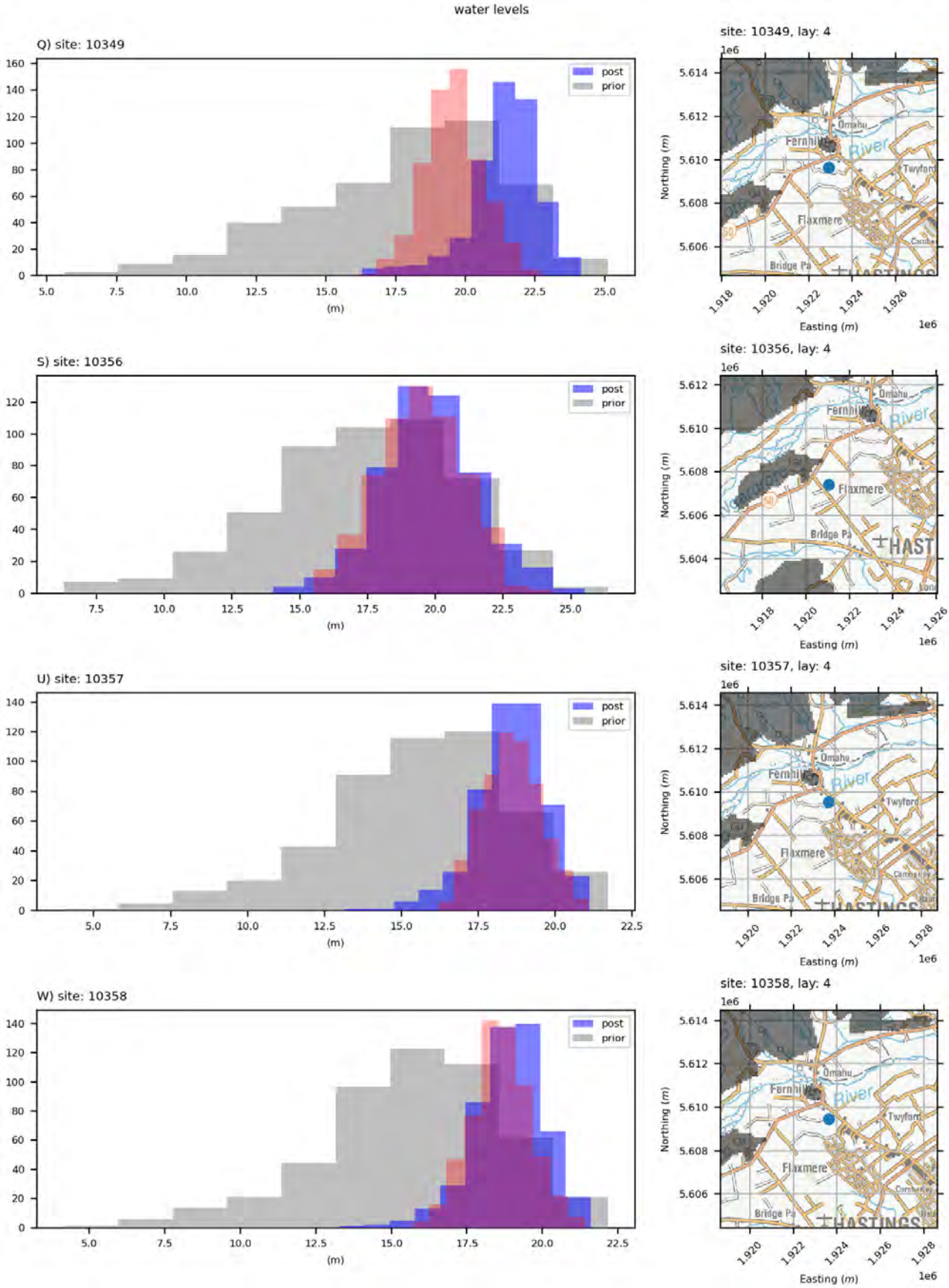
water levels
Q) site: 10349
post
prior
(m)
site: 10349, lay: 4
1e6
Northing (m)
Easting (m)
Omahu
Fernhill
River
Twyford
Flaxmere
Bridge Pa
S) site: 10356
site: 10356, lay: 4
U) site: 10357
site: 10357, lay: 4
W) site: 10358
site: 10358, lay: 4

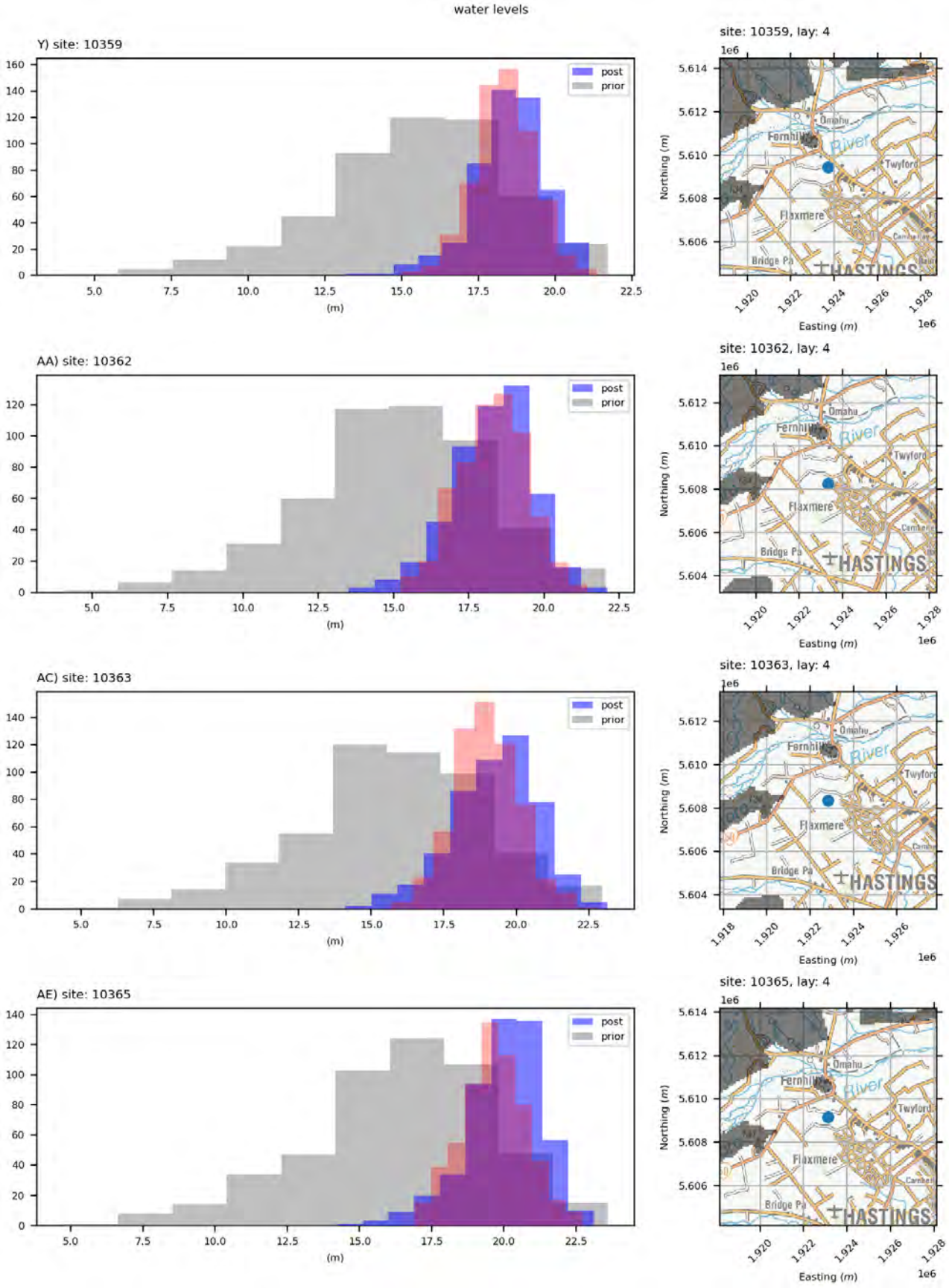
water levels
Y) site: 10359
post
prior
(m)
site: 10359, lay: 4
1e6
Northing (m)
Easting (m)
Omahu
Fernhill
River
Twyford
Flaxmere
Bridge Pa
HASTINGS
AA) site: 10362
site: 10362, lay: 4
AC) site: 10363
site: 10363, lay: 4
AE) site: 10365
site: 10365, lay: 4

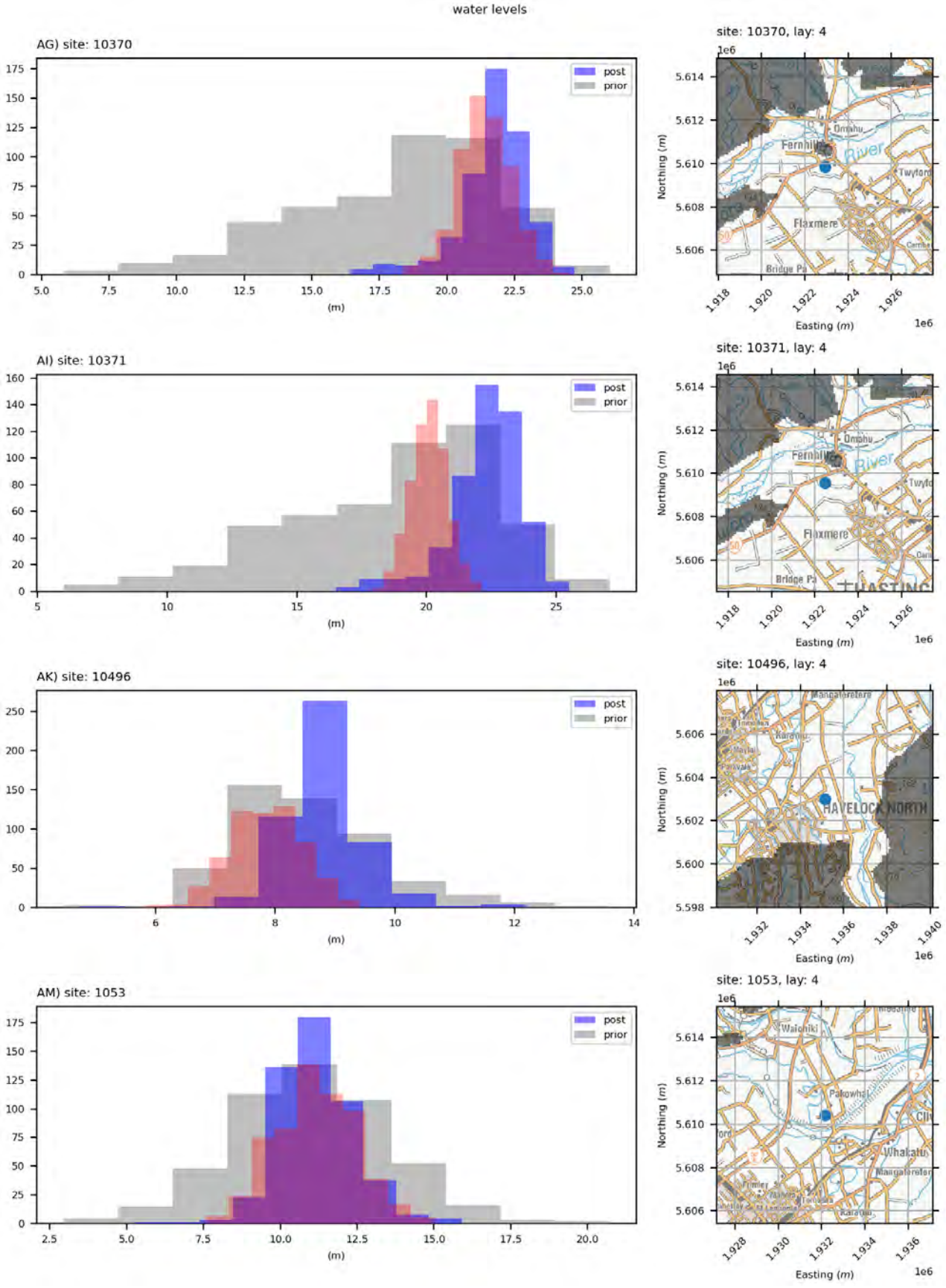
water levels
AG) site: 10370
post
prior
(m)
site: 10370, lay: 4
Northing (m)
Easting (m)
1e6
AI) site: 10371
post
prior
(m)
site: 10371, lay: 4
Northing (m)
Easting (m)
1e6
AK) site: 10496
post
prior
(m)
site: 10496, lay: 4
HAVELOCK NORTH
Northing (m)
Easting (m)
1e6
AM) site: 1053
post
prior
(m)
site: 1053, lay: 4
Northing (m)
Easting (m)
1e6

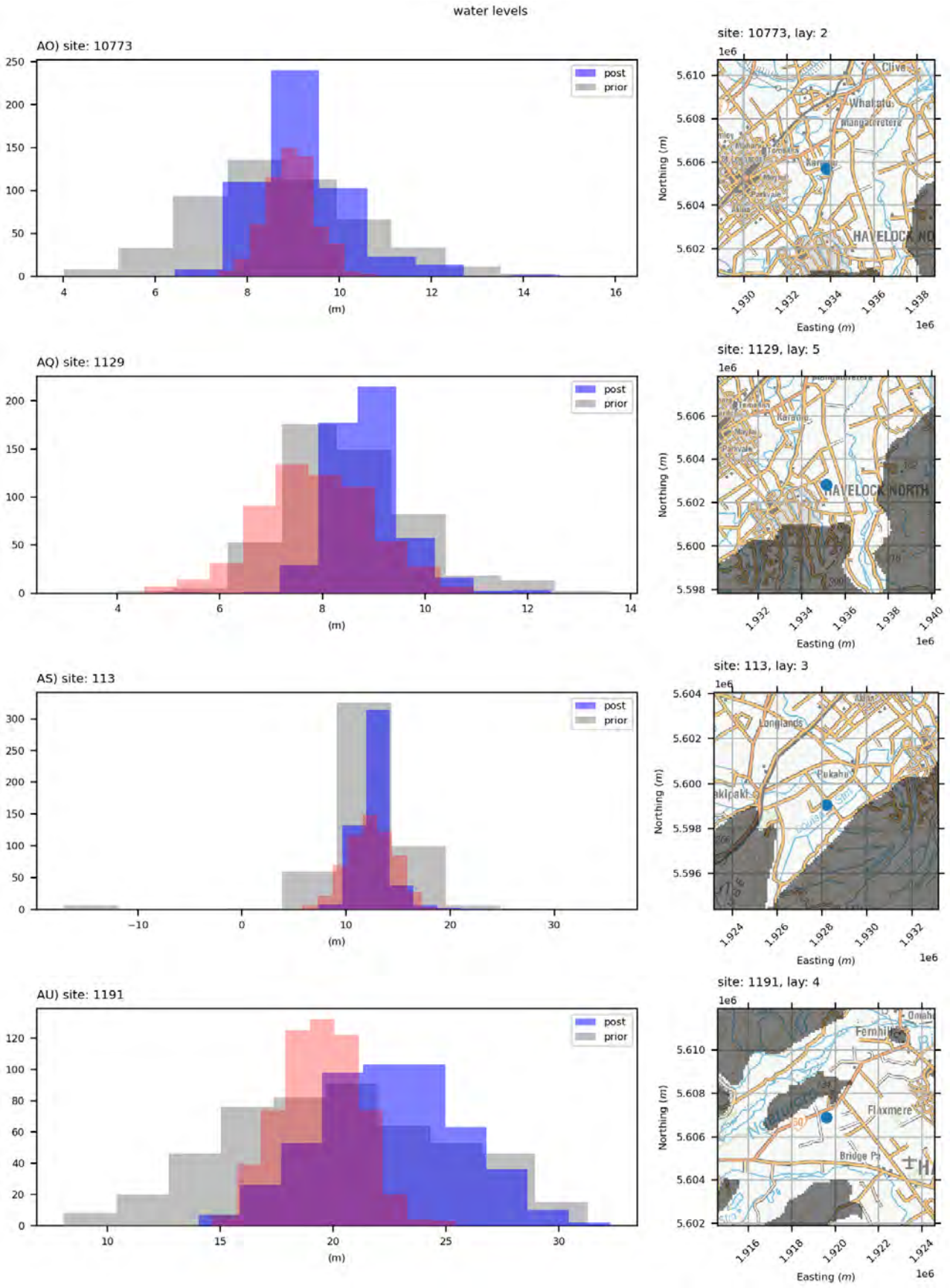
water levels
AO) site: 10773
post
prior
(m)
site: 10773, lay: 2
1e6
Northing (m)
Easting (m)
AQ) site: 1129
site: 1129, lay: 5
AS) site: 113
site: 113, lay: 3
AU) site: 1191
site: 1191, lay: 4

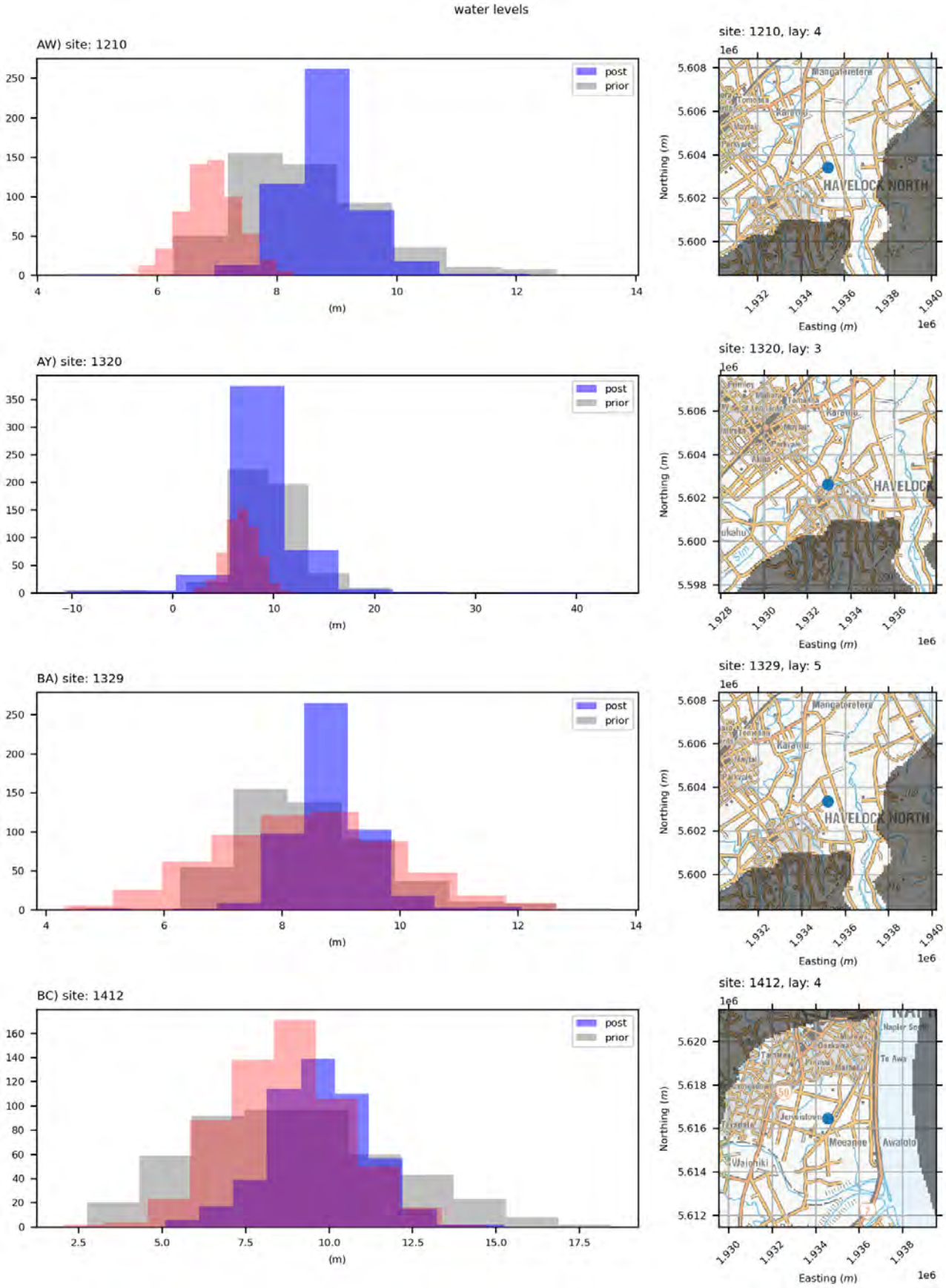
water levels
AW) site: 1210
post
prior
(m)
site: 1210, lay: 4
1e6
Northing (m)
Easting (m)
HAVELOCK NORTH
AY) site: 1320
site: 1320, lay: 3
HAVELOCK
BA) site: 1329
site: 1329, lay: 5
BC) site: 1412
site: 1412, lay: 4
Napier South
Te Awa
Meeanee
Awatoto

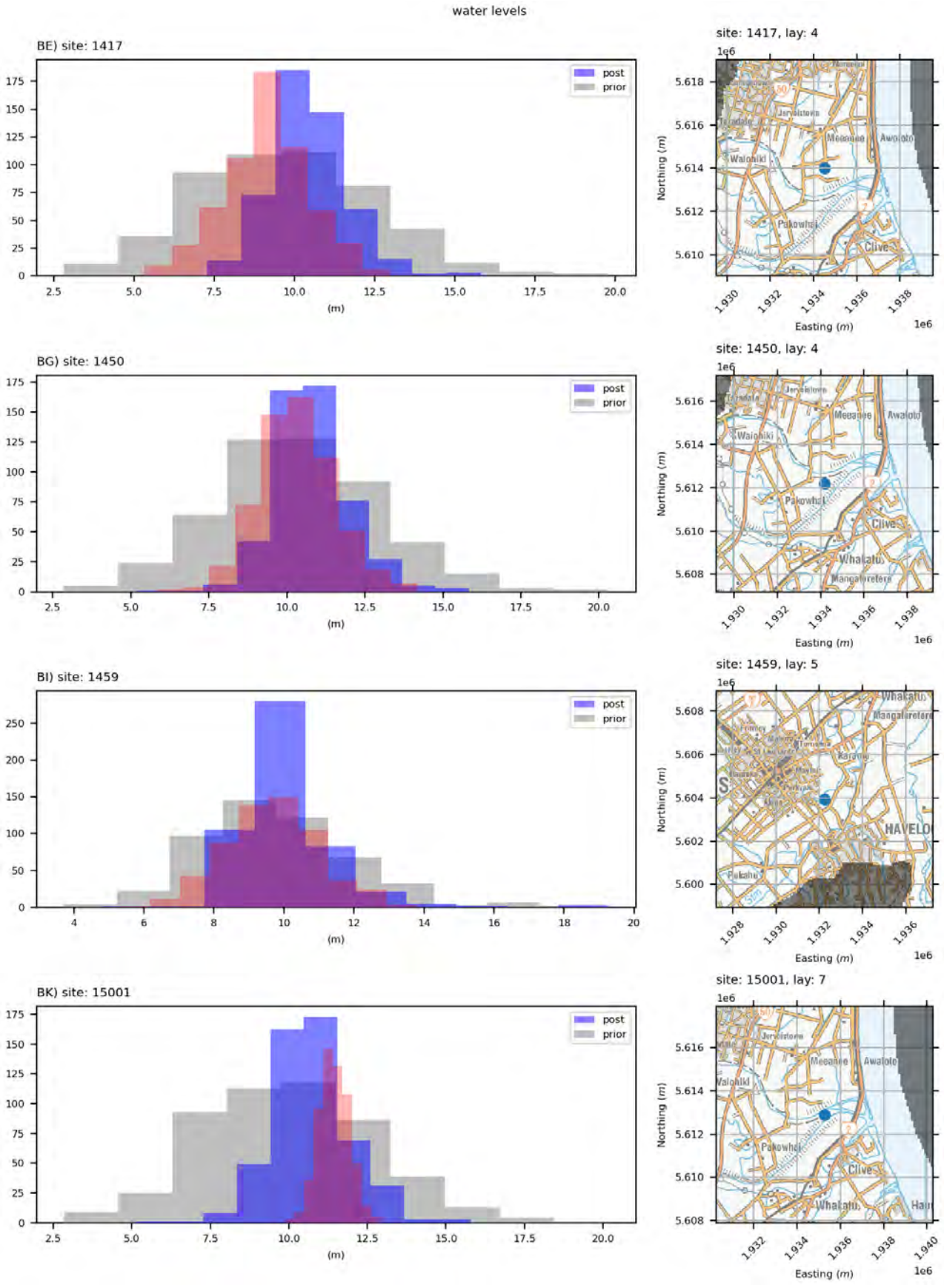
water levels
BE) site: 1417
post
prior
(m)
site: 1417, lay: 4
1e6
Northing (m)
Easting (m)
Jervistown
Meeanee
Awaloto
Waiohiki
Pakowhai
Clive
BG) site: 1450
site: 1450, lay: 4
Whakatu
Mangateretere
BI) site: 1459
site: 1459, lay: 5
HAVELO
BK) site: 15001
site: 15001, lay: 7

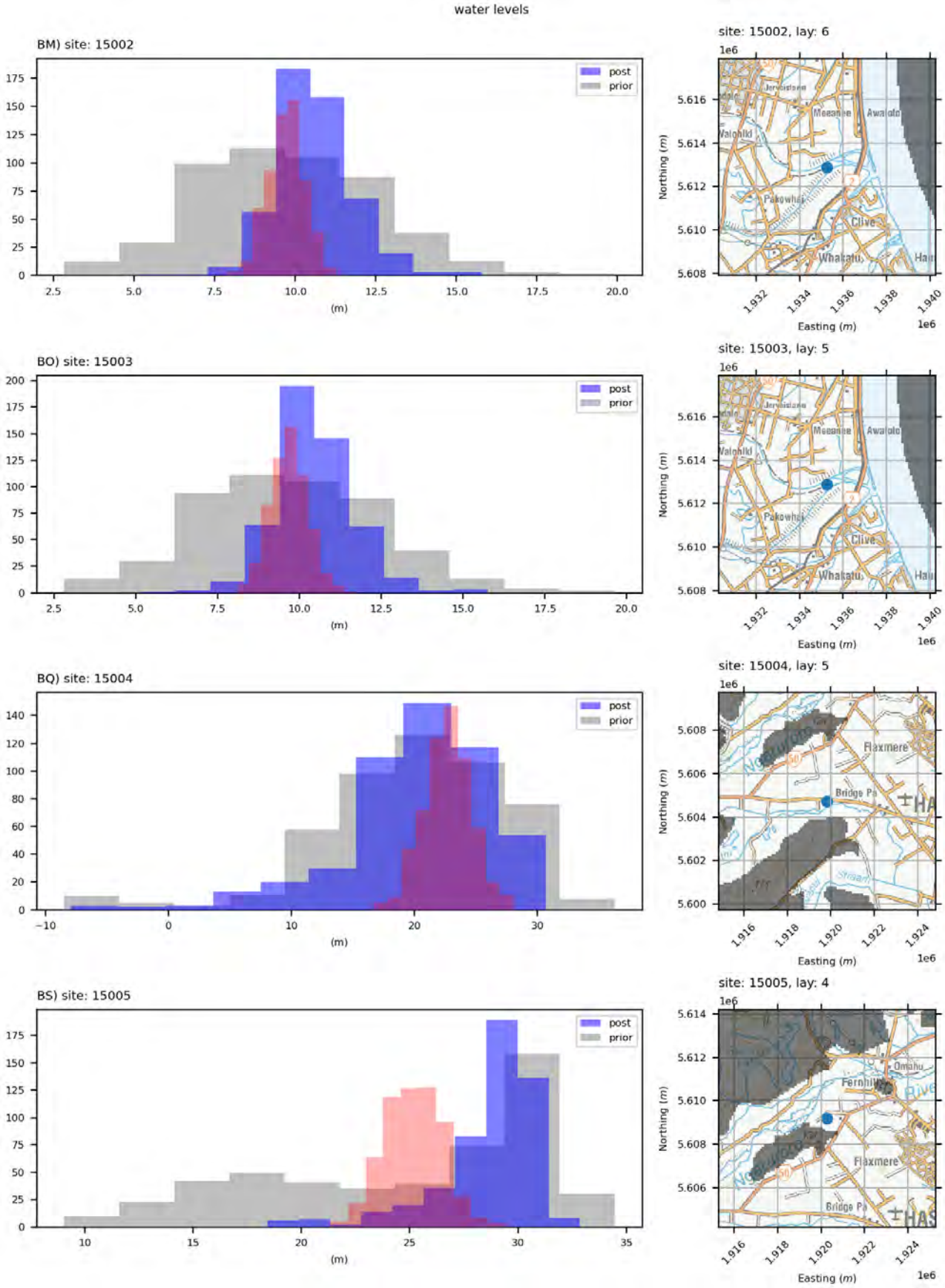
water levels
BM) site: 15002
post
prior
(m)
site: 15002, lay: 6
1e6
Northing (m)
Easting (m)
Meeanee
Awatoto
Clive
Whakatu
BO) site: 15003
site: 15003, lay: 5
BQ) site: 15004
site: 15004, lay: 5
Flaxmere
Bridge Pa
BS) site: 15005
site: 15005, lay: 4
Omahu
Fernhill
Flaxmere
Bridge Pa

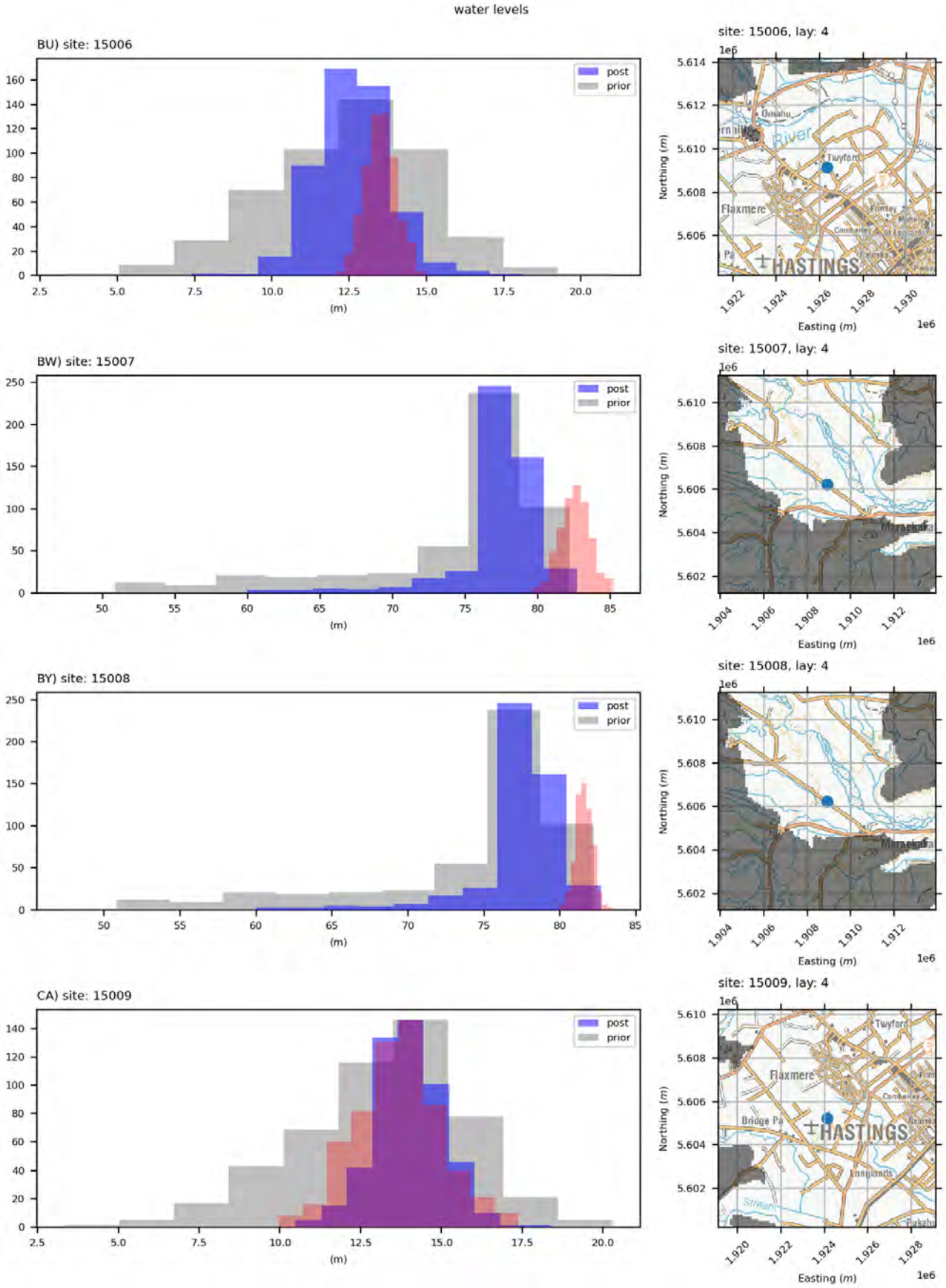
water levels
BU) site: 15006
post
prior
(m)
site: 15006, lay: 4
1e6
Northing (m)
Easting (m)
Omahu
River
Twyford
Flaxmere
Frimley
HASTINGS
BW) site: 15007
site: 15007, lay: 4
Maraekaka
BY) site: 15008
site: 15008, lay: 4
CA) site: 15009
site: 15009, lay: 4
Bridge Pa
Lyndhurst

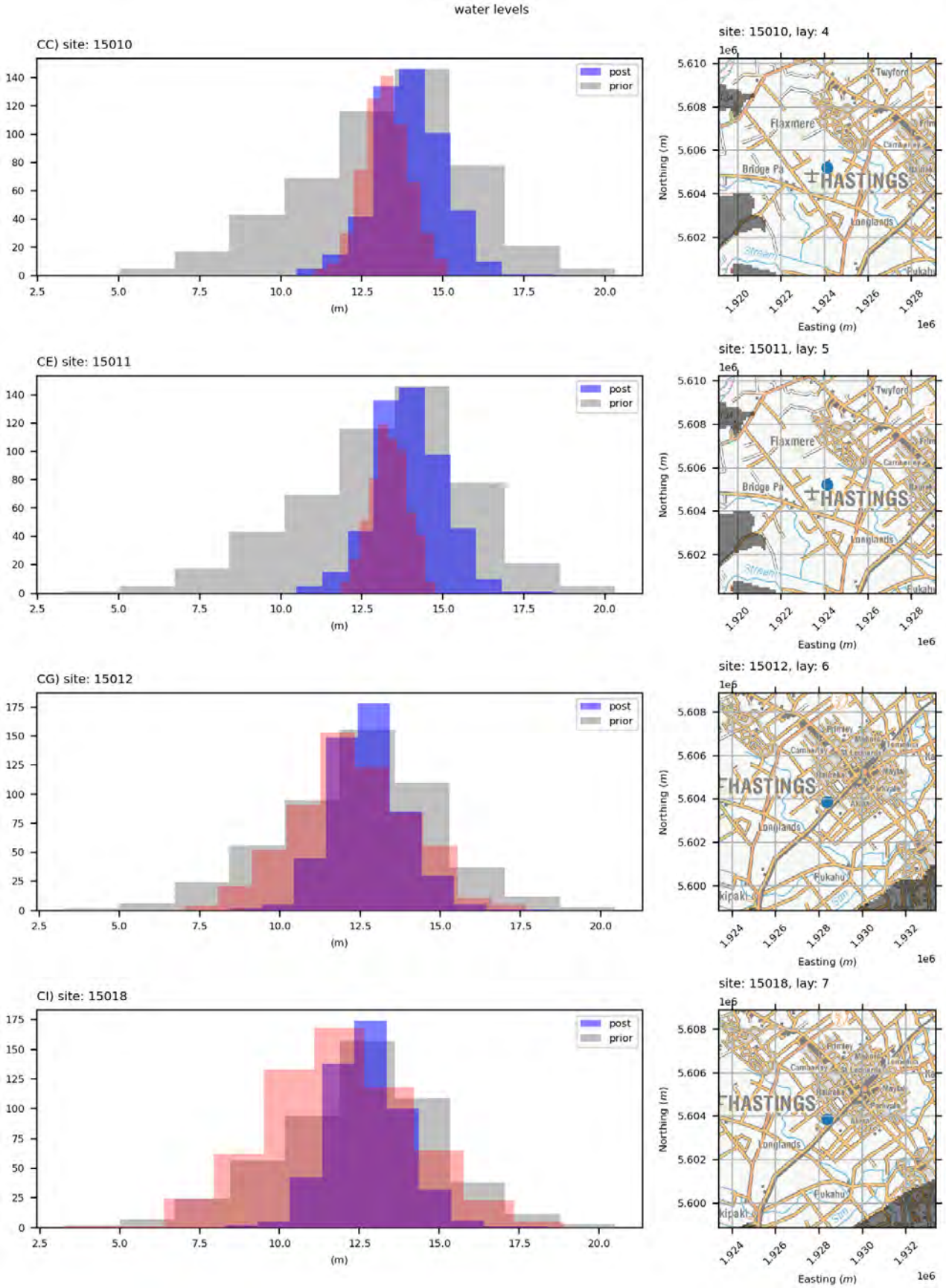
water levels
CC) site: 15010
post
prior
(m)
site: 15010, lay: 4
1e6
Northing (m)
Easting (m)
Twyford
Flaxmere
Bridge Pa
HASTINGS
Longlands
Fukahu
CE) site: 15011
site: 15011, lay: 5
CG) site: 15012
site: 15012, lay: 6
CI) site: 15018
site: 15018, lay: 7

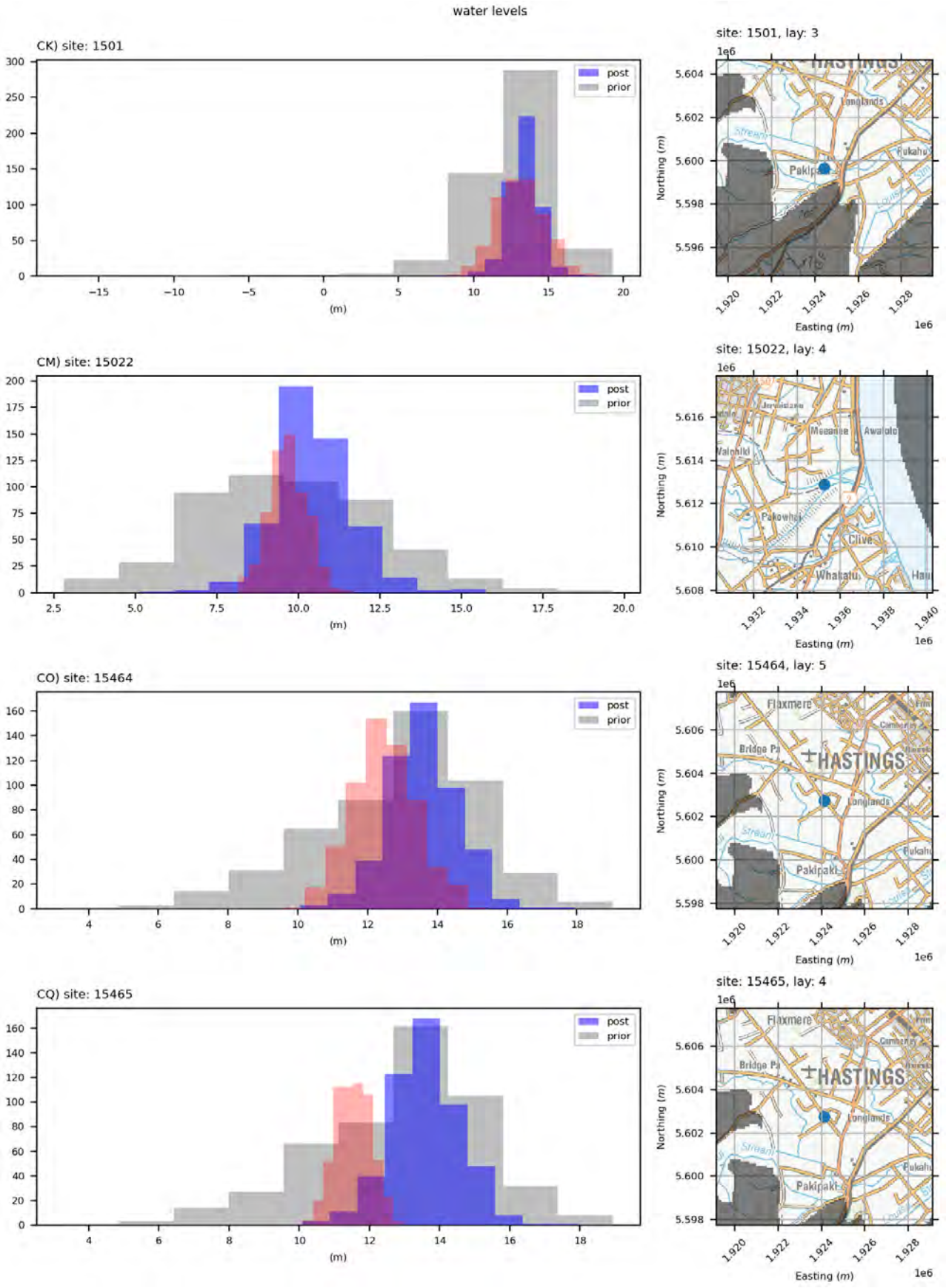
water levels
CK) site: 1501
post
prior
(m)
site: 1501, lay: 3
1e6
Northing (m)
Easting (m)
CM) site: 15022
site: 15022, lay: 4
CO) site: 15464
site: 15464, lay: 5
CQ) site: 15465
site: 15465, lay: 4
HASTINGS
Flaxmere
Longlands
Pakipaki
Clive
Whakatu

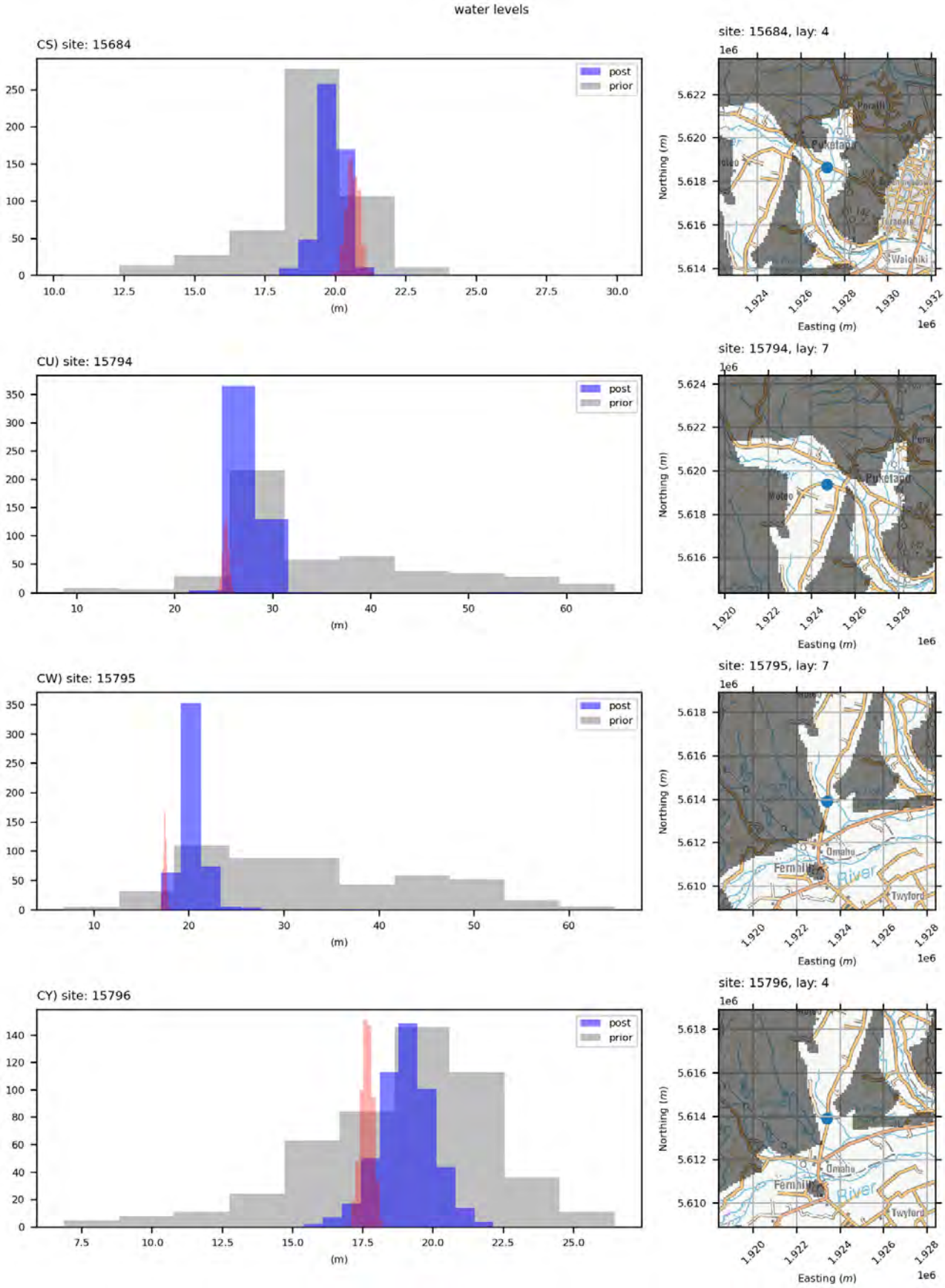
water levels
CS) site: 15684
post
prior
(m)
site: 15684, lay: 4
1e6
Northing (m)
Easting (m)
Pukekapia
Waiohiki
CU) site: 15794
site: 15794, lay: 7
Pukekapia
Woleo
CW) site: 15795
site: 15795, lay: 7
Omahu
Fernhill
River
Twyford
CY) site: 15796
site: 15796, lay: 4

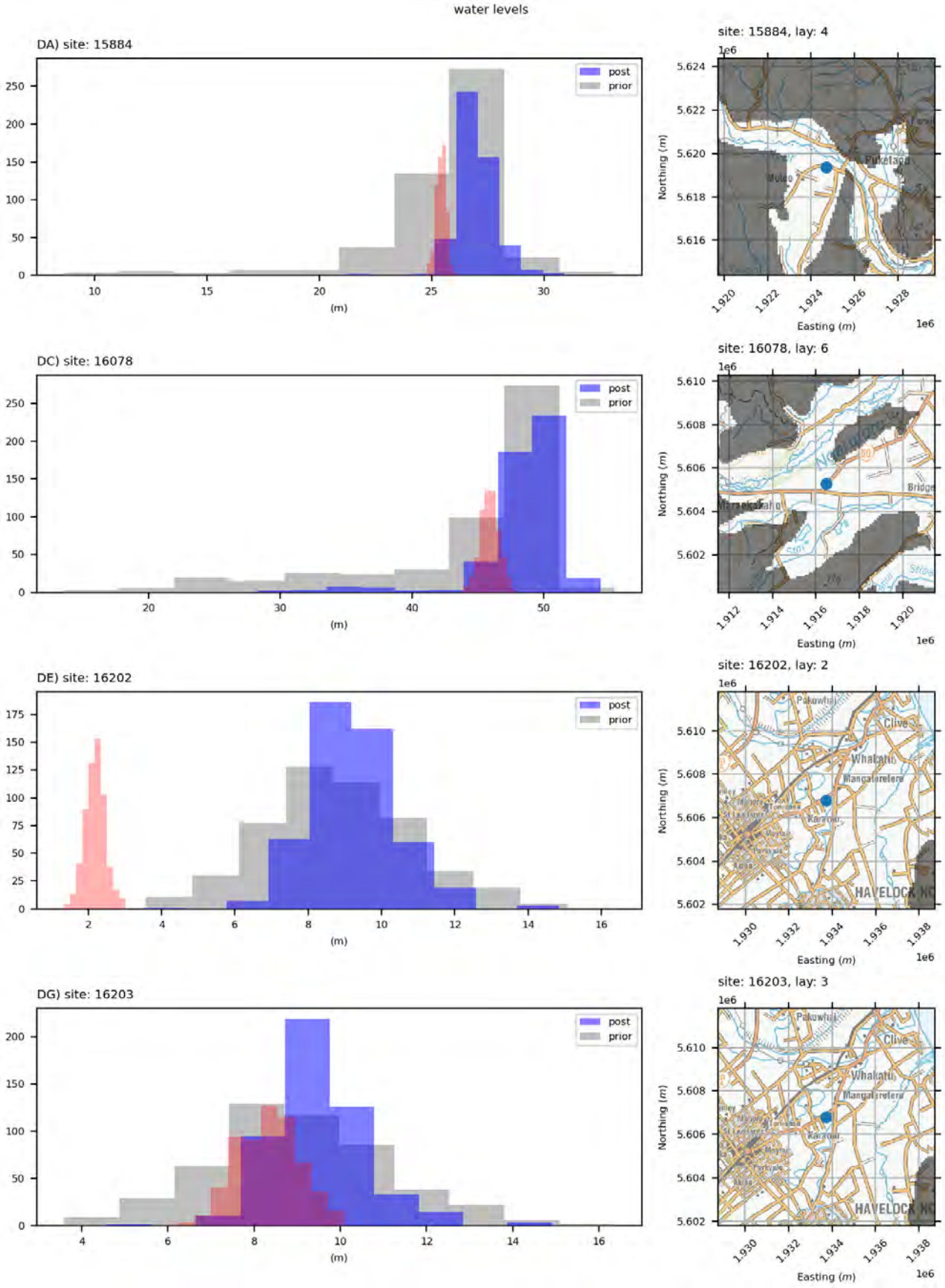
water levels
DA) site: 15884
post
prior
(m)
site: 15884, lay: 4
1e6
Northing (m)
Easting (m)
DC) site: 16078
site: 16078, lay: 6
DE) site: 16202
site: 16202, lay: 2
Clive
Whakatu
Mangateretere
HAVELOCK NO
DG) site: 16203
site: 16203, lay: 3

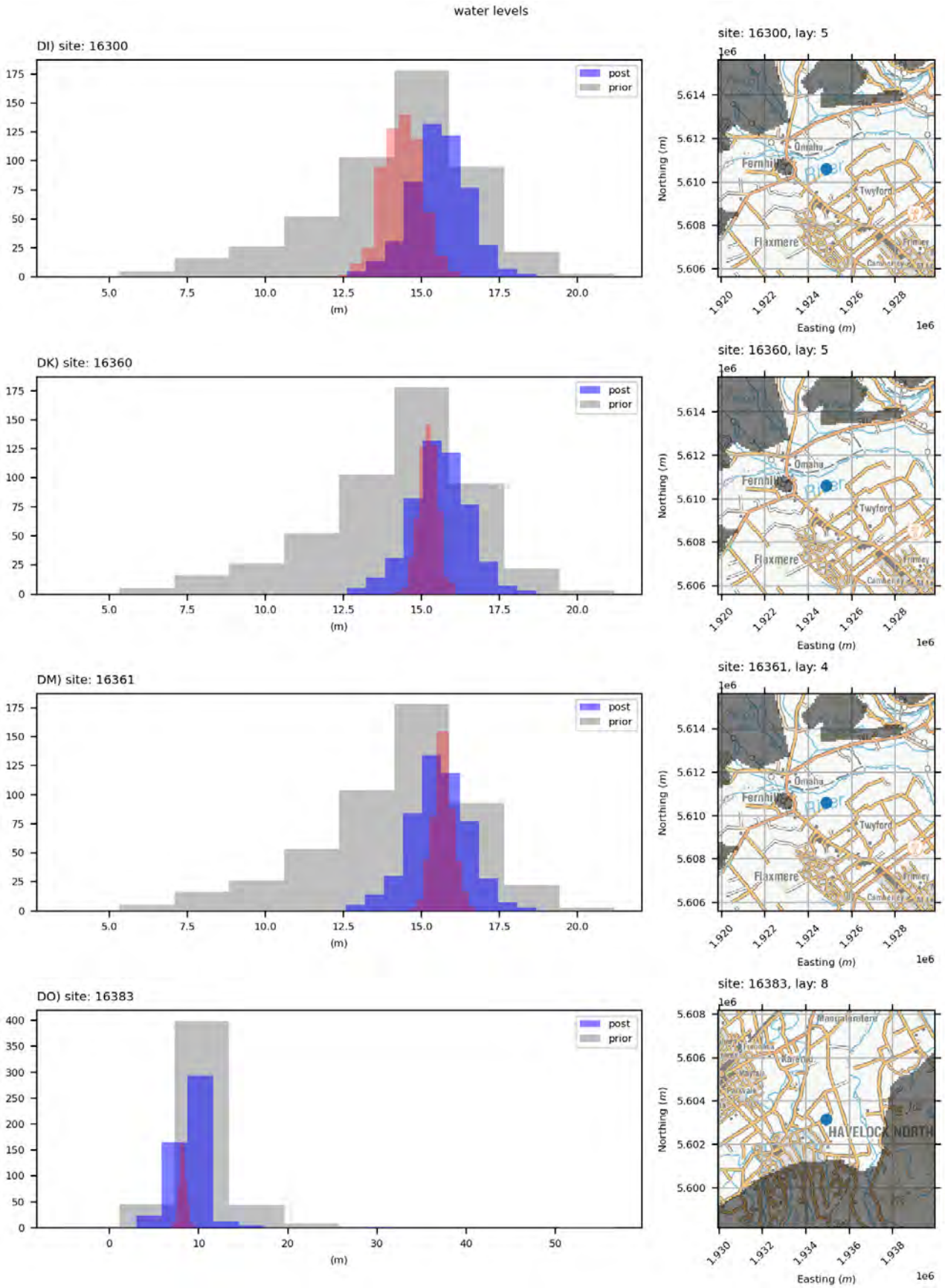
water levels
DI) site: 16300
DK) site: 16360
DM) site: 16361
DO) site: 16383
post
prior
(m)
site: 16300, lay: 5
site: 16360, lay: 5
site: 16361, lay: 4
site: 16383, lay: 8
Northing (m)
Easting (m)
1e6
Omahu
Twyford
Flaxmere
Frimley
HAVELOCK NORTH

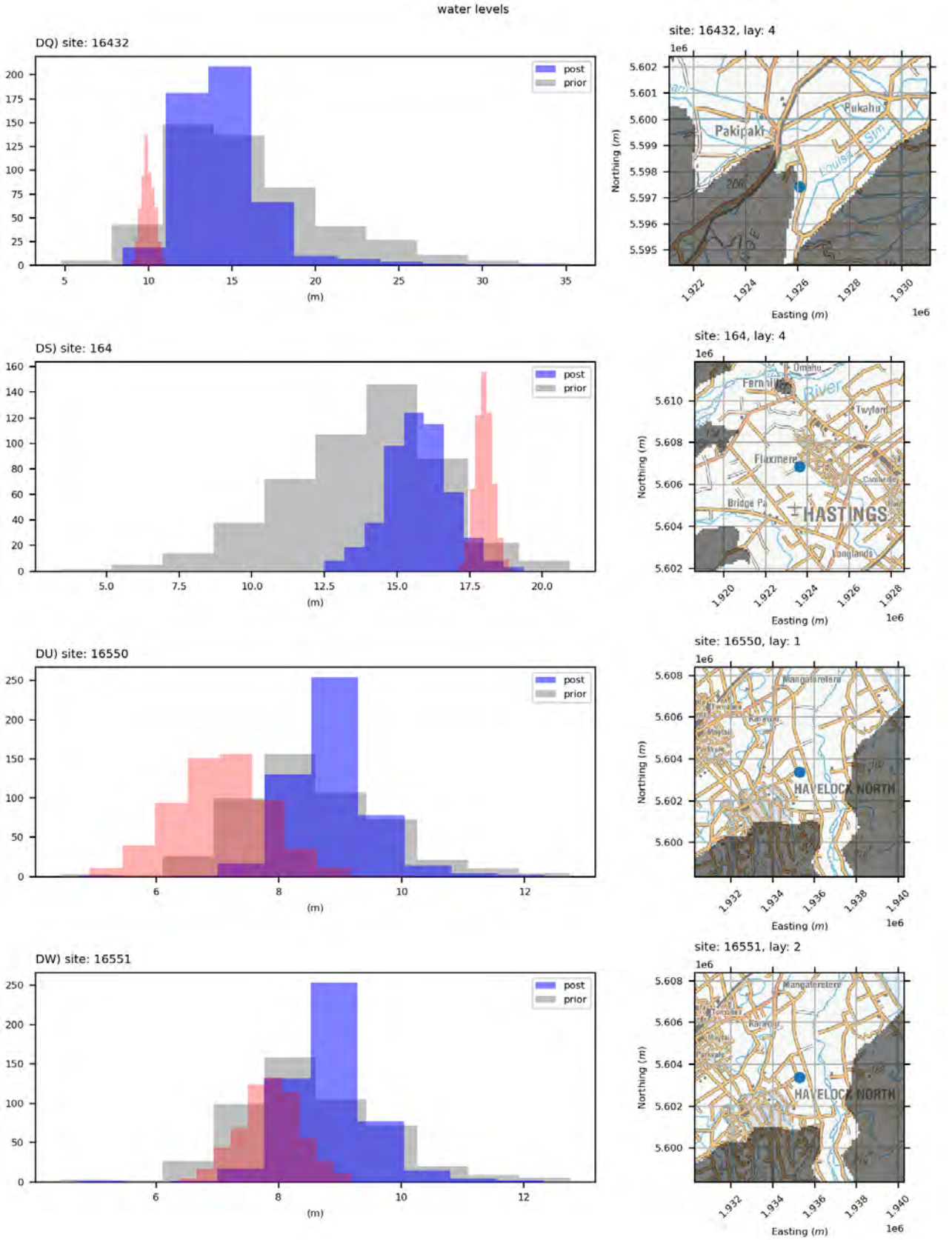
water levels
DQ) site: 16432
post
prior
(m)
site: 16432, lay: 4
1e6
Pukahu
Pakipaki
Northing (m)
Easting (m)
DS) site: 164
site: 164, lay: 4
Omahu
Fernhill
River
Twyford
Flaxmere
Bridge Pa
HASTINGS
Longlands
DU) site: 16550
site: 16550, lay: 1
Mangateretere
HAVELOCK NORTH
DW) site: 16551
site: 16551, lay: 2

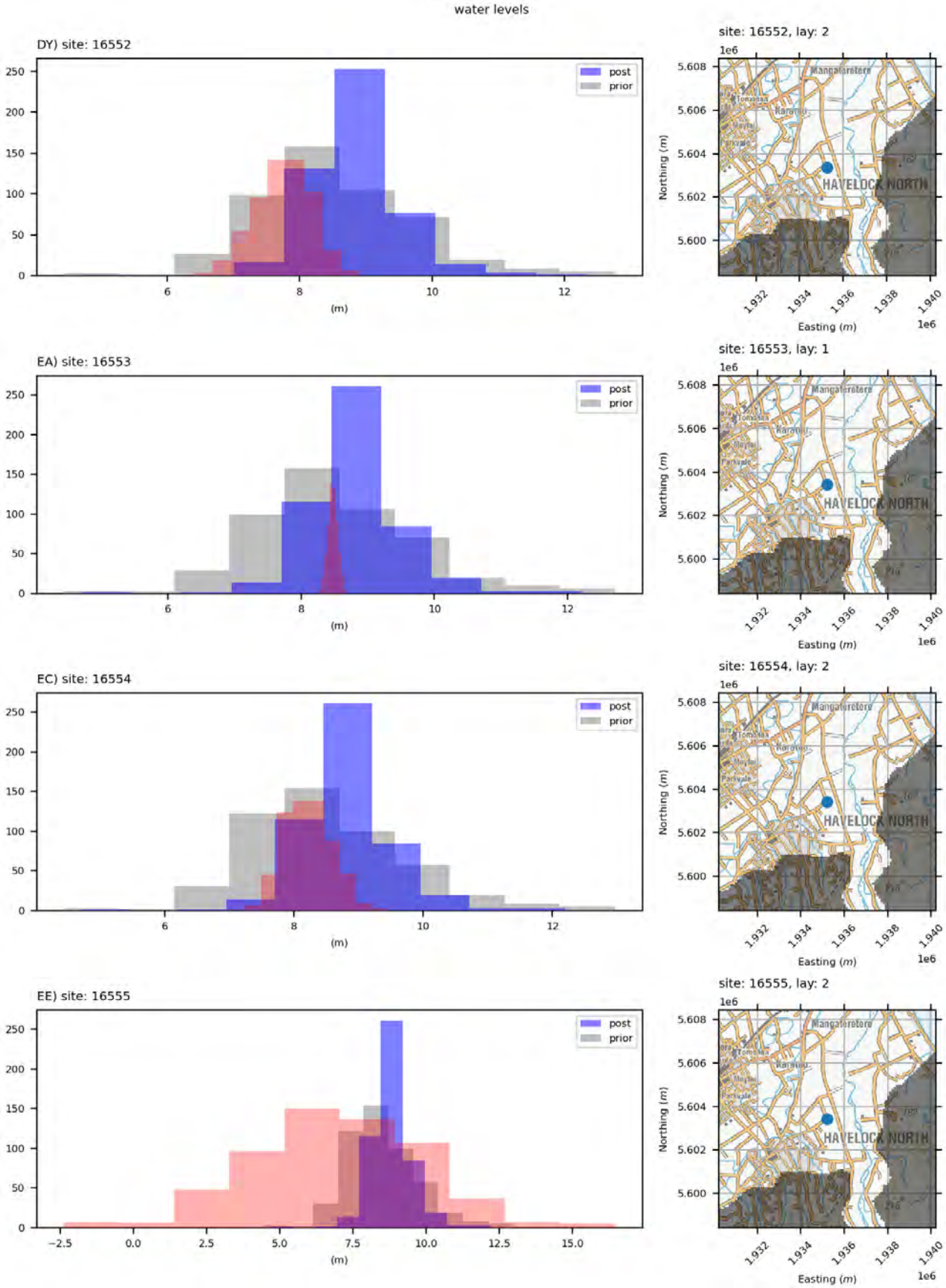
water levels
DY) site: 16552
post
prior
(m)
site: 16552, lay: 2
1e6
Northing (m)
Easting (m)
HAVELOCK NORTH
EA) site: 16553
site: 16553, lay: 1
EC) site: 16554
site: 16554, lay: 2
EE) site: 16555
site: 16555, lay: 2

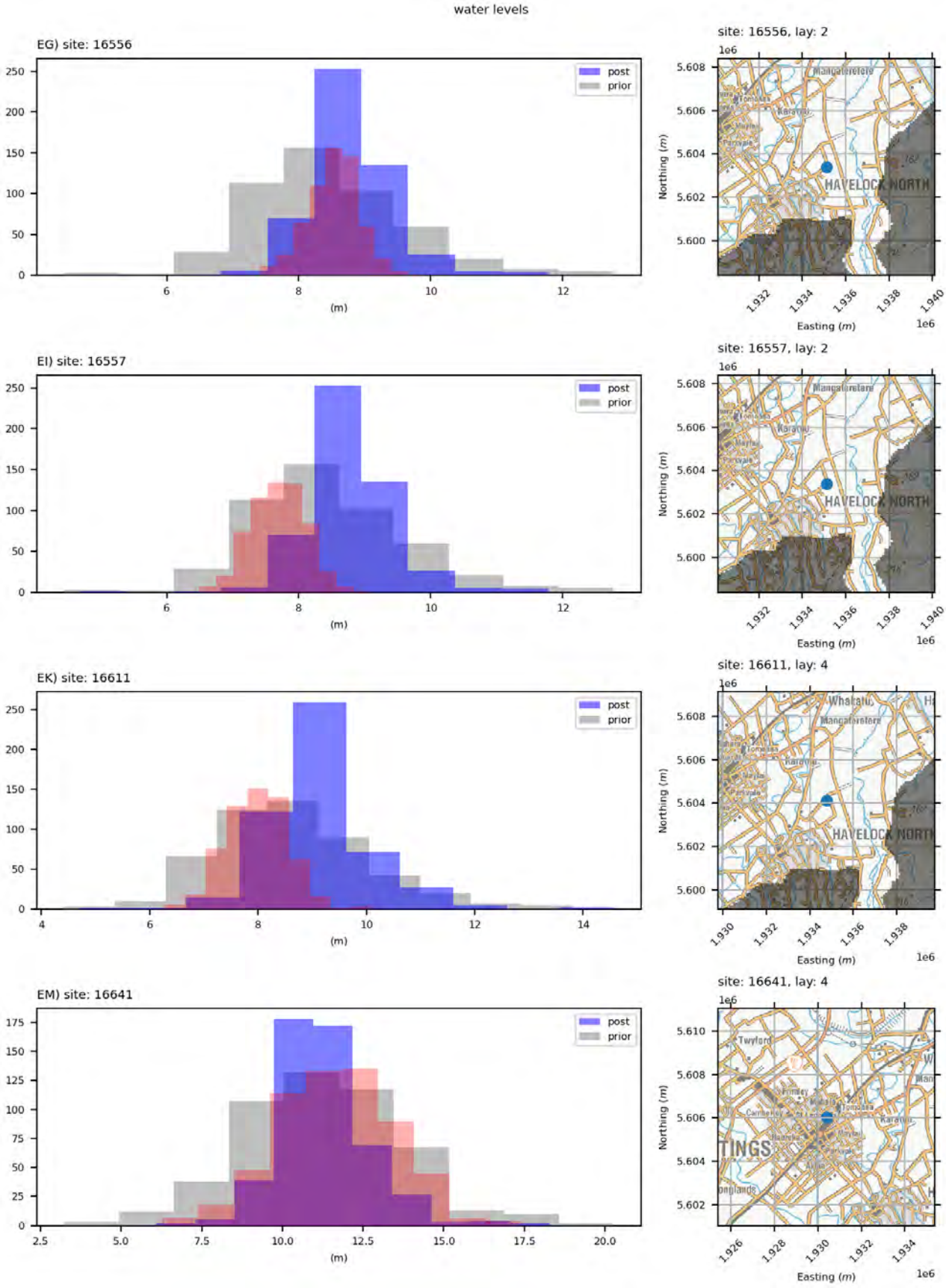
water levels
EG) site: 16556
post
prior
(m)
site: 16556, lay: 2
1e6
Northing (m)
Easting (m)
HAVELOCK NORTH
EI) site: 16557
post
prior
(m)
site: 16557, lay: 2
1e6
Northing (m)
Easting (m)
HAVELOCK NORTH
EK) site: 16611
post
prior
(m)
site: 16611, lay: 4
1e6
Northing (m)
Easting (m)
HAVELOCK NORTH
EM) site: 16641
post
prior
(m)
site: 16641, lay: 4
1e6
Northing (m)
Easting (m)
TINGS

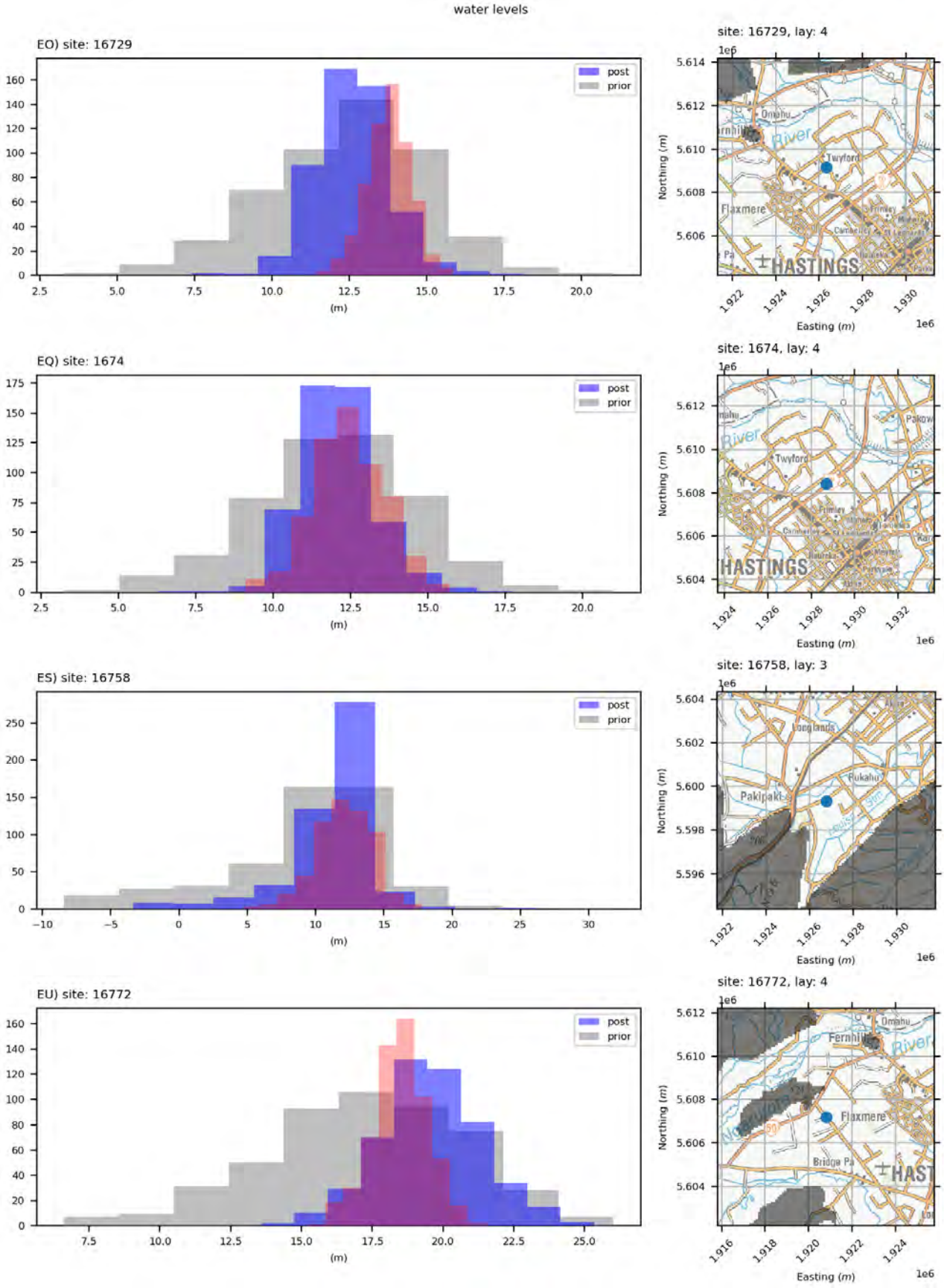
water levels
EO) site: 16729
post
prior
(m)
site: 16729, lay: 4
1e6
Northing (m)
Easting (m)
Omahu
Twyford
Flaxmere
HASTINGS
EQ) site: 1674
site: 1674, lay: 4
ES) site: 16758
site: 16758, lay: 3
Pukahu
EU) site: 16772
site: 16772, lay: 4
Fernhill
Bridge Pa

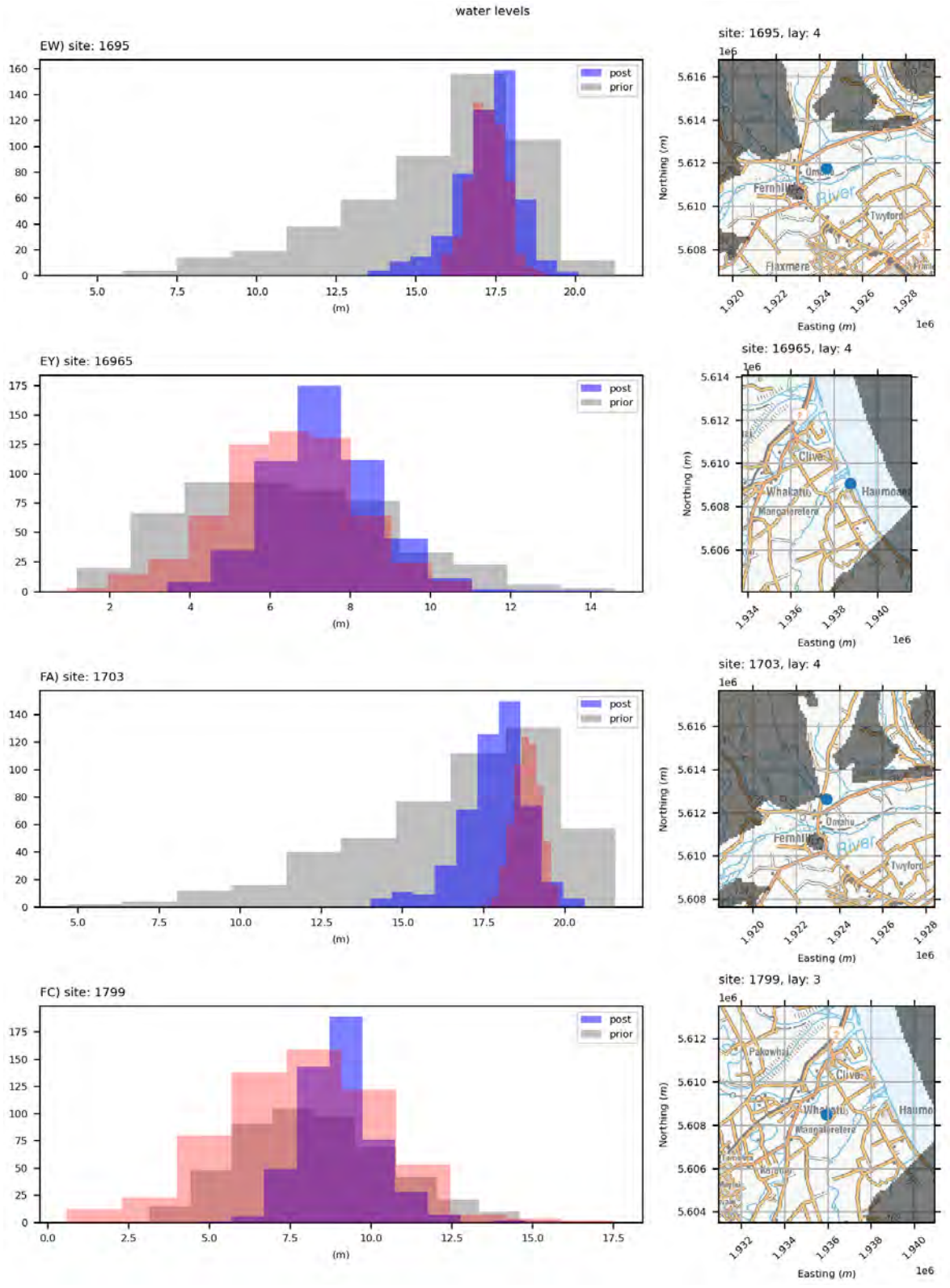
water levels
EW) site: 1695
post
prior
(m)
site: 1695, lay: 4
1e6
Northing (m)
Easting (m)
Fernhill
River
Twyford
Flaxmere
EY) site: 16965
site: 16965, lay: 4
Clive
Whakatu
Haumoana
Mangateretere
FA) site: 1703
site: 1703, lay: 4
Omahu
FC) site: 1799
site: 1799, lay: 3
Pakowhai

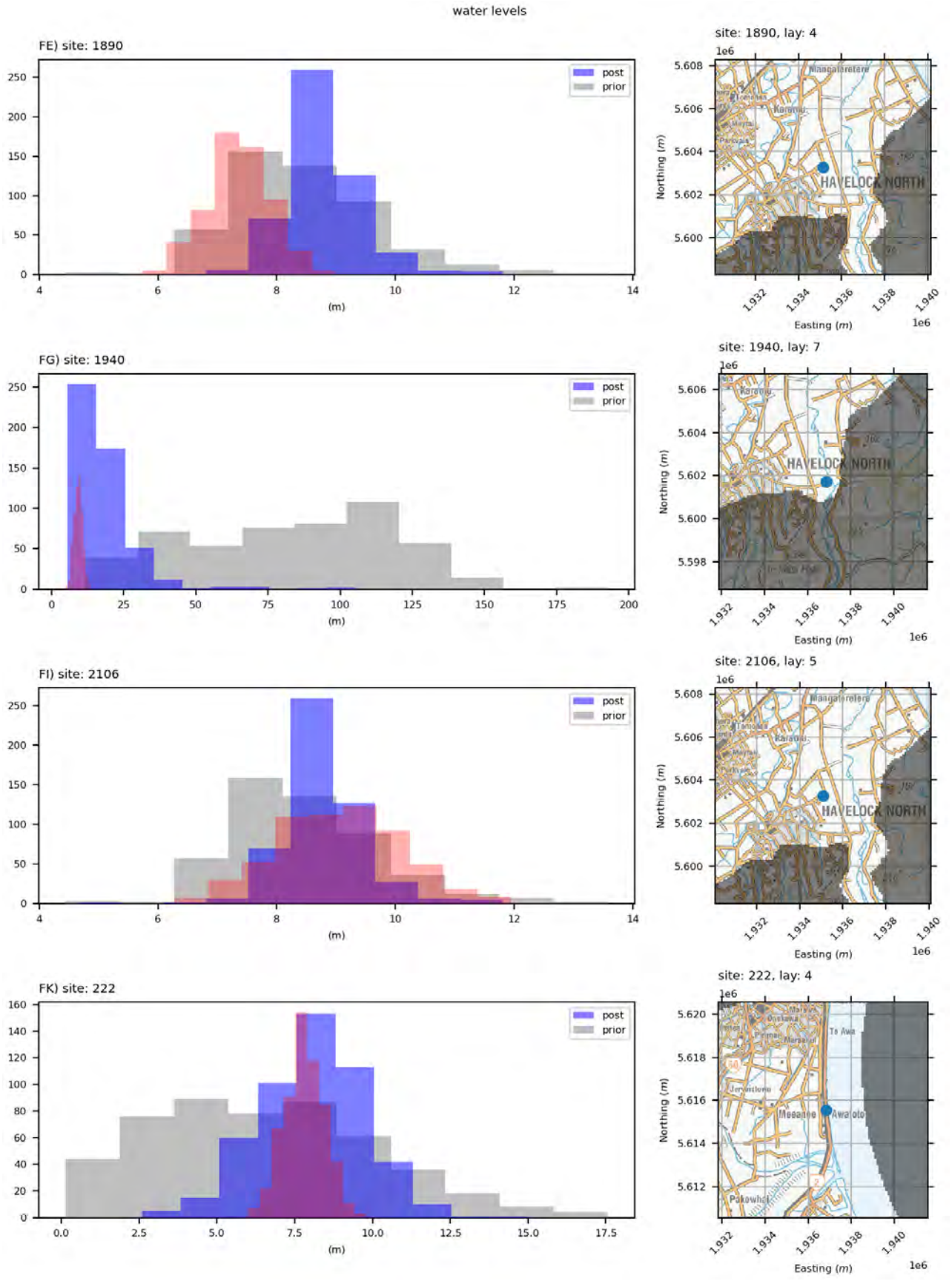
water levels
FE) site: 1890
post
prior
(m)
site: 1890, lay: 4
1e6
Northing (m)
Easting (m)
HAVELOCK NORTH
FG) site: 1940
post
prior
(m)
site: 1940, lay: 7
1e6
Northing (m)
Easting (m)
HAVELOCK NORTH
FI) site: 2106
post
prior
(m)
site: 2106, lay: 5
1e6
Northing (m)
Easting (m)
HAVELOCK NORTH
FK) site: 222
post
prior
(m)
site: 222, lay: 4
1e6
Northing (m)
Easting (m)
Te Awa
Meeanee
Awa oto
Pakowhai

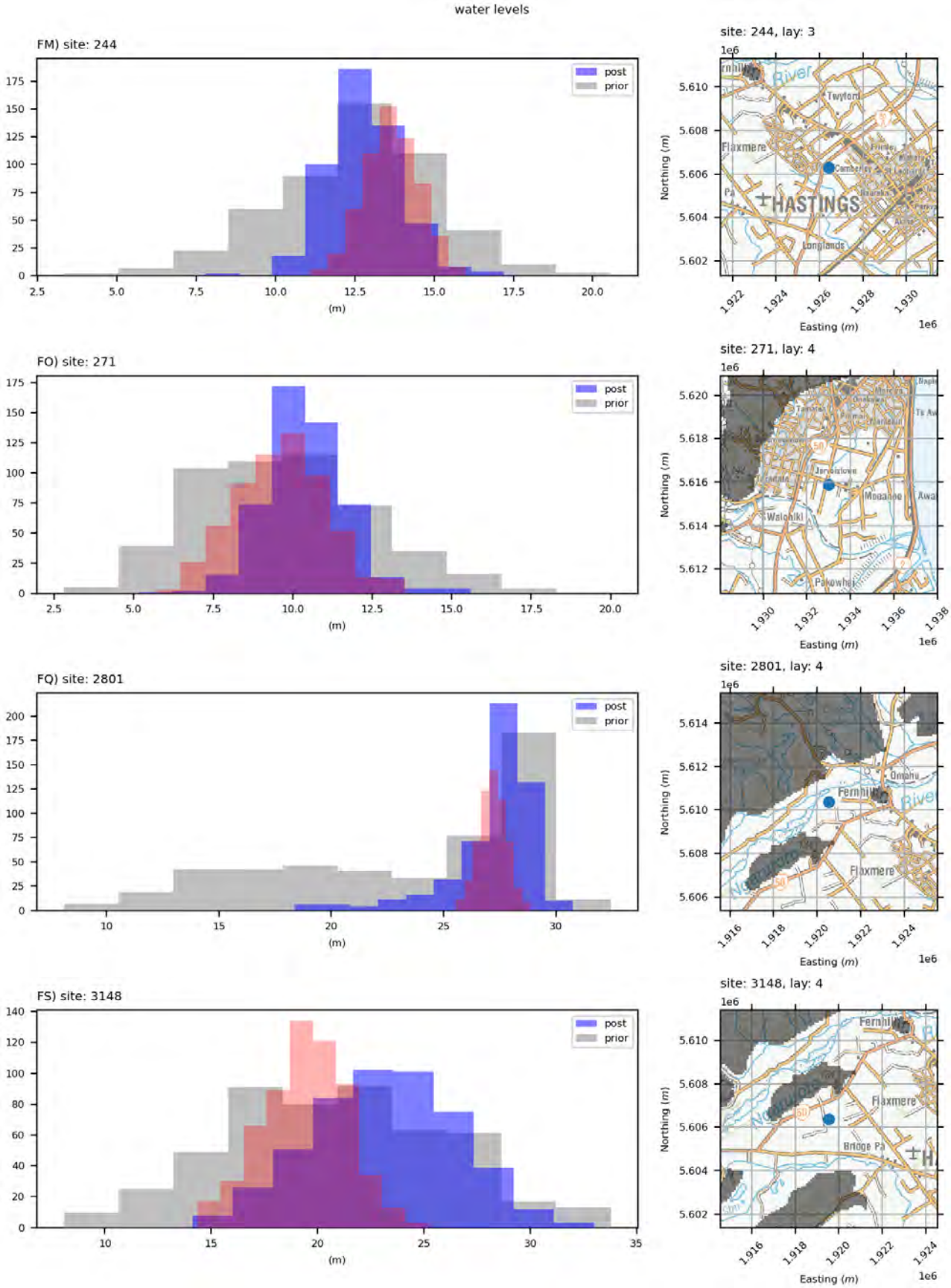
water levels
FM) site: 244
post
prior
(m)
site: 244, lay: 3
1e6
Northing (m)
Easting (m)
HASTINGS
Flaxmere
FO) site: 271
site: 271, lay: 4
FQ) site: 2801
site: 2801, lay: 4
Fernhill
FS) site: 3148
site: 3148, lay: 4

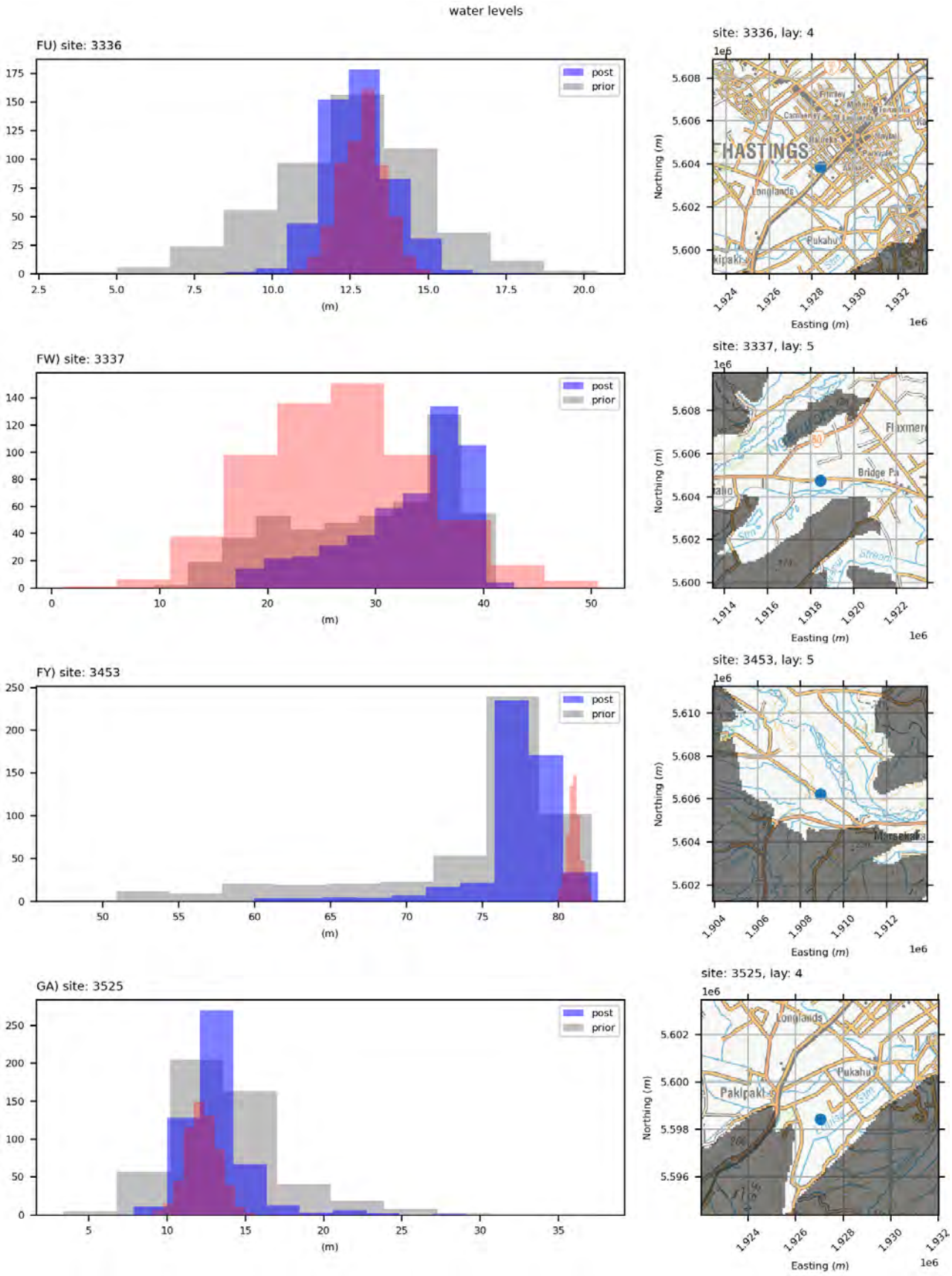
water levels
FU) site: 3336
post
prior
(m)
site: 3336, lay: 4
1e6
HASTINGS
Longlands
Pukahu
Northing (m)
Easting (m)
FW) site: 3337
site: 3337, lay: 5
Bridge Pa
FY) site: 3453
site: 3453, lay: 5
GA) site: 3525
site: 3525, lay: 4
Pakipaki

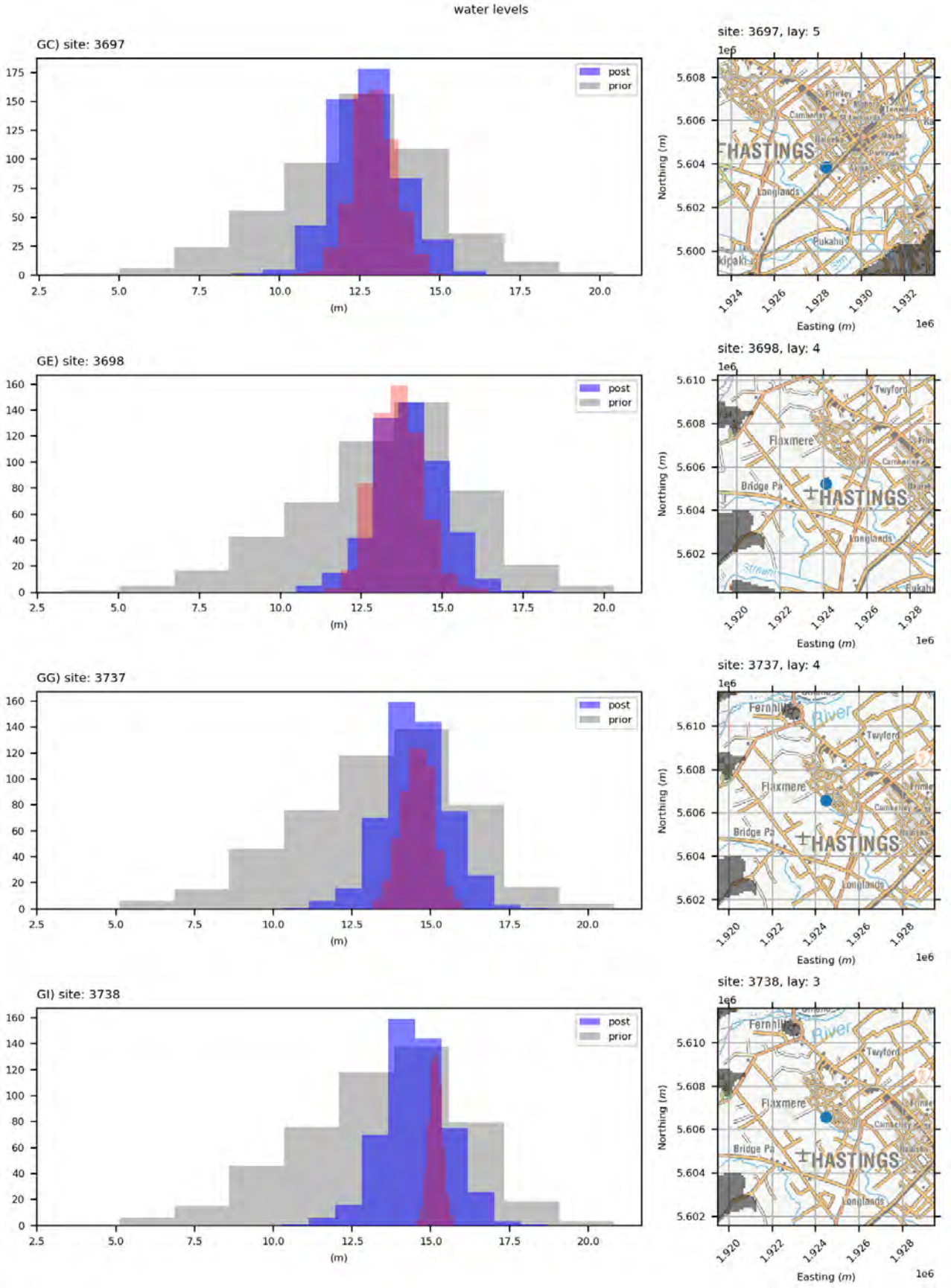
water levels
GC) site: 3697
post
prior
(m)
site: 3697, lay: 5
1e6
HASTINGS
Longlands
Pukahu
Northing (m)
Easting (m)
GE) site: 3698
site: 3698, lay: 4
Twyford
Flaxmere
Bridge Pa
GG) site: 3737
site: 3737, lay: 4
River
GI) site: 3738
site: 3738, lay: 3

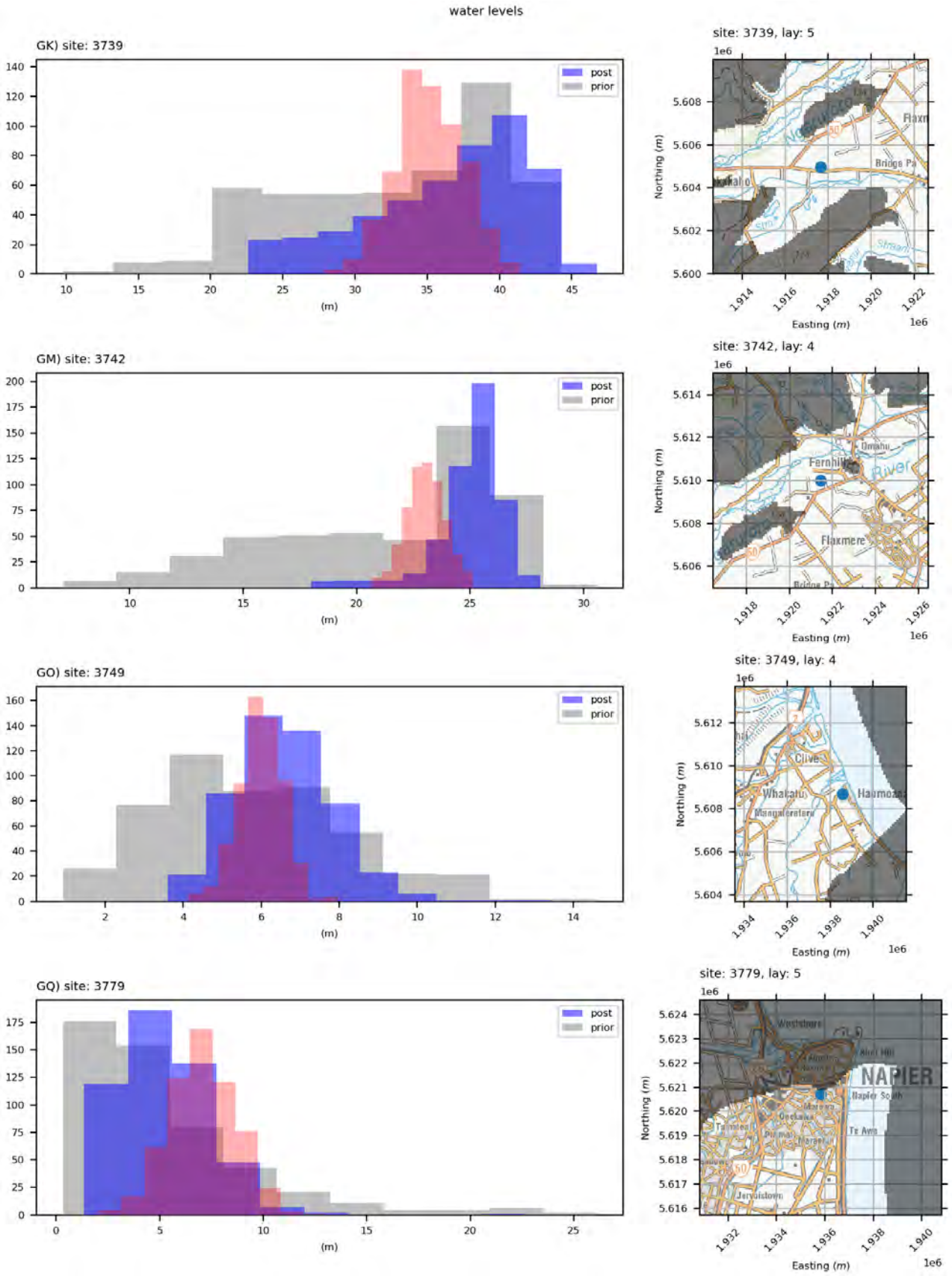
water levels
GK) site: 3739
post
prior
(m)
site: 3739, lay: 5
1e6
Northing (m)
Easting (m)
GM) site: 3742
post
prior
(m)
site: 3742, lay: 4
1e6
Northing (m)
Easting (m)
GO) site: 3749
post
prior
(m)
site: 3749, lay: 4
1e6
Northing (m)
Easting (m)
GQ) site: 3779
post
prior
(m)
site: 3779, lay: 5
1e6
Northing (m)
Easting (m)

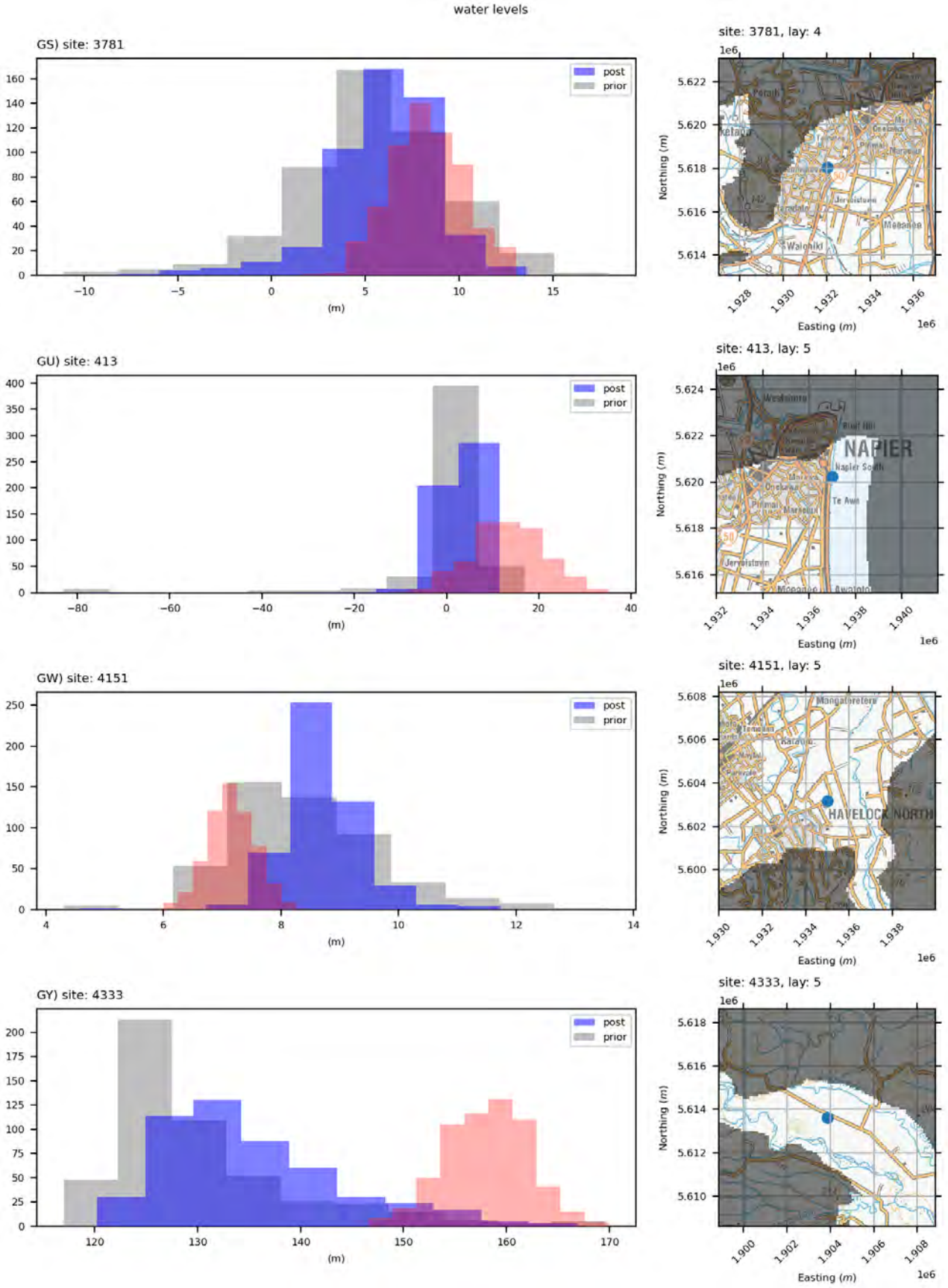
water levels
GS) site: 3781
post
prior
(m)
site: 3781, lay: 4
1e6
Northing (m)
Easting (m)
GU) site: 413
site: 413, lay: 5
NAPIER
GW) site: 4151
site: 4151, lay: 5
HAVELOCK NORTH
GY) site: 4333
site: 4333, lay: 5

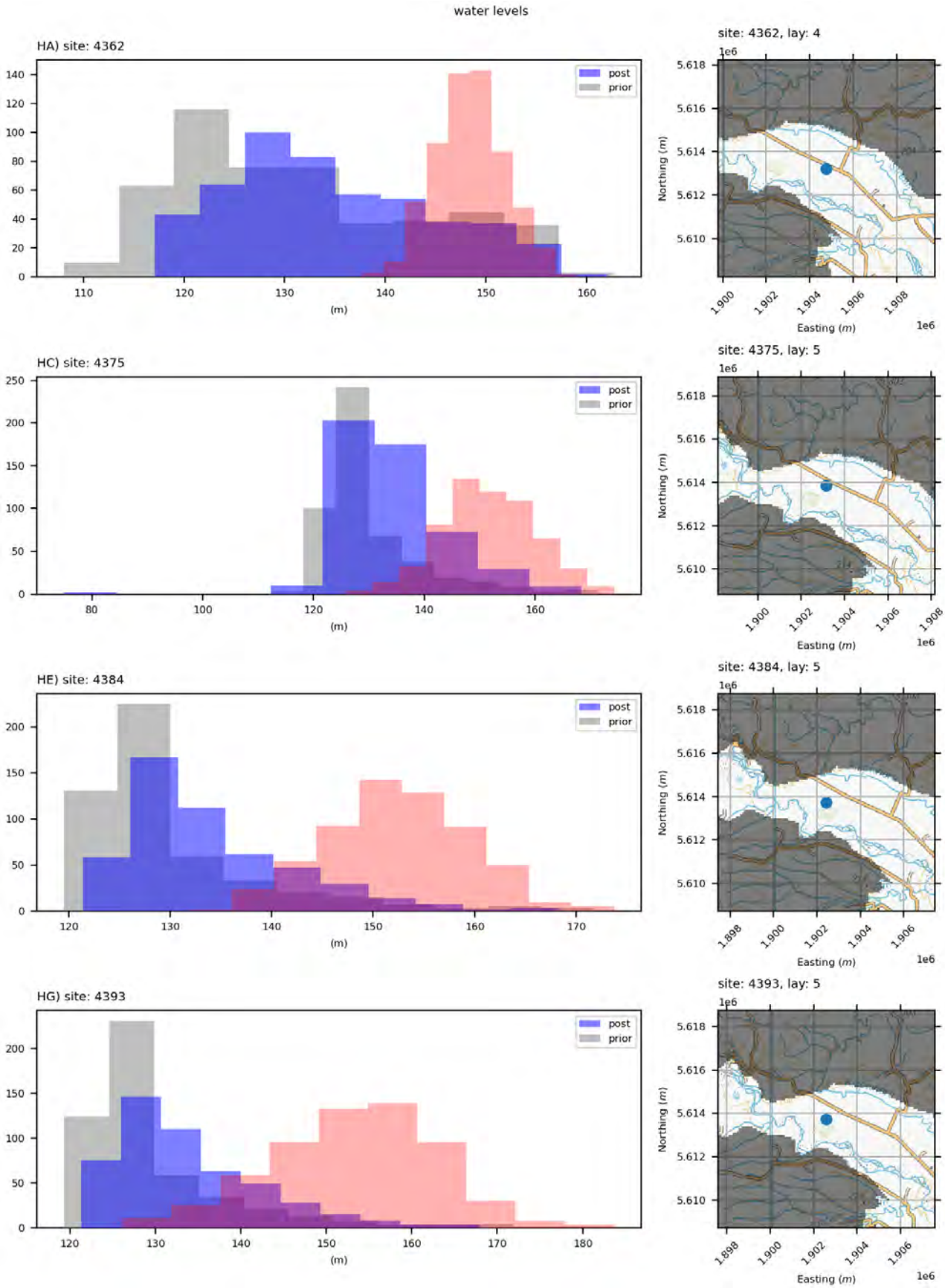
water levels
HA) site: 4362
post
prior
(m)
site: 4362, lay: 4
1e6
Northing (m)
Easting (m)
HC) site: 4375
site: 4375, lay: 5
HE) site: 4384
site: 4384, lay: 5
HG) site: 4393
site: 4393, lay: 5

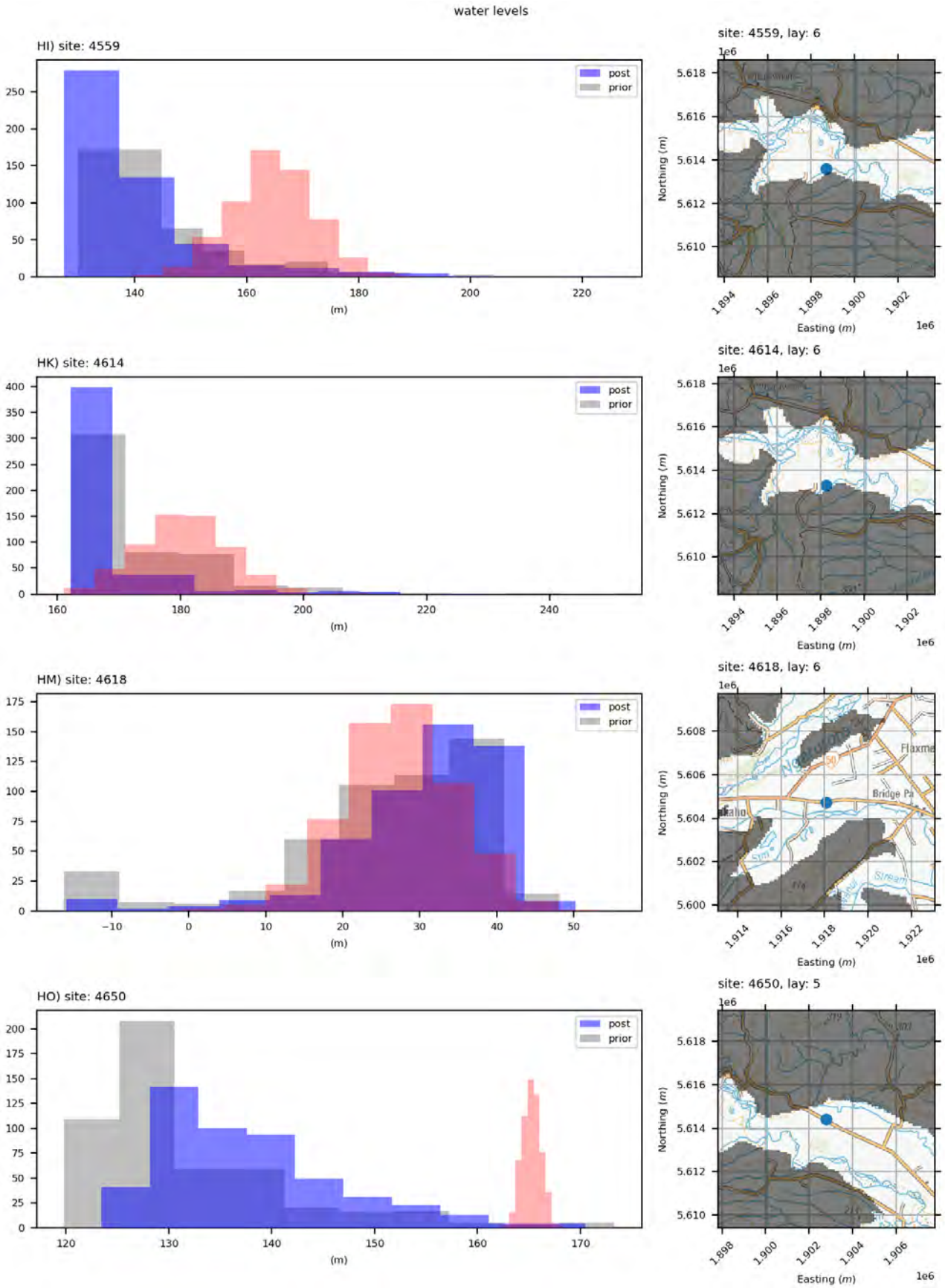
water levels
HI) site: 4559
post
prior
(m)
site: 4559, lay: 6
Northing (m)
Easting (m)
1e6
HK) site: 4614
site: 4614, lay: 6
HM) site: 4618
site: 4618, lay: 6
HO) site: 4650
site: 4650, lay: 5

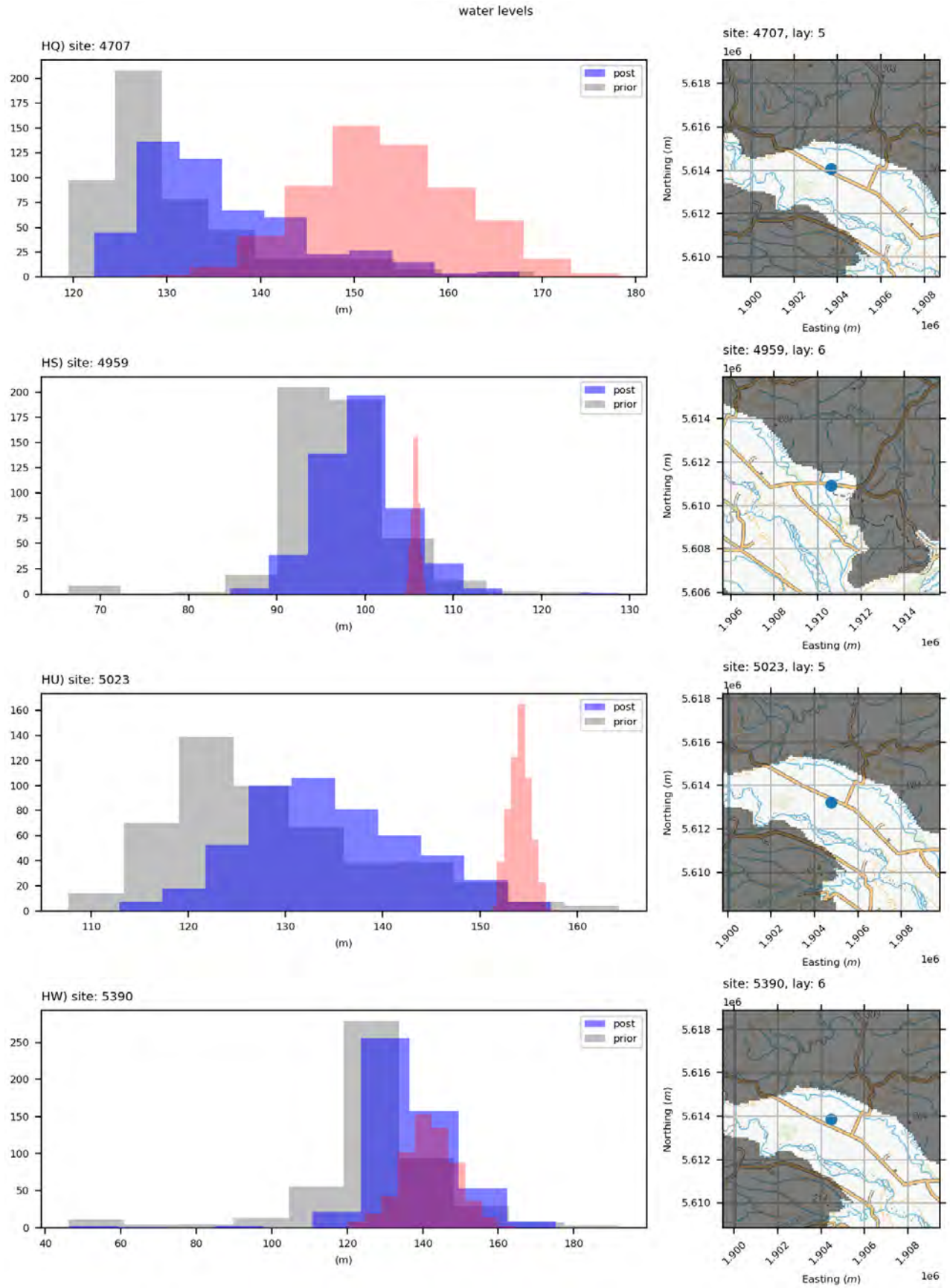
water levels
HQ) site: 4707
post
prior
(m)
site: 4707, lay: 5
1e6
Northing (m)
Easting (m)
HS) site: 4959
post
prior
(m)
site: 4959, lay: 6
1e6
Northing (m)
Easting (m)
HU) site: 5023
post
prior
(m)
site: 5023, lay: 5
1e6
Northing (m)
Easting (m)
HW) site: 5390
post
prior
(m)
site: 5390, lay: 6
1e6
Northing (m)
Easting (m)

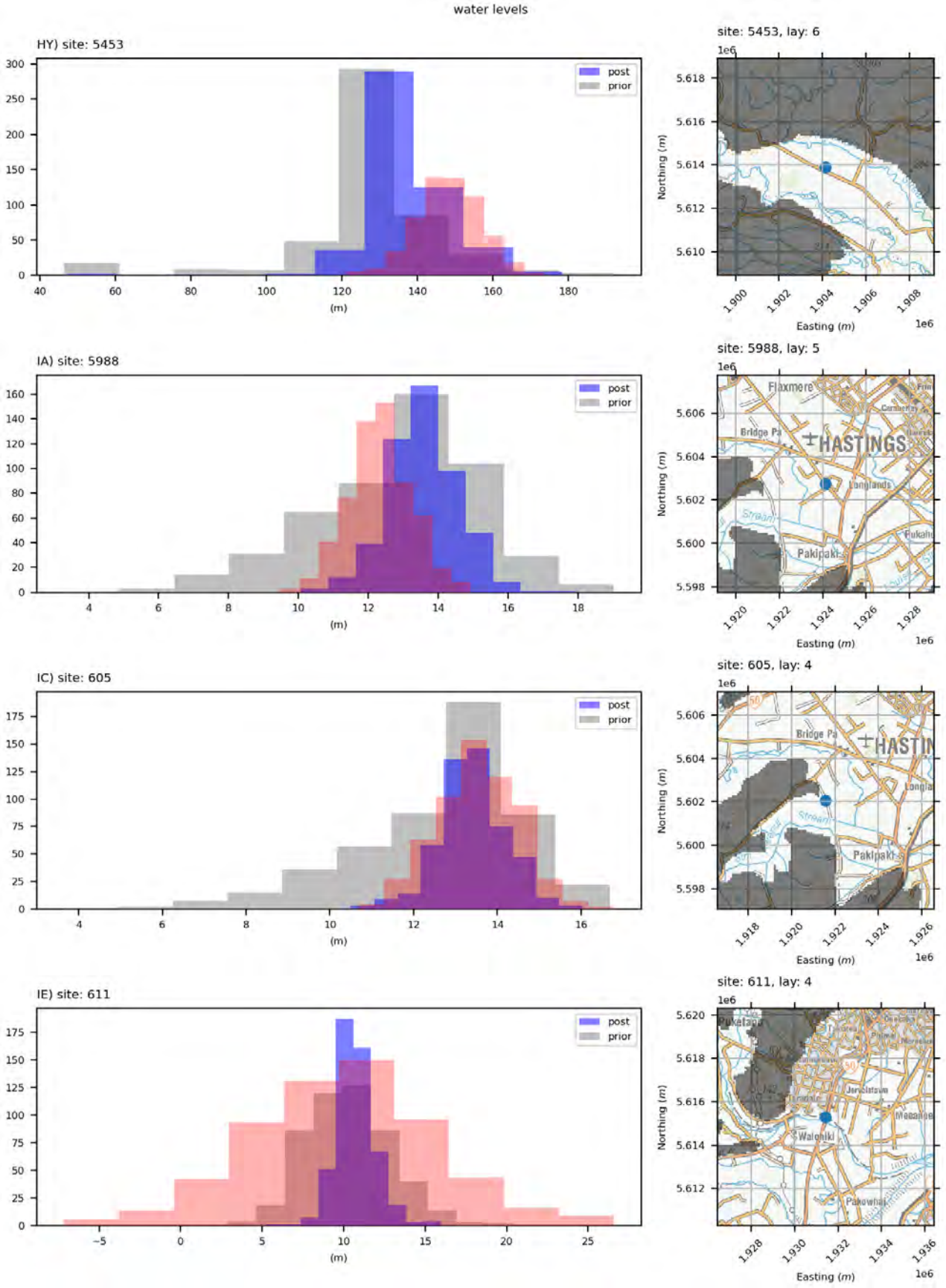
water levels
HY) site: 5453
post
prior
(m)
site: 5453, lay: 6
1e6
Northing (m)
Easting (m)
IA) site: 5988
site: 5988, lay: 5
Flaxmere
Bridge Pa
HASTINGS
Longlands
Pakipaki
IC) site: 605
site: 605, lay: 4
IE) site: 611
site: 611, lay: 4
Waipukurau
Waitoiki

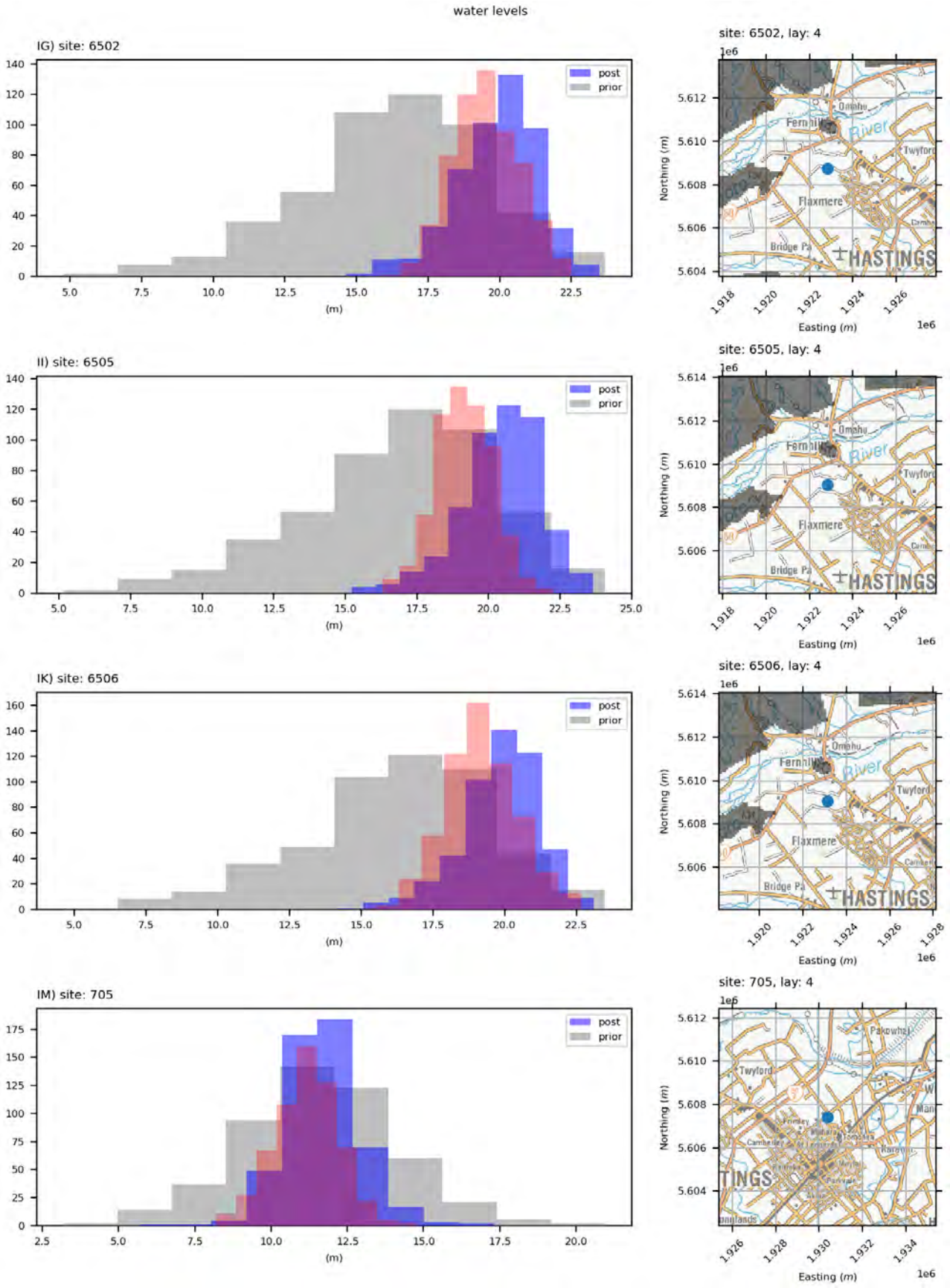
water levels
IG) site: 6502
post
prior
(m)
site: 6502, lay: 4
Northing (m)
Easting (m)
1e6
II) site: 6505
site: 6505, lay: 4
IK) site: 6506
site: 6506, lay: 4
IM) site: 705
site: 705, lay: 4
HASTINGS
Flaxmere
Twyford
Bridge Pa

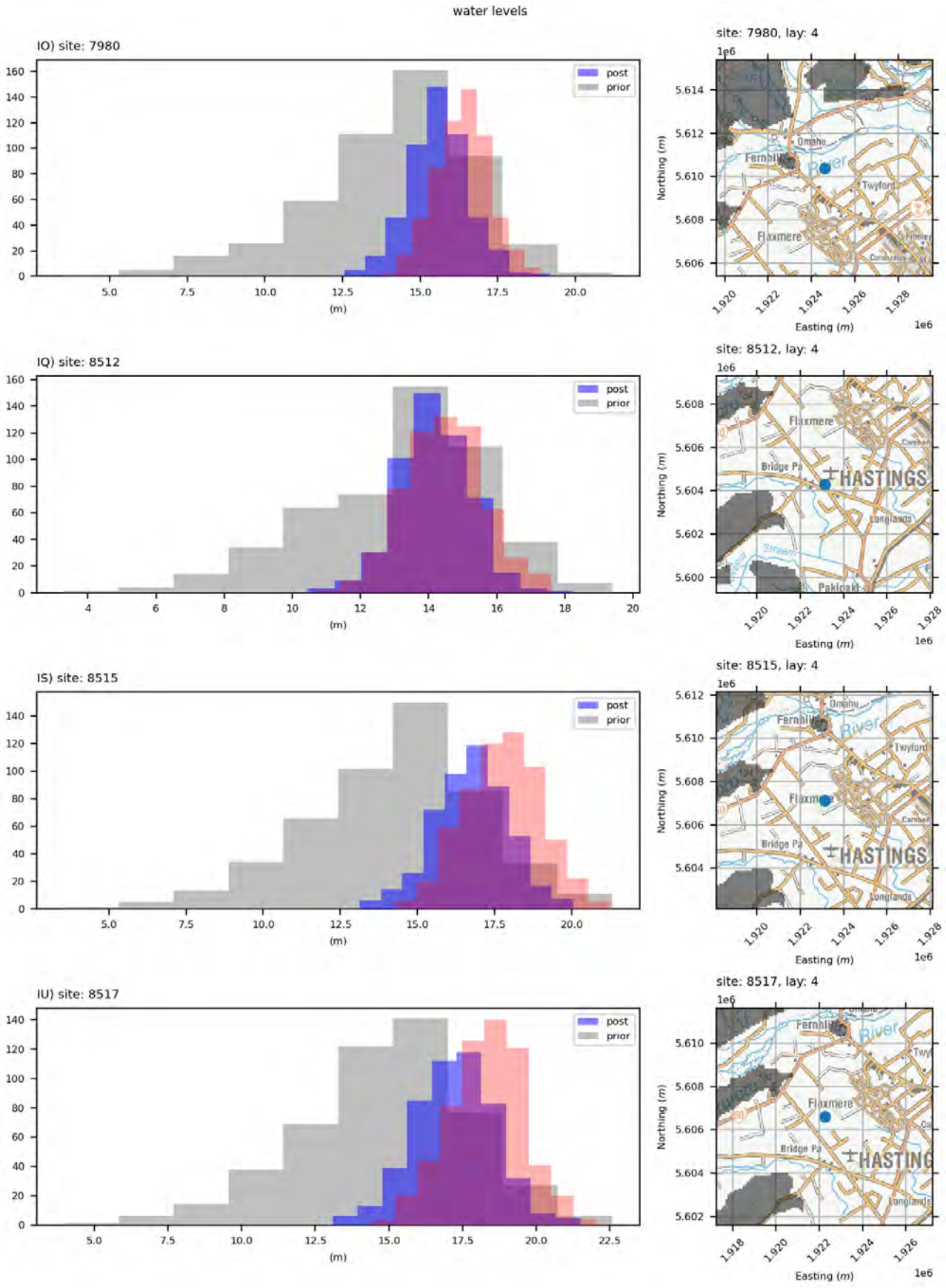
water levels
IO) site: 7980
post
prior
(m)
site: 7980, lay: 4
1e6
Northing (m)
Easting (m)
IQ) site: 8512
site: 8512, lay: 4
HASTINGS
IS) site: 8515
site: 8515, lay: 4
IU) site: 8517
site: 8517, lay: 4

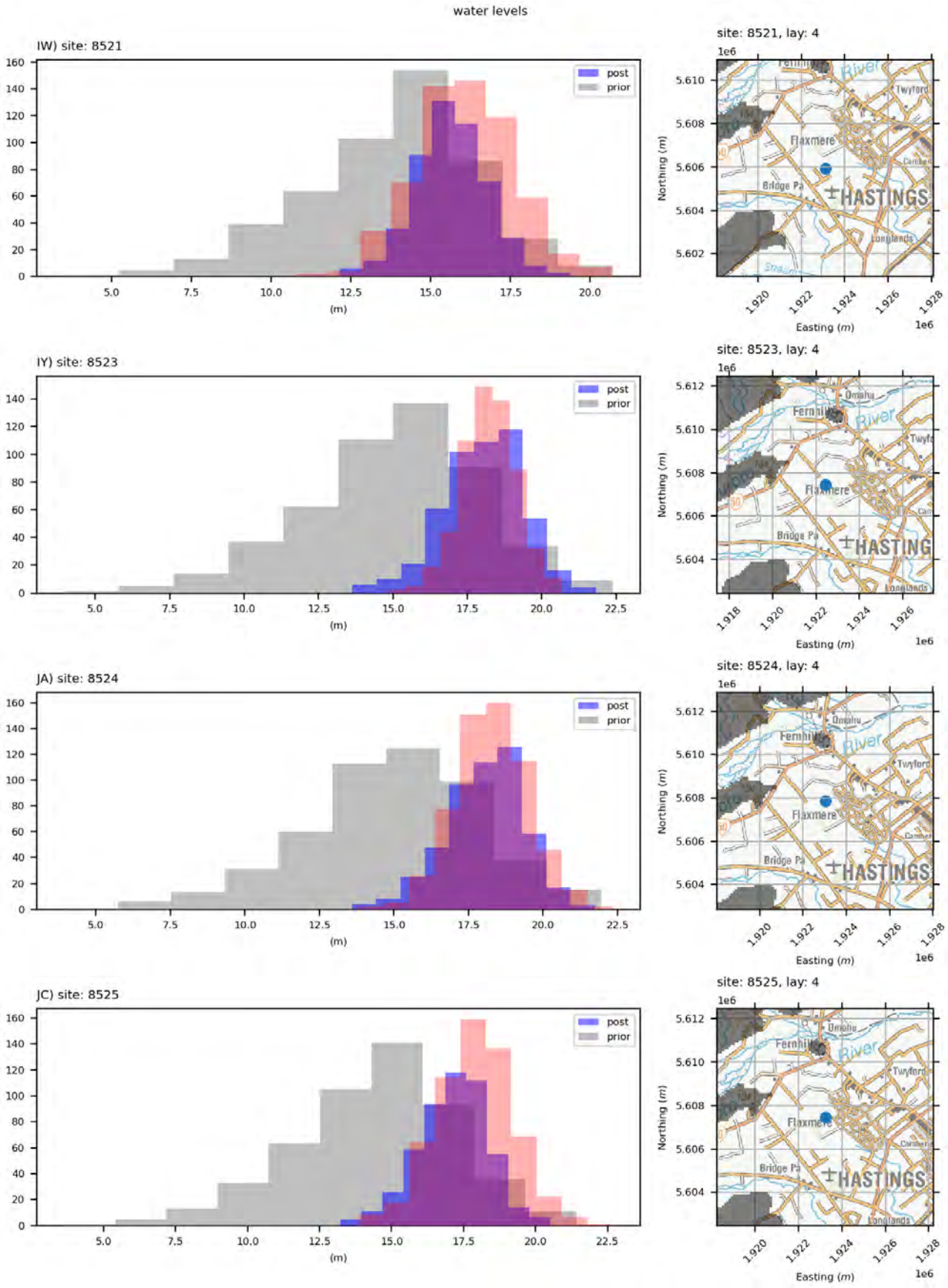
water levels
IW) site: 8521
post
prior
(m)
site: 8521, lay: 4
1e6
Northing (m)
Easting (m)
Flaxmere
Twyford
Bridge Pa
HASTINGS
IY) site: 8523
site: 8523, lay: 4
JA) site: 8524
site: 8524, lay: 4
JC) site: 8525
site: 8525, lay: 4

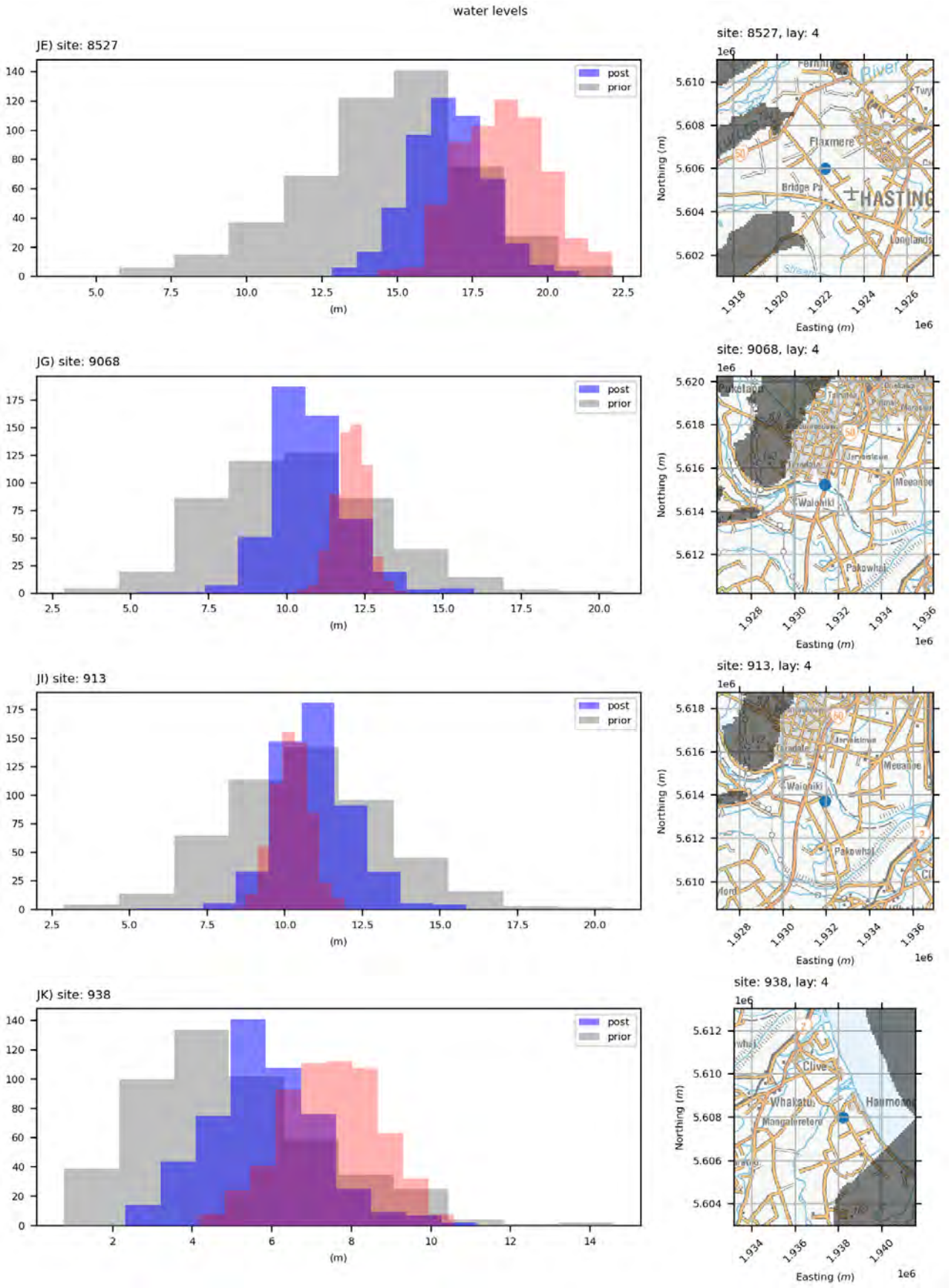
water levels
JE) site: 8527
post
prior
(m)
site: 8527, lay: 4
1e6
Northing (m)
Easting (m)
Flaxmere
HASTING
JG) site: 9068
site: 9068, lay: 4
Waiohiki
Pakowhai
JI) site: 913
site: 913, lay: 4
JK) site: 938
site: 938, lay: 4
Clive
Whakatu
Haumoana
Mangateretere

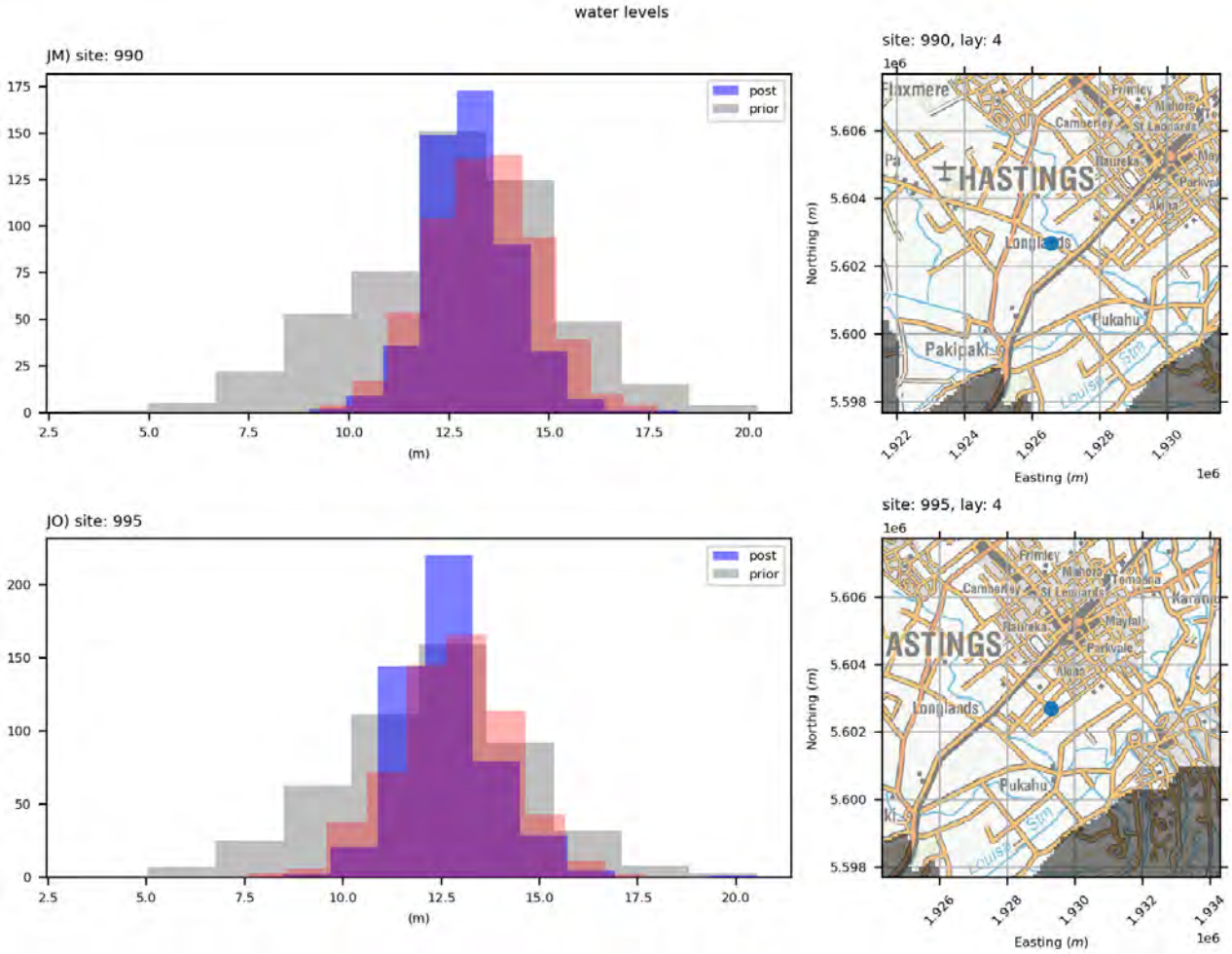
water levels
JM) site: 990
post
prior
(m)
site: 990, lay: 4
1e6
Flaxmere
HASTINGS
Longlands
Pukahu
Pakipaki
Northing (m)
Easting (m)
JO) site: 995
post
prior
(m)
site: 995, lay: 4
1e6
ASTINGS
Longlands
Pukahu
Northing (m)
Easting (m)

A3.2.4.2 Stream Flows

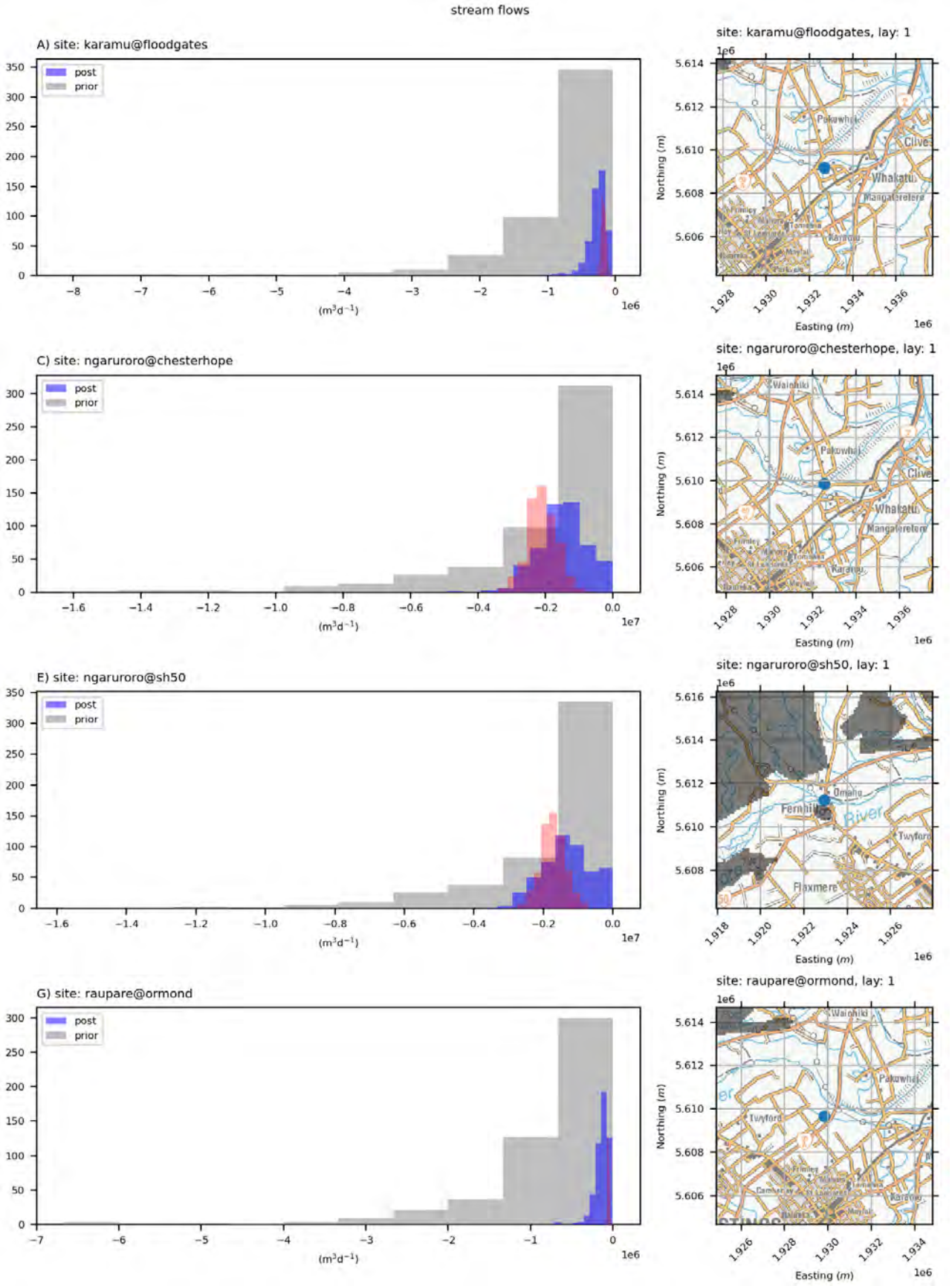

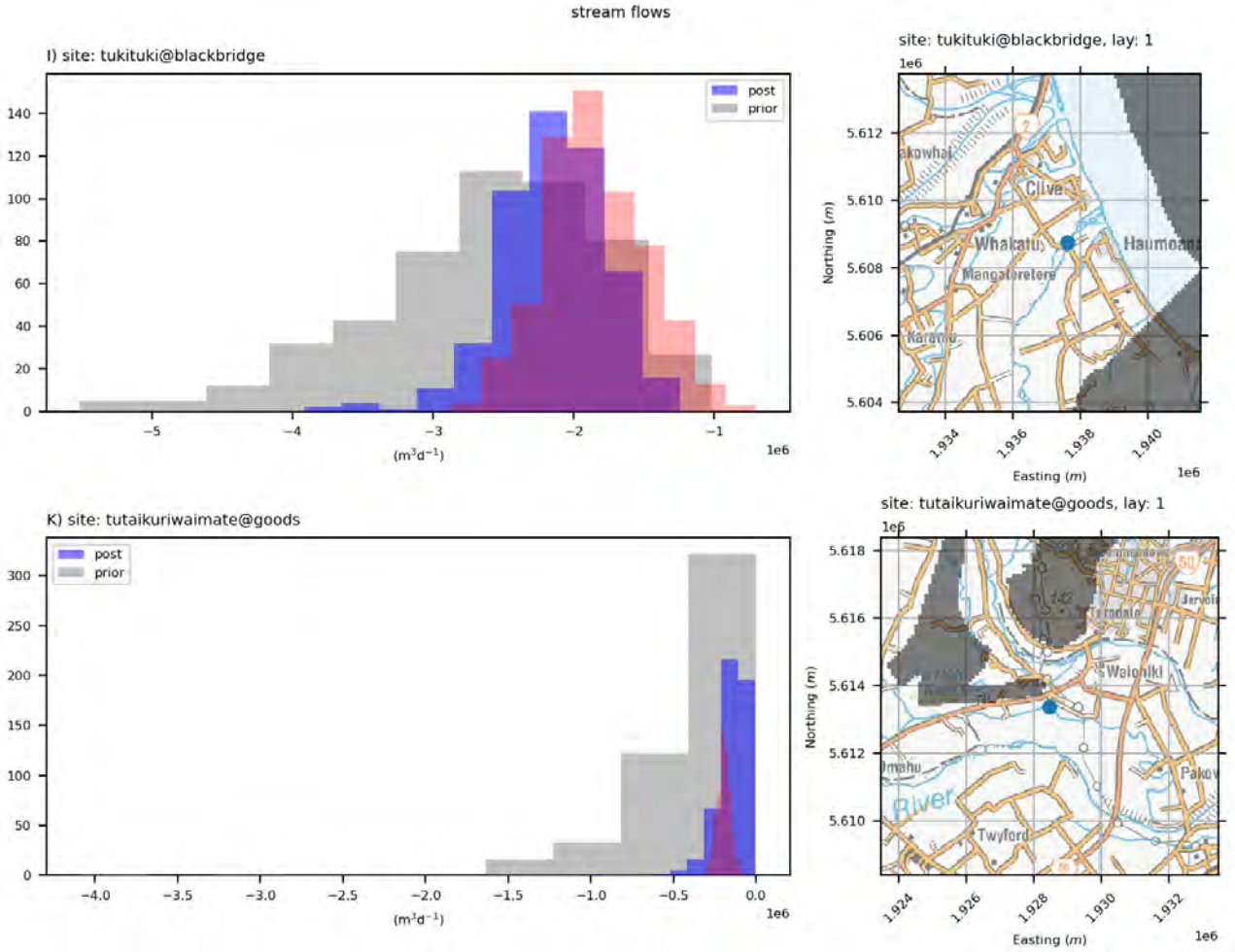
stream flows
I) site: tukituki@blackbridge
post
prior
(m³d⁻¹)
1e6
site: tukituki@blackbridge, lay: 1
Northing (m)
Easting (m)
Clive
Whakatu
Mangateretere
K) site: tutaikuriwaimate@goods
site: tutaikuriwaimate@goods, lay: 1
Waipiki
Twyford
River

A3.2.4.3 Surface-Water–Groundwater Exchange

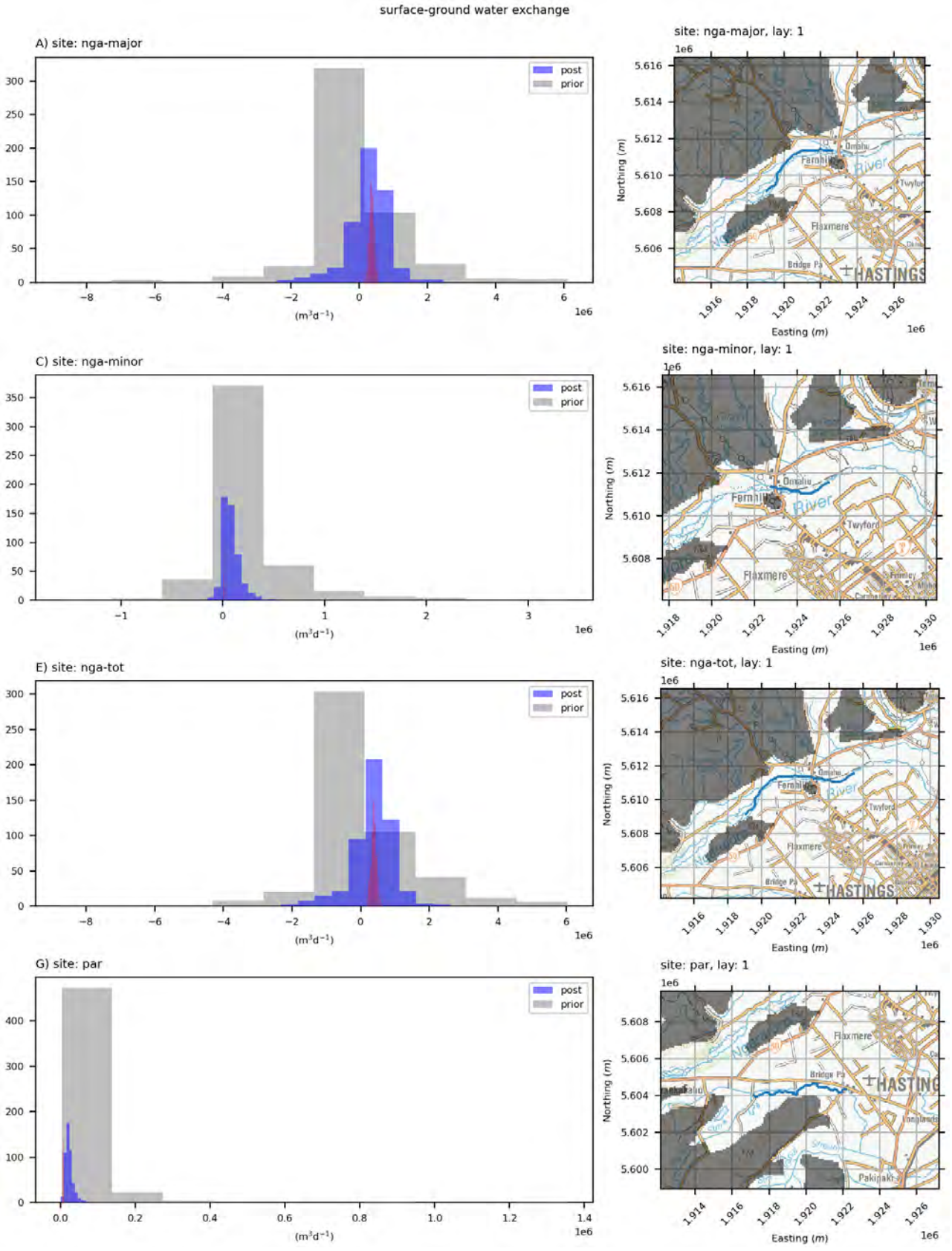

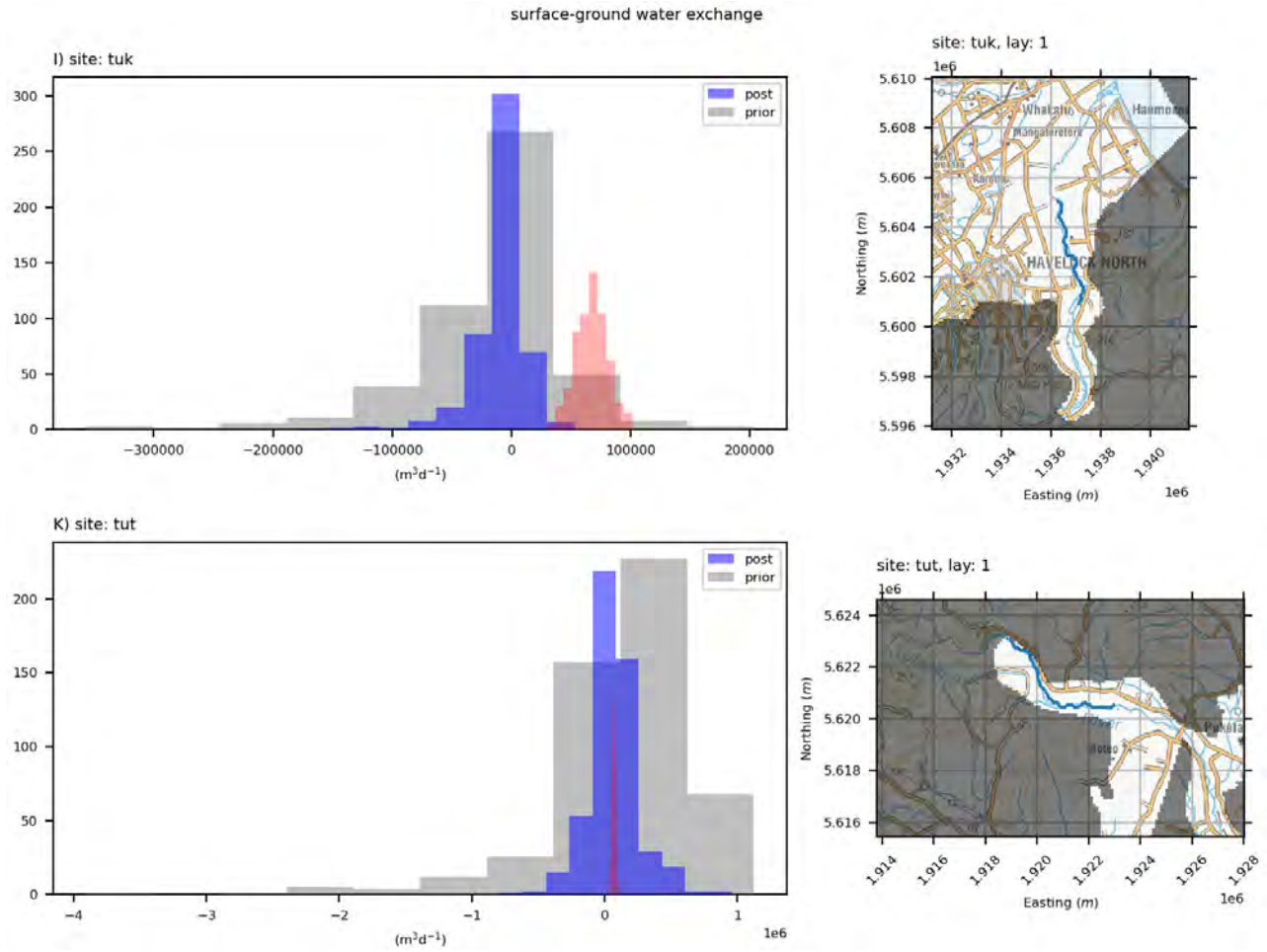
surface-ground water exchange
I) site: tuk
post
prior
(m³d⁻¹)
site: tuk, lay: 1
1e6
Northing (m)
Easting (m)
HAVELOCK NORTH
K) site: tut
post
prior
(m³d⁻¹)
1e6
site: tut, lay: 1
1e6
Northing (m)
Easting (m)
1e6

APPENDIX 4 Predictive Results

A4.1 Mapped Simulated Outputs

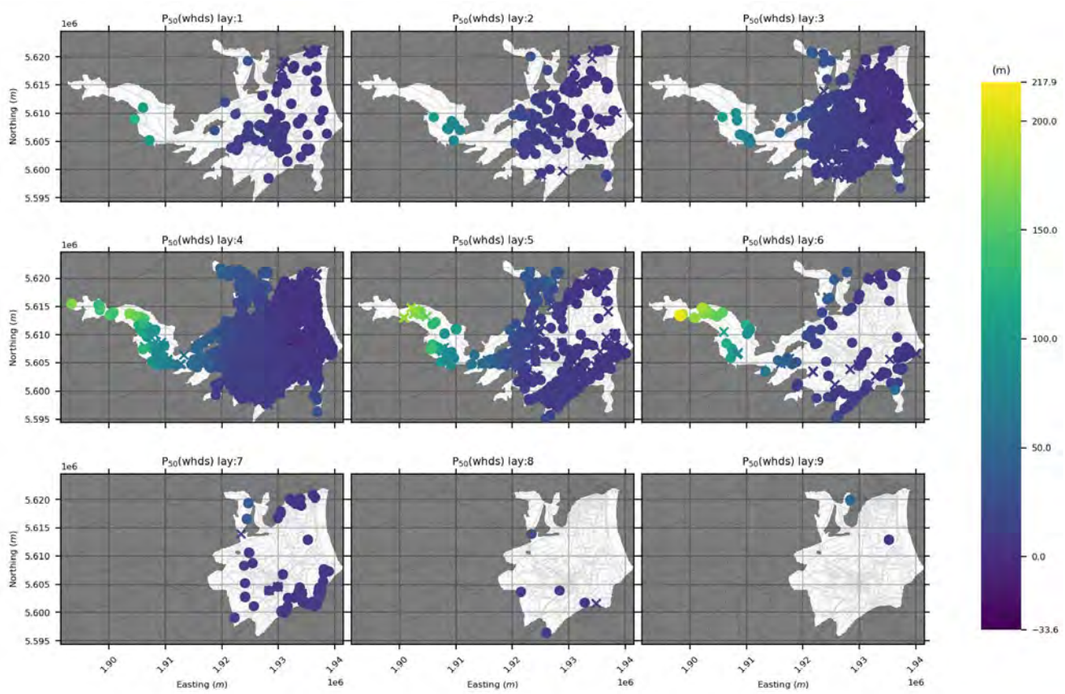

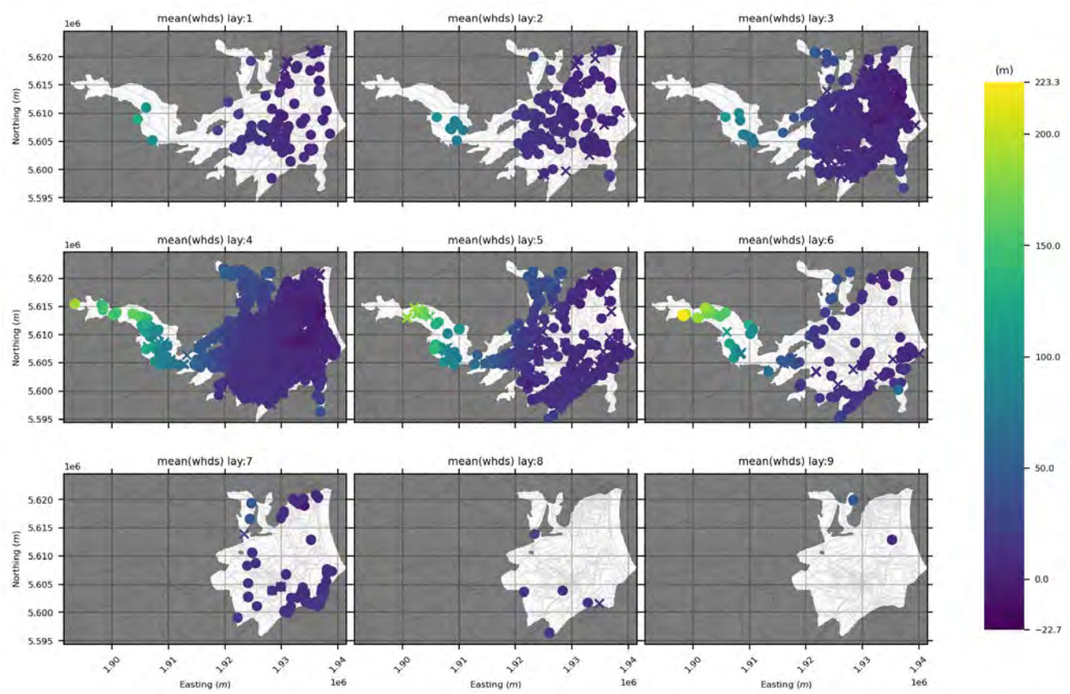

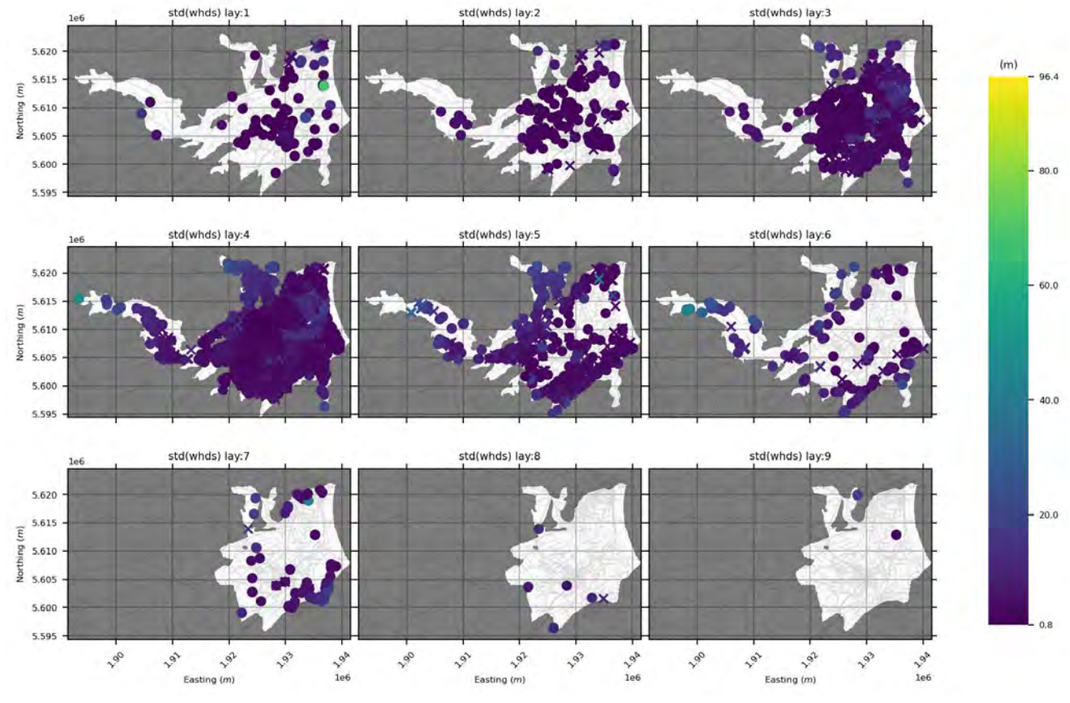

Figure A4.1 *geo* model prior ensemble median (upper left), mean (upper right) and standard deviation (right) for all water-level simulated outputs.

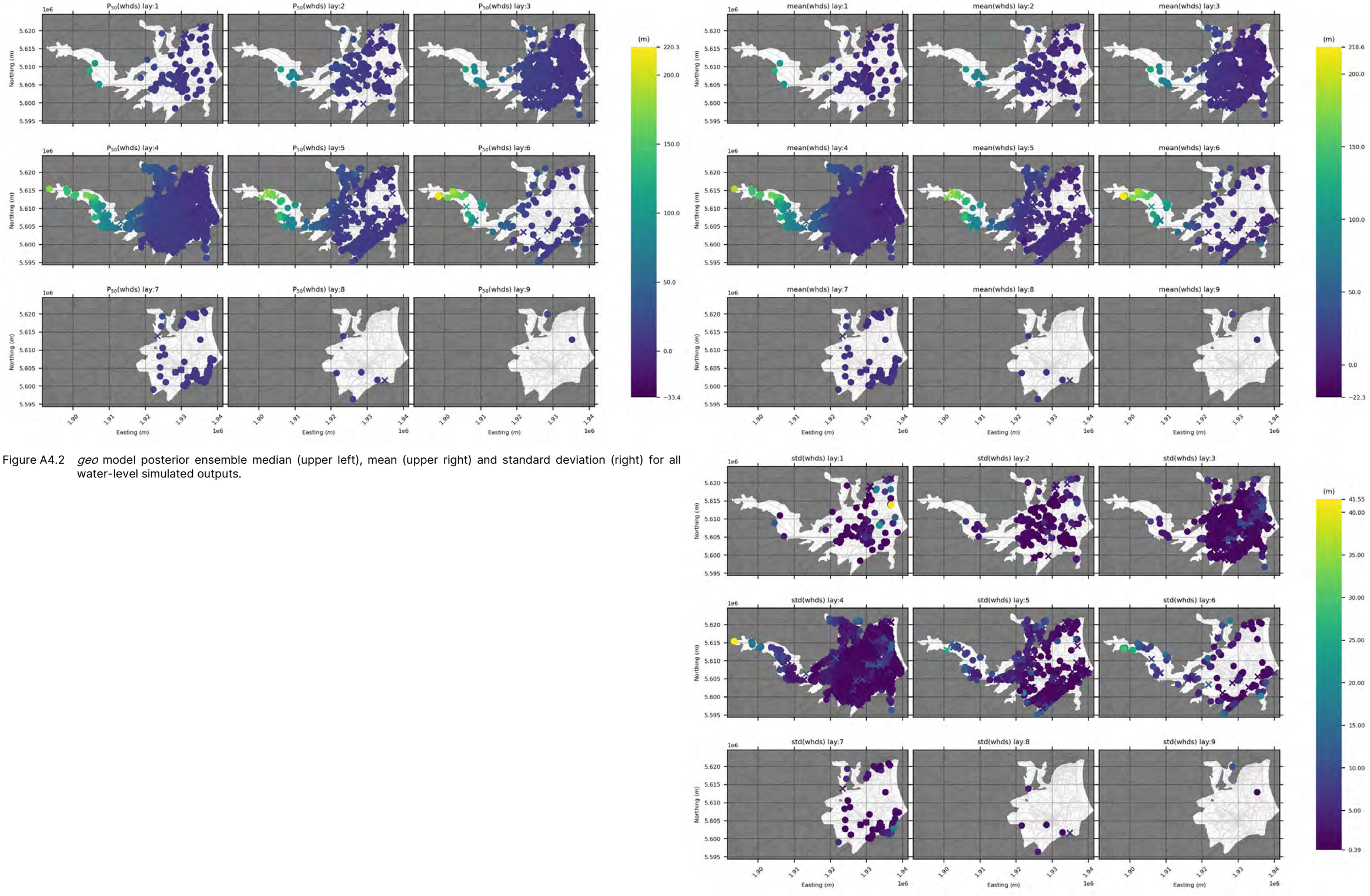

Figure A4.2 *geo* model posterior ensemble median (upper left), mean (upper right) and standard deviation (right) for all water-level simulated outputs.

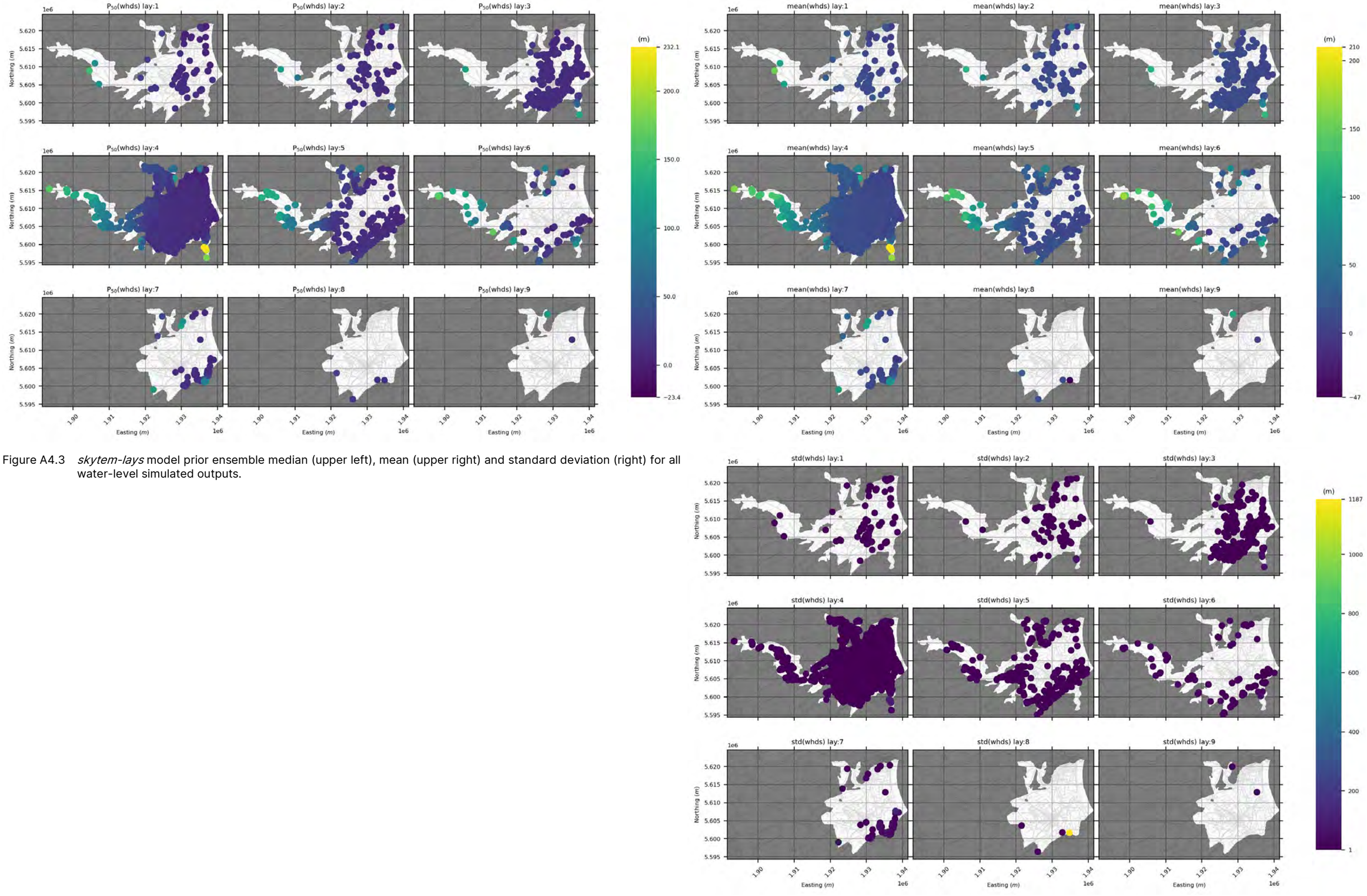

Figure A4.3 *skytem-lays* model prior ensemble median (upper left), mean (upper right) and standard deviation (right) for all water-level simulated outputs.

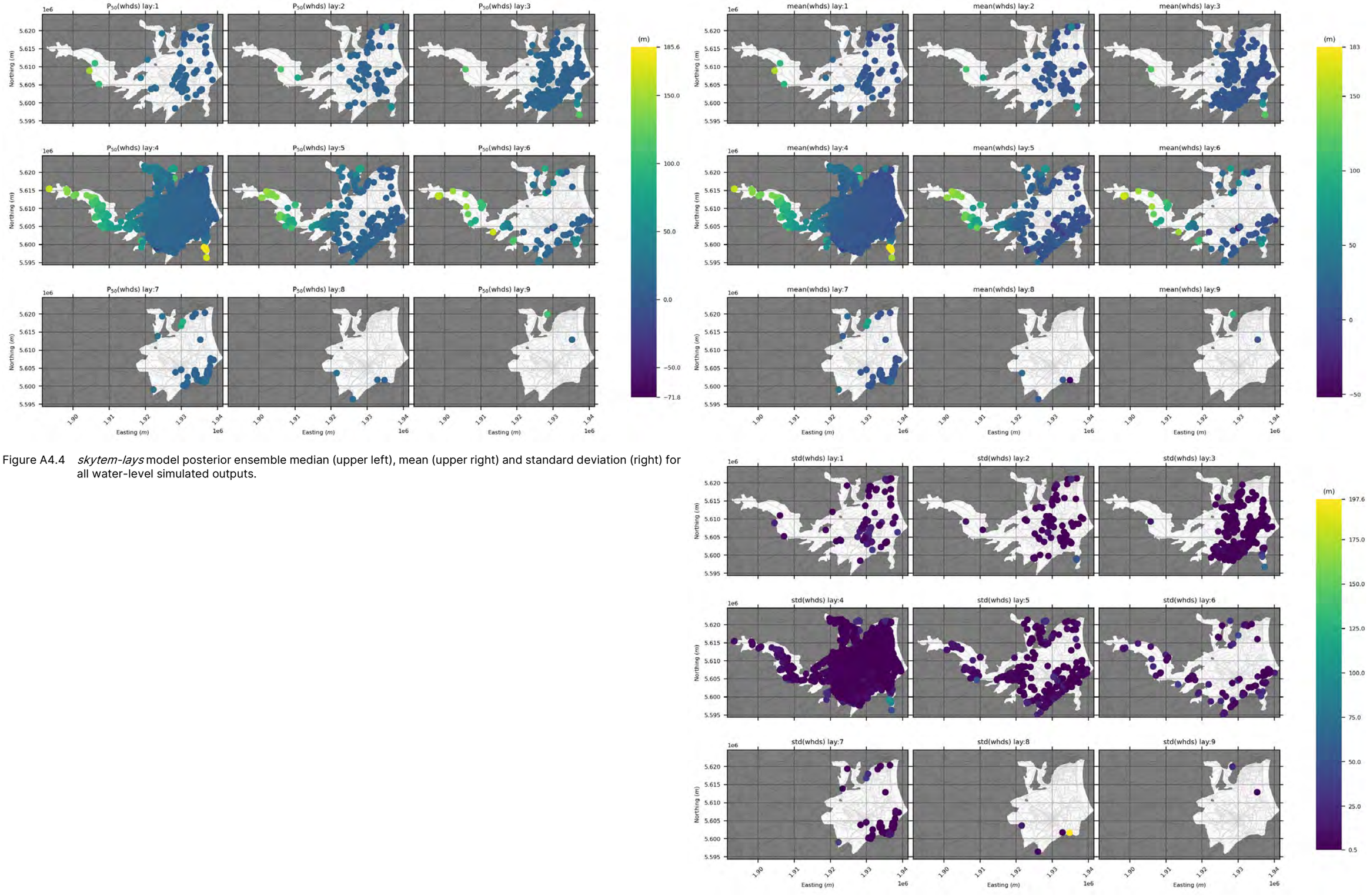

Figure A4.4 *skytem-lays* model posterior ensemble median (upper left), mean (upper right) and standard deviation (right) for all water-level simulated outputs.

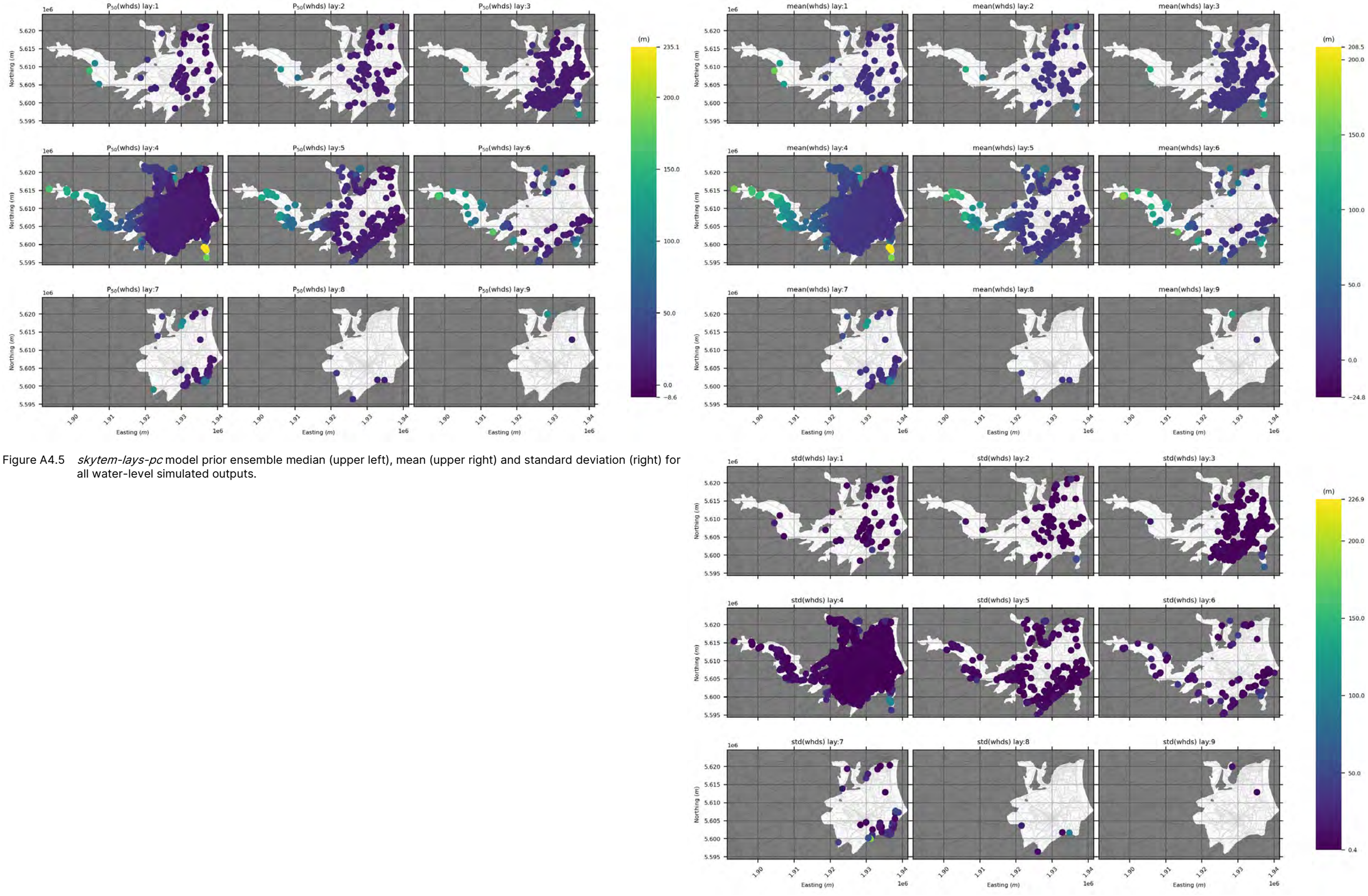

Figure A4.5 *skytem-lays-pc* model prior ensemble median (upper left), mean (upper right) and standard deviation (right) for all water-level simulated outputs.

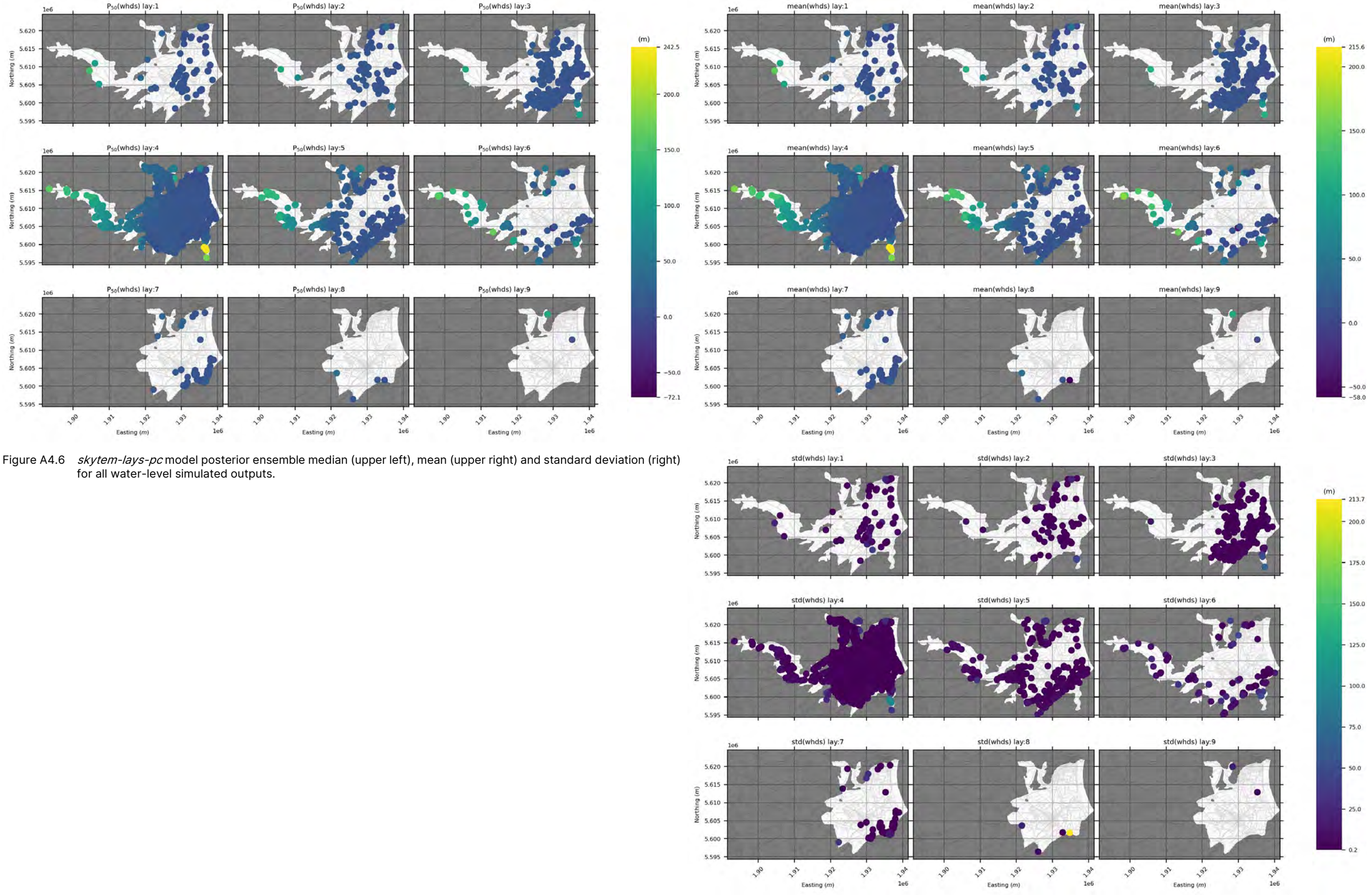

Figure A4.6 *skytem-lays-pc* model posterior ensemble median (upper left), mean (upper right) and standard deviation (right) for all water-level simulated outputs.

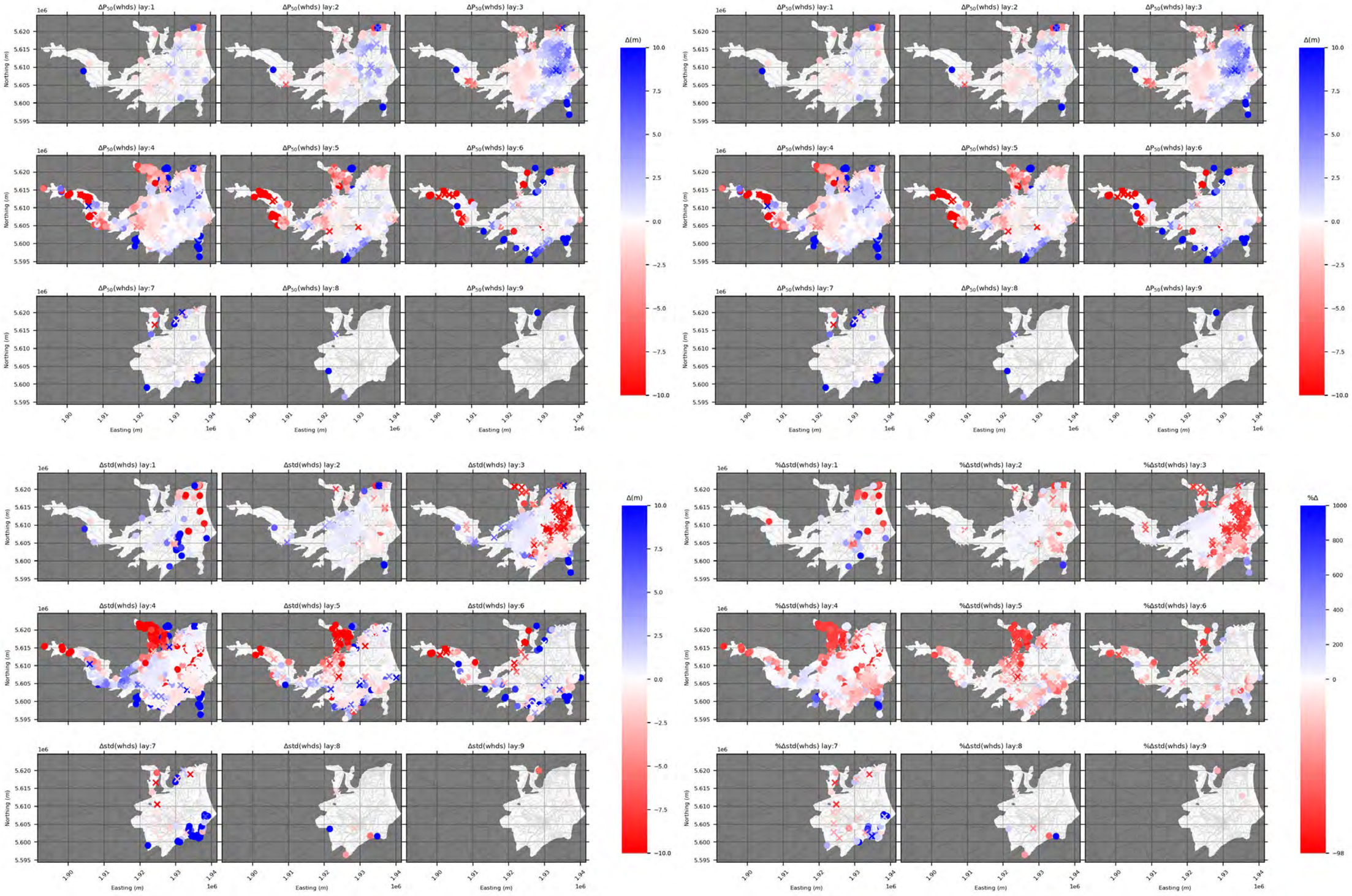

Figure A4.7 Difference between ensemble median (upper left), mean (upper right), standard deviation (lower left) and standard deviation percentage difference (lower right) for the *skytem-lays* model prior, relative to the *geo* prior, for all water-level simulated outputs. Note: crosses relate to well locations that are present in a different model layer in the *geo* model. Colour scales are clipped to ±10 m for difference plots and +1000% for standard deviation percent difference.

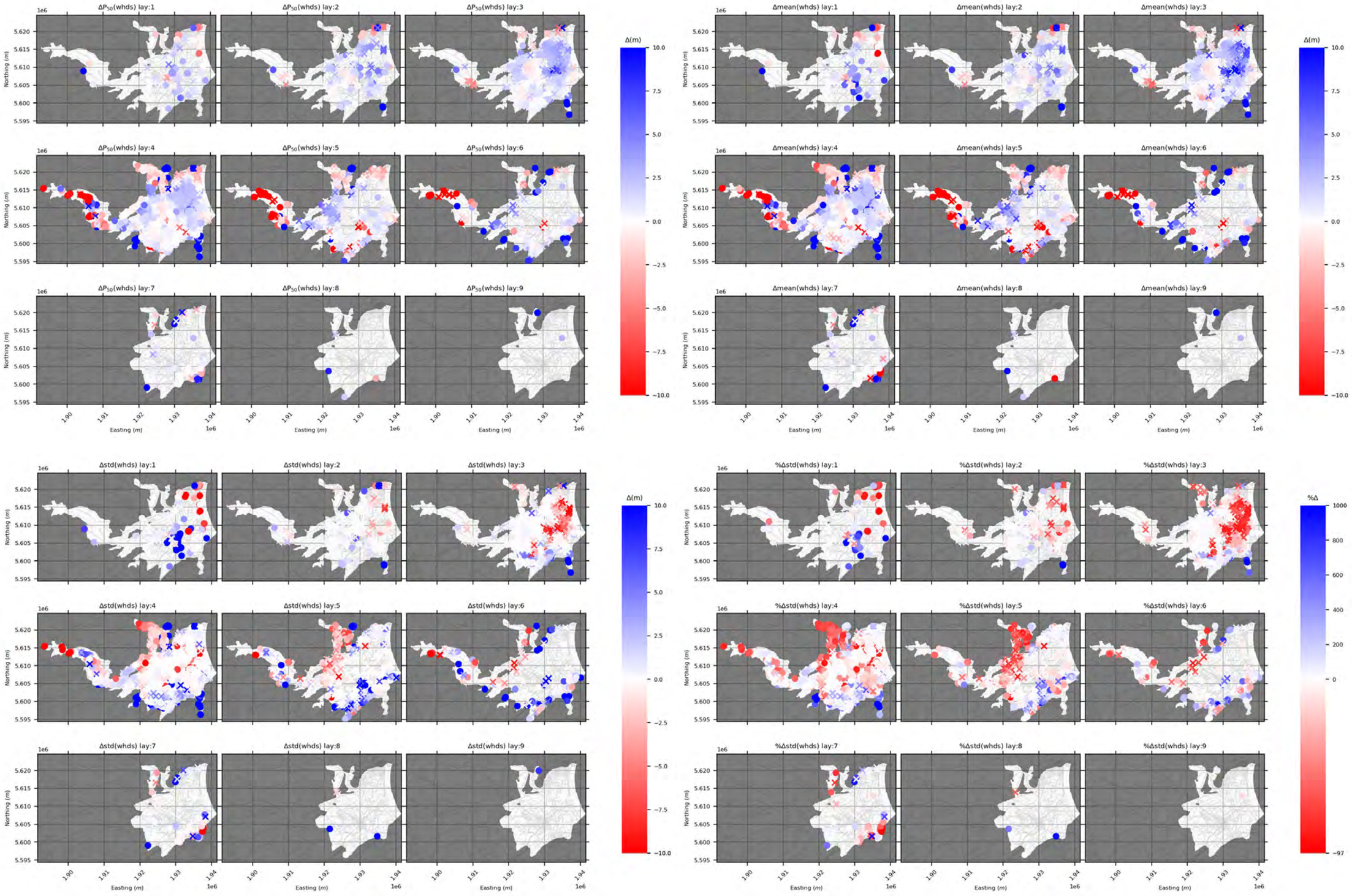

Figure A4.8 Difference between ensemble median (upper left), mean (upper right), standard deviation (lower left) and standard deviation percentage difference (lower right) for the *skytem-lays* model posterior, relative to the *geo* posterior, for all water-level simulated outputs. Note: crosses relate to well locations that are present in a different model layer in the *geo* model. Colour scales are clipped to ±10 m for difference plots and +1000% for standard deviation percent difference.

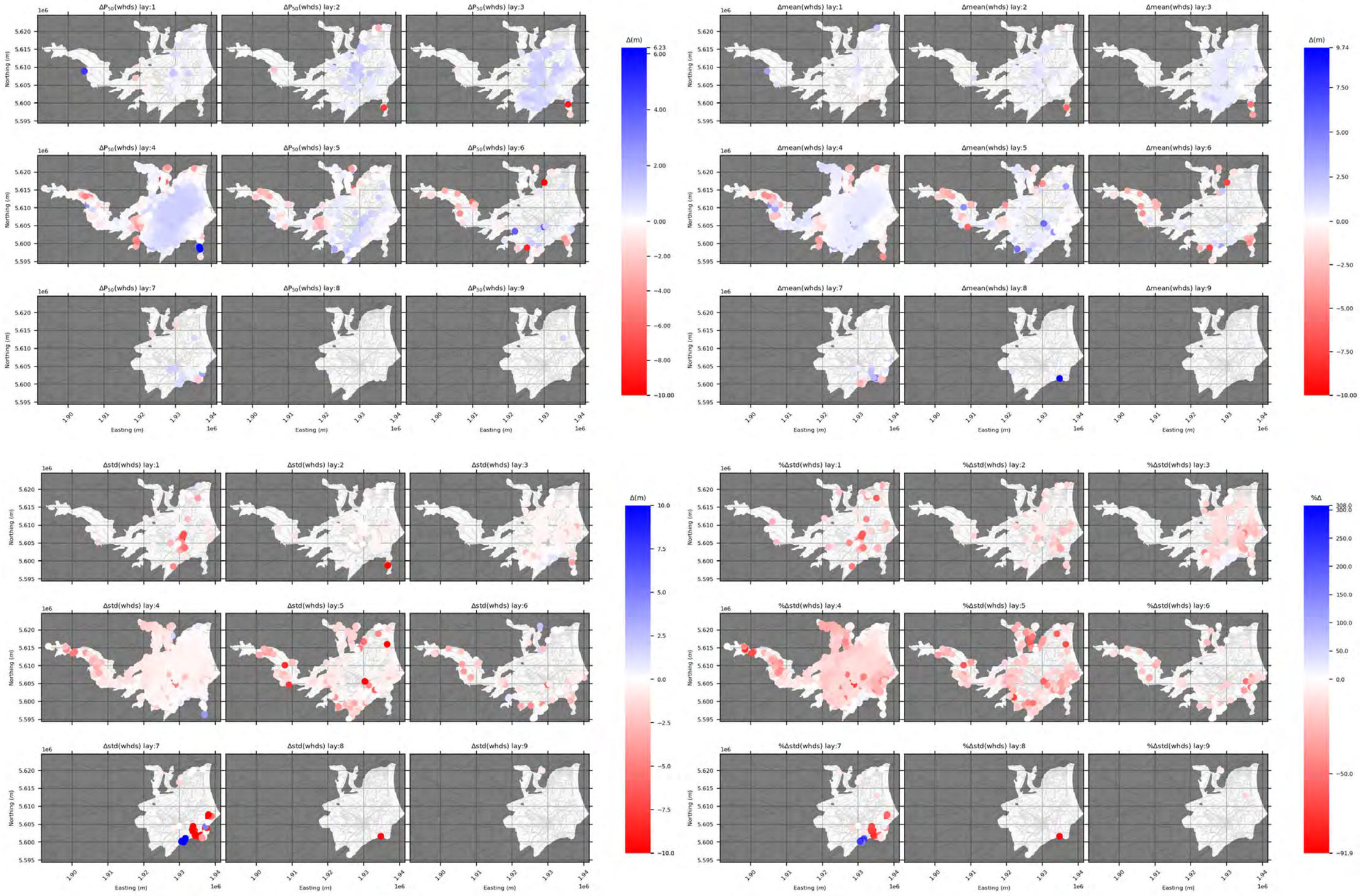

Figure A4.9 Difference between ensemble median (upper left), mean (upper right), standard deviation (lower left) and standard deviation percentage difference (lower right) for the *skytem-lays-pc* model prior, relative to the *skytem-lays* prior, for all water-level simulated outputs. Note: colour scales are clipped to ±10 m for difference plots.

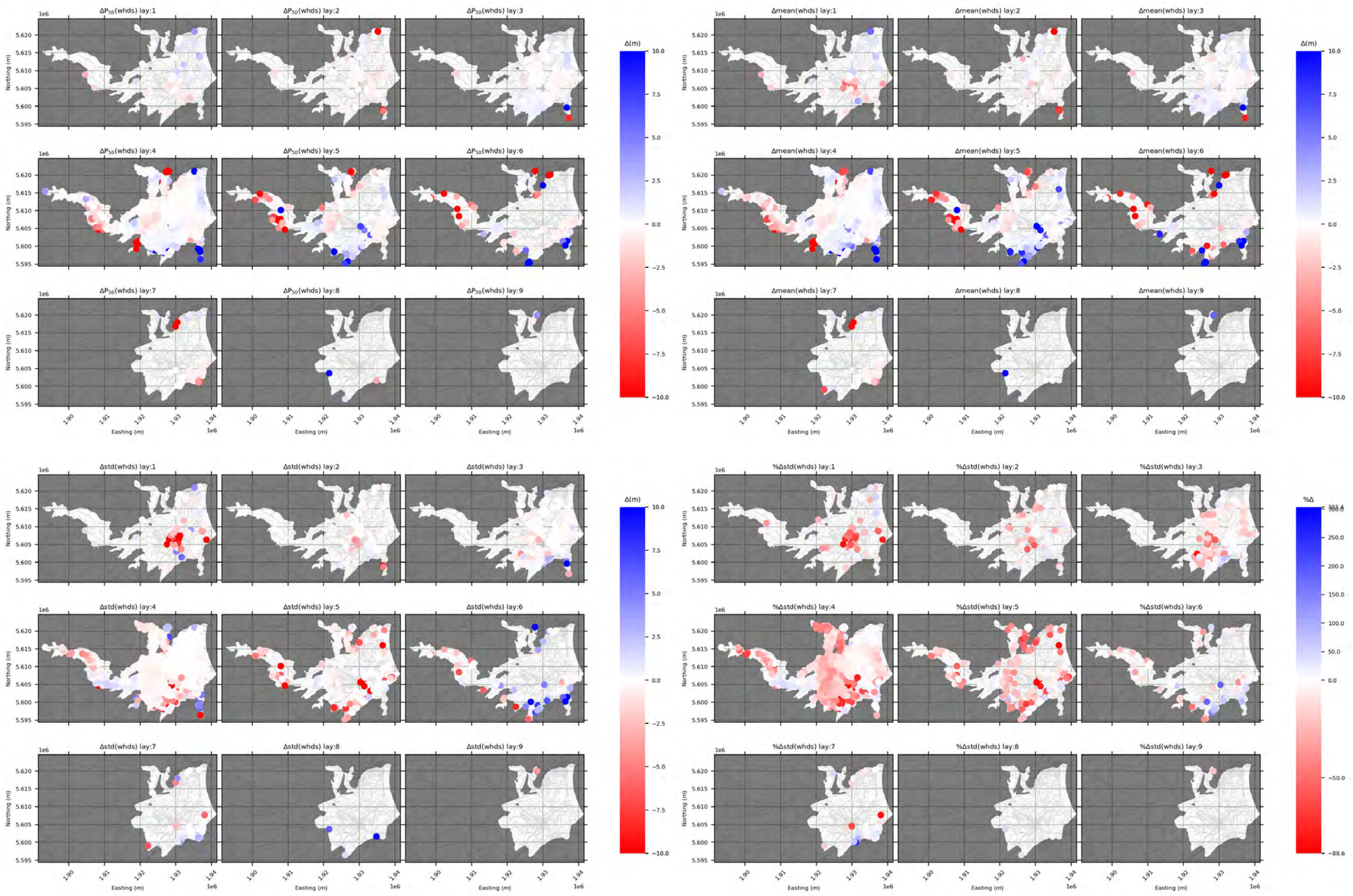

Figure A4.10 Difference between ensemble median (upper left), mean (upper right), standard deviation (lower left) and standard deviation percentage difference (lower right) for the *skytem-lays-pc* model posterior, relative to the *skytem-lays* posterior, for all water-level simulated outputs. Note: colour scales are clipped to ±10 m for difference plots.

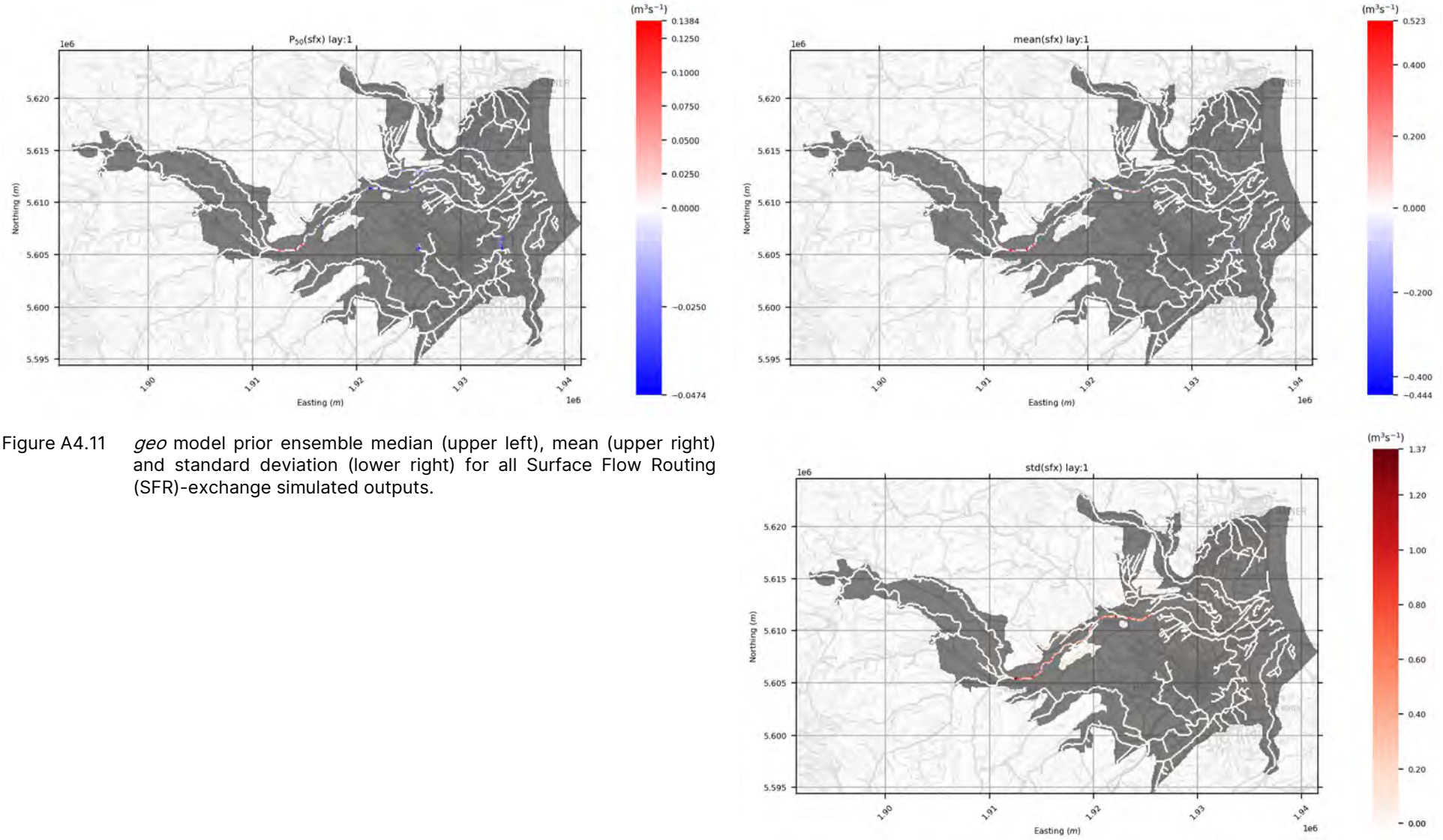

Figure A4.11 *geo* model prior ensemble median (upper left), mean (upper right) and standard deviation (lower right) for all Surface Flow Routing (SFR)-exchange simulated outputs.

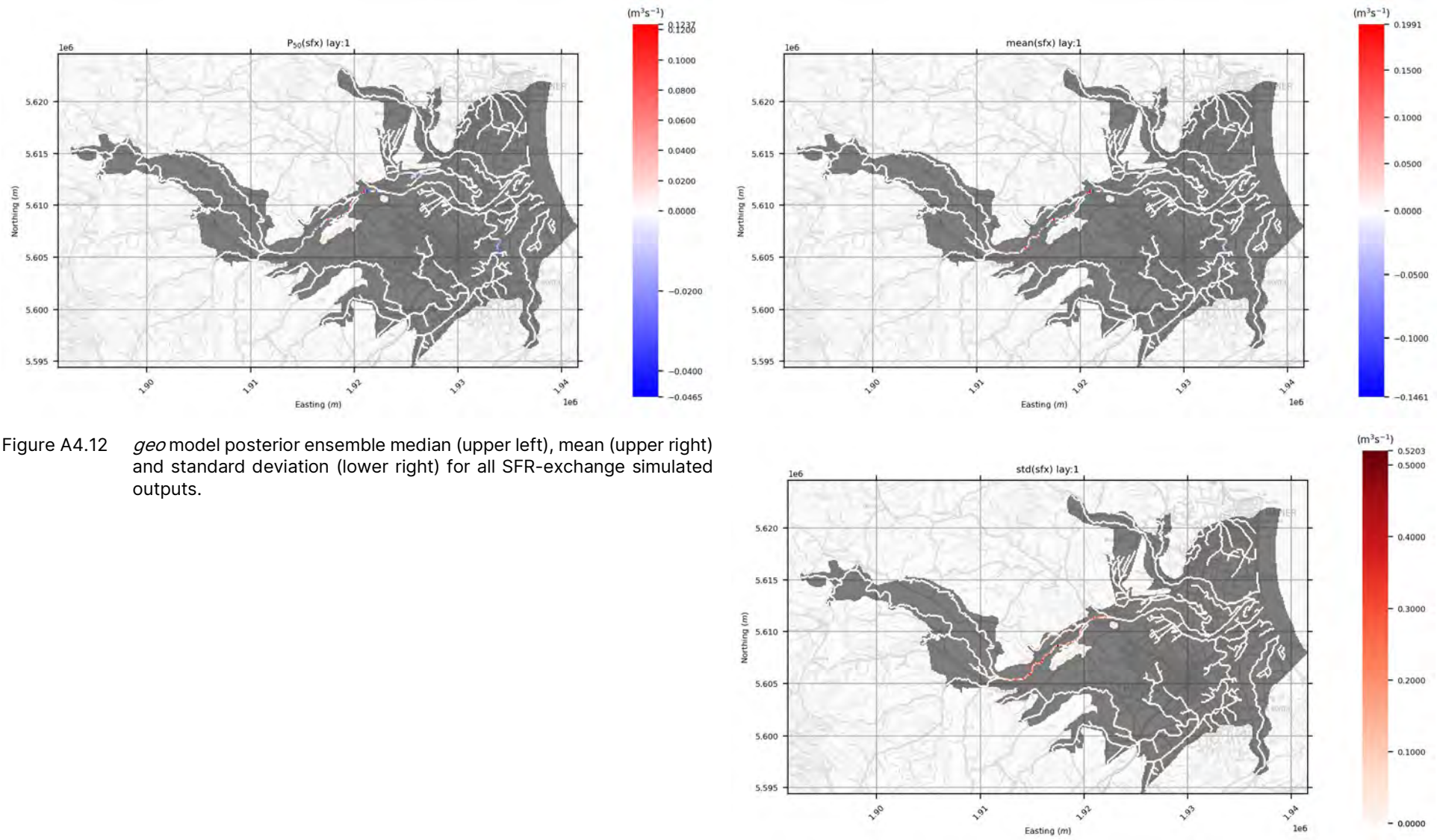

Figure A4.12 *geo* model posterior ensemble median (upper left), mean (upper right) and standard deviation (lower right) for all SFR-exchange simulated outputs.

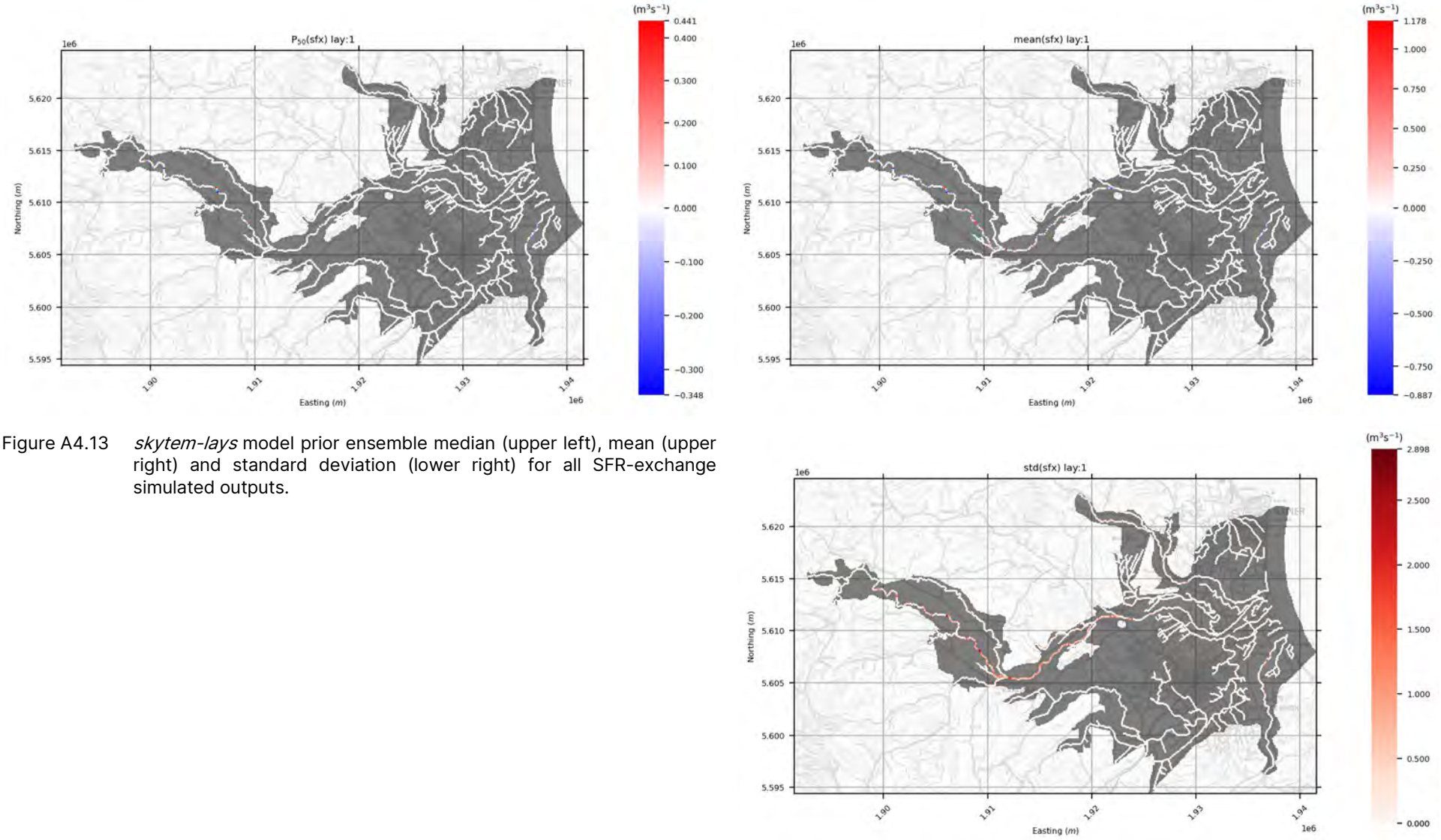

Figure A4.13 *skytem-lays* model prior ensemble median (upper left), mean (upper right) and standard deviation (lower right) for all SFR-exchange simulated outputs.

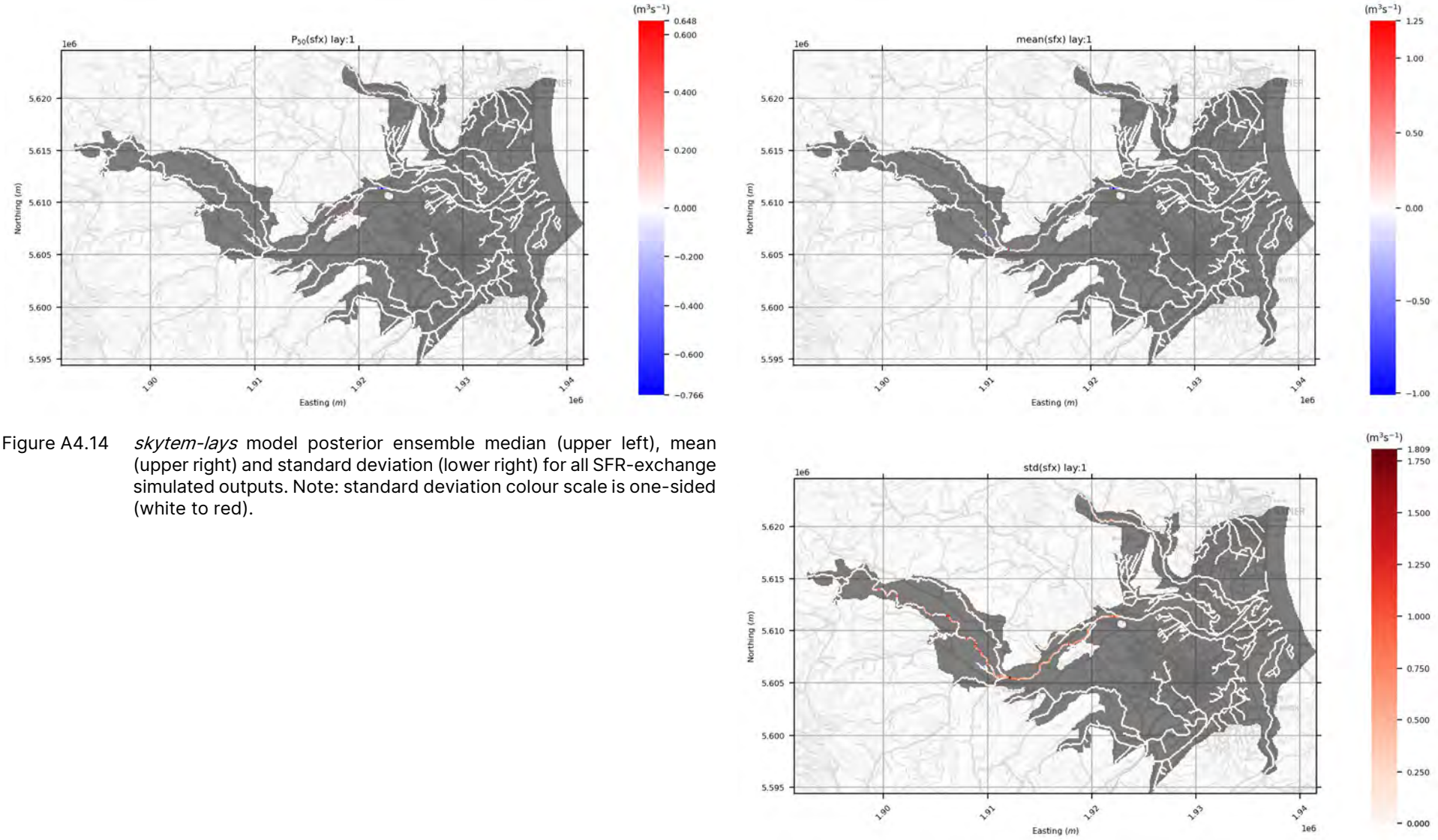

Figure A4.14 *skytem-lays* model posterior ensemble median (upper left), mean (upper right) and standard deviation (lower right) for all SFR-exchange simulated outputs. Note: standard deviation colour scale is one-sided (white to red).

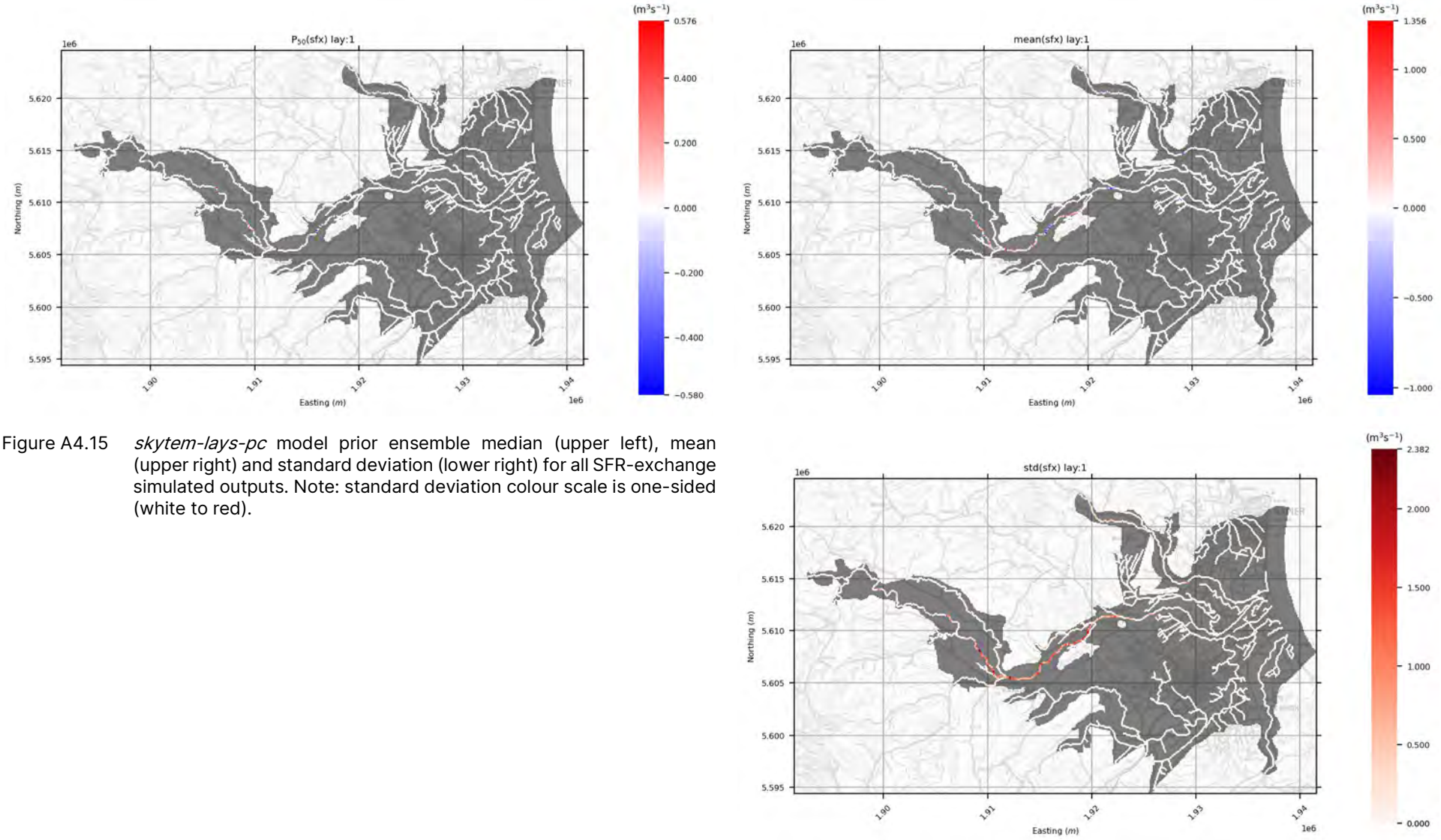

Figure A4.15 *skytem-lays-pc* model prior ensemble median (upper left), mean (upper right) and standard deviation (lower right) for all SFR-exchange simulated outputs. Note: standard deviation colour scale is one-sided (white to red).

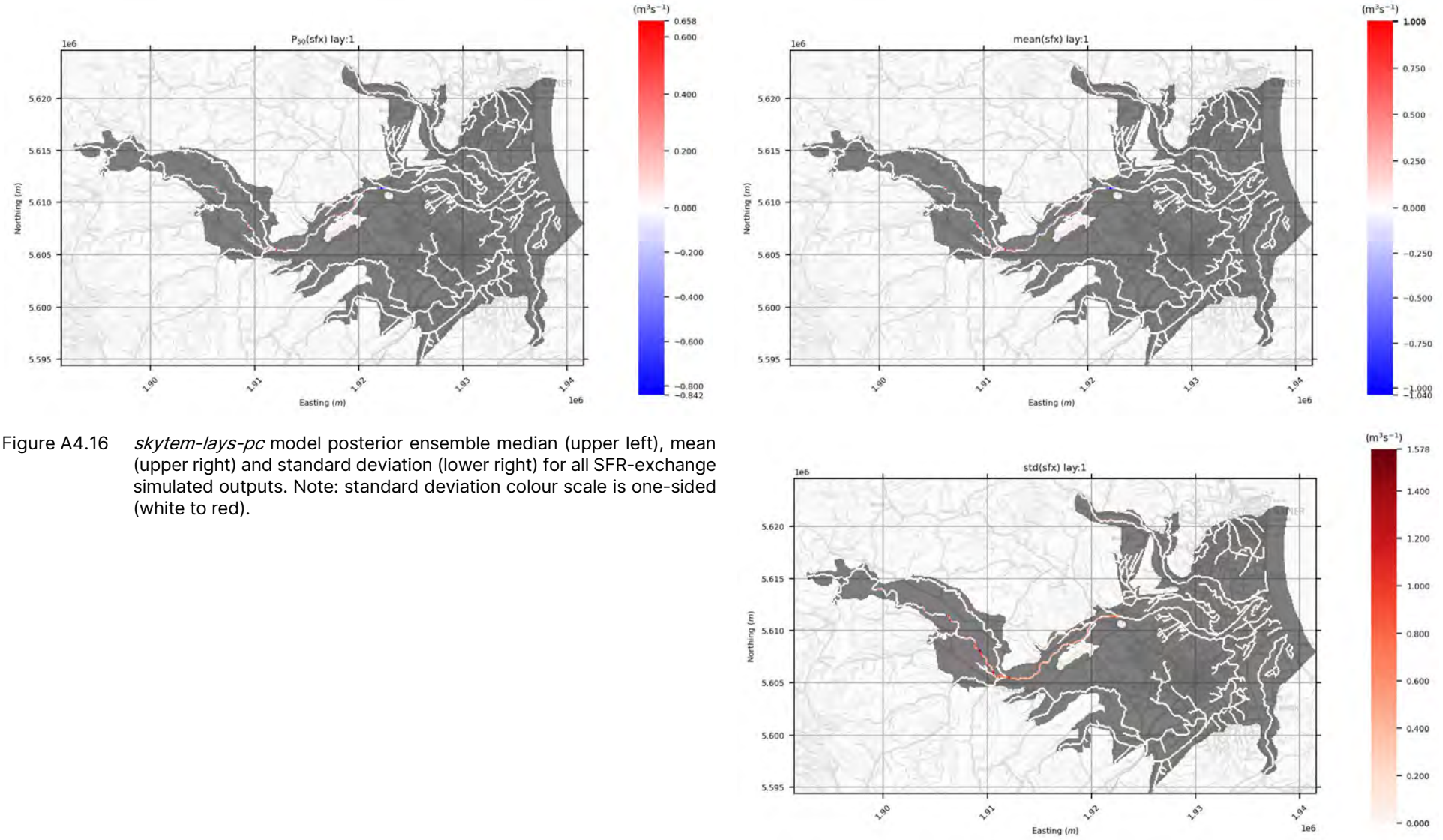

Figure A4.16 *skytem-lays-pc* model posterior ensemble median (upper left), mean (upper right) and standard deviation (lower right) for all SFR-exchange simulated outputs. Note: standard deviation colour scale is one-sided (white to red).

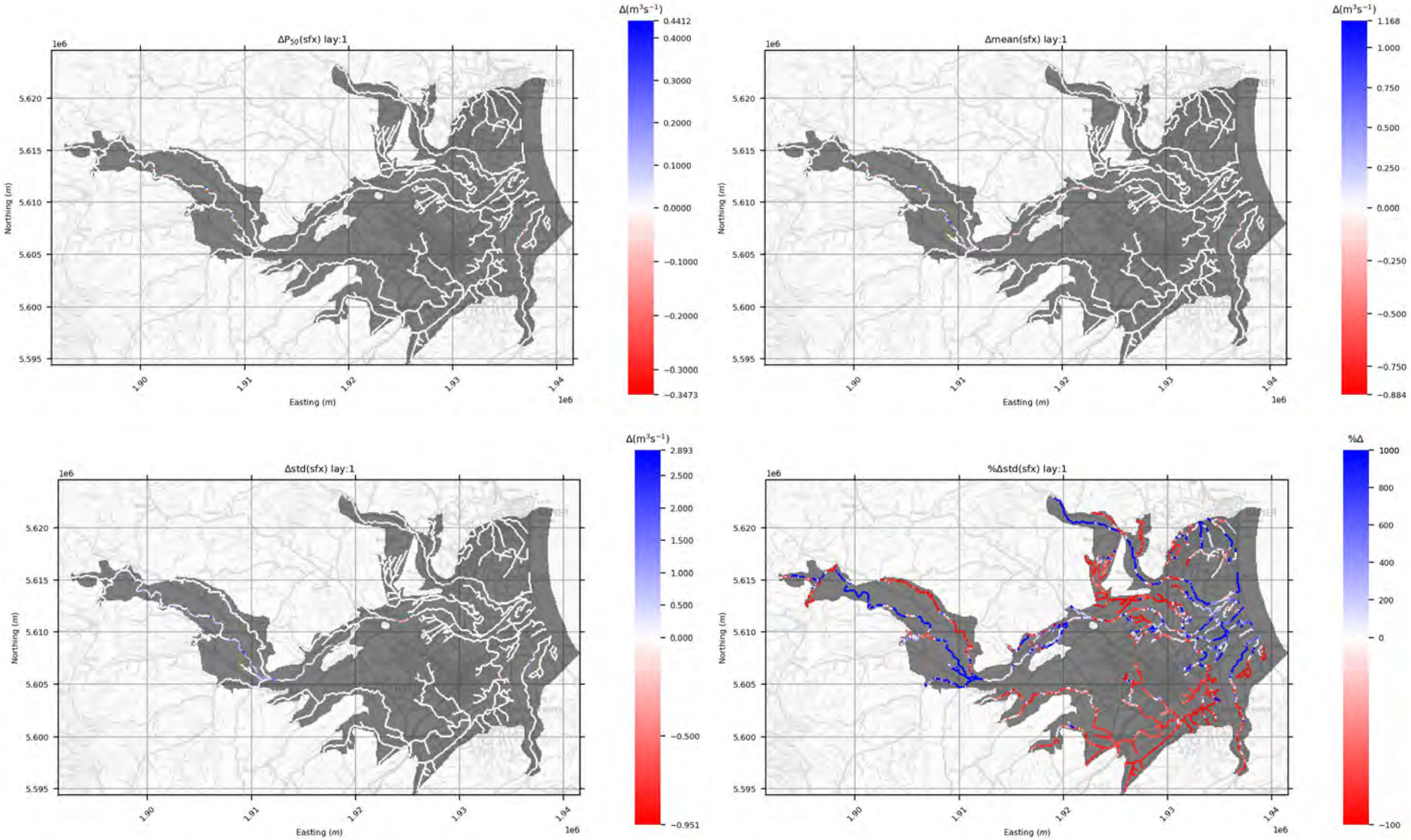

Figure A4.17 Difference between ensemble median (upper left), mean (upper right), standard deviation (lower left) and standard deviation percentage difference (lower right) for the *skytem-lays* model prior, relative to the *geo* prior, for all SFR-exchange simulated outputs. Note: standard deviation percent difference colour scale is clipped at +1000%.

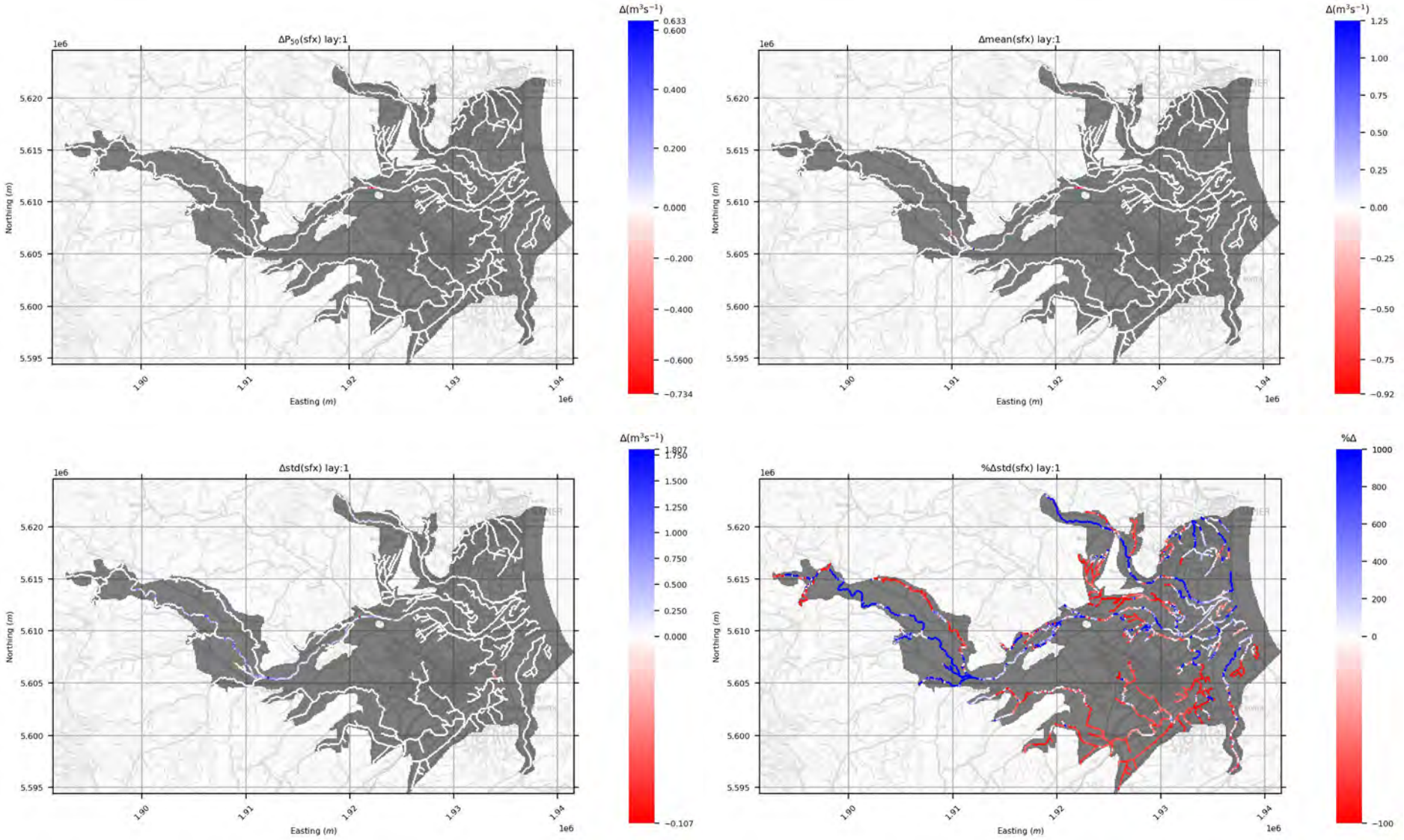

Figure A4.18 Difference between ensemble median (upper left), mean (upper right), standard deviation (lower left) and standard deviation percentage difference (lower right) for the *skytem-lays* model posterior, relative to the *geo* posterior, for all SFR-exchange simulated outputs. Note: standard deviation percent difference colour scale is clipped at +1000%.

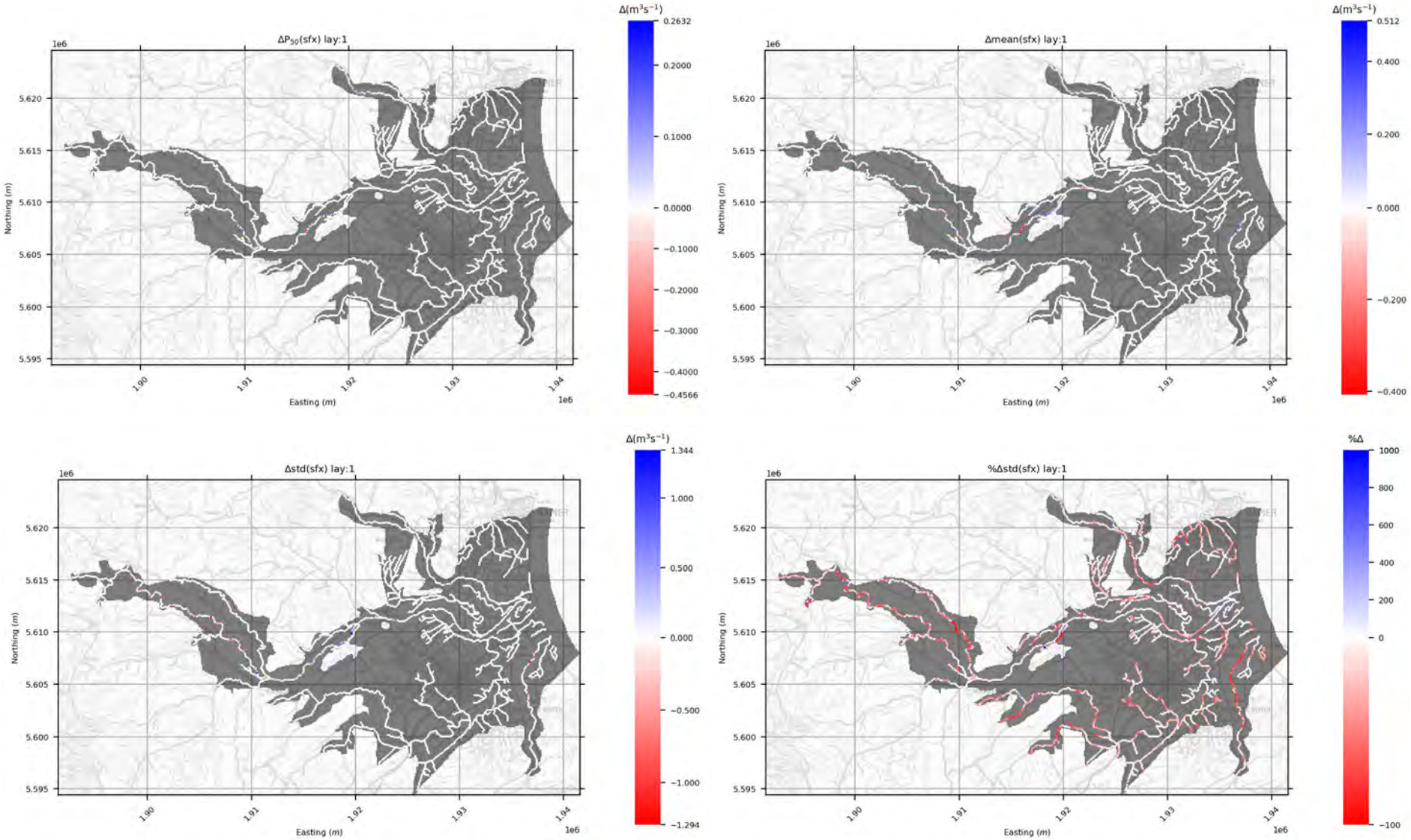

Figure A4.19 Difference between ensemble median (upper left), mean (upper right), standard deviation (lower left) and standard deviation percentage difference (lower right) for the *skytem-lays-pc* model prior, relative to the *skytem-lays* prior, for all SFR-exchange simulated outputs. Note: standard deviation percent difference colour scale is clipped at +1000%.

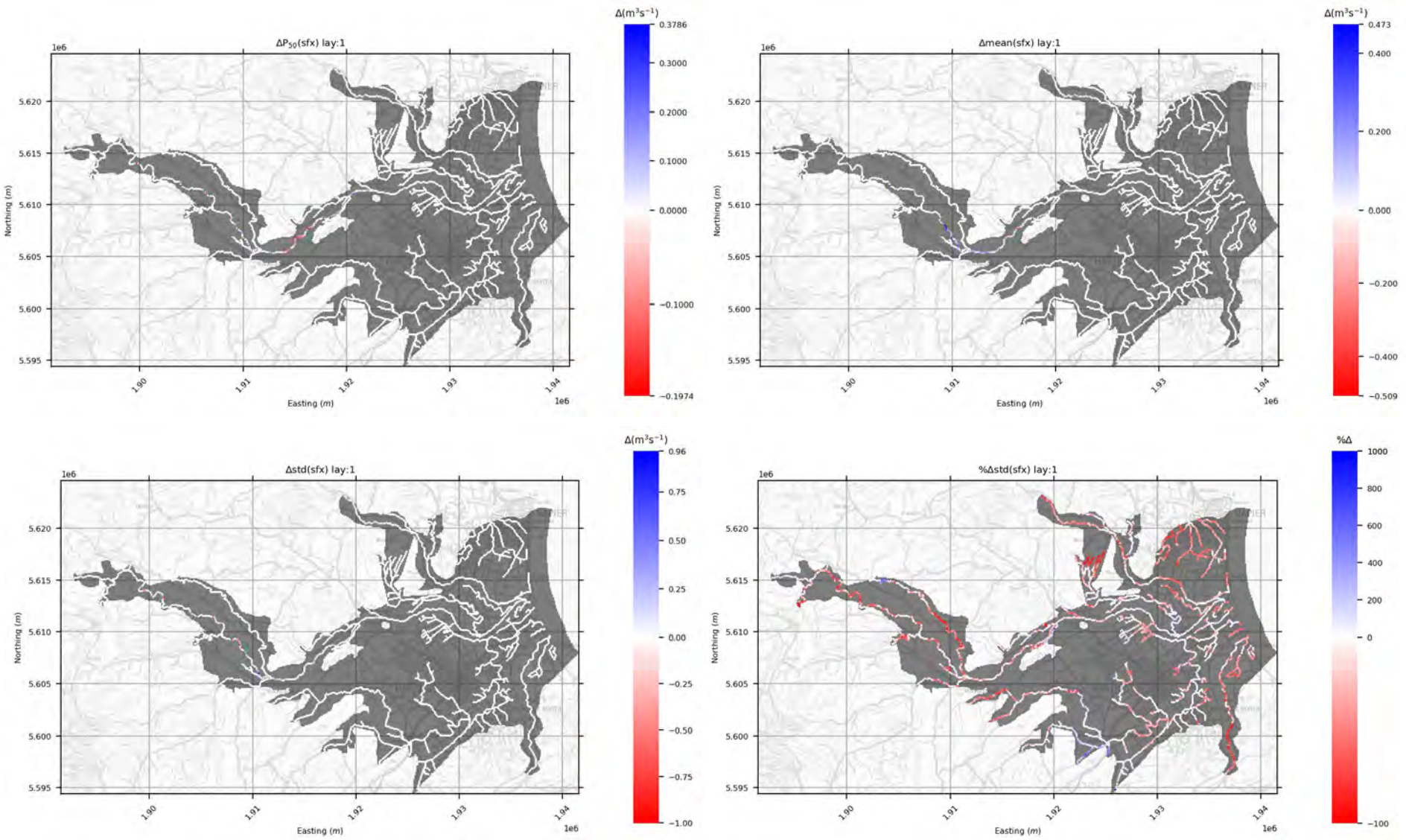

Figure A4.20 Difference between ensemble median (upper left), mean (upper right), standard deviation (lower left) and standard deviation percentage difference (lower right) for the *skytem-lays-pc* model posterior, relative to the *skytem-lays* posterior, for all SFR-exchange simulated outputs. Note: standard deviation percent difference colour scale is clipped at +1000%.

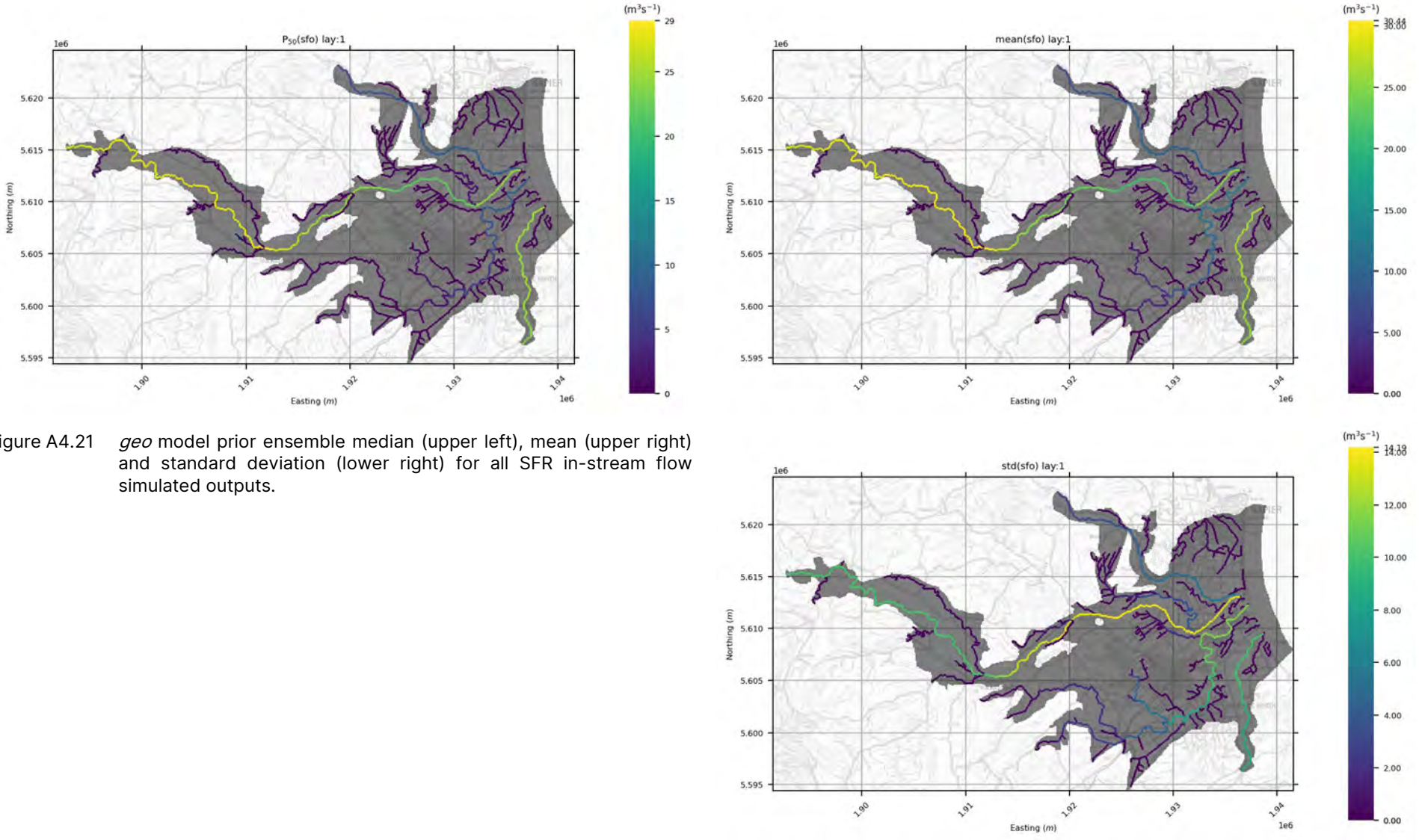

Figure A4.21 *geo* model prior ensemble median (upper left), mean (upper right) and standard deviation (lower right) for all SFR in-stream flow simulated outputs.

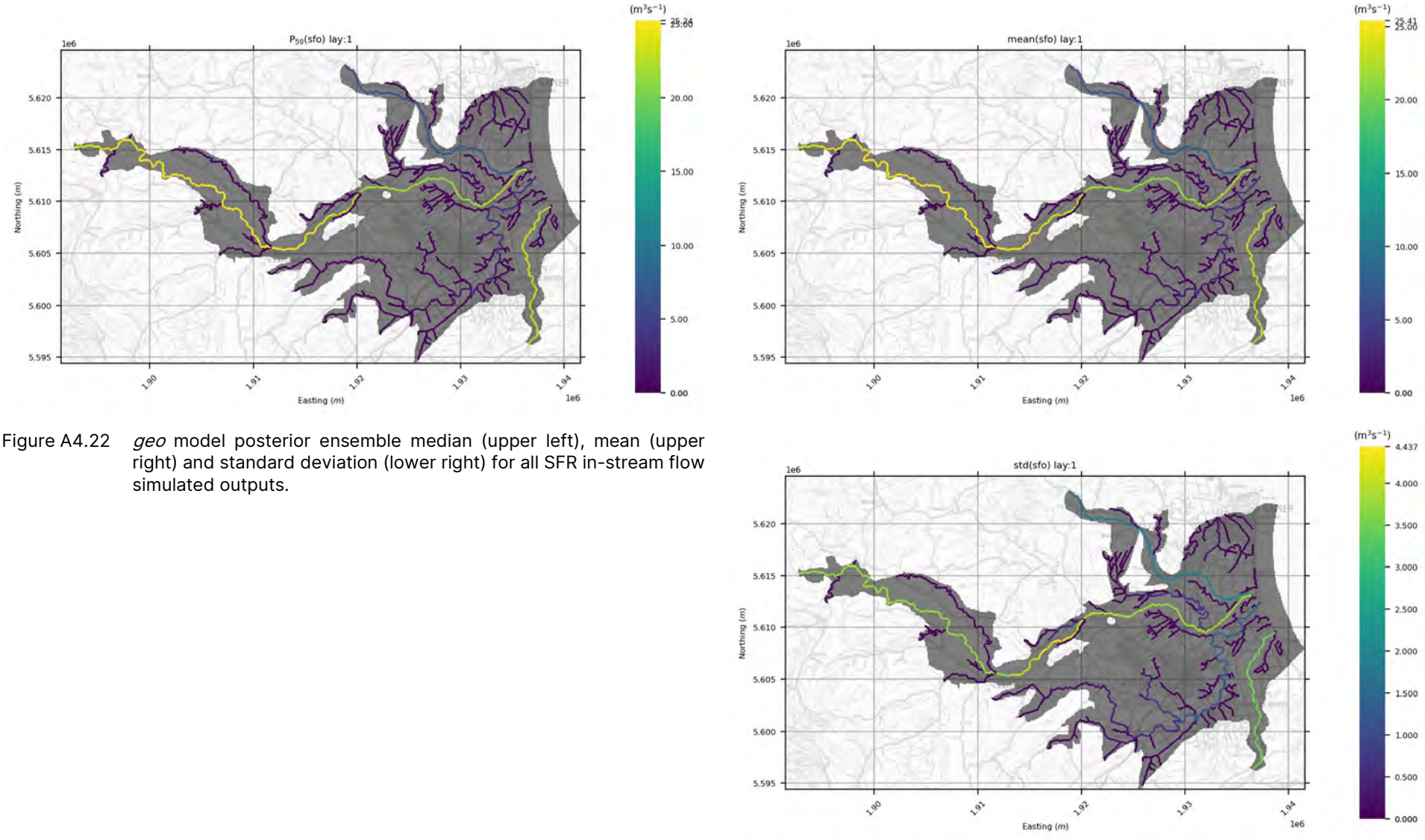

Figure A4.22 *geo* model posterior ensemble median (upper left), mean (upper right) and standard deviation (lower right) for all SFR in-stream flow simulated outputs.

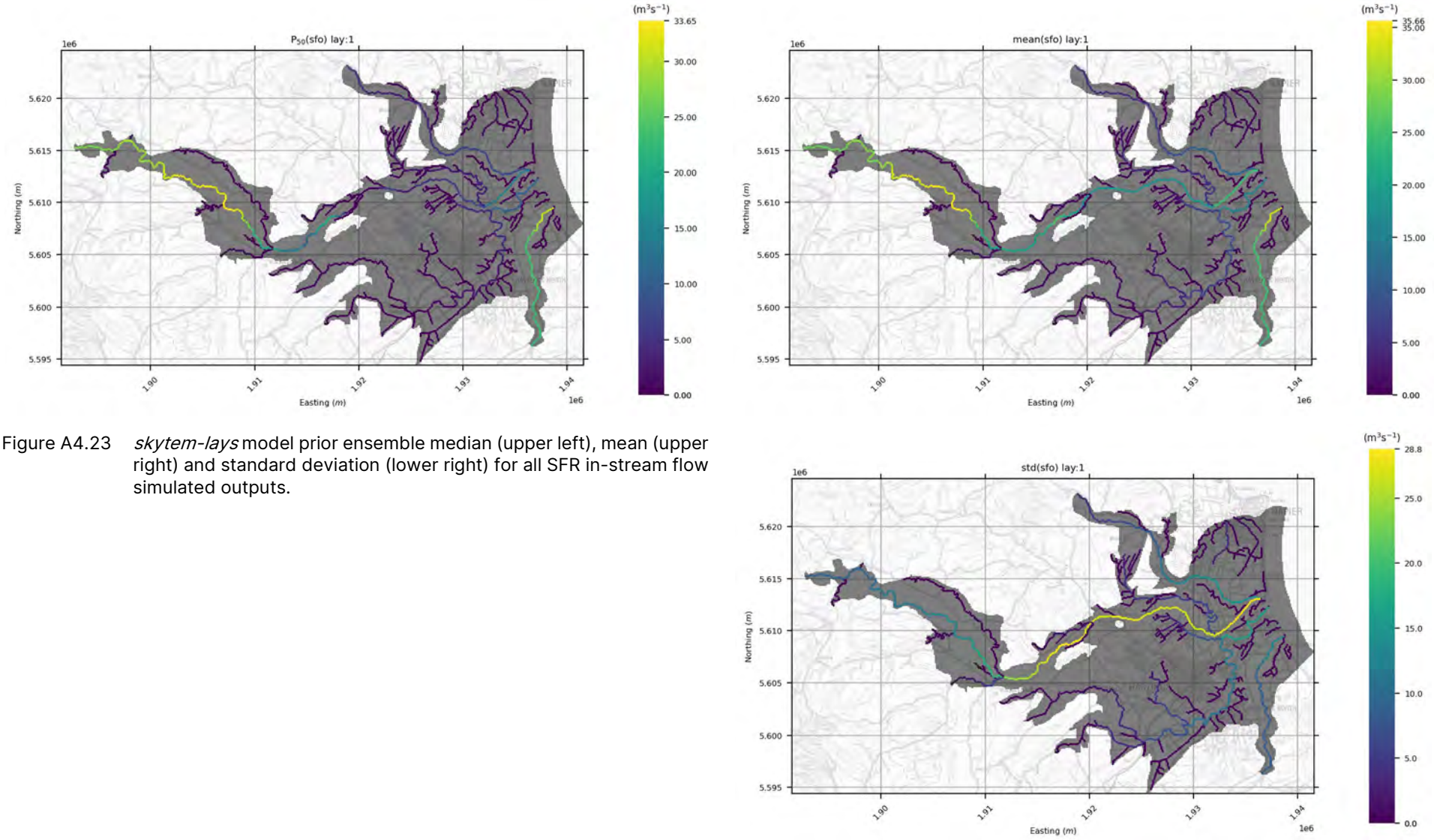

Figure A4.23 *skytem-lays* model prior ensemble median (upper left), mean (upper right) and standard deviation (lower right) for all SFR in-stream flow simulated outputs.

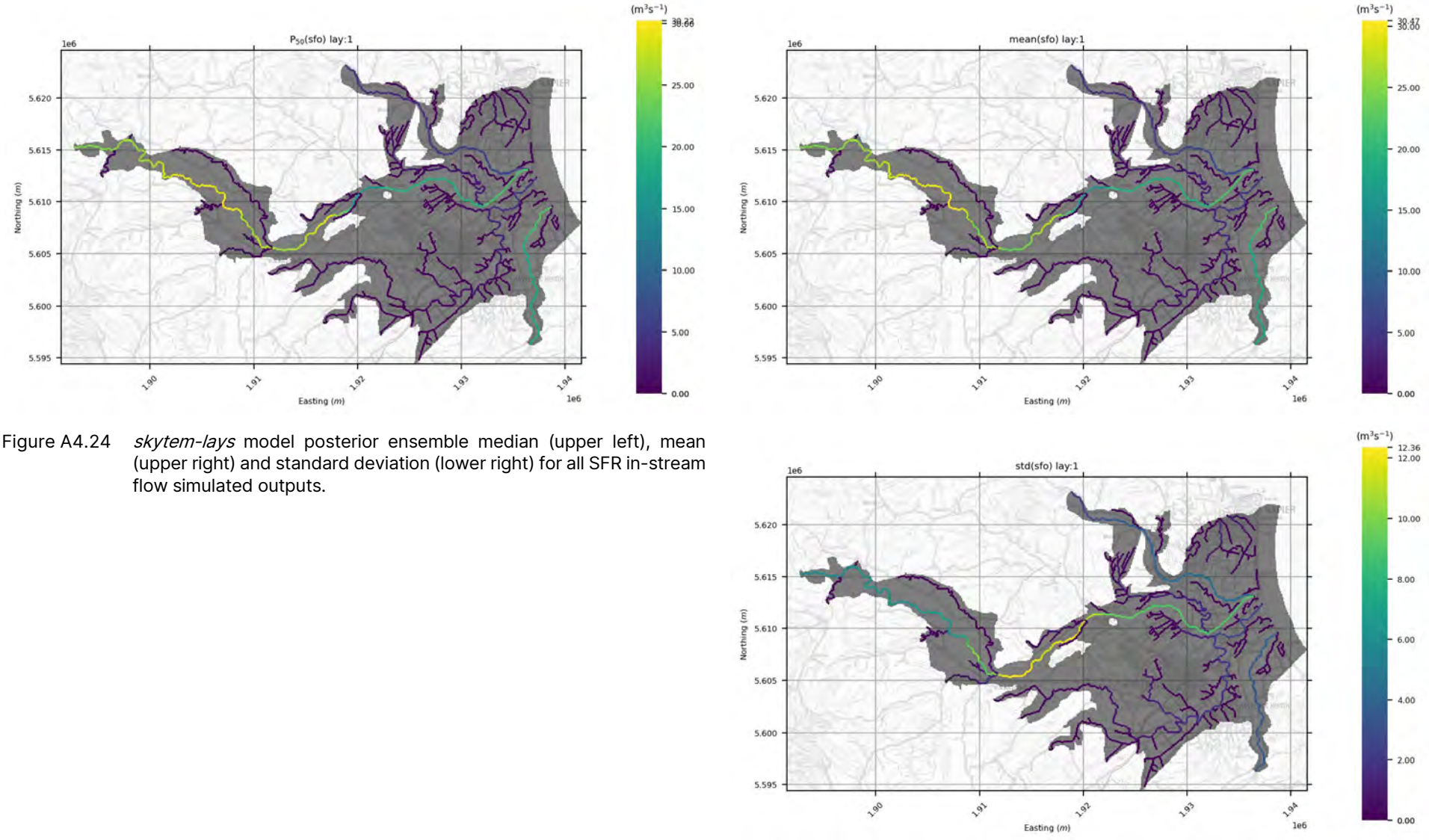

Figure A4.24 *skytem-lays* model posterior ensemble median (upper left), mean (upper right) and standard deviation (lower right) for all SFR in-stream flow simulated outputs.

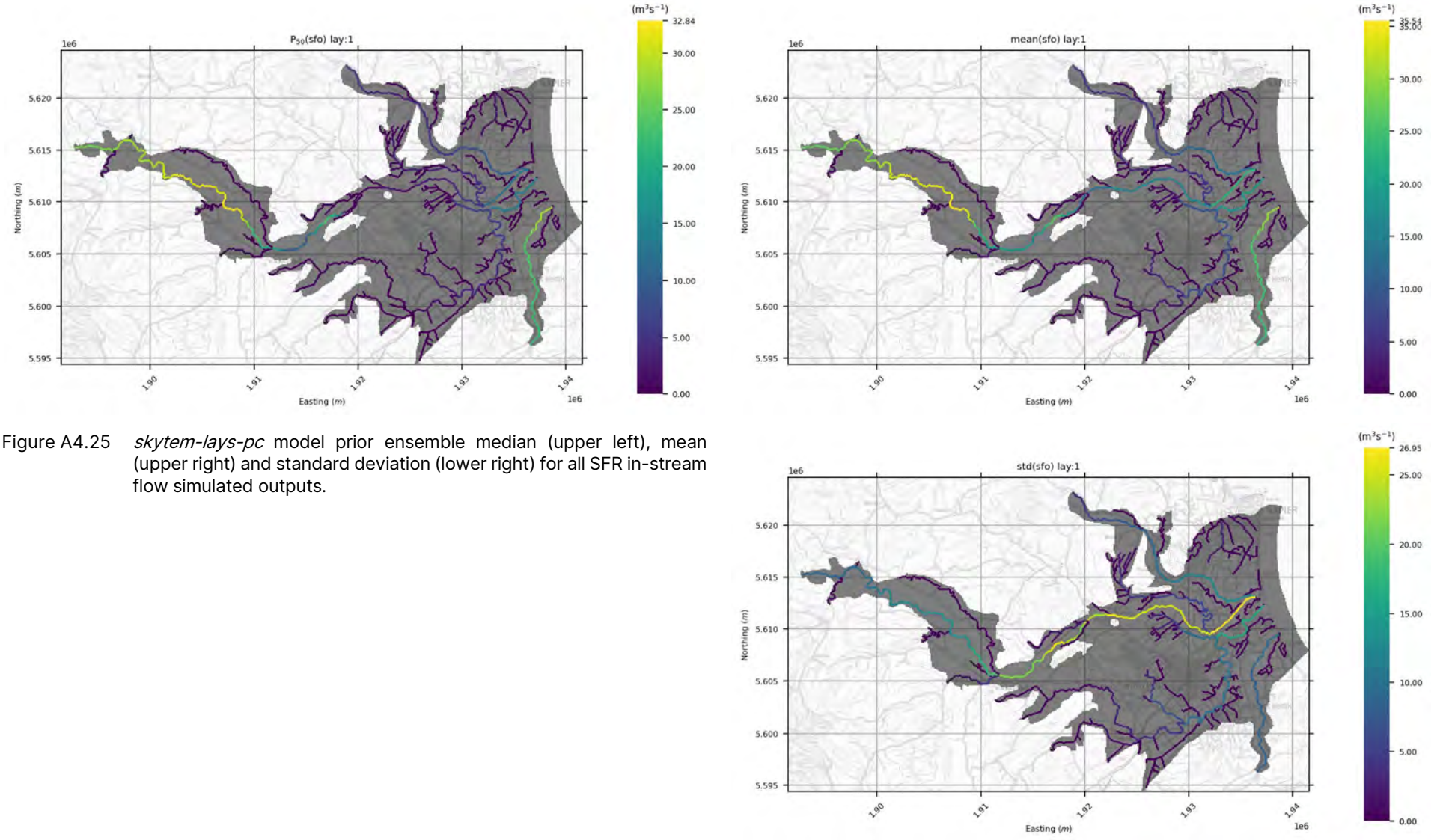

Figure A4.25 *skytem-lays-pc* model prior ensemble median (upper left), mean (upper right) and standard deviation (lower right) for all SFR in-stream flow simulated outputs.

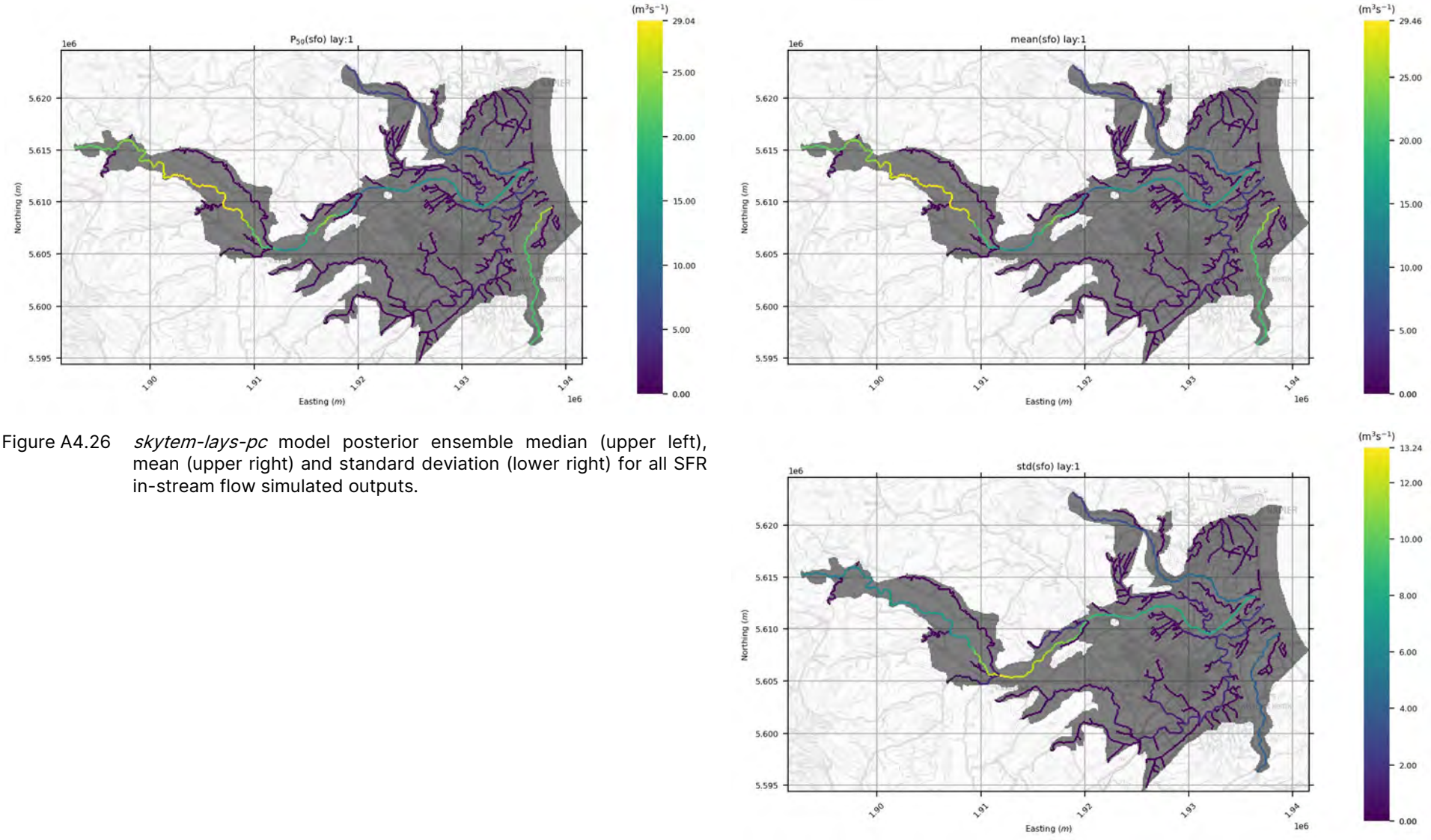

Figure A4.26 *skytem-lays-pc* model posterior ensemble median (upper left), mean (upper right) and standard deviation (lower right) for all SFR in-stream flow simulated outputs.

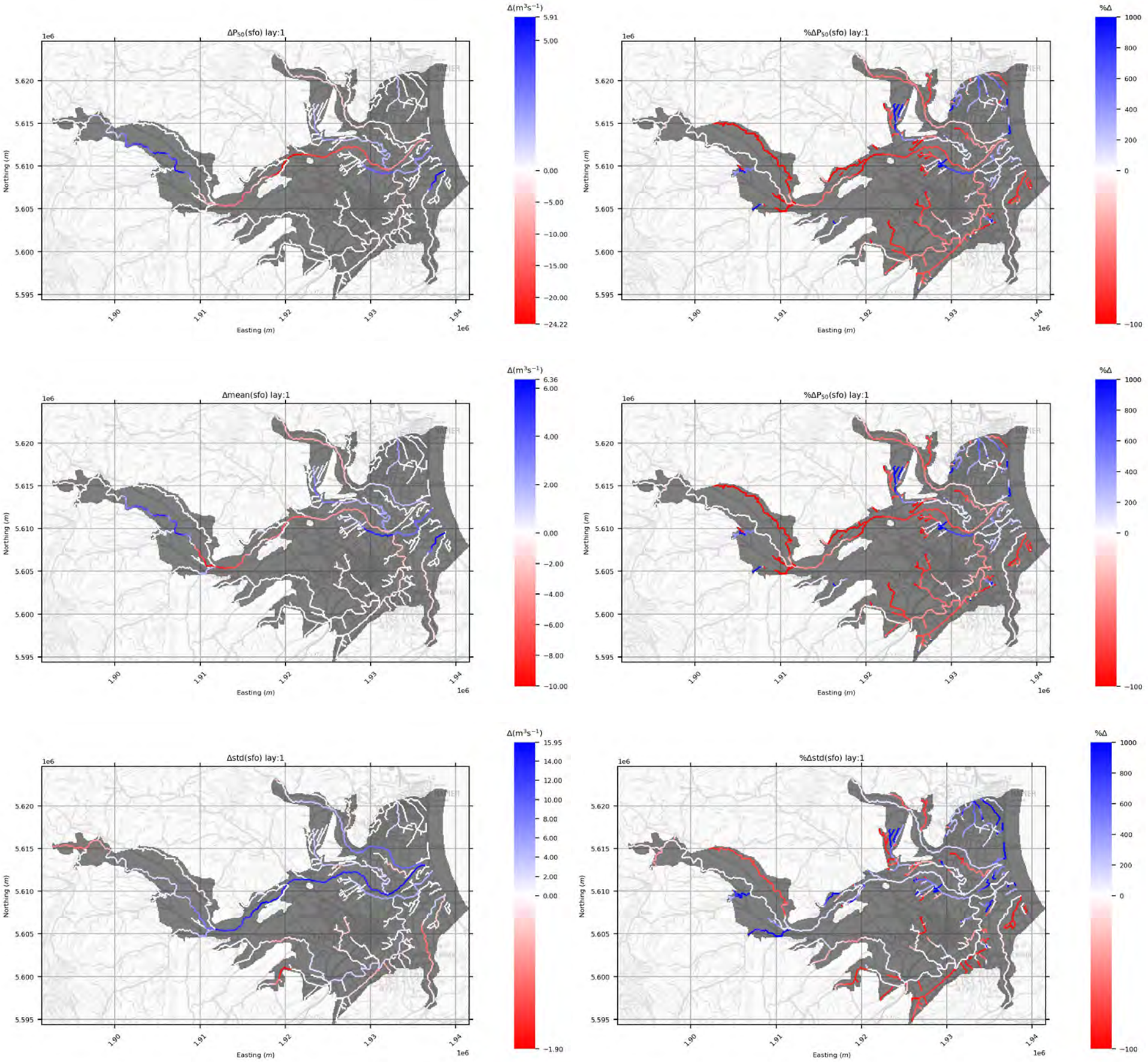

Figure A4.27 Difference (left) and percentage difference (right) between ensemble median (top), mean (middle) and standard deviation (bottom) for the *skytem-lays* model prior, relative to the *geo* prior, for SFR in-stream flow simulated outputs. Note: percent difference colour scales are clipped at +1000%.

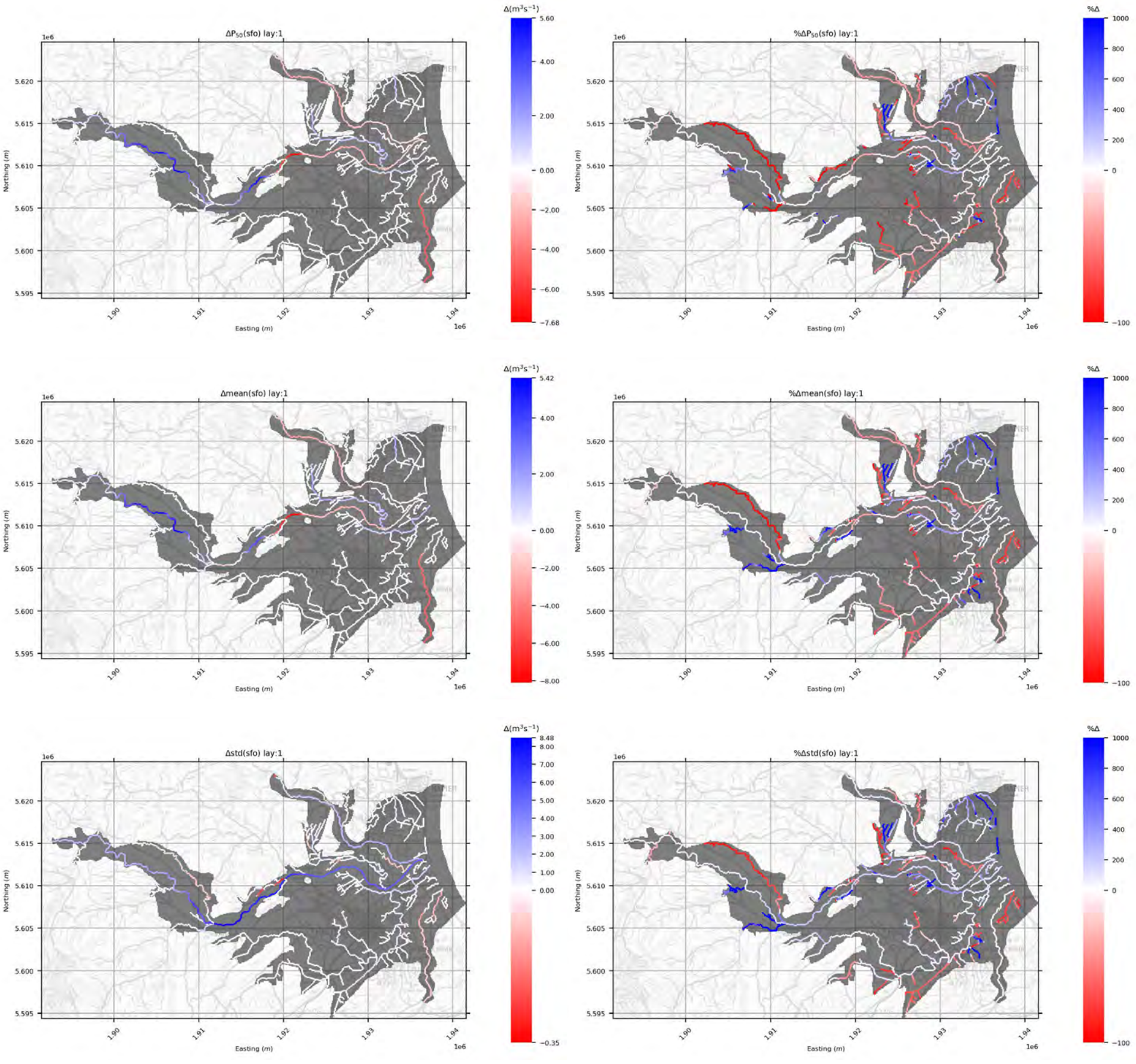

Figure A4.28 Difference (left) and percentage difference (right) between ensemble median (top), mean (middle) and standard deviation (bottom) for the *skytem-lays* model posterior, relative to the *geo* posterior, for SFR in-stream flow simulated outputs. Note: percent difference colour scales are clipped at +1000%.

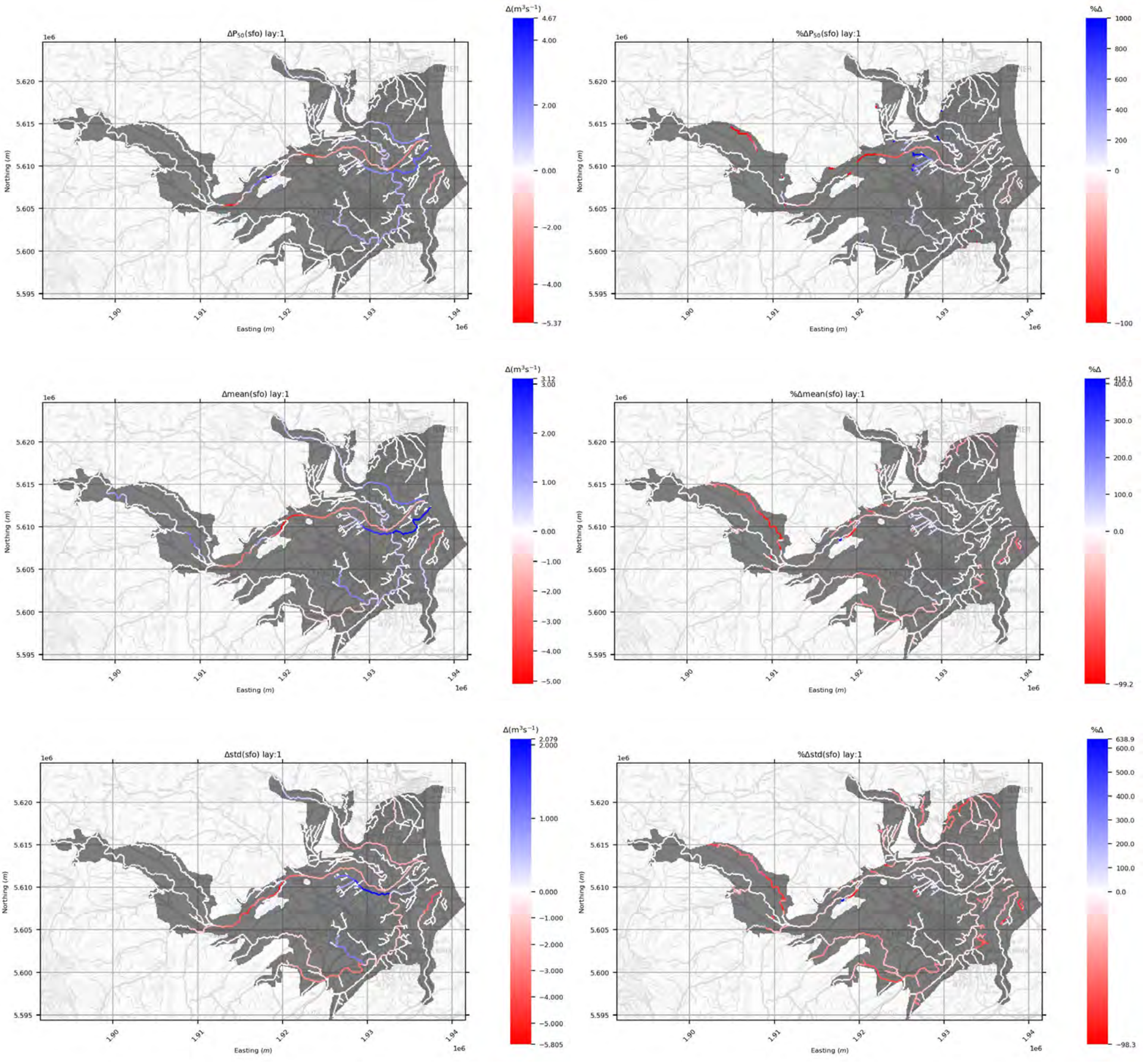

Figure A4.29 Difference (left) and percentage difference (right) between ensemble median (top), mean (middle) and standard deviation (bottom) for the *skytem-lays-pc* model prior, relative to the *skytem-lays* prior, for SFR in-stream flow simulated outputs. Note: percent difference colour scales are clipped at +1000%.

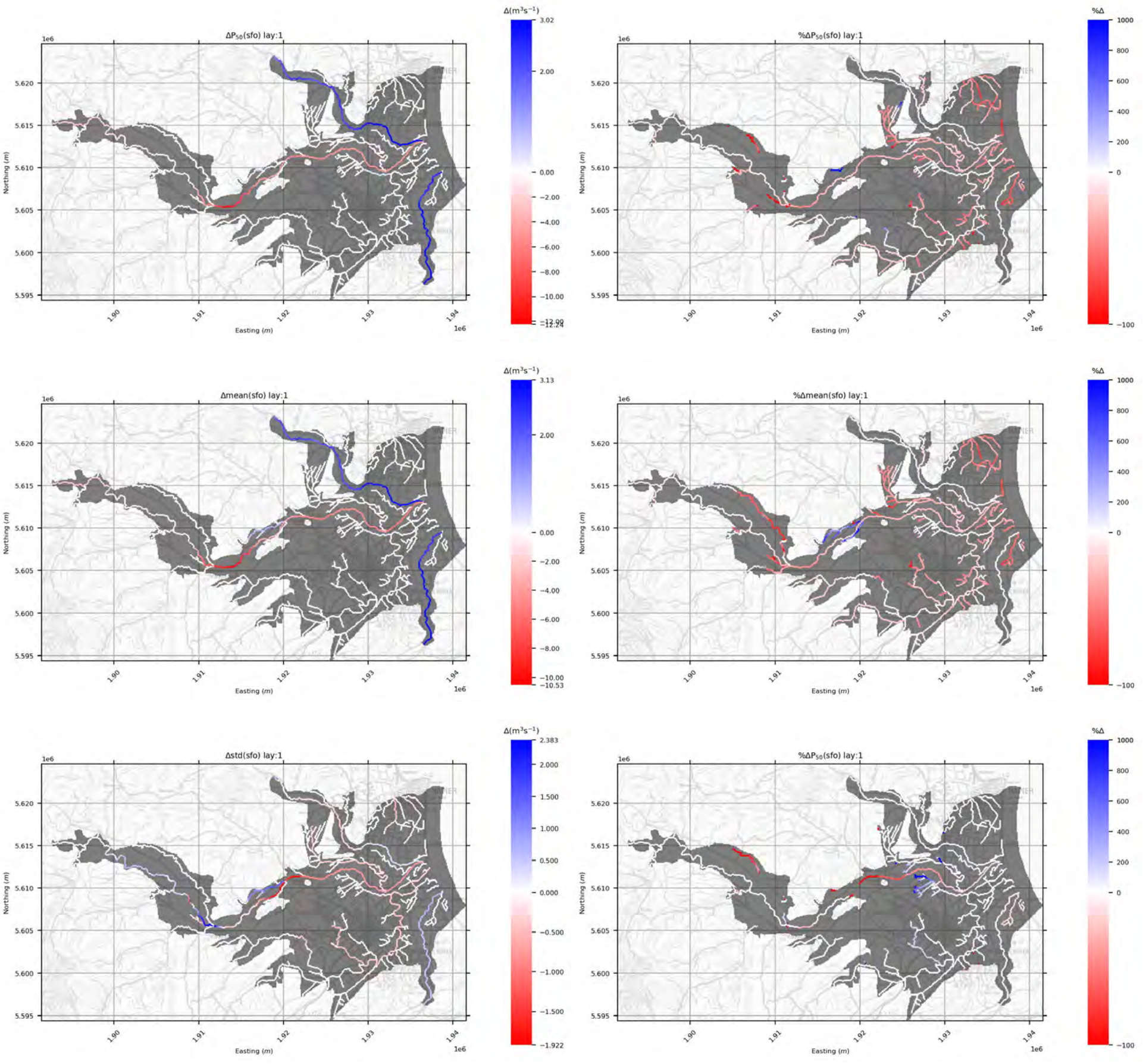

Figure A4.30 Difference (left) and percentage difference (right) between ensemble median (top), mean (middle) and standard deviation (bottom) for the *skytem-lays-pc* model posterior, relative to the *skytem-lays* posterior, for SFR in-stream flow simulated outputs. Note: percent difference colour scales are clipped at +1000%.

A4.2 *skytem-lays* Models

A4.2.1 Wet Scenario

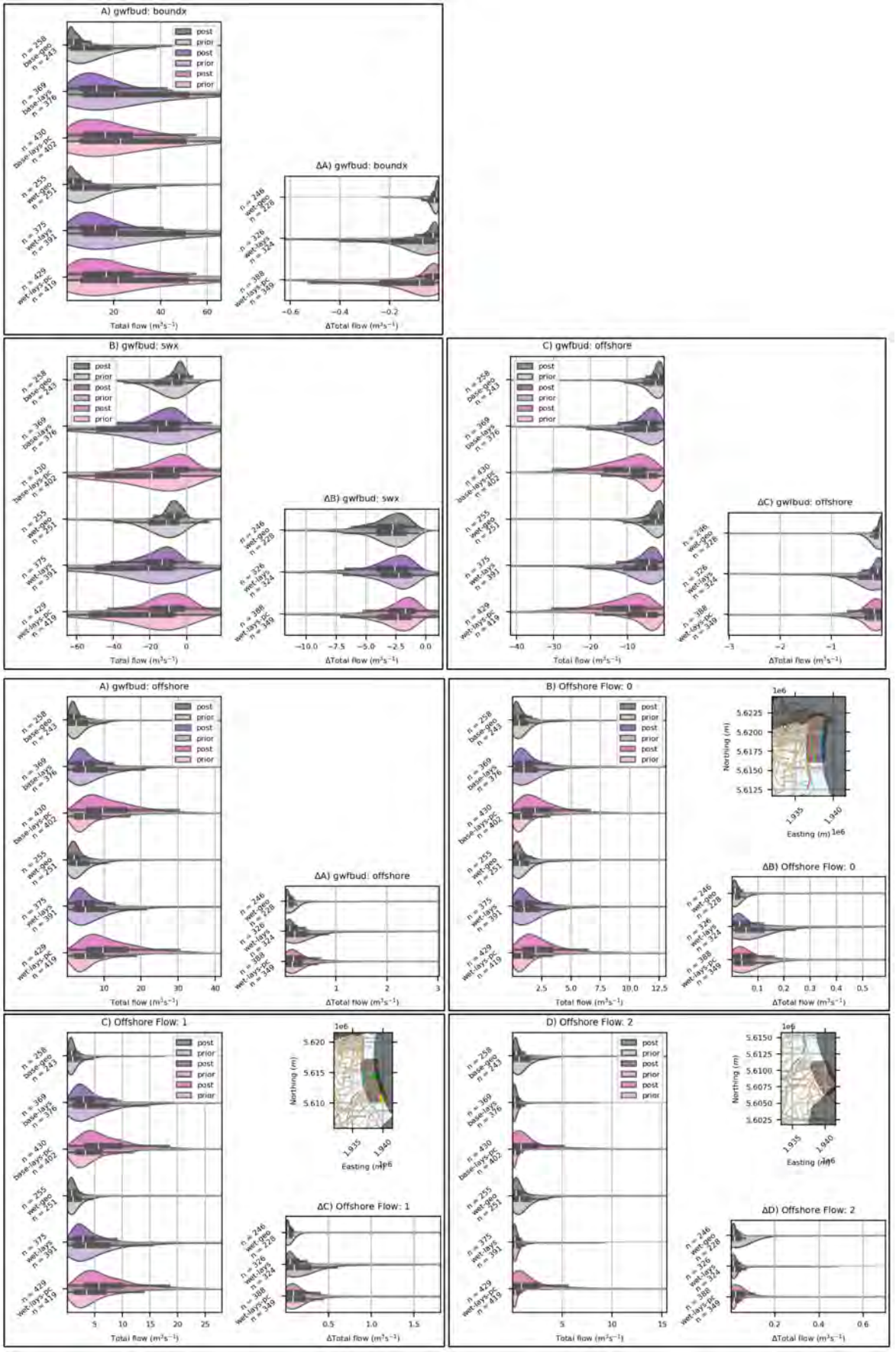

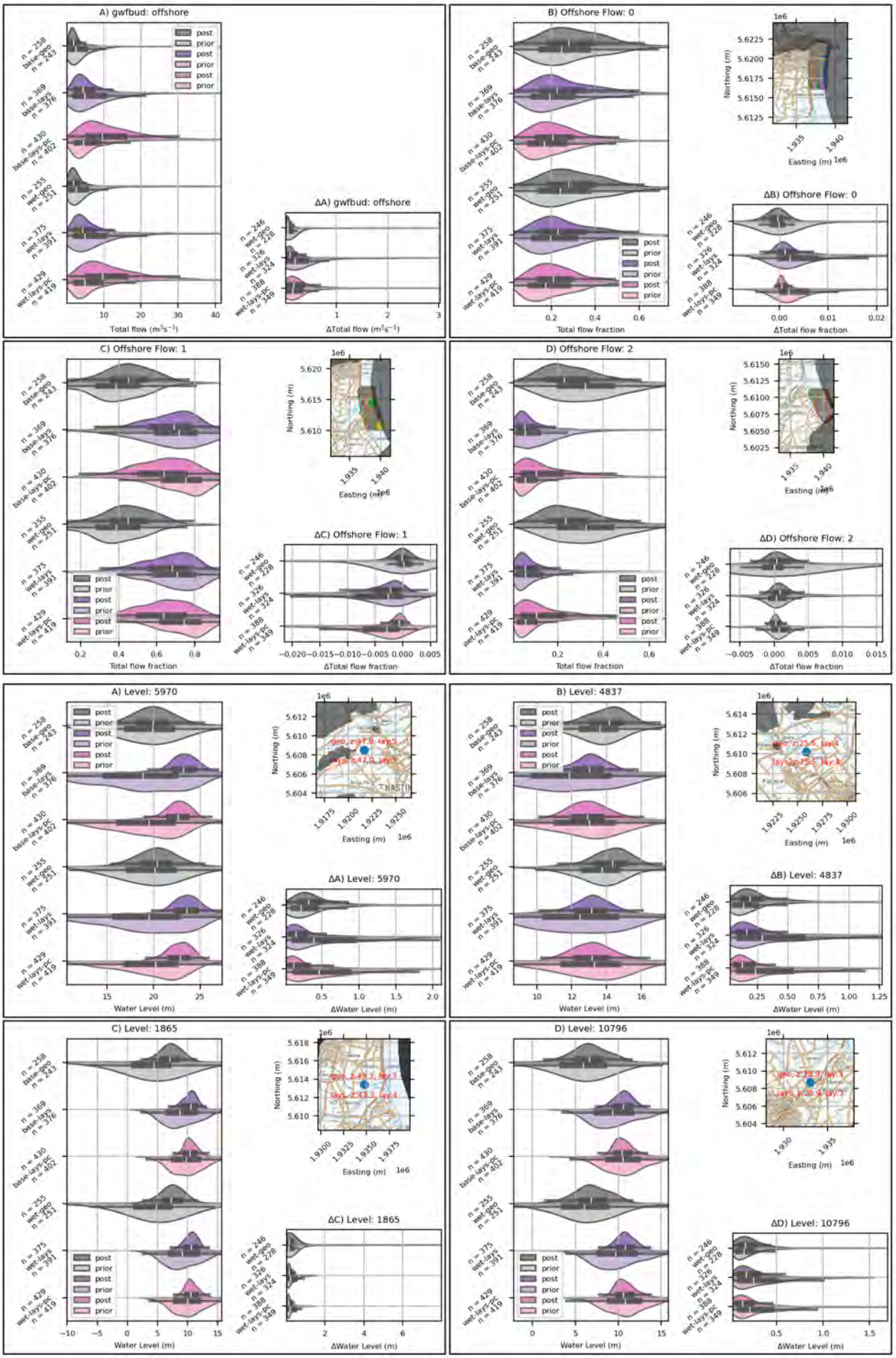
A) gwfbud: offshore
ΔA) gwfbud: offshore
B) Offshore Flow: 0
ΔB) Offshore Flow: 0
C) Offshore Flow: 1
ΔC) Offshore Flow: 1
D) Offshore Flow: 2
ΔD) Offshore Flow: 2
A) Level: 5970
ΔA) Level: 5970
B) Level: 4837
ΔB) Level: 4837
C) Level: 1865
ΔC) Level: 1865
D) Level: 10796
ΔD) Level: 10796
post
prior
Total flow (m³s⁻¹)
ΔTotal flow (m³s⁻¹)
Total flow fraction
ΔTotal flow fraction
Water Level (m)
ΔWater Level (m)
Northing (m)
Easting (m)
1e6

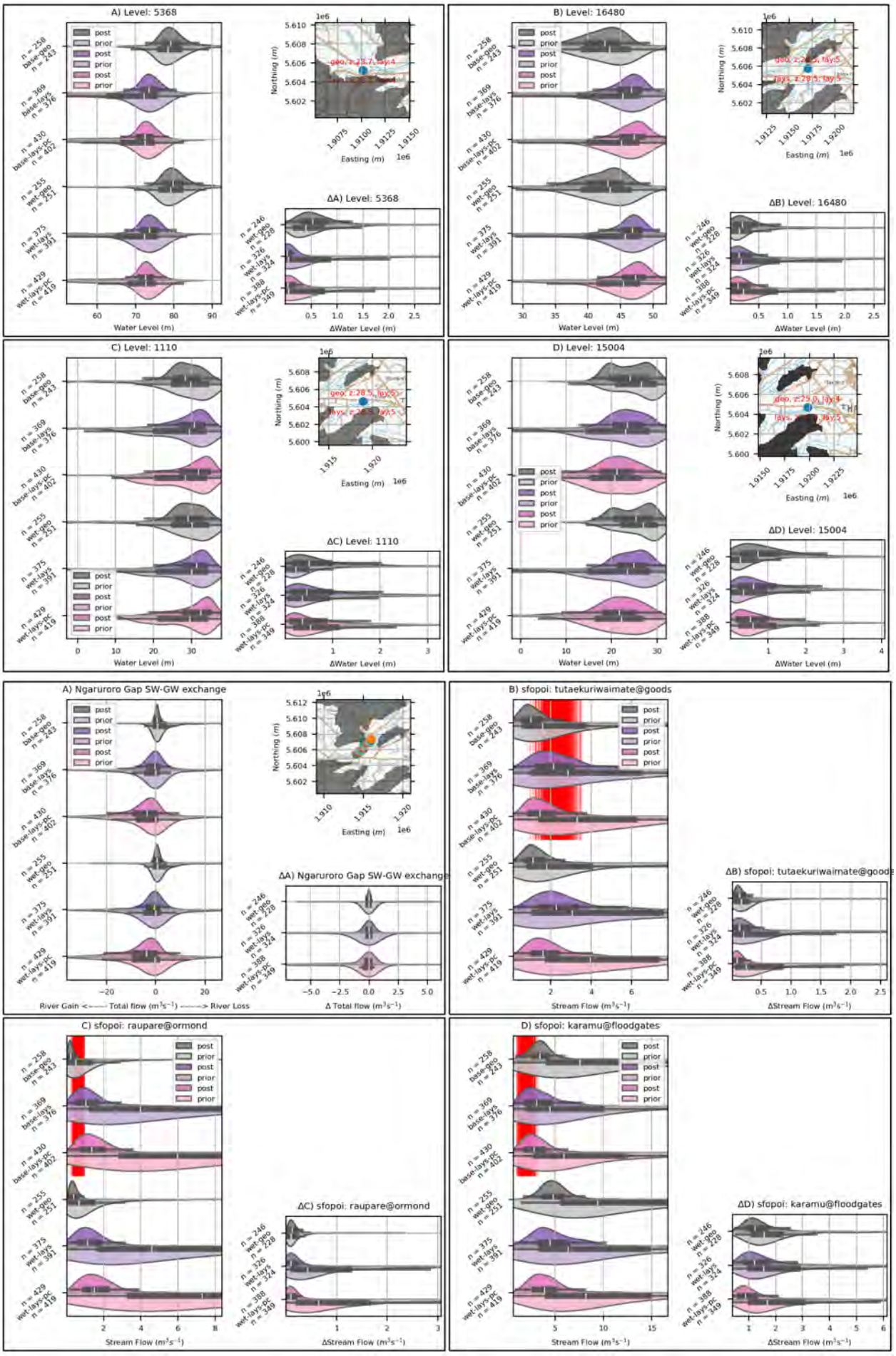
A) Level: 5368
B) Level: 16480
C) Level: 1110
D) Level: 15004
ΔA) Level: 5368
ΔB) Level: 16480
ΔC) Level: 1110
ΔD) Level: 15004
A) Ngaruroro Gap SW-GW exchange
B) sfopoi: tutaekuriwaimate@goods
C) sfopoi: raupare@ormond
D) sfopoi: karamu@floodgates
ΔA) Ngaruroro Gap SW-GW exchange
ΔB) sfopoi: tutaekuriwaimate@goods
ΔC) sfopoi: raupare@ormond
ΔD) sfopoi: karamu@floodgates
post
prior
Water Level (m)
ΔWater Level (m)
Stream Flow (m³s⁻¹)
ΔStream Flow (m³s⁻¹)
Easting (m)
Northing (m)
River Gain <—— Total flow (m³s⁻¹) ——> River Loss
Δ Total flow (m³s⁻¹)

A4.2.2 20% Pumping Increase Scenario

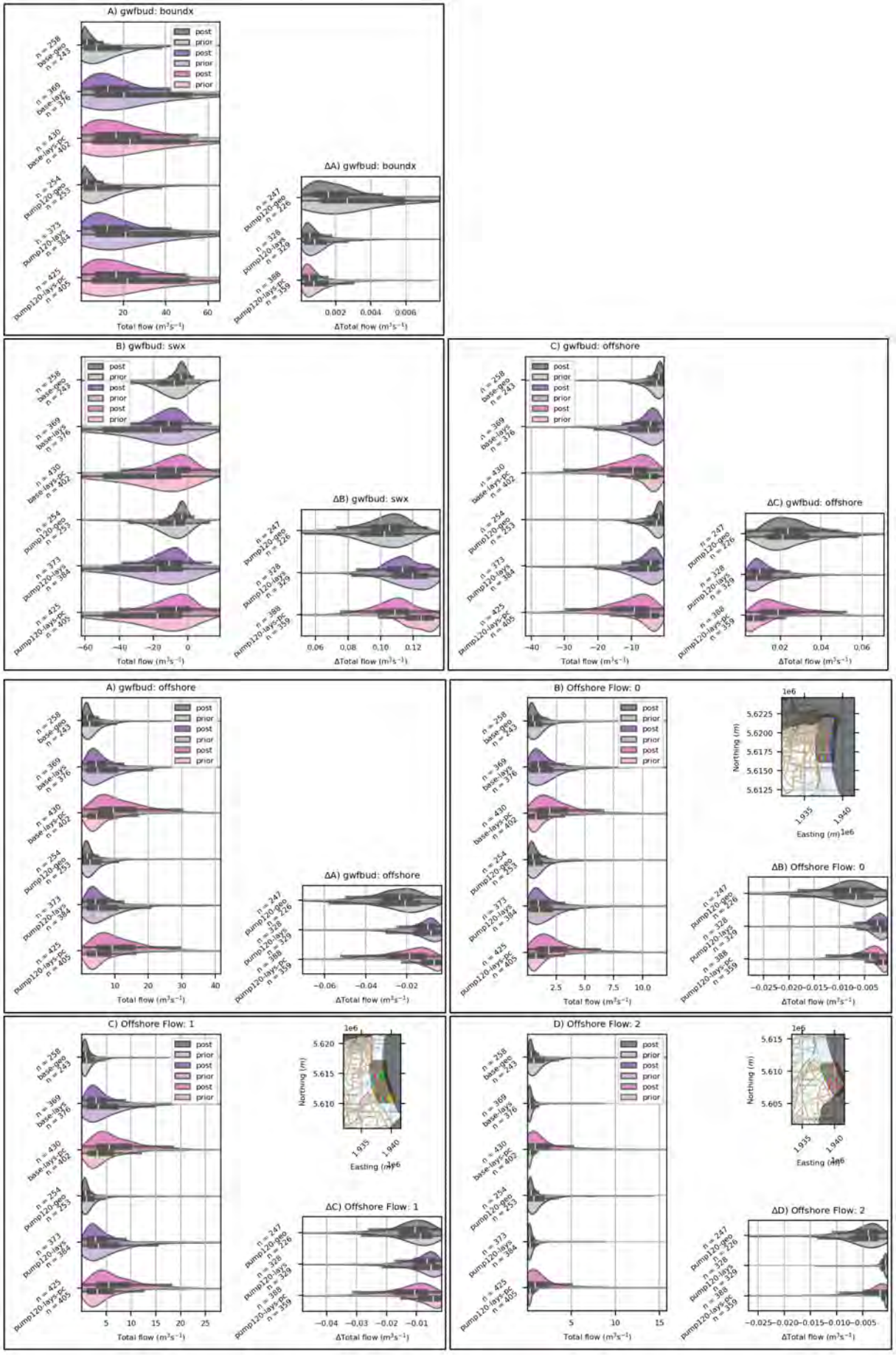

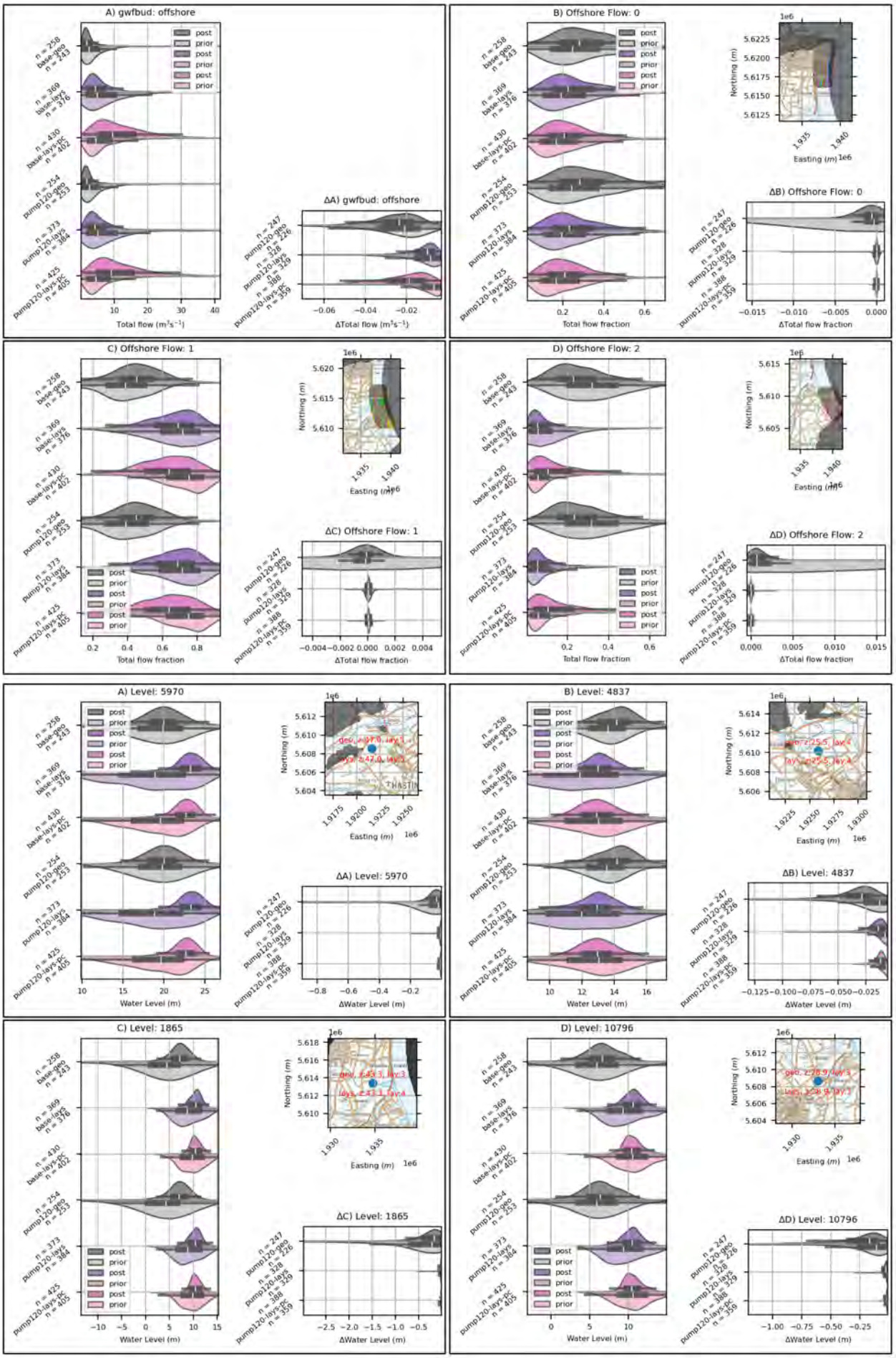
A) gwfbud: offshore
ΔA) gwfbud: offshore
B) Offshore Flow: 0
ΔB) Offshore Flow: 0
C) Offshore Flow: 1
ΔC) Offshore Flow: 1
D) Offshore Flow: 2
ΔD) Offshore Flow: 2
A) Level: 5970
ΔA) Level: 5970
B) Level: 4837
ΔB) Level: 4837
C) Level: 1865
ΔC) Level: 1865
D) Level: 10796
ΔD) Level: 10796
post
prior
Total flow (m³s⁻¹)
ΔTotal flow (m³s⁻¹)
Total flow fraction
ΔTotal flow fraction
Water Level (m)
ΔWater Level (m)
Northing (m)
Easting (m)

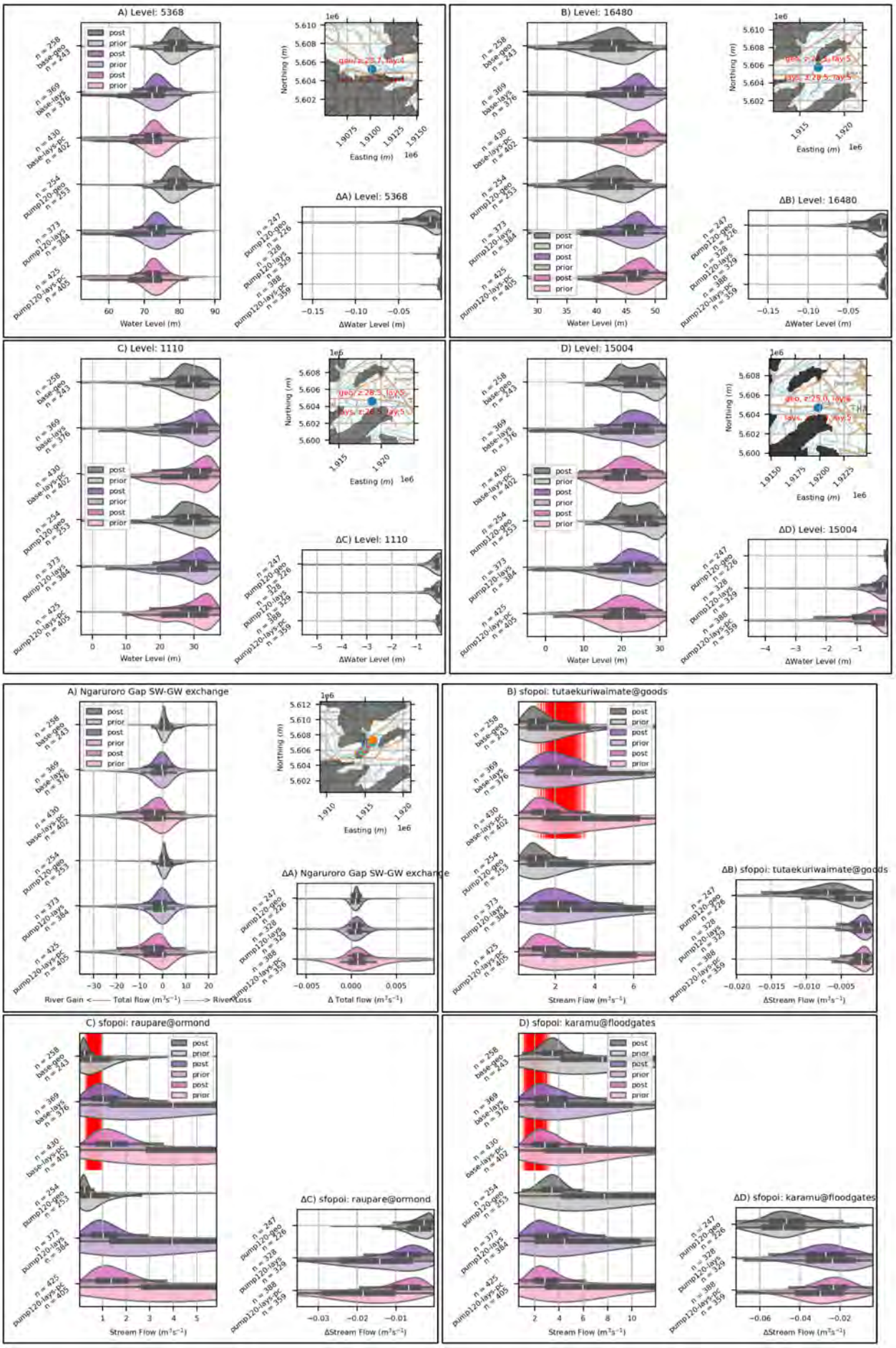
A) Level: 5368
B) Level: 16480
C) Level: 1110
D) Level: 15004
ΔA) Level: 5368
ΔB) Level: 16480
ΔC) Level: 1110
ΔD) Level: 15004
Water Level (m)
ΔWater Level (m)
Easting (m)
Northing (m)
A) Ngaruroro Gap SW-GW exchange
B) sfopoi: tutaekuriwaimate@goods
C) sfopoi: raupare@ormond
D) sfopoi: karamu@floodgates
ΔA) Ngaruroro Gap SW-GW exchange
ΔB) sfopoi: tutaekuriwaimate@goods
ΔC) sfopoi: raupare@ormond
ΔD) sfopoi: karamu@floodgates
River Gain <—— Total flow (m³s⁻¹) ——> River Loss
Δ Total flow (m³s⁻¹)
Stream Flow (m³s⁻¹)
ΔStream Flow (m³s⁻¹)
post
prior

A4.2.3 20% Pumping Decrease Scenario

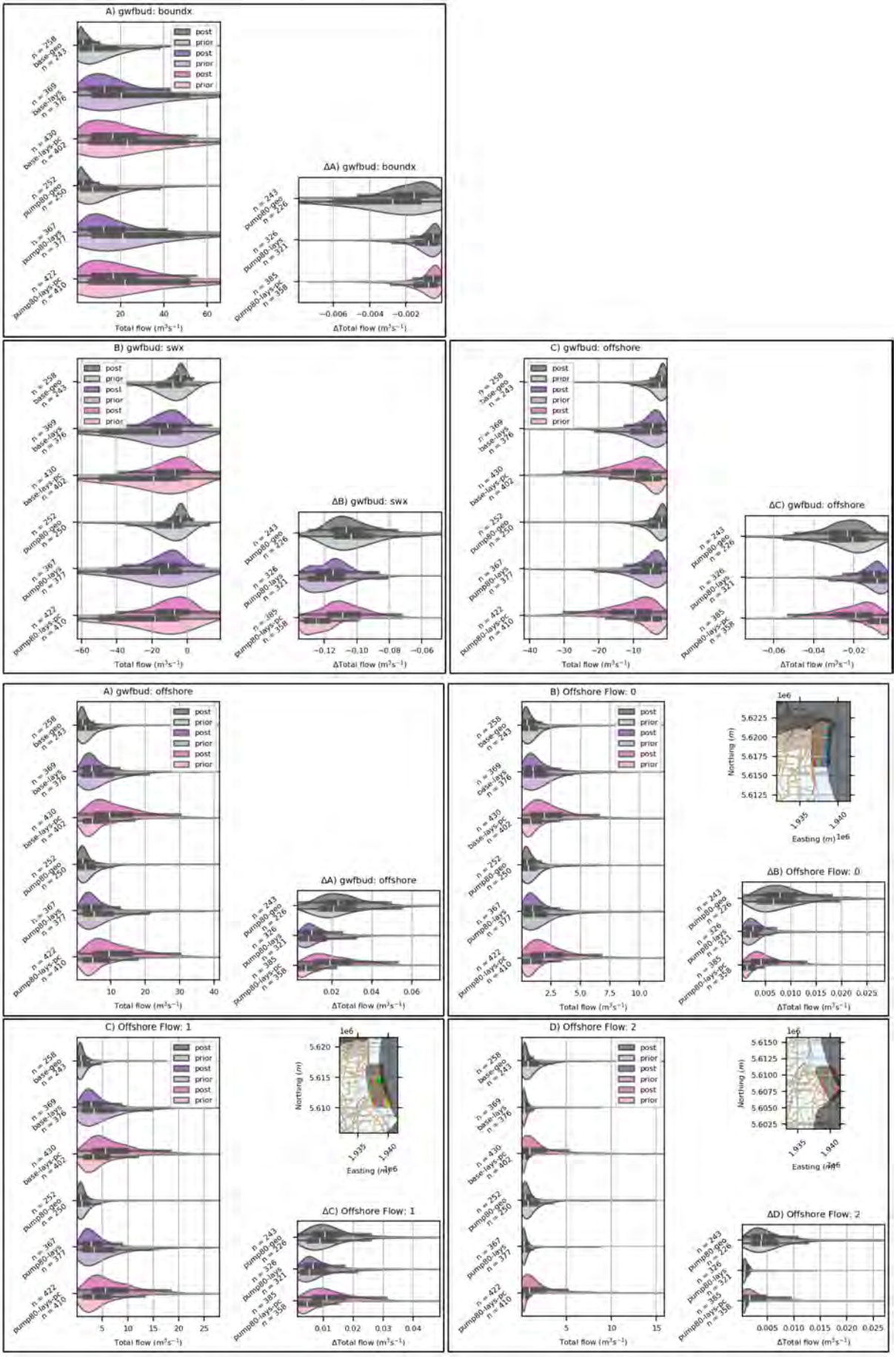

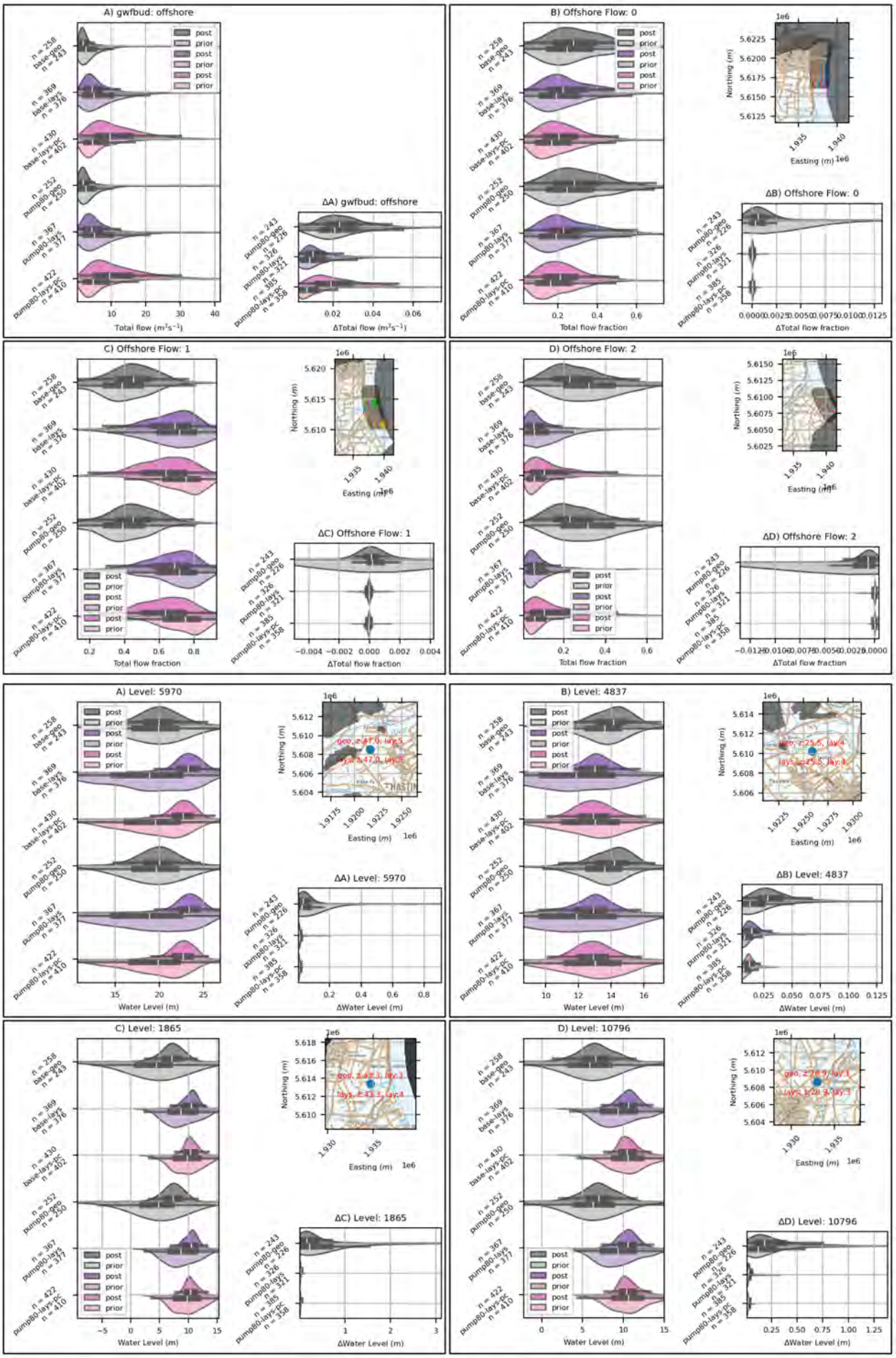
A) gwfbud: offshore
ΔA) gwfbud: offshore
B) Offshore Flow: 0
ΔB) Offshore Flow: 0
C) Offshore Flow: 1
ΔC) Offshore Flow: 1
D) Offshore Flow: 2
ΔD) Offshore Flow: 2
A) Level: 5970
ΔA) Level: 5970
B) Level: 4837
ΔB) Level: 4837
C) Level: 1865
ΔC) Level: 1865
D) Level: 10796
ΔD) Level: 10796
post
prior
Total flow (m³s⁻¹)
ΔTotal flow (m³s⁻¹)
Total flow fraction
ΔTotal flow fraction
Water Level (m)
ΔWater Level (m)
Northing (m)
Easting (m)
1e6

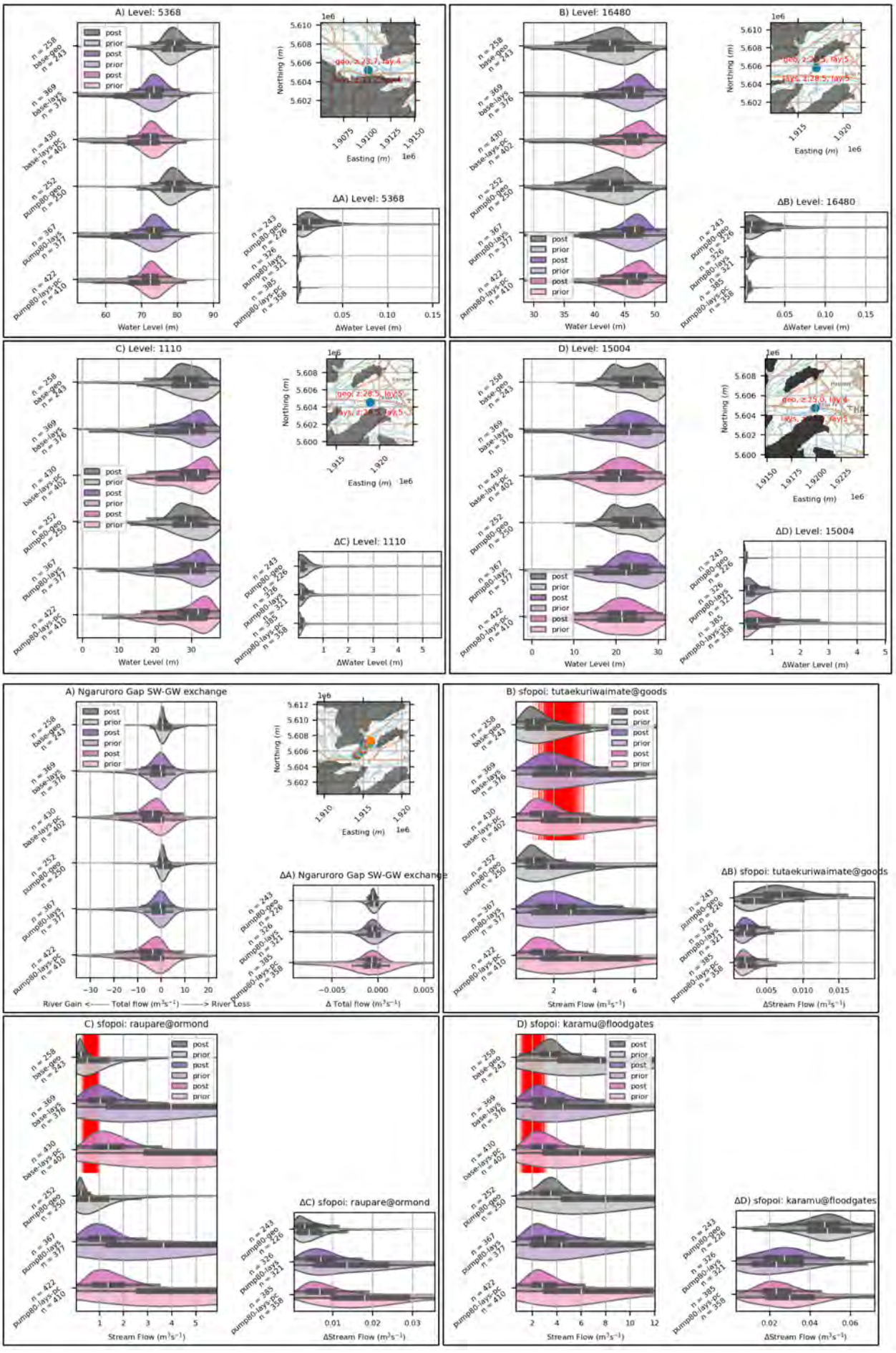
A) Level: 5368
B) Level: 16480
C) Level: 1110
D) Level: 15004
ΔA) Level: 5368
ΔB) Level: 16480
ΔC) Level: 1110
ΔD) Level: 15004
Water Level (m)
ΔWater Level (m)
Northing (m)
Easting (m)
A) Ngaruroro Gap SW-GW exchange
B) sfopoi: tutaekuriwaimate@goods
C) sfopoi: raupare@ormond
D) sfopoi: karamu@floodgates
ΔA) Ngaruroro Gap SW-GW exchange
ΔB) sfopoi: tutaekuriwaimate@goods
ΔC) sfopoi: raupare@ormond
ΔD) sfopoi: karamu@floodgates
River Gain <—— Total flow (m³s⁻¹) ——> River Loss
Δ Total flow (m³s⁻¹)
Stream Flow (m³s⁻¹)
ΔStream Flow (m³s⁻¹)

A4.3 *skytem-k* Models

A4.3.1 Dry Scenario

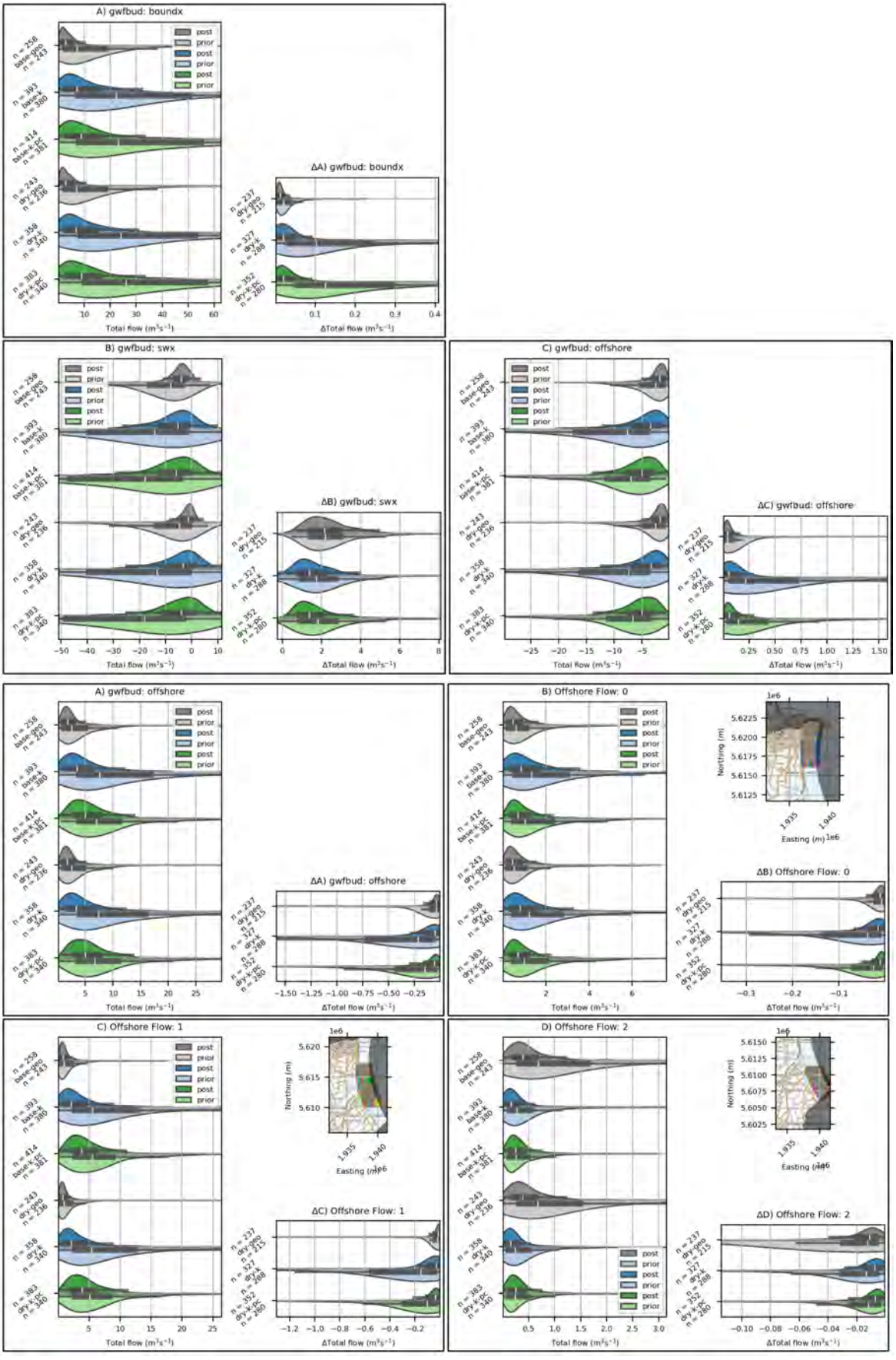

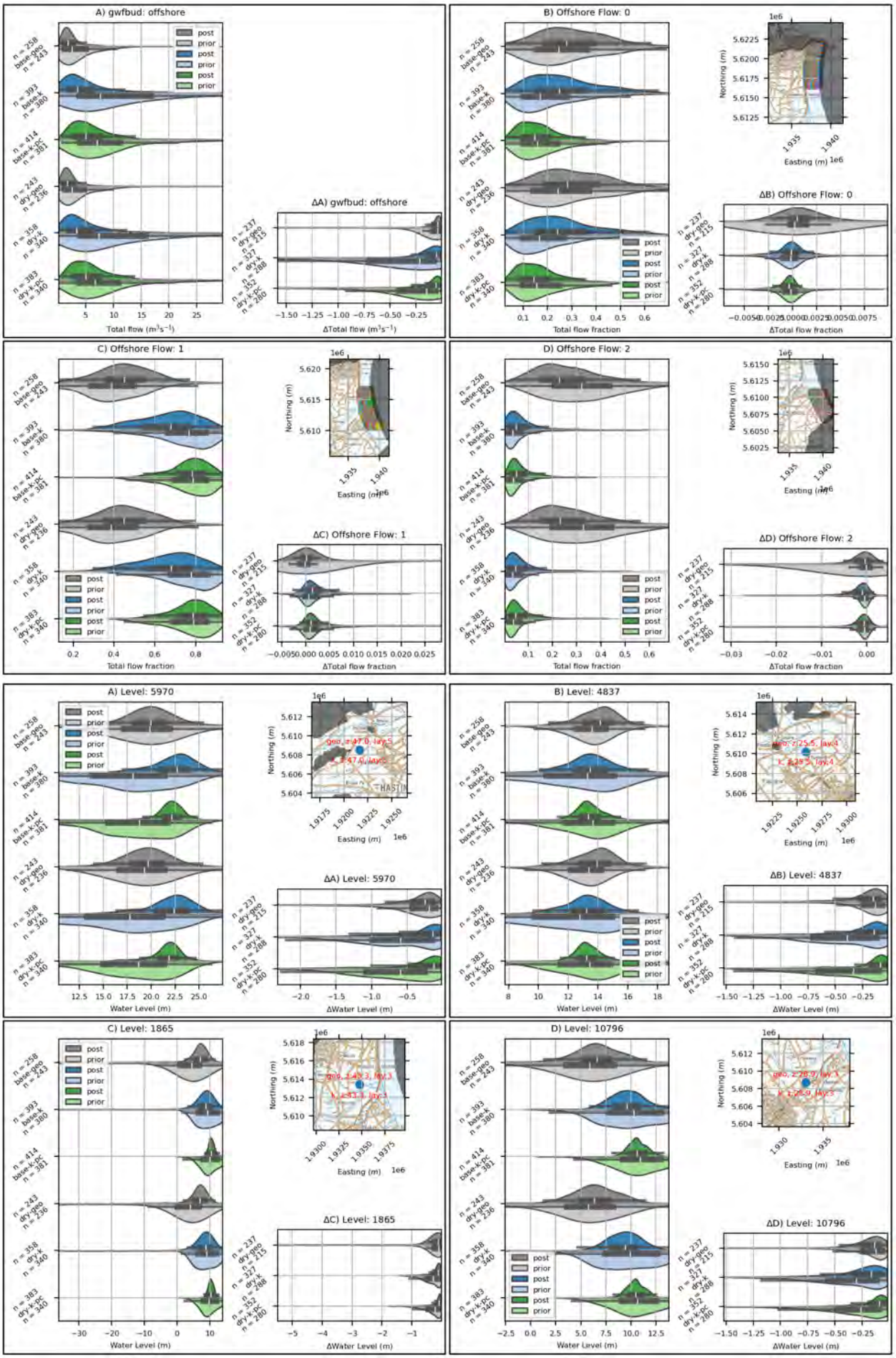
A) gwfbud: offshore
ΔA) gwfbud: offshore
B) Offshore Flow: 0
ΔB) Offshore Flow: 0
C) Offshore Flow: 1
ΔC) Offshore Flow: 1
D) Offshore Flow: 2
ΔD) Offshore Flow: 2
A) Level: 5970
ΔA) Level: 5970
B) Level: 4837
ΔB) Level: 4837
C) Level: 1865
ΔC) Level: 1865
D) Level: 10796
ΔD) Level: 10796
post
prior
Total flow (m³s⁻¹)
ΔTotal flow (m³s⁻¹)
Total flow fraction
ΔTotal flow fraction
Water Level (m)
ΔWater Level (m)
Northing (m)
Easting (m)
1e6

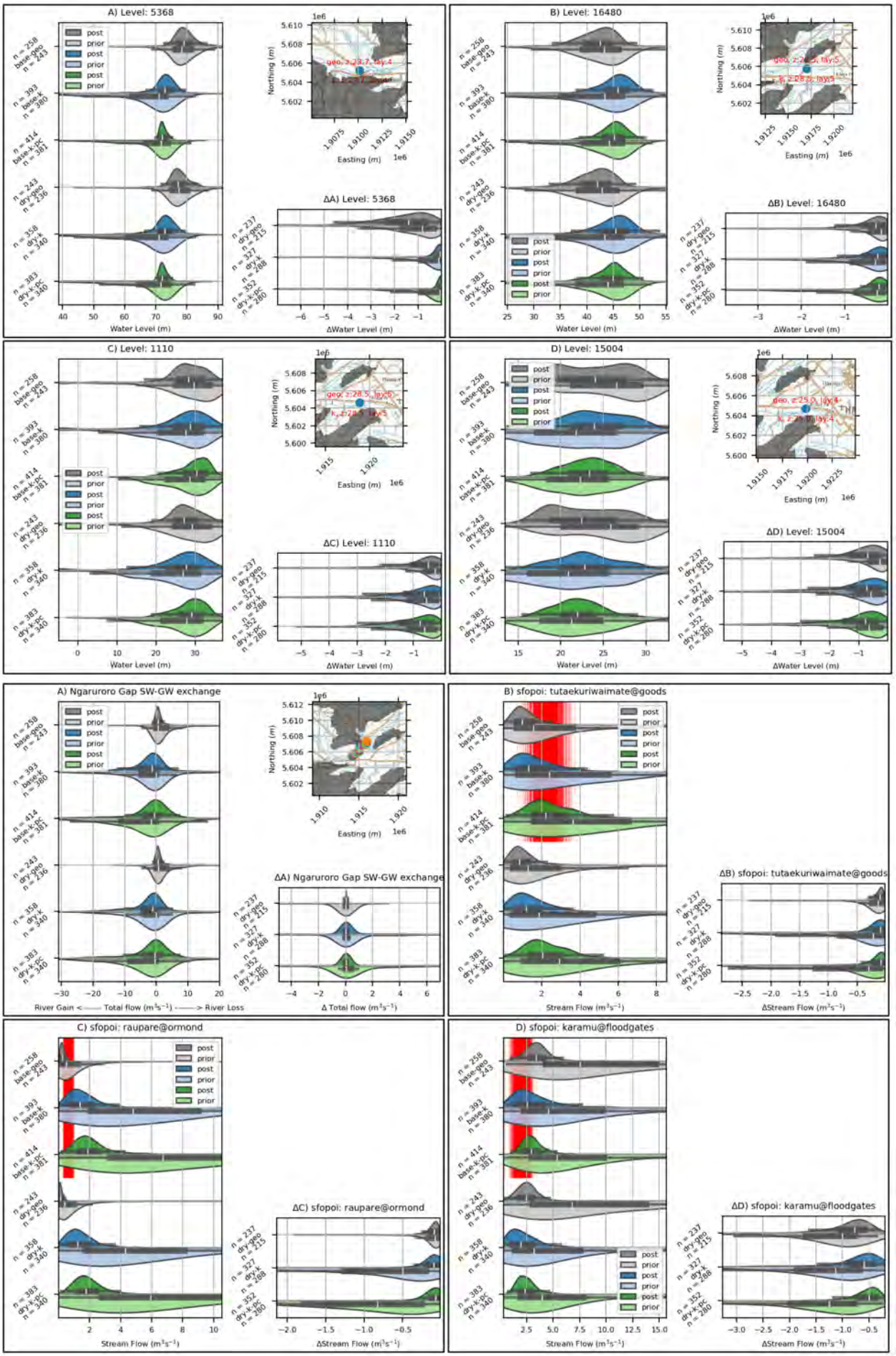
A) Level: 5368
B) Level: 16480
C) Level: 1110
D) Level: 15004
ΔA) Level: 5368
ΔB) Level: 16480
ΔC) Level: 1110
ΔD) Level: 15004
Water Level (m)
ΔWater Level (m)
Easting (m)
Northing (m)
A) Ngaruroro Gap SW-GW exchange
B) sfopoi: tutaekuriwaimate@goods
C) sfopoi: raupare@ormond
D) sfopoi: karamu@floodgates
ΔA) Ngaruroro Gap SW-GW exchange
ΔB) sfopoi: tutaekuriwaimate@goods
ΔC) sfopoi: raupare@ormond
ΔD) sfopoi: karamu@floodgates
River Gain <—— Total flow (m³s⁻¹) ——> River Loss
Δ Total flow (m³s⁻¹)
Stream Flow (m³s⁻¹)
ΔStream Flow (m³s⁻¹)
post
prior

A4.3.2 Wet Scenario

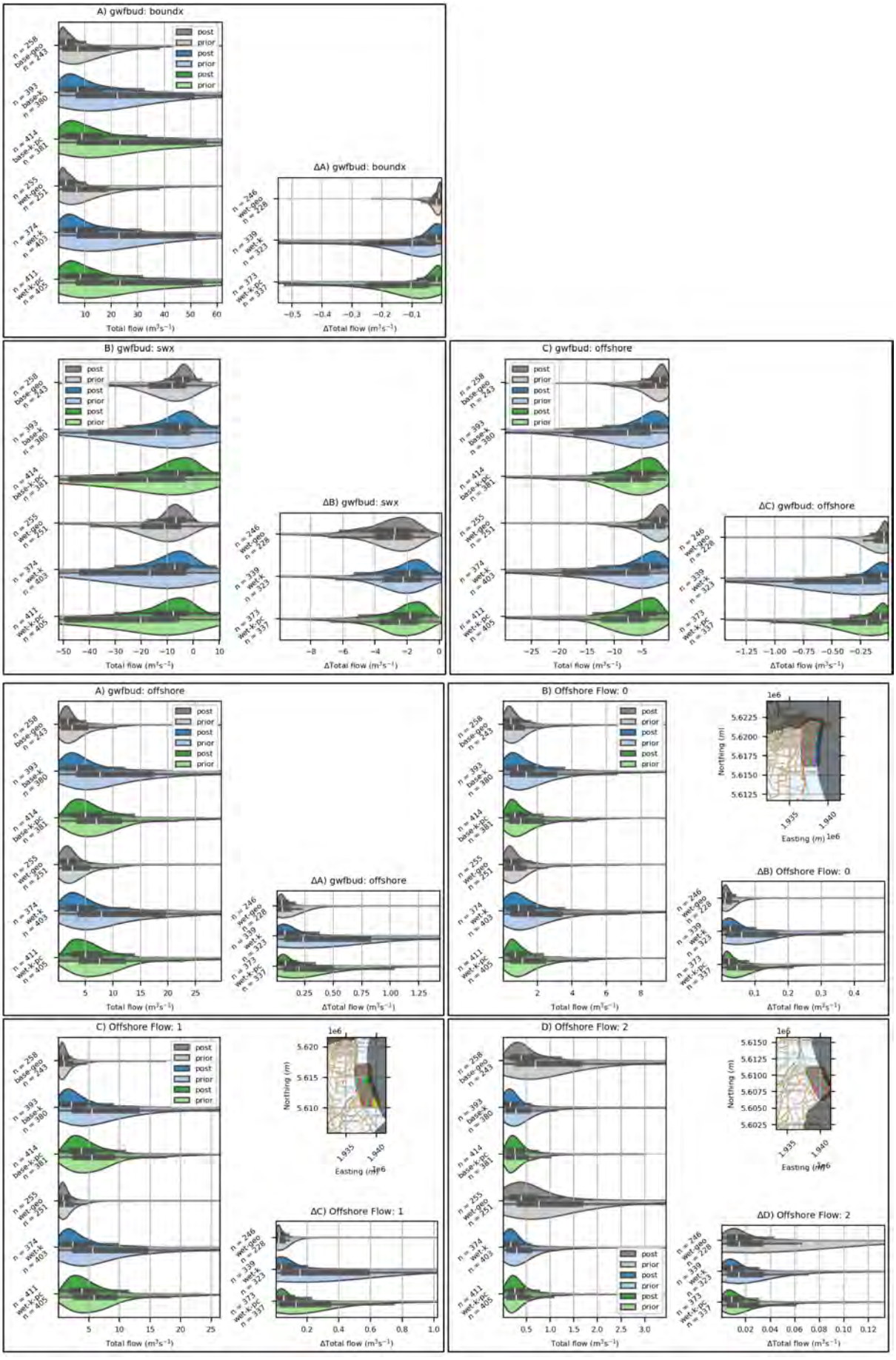

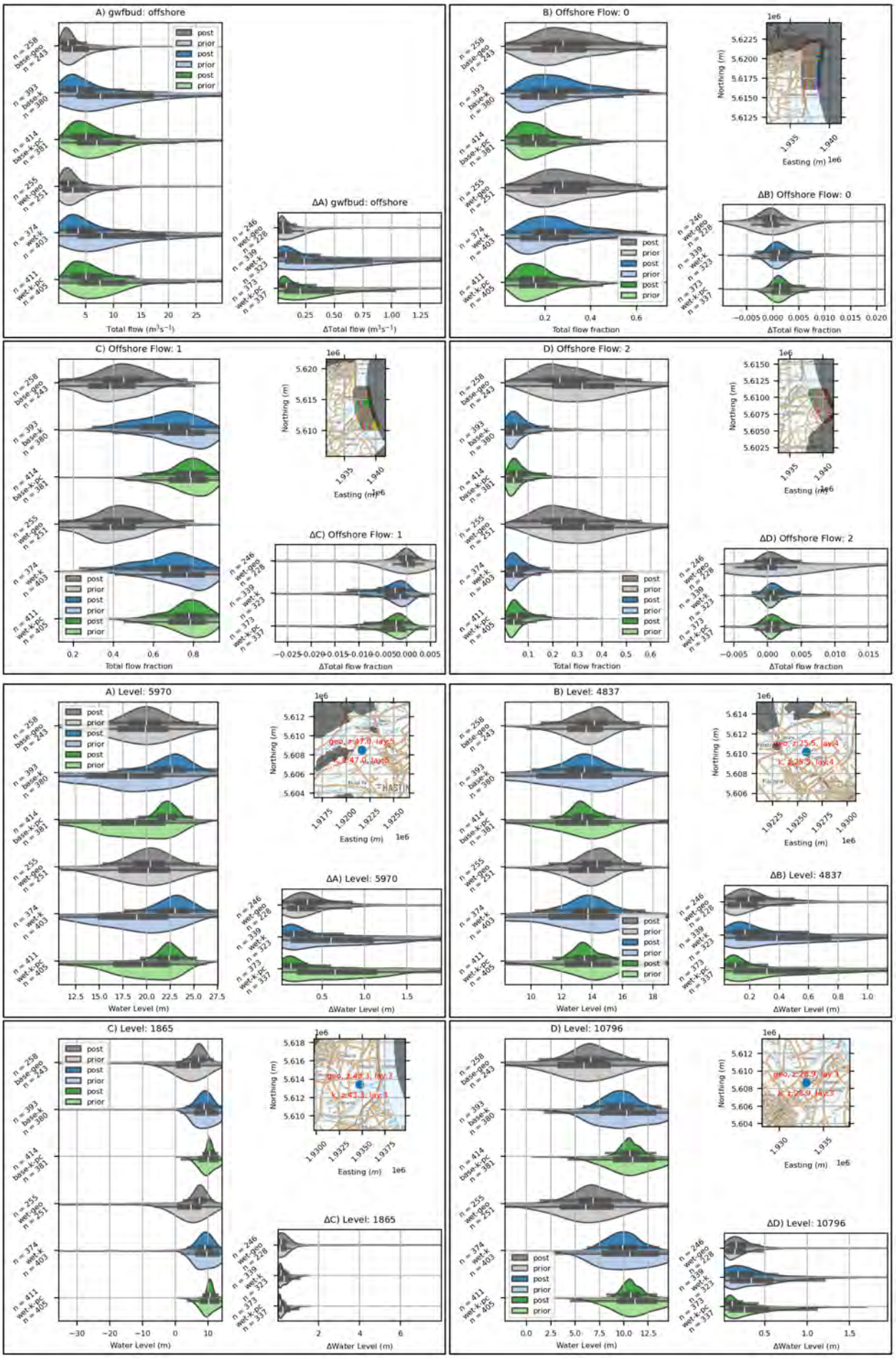
A) gwfbud: offshore
ΔA) gwfbud: offshore
B) Offshore Flow: 0
ΔB) Offshore Flow: 0
C) Offshore Flow: 1
ΔC) Offshore Flow: 1
D) Offshore Flow: 2
ΔD) Offshore Flow: 2
A) Level: 5970
ΔA) Level: 5970
B) Level: 4837
ΔB) Level: 4837
C) Level: 1865
ΔC) Level: 1865
D) Level: 10796
ΔD) Level: 10796
post
prior
Total flow (m³s⁻¹)
ΔTotal flow (m³s⁻¹)
Total flow fraction
ΔTotal flow fraction
Water Level (m)
ΔWater Level (m)
Northing (m)
Easting (m)
1e6

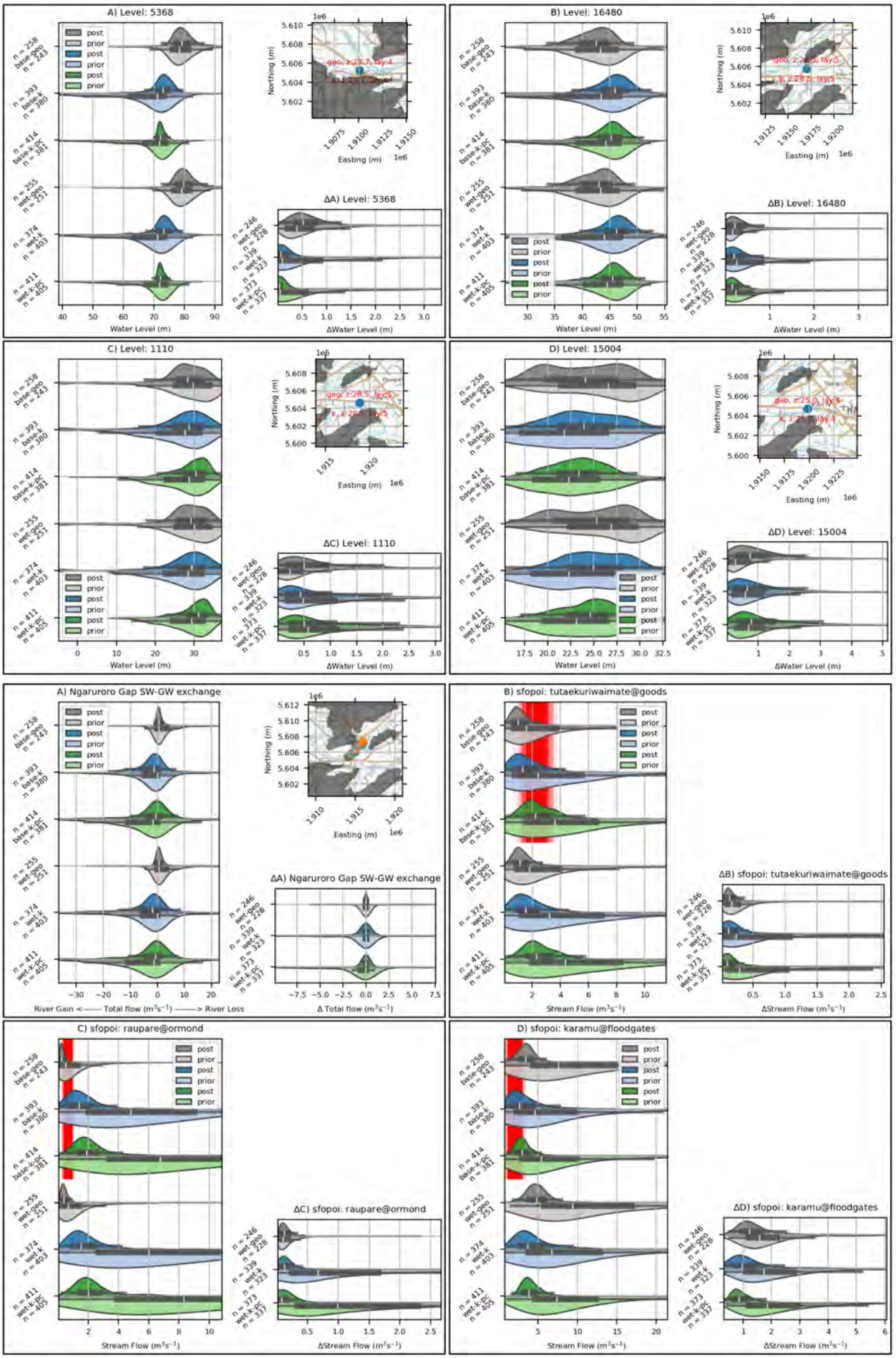
A) Level: 5368
B) Level: 16480
C) Level: 1110
D) Level: 15004
ΔA) Level: 5368
ΔB) Level: 16480
ΔC) Level: 1110
ΔD) Level: 15004
Water Level (m)
ΔWater Level (m)
Easting (m)
Northing (m)
A) Ngaruroro Gap SW-GW exchange
B) sfopoi: tutaekuriwaimate@goods
C) sfopoi: raupare@ormond
D) sfopoi: karamu@floodgates
ΔA) Ngaruroro Gap SW-GW exchange
ΔB) sfopoi: tutaekuriwaimate@goods
ΔC) sfopoi: raupare@ormond
ΔD) sfopoi: karamu@floodgates
River Gain <—— Total flow (m³s⁻¹) ——> River Loss
Δ Total flow (m³s⁻¹)
Stream Flow (m³s⁻¹)
ΔStream Flow (m³s⁻¹)
post
prior

A4.3.3 20% Increase in Pumping

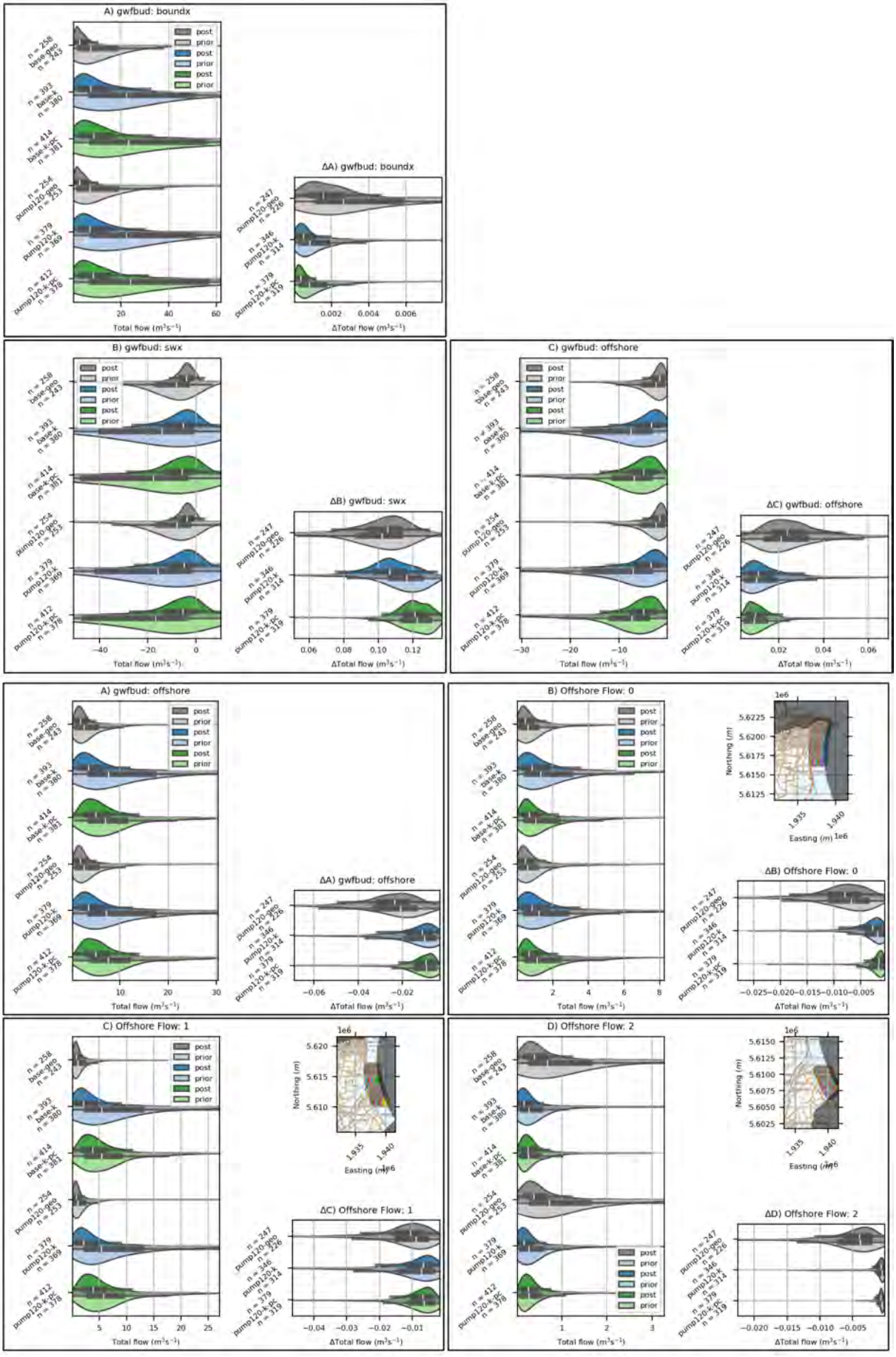

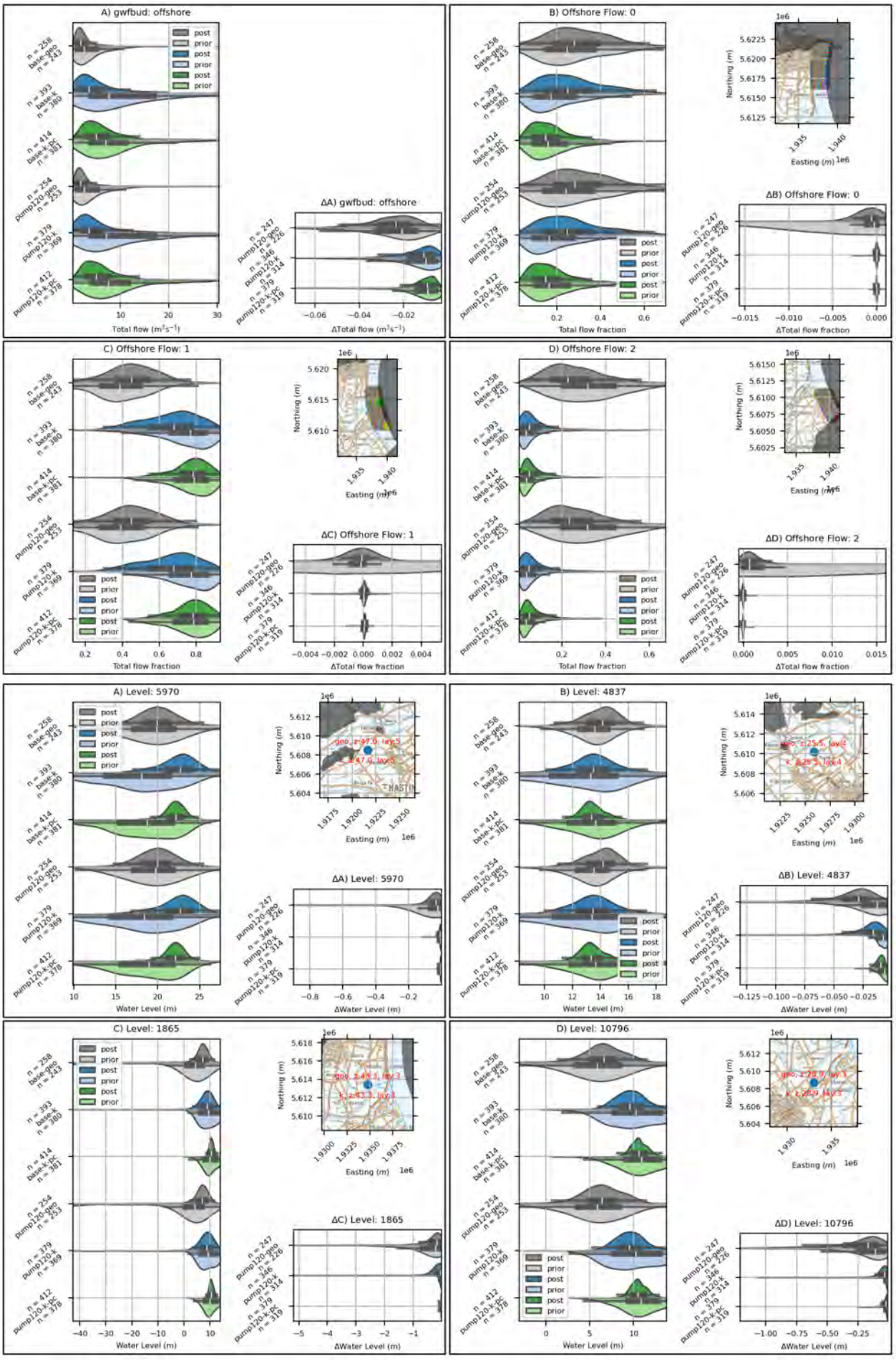
A) gwfbud: offshore
ΔA) gwfbud: offshore
B) Offshore Flow: 0
ΔB) Offshore Flow: 0
C) Offshore Flow: 1
ΔC) Offshore Flow: 1
D) Offshore Flow: 2
ΔD) Offshore Flow: 2
A) Level: 5970
ΔA) Level: 5970
B) Level: 4837
ΔB) Level: 4837
C) Level: 1865
ΔC) Level: 1865
D) Level: 10796
ΔD) Level: 10796
Total flow (m³s⁻¹)
ΔTotal flow (m³s⁻¹)
Total flow fraction
ΔTotal flow fraction
Water Level (m)
ΔWater Level (m)
Northing (m)
Easting (m)
post
prior

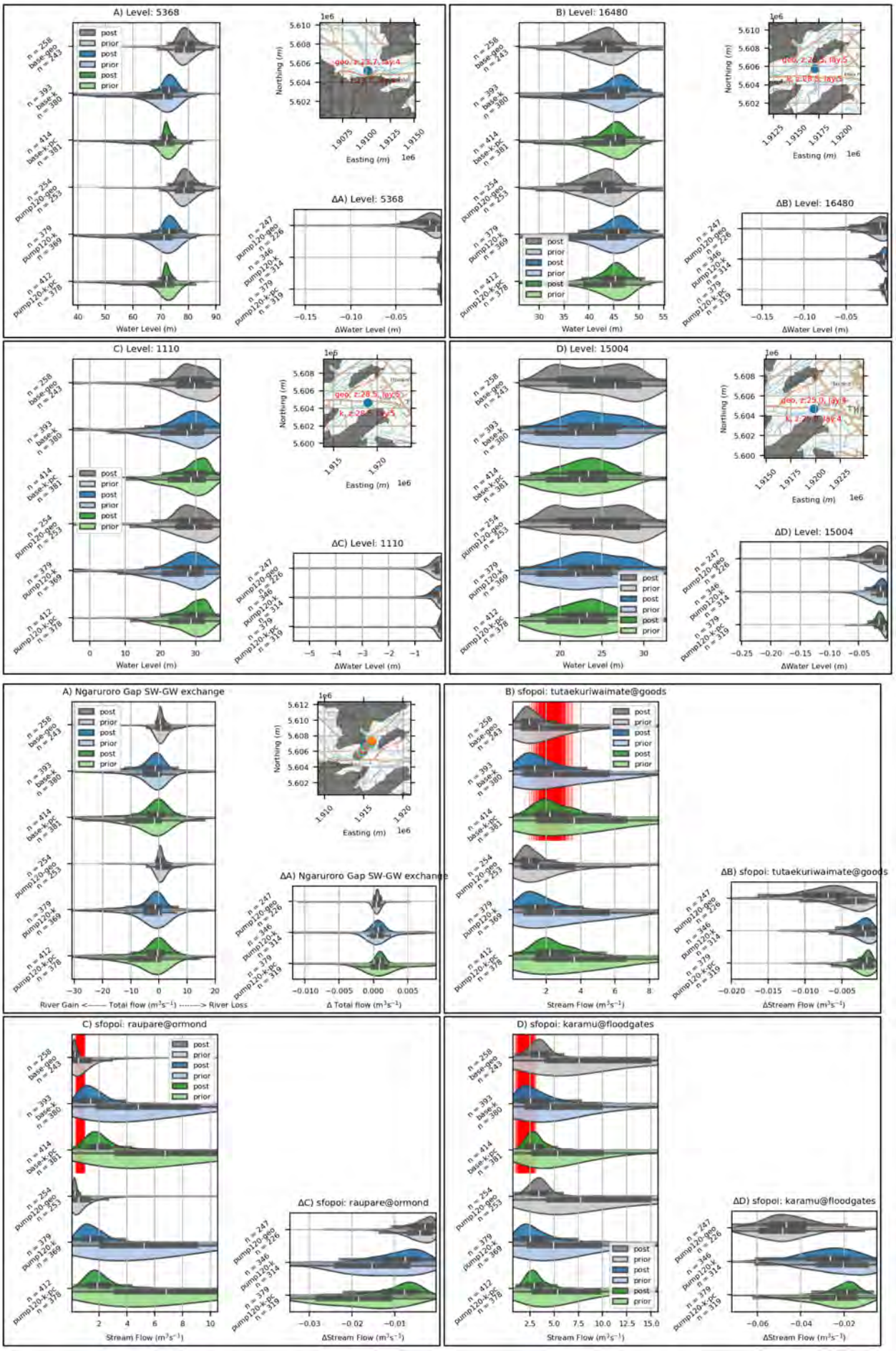
A) Level: 5368
B) Level: 16480
C) Level: 1110
D) Level: 15004
ΔA) Level: 5368
ΔB) Level: 16480
ΔC) Level: 1110
ΔD) Level: 15004
Water Level (m)
ΔWater Level (m)
Northing (m)
Easting (m)
A) Ngaruroro Gap SW-GW exchange
B) sfopoi: tutaekuriwaimate@goods
C) sfopoi: raupare@ormond
D) sfopoi: karamu@floodgates
ΔA) Ngaruroro Gap SW-GW exchange
ΔB) sfopoi: tutaekuriwaimate@goods
ΔC) sfopoi: raupare@ormond
ΔD) sfopoi: karamu@floodgates
River Gain <—— Total flow (m³s⁻¹) ——> River Loss
Δ Total flow (m³s⁻¹)
Stream Flow (m³s⁻¹)
ΔStream Flow (m³s⁻¹)

A4.3.4 20% Decrease in Pumping

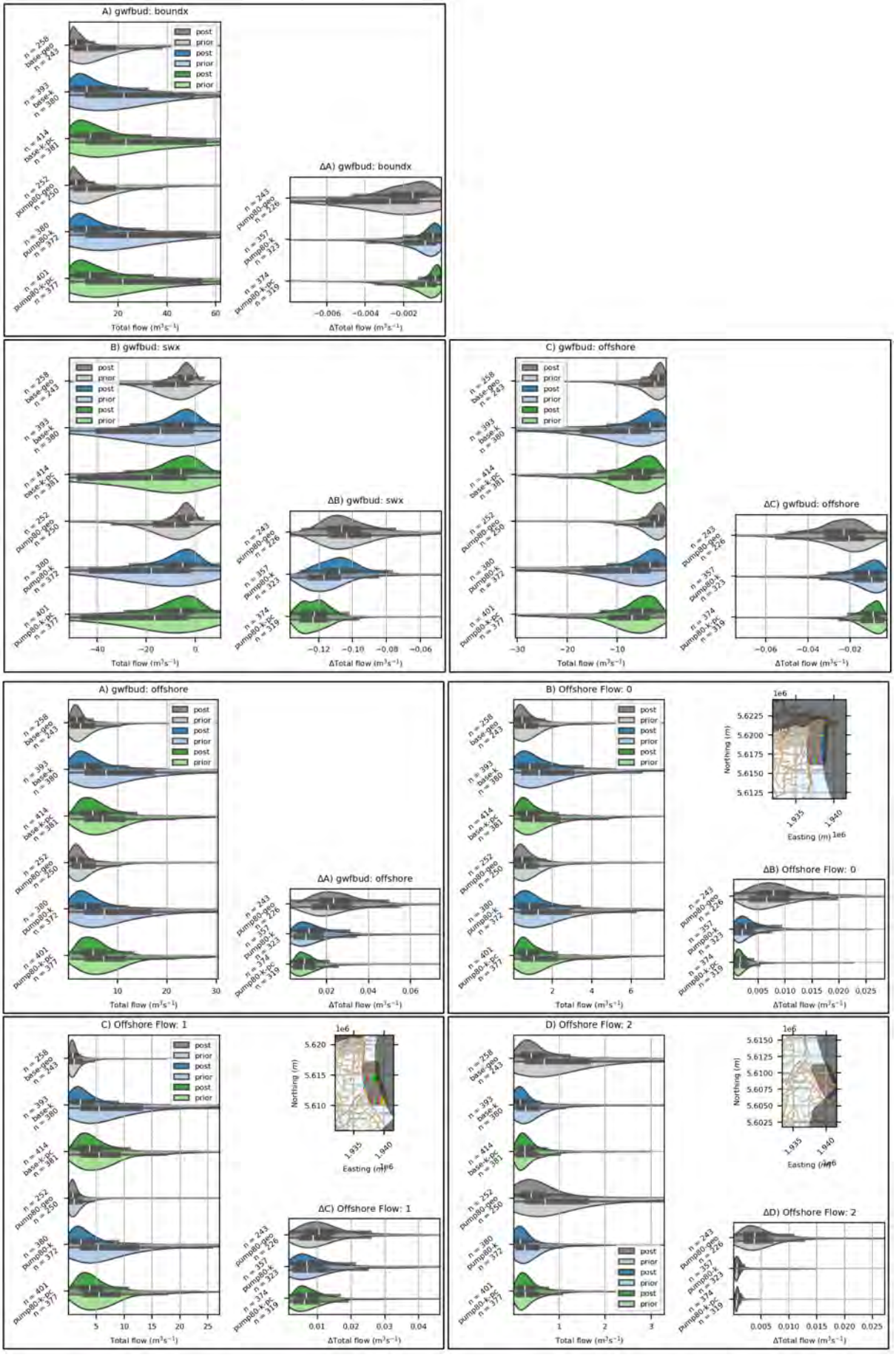

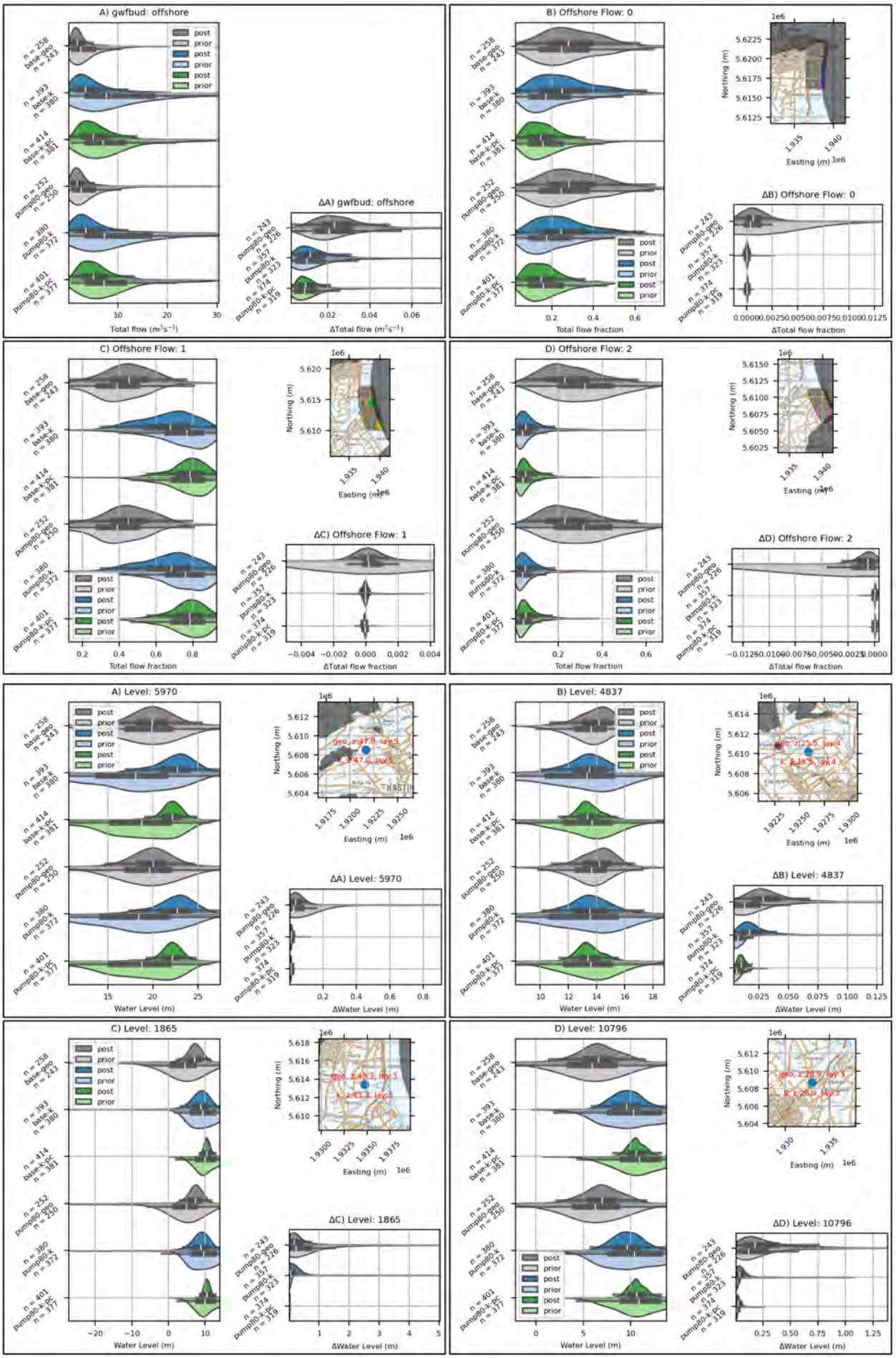
A) gwfbud: offshore
ΔA) gwfbud: offshore
B) Offshore Flow: 0
ΔB) Offshore Flow: 0
C) Offshore Flow: 1
ΔC) Offshore Flow: 1
D) Offshore Flow: 2
ΔD) Offshore Flow: 2
A) Level: 5970
ΔA) Level: 5970
B) Level: 4837
ΔB) Level: 4837
C) Level: 1865
ΔC) Level: 1865
D) Level: 10796
ΔD) Level: 10796
post
prior
Total flow (m³s⁻¹)
ΔTotal flow (m³s⁻¹)
Total flow fraction
ΔTotal flow fraction
Water Level (m)
ΔWater Level (m)
Northing (m)
Easting (m)
1e6

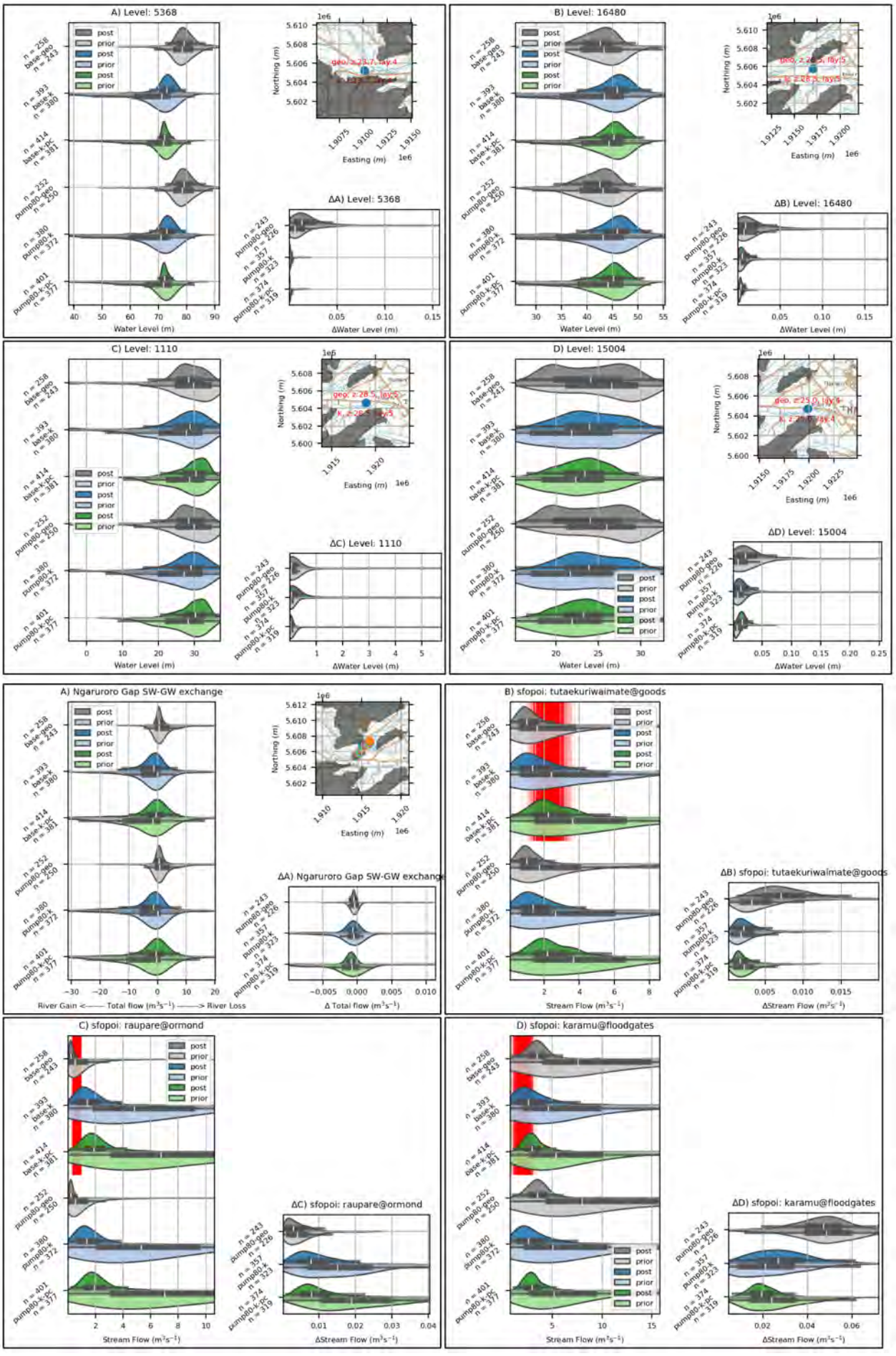
A) Level: 5368
B) Level: 16480
C) Level: 1110
D) Level: 15004
ΔA) Level: 5368
ΔB) Level: 16480
ΔC) Level: 1110
ΔD) Level: 15004
Water Level (m)
ΔWater Level (m)
Easting (m)
Northing (m)
A) Ngaruroro Gap SW-GW exchange
B) sfopoi: tutaekuriwaimate@goods
C) sfopoi: raupare@ormond
D) sfopoi: karamu@floodgates
ΔA) Ngaruroro Gap SW-GW exchange
ΔB) sfopoi: tutaekuriwaimate@goods
ΔC) sfopoi: raupare@ormond
ΔD) sfopoi: karamu@floodgates
River Gain <—— Total flow (m³s⁻¹) ——> River Loss
Δ Total flow (m³s⁻¹)
Stream Flow (m³s⁻¹)
ΔStream Flow (m³s⁻¹)

1 Fairway Drive, Avalon 5011
PO Box 30368, Lower Hutt 5040

gns.cri.nz